Evolution of Volcanism and Hydrothermal Activity in the Yanacocha Mining District, Northern Perú

By
Anthony A. Longo

Ph.D. Geology Dissertation
Department of Geosciences

Doctoral Defense
April 7, 2005
COAS Admin Conference Rm 106

AN ABSTRACT OF THE DISSERTATION OF

Anthony A. Longo for the degree of Doctor of Philosophy in Geology
presented on April 7, 2005.
Title: Evolution of Volcanism and Hydrothermal Activity in the Yanacocha Mining
    District, Northern Perú

Abstract approved:

_____

John H. Dilles   Anita L. Grunder

The Yanacocha Mining District in northern Perú is considered the largest group of high-sulfidation style epithermal gold deposits in the world. District-scale geologic mapping coupled with detailed $^{40}Ar/^{39}Ar$ geochronology, geochemistry and petrography establish the volcanic history of the area and analyze the temporal and spatial evolution of volcanism, hypogene advanced argillic alteration, and Au-Cu-Ag mineralization. Volcanic rocks spanned from ~19.5 to 8.4 Ma and evolved temporally from andesite (60% SiO_2) to rhyolite (71% SiO_2). Rocks older than 15 Ma erupted from pre-Yanacocha volcanic centers outside the district. Volcanic rocks of the Yanacocha Volcanic Field erupted in the district from 14.5 to 8.4 Ma contemporaneous with magmatic-hydrothermal quartz-alunite that is directly associated with the deposition of gold ore. Alunite ages define several discrete pulses of hydrothermal activity that spanned 5.4 m.y., from 13.6 to 8.2 Ma.

Magmatism and hydrothermal activity progressed northeast through time across the district. Five periods of magmatic activity with volcanism and six pulses of hydrothermal activity have been interpreted from the volcanic stratigraphy and age data. Volcanism alternated between dominantly effusive and explosive stages. Eruptions began 14.52±0.13 Ma with the Lower Yanacocha andesite lavas in the west and ended by 11.22±0.08 Ma with the explosive eruption in the east of the dacitic San Jose ignimbrite. Magmatism then shifted to highly oxidized dacite to rhyolite magmas characterized by domes and isolated intrusions of porphyry plugs, and ended in the final explosive

eruption of the Negritos rhyolite ignimbrite at 8.43±0.04 Ma. Volumes and rates of eruption peaked from 14.5 to 11.2 Ma during eruptions of the Lower Yanacocha andesite and the San Jose ignimbrite, and then decreased dramatically after ~11 Ma.

Alunite ages indicate hydrothermal activity began in the west at the Cerro Negro Oeste and Quilish deposits from 13.56±0.24 to 12.64±0.61 Ma, and migrated east to the Carachugo and Maqui Maqui deposits where separate pulses developed from 11.01±0.09 to 10.73±0.05 Ma and 10.24±0.14 to 9.95±0.14 Ma. Activity then became centered at the Cerro Yanacocha deposit from 9.25±0.10 to 8.22±0.46 Ma. Comparisons of volcanic and alunite ages suggest that most gold deposition events correlate with periods of low volcanic eruption rates. Rates of gold deposition increased dramatically after ~11 Ma when eruptive output decreased and magmatic SiO_2 content increased.

The $^{40}Ar/^{39}Ar$ dates demonstrate that magmatic and hydrothermal activity lasted 2.2 and 4.8 m.y. longer than previously hypothesized for Yanacocha.

Evolution of Volcanism and Hydrothermal Activity in
the Yanacocha Mining District, Northern Perú

by

Anthony A. Longo

A DISSERTATION

submitted to

Oregon State University

In partial fulfillment of
the requirements for the
degree of

Doctor of Philosophy

Presented April 7, 2005
Commencement June 2006

Doctor of Philosophy dissertation of Anthony A. Longo
Presented on April 7, 2005.

APPROVED:

_____

Co-Major Professor, representing Geology

_____

Co-Major Professor, representing Geology

_____

Chair of the Department of Geosciences

_____

Dean of the Graduate School

I understand that my dissertation will become part of the permanent collection of Oregon
State University libraries. My signature below authorizes release of my dissertation to
any reader upon request.

_____

Anthony A. Longo, Author

ACKNOWLEDGEMENTS

Lastly, I wish to thank my family for their love, understanding, and support throughout the last 4 ½ years. I express my greatest thanks to my wife Bernadette for her love and support, and all her work at home as a mother while I was bent over the computer or living in the Noble Gas Laboratory. Most of all I thank my daughter Shasta. She patiently spent many hours waiting for me to come home night after night. She was able to join me for my field seasons in Perú. She moved from her home in Philomath to Hawaii, Michigan, and back to Oregon, experiencing Kindergarden in three schools so that her dad could finish the Ph.D. She waited one year to start her new life in Perú and is a very accepting, easy going, and a wonderful child. I wish to dedicate this thesis to her.

CONTRIBUTION OF AUTHORS

All these data were collected solely by the author. Prof. John Dilles and Prof. Anita Grunder assisted with the study design, the interpretations of field work and analytical data, along with the writing of Chapter's 2, 3, and 4. The author prepared samples and performed age and microprobe analysis in facilities at Oregon State University. Prof. Robert Duncan supervised the ^{40}Ar/^{39}Ar dating of these rocks, and assisted with interpretation of these data and the writing of Chapter 2.

TABLE OF CONTENTS

CHAPTER I

CHAPTER II

CHAPTER III

TABLE OF CONTENTS (Continued)

CHAPTER IV

GEOCHEMICAL VARIATION WITH TIME OF CENOZOIC
VOLCANISM IN THE YANACOCHA DISTRICT,
NORTHERN PERÚ ………………………………………..… 206

CHAPTER V

TABLE OF CONTENTS (Continued)

LIST OF FIGURES

LIST OF FIGURES (Continued)

LIST OF FIGURES (Continued)

LIST OF FIGURES (Continued)

LIST OF FIGURES (Continued)

LIST OF FIGURES (Continued)

LIST OF FIGURES (Continued)

LIST OF FIGURES (Continued)

LIST OF FIGURES (Continued)

LIST OF FIGURES (Continued)

LIST OF TABLES

LIST OF TABLES (Continued)

LIST OF TABLES (Continued)

LIST OF PLATES

Map Inserts:

LIST OF APPENDICES

LIST OF APPENDIX FIGURES

LIST OF APPENDIX FIGURES (Continued)

LIST OF APPENDIX TABLES

LIST OF CD APPENDICES

LIST OF CD PLATES

This Dissertation is dedicated to my loving daughter Shasta Rosa Longo.

Shasta and the author mapping volcanic rocks in the Lower Yanacocha volcanic sequence near Cerro Atazaico, west district of Yanacocha, Perú (July, 2001).

EVOLUTION OF VOLCANISM AND HYDROTHERMAL ACTIVITY IN THE YANACOCHA MINING DISTRICT, NORTHERN PERÚ

INTRODUCTION

Yanacocha is a world-class mining district in the Cajamarca Province of northern Perú (Figure 1.1) with reserves and production of more than 50 million ounces of gold in oxide ore and an unknown resource of gold and copper in sulfide (Myers and Williams, 2000). The property is owned and operated by Minera Yanacocha S.R.L., a joint venture with 51.35% Newmont Mining Corporation, 43.65% Compania de Minas Buenaventura, S.A.A., and 5% International Financial Corporation (Newmont Annual Report, 2004). In 2003, Newmont reported a gold reserve of 31.7 million ounces with a heap leach grade of 0.03 ounces/ton calculated at 325 USD per ounce gold price (Newmont, 2004; p. 51). Since mining activity began in 1993, gold production has exceeded 14.5 million ounces (a value of >$6 billion at the 2005 average price of 425 USD per ounce Au) from mines in the core of the district (Leng, 1999; Hall, 2000; Newmont, 2003, p. 26; Newmont, 2004, p. 32) earning Yanacocha the reputation as the leading gold producer in South America, and the largest and most productive group of high-sulfidation style epithermal gold deposits in the world.

The district was first worked by native Peruvians during pre-Incan time, and pits were dug in nearly every site that present day exploration has discovered a gold deposit. It is believed that the pre-Incan and Incan cultures fashioned a technology for exploiting clays and silica for ceramics, cinnabar, and native gold from Yanacocha. The district was forgotten until 1968 when exploration for porphyry copper deposits was near its peak, and the Japanese spent over 2 years testing the base metal potential around Cerro Yanacocha. The district was subsequently explored by the British Geological Survey and the French government, and in 1983 Yanacocha was acquired by Newmont Mining Corporation (Pavard and Bowerman, 1994). Exploration began in 1984, and mining operations were inaugurated at the Carachugo Sur gold deposit in 1993 (Pavard and Bowerman, 1994).

Miocene volcanic rocks at Yanacocha represent a large volcanic field known as the Yanacocha Volcanic Field (YVF) with compositional variations that typify a continental subduction-related, calc-alkaline rock suite. Rocks in the Miocene YVF are host to Au ore and are temporally and spatially associated with the hydrothermal activity. The district represents a series of high-sulfidation epithermal ore deposits characterized by the presence of hydrothermal alteration with alunite ± pyrophyllite + quartz, vuggy quartz, granular quartz, and massive quartz with gold ± copper ± silver (Turner, 1997; Harvey et al., 1999; Longo, 2000). High-sulfidation style epithermal deposits worldwide are characterized by the presence of zones with alunite + quartz ± pyrophyllite and other minerals typical of hypogene advanced argillic alteration at relatively low temperature (~150-350°C), and ore minerals with relatively high sulfur content that form under highly acidic, oxidized, and sulfidized hydrothermal conditions (Arribas, 1995). At Yanacocha, high-sulfidation epithermal gold deposits developed as clusters aligned in a N50°E direction over a 15 km distance. Intense and widespread hydrothermal alteration related to the ore deposits was developed over a zone as wide as 8 kilometers and covers an area of over 100 km^2 (Harvey et al., 1999). On a local scale, the ore deposits cluster in trends that follow E-W, northwest and northeast directions. Deposit clusters include (1) the westernmost Cerro Negro Oeste and Este deposits, and the Cerro Quilish complex; (2) the centrally located Corimayo-Tapado complex and the Cerros Yanacocha complex; (3) the San Jose deposit and the Carachugo-Chaquicocha-Quecher Complex; and (4) the Maqui Maqui and Arnacocha deposits to the northeast (Figure 1.2). La Quinua is a deposit of gold ore-bearing glacial outwash gravels eroded from the Cerros Yanacocha Complex that fills a graben and covers a deeper bedrock deposit at Corimayo-Tapado (Williams and Calderón, 2000; Mallette et al., 2003). The bedrock deposits range in size from 400,000 to over 4 million ounces of gold (Harvey et al., 1999; Teal et al., 2002). Six mines presently in production are Cerro Negro, La Quinua, Cerro Yanacocha, Carachugo, San Jose, and Maqui Maqui.
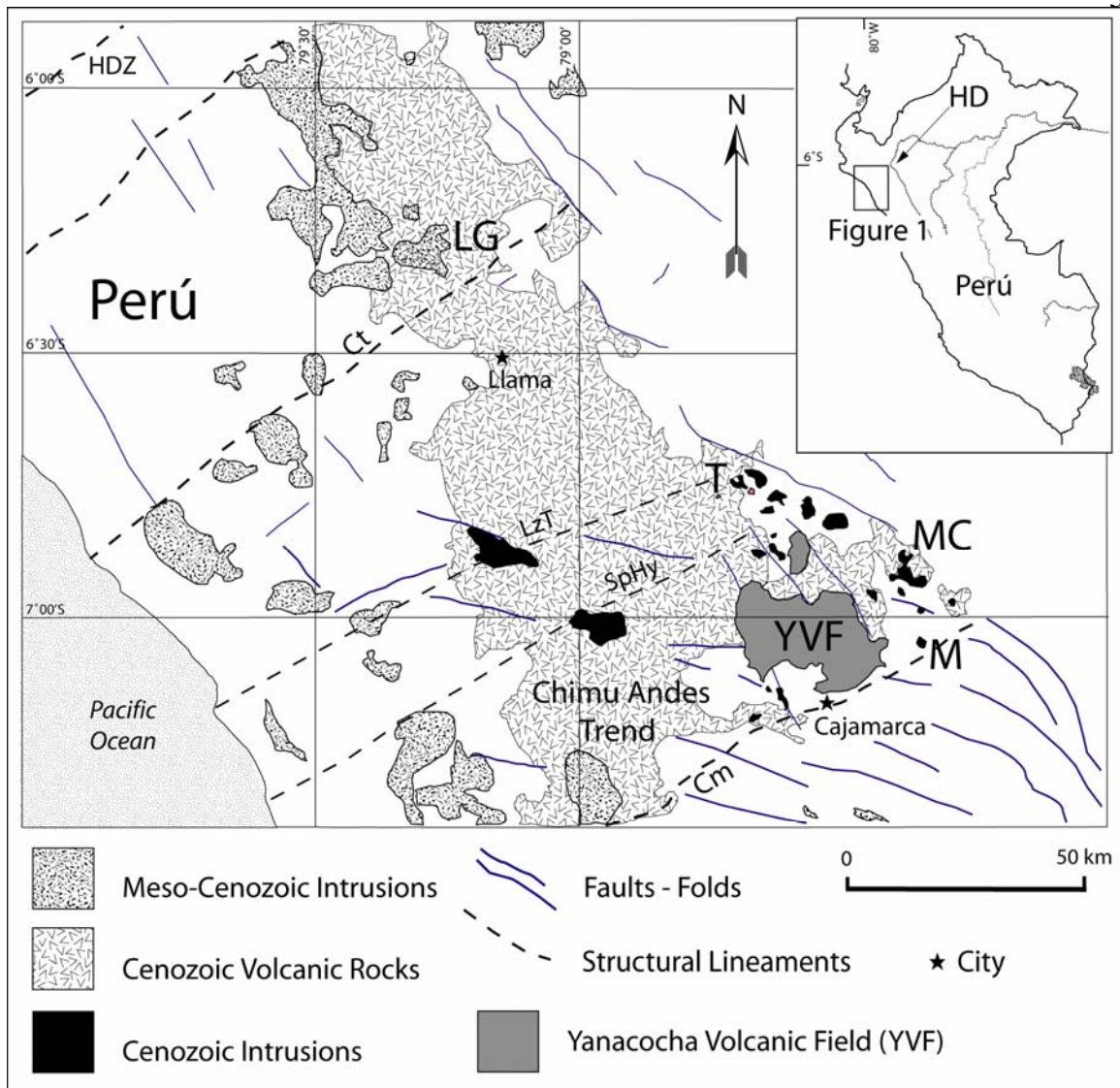
Figure 1.1 Location map of the Yanacocha Mining District located in the Yanacocha Volcanic Field (YVF) in northern Perú. The figure also displays the locations of various areas and districts mentioned in the text. Porphyry Cu-Au and other Au and base metal systems define a northwest trend from the Michiquillay (M) and Minas Congas (MC) porphyry Cu-Au deposits, to the Tantahuatay (T) high-sulfidation gold deposit. The trend could extend to the La Granja (LG) base metal district. HDZ represents a projected northeast trend to the Huancabamba deflection (location in the map inset as HD). The Chimu Andes trend of fold axes and faults extends below the YVF and continues west-northwest across the LzT. The Chicama-Yanacocha structural corridor is delineated by the La Zanja-Tantahuatay Lineament (LzT) and the Cajamarca Lineament (Cm). The Cutervo Lineament (Ct) is also shown and may represent the northwest boundary of the Chimu Andes Trend.

Scope of the Study

This dissertation comprises three manuscripts (Chapters 2, 3, and 4) that present results from district-scale geologic mapping over a study area of ~1000 km^2 centered at Yanacocha, 65 radiometric ^{40}Ar/^{39}Ar ages, 185 geochemical and petrographic analyses, and microprobe analyses on hornblende and pyroxene (including preliminary analyses on apatite from two important ash-flow tuffs). These data have resulted in major revisions to the volcanic stratigraphy, the timing of mineralization, and the district geologic model. It is the first study to describe in detail the volcanic stratigraphy of the Yanacocha district with the perspective and insight gleaned from extensive geologic mapping of the fresh rocks outside the halo of hydrothermal alteration. It also is the first study to test the spatial and temporal relationship of the volcanic and intrusive rocks with the hydrothermal alteration across the entire 15 km length of the district.

Purpose and Methodology

Volcanic rocks at Yanacocha belong to a large volcanic field known as the Yanacocha Volcanic Field with compositional variations that typify a continental subduction-related, calc-alkaline rock suite. These rocks are host to Au ore and are temporally and spatially associated with the hydrothermal activity. The economic importance and incredible magnitude of the high-sulfidation Au deposits at Yanacocha has generated great interest and the continued study of the volcanic and intrusive rocks. The present study describes the volcanic stratigraphy of the Yanacocha District and unravels the temporal relationship of volcanism to hypogene advanced argillic alteration and Au-Ag-Cu mineralization. The study documents the sequence of volcanic events that shaped Yanacocha, establishes the volcanic history of the area, and analyzes the temporal and spatial evolution of volcanism, hypogene advanced argillic alteration, and mineralization. An analysis of the timing and association of volcanism with alteration developed an understanding for the petrologic history of the igneous rocks and helped to identify the magmatic processes related to mineralization. The study integrated field geology with ^{40}Ar/^{39}Ar and petrologic analyses in order to define more clearly the stratigraphy, the type of volcanic system, and the timing of volcanism and mineralization.

The work is relevant to assessing the remaining mineral potential of the greater Yanacocha District, and so of direct benefit to Minera Yanacocha, S.A. and Newmont Mining Corporation.

Design Overview

Extensive field mapping, core logging, and radiometric $^{40}Ar/^{39}Ar$ dating were used to establish the volcanic stratigraphy and temporal framework of volcanism and Au-Cu mineralization within the Yanacocha District and surrounding region. Detailed petrography, bulk rock oxide and trace element chemistry, and microprobe mineral analyses were undertaken in order to examine the magmatic chemistry and petrologic evolution, and assist in defining the stratigraphy as outlined in this study. These data document the composition of the volcanic rocks and how they vary with stratigraphic position and time. The study allows a test of the hypothesis that volcanism and mineralization are coeval Miocene events. Work focused on the fresh volcanic rocks that surround the zone of intense hypogene advanced argillic alteration. A field program was designed that included field mapping at 1:25,000 scale, sampling, and detailed core logging of the igneous rocks within and around Yanacocha District. Fieldwork began by mapping fresh volcanic rocks beyond the limits of the district. These rocks are the unaltered analogs of the volcanic rocks that host gold, silver, and copper ore within the Yanacocha District and were mapped from outside district boundaries into the core of the district (termed the "outside-in" mapping concept during the fieldwork). Least-altered volcanic and intrusive rocks were sampled from areas within and surrounding the Yanacocha District for radiometric dating and petrologic analysis. Alunite was collected from zones of quartz-alunite alteration within and surrounding the ore zones of each major Yanacocha deposit. Isotopic analyses of sulfur from alunites in this study were used to demonstrate whether alunite was formed by hypogene versus supergene processes.

Results of this study produced the following products:

(1) A geologic map and two cross sections (north-south and east-west across the map area) at 1:50,000 scale that include the Yanacocha district and surrounding volcanic terrane.

(2) Detailed field and petrographic descriptions of each rock sequence outlined in the study designed in chart and graphical formats that may be useful in the field.

(3) A generalized stratigraphic section of the volcanic and intrusive rocks for the district.

(4) A composite chronostratigraphic summary that shows temporal and spatial relationships of the volcanic stratigraphy, intrusions and gold-copper ore at Yanacocha.

(5) Detailed stratigraphic columns from specific locations across the district that detail the volcanic stratigraphy and unit thicknesses.

(6) A comparison of past stratigraphic models with the revised stratigraphic model of this study.

(7) A geochronological summary of the rock units, alteration and mineralization from across the district.

(8) Descriptive geochemical and microprobe analyses for each rock sequence that include visual modeling with major element oxide and trace element variation and Pierce variation diagrams combined with detailed petrographic descriptions and geology in an attempt to characterize the magmatic processes related to mineralization.

(9) A hypothesis that relates the petrology, geochemistry, and age of volcanic rocks to the temporal and spatial relationship to the Au-Cu mineralization, and the hypogene advanced argillic alteration that halos the high-sulfidation gold deposits.

This study has several scientific outcomes that may provide potential economic benefit to Minera Yanacocha, S.A. and Newmont Mining Corporation. Potential benefits include the following:

1. Identification and preliminary evaluation of additional prospective zones of alteration outside the current district boundaries was accomplished during the field geology portion of this study. Areas identified included a 6 kilometer-long *Yanacocha Parallel Trend* that lies to the southeast of the San Jose-Carachugo-Chaquicocha-Quecher trend from Bosque de Piedra to Opalita Sur to Pozo de Azufre and Combayo (Longo, 2001).

2. A detailed model of volcanic stratigraphy and facies (via extensive field mapping, core logging, radiometric $^{40}Ar/^{39}Ar$ dating, and petrologic analyses) that may be useful for exploration of conceptual targets covered by fresh volcanic rocks within district boundaries such as along the Quilish-Corimayo trend at Pampa Corimayo (Longo, 2004).

3. Recognition of favorable lithologic and volcano-tectonic controls to gold ore that may lead to important target concepts and could be applied to regional exploration.

4. Development of a petrologic history for the igneous rocks at Yanacocha that may identify the magmatic processes related to mineralization;

5. A comprehensive model for the evolution of volcanism and the temporal relationship of volcanism to acid-sulfate alteration and Au-Cu mineralization at Yanacocha that will improve the quality of conceptual targeting, project mapping, and ultimately, better exploration models.

6. A volcanic exploration model that may be exported worldwide to similar geologic settings.

Tectonic and Geologic Setting

Tectonics and Magmatism of Northern Perú

Tectonic episodes of the Andean Cycle in Perú (Cobb et al., 1981; Megard, 1984) began with the subduction of the Farallon Plate in the early Mesozoic and have lasted for more than 200 million years (Petford and Atherton, 1995). Several episodes of compression and uplift followed by various magmatic events and their coeval phases of extension shaped the Andes of northern Perú beginning in Late Triassic and ending late Miocene. Much of this understanding comes from work done in central and southern Perú (Noble et al., 1974; Noble et al., 1985), and only a smattering of data exist to explain the tectonism and the magmatic history in northern Perú (Noble et al., 1990).

Four major structural settings have been recognized in northern Perú (Figure 1.1). Near the location of Cajamarca a major bend is present and the trend of fold axes in the Mesozoic basement diverge from their characteristic northwest Andes Cordillera Trend to a set of west and west-northwest striking fold axes and faults that extend below the Yanacocha Volcanic Field. This deflection in the Andes fold belt is known as the Chimu Andes Trend and is attributed to the early Cenozoic Inciac I fold and thrust belt (Benavides, 1999). The characteristic northwest Andes Trend continues north of the Chimu trend at approximately 6°30'S. A second major bend in the Andes Cordillera known as the Huancabamba Deflection is present ~200 km north of Cajamarca situated at 4°S (Mitouard et al., 1990). In this area the northwest trending Andes Cordillera at 140°

bends to the northeast at 20°. An important structural corridor defined by prominent northeast trending faults and fracture zones extends for 120 km from the Cutervo Lineament to the Cajamarca Lineament and hosts several significant metal deposits. The Cutervo-Cajamarca zone accommodates three major structural blocks defined by the two major lineaments and two intermediate lineaments informally known as the La Zanja-Tantahuatay lineament and the Sipan-Hualgayoc lineament. The Chicama-Yanacocha structural corridor represents the southeast half of the Cutervo-Cajamarca structural zone and hosts the most important ore deposits in the region including the Yanacocha district (Quiros, 1997; Turner, 1999; Torres et al., 2001). Finally, a northwest trend defined by eight separate porphyry Cu-Au systems is situated 20 km northeast of the Yanacocha district and may extend for nearly 125 km from Michiquillay to La Granja (Llosa et al., 1999; Torres et al., 2001).

Deformation that led to the development of the Mesozoic fold belt represents the initial stage of the Andean Cycle. Four compressional events have been recognized since the Triassic period that produced intense pre-Cenozoic deformation and folds that trend predominately west-northwest to northwest in northern Perú (Reyes, 1980; Cobbing et al., 1981; Wilson, 1984; and Megard, 1984 and 1987). Four additional compressional events followed in the Cenozoic Era and spanned ~ 50 m.y. from ~ 60 to 10 Ma (Noble et al., 1974; Cobbing et al., 1981; McKee and Noble, 1982; Noble et al., 1985 and 1990; and Benavides, 1999). The compressional events recognized in northern Peru are listed as follows: (1) Late Triassic compression and uplift in the eastern cordillera, (2) Middle Jurassic Vicusian Orogeny in northern Peru and southern Ecuador, (3) Cretaceous Mochica or Subhercycian Orogeny (100-95 Ma), (4) Cretaceous-Paleocene Peruvian Orogeny (90-60? Ma), (5) Paleocene-Eocene Incaic I Orogeny (59-55 Ma), (6) Eocene Incaic II Orogeny (43-42 Ma), (7) Miocene Quechua I Orogeny (23 Ma in northern Peru), and (8) Miocene Quechua II Orogeny (12-11 Ma in northern Peru).
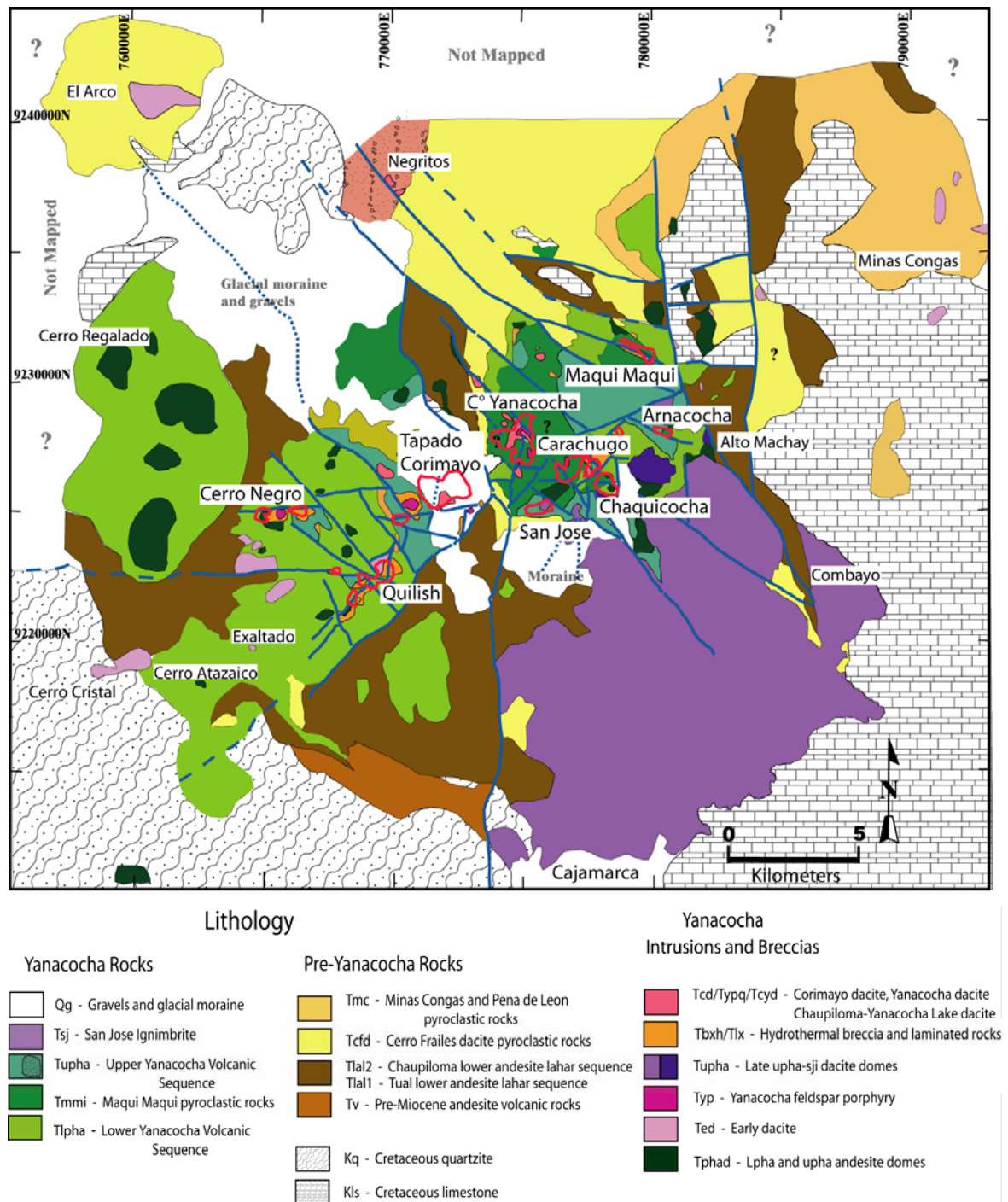
Figure 1.2. Simplified geologic map of the Yanacocha district including the location of the high sulfidation gold deposits outlined in red. The geologic interpretation is based on field geology and the geologic map from this study discussed in detail in later sections.

Early volcanism of the Andean Cycle (Zeil, 1979; Cobbing et al., 1981; Palacios et al., 1995; Quiroz, 1997; Atherton, 1990; Petford and Atherton, 1995) began with Late Triassic-Early Jurassic Mariana-style island-arc magmatism and back-arc extension. Late Jurassic extension developed the western basins, and an island arc erupted in northern Peru. Magmatism then moved from island arc to continental arc coeval with Early Cretaceous extension and the emplacement of the Coastal Batholith (100-55 Ma) and began with the eruption of tholeiites of the Casma Volcanic Sequence that crop out along the coast in northern Peru from Lima and Trujillo. Between the Peruvian and Incaic Orogenys (~60 Ma) magmatism migrated southward to form the Toquepala Volcanic Sequence of southern Perú.

The $^{40}Ar/^{39}Ar$ and K/Ar ages (Table 1.1) from northern Perú (Noble et al., 1990) indicate four periods of Cenozoic volcanism beginning in the Early Eocene (55 Ma) and ending in the Late Miocene (8.2 Ma). Each magmatic event is separated by a period of erosion marked by an unconformity. These unconformities are interpreted by Noble et al. (1990) as correlative with five periods of subduction-driven compression defined by geologic mapping and radiometric dating along various transects through central and southern Perú (McKee and Noble, 1982; Noble et al., 1985, 1990).

Cenozoic volcanism in northern Perú (Cobbing et al., 1981; Noble et al., 1990; Turner, 1997; Noble and McKee, 1999; Benevides, 1999) began with eruptions of the Llama and Calipuy Volcanic Sequences at ~ 55 Ma after the Incaic I Orogeny. Volcanism flared up once again after the Incaic II Orogeny (~44 Ma) with eruptions of volcanic rocks of the Porculla Formation (39 Ma) and Huambos Formation (35.4 Ma). During the Oligocene Epoch, northern Perú experienced a quiescence of volcanism, and magmatism again migrated southward and is represented by the lower Tacaza Volcanic Sequence in southern Perú (Noble and McKee, 1982). Following the Quechua I phase deformation at ~23 Ma volcanism flared up, and the development of the Miocene arc began near Yanacocha. Conglomerates, volcaniclastic rocks and air-fall tuff of the Chala sequence (23.2 Ma; Table 1.1) were deposited over the Huambos Formation above an angular unconformity (Noble et al., 1990). Early Miocene volcanism progressed from 19.5 to 16.0 Ma (this study) with the eruption of andesite lava flows and lahars from eroded stratovolcanoes. These rock units filled deep, southwest-draining valleys such as

Rio Porcon north of Cajamarca. An extensive sequence of dacite tuffs and lahars was erupted at 15.5 Ma (this study), and these rocks overlie the Early Miocene andesite lahars and lava flows. Volcanism continued during Middle and Late Miocene with eruption of the Yanacocha Volcanic Field (14.5 to 8.4 Ma; this study). At ~ 8.4 Ma arc volcanism ceased with the initiation of flat-slab tectonics and associated volcanic gap from 2°S – 15°S in northern Peru (Gutscher et al., 1999). Magmatism shifted south to central Peru where Late Miocene to Pliocene volcanism and associated back-arc extension followed the Quechua II and Quecha III orogenic phases (Noble et al., 1985) and emplacement of the main part of the Cordillera Blanca Batholith (Pitcher, 1974; Atherton and Petford, 1996). Currently, volcanism is active ~650 km north of Yanacocha in the Northern Volcanic Zone from 2°S to 5°N and in the Central Volcanic Zone from 15°S in southern Peru to 27°S in northern Chile.

Structure

The tectonic events that led to the development of the major structural features at Yanacocha are poorly understood in northern Peru. The Chimu trend (Figure 1.1) of folds and faults, related to the Mesozoic fold belt east of Cajamarca, trend west northwest to northwest (Reyes, 1980; Wilson, 1984) beneath Yanacocha and may have been reactivated forming a zone of faults and fractures in the Miocene volcanic section at Yanacocha. The lithology of pre-Cenozoic basement rocks below the Yanacocha volcanic rocks is not known, however, the presence of rare quartzite and black hornfels and argillite fragments found in the intrusive rocks, pyroclastic rocks, and pebble dikes throughout the district suggests that quartzite and argillite underlie the district. The depth to basement is not well known and only estimated by geophysical data (Goldie, 2000) and a few widely scattered drill hole intercepts. Furthermore, thick-bedded micritic limestone crops out northeast of the Maqui Maqui gold deposit and along the La Quinua fault at Tatiana ~3 km north of Corimayo in the central portion of the district (Figure 1.2).

Three major trends of faults and fracture sets are recognized as important controls for gold ore at Yanacocha and include N35-50ºW, N40-60ºE, and east-west (Edwards,

2000; Longo, 2000; Harvey et al., 1999: Myers, 1997b). Other structures of importance include north-south to north-northwest trends interpreted as faults. These faults have been recognized by Myers (1997b), Klein et al. (1999), Edwards (2000), and Klein (2000) in the West District especially at Quilish and Cerro Negro. Alunite alteration of the volcanic rocks along the faults is assumed to be associated with the main high-sulfidation event and gold ore (Turner, 1997; Harvey et al., 1999; Prihar, 1998).

Problems with the Regional Volcanic Stratigraphy

The region surrounding Yanacocha was first mapped by Reyes (1980), Wilson (1984), and Cobbing et al. (1981). Volcanic units mapped by Reyes (1980) as mid-Tertiary San Pablo volcanics in the south do not conform to the volcanic units mapped as early Tertiary Llama Formation by Wilson (1984) in the north. Cobbing et al. (1981) resolved this discrepancy and combined both units as Porculla Volcanics but ignored erosional unconformities proposed by Reyes (1980) and Wilson (1984).

All major dacite to rhyolite ash-flow sheets in the region that cap ridge tops and fill valleys have been classified as Huambos Formation by Wilson (1984). He assumed a Late Neogene age and linked the Huambos tuff with a late period of pyroclastic eruptions that covered enormous areas of the Andes after uplift. Noble et al. (1990) collected a suite of samples for K/Ar dating along a traverse north of Yanacocha from Llama to Bambamarca (Figures 1.1 and 1.3). Their work resulted in major revisions to the stratigraphy of Wilson (1984) by confirming a Late Eocene age of 39.3 Ma for the Huambos Formation at its type area.

Many problems and confusion still exist in how the volcanic sections are correlated across the region. Surrounding Yanacocha on many ridge tops are spectacular columns of weathered ash-flow tuffs and lahars that local geologists call "Huambos" or "Frailones" tuff because the columnar outcrops resemble kneeling monks praying (los frailes). Wilson (1984; p. 57) stated "the topographic expression of the Huambos volcanics is very characteristic and generally forms plains bordered by escarpments of irregular columns or cliffs and incised by systems of dendritic drainages." The tuffs of the "Huambos" volcanics also have the property to be easily worked by simple tools, and

the pre-Inca people carved numerous cavities for tombs in horizontal lines in cliff faces that look like windows called *ventanillas.* The tuff was used for stone construction of buildings in Cajamarca (Wilson, 1984), and is presently mixed with other materials to make bricks. These characteristics for identifying "Huambos" volcanic rocks are widely accepted by local geologists. Consequently, all volcanic rocks that crop out in weathered columns or have "ventanillas" have been termed the "Frailones" and "Huambos" tuff regardless of composition and mineralogy.

Outcrop patterns and general appearance of these volcanic rocks are similar throughout the region around Cajamarca. North-northeast of Cajamarca and south of Yanacocha are thick sequences of ash-flow tuffs referred to as the "Otuzco" tuff. These ash-flow sheets form spectacular cliff faces that house the famous Ventanillas de Otuzco and Combayo. Turner (1997) recognized the "Otuzco" and "Frailones" as two distinct sequences that erupted from separate centers and categorized them as two separate members of the "Huambos" Formation. Turner (1997 and 1999) also described a biotite- and quartz-bearing felsic ash-flow tuff that crops out north-northeast of Maqui Maqui and overlies "Regalado" andesite lava, which he interpreted as the "Frailones" tuff. In these correlations, all ash-flow tuffs referred to as "Huambos," "Otuzco" and "Frailones" were considered to post-date the Yanacocha age gold mineralization, and therefore should be unaffected by the Middle to Late Miocene high sulfidation hydrothermal alteration.
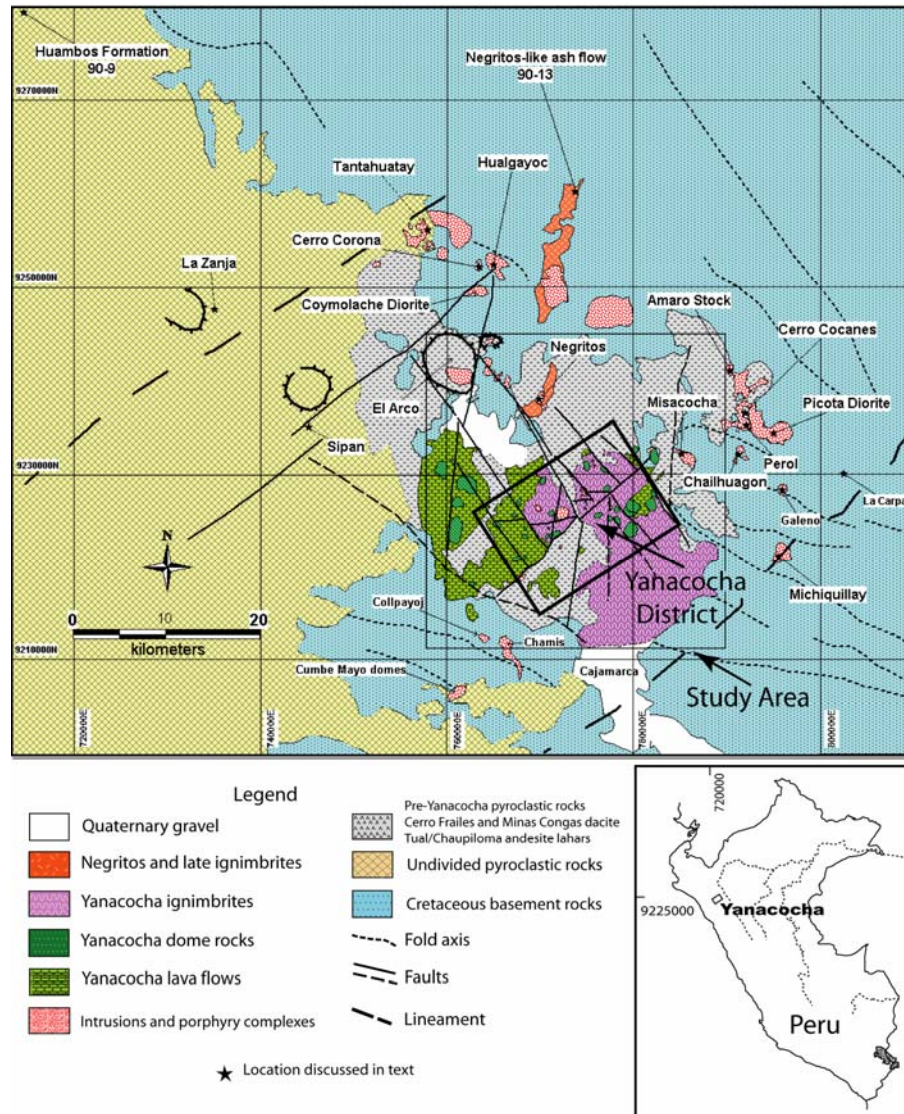
Figure 1.3. Location map of the Yanacocha District and other mineral districts in northern Perú that lie within a structural corridor defined by the Cajamarca and La Zanja-Tantahuatay lineaments (bold dashed lines). The map is modified after Cobbing et al. (1981) with geology from the present study. Ages of mineralization are as follows for districts and locations shown on the map: Michiquillay (20.6 Ma; Laughlin et al, 1968; and 20.1 Ma; Noble, 2002; Noble et al., 2004), Minas Congas-Cerro Cocanes at Perol (16.1 Ma; Noble, 2002; Noble et al., 2004), and Minas Congas-Chailhuagon (15.3 Ma; Noble, 2002), Cerro Corona (13.5 Ma; Macfarlane et al., 1994), Tantahuatay (13.3 – 11.0 Ma; Prihar, 1998), and Yanacocha (13.6 – 8.2 Ma; This study). The range of ages for late Cenozoic magmatism in northern Peru are as follows: Llama Formation (sample 90-1 that lies 8 km west of 90-9; 54.8 to 44.2 Ma; Noble et al., 1990), Michiquillay (46.4 Ma; Laughlin et al, 1968), Picota Diorite (43.6 Ma; Laughlin et al, 1968), Huambos Formation (36.4 Ma; sample 90-9; Noble et al., 1990), Misacocha (20.8 Ma; Llosa et al., 1999), the Minas Congas district from Chailhuagon to the Amaro stock (15.9 Ma; Chauvet and Bailly, 2001), Cerro Corona (14.4 Ma; James, 1998), Cerro Coimolache (14.3 Ma; James, 1998), Cerro Hualgayoc (14.3 Ma; Borredon, 1992; and 9.1 Ma; Macfarlane et al., 1994),Yanacocha (19.5 – 8.4 Ma), Tantahuatay (13.2 – 8.3; Prihar, 1998; Noble and McKee, 1999), and a Negritos-like rhyolite ignimbrite (8.2 Ma; sample 90-13; Noble et al., 1990).

A sequence of andesite lava flows, pyroclastic rocks, and domes at Yanacocha were named the "Regalado" formation by Turner (1997). This name was applied to little altered and fresh andesite lavas and tuffs at Yanacocha and to domes west of Cerro Negro (Figures 1.1, 1.2, and 1.3). Turner (1997) believed the rocks overlay the high-sulfidation gold zones, but later agreed the "Regalado" andesites are part of the Yanacocha Volcanic Field and should not be given separate formation status (Turner, 1999). The Yanacocha andesite volcanics also have been interpreted to correspond to the Porculla Formation. However, $^{40}Ar/^{39}Ar$ dates of Turner (1997) showed that the Yanacocha volcanics are a sequence of Middle Miocene volcanic rocks, whereas the volcanic rocks of the Porculla Formation are Eocene (Noble et al., 1990).

Noble et al. (1974 and 1990) and McKee and Noble (1982) recognized some of the problems in the timing of volcanism and tectonic events in the Central Andes and clarified the ages for some Cenozoic volcanic rocks along a traverse from Llama to Bambamarca north of Yanacocha. K-Ar dates from Noble et al. (1990) confirm Eocene ages of 56.6 to 43 Ma for rhyolite tuffs of the Llama Formation, and 40.3 to 34.2 Ma for tuffs in the type section of the Huambos Formation (Table 1.1d). Wilson (1984) recognized the volcanics of Porculla overlie the Llama Formation and underlie Huambos but assumed a Late Miocene to Pliocene age for the Huambos Formation. These same ash-flow tuffs classified as Huambos Formation by Wilson (1984) are Eocene in age. Moreover, Noble et al. (1990) suggested that the contact between Llama and Porculla is a regional angular unconformity (Inciac II) and that the volcanic rocks of Porculla and Huambos may be conformable.

Stratigraphic Models and Past Work

Prior to the present study, various models (Figure 1.4) for the volcanic stratigraphy and deposit evolution at Yanacocha were proposed by Turner (1997), Harvey et al. (1999), Edwards (2000), Klein (2000), and Longo (2000). In general, all stratigraphic models describe a lower sequence of andesite lava and pyroclastic rocks, a middle sequence of dacite and andesite pyroclastic rocks with water-lain tuffs and volcaniclastic sedimentary rocks, and an upper sequence of andesite lava flows,

pyroclastic rocks, and domes. Turner (1997 and 1999) describes the middle sequence as an andesitic flow-dome complex of porphyritic and pyroclastic rocks and classified them the Yanacocha Volcanic Complex. Turner (1997) and Klein (2000) describe a basal sequence of debris flows, volcaniclastic sediments, and andesite pyroclastic rocks along the Bambamarca road near Cajamarca as pre-Yanacocha Calipuy Group rocks or Llama formation that rest unconformably over Cretaceous basement quartzite and limestone. Some models describe the upper sequence as post-Yanacocha hornblende andesite flow-dome sequence called "Regalado" (Turner, 1997; Harvey et al., 1999) or late porphyritic andesite lava and andesite porphyry (Klein, 2000; Edwards, 2000). Four rock sequences were recognized at Chaquicocha that consisted from oldest to youngest of a lower andesite sequence, laminated rocks, an upper pyroclastic sequence including the
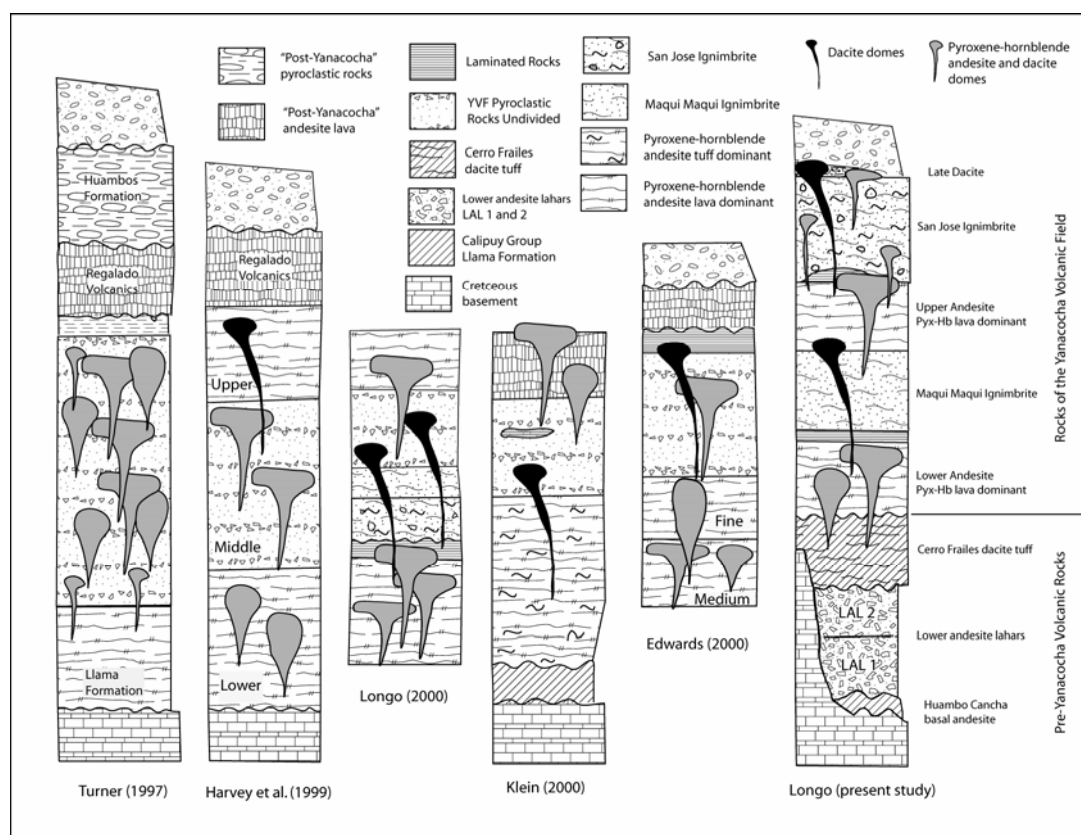
Figure 1.4. Comparison of the past stratigraphic models for Yanacocha to the stratitgraphic model presented in the present study. Thicknesses for the pile of Cenozoic volcanics range from 265 meters to 1.7 km.

San Jose ignimbrite, and upper dacite domes and related pyroclastic rocks (Longo et al., 2000). Phreatic breccias, and upper (late) feldspar porphyries and diatremes crosscut the volcanic and related-dome sequences (Longo et al., 2000; Longo, 2000). All models agree that there were multiple stages of intrusive activity and brecciation culminating with late diatremes and unaltered rhyodacite plugs.

Ignimbrites have long been recognized as an integral part of the volcanic stratigraphy at Yanacocha. Abarca and Harvey (1997) described a pyroclastic sequence at the Encajon deposit on Cerro Yanacocha (now part of the Cerro Yanacocha deposit complex) that contains lithic tuff and eutaxitic textured ignimbrite. Ignimbrites at Cerro Yanacocha are crosscut by heterolithic and matrix-supported breccia plugs termed diatreme (Abarca and Harvey, 1997). Myers et al. (1997) observed a thick sequence of pyroclastic rocks at Carachugo intruded by 11.8 Ma andesite flow-dome complexes and later diatremes. Klein and Barreda (1997) recognized a pyroclastic unit with strong eutaxitic texture overlying porphyritic andesite lava and lithic tuff at the San Jose deposit. This ignimbrite is up to 150 meters thick with large fiamme several centimeters in length (Klein and Barreda, 1997) and was subsequently named the San Jose ignimbrite. The ignimbrite at San Jose was later split into two members that includes an upper fresh to propylitically altered ignimbrite and a lower, strongly acid leached, ignimbrite with advanced argillic alteration, granular and vuggy quartz, massive quartz, and gold ore (Schnell et al., 2000). The upper unit is separated from the lower unit by a narrow, horizontal layer of clay considered altered vitrophyre, and therefore, the ignimbrite was classified post-mineral by some Yanacocha geologists. Noble (1997) analyzed the "fresh" vitrophyre and found that it was opaline amorphous silica alteration within the ignimbrite. Ignimbrites with previously altered accidental fragments, eutaxitic textures, and rare rheomorphic textures were observed at San Jose (Klein and Pinto, 1999), Cerro Baul (Barreda, 1999; Longo et al., 1999), Chaquicocha (Longo et al., 1999a; Longo et al. 2000; Longo, 2000), Corimayo (Gomez, 2000), Arnacocha (Longo et al., 1999b; Masterman and Bartra, 2000), and Maqui Maqui (Quiroz et al., 1995; Bartra et al., 1999).

Previous Geochronology Work and Studies

Numerous radiometric ages of unaltered volcanic and intrusive rocks and hydrothermally altered rocks from other mineral districts throughout the region are summarized in figure 1.3. All ages are reported with their estimated analytical error. These data indicate that the first pulse of magmatic activity was Eocene age and includes rhyolite and dacite ash-flow tuffs of the Llama Formation and the Huambos Formation (Noble et al., 1990). Over 55 km southeast, the Minas Congas and Michiquillay districts have diorite stocks that span 4 m.y. of Middle Eocene time (Laughlin, 1968; Thompson, 2002). Volcanism of Oligocene age is presumed absent in northern Peru (Noble et al., 1990), and the next pulse of magmatism was in early to Middle Miocene that spanned ~ 4.9 m.y. from Misacocha and Amaro to Chailhuagon (Llosa et al., 1999; Chavet and Bailly, 2001; Thompson, 2002). Magmatism during the Middle Miocene was widespread over 25 km from Chailhuagon to the Tantahuatay district. Combined ages from Tantahuatay, Cerro Corona and Hualgayoc districts span 6.2 million years from 14.5 to 8.3 Ma (MacFarlane et al., 1994, James, 1998, Prihar, 1998). Hydrothermal activity associated with the ore deposits in districts around Yanacocha is also of Miocene age and range from 20.1 to 11.0 Ma (Figure 1.1). These include porphyry Cu-Au mineralization at Michiquillay, Chailhuagon and Perol, and Cerro Corona that range in age from 20.1 to 13.5 Ma (MacFarlane et al., 1994; Llosa et al., 1999; Noble, 2002). High-sulfidation style epithermal deposits are younger and spanned 2.3 million years from 13.3 to 11.0 Ma in the Tantahuatay district (Prihar, 1998).

At Yanacocha, previous K/Ar (Noble et al., 1990; Noble, 1999) and ^{40}Ar/^{39}Ar dates (Turner, 1997) defined a sequence of Middle Miocene volcanic rocks that ranged from 12.5 to 11.4 Ma. Alunite alteration of the volcanic rocks spanned 0.6 million years from 11.5 to 10.9 Ma (Turner, 1997) and was associated with the main high-sulfidation mineralization event and gold ore (Turner, 1997; Harvey et al., 1999). Late dacite and rhyodacite dikes intruded the volcanic rocks from 9.9 to 8.4 Ma (Turner, 1997). These age data suggested volcanic activity spanned 1.1 million years followed by 600,000 years of hydrothermal alteration culminating with post-mineral magmatic activity of dacitic composition that lasted 1.5 million years. The conclusions were based on 12 radiometric

ages including seven ages from volcanic and dome rocks, two ages from dacite intrusions, and three ages from alunites. Sampling for geochronology was confined to the northeast portion of the district, and two alunites came from the Carachugo deposit (10.92 Ma, Turner, 1997; 10.95 Ma, Noble, 1999). A third alunite dated advanced argillic alteration with trace gold at Cerro Azufre southwest of the Maqui Maqui deposit (11.5 Ma; Turner, 1997).

Concurrent Work at Yanacocha

Many geologists have contributed to the understanding of the geology and volcanic stratigraphy in the Yanacocha district during the course of this study. Geologists whose work contributed to the interpretation of the stratigraphy, that began in earnest in 1999 and continued concurrently with the present study, include Jorge Barreda, Rafael Bartra, Peter Bell, Juan Escalante, Jeff Edwards, Elmer Flores, Jaime Gomez, Bruce Harvey, Thomas Klein, Carlos Loayza, Steve Moore, Stan Myers, Hernando Terrones, Peter Rogowski, Miguel Rutti, Eric Saderholm, Lewis Teal, Cesar Velasco, Cindy Williams, and the author of this dissertation whose work at Yanacocha as a geologist spanned nearly four years from 1997-2001 prior to this study.

The current understanding of the volcanic stratigraphy is the result of a compilation of over four years of extensive core logging and field mapping. In 1999 at Chaquicocha Sur, a team of exploration geologists recognized distinct lithologic characteristics in outcrops and drill core. As work progressed, the understanding of the volcanic stratigraphy in the Yanacocha district advanced concurrently with the work as presented in this study. Moore and Saderholm (2002a and b) presented the volcanic stratigraphy for the entire Yanacocha district and compiled stratigraphic columns for twelve sites that included Corimayo, Tapado-Rocio, San Jose-Punto Negro, San Jose Norte-Baul, Yanacocha-Carachugo-Chaquicocha, Quecher, Barranco, Hornamo-Cori Cashpa, Quebrada Pampa Larga-Huayhua, Colorado-Maqui Maqui, Arnacocha-Maqui Maqui Sur, and Huacataz. Three interpretive district-wide cross sections were compiled that demonstrated the continuity of the volcanic rock sequences as proposed by Saderholm and Moore (2002b). As noted in Figure 1.5, most of the stratigraphic units and correlations are broadly equivalent with those reported in this study.
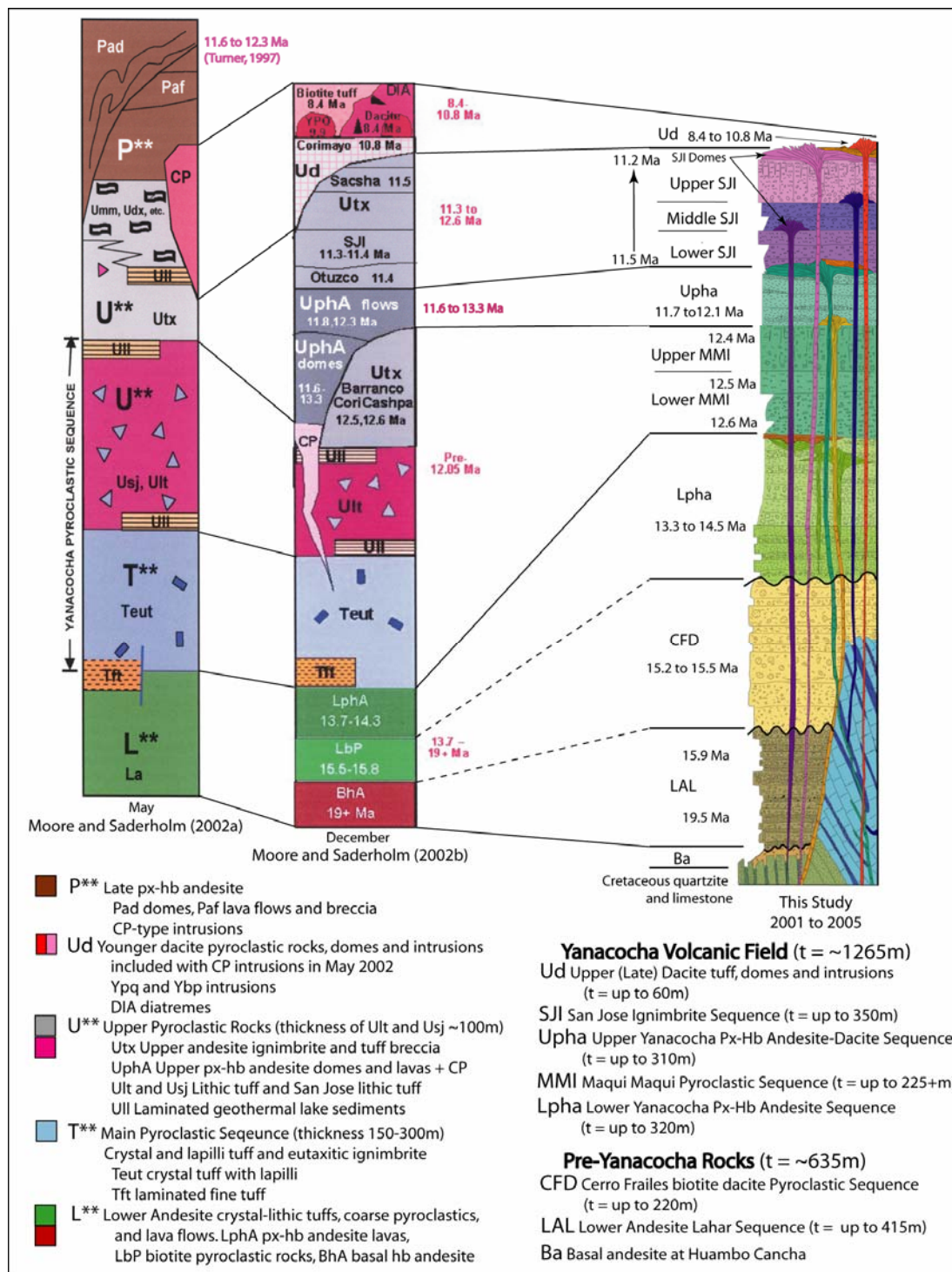
Figure 1.5 Comparison of the volcanic stratigraphy at Yanacocha from this study and two versions from Moore and Saderholm (2002). Thicknesses (t) are reported as maximum thicknesses estimated from the field geology. The May 2002 section is the interpretation before applying the ^{40}Ar/^{39}Ar dates from this study, and the December 2002 section is after the dates were applied resulting in similarities to the stratigraphy of this study.

Two versions of the volcanic stratigraphy from Moore and Saderholm (2002a; 2002b) are presented in Figure 1.5 for comparison to the volcanic stratigraphy from this study. The early version of Moore and Saderholm (2002a) is the stratigraphic interpretation before applying the $^{40}Ar/^{39}Ar$ dates from this study. This version (May 2002) displays three distinct volcanic lithologies with similarities to the previous models in Figure 1.4 as follows: (1) a lower andesite sequence with lavas and pyroclastic rocks (La), (2) a middle sequence of Yanacocha andesite to dacite pyroclastic rocks with interlayered fine laminated tuffs and volcaniclastic sedimentary rocks (Teut and U**), and (3) an upper (late) sequence of andesite lava flows, pyroclastic rocks, and domes (P**). All upper sequence P rocks are presented as pyroxene-hornblende andesites with ages that range from 11.6 to 12.3 Ma (Turner, 1997). The middle pyroclastic sequence is further divided into two sub-units that include: (1) a main pyroclastic sequence (Teut) of poorly welded crystal and lapilli tuffs with accidental basement fragments quartzite and argillite that are locally welded with distinct eutaxitic textures (hence the name Teut for "transitional" eutaxitic), and (2) an upper lithic-rich pyroclastic sequence (Utx) with interbedded laminated rocks and the well-known ignimbrites of the San Jose (Usj) and Maqui Maqui (Umm).

The stratigraphic section from Moore and Saderholm (2002b) is a later version after applying the new $^{40}Ar/^{39}Ar$ dates obtained by this study. This version (December 2002) has many similarities to the stratigraphic interpretation that has evolved from 2001 to present as part of this study. Figure 1.5 examines these relationships in detail, and the Moore and Saderholm (2002b) units equate to the units of this study as follows:

(1) The Lower Andesite sequence from Moore and Saderholm (2002b) is separated into three units that correspond to this study's pre-Yanacocha rocks (LAL and CDF) and the Lower Yanacocha andesite sequence (Lpha).

(2) The Teut, Ult, and the Utx Barranco and Cori Cashpa tuffs correspond to this study's upper and lower Maqui Maqui pyroclastic sequence (MMI).

(3) The UphA sequence of Moore and Saderholm (2002b) is equivalent to the Upper Yanacocha pyroxene-hornblende andesite and dacite sequence (Upha) of this study.

(4) Overlying the UphA are a sequence andesite pyroclastic rocks with ignimbrites named Utx pyroclastics by Moore and Saderholm (2002b). These rocks are equivalent

to the San Jose ignimbrite sequence (SJI) of this study, and include the Sacsha breccia, the SJI, the Umm, and the Otuzco tuff. These Moore and Saderholm (2002b) units equate to the units of this study as follows: the Sacsha breccia is equivalent to the Upper San Jose spatter ignimbrite (Upper SJI); the Otuzco tuff and SJI are equivalent to the Lower and Middle members of the San Jose ignimbrite sequence Middle and Lower SJI); and the Umm is the Maqui Maqui ignimbrite (MMI).

(5) Overlying and intruding the Utx are younger dacite pyroclastics and intrusions (Ud) (Moore and Saderholm, 2002b). These include dacite domes and lava flows at Corimayo, Rocio, San Jose and Punto Negro; the Yanacocha quartz porphyry (Ypq) and the Yanacocha biotite porphyry (Ybp) dacite and rhyolite plugs at Cerro Yanacocha, phreatomagmatic diatreme breccias, and coeval biotite dacite tuffs at China Linda. These rocks are equivalent to units named in this study as the Upper (late) Dacite that includes the Corimayo and La Quinua dacite domes and related dacite pyroclastic rocks, the Yanacocha and Chaquicocha quartz porphyry plugs, the Punta Negra dacite plug, the Cori Cashpa dacite plug and breccia, and the Chaupiloma – Yanacocha Lake rhyolite dikes and plugs. As discussed below, this study correlates the dacite tuffs at China Linda as part of the older ignimbrites of Peña de Leon near Minas Congas and the pre-Yanacocha Cerro Frailes dacite pyroclastic sequence (refer to Chapter 3).

Flores et al. (2003) developed a lithologic and structural model for the Quilish deposit, and defined the volcanic stratigraphy for the west district, by logging thousands of meters drill core. The stratigraphy was described as lower "bimodal" andesite porphyry and an overlying lithic-crystal tuff intruded by andesite dikes, quartz dacite porphyry and large breccia bodies described as phreatic, hydrothermal and silica oxide breccia.

Bell et al. (2004) captured the concept of shallow-level porphyry plugs, diatremes, and the margins of domes as controls that influenced mineralization in the Yanacocha district, and discuss another version of the volcanic stratigraphy. They described the volcanic stratigraphy in terms of three depositional phases that include the following: (1) a lower andesite that rests unconformably over Creataceous basement rocks, (2) a middle sequence of pyroclastic rocks that include lower crystal-rich tuffs and upper lithic-rich

tuffs, and (3) upper andesite lava flows, domes and minor pyroclastic rocks that overlie the middle sequence pyroclastic rocks. Bell et al. (2004) concurred with many workers in the district that the entire volcanic section at Yanacocha is intruded by multiple phases of andesite and dacite, and that quartz dacite plugs and dikes are associated with the deeper porphyry style gold-copper mineralization.

Important work conducted by consultants included studies by Meldrum (2001) and Rehrig and Hardy (2001). Patterns of geochemical zonation around the Cerro Yanacocha gold-silver deposit and the Corimayo gold deposit were studied and modeled by Meldrum (2001). Rehrig and Hardy (2001) completed an in-depth structural analysis of the central Yanacocha gold district, and over 8,000 structural measurements were recorded from numerous exposures in road cuts, open pits, and natural outcrops. These works led to continued studies and reevaluations of many areas of known mineral resources within the district.

One such area was the small high-grade deposit at Chaquicocha Alta. This deposit was discovered Fall of 1999 by a MYSA team of geologists after detailed geologic mapping and surface sampling at the scale of 1:2,000. They defined a stockwork zone of rib-like veinlets with coinciding barium, mercury, arsenic and tin anomalies (see Longo et al., 2000). The veinlets developed within a northwest corridor and displayed northwest, east-west, and north-south trends, and they were interpreted as quartz-alunite overprinted with granular quartz alteration. A high-grade gold surface sample (10 g/t Au) collected from a pre-Incan prospect led to the initial core drilling and discovery hole CHQ-93 where visible gold with barite was found only 25 meters below barren quartz alteration. Gomez (2002a) continued the study of the Chaquicocha Alta high-grade gold deposit with detailed mapping at a scale of 1:500. He described the structural setting and hydrothermal system in much greater detail than all previous work and developed an exploration model useful for finding high-grade gold in high-sulfidation gold systems.

University studies conducted concurrently with the present study include Loayza (2002), Pinto (2002), and Gomez (2002). Below are brief descriptions for these studies. (1) Pinto (2002) was first to document the Kupfertal porphyry Cu-Au system at Yanacocha and suggest that the hydrothermal advanced argillic alteration associated

with the high-sulfidation gold deposits is gradational with depth and in transition with the deeper porphyry-style hydrothermal biotite alteration at Kupfertal.

(2) Loayza (2002) completed a geologic study on the Cerro Yanacocha deposit and recognized four stages of mineralization closely associated with hydrothermal alteration related to high-sulfidation events. His study suggested that the host rocks to the Cu-Ag mineralization and gold ore belong to a volcaniclastic sequence over 700 meters thick. The base of the section is described as an andesite porphyry sequence overlain by a eutaxitic-textured ignimbrite with sparse porphyritic accidental fragments. Both units display intermediate to advanced argillic and propylitic alteration. The basal sequence is overlain by a strongly silicified intermediate sequence of rocks interpreted to be pyroclastic consisting of crystal-lithic tuffs and ignimbrites; however, the hydrothermal alteration destroys the original textures. An upper sequence of moderately to strongly altered fragmental rocks is described as lithic tuffs and ignimbrite with large fiamme. Andesite domes intruded the volcaniclastic sequence and andesite lava flows overlie the pyroclastic rocks. Loayza (2002) stated that the volcanic stratigraphy is intruded by several generations of breccias and intrusions.

(3) Gomez (2002b) documented the geology of the Corimayo gold deposit and described a maar-like setting with volcaniclastic sediments and a related pyroclastic apron intruded by a dacite dome. He described the annular pattern for gold ore around the dacite dome and many of the altered fragmental rocks at depth that host ore as tuffs and tuff breccias.

The stratigraphic interpretation as presented in this study is the authors, but draws on all district knowledge gathered by Minera Yanacocha S.R.L. (MYSA). The interpretation (Figures 1.4 and 1.5) is based on new geologic mapping, $^{40}Ar/^{39}Ar$ dating, geochemistry, and petrography presented in this study, and includes my knowledge gleaned from four years of work with MYSA prior to the present study. I wish to acknowledge both named and unnamed contributions of all geological workers, and apologize for any omissions. The improved stratigraphic understanding offered here and by Moore and Saderholm (2002a and b) is the result of a MYSA team effort.

Table 1.1a Age determinations from previous work in the Yanacocha Region: Cerro Corona, Tantahuatay and Hualgayoc

Sample	Location	Easting	Northing	Age (Ma)	Mineral	Analytical Technique	References
Andesite porphyry	Cerro Jesus de Hualgayoc	No data	No data	14.30±0.70	No data	K-Ar	Borredon (1982)
Quartz diorite	Cerro Corona	763480	9252260	14.4±0.10	Zircon	U-Pb date	James (1998)
Diorite Stock	Cerro Coimolache	762000	9250000	14.3±0.10	Zircon	U-Pb date	James (1998)
Hydrothermal biotite	Cerro Corona	763300	9252260	13.5±0.27*	Biotite	K-Ar	Macfarlane et al. (1994)
Hydrothermal biotite from a small intrusion	near Cerro Corona	763550	9252840	13.4±0.30*	Biotite	K-Ar	Macfarlane et al. (1994)
DDH A-10 altered andesite	Pena de las Aguilas, Tantahuatay	756500	9252500	13.30±0.06**	Alunite	$^{40}Ar/^{39}Ar$	Prihar (1998)
Phyllic altered granodiorite(?)	Quebrada Puente de la Hierba, Tantahuatay			13.28±0.14**	Sericite	$^{40}Ar/^{39}Ar$	Prihar (1998)
Andesite dome	Cerro Mirador Sur, Tantahuatay	756965	9254660	13.20±0.20	Zircon	U-Pb date	James (1998)
DDH M-9, 138.2m, Altered andesite, Norte	Cerro Mirador, Tantahuatay	756500	9254500	12.90±0.06**	Alunite	$^{40}Ar/^{39}Ar$	Prihar (1998)
Andesite dome	Cerro Pirata, Tantahuatay	752300	9252450	12.78±0.69**	Hornblende	$^{40}Ar/^{39}Ar$	Prihar (1998)
Andesite surge tuff	south Cerro Cienaga, Tantahuatay	752600	9252450	12.74±0.09**	Biotite and Hornblende	$^{40}Ar/^{39}Ar$	Prihar (1998)
Monzodiorite	north Quebrada Puente de la Hierba, Tantahuatay	757500	9254350	12.73±0.08**	Biotite	$^{40}Ar/^{39}Ar$	Prihar (1998)
DDH C-29, 237m, Altered andesite	Cerro Cienaga Norte, Tantahuatay	754500	9255000	12.71±0.06**	Alunite	$^{40}Ar/^{39}Ar$	Prihar (1998)
Late to post mineral andesite dike	Cerro Mirador Sur, Tantahuatay	756850	9254550	12.64±0.08**	Biotite	$^{40}Ar/^{39}Ar$	Prihar (1998)
HT-2	Tantahuatay Zone, Hualgayoc, Cerro Tantahuatay	758869	9256023	12.4±0.4*	Alunite	K-Ar	Noble and Mckee (1999)
DDH T-10, 32.0m, enargite-pyrite-alunite vein crosscutting altered andesite	Cerro Tantahuatay 2	758000	9256000	11.01±0.08**	Alunite	$^{40}Ar/^{39}Ar$	Prihar (1998)
Rhyodacite tuff	Cerro Tantahuatay 1	758760	9256050	9.59±0.06**	Biotite	$^{40}Ar/^{39}Ar$	Prihar (1998)
Rhydacite plug-dome	Cerro Hualgayoc	764570	9254640	9.05±0.21*	Biotite	K-Ar	Macfarlane et al. (1994)
TANTADIKE	Dacite dike from the Tantahuatay Zone, Hualgayoc district that cuts mineralized rock	757951	9256950	8.5±0.3* 8.7±0.3*	Biotite	K-Ar	Noble and Mckee (1999)
Rhydacite plug-dome	Cerro Palo de Fierro, Tantahuatay	759570	9253350	8.31±0.03*	Sanidine	$^{40}Ar/^{39}Ar$	Prihar (1998)

* Errors are stated at the 1σ level. ** Errors are stated at the 2σ level. No asterisk means the error level was not reported.

Table 1.1b Age determinations from previous work in the Yanacocha Region: Yanacocha Area

Sample	Location/Notes	Easting	Northing	Age (Ma)	Mineral	Analytical Technique	References
YC-1	Rhyodacite tuff northeast of Maqui Maqui – (should be MM-11)	779730	9232920	15.78±0.17**	Biotite	^{40}Ar/^{39}Ar	Turner (1997)
PL-36	Pampa Larga Yanacocha Flow-Dome	777612	9230540	12.26±0.12**	Hornblende	^{40}Ar/^{39}Ar	Turner (1997)
YB-HBL	Hbl-biotite dacite near Yanacocha Norte exact location unknown	775500	9227500	12.07±0.50*	Hornblende	K-Ar	Noble (1997)
PL-48	Pampa Larga Regalado	777146	9228585	11.79±0.14**	Hornblende	^{40}Ar/^{39}Ar	Turner (1997)
QU-114	alunite at Cerro Azufre ? south of Maqui-Maqui	779500	9228925	11.46±0.15**	Alunite	^{40}Ar/^{39}Ar	Turner (1997)
90-12	Ventanillas de Otuzco - Otuzco Tuff	781126	9212018	11.40±0.60*	Hornblende	K-Ar	Noble et al. (1990)
YB-ALUN	Alunite at Carachugo Sur from Noble in 1997	776400 776970	9226625 9227164	10.95±0.40*	Alunite	K-Ar	Noble (1997)
CA-SUR	Carachugo Sur alunite	776925	9226175	10.92±0.09**	Alunite	^{40}Ar/^{39}Ar	Turner (1997)
YA-74	Rhyodacite intrusion Yanacocha	774790	9228320	9.9±0.05**	Biotite	^{40}Ar/^{39}Ar	Turner (1997)
MM-11	Rhyodacite tuff at Negritos (I believe this sample was mixed up with YC-1 and should have been YC-1 that was collected at Negritos)	770000	9239000	8.42±0.05** 8.79±0.08**	Biotite and Hornblende	^{40}Ar/^{39}Ar	Turner (1997) unknown location NE of Yanacocha and NW of Maqui-Maqui on Crown Tenement
YS-2	Rhyodacite intrusion Yanacocha	775300	9227378	8.4±0.06**	Biotite	^{40}Ar/^{39}Ar	Turner (1997)

* Errors are stated at the 1σ level. ** Errors are stated at the 2σ level.

Table 1.1c Age determinations from previous work in the Yanacocha Region: Minas Congas, Michiquillay, and the Picota Diorite

Sample	Location	Easting	Northing	Age (Ma)	Mineral	Analytical Technique	References
Michiquillay diorite	Michiquillay	No data	No data	46.40±1.8	Hornblende	K-Ar	Laughlin et al. (1968)
Picota diorite	Cocanes Este, Minas Congas	No data	No data	43.60±3.7	Hornblende	K-Ar	Llosa et al. (1999)
T-7-27-4, Minas Congas	Picota Hornblende Diorite	No data	No data	42.03±0.46**	Hornblende	$^{40}Ar/^{39}Ar$	Thompson (2002)
Chailhuagon	Chailhuagon, Minas Congas	No data	No data	23.20±2.1	unknown	K-Ar	Llosa et al. (1999)
Andesite Stock	Misacocha	No data	No data	20.80±1.9	unknown	K-Ar	Llosa et al. (1999)
Michiquillay hydrothermal biotite	Michiquillay	No data	No data	20.60±0.60	Biotite	K-Ar	Laughlin et al. (1968)
J-28/584, Minas Congas	Michiquillay, weak potassic	No data	No data	20.10±0.13**	Biotite	$^{40}Ar/^{39}Ar$	Noble (2002)
T-7-18-1, Minas Congas	Dike: Amaro Stock	No data	No data	17.30±0.21**	Hornblende	$^{40}Ar/^{39}Ar$	Thompson (2002)
T-8-8-1, Minas Congas	Dacite Dome - dacitic porphyry dome in the northeastern part of the map area	No data	No data	17.08±0.03**	Hornblende	$^{40}Ar/^{39}Ar$	Thompson (2002)
T-8-8-2, Minas Congas	Condor Cana Dome Outflow	No data	No data	16.52±0.07**	Hornblende	$^{40}Ar/^{39}Ar$	Thompson (2002)
O-34-96, Minas Congas	Cocanes advanced argillic alteration	No data	No data	16.11±0.18**	Alunite	$^{40}Ar/^{39}Ar$	Noble (2002)
T-7-27-2, Minas Congas	Upper Minas Conga Dome	No data	No data	16.00±0.15**	Alunite	$^{40}Ar/^{39}Ar$	Thompson (2002)
CHA-03 DDH J3-19m	Chailhuagon stock, Minas Congas	No data	No data	15.90±0.20	Hornblende	K-Ar	Chauvet and Bailly (2001)
CHA-08 DDH J3-34.5m	Chailhuagon stock, Minas Congas	No data	No data	15.90±0.20	Hornblende	K-Ar	Chauvet and Bailly (2001)
H18-500m	Chailhuagon stock, Minas Congas	No data	No data	15.50±0.20	Hornblende	K-Ar	Chauvet and Bailly (2001)
H-46/535, Minas Congas	Perol potassic alteration	No data	No data	15.86±0.10**	Orthoclase	$^{40}Ar/^{39}Ar$	Noble (2002)
N-21/235, Minas Congas	Chailhuagon, Potassic alteration	No data	No data	15.35±0.12**	Biotite	$^{40}Ar/^{39}Ar$	Noble (2002)
Granodiorite	Chailhuagon, Minas Congas	No data	No data	14.20±1.3	unknown	K-Ar	Llosa et al. (1999)

* Errors are stated at the 1σ level. ** Errors are stated at the 2σ level. No asterisk means the error level was not reported.

Table 1.1d Age determinations from previous work in the Yanacocha Region: Regional Area

Sample	Location	Easting	Northing	Age (Ma)	Mineral	Analytical Technique	References
90-1	Llama, rhyolite	707712	9278550	54.8±1.8*	Plagioclase	K-Ar	Noble et al. (1990)
90-6	Llama, rhyolite ash-flow tuff	731324	9281222	44.2±1.2*	Sanidine	K-Ar	Noble et al. (1990)
90-8	Huambos, basal ash-flow sheet	712504	9277978	39.30±1.0*	Sanidine	$^{40}Ar/^{39}Ar$, total fusion	Noble et al. (1990)
90-9	Huambos, basal dacitic ash flow sheet Huambos Formation	714354	9279815	36.40±1.0*	Sanidine	K-Ar	Noble et al. (1990)
90-11	Bambamarca, "Chala" sequence	776035	9259996	23.2±1.5*	Plagioclase	K-Ar	Noble et al. (1990)
90-13	Negritos equivalent - SW of Bambamarca., phenocryst-rich rhyolite ash flow containing biotite and abundant sanidine and quartz.	773458	9260931	8.20±0.20*	Sanidine	K-Ar	Noble et al. (1990)

* Errors are stated at the 1σ level.

THE DURATION OF MAGMATISM AND HYDROTHERMAL ACTIVITY IN THE YANACOCHA GOLD DISTRICT, NORTHERN PERÚ

Anthony A. Longo

John H. Dilles

Robert Duncan

Anita L. Grunder

Abstract

The Yanacocha Mining District in northern Perú is considered the largest and most productive group of high-sulfidation style epithermal gold deposits in the world. This paper documents the sequence of volcanic and hydrothermal events that shaped Yanacocha by using district-scale geologic mapping coupled with detailed radiometric $^{40}Ar/^{39}Ar$ incremental heating geochronology. These new data serve as the basis to establish the volcanic history of the area and analyze the temporal and spatial evolution of volcanism, acid sulfate alteration, and Au-Cu mineralization. The $^{40}Ar/^{39}Ar$ ages indicate that the late Cenozoic magmatic activity in the 1000 km^2 study area spanned 11.1 m.y., from 19.5 to 8.4 Ma. Eight volcanic sequences have been recognized, each with a distinctive mineralogy and composition. They represent a calc-alkaline rock suite that temporally evolved from andesite to rhyolite. Rocks older than 15 Ma erupted from pre-Yanacocha volcanic centers outside the district and underlie volcanic rocks from the Yanacocha Volcanic Field (YVF) centered in the district. Volcanic rocks of the YVF erupted over an interval of 6.1 m.y. from 14.5 to 8.4 Ma, contemporaneous with hydrothermal processes that spanned 5.4 m.y. from 13.6 to 8.2 Ma and led to the deposition of gold ore.

Magmatism and hydrothermal activity migrated ~15 km from southwest to northeast over ~6 m.y. across the district. Volcanism began in the west at 14.5 Ma with monogenetic effusive eruptions of pyroxene-hornblende andesite lavas forming a series of stratocones. Andesite dome-building and minor explosive eruptions followed the early effusive activity, and with time volcanism migrated to the northeast becoming dominantly explosive and dacitic in composition with eruptions of the Maqui Maqui ignimbrite (12.63 to 12.40 Ma). At 12 Ma a second stage of effusive eruptions characterized by numerous andesite domes began in the northeastern area from Cerro Negro to Maqui Maqui. A second stage of explosive volcanism followed the effusive eruptions and is characterized by three separate ash-flow tuff eruptions of the San Jose ignimbrite (11.54 to 11.22 Ma). Magmatism then shifted to a stage of small volume highly oxidized dacite to rhyolite magmas that produced three sets of domes and isolated

intrusions of porphyry plugs in the interval from 10.8 to 8.4 Ma. Volcanism ended in a final explosive event with the eruption of the Negritos ignimbrite at 8.4 Ma.

The duration of magmatic and hydrothermal activity was longer and more persistent than previously hypothesized. Hydrothermal activity that formed gold deposits began in the west at Cerro Negro Oeste at 13.5 Ma, migrated 5 km east to Quilish by 12.6 Ma, and then 15 km east northeast to Carachugo and Maqui Maqui. By 10.8 Ma, high-sulfidation gold mineralization became widespread in the east district in a northeast elongated area ~10 km by 5 km from Corimayo to Maqui-Maqui and continued for 700,000 years until 10.1 Ma. Activity then became centered at Cerro Yanacocha by 9.3 Ma for a duration of 1.1 m.y. and ended by 8.2 Ma. The bulk the hydrothermal activity and gold ores are associated with the youngest, small-volume dacite and rhyolite with ages ranging from 10.8 to 8.4 Ma.

Introduction

Yanacocha Overview

Yanacocha is a world-class mining district in the Cajamarca Province of northern Perú (Fig. 2.1) with more than 50 million ounces of gold in oxide ore and an unknown resource of gold and copper in sulfide ore (Myers and Williams, 2000). The district was first worked by native Peruvians during pre-Incan time, and pits were dug in nearly every site that present day exploration has discovered a gold deposit. It is believed that the pre-Incan and Incan cultures fashioned a technology for exploiting clays and silica for ceramics, cinnabar, and native gold from Yanacocha. The district was forgotten until 1968 when exploration for porphyry copper deposits was near its peak, and a Japanese company Nippon Mining spent over 2 years testing the base metal potential around Cerros Yanacocha. The district was subsequently explored by the British Geological Survey and the French government CEDIMIN, and in 1983 Yanacocha was acquired by Newmont Mining Corporation and Compania de Minas Buenaventura (Pavard and Bowerman, 1994). Exploration began in 1984, and mining operations were inaugurated at the Carachugo Sur gold deposit in 1993 (Pavard and Bowerman, 1994).

Miocene volcanic rocks at Yanacocha represent a large volcanic field known as the Yanacocha Volcanic Field (YVF) with compositional variations that typify a continental subduction-related calc-alkaline rock suite. Rocks in the Miocene YVF are host to Au ore and are temporally and spatially associated with the hydrothermal activity. The district represents a series of high-sulfidation epithermal ore deposits characterized by the presence of hydrothermal alteration with alunite ± pyrophyllite + quartz and residual quartz with gold ± copper ± silver (Turner, 1997). High-sulfidation style epithermal deposits worldwide are characterized by the presence of zones with alunite + quartz ± pyrophyllite and other minerals typical of hypogene advanced argillic alteration at relatively low temperature (~150-350°C), and ore minerals with relatively high sulfur content that form under highly acidic, oxidized, and sulfidized hydrothermal conditions (Arribas, 1995).

At Yanacocha, high-sulfidation epithermal gold deposits developed as clusters aligned in a N50°E direction for 15 km. Intense and widespread hydrothermal alteration related to the ore deposits was developed over a zone as wide as 8 kilometers and covers an area of over 100 km^2 (Harvey et al., 1999). On a local scale, the ore deposits cluster in trends that follow E-W, northwest and northeast directions. Deposit clusters include (1) the western-most Cerro Negro Oeste and Este deposits and Cerro Quilish complex; (2) the centrally located Corimayo-Tapado complex and the Cerros Yanacocha complex; (3) the San Jose deposit and the Carachugo-Chaquicocha-Quecher Complex; and (4) the Maqui Maqui and Arnacocha deposits to the northeast (Fig. 2). La Quinua is a +10 million ounce gold deposit of ore-bearing glacial outwash gravels eroded from the Cerro Yanacocha Complex that fill a graben and covers a deeper bedrock deposit at Corimayo-Tapado (Williams and Calderón, 2000). The bedrock deposits range in size from 400,000 to over 4 million ounces of gold (Harvey et al., 1999; Teal et al., 2002). Six mines presently in production are Cerro Negro, La Quinua, Cerro Yanacocha, Carachugo, San Jose, and Maqui Maqui. Newmont reported an existing gold reserve of 31.7 million ounces in December, 2003, with a heap leach grade of 0.03 ounces/ton calculated at 325 USD per ounce gold price (Newmont, 2004; p. 51). Since mining activity began in 1993, gold production has exceeded 14.5 million ounces from mines in the core of the district (Leng, 1999; Hall, 2000; Newmont, 2003, p. 26; Newmont, 2004, p. 32) earning

Yanacocha the reputation as the leading gold producer in South America, and the largest and most productive group of high-sulfidation style epithermal gold deposits in the world.

Three major structural trends are recognized as important controls for gold ore at Yanacocha and include N35-50ºW, N40-60ºE, and west-northwest to east-west (Edwards, 2000; Longo, 2000; Harvey et al., 1999: Myers, 1997b). Structures related to the Mesozoic fold belt in the Yanacocha area trend west-northwest to northwest (Rivera, 1980; Wilson, 1984) and may be translated upward into the Yanacocha volcanic section. Other structures of importance are interpreted as faults that strike north-south to north-northwest. These faults have been recognized by Myers (1997b), Klein et al. (1999), Edwards (2000), and Klein (2000) in the west district and control ore at the Quilish complex and Cerro Negro. Alunite alteration of the volcanic rocks along the faults is assumed to be associated with the main high-sulfidation event and gold ore (Turner, 1997; Harvey et al., 1999, Prihar, 1999). The tectonic events that led to the development of the major structural features at Yanacocha are poorly understood in northern Peru.

Purpose

Volcanic rocks at Yanacocha belong to a large volcanic field known as the Yanacocha Volcanic Field (YVF) with compositional variations that typify a continental subduction-related calc-alkaline rock suite. These rocks are host to Au ore and are temporally and spatially associated with the hydrothermal activity. The economic importance and incredible magnitude of the high-sulfidation Au deposits at Yanacocha has generated great interest and the continued study of the volcanic and intrusive rocks. The present study was designed to test the hypothesis that volcanism and Au-Ag-Cu mineralization were coeval Miocene events. Metal ratios at Yanacocha display a wide range in values with Cu/Au from <1 to >12000 and Ag/Au from <1 to >50 that vary through time. This study was undertaken to establish the volcanic and mineralization history of the area by documenting the sequence of volcanic events that shaped Yanacocha and analyzing the temporal and spatial evolution of volcanism, acid-sulfate alteration, and mineralization.
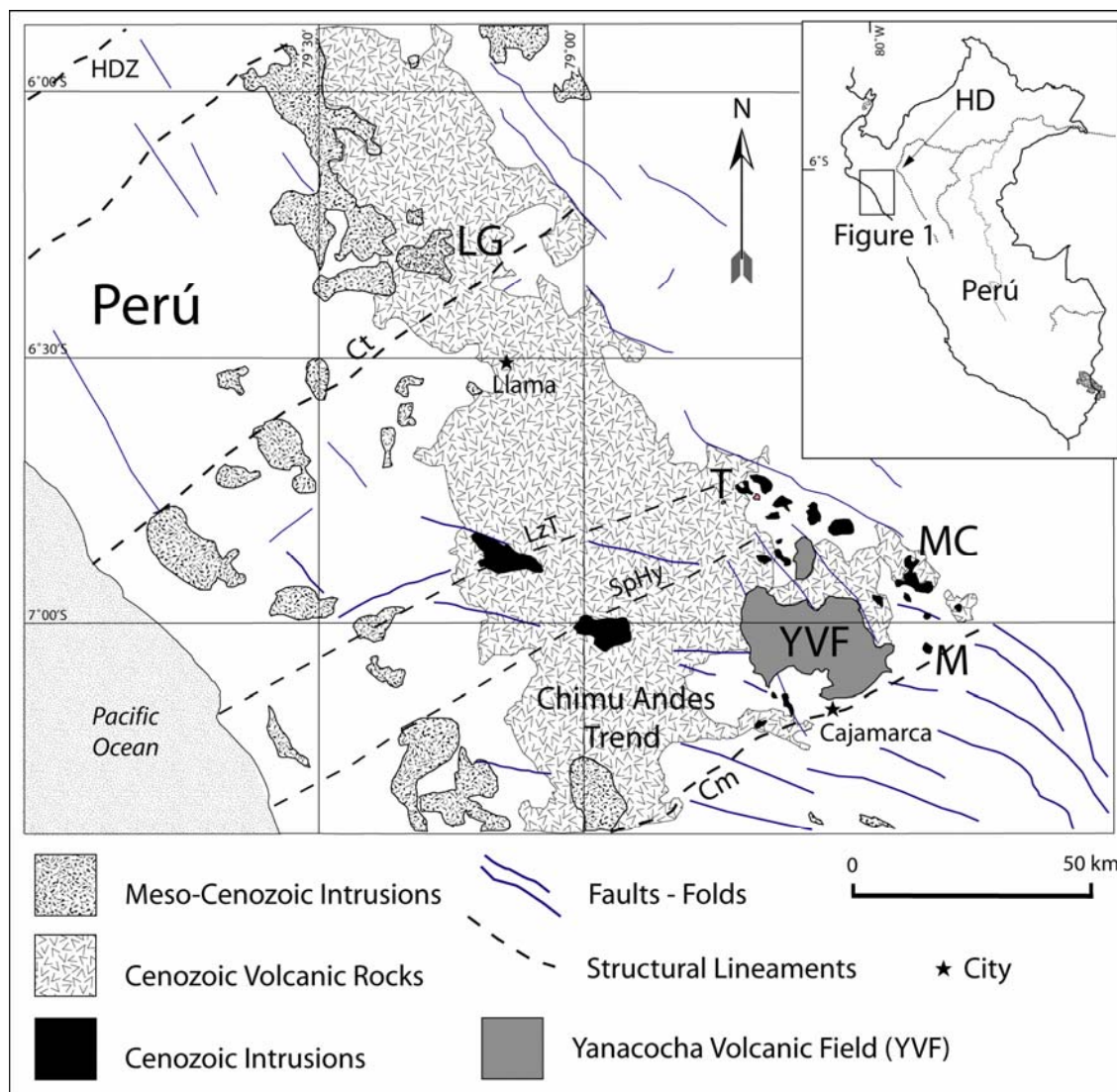
Figure 2.1 Location map of the Yanacocha Mining District located in the Yanacocha Volcanic Field, northern Perú. The figure also displays the locations of various areas and districts mentioned in the text. Porphyry Cu-Au and other Au and base metal systems define a northwest trend from the Michiquillay (M) and Minas Congas (MC) porphyry Cu-Au deposits, to the Tantahuatay (T) high-sulfidation gold deposit. The trend could extend to the La Granja (LG) base metal district. HDZ represents a projected northeast trend to the Huancabamba deflection (location in the map inset as HD). The Chimu Andes trend of fold axes and faults extends below the YVF and continues west-northwest across the LzT. The Chicama-Yanacocha structural corridor is delineated by the La Zanja-Tantahuatay Lineament (LzT) and the Cajamarca Lineament (Cm). The Cutervo Lineament (Ct) is also shown and may represent the northwest boundary of the Chimu Andes Trend.

Field geology integrated with radiometric ^{40}Ar/^{39}Ar age determinations were employed to define the volcanic stratigraphy and the age of volcanism and mineralization. District-wide field mapping at 1:25,000 scale, core logging, and ^{40}Ar/^{39}Ar dating were used to establish the volcanic stratigraphy and temporal framework of volcanism and mineralization within the Yanacocha district. This study discusses new results that include 69 radiometric ^{40}Ar/^{39}Ar ages and district-scale geologic mapping over a study area of ~1000 km^2 centered at Yanacocha. These data have resulted in major revisions to the volcanic stratigraphy, the timing of mineralization, and the district geologic model. The work is relevant to assessing the remaining mineral potential of the greater Yanacocha district, and so of direct benefit for exploration of epithermal high-sulfidation systems worldwide.

Geologic Setting

District-scale geologic mapping and detailed core logging of geology from the Yanacocha ore deposits have resulted in major revisions to the Cenozoic volcanic stratigraphy (Figure 2.2). New stratigraphic relationships at Yanacocha define eight rock packages that include three pre-Yanacocha volcanic sequences and five local volcanic sequences that represent the Yanacocha Volcanic Field as summarized in Chapter III. Rock packages considered pre-Yanacocha include the following in stratigraphic order:

(1) Huambo Cancha andesite lavas and pyroclastic rocks referred to as basal andesite unconformably overlie the Cretaceous basement and early unconformity in the Rio Porcon Valley. These rocks may belong to the Llama (55-44 Ma) or Huambos (39-36 Ma) volcanic sequences as discussed by Noble et al. (1990). The time of the uncomformity at the base of the Huambo Cancha andesite is unknown, but may have resulted during the Cretaceous-Paleocene Peruvian Orogeny (90-60? Ma) and the Paleocene-Eocene Inciac I Orogeny (59-55 Ma) (Cobbing, 1981; Megard, 1984 and 1987; Noble et al., 1985 and 1990).

(2) The Tual and Chaupiloma lower andesite lahar sequence of pumice-rich lahars, debris flows, volcaniclastic sediment, and andesite lava flows and filled paleo-channels in the Huambo Cancha andesite. An unconformity after the Huambo Cancha andesite is
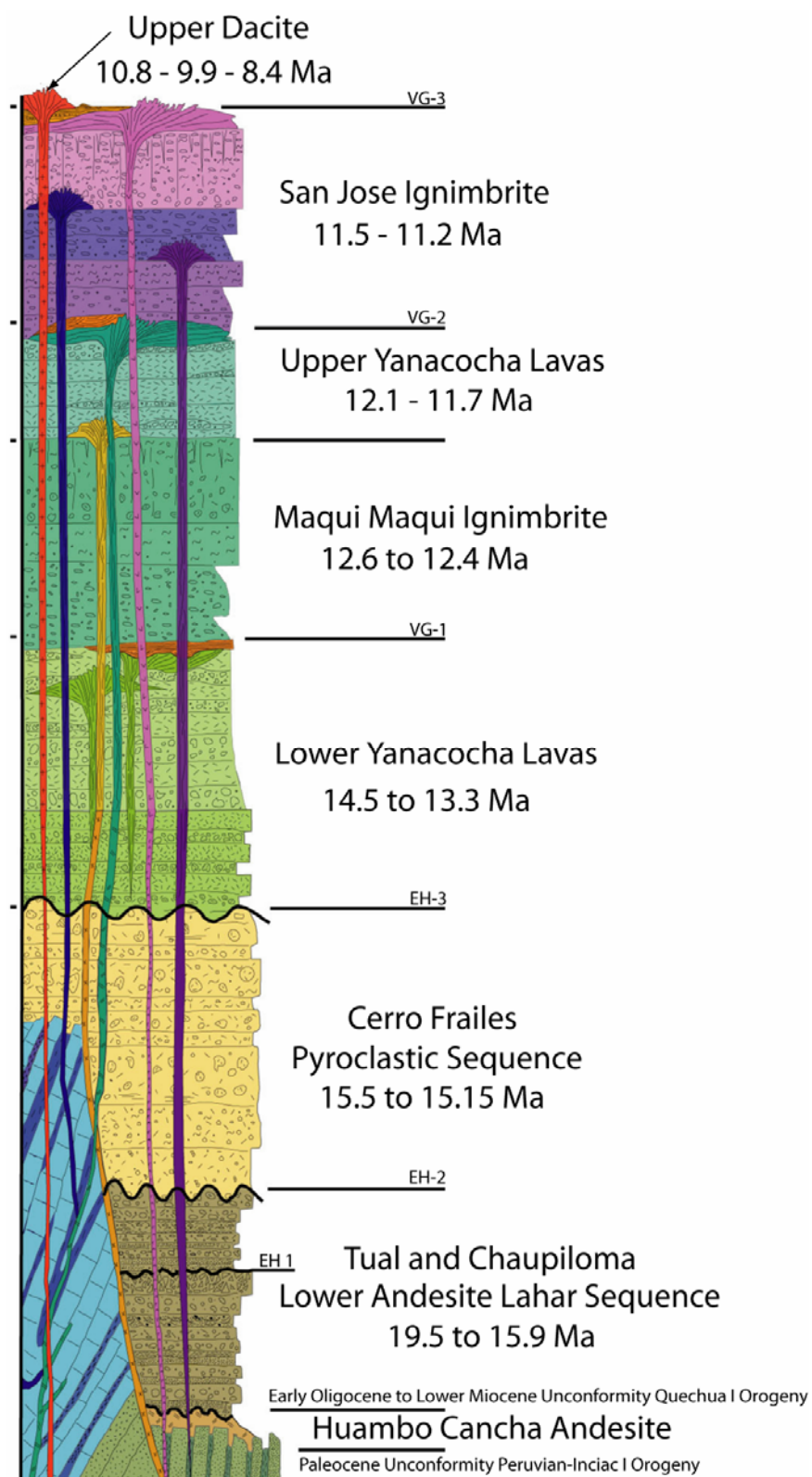
Figure 2.2. Generalized stratigraphic column showing the volcanic stratigraphy as presented in this study. EH – erosional hiatus VG – volcanic gap.

contemporaneous with the Eocene Inciac II or Oligocene Quechua I Orogenies of McKee and Noble (1982), Noble et al. (1985), and Noble et al. (1990).

(3) The Cerro Frailes dacite pyroclastic sequence with coarse biotite-rich dacite lithic ash-flow tuffs and debris flows was erupted and deposited over an erosional hiatus marked by stream channels cut into the andesite lahar sequence. After eruptions of the Cerro Frailes ash-flow tuff the Yanacocha area experienced gentle folding and an erosional hiatus.

Rock sequences that belong to the Yanacocha Volcanic Field (YVF) represent volcanic and intrusive rocks from five contiguous episodes of magmatism centered at Yanacocha. Compositional variations are typical of a calc-alkaline rock suite with a complex magmatic system that progressed from andesite to rhyolite. These rocks evolved from spatially and temporally distinct centers and developed a northeast-trending corridor of Middle Miocene volcanism 25 km long that covered more than 500 km^2 with lava flows and pyroclastic rocks. These relationships genetically link five episodes of volcanism and associated rocks at Yanacocha to the Yanacocha Volcanic Field.

Volcanism began with two periods of dominantly effusive eruptions of andesite composition that culminated in two periods of dominantly explosive eruptions of dacitic composition. The early styles of YVF volcanism were followed by rocks with compositional variations from dacite to rhyolite. These rocks are distinct from older ones and contain the mineral assemblage of sphene + magnetite + quartz implying relatively high oxygen fugacities (Wones, 1989). This late episode of highly oxidized felsic magmas developed porphyritic domes with minor lavas and pyroclastic aprons, and isolated intrusions of dacite porphyry plugs. Volcanism ended in a final explosive event with the eruption of the Negritos rhyolite ignimbrite. Eruption of the Negritos ignimbrite was followed by a cessation of arc volcanism in the Yanacocha area and the initiation of flat-slab tectonics and associated volcanic gap from 2°S – 15°S in northern Perú (Gutscher et al., 1999).

Laminated rocks are present at three levels in the volcanic stratigraphy. Some are distinctly pyroclastic, whereas others have thin and planar laminations of dense silica. They are interpreted as laminated water-lain tuffs and surge deposits within a package of

pyroclastic rocks (Edwards, 2000) and accumulations of colloidal silica that deposited in acid lakes associated with hydrothermal and volcanic vent areas (Longo, 2000).

Rocks of the YVF are as follows in stratigraphic order (Figure 2.2):

(1) The lower Yanacocha pyroxene-hornblende andesite volcanic sequence with lavas and minor pyroclastic rocks from an early period of effusive volcanism and dome building called *effusive stage 1*.

(2) The middle Yanacocha Maqui Maqui pyroclastic sequence with laminated rocks, the lower and upper Maqui-Maqui ignimbrite sequence, and early hornblende andesite and dacite porphyry intrusions. The Maqui Maqui ignimbrite sequence consisted of hornblende ± biotite andesite, trachyandesite, and dacite ignimbrites that represent an early period of explosive volcanism called *explosive stage 1*. These rocks post date and are temporally related to porphyritic intrusions, feldspar porphyry plugs and diatremes with the similar mineral assemblages to the Maqui Maqui ignimbrite. A period of early dacite intrusions with quartz + hornblende + biotite phenocrysts intruded the lower Yanacocha volcanic sequence in the west district.

(3) The upper Yanacocha porphyritic sequence with pyroxene-hornblende andesite and dacite lavas and pyroclastic rocks from a second period of effusive volcanism associated with numerous andesite dome related systems called *effusive stage 2*

(4) The San Jose ignimbrite sequence with hornblende ± pyroxene ± biotite dacite ignimbrites from a second period of explosive volcanism called *explosive stage 2*. Pyroxene-hornblende endogenous dacite domes with compositions similar to the upper Yanacocha volcanic sequence followed the explosive eruptions and may correspond to ignimbrite vent areas.

(5) Upper hornblende-biotite dacite domes and pyroclastic rocks of Corimayo-Tapado, the quartz porphyry dacite plugs of Yanacocha, and the rhyodacite dikes and domes of Chaupiloma-Yanacocha Lake represent the final, highly oxidized, magmatic phase spatially and temporally associated with the ore deposits at Yanacocha.Volcanism ended in a final explosive event with the eruption of the

Negritos rhyolite ignimbrite that may have vented from a fissure near the location of the Chaupiloma and Yanacocha lake rhyodacite dikes (*explosive stage 3*).

Five unconformities, three intervals of erosion or disconformities, and three brief cessations of volcanism were recognized in the field and listed below as follows (Figure 2.2):

(1) A late Cretaceous - early Cenozoic angular uncomformity resulted during the Cretaceous-Paleocene Peruvian Orogeny (90-60? Ma) and the Paleocene-Eocene Inciac I Orogeny (59-55 Ma) (Cobbing, 1981; Megard, 1984 and 1987; Noble et al., 1985 and 1990). All pre-Yanacocha rock packages the Humabo Cancha volcanics, Tual-Chuapiloma lahars, and Cerro Frailes dacite tuffs have been observed to overlie Cretaceous limestone and quartzite with angular unconformity.

(2) An unconformity atop the Huambo Cancha volcanic rocks and below the Tual lahar sequence may be contemporaneous with the late Eocene Inciac II or early Oligocene to lower Miocene Quechua I Orogenies (McKee and Noble, 1982; Noble et al., 1985; and Noble et al., 1990) where andesite lahars of the Tual sequence filled channels from a drainage system that incised the Tv,

(3) *Erosional hiatus 1* may represent a temporal gap and interval of erosion between the Tual member and the Chaupiloma member of the lower andesite lahar sequence. The gap may correspond to a lower Miocene disconformity before the deposition of the Chaupiloma member. Lahars, volcaniclastic sediments and lava flows of the Chaupiloma member have been observed to fill channels that cut down into the Tual member.

(4) *Erosional hiatus 2* represents a second interval of erosion marked by a disconformity between the Tual-Chaupiloma lahar sequences and the overlying Cerro Frailes dacite tuffs. Lahars and tuffs of Cerro Frailes dacite were deposited and filled channels carved into Tual and Chaupiloma lahar sequence. This hiatus is early mid-Miocene and may correspond to a second disconformity.

(5) *Erosional hiatus 3* marks a gap in the stratigraphy and distinct change in the composition of the volcanic rocks at Yanacocha from biotite dacite to pyroxene andesite. After eruptions of the Cerro Frailes pyroclastic rocks, the Yanacocha area experienced gentle folding with an erosional hiatus that may represent a gentle angular unconformity of Middle Miocene. Andesite lava flows of lower Yanacocha volcanic sequence were channeled into a drainage system that cut canyons into the Cerro Frailes tuffs and Tual-Chaupiloma lahars.

In the Yanacocha Volcanic Field, laminated rocks mark apparent time gaps in the volcanic stratigraphy. Laminated rocks consist of a sequence of thinly laminated siliceous rocks interpreted as accumulations of colloidal silica that were deposited in acid lakes intercalated with thin bedded, fine-grained tuffs. These volcanic gaps are as follows (Figure 2.2):

(1) *Volcanic gap 1* is bracketed by Lower Yanacocha andesite lava and a lower Maqui Maqui ash-flow tuff. The gap contains thin laminated siliceous rocks and thin ash layers that lie below the Maqui Maqui pyroclastic sequence.

(2) *Volcanic gap 2* is bracketed by lava flows of the Upper Yanacocha volcanic rocks and the oldest known ignimbrite of the San Jose sequence. The hiatus is marked in some areas by siliceous and opaline laminated rocks below the San Jose ignimbrite sequence. These rocks crop out north of Cerro Paquerumi on the west slope of Quebrada Chaquicocha, below the ignimbrite on Cerro Baul, and at Cerro Chaquicocha. They also were found in drill holes at Huacataz and San Jose Sur. Youngest fresh domes of the Upper Yanacocha sequence lack any outcrop evidence of overlying laminated rocks.

(3) *Volcanic gap 3* represents a time interval after a cessation of San Jose ignimbrite volcanism and before the earliest known dacite dome at Corimayo with an age of ~10.8 Ma. At Corimayo and Rosas, siliceous laminated rocks, tuffaceous lacustrine sediments, and thin bedded tuffs lie below dacite lavas from the Corimayo dome.

Method

Sulfur Isotope Methods

Alunite samples used for geochronology in this study were analyzed for the $^{34}S/^{32}S$ isotopic ratios to test for hypogene origin for each alunite. Coarse alunite samples were hand picked to 80-90% purity, and fine samples where sieved -80+100 mesh removing coarse contaminants (55-65% purity). All samples were analyzed by X-ray diffraction to check purity. A total of 26 samples were submitted for analysis. Duplicates were analyzed for CQ-37, QN-1 and CN-1, and sample TAP-169 had two analyses; one with alunite and some pyrite (TAP-169-1) and another of pure alunite (TAP-169-2A). Also, two samples of pyrite coexisting with alunite were collected from samples YN-105 (Yanacocha Norte) and TAP-169 (Tapado) and analyzed. Results are presented in standard permil notation relative to Canyon Diablo trolite standard ($\delta^{34}S_{cdt}$) in Table 2.3 and figure 2.20.

Samples were analyzed at the G.G. Hatch Isotope Laboratories at the University of Ottawa (Ottawa, Ontario, Canada) employing a FinniganMAT Delta^{plus} mass spectrometer with online GC/C and EA. The mass spectrometer is operated in dual-inlet and continuous-flow modes and is coupled with an elemental analyzer for on-line combustion, a PreCon device, and a gas chromatograph for separation of carbon, nitrogen, and sulfur gases for isotopic analyses. The elemental analyzer provides the mass spectrometer with a bulk sample preparation and inlet system that can handle microgram quantities of sample. It is a furnace that converts sulfur-bearing compounds to SO_2, carbon-bearing compounds to CO_2, and nitrogen-bearing compounds to N_2, which are then analyzed for their isotope ratios.

Each sample was weighed and mixed with V_2O_5 (1:3 weight ratio). The mixture was placed in tin foil and injected into a CE Elemental Analyzer. The samples were combusted at ~1700°C to release SO_2 gas. The gas was passed through 7ml of silicate at 1000°C and a Cu-filter at 600°C to buffer the oxygen isotope composition and reduce any SO_3 to SO_2. Pure SO_2 gas was than introduced to a Finnigan-MAT Delta^{plus} mass spectrometer for the isotope analysis. Standards used were IAEA-S1 (-0.3 permil

$\delta^{34}S_{CDT}$) and IAES-S2 (+21.7 permil $\delta^{34}S_{CDT}$). Laboratory support was provided by Dr. Keiko H. Hattori, Paul Middlestead, and Wendy Abdi.

^{40}Ar/^{39}Ar Methodology

A total of 69 samples were selected from volcanic and intrusive rocks collected throughout the Yanacocha district and dated via the ^{40}Ar/^{39}Ar method. Samples included 48 fresh rocks and 21 hydrothermally altered rocks. The age of volcanism was determined from 23 plagioclase, 1 sanidine, 5 hornblende, 5 biotite and 3 whole rock samples, collected from a variety of ash-flow tuffs and lava flows complemented with 11 samples (6 plagioclase, 2 hornblende, 2 biotite, and 1 whole rock) from domes and intrusions across the region. Petrographic analysis confirmed that 85% of the fresh rocks sampled for radiometric dating were completely undisturbed by the later hydrothermal event responsible for the gold deposits.

Alunite alteration of the Yanacocha rocks is commonly associated with the main high-sulfidation alteration and gold ore (Turner, 1997; Harvey et al., 1999, Prihar, 1999, Hedenquist, 2000). Therefore, ages for mineralization are estimated via dating 20 alunites collected across Yanacocha and represent the following deposits from west to east (Fig 2.4): (1) Cerro Negro Oeste, (2) Cerro Quilish Norte, (3) Corimayo and Tapado, (4) the Cerros Yanacocha Complex, (5) Chaquicocha and Cerro Baul, and (6) Maqui Maqui. Hydrothermal biotite associated with anomalous gold, copper and molybdenum was collected from a diamond drill hole at Kupfertal (Figure 2.4) and provides an age for the hypothesized porphyry system that lies at depth between the Cerros Yanacocha Complex and the San Jose gold deposits.

Sample Selection

Detailed geologic field studies are necessary for an assessment of ^{40}Ar/^{39}Ar geochronology. All ^{40}Ar/^{39}Ar age determinations at Yanacocha are consistent with stratigraphic and intrusive relationships observed in the field and no inconsistencies were found that place major uncertainties in the ages. These relationships were documented by geologic mapping and include obvious contacts above unconformities, distinct differences in mineralogy and composition, and distinct textural features that distinguish

lava dominant sequences versus pyroclastic sequences (Figure 2.2). Samples of the igneous rocks were collected in sites where stratigraphic relationships could be observed in the field. Sampling methodology is reviewed below for each volcanic sequence, and the sample locations are located on Plate 4 with coordinates for each sample in Appendix VI.

Tual and Chaupiloma Lahar Sequences

The age of the Tual lahar sequence (LAL-1) was determined on plagioclase from a pumice-rich andesite lahar (CC-18). The sample was collected from a basal section of the sequence that overlies the Huambo Cancha andesite and the angular unconformity above the Cretaceous quartzite basement at Tual. This is the lowest stratigraphic unit dated of the pre-Yanacocha rocks and it overlies the Huambo Cancha andesite.

Two additional samples represent the Chuapiloma lahar sequence (LAL-2) stratigraphically below Cerro Frailes pyroclastic rocks. These rocks appear to overlie the Tual lahars with an erosional discontinuity. Ages were determined on plagioclase (DN-84) from a glomeroporphyritic andesite lava flow near the top of the LAL-2 section north of Maqui Maqui, and a hornblende (CC-18) from a lahar south of Corimayo at Cerro Collotan.

Cerro Frailes Dacite Pyroclastic Sequence

Ages for the Cerro Frailes dacite pyroclastic sequence were determined from four biotites and one plagioclase collocated from four separate locations around Yanacocha. Samples include basal dacite ash-flow tuffs (DN-12 and DN-71) that overlie prominent outcrops of LAL at Chaupiloma and Maqui Maqui Norte. An ash-flow tuff (Fraile-2) also was sampled north of Maqui Maqui at Cerro de Los Frailes where well bedded dacite tuff breccia and pyroclastic breccia overlie andesite lahars of LAL-2. South of the district boundaries at Combayo, a sample of biotite-rich lapilli tuff (CB-35) was collected from rocks that crop out below the San Jose ignimbrite and west of outcrops of andesite lahars that resemble the Chaupiloma lahar sequence.

Lower Yanacocha Volcanic Sequence

Ages for the Lower Yanacocha pyroxene andesite volcanic sequence were determined for five plagioclases and one whole rock sample that were selected from samples of lava flows and domes collected from across the district. In the west, samples were collected from four locations and include: (1) a quartz-bearing andesite dome (CR-4) that intruded Cretaceous basement rocks and andesite lahars at Cerro Regalado, (2) a pyroxene andesite dome on the summit of Cerro Atazaico (Atazaico), (3) a fine-grained pyroxene andesite lava flow below pyroclastic rocks on the south side of Cerro Quilish (DO-43), and (4) a medium-grained porphyritic pyroxene andesite lava flow in Pampa Cerro Negro (CNN-1) that overlies andesite lahars. In the east district, samples were collected from an andesite tuff breccia at Alta Machay (CB-5) that crops out northeast of Arnacocha adjacent to LAL-2, and a porphyritic andesite lava flow south of Arnacocha (AZU-1) that crops out adjacent vertically flow-banded pyroxene andesite from the Ocucho dome.

Maqui Maqui Pyroclastic Sequence

Ages for the Maqui Maqui pyroclastic sequence were determined from three plagioclases and one biotite in four separate areas of the east district. One sample (DN-30) was collected from the Cori Coshpa ash-flow tuff that overlies the Cerro Frailes dacite sequence ~ 3 km north of Cerros Yanacocha. Other samples came from a crystal-rich, lithic-poor tuff adjacent the Maqui Maqui Norte gold deposit (DN-52), and a eutaxitic-textured ignimbrite below pilotaxitic-textured Upha pyroxene andesite lavas in the Rio Colorado graben west of Maqui Maqui (MM-342). Another eutaxitic-textured dacite ignimbrite (DN-7) was sampled ~ 1.5 km north of Cerros Yanacocha and Barranco and overlies dacite lapilli tuff (DN-12) interpreted as an ash-flow tuff in the Cerro Frailes dacite sequence at Chaupiloma.

Upper Yanacocha Volcanic Sequence

Rocks dated from the Upper Yanacocha volcanic sequence include eight samples of pyroxene andesite and dacite collected from domes, lava flows and a monolithic tuff

breccia. These rocks belong to a thick monotonous section of porphyritic and trachytic pyroxene andesite lavas with associated andesite and dacite domes. Ages were determined on three plagioclases and one hornblende that include: (1) a monolithic tuff (DN-83) in the Rio Colorado graben adjacent an andesite dome at Antonio, and (2) three pyroxene andesite to dacite lava flows from across the district (DO-60, COR-7, CHQS-2). Additional age determinations from plagioclase were selected from four samples collected of andesite and dacite domes in the east district and include: (1) the dacite dome at Machay (CB-65), (2) the pyroxene andesite dome at Ocucho (AZU-2 and DE-2), and the pyroxene dacite dome at Chaquicocha Sur (CHQS-1).

Miscellaneous Yanacocha Porphyritic Rocks

The ^{40}Ar/^{39}Ar dates in this group incorporated samples interpreted as andesite domes, intrusions, and lava flows with rare quartz phenocrysts or an absence of pyroxene. Ages were determined on two plagioclases, two hornblendes and a whole rock, and include the following rocks: (1) a quartz-bearing andesite intrusion (YSBD) surrounded by hydrothermal alteration and fragmental rocks associated with the high-sulfidation gold system at Cerro Yanacocha, (2) porphyritic hornblende andesite lavas (YS-370) that overlie intense hydrothermal alteration and fragmental rocks related to the at Yanacocha Sur high-sulfidation gold system, (3) a porphyritic hornblende andesite plug (DN-77) that intruded Cerro Frailes dacite pyroclastic rocks and Maqui Maqui ignimbrite at Maqui Maqui Norte, (4) a trachytic hornblende andesite dike (SLT-02) that intruded pyroxene andesite lavas at Corimayo, and (5) a porphyritic hornblende dacite dome (CB-3) at Alto Machay. Minera Yanacocha geologists interpreted the porphyritic rocks of YS-370 as a sill of Yp feldspar porphyry and the YSBD as a post-mineral black dike in the Yanacocha Sur deposit.

San Jose Ignimbrite Sequence

Ash-flow tuffs mapped in the field as the San Jose ignimbrite represent a thick package of rocks in the southeast portion of the district. Deep canyons expose excellent sections into the sequence, and it was possible to assemble a suite of samples that represent ignimbrites from the base to the top of the section. Ages were determined on

nine plagioclases, three hornblendes, and two whole rocks. Samples that represent the basal portions of the section included: (1) plagioclase from a pyroxene dacite ignimbrite with glassy juvenile blobs (CB-44) that overlies porphyritic andesite and Maqui Maqui ignimbrite at Arnacocha, and (2) plagioclase from a white pumice-rich lapilli tuff that unconformably overlies Creataceous limestone below the Ventanillas de Combayo. Samples that represent ignimbrites from middle portions of the section include: (1) plagioclase from a welded and devitrified eutaxitic textured, pyroxene-poor, dacite ignimbrite (CB-56) from Quebrada Azufre west of Combayo, (2) two whole rock samples from a welded eutaxitic textured, pyroxene-poor, dacite ignimbrite (SJS-79A) with altered accidental fragments that overlies gold ore at the San Jose deposit, (3) plagioclase from a devitrified, pyroxene-poor, dacite ash-flow tuff (CB-74), with abundant sanidine-andalusite-quartz and massive quartz altered accidental fragments, that overlies a disconformity and the pyroxene andesite Machay dome, (4) plagioclase and hornblende from a eutaxitic textured, pyroxene dacite ignimbrite (CB-38) that underlies the upper spatter ignimbrite, (5) plagioclase from a lapilli dacite ash-flow tuff (CB-59) that overlies the basal flows of VC-4 and underlies upper flows of VC-1 ~6 km southeast of the district, and (6) hornblende from a lapilli dacite ash-flow tuff (RC-6) that overlies Cretaceous limestone ~8 km southeast of the district in outcrop above Rio Chonta. Upper ignimbrites include: (1) a large megacryst of hornblende from the pyroxene dacite spatter ignimbrite (BS-3) at Sacsha, (2) plagioclase from the pyroxene dacite spatter ignimbrite (DE-36) ~1.5 km south of Ocucho dome, (3) plagioclase from the fiamme-poor and crystal-rich tuff (SJS-78A) that overlies the eutaxitic ignimbrite (SJS-79A) at San Jose, and (4) plagioclase from the upper white, lapilli dacite tuff (VC-1, white tuff) that caps the ridge south of the Ventanillas de Combayo and overlies VC-4 and CB-59.

Late Yanacocha Dacite

Porphyritic- and porphyry-textured rocks of dacite to rhyolite composition were dated from three separate sites at Yanacocha. Ages were determined on one sanidine and two biotites, and the rocks include the Corimayo dacite dome (COR-1, biotite) below La Quinua gravels at Corimayo, the Yanacocha dacite porphyry (YN-1A, biotite) from

Yanacocha Norte at Cerro Yanacocha, and the Negritos ignimbrite (NG-5, sanidine)
collected 8 km north of the mine site at Cerros de Los Negritos.

Altered Rock Samples

Age of alteration at Yanacocha was determined for 20 alunites and one
hydrothermal biotite collected from eight deposits across the district. All alunite samples
were analyzed in the X-ray diffraction (XRD) laboratory at Oregon State University with
a Philips XRG 3100 (Appendix If) to confirm the presence of alunite, and determine its
composition and purity prior to $^{40}Ar/^{39}Ar$ dating. Sample results and XRD patterns with
the °2θ peak intensities can be viewed in Appendix If. Two general varieties of alunite
found at Yanacocha included Na-rich natroalunite and K-rich alunite. Alunite
compositions are classified as natroalunite with of molar K/(Na+K)< 0.5 and K-rich
alunite with molar K/(Na+K)> 0.5 (Lipske, 2002). XRD patterns typical of Na-rich
alunites display some peak intensities that are offset to higher degrees 2θ positions with
respect to K-rich varieties. Peak shifts used to identify the K-rich and Na-rich end
members occur at two distinct °2θ positions as follows: (1) K-rich endmenber at 31°2θ
and the Na-rich endmeber at 32°2θ, and (2) the K-rich endmember at 39.3°2θ and the Na-
rich endmember at 40.6°2θ. Mixed K-Na alunite compositions that have peak intensities
nearest the Na-endmember were observed in five samples (Baul-1, CLL-1, MM-46377,
SJS-1, and YO-1), and all remaining samples contained a K-rich variety of alunite. MM-
46377 has a distinct composition and the mineral is an unknown variety of alunite closer
to the Na-rich endmember (possibly similar to minamiite or huangite).

Sample Preparation

All samples were individually crushed and pulverized to -30+50 mesh, then a
hand magnet was stirred through each sample to remove magnetite. Alunite separates
TAP-169, ENC-6, PNE-3, and MM-314 were sieved to -80+100 and -120 mesh due to
the fine nature of the alunite. All other alunites were sieved to -30+50 mesh and
handpicked for purity. Plagioclase and amphibole were separated using a Frantz
isodynamic magnetic separator Model L-1, and the vibrator control and sample holder
were adjusted to a setting that allowed for a steady stream one to two crystals wide (68-

70 on the vibrator control and a couple of turns on the sample cone to loosen the sample holder) for 2 to 4 hours. Plagioclase separation began at 0.15 amps and was increased stepwise by 0.15 to 0.30 amps until a maximum of 1.9 amps was reached, and the nonmagnetic concentrate was nearly all feldspar. During amphibole separation the power was increased stepwise from 0.1 to 0.7 the magnetic separates of the initial steps were discarded until visible amphibole was dropping out. Both plagioclase and amphibole then were handpicked to assure 100% purity. All mineral separates were washed in distilled/de-ionized water with an ultrasonic cleaner for 5 to 10 minutes until clear, then decanted, and finally dried overnight at 70° C. Plagioclase mineral separates were washed in 5% HF for 1 minute, and 5% HNO_3 for 15 minutes, and then washed in de-ionized water as described above.

Biotite was separated using a technique of decantation. The pulverized sample containing biotite was poured into a large +1.0 liter-sized beaker. The beaker was rapidly filled with de-ionized water and decanted halfway into a second large beaker. Biotites momentarily float in the upper portion of the beaker while all other minerals rapidly settle out. The second beaker is allowed to sit until all the sample settles and then was decanted of the water. This procedure was repeated several times, allowing concentration of biotite in the second beaker. Biotite concentrates were dried overnight at 70° C and then handpicked for purity.

Yanacocha mineral separates were weighed and 92-100 mg of plagioclase, 28-43 mg of alunite (the optimum amount of alunite), 20-30 mg of biotite, 30-50 mg of hornblende were each placed in separate copper-foil containers and labeled with a sample ID. All samples were irradiated in the Oregon State University Triga Reactor at 1 megawatt for 6 hours in evacuated quartz vials loaded in Al-Triga tubes. Sample height in millimeters is recorded for each sample. The neutron flux (J) is monitored with several 2.5 to 10 mg samples of Fish Creek Tuff FCT-3 biotite standard with an age of 28.03±0.12 Ma (Renne et al., 1998). The FCT-3 monitor is placed at regular intervals in the quartz vials, monitor height is recorded as for the samples, the J is calculated for each monitor, and a second-degree polynomial fitted to the measured J's that can be used for each sample distance from the neutron source.

Laboratory Procedures

^{40}Ar/^{39}Ar radiometric ages reported in this study were determined in the noble gas mass spectrometry lab of the College of Oceanic and Atmospheric Sciences at Oregon State University. Two gas extration methods were used and discussed below: (1) incremental heating with a furnace for whole rock, plagioclase, hornblende, biotite and one alunite sample, and (2) step heating by laser fusion for 19 alunites.

Furnace Method

Age analyses on mineral separates of plagioclase, biotite, hornblende, whole rock mini-cores, and one alunite were accomplished using stepwise or incremental heating with a furnace in the noble gas mass spectrometry lab. The system is equipped with a Heine low-blank, double-vacuum resistant furnace with a Mo-lined, Ta-Nb crucible (Huard, 2003). Gas extraction in plagioclase, hornblende, biotite and whole rock samples is achieved by incremental heating in the furnace. Irradiated samples, individually wrapped in Cu foil, and whole rock mini-cores are loaded into a glass sample holder attached to the furnace manifold and an all metal, vacuum sealed extraction line system fixed with Varian valves. At the onset of an incremental heating experiment, samples are separately dropped from the manifold into the furnace crucible. Temperatures in the crucible are controlled by a programmable power supply thermocouple system (Huard, 2003). All samples were degassed at the start of the experiment at 400°C and the end at a ~1500°C final degas between samples. During the degas stage and between heating steps the extraction lines are pumped out with two ion pumps at 150L/s and 200L/s. During a heating step the gas is exposed for 15 minutes to the ST 101 Zr-Al primary getter. On cool down after 2½ minutes the gas is exposed to the ST 172 Zr-V-Fe final getters for approximately 4 minutes. The gas is slowly released through the inlet valve into a Mass Analyser Products model 215-50 rare gas mass spectrometer for ^{40}Ar/^{39}Ar analyses and the age calculations begin for all isotopes of argon (Huard, 2003).

Laser Fusion Method

Incremental heating experiments for 19 alunite mineral separates were conducted by a Merchantek 30 watt CO_2 laser system with a microscopic infrared pyrometer API Micro Probe model MSP-200G that monitors the temperature of a 50 micron spot on the sample over a temperature range of 400-1500°C (Huard, 2003). The system is computer operated and temperatures are controlled with percent laser power by the computer. As with the furnace, gas extractions are cleaned for 15 minutes in a ST 101 Zr-Al primary getter. One minute after heating is complete the gas is exposed to the ST 172 Zr-V-Fe final getters for the remaining 4 minutes before the gas is expanded into the spectrometer. Both the primary and final getters were degassed for one hour after every sample and the extraction line system was vented for an additional hour to prevent contamination.

Alunite $((K,Na)Al_3(SO_4)_2(OH)_6)$ is a sulfate that will release SO_2, SO_3, and OH radicals into the extraction line system during incremental step heating experiments. The getters are unable to adequately clean these gases before admittance into the spectrometer, and the desulfatization reaction can potentially damage the extraction line system. Release of radiogenic $^{40}Ar_{(r)}$ from alunite occurs during the dehydroxylation reaction associated with the thermal decomposition of alunite to alum $(KAl(SO_4)_2)$ and alumina (Al_2O_3) (Itaya et al., 1996). Incremental heating experiments on alunite from 100 to 1000°C were conducted by Itaya et al. (1996) at intervals of 100°C defining the quantitative release patterns of radiogenic $^{40}Ar_{(r)}$ and nonradiogenic Ar. Optimum release of $^{40}Ar_{(r)}$ exists at temperatures >400°C and <750°C, and minimum release occurs at 400°C and 800°C. Therefore, step heating must be achieved by using small incremental amounts of laser power between the critical temperature range 400-750°C of gas release to minimize contamination. All alunite samples in this study required a three minute period for the final clean up of the gases in the spectrometer getter before starting the timer to record data.

Approximately 10-20 mg of the irradiated alunite sample was loaded into separate pans in a Cu-planchette. Sample sizes >20 mg were problematic due to large amounts of SO_2 and SO_3 gases. The planchette is capped with a coverslip that is transparent to the CO_2 laser wave. Coverslips used in 2002 analyses were KBr, and these easily fogged

while alunite was heated during the higher power steps. During the 2003 analyses, smaller samples of 10-15 grams were loaded into the planchette, and a BaF coverslip was employed that did not readily fog. Once fogged, the ability to transmit the CO_2 laser wave was severely diminished and laser power had to be greatly increased to heat the sample. Required temperatures are not reached with fogged coverslips, and therefore, the experiments are terminated and finished at a later date after replacing the coverslip during sample reloads.

Typical incremental heating procedures for alunite began with a 15 minute laser blank for calibration. Thereafter, a 15 minute laser blank was run following two to three heating stages during an experiment. Alunite heating experiments consisted of seven heating increments that began at 400°C, increased to 500°C, and than increased slowly by 50°C until 700°C. The final heating stage used was 800°C, and in a few cases a 900°C step was added to test the potential gas release. Temperatures above 800°C leads to further release of SO_3 and the formation of H_2SO_4 that damage the extraction-line system (Itaya et al., 1996). The temperature range for the optimum release of $^{40}Ar_{(r)}$ and $^{39}Ar_{(K)}$ gas in the alunite from this study was generally from 500°C through 700°C, however, each sample behaved differently and in some samples gas was released over smaller temperature intervals. Optimal temperatures for the release of $^{40}Ar_{(r)}$ in alunite were at 600° and 650°C, however, in some samples the greatest amount of $^{40}Ar_{(r)}$ was released at 550°C and others at 700°C.

Temperatures were controlled by laser power, monitored with an infrared pyrometer, and reported as degrees centigrade. A variation in sample size and size fractions also affects the heating procedures. Smaller size fractions and larger samples generally require more laser power to reach the required temperature, but as a "rule of thumb" the starting temperature of 400°C was reached with 2 – 2.5% laser power (<0.1 watts), and an increase in laser power of 0.7% and 1% to ~3.0% (0.18 watts) was required to reach the 500°C step. Laser power was increased 0.4% to 0.8% (0.15-0.75 watts) for each consecutive 50°C interval to 700°C and to 9.5% and 10.0% (1.55-1.65 watts) to reach the final 800°C heating stage. A "dual-step" heating procedure was employed after the 400°C heating step. During each consecutive heating increment the laser power was increased in two stages with two separate scans across the sample tray.

This technique helped prevent the fogging problem from a single large release of gas that will end the experiment. The dual-step heating procedure is described as follows: (1) a 15 minute timer is started, (2) laser power is increased until half of the temperature required for the heating stage is reached, (3) the sample is scanned and the gas is released to the getters, (4) the power is increased to the total required temperature for the heating increment, and (5) the sample is scanned a second time releasing the remaining gas to the getters. The entire dual-step heating procedure must be no more than 10 minutes and provides for a one minute pause after heating and four minute exposure to the final getters. The final procedure for all alunite samples was to open the inlet valve and wait one minute while the gas expands into the spectrometer. After the inlet valve was closed a period of approximately three minutes was allowed as the peak intensity climbed and stabilized before starting the timer and collecting data at the computer. This is due to SO_2 and SO_3 contaminants and the abundant OH radicals in the alunites and the ineffectiveness of the getters to thoroughly getter these gases.

Data Analysis and Presentation

The $^{40}Ar/^{39}Ar$ ages were calculated with ArArCALC v2.2 software from Koppers (2002) and the ages are reported within the limits of a 2σ error (95% confidence interval). Data regressions from the mass spectrometer measured peak intensities for all argon isotopes are calculated with respect to inlet time of the argon gas. Regressions are calculated over time for each isotope of argon (^{36}Ar, ^{37}Ar, ^{38}Ar, ^{39}Ar and ^{40}Ar). Reductions to these data involved the removal of excessive outliers radically inconsistent within a linear cluster of data, or removal of data with unusually high error. Aggressive data reduction can be applied to force a heating step on a plateau; however, this method is not acceptable within the limits of statistical models, adds uncertainty to the age, and threatens reliability of the study. Therefore, minimal data reduction was applied in all the age experiments for this study. Examples are presented and discussed in Appendix II.

The data for each sample are presented graphically as age spectrum and isochron diagrams. The age spectrum diagram plots the age for each heating step versus the cumulative percent of $^{39}Ar_K$ released from the sample, and the initial ratio $^{40}Ar/^{36}Ar$ is assumed to be trapped argon of atmospheric composition ($^{40}Ar/^{36}Ar$=295.5). Both normal

and inverse isochron diagrams (isotope correlation diagrams) further test the validity of the results by requiring a best-fit straight line test to the data (linear correlation). The normal isochron diagrams plot isotope ratios of ^{39}Ar/^{36}Ar versus ^{40}Ar/^{36}Ar for each heating step. The slope of the line is equivalent to the age since crystallization (closure age) and the y axis intercept is the initial ^{40}Ar/^{36}Ar composition of trapped argon in the sample at closure, usually within error of the atmospheric value. The inverse isochron diagrams plot the ratios ^{36}Ar/^{40}Ar versus ^{39}Ar/^{40}Ar for each step and have an advantage over normal isochron plots in that the most abundant isotope ^{40}Ar is in the denominator of both axes, thereby minimizing error while calculating age and initial argon composition.

A weighted mean plateau age as defined by McDougall and Harrison (1999) is the mean of the steps comprising the plateau weighted by the inverse of the variance, and the error for the mean of all the heating steps on the plateau is less than the error for a single step. A variety of criteria discussed by McDougall and Harrison (1999; p. 111) have been proposed to define an acceptable crystallization age. In some cases additional criteria have been presented that complement a specific set of data. In this study, ages are accepted as closure ages when the following criteria from Dalyrymple and Lanphere (1974), Duncan et al. (1997), Tegner and Duncan (1999), and Frey et al. (2004) are met:

1. The plateau age is a part of an age spectrum that has a minimum of three contiguous and concordant heating steps with ≥50% of the total ^{39}Ar$_K$ released from the sample. The term concordant is defined as the apparent ages for each heating step in the plateau are the same within the limits of a 2σ error.

2. The MSWD (mean square of weighted deviates) of the weighted plateau age is within acceptable limits. An ideal MSWD equals 1, whereas wieghted mean plateau ages are not acceptable with an MSWD > 2.5 or approaching 0 [1].

3. The steps that form the plateau also produce a well-defined isochron with acceptable MSWD's.

4. The plateau and isochron ages are concordant,

5. The initial ^{40}Ar/^{36}Ar ratio is within the limits of a 2σ error of $(^{40}$Ar/^{36}Ar$)_A = 295.5$ for trapped argon of atmospheric composition.

[1] MSWD (mean square of the weighted deviates) "a goodness-of-fit parameter that tests whether all the data are sampling the same mean value. Indicates how well the data, normalized by the analytical errors, fit the calculated least-squares straight line. An MSWD much less than the expected value of 1 suggests that experimental errors may be overestimated. MSWD values > 1 indicate the experimental errors may be underestimated or a linear relationship between the data may not exist" (McDougall and Harrison, 1999; p135-136.). The MSWD tests for the variation of the mean for each heating step by comparing the mean value and the variability of the data around the mean within the limits of a 95% confidence interval for each step. MSWD = x^2/n-1 = $1/n$-1$\sum(X_i- \mu_x)^2/\sigma_i^2$ (McIntyre et al., 1966).

Most samples in the present study produced an undisturbed age spectrum with plateaus that represent simple argon closure, hence, they produced acceptable plateau ages that are reported as *preferred* ages. The preferred age for each sample is considered the closure age at the time of crystallization when the initial $^{40}Ar/^{36}Ar$ composition became trapped and isolated in a closed system. Plateau ages are the weighted mean of three to eight contiguous and concordant heating steps. They are generally reported as the *preferred* age; however, isochron ages and total fusion or integrated ages are considered as *preferred* ages in cases where the plateau age does not meet the above criteria 1 and 2.

Most results show slightly discordant low and high temperature step ages that reflect effects of Ar-loss, excess Ar, and Ar-recoil. Intervening concordant plateaus meet the criteria for an acceptable age. Some age analyses of the Yanacocha rocks, however, experienced more pronounced effects that produced discordant age spectra from which no acceptable plateau age could be inferred. Excess Ar results from the accumulation of non-atmospheric Ar into phases that experienced complex thermal histories after the initial closure temperature (Kelly, 2002). Ar-loss is common in the initial low temperature steps and reflects the presence of late low-temperature alteration minerals with higher K/Ca ($^{39}Ar/^{37}Ar$) and younger ages. Duncan et al. (1997) explained that the data from the Karoo volcanic suite were suspected of Ar-loss when the total fusion age was significantly younger than the plateau age, and excess Ar when the total fusion age was significantly older than the plateau age. The initial $^{40}Ar/^{36}Ar$ ratio may reflect the artifacts of excess Ar and Ar-loss. Duncan et al. (1997) noted that tight clustering of the step data in isochron diagrams lead to imprecise regressions and large uncertainties in the $^{40}Ar/^{36}Ar$ intercepts and the age. In these cases, the plateau age is preferred over the isochron age. Many samples showed minor effects of Ar loss and excess Ar, and their intervening plateaus met the above conditions for a preferred age. A few alunite samples

experienced a tight data clustering combined with Ar-loss and excess Ar. Uncertainties resulting from the combination from these effects necessitate a best estimate of the age using all available age data and geology.

Experimental effects that can be detrimental to the age of a sample result during the process of Ar recoil. Ar recoil is an effect produced during irradiation that results in progressively younger step ages during the course of incremental heating. Duncan et al. (1997) described the resulting age spectra as an "inverse staircase" pattern of decreasing step ages with %^{39}Ar released from the sample. Recoil takes place during the production of ^{39}Ar and ^{37}Ar from ^{39}K and ^{40}Ca, respectively, while samples are irradiated in the nuclear reactor (McDougall and Harrison, 1999). Isotopes of ^{39}Ar and ^{37}Ar move from K- and Ca-rich minerals to K- and Ca-poor minerals. Yanacocha rocks that display effects of Ar recoil are whole rock and biotite samples that were affected by weak low temperature hydrothermal alteration. The loss of ^{39}Ar from the fine-grained K- and Ca-rich alteration minerals produces an increased age in the low temperature phases (Duncan et al., 1997; McDougall and Harrison, 1999). Consequently, atoms are transferred from the lower temperature phases to the higher temperature phases and produce a decrease in age with increased step temperatures. The age spectrum displays an inverse staircase pattern with the oldest ages in the low temperature steps. In samples that experienced recoil throughout the age spectra and plateau, the best estimate of age is the total fusion age (Duncan et al., 1997).

Sulfur Isotope Analyses

Sulfur Isotope Results

Sulfur isotopic compositions (δ^{34}S values) in the Yanacocha alunites range from +11.4‰ to +25.9‰ (Figure 2.3). The δ^{34}S values of coexisting alunite and pyrite in samples 18 and 21 are 16.0 to 16.8‰ and -2.4‰ to -14.5‰ respectively (Figure 2.3). One alunite (sample 10) has a δ^{34}S value anomalously lighter (+11.4‰) than other alunites in this study (Table 2.3) and may have been contaminated with isotopically light sulfide and native sulfur. It is a sample of patchy- to wormy-textured quartz alunite, with

trace amounts of sulfide and native sulfur, from 260 meters depth in diamond drill hole MM-314 at the bottom of the Maqui Maqui open pit. Sulfate-sulfide fractionation curves from Field and Fifarek (1986) suggest that the sulfur in samples 18 and 21 (Table 2.3) fractionated and isotopically equilibrated at temperatures of ~200°C and ~320°C, respectively. During isotopic fractionation, the heavy sulfur isotope is preferentially enriched in that phase having the strongest bond; that is, as sulfides oxidize to SO_4^{-2} the
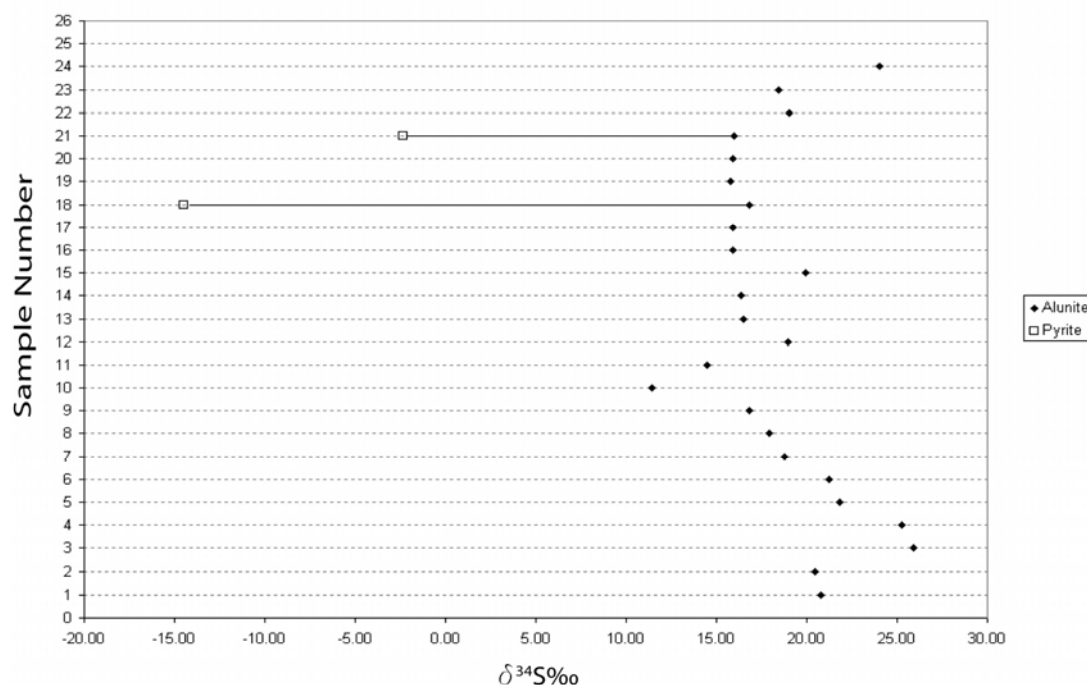
Figure 2.3. Plot of sulfur isotopic compositions.

fractionated sulfur would yield enrichments in ^{34}S and depletions in ^{32}S (^{34}S is enriched from $S^{+6} > S^{+4} > S^0 > S^{-2}$). As a general rule, sulfur in hypogene epithermal systems isotopically equilibrates at temperatures ≥300°C (Field and Fifarek, 1986). However, at the Pierina high-sulfidation gold deposit, SO_2 disproportionates to HSO_4^- and H_2S between 320 to 180°C (Fifarek and Rye, 2005) suggesting that sample 18 is within acceptable ranges.

Alunites at Yanacocha are of magmatic-hydrothermal origin as defined by Rye (2005), and their sulfur isotopic compositions are heavy ($\delta^{34}S > +11‰$). Yanacocha

sulfur isotopic compositions are similar to magmatic-hydrothermal alunites from other high-sulfidation epithermal systems as follows: Pierina, Perú (+8.5 to +31.7‰; Fifarek and Rye, 2005); Tambo (El Indio), Chile (24-27‰; Deyell et al., 2005); Julcani, Perú (+22.7 to +28.1‰; Rye et al., 1992); and Summitville, Colorado (+13.4 to +24.6‰; Rye et al., 1992; and +18.2 to +24.5‰ with coexisting pyrite at –8.1 to –2.2‰; Bethke et al., 2005). Other hypogene sulfates from porphyry Cu-Au systems in the Andean Cordillera have $\delta^{34}S$ values that range from +7 to +25‰ (Field and Gustafson, 1976; Field et al., 1983). Supergene sulfate minerals derived in near surface non-equilibrium conditions during the oxidation of isotopically light sulfide typically will have $\delta^{34}S$ values that range from -15 to -3‰ (Rye et al. 1992). These sulfates inherit the sulfur isotopic compositions near that of the oxidized sulfide. Therefore, alunite derived through shallow supergene processes would be ^{34}S-depleted, and at Yanacocha, they would have $\delta^{34}S$ values < 0‰ and nearer the sulfur isotopic composition of the pyrite at Yanacocha Norte (sample YN-105, -2.4‰).

Alunite Composition

Samples were analyzed with XRD to verify the presence of alunite, its composition and its purity prior to $^{40}Ar/^{39}Ar$ dating and sulfur isotope analysis (Appendix VIII, Table A1.5). Most samples analyzed were alunite and natroalunite contaminated by quartz (5-60%) and rutile. Some samples were also contaminated with pyrophyllite, trace jarosite and diaspore. Alunite grain size is quite variable throughout the deposits, and crystals range from coarse-grained (0.25-2.0mm, Table 2.2) euhedral and vug-filling to massive, fine-grained, subhedral and anhedral varieties ≤0.05mm (≤50μm, Table 2.2). Color and grain size are not distinctive of either alunite or natroalunite and both compositions can be white, tan, or pink, and coarse- or fine-grained. Based on bulk rock chemical analyses, alunites at Yanacocha display mixed compositions and are generally K-rich. Molar K/K+Na ratios range 0.92 to 0.55 and molar Ca/Ca+K+Na ratios range 0.11 to 0.01 for the alunite-rich rock samples at Yanacocha analyzed in this study. These ratios are presented in Figure 2.4 and indicate that west district alunites are generally K-rich with very low Ca, Cerros Yanacocha alunites are both K-rich and slightly enriched in Ca and Na, and alunite in the east district has the most sodic-rich varieties.
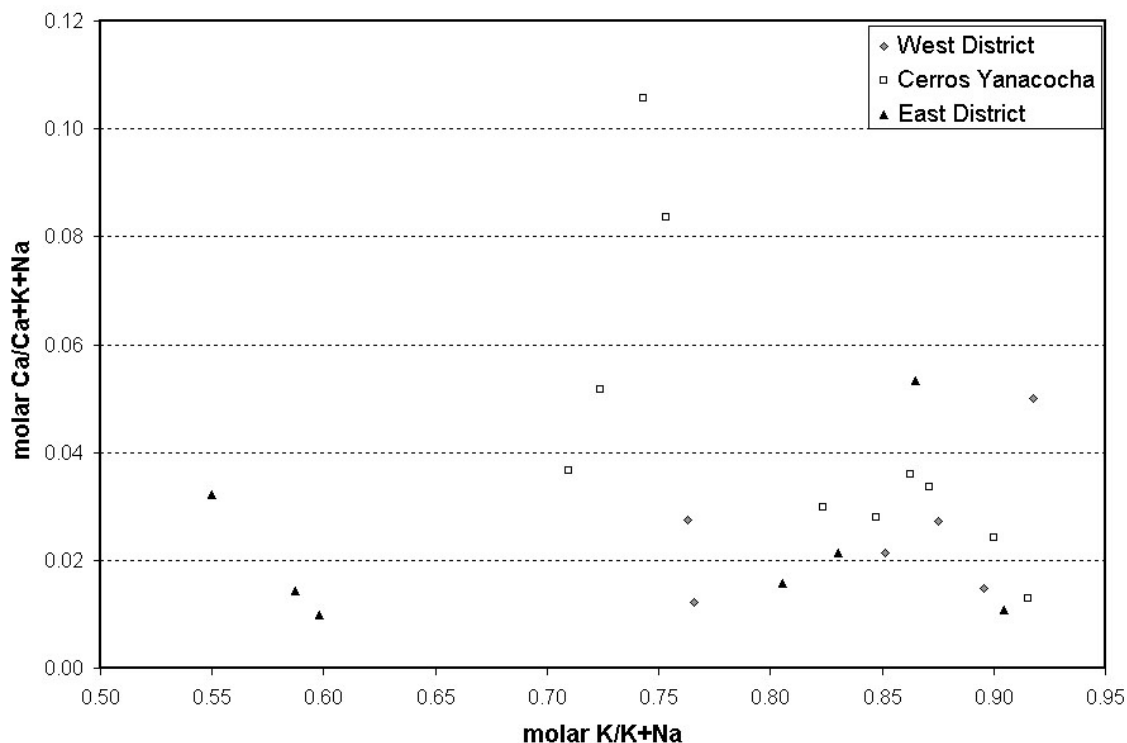
Figure 2.4. Scatter plot showing the variation between molar K/K+Na and molar Ca/Ca+K+Na in the alunites analyzed at Yanacocha. The alunites are grouped with respect to their sample area and these data suggest the west district alunite compositions are most K-rich whereas the east district alunites are both K-rich alunites and Na-rich natroalunites. Cerros Yanacocha have some Ca-rich varieties.

$^{40}Ar/^{39}Ar$ Geochronology

$^{40}Ar/^{39}Ar$ Results

Results of the $^{40}Ar/^{39}Ar$ age determinations are summarized in Tables 2.1 and presented in Figures 2.5 through 2.26. All data for each analysis can be found in CD Appendix I. Results for the acceptable ages are presented below grouped by mineral or sample type. Age spectra that produced unacceptable plateau ages generally experienced combined effects from Ar-loss, excess Ar, and Ar recoil, or elevated analytical error. These included six fresh volcanic rocks and ten alunites whose ages were estimated from the age spectra and isochron plots. These results are considered *discordant* and include: (1) six fresh rocks discussed in stratigraphic order, (2) analyses of alunite from cover-slip

fogging, and (3) analyses of alunite not affected by fogging. Valid age estimates are still possible in these cases and are examined in detail below.

Precision and reliability of the ^{40}Ar/^{39}Ar age analyses were tested with duplicate samples from three separate and critical sites at Yanacocha (Table 2.1, Figure 2.5, CD Appendix I). Paired samples include: (1) plagioclase and a hornblende from tha same sample (CB-38) of San Jose ignimbrite, (2) two whole rock analyses from samples collected 3 meters apart from the same ignimbrite flow unit in diamond drill hole SJS-79A above the San Jose gold deposit (SJS-79A 20.3m, SJS-79A 23.4m), and (3) biotite and plagioclase from the same sample of the Cerro Frailes dacite tuff at Chaupiloma (DN-12). Plateau and isochron ages for each pair of duplicate samples were similar providing an overall mean relative deviation of ±0.5% and within the limits of a 2σ error (Figure 2.3). The CB-38 paired samples produced ages of 11.27±0.07 for the plagioclase and 11.29±0.15 for the hornblende providing ±0.1% mean relative deviation. Whole rock samples in diamond drill hole SJS-79A have similar ages of 11.43±0.11 and 11.30±0.08 and provided a mean relative deviation of ±0.6%. Finally, DN-12 biotite gave an isochron age of 15.37±0.22 and plagioclase from the same rock had a plateau age of 15.18±0.14, producing a mean relative deviation of ±0.7%.
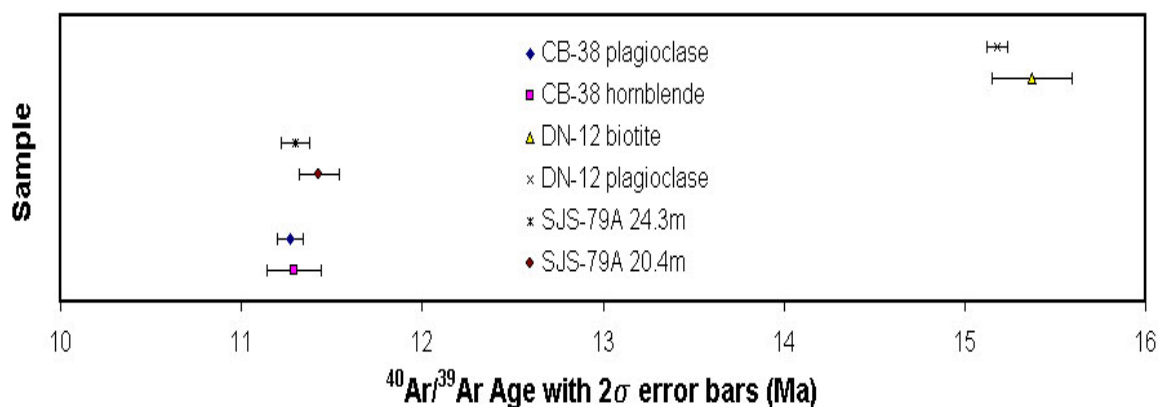
Figure 2.5 Results of the paired samples to test the precision of the ^{40}Ar/^{39}Ar dating at Yanacocha.

K/Ca Ratios

Plots of the K/Ca ratios are presented along side the respective normal isochron plots for representative samples of fresh rocks and samples with weak hydrothermal alteration collected near and within the gold deposits. Fresh rocks at Yanacocha display the following patterns in the K/Ca plots (Figures 2.6 and 2.7).

(1) In the fresh rocks, K/Ca ratios are <0.4 for plagioclase and hornblende analyses, and K/Ca ratios for biotite are >>1.

(2) K/Ca ratios for plagioclase and hornblende are typically higher in the initial low temperature steps and range from 0.15 to 0.25 for plagioclase and 0.2 to 0.4 for hornblende.

(3) K/Ca ratios for plagioclase and hornblende are lower and generally <0.10 within the range of the plateau age.

(4) Plots of K/Ca for biotite display an inverse saddle-shape with decreased K/Ca in the initial low temperature steps and increased K/Ca in the range of the plateau age opposite of the plagioclase and hornblende.

(5) Ranges of K/Ca for biotite are typically >2 to 10 for low temperature steps and >10 to >50 for the range of the plateau age.

Rocks near hydrothermal systems affected by weak clay (illite?), calcite and chlorite alteration display patterns with both high K/Ca and low K/Ca in the low temperature steps as follows (Figure 2.8):

(1) K/Ca ratios for plagioclase (DN-52) and hornblende analyses in altered rocks are typically higher in the initial low temperature steps than for the fresh rocks in this study, and range from 0.2 to >1.0.

(2) K/Ca ratios for biotite are generally >>1 with similar patterns to the fresh rocks. The ranges are more dramatic and approach 0 in the low temperature steps and up to 150 in the range for the plateau age as displayed by sample YN-1A and COR-1 (Figure 2.6).

(3) Whole rock samples with weak hydrothermal alteration display two patterns. Inverse stairstep patterns related to Ar recoil with high K/Ca that range from 1 to 2 in the low temperature steps (Figure 2.6, samples CB-5 and SJS-79A), and low

K/Ca in the low temperature steps that follows an inverse stairstep pattern of Ar recoil and then increases in a normal stairstep pattern with each temperature increment (Figure 2.9, sample YSBD).

Inverse stairstep patterns in K/Ca ratios are directly related to Ar recoil and can be referenced as a *recoil test* when issues for recoil arise in an age spectrum.

Differences in the K/Ca ratio between fresh and altered samples are subtle but observable. Plagioclase and hornblende from altered rocks have slightly higher K/Ca ratios, and biotite has lower K/Ca ratios in the low temperature range than fresh rocks. In the altered rocks, the higher K/Ca at low temperatures may be an artifact of nuclear recoil as observed in the whole rock samples CB-5 and SJS-79A (Figure 2.8). Increased K/Ca in the intial steps may be related to low temperature potassium metasomatism in to the rims and along fractures in the grain as in the hornblende of DE-18 and the plagioclase of DN-52. Lower K/Ca at low temperatures may indicate the presence of low temperature Ca-bearing clay minerals and calcite (Figure 2.9).

Patterns of Ar-loss, excess Ar and Ar recoil in the initial low temperature steps of the age spectra are likely related to low temperature hydrothermal alteration and the presence of minor fine-grained clay minerals. This interpretation is supported by petrography, and the lower $^{39}Ar/^{37}Ar$ ratio and lower K/Ca ratio in the low temperature steps. Generally, the lower isotopic ratio $^{39}Ar/^{37}Ar$ reflects the lower K/Ca of clay minerals (eg., the lower temperature steps in the clay-calcite-pyrite altered YSBD, Figure 2.9). The lower K/Ca in the initial steps of the Yanacocha dacite porphyry (Figure 2.9, YN-1A) may reflect the presence of minor calcite alteration observed in thin section. YN-1A may have equilibrated with hydrothermal fluids, and diffusion of Ar from the hydrothermal fluid into the margins of the biotite during alteration may explain the excess in the low temperature steps. Ar-loss in the Corimayo dacite may be due to its close proximity to the Corimayo gold deposit. In reference to the $^{39}Ar/^{37}Ar$ ratios, the low K/Ca ratios in the initial steps suggest the presence of low temperature Ca-bearing clay minerals that produce the effects of Ar-loss and younger ages. Higher K/Ca in the initial heating steps may reflect Ar-recoil or excess Ar. In the case of biotite, the K/Ca ratios for calcite and clay alteration would be much lower than the K/Ca ratios for the biotite (Figure 2.9; Table IIa, CD Appendix II, K/Ca ratios).
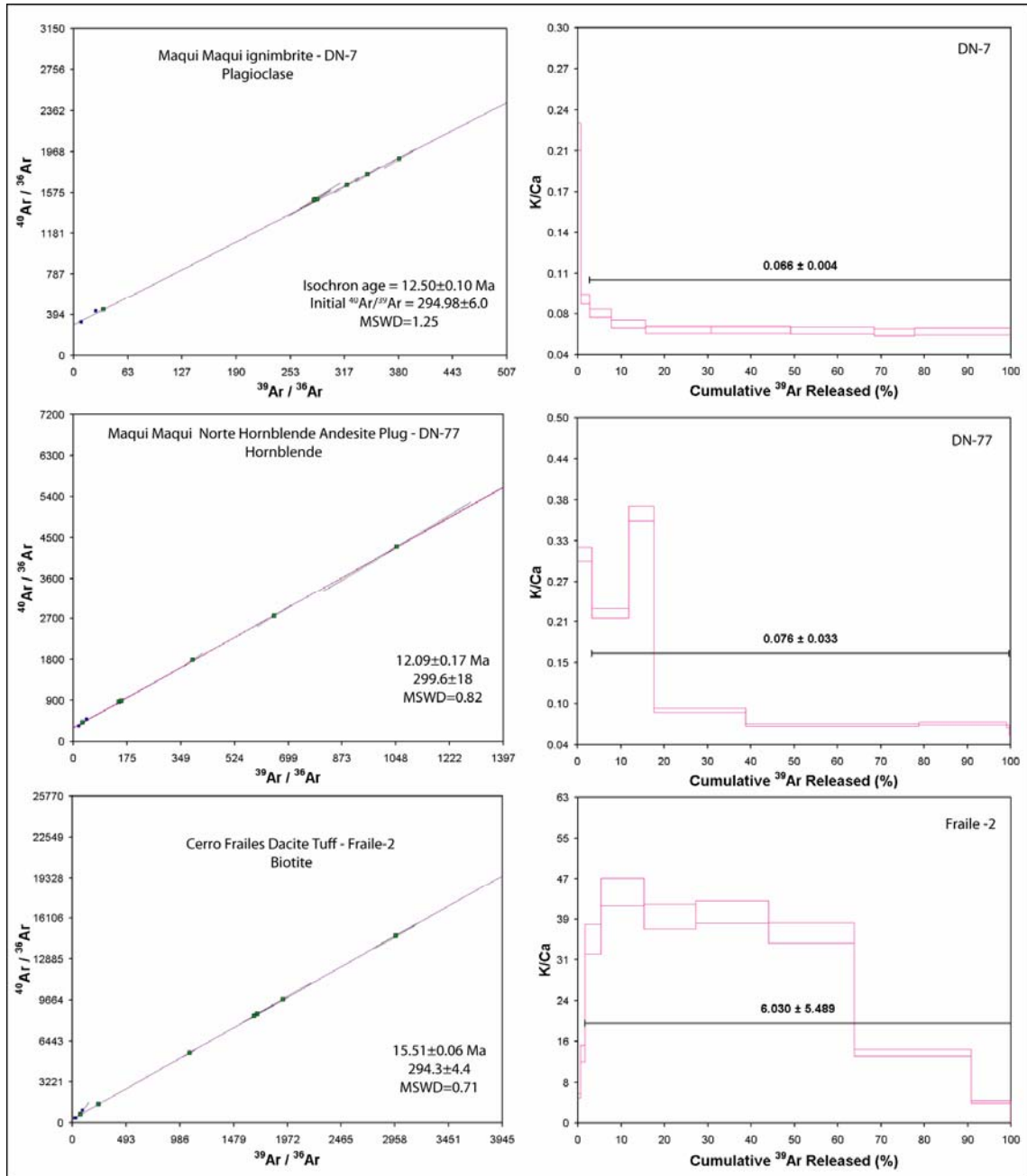
Figure 2.6. Normal isochron and K/Ca plots for unaltered Yanacocha samples. Normal isochron plots on the left and K/Ca plots on the right.
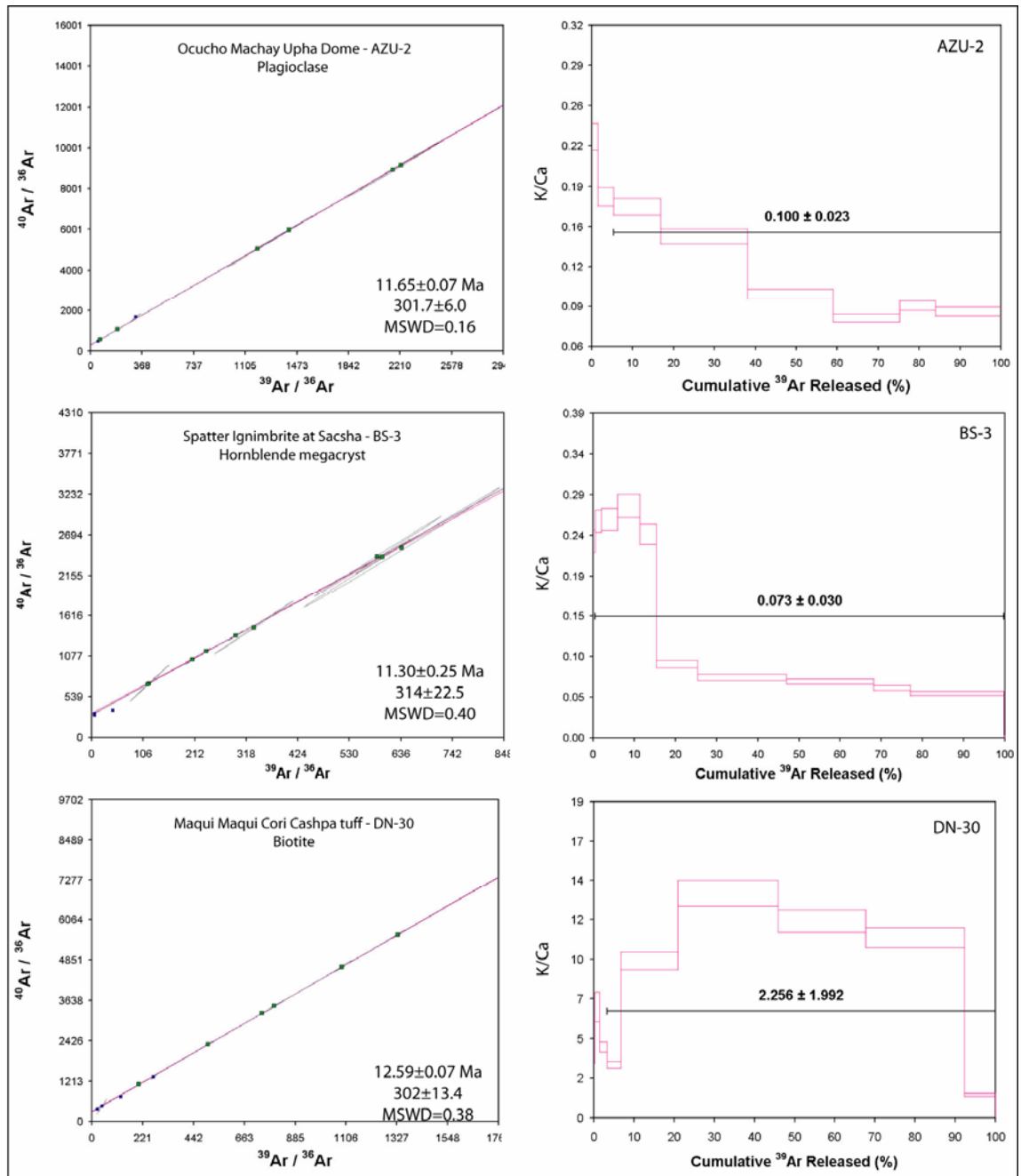
Figure 2.7 Additional normal isochron and K/Ca plots for unaltered rocks at Yanacocha. The plots show typical patterns in the K/Ca ratio for plagioclase, hornblende and biotite that are not affected by hydrothermal alteration.
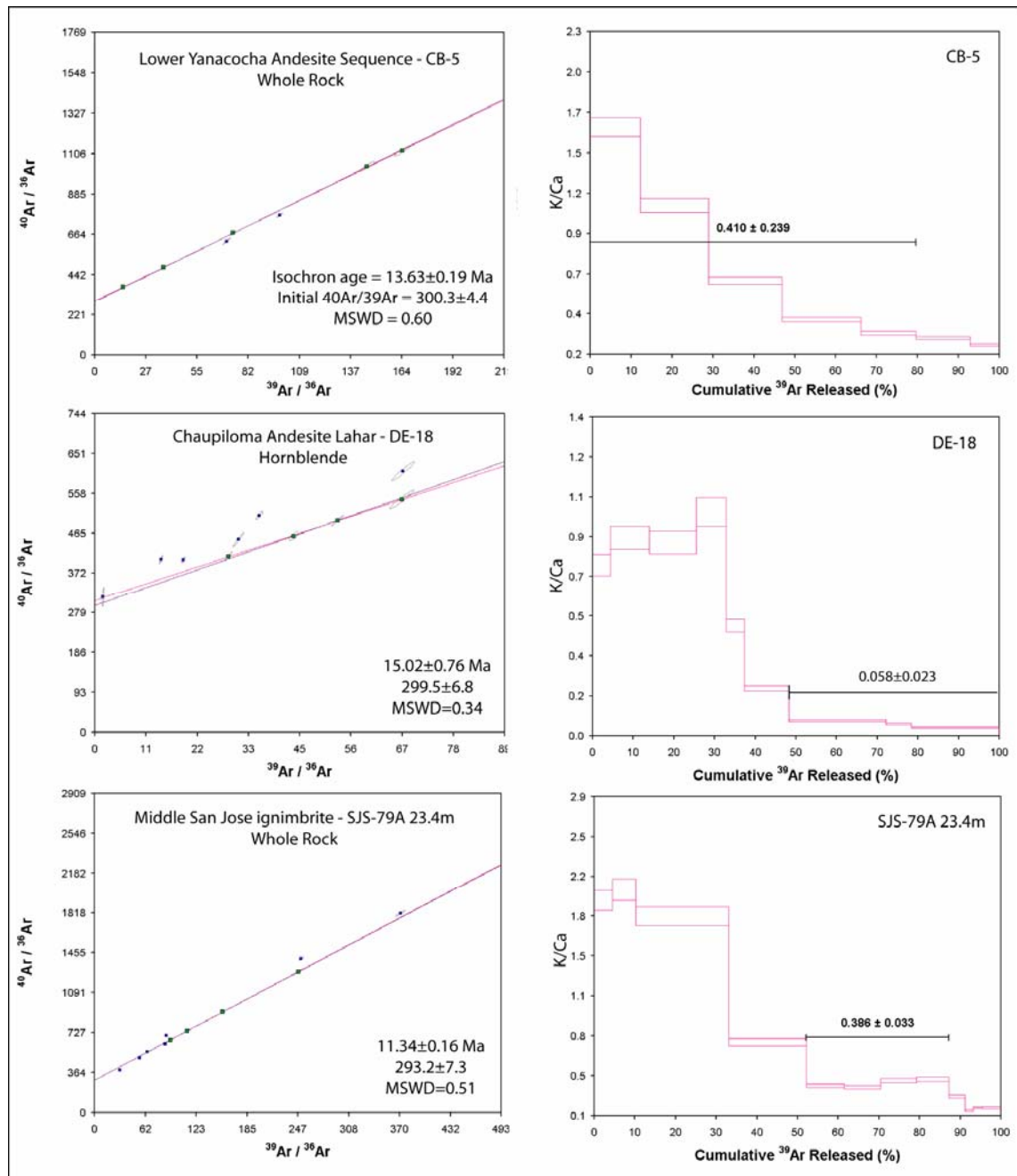
Figure 2.8 Normal isochron and K/Ca plots for altered Yanacocha rocks. The diagram compares whole rock and hornblende samples from volcanic rocks with weak alteration at Alto Machay (CB-5), Cerro Collotan (DE-18), and the San Jose Au deposit. These rocks are affected by weak intermediate argillic with calcite ± chlorite alteration; however the low temperature steps have anomalously high K/Ca ratios relative to the plateau indicating some low-temperature K-metasomatism.
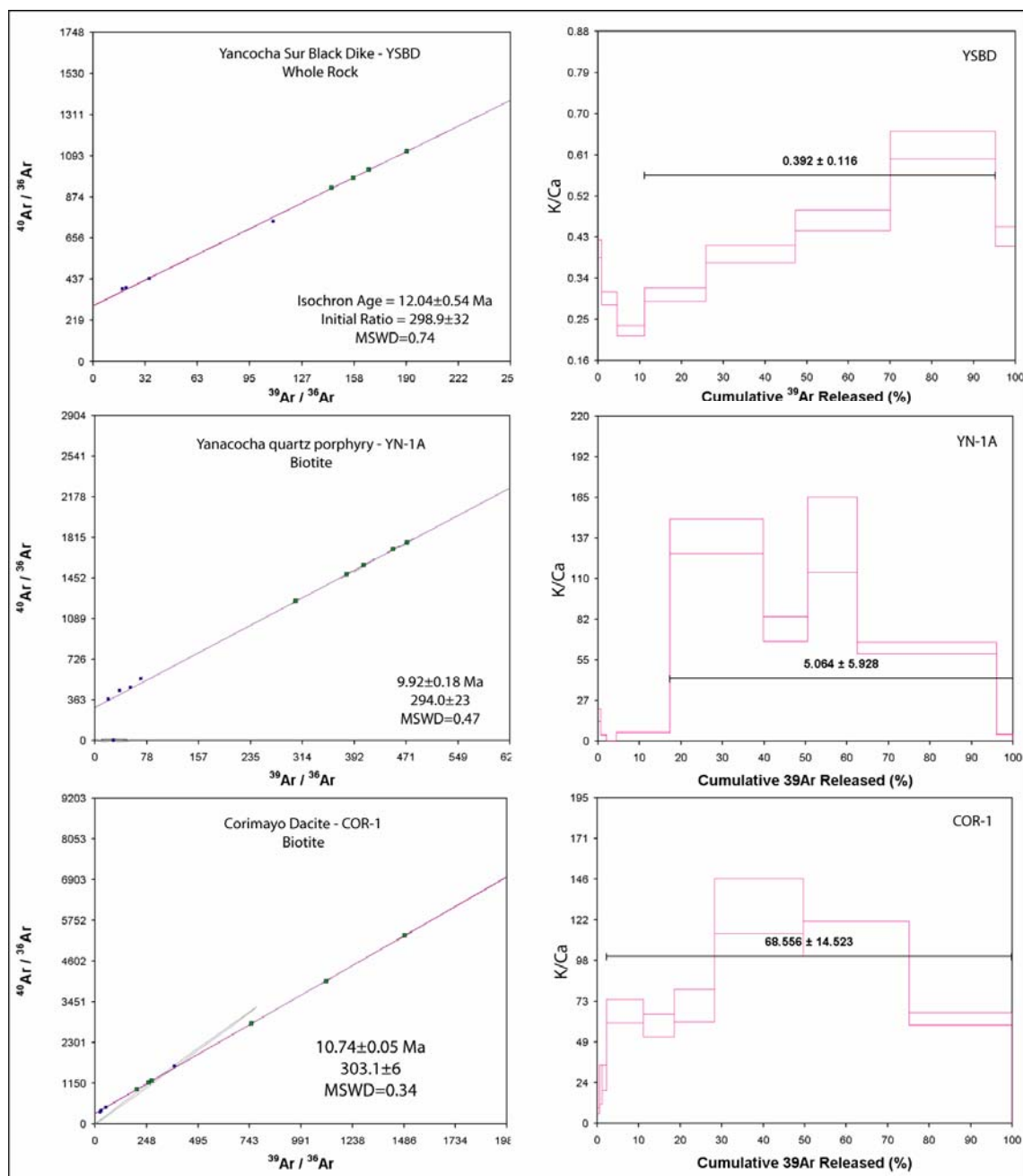
Figure 2.9 Additional normal isochron and K/Ca plots of altered rocks at Yanacocha. The diagram compares plots of fresh intrusions found in the ore deposits at Cerro Yanacocha and Corimayo. Samples include the YSBD dike, the Corimayo dacite and the Yanacocha quartz porphyry. Alteration is weak illite (clays) ± pyrite ± calcite.

Acceptable Ages

Age spectra from 77% (n=53) of the Yanacocha samples are undisturbed and produced plateau ages that meet the above criteria for an acceptable age determination. These samples display age spectra with concordant plateaus bordered by patterns in heating steps that display the effects of minor argon loss (Ar-loss) and excess argon (excess Ar). Age spectra with excess Ar have total fusion ages older than the plateau age, and age spectra with Ar-loss have total fusion ages younger than the plateau age. Each mineral behaves differently and displays age spectra characteristic for the mineral and rock package. All plateau and isochron age data are concordant in each sample and meet the conditions for an acceptable age.

Plagioclase

Age analyses were preformed on 34 plagioclases throughout the stratigraphic section at Yanacocha. Plateau ages were chosen as the preferred age on all but two problematic samples. Plagioclase age spectra show five distinct patterns that include (Figs. 2.10 and 2.11, Table 2.1): (1) excess Ar in the initial low temperature steps and the final high temperature steps (Fig 2.8 d and f) and subtle saddle-shaped spectrum (Fig. 2.8f), (2) combined effects of Ar-loss and excess Ar in the initial steps (Figs. 2.10a and 2.11b), (3) combined effects of Ar-loss in the initial steps and excess argon in the final high temperature steps (Fig 2.10b), (4) excess argon in the final high temperature steps (Fig. 2.10c), and (5) Ar recoil in the initial steps resulting in a *inverse stair step* pattern (Fig. 2.10e). Plateaus vary with four to seven intervening steps on the plateau and 60-95% of the $^{39}Ar_{(K)}$ released. All have total fusion ages that are slightly older than the plateau age.

Samples from the Lower Yanacocha andesite sequence (Lpha; CNN-1, Figure 2.10c), Upper Yanacocha andesite sequence (Upha dome, Figure 2.10d), and the San Jose ignimbrite (CB-56, Figure 2.10f) have plagioclase with age spectra that show patterns of excess Ar in the initial low temperature steps and the final high temperature steps. San Jose ignimbrite and the Maqui Maqui porphyritic rocks also display age spectra with excess Ar in the initial steps and slight stair step upward pattern of excess Ar in the final steps (Figures 2.10f and 2.11c). Upper Yanacocha andesites (Upha) display Ar-
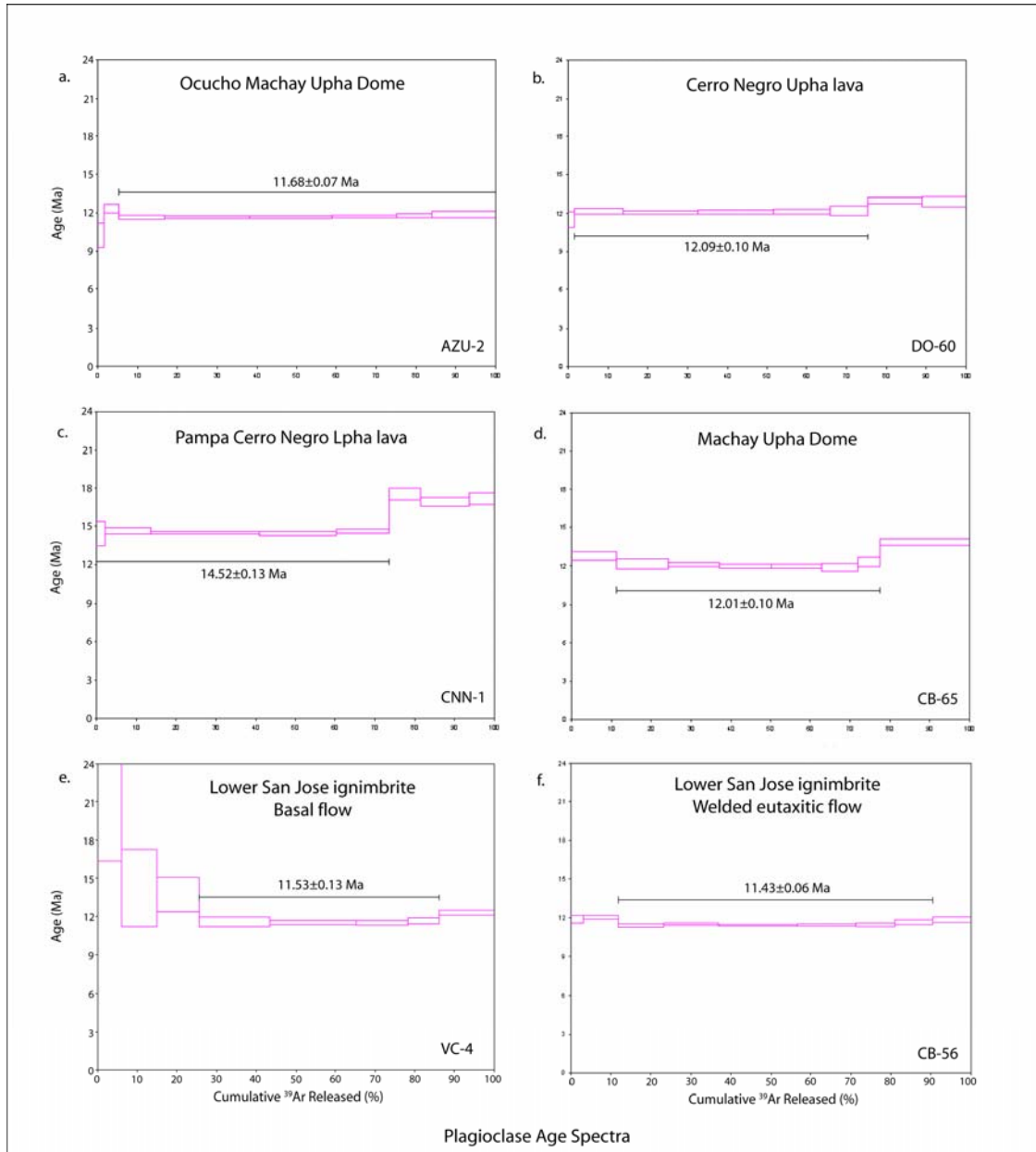
Figure 2.10 Experimental $^{40}Ar/^{39}Ar$ age data for plagioclase plotted as plateau age spectrum diagrams. Each heating step is represented by a horizontal rectangle whose height is $\pm 2\sigma$ uncertainty of the step age.
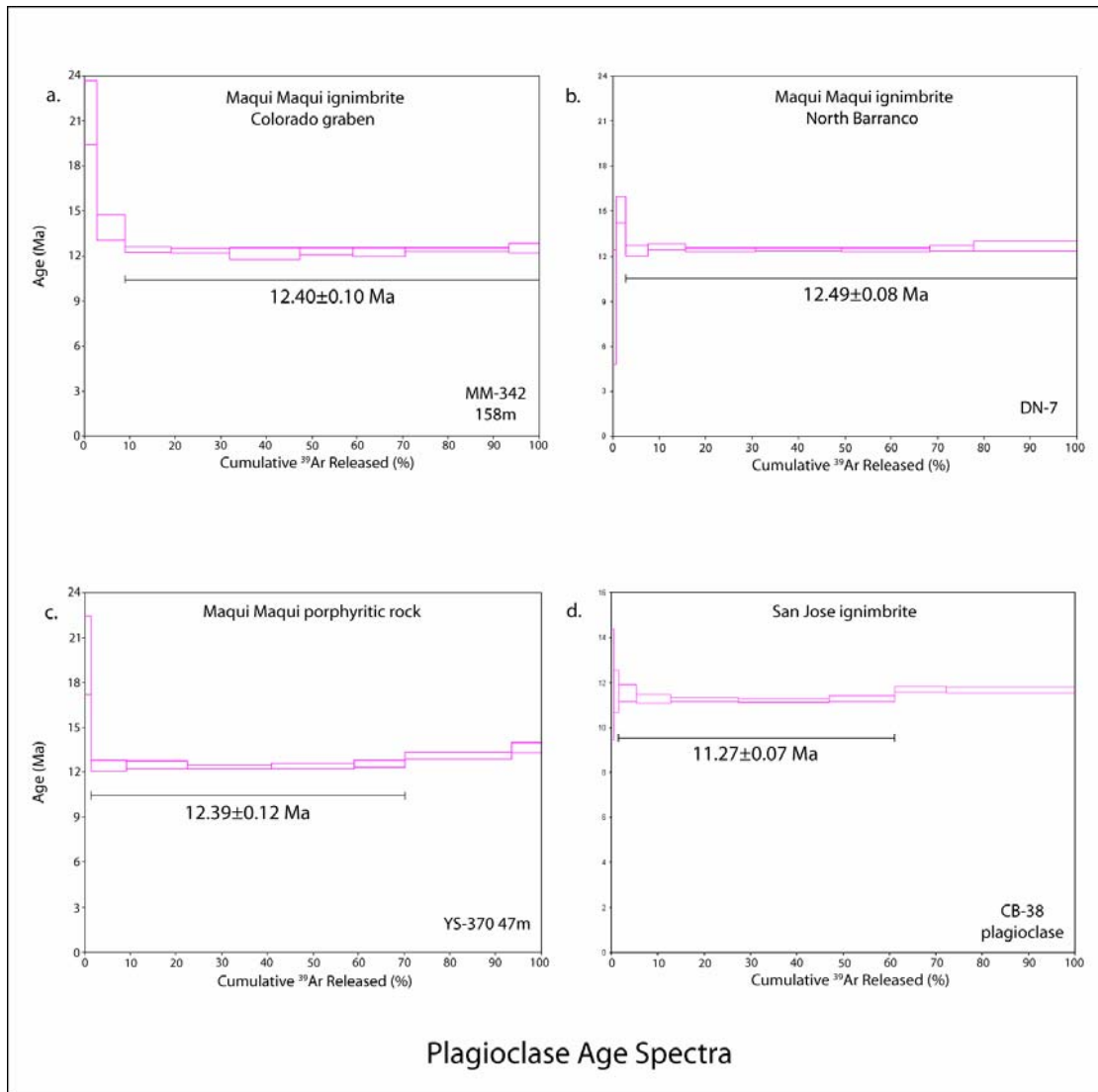
Figure 2.11 Experimental ^{40}Ar/^{39}Ar age data for plagioclase from the Maqui Maqui and San Jose ignimbrites plotted as plateau age spectrum diagrams. Each heating step is represented by a horizontal rectangle whose height is ± 2σ uncertainty of the step age.

loss in the initial steps and excess argon in the final steps (Figures 2.10a and b). San Jose and Maqui Maqui ignimbrites have age spectra with subtle saddle shapes and slight excess Ar in the initial low temperature steps and the final high temperature steps (Figures 2.10f, 2.11b and 2.11d). The Maqui Maqui ignimbrite in Figure 2.11a displays an example of age spectra that show patterns of excess Ar in the initial low temperature steps only. The inverse stairstep pattern of Ar-recoil is displayed in the initial low

temperature steps in sample VC-4 of the San Jose ignimbrite (Figure 2.10e). The age spectrum developed a saddle-shape pattern with an acceptable intervening four step plateau and 61% $^{39}Ar_K$. The isotopic ratio $^{39}Ar/^{37}Ar$ is higher and $^{39}Ar_K$ is lower in the first three initial steps, which suggests the presence of low temperature clay minerals and loss of $^{39}Ar_K$ through nuclear recoil.

Sanidine

One sanidine was analyzed in the study from the Negritos rhyolite ignimbrite (NG-5). The age spectrum showed a concave upward, saddle-shaped spectrum with excess Ar in the initial low temperature steps and slight excess Ar in the final high temperature steps, and an intervening plateau with four steps and 74% of the $^{39}Ar_{(K)}$. The final steps with excess Ar are concordant with the plateau and included in the calculation of the plateau age (Figure 2.12 a, Table 2.1 h). This changed the age of NG-5 slightly to 8.43±0.04 Ma over the isochron age of 8.48±0.04 Ma, but it is essentially the same age within the 2σ error. With the addition of the high temperature steps in the plateau age, the MSWD became elevated to 2.0 and is acceptable within the limits of criteria 2 and 3.

Biotite

Age analyses were realized on seven biotites from pyroclastic rocks of the Maqui Maqui and Cerro Frailes pyroclastic sequences, and domes and intrusions of the late dacite at Corimayo and Cerro Yanacocha (Figs. 2.12 b-f). Age spectra from biotite of the Cerro Frailes and Maqui Maqui (Figs. 2.12b and c) show patterns of Ar-loss in the initial low temperature steps followed by three to six contiguous steps and 82.5% to 97% $^{39}Ar_{(K)}$. Total fusion ages are younger than the plateau ages. Biotite from the Cerro Frailes ash-flow tuff (CB-35, Fig. 2.12c) at Combayo displays an age spectra with combined effects of Ar-loss and subsequent excess argon with slight recoil in the initial steps followed by a three step plateau with 82.5 % $^{39}Ar_{(K)}$. Biotite age spectra for the late dacite at Yanacocha display two distinct patterns. The Corimayo dome (COR-1, Fig. 2.12e) shows a pattern of Ar-loss in the low temperature steps followed by a plateau that is concordant with six contiguous steps, and the Yanacocha dacite porphyry displays a
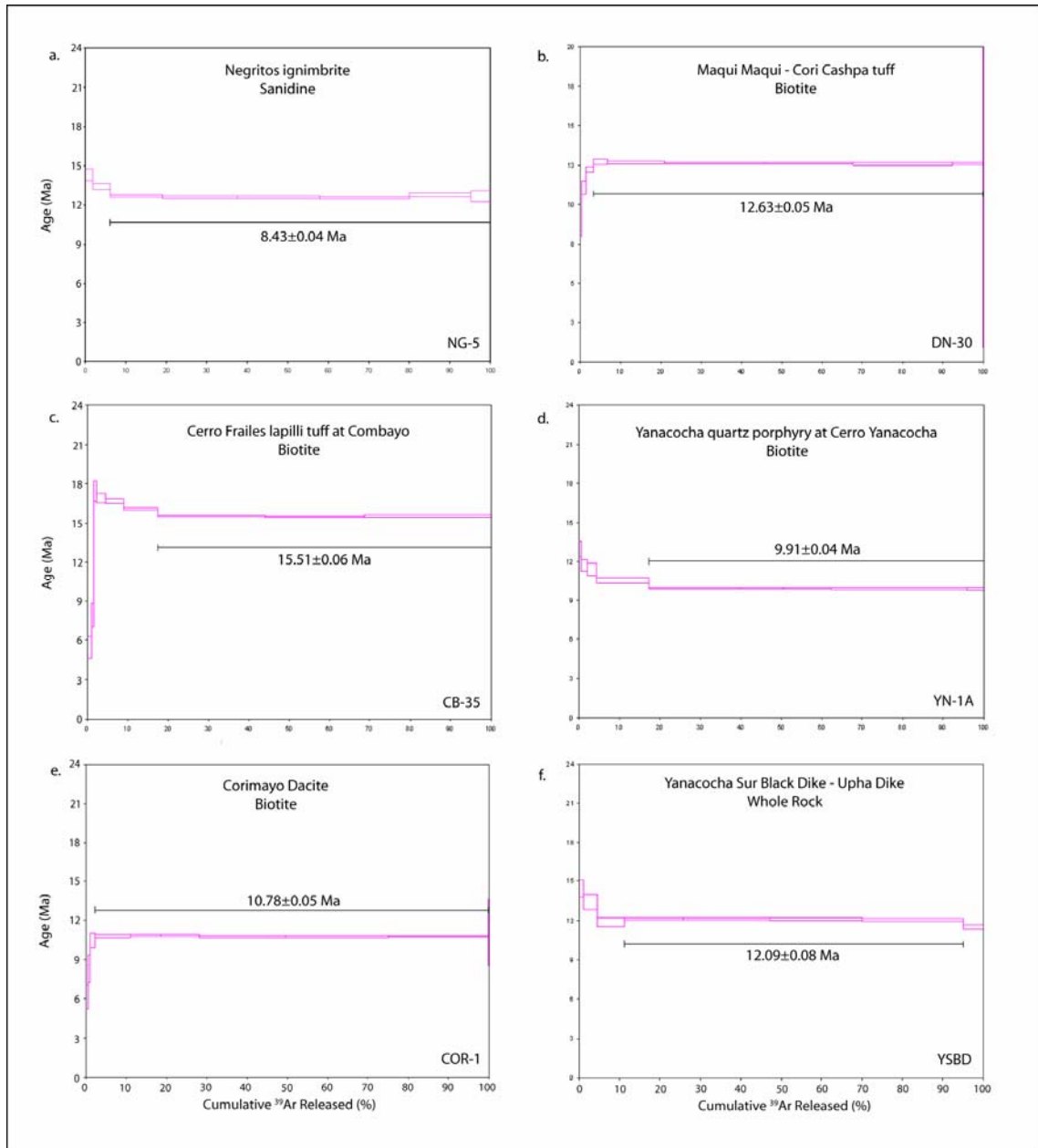
Figure 2.12 Age spectra for sanidine and biotite in the Maqui Maqui ignimbrite, Cerro Frailes tuff, and late Dacites at Yanacocha. Sample NG-5 is sanidine from a late rhyolite ignimbrite and YSBD is a whole rock sample of the black dike at Yanacocha Sur. The remaining samples are biotites from Cerro Frailes CB-35, Maqui Maqui DN-30, and the late dacites at Corimayo and Cerros Yanacocha. Each heating step is represented by a horizontal rectangle whose height is ± 2σ uncertainty of the step age.

pattern of excess Ar and slight recoil followed by a plateau concordant with five contiguous steps.

Hornblende

Seven hornblendes were analyzed from samples of the San Jose ignimbrite (Figure 2.13 a-c), coarsely porphyritic hornblende andesite intrusive rocks (Figure 2.13d and e), and an Upper Yanacocha andesite lava (Fig. 2.13f). Porphyritic hornblende andesite intrusive rocks dated in this study may be the fresh equivalent to Yp and Cp dikes and plugs. Hornblende in the Upper Yanacocha lava (CHQS-2) displayed excess Ar in the low temperature and high temperature steps, resulting in the total fusion age being greater than the plateau age. Age spectra from the hornblende in intrusions (Figs. 2.13d and e) displayed slight excess Ar and elevated 2σ error in the low and high temperature steps. Hornblende age spectra of the San Jose ignimbrite display excess Ar in the initial low temperature step and Ar-loss in the final high temperature step of BS-3 and CB-38 (Figs 2.13a and b). The most significant steps are the middle and high temperatures that range from 1100-1300°C. As expected, apparent ages in the most significant heating steps approach the preferred age of the plateau. These patterns are typical of the hornblendes analyzed at Yanacocha in that most $^{40}Ar_{(r)}$ and $^{39}Ar_{(K)}$ gas was released in the middle temperature range from ~1050 to 1200°C (Figures 2.13b, c, d and f) leaving age spectra with only one to four significant intervening steps. Significant steps are bordered by heating steps that produced only small amounts of argon gas. These steps show large uncertainties in their apparent age, but may be included in the calculation of plateau ages to secure an acceptable plateau. In general, hornblende plateaus display patterns typical of mineral separates and generally have much smaller temperature range for gas release (eg., 80%-99% of the $^{39}Ar_{(K)}$ is released from three to nine intervening steps). All hornblendes have total fusion ages older than the plateau ages due to excess Ar or Ar recoil in the initial steps.

Whole Rock

Four whole rock samples were analyzed in this study in cases with small sample sizes or fine-grained textures prevented an adequate mineral separate. YSBD (*Black Dike*) is an intrusion surrounded by altered and brecciated rocks in the Yanacocha Sur
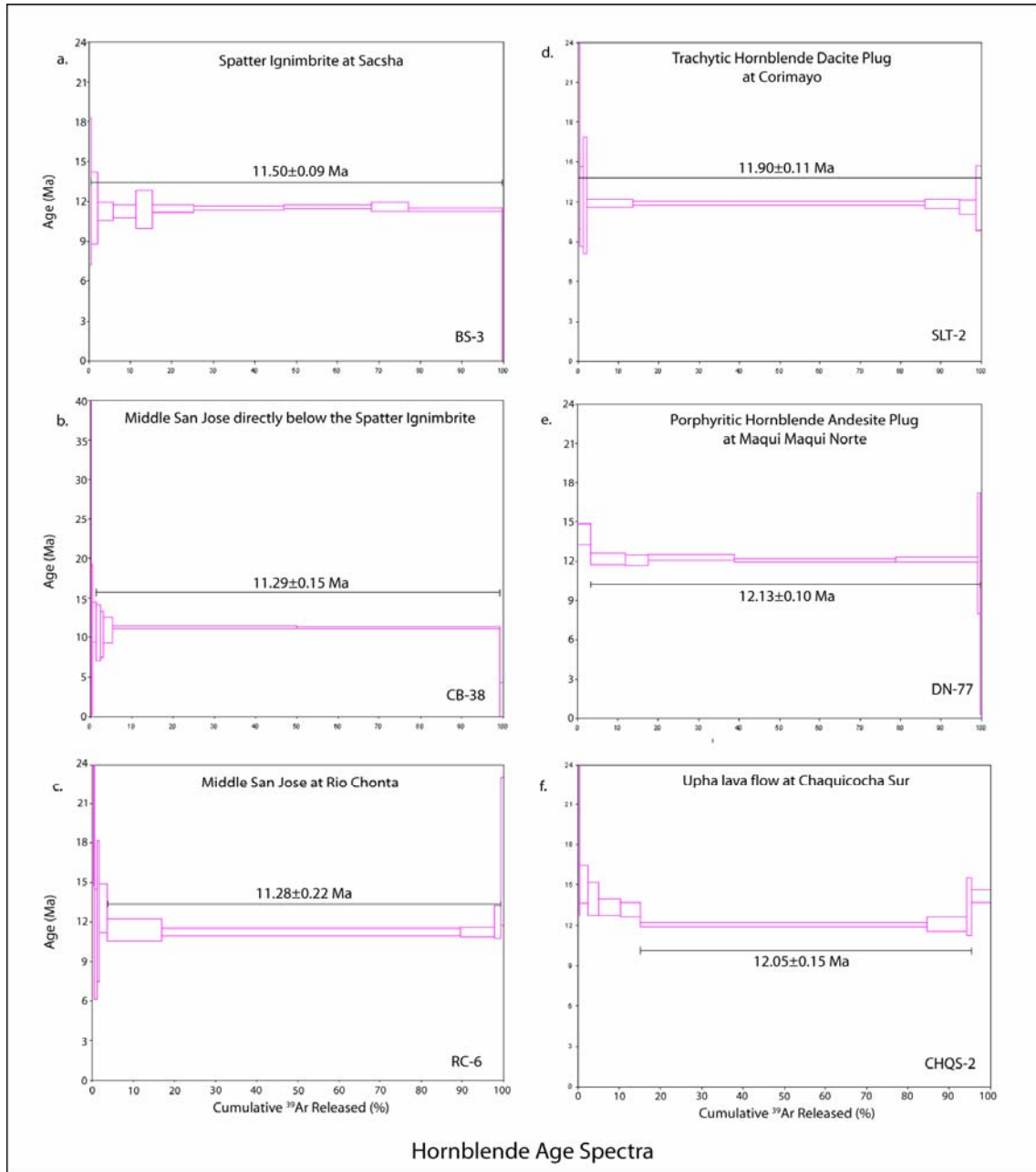
Figure 2.13 Hornblende age spectra that display acceptable plateau ages for samples at Yanacocha. Each heating step is represented by a horizontal rectangle whose height is ± 2σ uncertainty of the step age.

deposit that produced an acceptable plateau age. The sample displays effects slight Ar recoil in the initial low temperature steps and Ar-loss in the final high temperature step with four intervening and contiguous steps on the plateau (Fig. 2.10f). Ar recoil is supported by the inverse stairstep pattern in low temperature steps of the K/Ca plot for YSBD (Figure 2.9). These effects are attributed to weak low temperature clay alteration that produced recoil in the initial steps. Whole rock samples CB-5 and SJS 79A require further discussion and the data are examined below and in the next section on discordant ages.

Sample CB-5 is a whole rock sample from the matrix of a Lower Yanacocha monolithic hornblende andesite tuff with weak calcite-chlorite alteration. The sample contained abundant small monolithic rock fragments (0.5-4.0mm) of porphyritic andesite distinctly coarser grained than the fine-grained groundmass. All mafics of hornblende and pyroxene were altered to calcite, plagioclase was dusted with clays, and the groundmass contains chlorite. The age spectrum in CB-5 displays decreasing step ages and an *inverse staircase* pattern characteristic of Ar recoil (Fig. 2.16a). The K/Ca plot supports Ar-recoil and also displays an inverse stairstep pattern (Figure 2.8). The Ar recoil effect results in a concordant plateau age older than the total fusion age. This increased age, or increase in the $^{40}Ar/^{39}Ar$ ratio, is produced in the low temperature steps by ^{39}Ar recoil transfer from the K-bearing fine-grained low temperature phases; a loss of ^{39}Ar from K-bearing fine-grained alteration minerals with ^{40}Ar remaining unchanged. All age estimates for CB-5 are essentially identical within a 2σ error; that is, the plateau age of 13.76 ± 0.17 Ma, the isochron age of 13.63 ± 0.19 Ma, and total fusion age 13.72 ± 0.17 Ma are concordant. The sample meets all criteria for a valid plateau age.

Alteration Age Spectra

Alunite

Age spectra of nine alunites produced acceptable plateau ages that require little explanation (Fig. 2.14 and 2.15), and include samples with compositions that range from natroalunite (Na-rich endmember) and alunite (K-rich endmember). Patterns in the alunite age spectra vary from sample to sample (Fig. 2.14) but, typically, they display patterns of argon loss in the initial and final heating steps (Figs. 2.14b, c, d), or irregular

patterns with excess argon in the initial step and Ar-loss in the final steps, and intervening plateaus with 4 to 8 contiguous steps. In these cases, the total fusion age is less than the plateau age. Concordant plateaus vary from 75% to 99% of the total $^{39}Ar_{(K)}$ released in the sample (Figure 2.14).

Baul-1 was the first alunite sample dated and the only alunite analyzed in the furnace. The sample was from a massive pink alunite vein on Cerro Baul that crosscuts a eutaxitic-textured dacite ignimbrite with previously-altered accidental fragments. Results from x-ray diffraction (XRD) analyses showed the sample was a Na-rich variety of alunite contaminated with 10% quartz and trace rutile (Appendix VIII, Table A1.5). A concordant plateau resulted in three heating steps between 600-750°C and 99.8% of the $^{39}Ar_{(K)}$ gas was released with all relevant $^{40}Ar_{(r)}$ gas in the sample (Figure 2.14). The 700°C step had 79.97% $^{39}Ar_{(K)}$ gas producing an age of 11.02±0.07 Ma, and was obviously the most significant step in determining the age of Baul-1. The plateau age of 11.01±0.09 Ma, isochron age of 11.01±0.11, and the total fusion age of 11.07±0.14 Ma are concordant within a 2σ error.

Argon release patterns for incremental step heating are well defined for alunite. Itaya et al. (1996) discovered the maximum and minimum release temperatures of radiogenic $^{40}Ar_{(r)}$ from magmatic-hydrothermal alunite. Maximum release occurs at 600°C with the next most significant release between 400°C and 500°C, and minimum release is well defined at 400°C and 800°C. Release of nonradiogenic $^{40}Ar_{(a)}$ is also maximized at temperatures between 400-700°C with the highest proportions of $^{40}Ar_{(a)}/$ $^{40}Ar_{(r)}$ ≤400°C and >750°C.

Lessons learned from Baul-1 are similar to Itaya et al. (1996) and include the following: (1) all relevant gas needed to calculate the age was released at temperatures ≤750°C, and the most significant step was at 600°C; (2) maximum release of $^{40}Ar_{(r)}$ was at 500-600°C and minimums were at 400°C and 800°C, therefore, alunite age experiments must begin at a temperature of 400°C; (3) the 126 mg sample used for Baul-1 was much too large and caused significant contamination to the extraction line system and subsequent alunite samples were re-proportioned and weighed to 10-20mg; (5) the furnace method is not appropriate for alunite due to contamination and specialized low temperature heating requirements; (6) alunites require detailed low
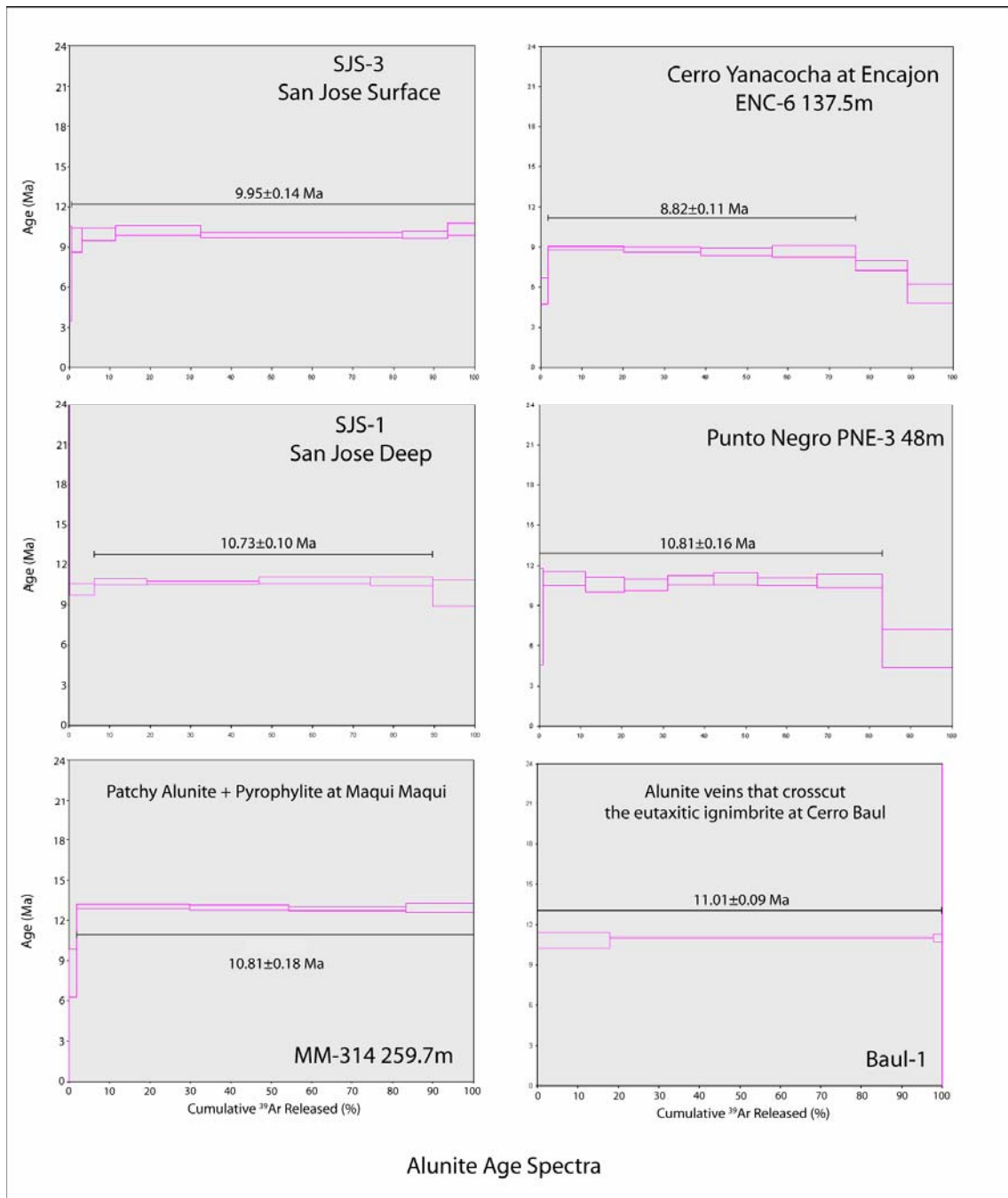
Figure 2.14 Experimental ^{40}Ar/^{39}Ar age data for alunite plotted as plateau age spectrum diagrams that meet the criteria for an acceptable plateau age. Each heating step is represented by a horizontal rectangle whose height is ± 2σ uncertainty of the step age.

temperature incremental heating between 400°-750°C, best accomplished with the laser method.

Hydrothermal Biotite

The age spectrum for hydrothermal biotite (Figure 2.15) displays a combined pattern of Ar-loss and Ar recoil in the initial low temperature steps, and Ar-loss in the final step, resulting in a total fusion age slightly lower than the weighted plateau age. A plateau contains six concordant and contiguous steps and 85% ^{39}Ar$_{(K)}$ (Table 2.1j), with an MSWD of 2.23 that is in the range of <2.5 for an acceptable plateau age (Tegner and Duncan, 1999; McDougall and Harrison, 1999) . Both the plateau age and the isochron age are concordant within a 2σ error and the same age. The isochron age yields a ^{40}Ar/^{36}Ar intercept with large uncertainty slightly greater than the atmospheric value of 295.5 (Figure 2.15; Table 2.1). The ^{40}Ar/^{36}Ar intercept is poorly defined in the KUP-3 biotite because the data plot in a tight cluster along the isochron due to very low amounts of ^{36}Ar (atmospheric) in steps of the weighted plateau age. The KUP-3 571m ages are all essentially the same age within the limits of a 2σ error. The crystallization age of the sample is probably slightly younger than the plateau age (10.73±0.05 Ma) and slightly older than the isochron age (10.68±0.06 Ma). The total fusion age of 10.70± 0.04 Ma lies between the plateau and isochron age, and is also identical to the most significant heating step that contained 28.3% ^{39}Ar$_{(K)}$ at 1175°C. All ages are essentially the same within the limits of a 2σ error and to maintain consistency the plateau as is chosen as the preferred age.
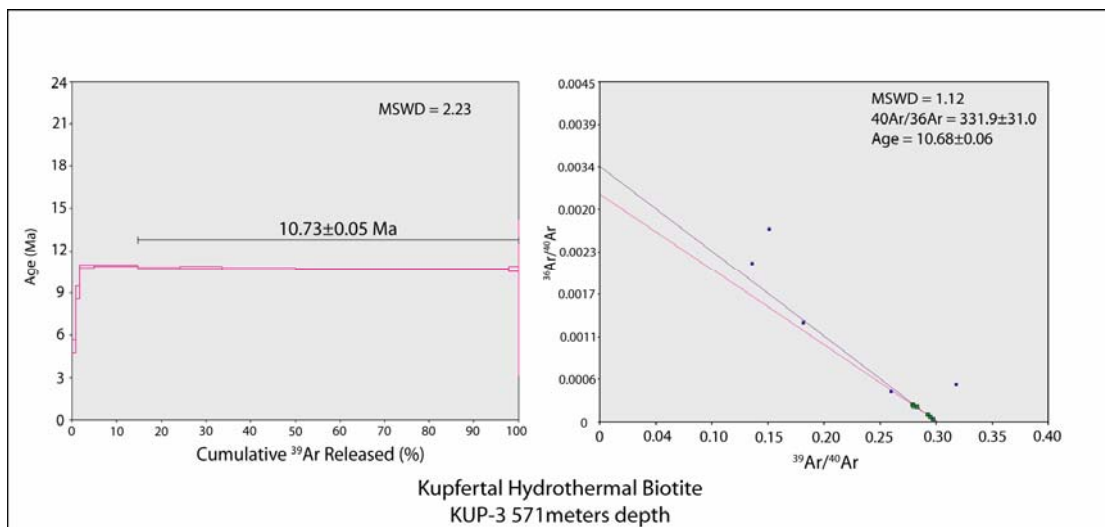
Figure 2.15 Experimental ^{40}Ar/^{39}Ar age data from the Kupfertal hydrothermal biotite. Sample collected at 571 meters in diamond drill hole KUP-3. Data are plotted as a plateau age spectrum and inverse isochron diagrams.

Discordant Ages

Discordant age spectra produced by the ^{40}Ar/^{39}Ar step heating experiments violate one or more of the plateau age criteria and are attributed to combined effects of Ar-loss, excess Ar, and Ar-recoil. Generally, the combined effects precluded a valid plateau age. Some samples also experienced data clustering along the isochron that produced uncertainties in the initial ratios and isochron ages. Large uncertainties present from these effects necessitate an estimation of the age using all available age data and field geology. Some of the Yanacocha samples failed to produce plateaus interpretable as crystallization ages. Six fresh rocks and ten alunites require explanations for the preferred ages accepted in this study (Figures 2.16, 217, 2.22-2.24; Table 2.1). Fresh samples are discussed in order of stratigraphic sequence (Figures 2.16 and 2.17). Discordant alunite ages are discussed as follows (Figures 2.23 and 2.24): (1) samples with analyses whose results were affected by the fogging of the coverslip during the experiment, and (2) samples with analyses whose results display large analytical error from effects other than fogging.

Chaupiloma Lahar Sequence

Hornblende (DE-18) from a Chaupiloma-like lahar at Cerro Collotan produced a *saddle-shape* pattern in the age spectrum characteristic of excess argon (^{40}Ar$_E$) (McDougall and Harrison, 1999; p. 123-125) with two distinct "plateaus" (Figure 2.16e

and f). The initial low temperature steps display slight inverse staircase effect from Ar recoil that is supported by high K/Ca ratios for the initial steps (Figure 2.8, DE-18). The isotopic composition ^{39}Ar/^{37}Ar ratio and the K/Ca ratio are elevated relative to the high temperature plateau and suggest that K-rich alteration minerals are present in the lower temperature steps where Ar recoil is suspect. At higher temperatures, three contiguous steps form an *upper* plateau with 52% of the ^{39}Ar$_K$ gas released and an age of 15.41±0.36 Ma. The corresponding isochron age of 15.02±0.76 Ma and the total fusion age 15.12±0.25 Ma are concordant within the limits of a 2σ error. The higher temperature plateau also includes the two most significant steps in the age spectrum (eg., the highest levels of ^{39}Ar$_K$ and ^{40}Ar$_r$ in a single step) and may be closest to the undisturbed closure age for DE-18.

Sample DE-18 was affected by a low temperature hydrothermal event as evidenced by clay (illite?), calcite, chlorite and magnetite alteration in the groundmass, plagioclase and hornblende. This may have resulted in excess argon for the lower two temperature increments by diffusion into the rims of the amphibole during the hydrothermal event that produced the K-rich alteration minerals. The low temperature "plateau" could have developed from Ar-loss from the late thermal event that caused the alteration, and its lowest two steps could reflect Ar recoil. This assumption is supported by consistently higher K/Ca ratios in the first four steps that decrease and pattern an inverse stairstep after step 4 (Figure 2.8, DE-18). The final steps have low K/Ca compositions more typical of fresh hornblende in the Yanacocha andesites (Figure 2.6).

The 1150°C step in the upper "plateau" contains 23.9% of the ^{39}Ar$_{(K)}$ and more ^{40}Ar$_{(r)}$ than any step in the lower plateau. The age of 15.29±0.54 Ma is closer to the predicted age of 15.9 Ma for the LAL-2 andesite lava flow (DN-84) than any single step on the lower "plateau". The high temperature plateau may be a remnant of the original pre-alteration isotopic composition for DE-18. The similarity of this plateau and isochron ages with the age of the 1150°C step give confidence to the older age of DE-18 greater than 15 Ma. Therefore, the high temperature plateau age 15.41±0.36 Ma was selected as the preferred age for DE-18.
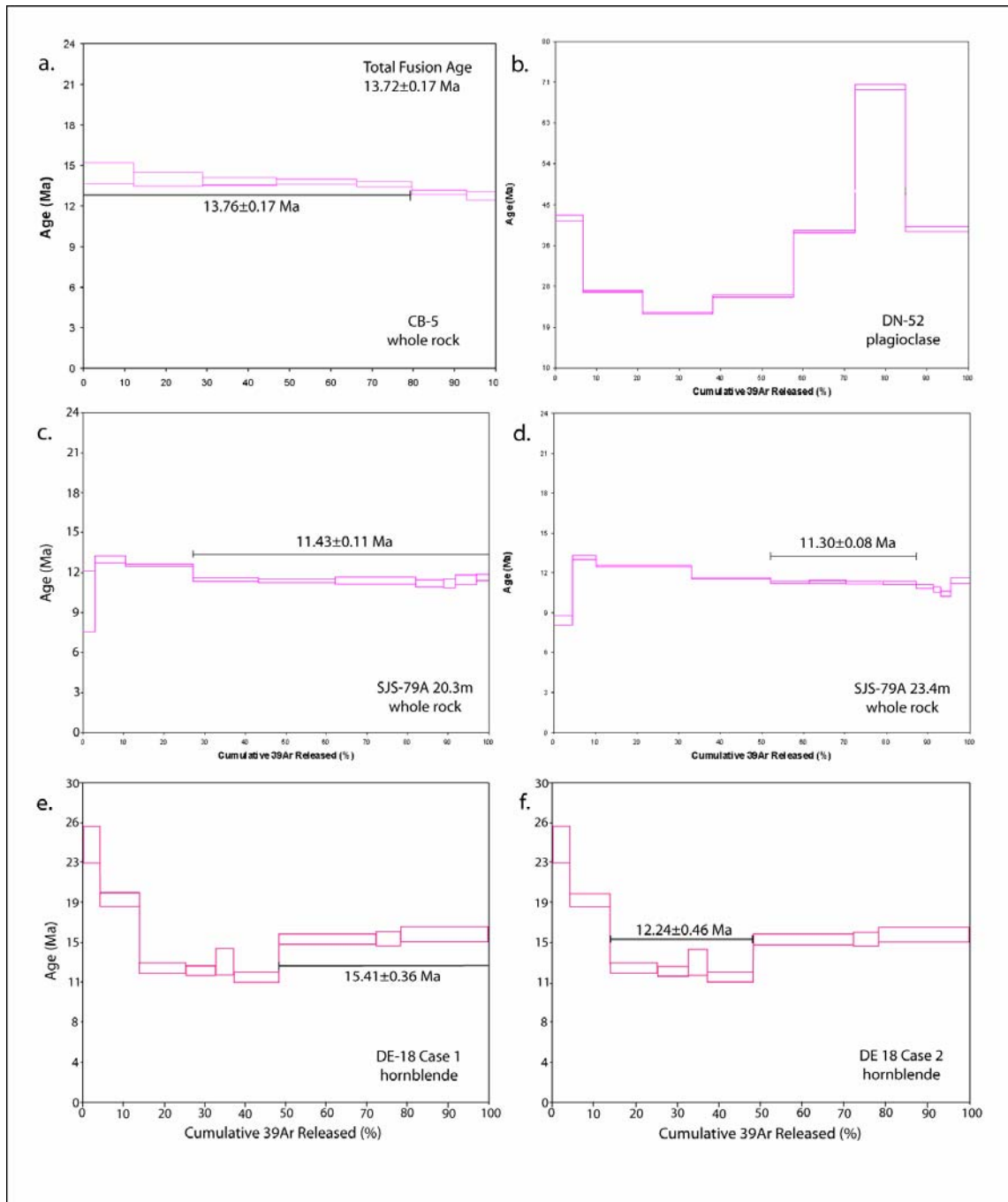
Figure 2.16 Experimental ^{40}Ar/^{39}Ar age data for discordant ages plotted as plateau age spectrum diagrams that produced extraneous effects from Ar-loss, excess Ar, and Ar recoil. Plateau ages do not meet the criteria for an acceptable age. Each heating step is represented by a horizontal rectangle whose height is ± 2σ uncertainty of the step age.

Cerro Frailes Pyroclastic Sequence

A sample of biotite dacite lapilli ash-flow tuff (DN-12) was collected from an ash flow tuff above the Chaupiloma andesite lahar sequence in the Chaupiloma area. Geologic mapping and field relationships suggest it is a basal tuff in the Cerro Frailes pyroclastic sequence, and it overlies andesite lahars of the Chaupiloma sequence (15.9 Ma, DN-84) and below the Maqui Maqui ignimbrite north of Barranco (12.5 Ma, DN-7). A predicted age of 15.5 Ma is based on field mapping and other $^{40}Ar/^{39}Ar$ dates for the Cerro Frailes tuff at Yanacocha. Dacite tuffs at Chaupiloma have been interpreted as the youngest ash flow tuffs in the district and part of a post-mineral upper dacite sequence as defined by Yanacocha geologists (Trujillo, 2004).

The crystallization age was estimated from $^{40}Ar/^{39}Ar$ analyses of both biotite and plagioclase from the same sample, and the $^{40}Ar/^{39}Ar$ dates from both minerals indicate that the DN-12 tuff is pre-Yanacocha and >15 Ma (Figure 2.17; CD Appendix I, 03C2722). Age results bracket the crystallization age between the youngest plateau age of 15.18±0.14 Ma for the plagioclase, the total fusion age for the biotite of 15.98±0.08 Ma (Figure 2.17). The Chaupiloma tuff is a part of the Cerro Frailes dacite pyroclastic sequence and not part of the Upper Dacite sequence at Yanacocha.

The tuff of sample DN-12 was affected by weak clay-chlorite-calcite alteration from a nearby hydrothermal system that affected the groundmass and biotites (Figure 2.16); therefore, both biotite and plagioclase were analyzed for a better resolution of the age. Plagioclase appeared unaltered in thin section, and the age spectrum produced an acceptable plateau age of 15.18±0.14 Ma with seven contiguous steps and 98.2% of the $^{39}Ar_{(K)}$ gas released (Figure 2.17, Table 2.1), and considered the preferred age for the DN-12 tuff. The isotopic $^{39}Ar/^{37}Ar$ plot shows a uniform low K/Ca ratio for the steps associated with the plateau age typical for fresh plagioclases (Figures 2.4 and 2.5) and these data suggest that plagioclase was not altered in DN-12.

The biotite has rare calcite alteration in the cleavage lamellae and tiny inclusions of feldspar and magnetite (Figure 2.18). The biotite age spectrum (Figure 2.17a) did not produce a plateau that meets the criteria for an acceptable plateau age, and four contiguous steps with 48.7 % of the $^{39}Ar_{(K)}$ gas released give an apparent age of

15.45±0.10 Ma (Figure 2.17) with an isochron age of 15.36±0.10 Ma (Table 2.1); both statistically similar to the plagioclase age within a 2σ error. A second isochron age of 15.38±0.09 Ma was estimated from six steps shaded gray in Figure 2.17 with 58.3% of the $^{39}Ar_{(K)}$ gas released (Figure 2.17; Table 2.1) that includes the four contiguous steps from the high temperature end of spectrum and two low temperature steps that are not contiguous, but have the same age. Data are spread out along the isochron and not clustered, and they have initial ratios within a 2σ error of atmospheric composition. The second isochron age with >50% of the $^{39}Ar_{(K)}$ gas released is statistically similar to the first isochron age. Both are closer to the plateau age for the plagioclase than the total fusion age for the biotite of 15.98±0.08 Ma. The second isochron age in Figure 2.17 is accepted as the preferred age for the biotite in sample DN-12.

Alteration is suspect in the biotites and the K/Ca plot in Figure 2.19 supports the petrographic observations in Figure 2.18 indicating the presence of calcite and Ca-clays
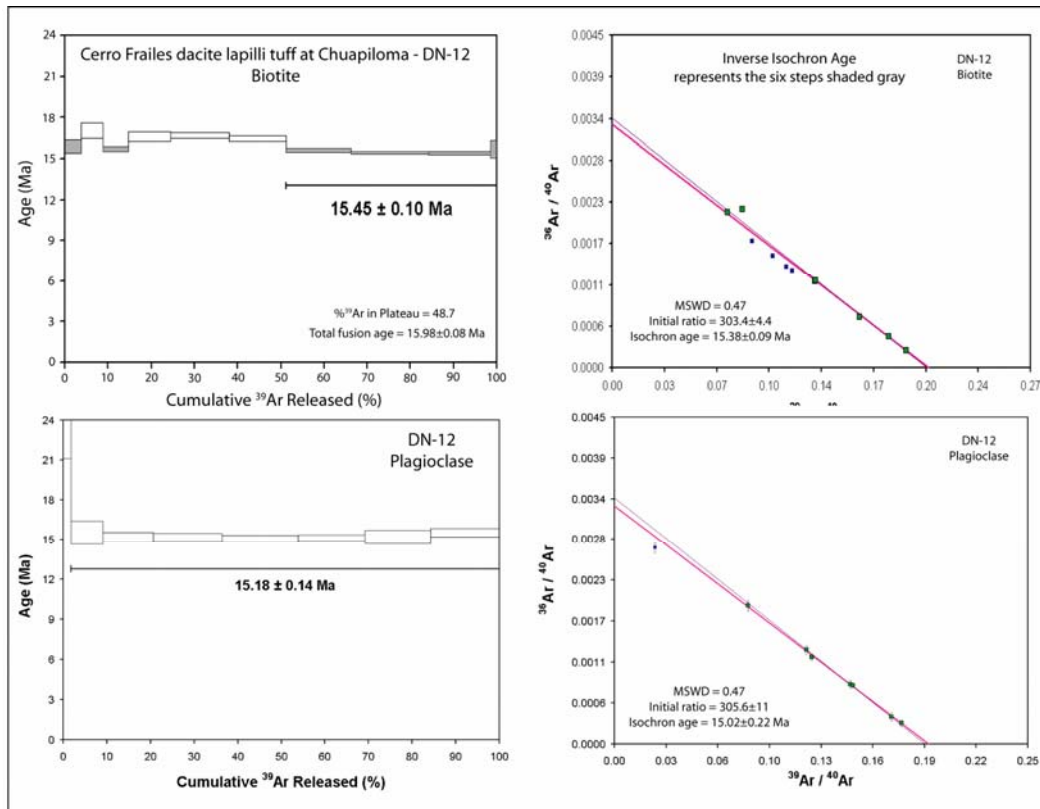
Figure 2.17 Age spectra and inverse isochron plots for the Cerro Frailes dacite lapilli tuff at Chaupiloma. Both plagioclase and biotite were analyzed for the same sample.
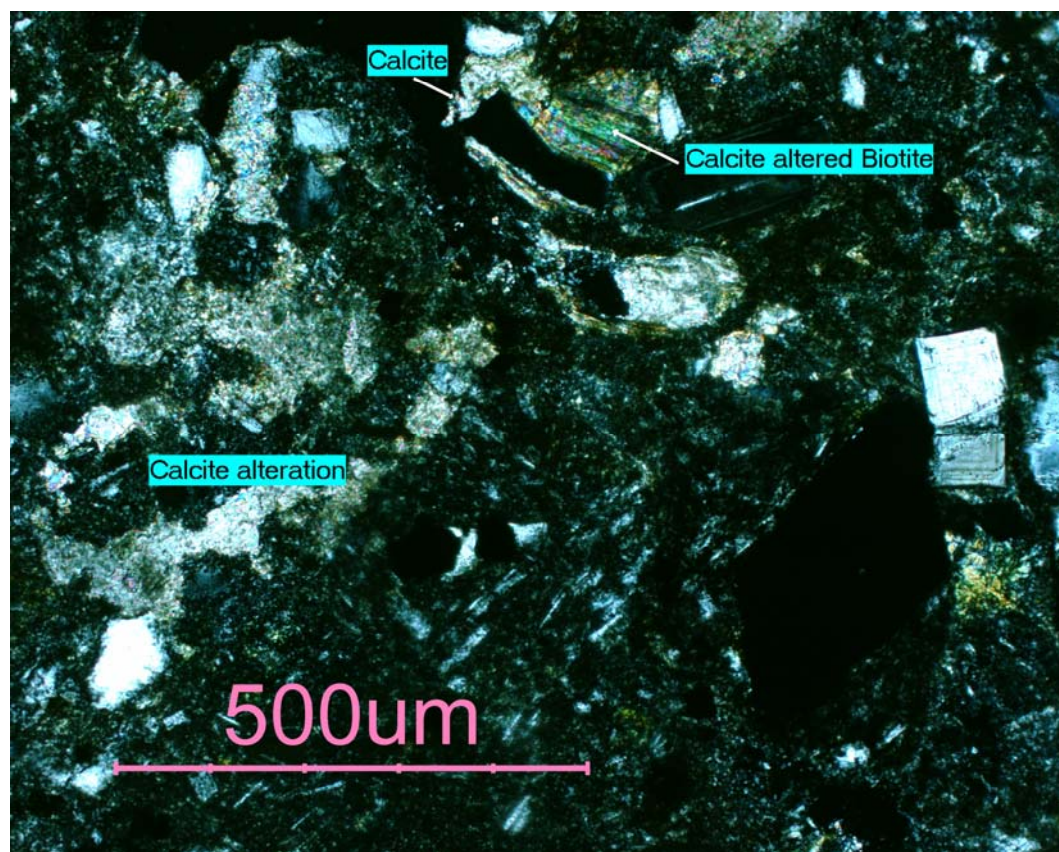
Figure 2.18 Photomicrograph with crossed polars showing calcite alteration in the DN-12 Cerro Frailes tuff at Chaupiloma.
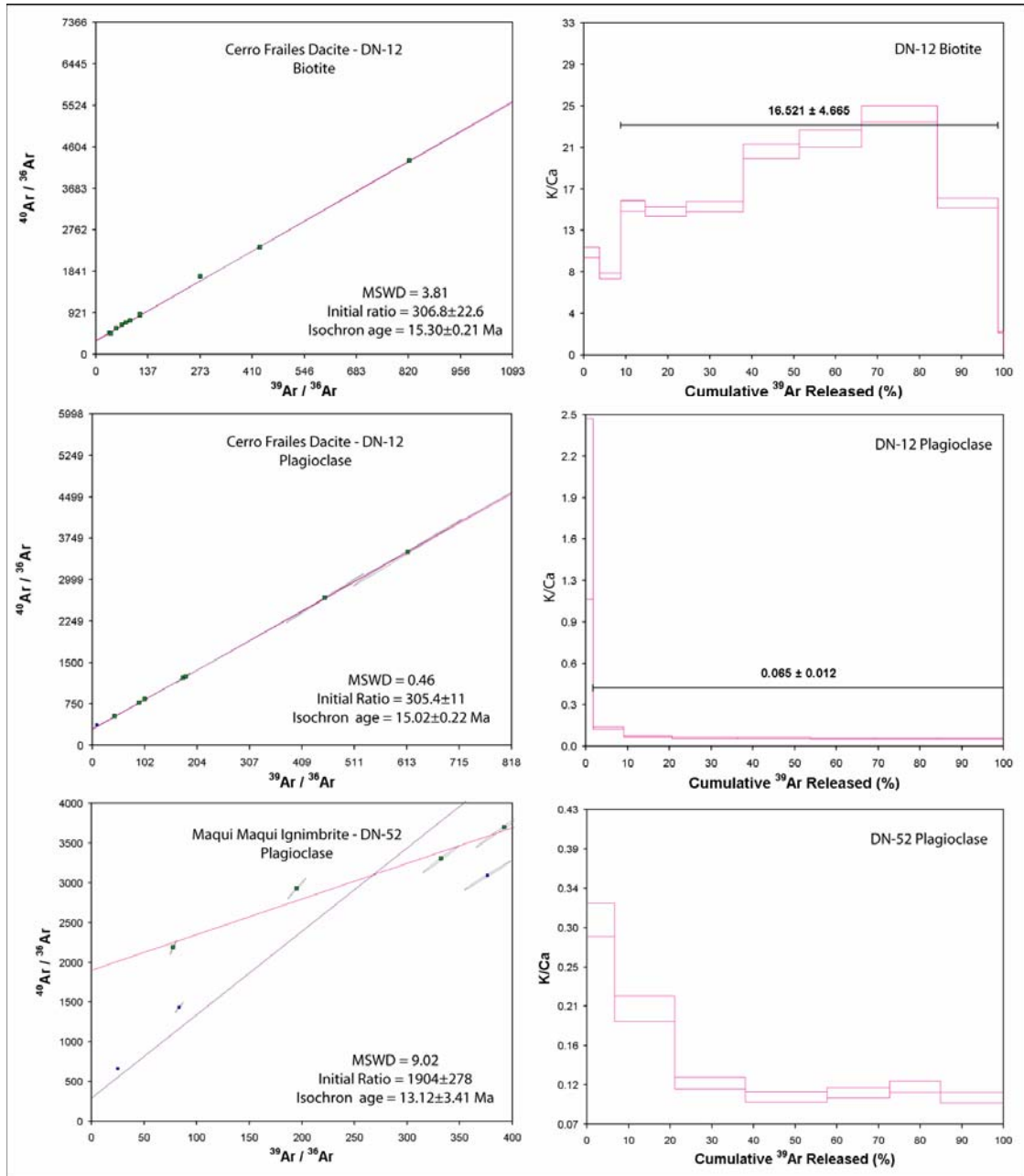
Figure 2.19 Normal isochron and K/Ca plots for discordant ages from the DN-12 Cerro Frailes biotite and plagioclase from the DN-52 Maqui Maqui ignimbrite. Plagioclase from DN-12 displays a concordant plateau age in Figure 2.15 and the K/Ca and isochron plots are presented for comparison. Calcite alteration is suspect in the biotite with decreased K/Ca in the initial low temperature steps, and K-metasomatism in plagioclase with increased K/Ca in the initial steps.

with lower K/Ca ratios in the initial low temperature steps. However, the K/Ca pattern is somewhat erratic and does not differ greatly from the K/Ca plots for fresh and altered biotites that produced acceptable plateau ages (Figures 2.6, 2.7, 2.9 and 2.12). In the initial low temperature steps (Figure 2.17), the lower (younger) two steps have similar ages to the two most significant final high temperature steps (highlighted in gray in Figure 2.17) and could represent an age closer to the crystallization age. The initial step has a younger apparent age with a low K/Ca ratio, and could represent Ar-loss as a result of the alteration (Figures 2.17 and 2.19). The third heating step has a similar age to the first step, and the K/Ca ratio is more typical of the biotite. The higher (oldest) steps reflect the effects of slight excess argon since the K/Ca plot lacks the low temperature K-enriched phases as in CB-5 and SJS-79A (Figure 2.8) and does not support Ar-recoil, or ^{39}Ar loss.

The age for DN-12 was influenced by results from both the biotite and plagioclase samples, and field mapping of the Cerro Frailes pyroclastic sequence into Chaupiloma. All age results indicate that the dacite tuff at Chaupiloma is older than 15 Ma and part of the Cerro Frailes pyroclastic sequence. The data show it is not a post-mineral ash flow tuff related to the late dacite.

Maqui Maqui Ignimbrite

Sample DN-52 was collected from the Maqui Maqui ignimbrite adjacent to the Maqui Maqui Norte gold deposit, and many mafic minerals were altered or decomposed from a later thermal event. Plagioclase from the sample displayed a saddle-shaped age spectrum characteristic of excess radiogenic argon (^{40}Ar$_E$) (Kelly, 2002; McDougall and Harrison, 1999; p. 123-125). Plagioclase phenocrysts are concentrically normal zoned and shock-fractured, and "sericite" veinlets crosscut many plagioclase crystals (Figures 2.20 and 2.21). Apparent ages from the low and high temperature steps and the calculated 2σ weighted mean age of 30.62±11.61 Ma greatly exceed the predicted age of 12.5 Ma for the Maqui Maqui ignimbrite from DN-7 and MM-342 (Table 2.1d). An age of 21.76±0.17 Ma was produced for the minimum step in the saddle-shaped spectrum, and this too is older than the predicted age. The initial ^{40}Ar/^{39}Ar reflects a trapped argon component much greater than 295.5 (atmospheric) indicating significant disturbances to

the age spectra that is not of atmospheric composition, and the normal isochron age was within the predicted age limit at 13.12±3.41 Ma (Figure 2.17, DN-52).

The K/Ca plot (^{39}Ar/^{37}Ar ratio) in Figure 2.19 displays high K/Ca ratios in the initial low temperature steps with an inverse stairstep pattern observable in samples with recoil. The high K/Ca ratios in the initial steps support the presence of sericite. The remaining K/Ca plot is low and characteristic of plagioclase.

Figure 2.20 Shock-fractured plagioclase (DN-52) characteristic in ash-flow tuffs. Examples of shock fracturing in phenocrysts are discussed by Best et al. (2003). Shock-fractured phenocrysts are also found related to hydrothermal activity.

Significant ^{40}Ar$_E$ is related to the presence of melt and fluid inclusions, and mineral inclusions, in low potassium minerals such as plagioclase, and argon solubility is higher in the hydrous fluids and silicate fluids relative to the mineral phase (Kelly, 2002). Therefore, ^{40}Ar$_E$ is released at both low and high temperatures from hydrothermal fluids and melt inclusions (Kelly, 2002). Possibly ^{40}Ar$_E$ from the hydrothermal fluids diffused into the higher temperature plagioclase cores and lower temperature rims during a

hydrothermal event that formed the alteration and secondary minerals found in fractures and veinlets that crosscut the sample. Another hypothesis could be the excess Ar was trapped at the time of crystallization and reflects compositions in the magma (Duncan pers comm., 2005).
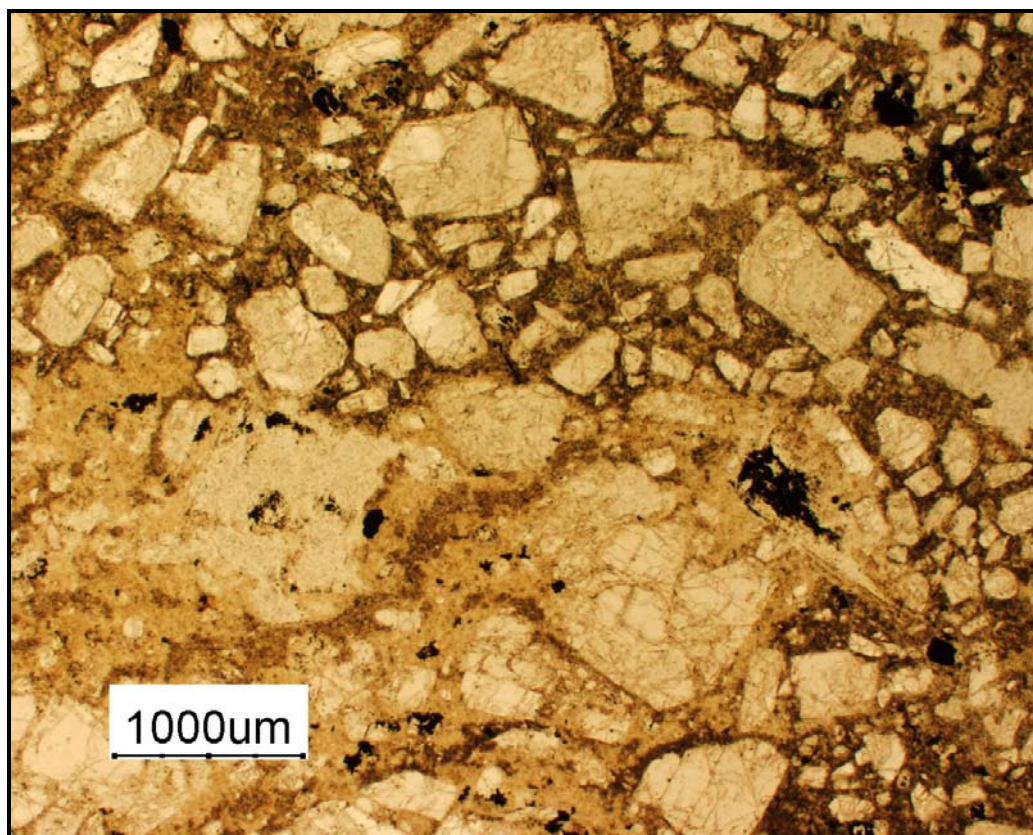
Figure 2.21 Example of weak intermediate argillic alteration in the Maqui Maqui ignimbrite. Clays replace groundmass glass, dust the rims of the plagioclase and fill fractures in the phenocrysts.

San Jose Ignimbrite

Whole rock samples were collected from drill core of a single unit of eutaxitic San Jose ignimbrite at 20.3 meters- and 23.4 meters-depth in diamond drill hole SJS-79A. The ignimbrite lies above gold ore at the San Jose deposit, and the samples displayed weak intermediate argillic alteration with unidentified clays, and chlorite and calcite pseudomorphs of pyroxene and hornblende. Petrographic studies indicate that the plagioclase was relatively unaltered, but some crystals were observed dusted with clays.

The whole rock mini-core sampled the groundmass in attempt to avoid altered mafic minerals and large plagioclase. The samples produced patterns in their age spectra from combined effects of Ar-loss and Ar recoil (Figure 2.16c and d) discussed below as follows:

(1) The age spectrum of the sample from 20.3 meters depth shows a pattern of combined effects from Ar-loss in the first heating step and Ar recoil, or ^{39}Ar loss, in the 700° and 800° C steps (Figure 2.16c). A plateau in higher temperature steps meets the criteria for an acceptable age, and produced a weighted plateau age of 11.43±0.11 Ma from seven contiguous steps. The isochron age of 11.51±0.23 Ma is concordant, but the total fusion age of 11.67±0.12 Ma is older reflecting the ^{39}Ar loss from the lower temperature steps.

(2) The second sample at 23.4 meters depth shows a pattern that combines the effects of Ar recoil with Ar-loss at the low temperature steps (Figure 2.16d). A small "plateau" developed in the higher temperature heating steps from 950-1100°C; however, the "plateau" was composed of only 35% of the ^{39}Ar$_K$ gas released in four steps and did not meet the acceptable criteria. A small inverse staircase pattern immediately follows the plateau suggesting continued Ar recoil in the high temperature steps. The effects of recoil are supported by the K/Ca plot in Figure 2.8 and decreasing K/Ca ratios develop an inverse staircase pattern for the same steps that indicate Ar recoil, or ^{39}Ar loss from the initial K-rich phases. The plateau age (11.30±0.08 Ma) and isochron age (11.34±0.16 Ma) are concordant, but the total fusion age is older at 11.56±0.07 Ma reflecting the ^{39}Ar loss in the low temperature steps. Heating steps <950°C contained most of the ^{39}Ar$_{(k)}$ and ^{40}Ar$_{(r)}$ gas and low error due to the abundance these isotopes, These initial steps display an inverse staircase pattern of Ar recoil and failed to match the plateau within a 2σ error. The apparent age for the most significant step is 12.49±0.07 Ma, older then the plateau age by over 1 m.y., and the age reflects the ^{39}Ar loss (Figure 2.22). An isochron age of 11.28±0.14 Ma estimated from five steps (shaded gray in Figure 2.22) with 40% ^{39}Ar released is preferred over the isochron from the "plateau".
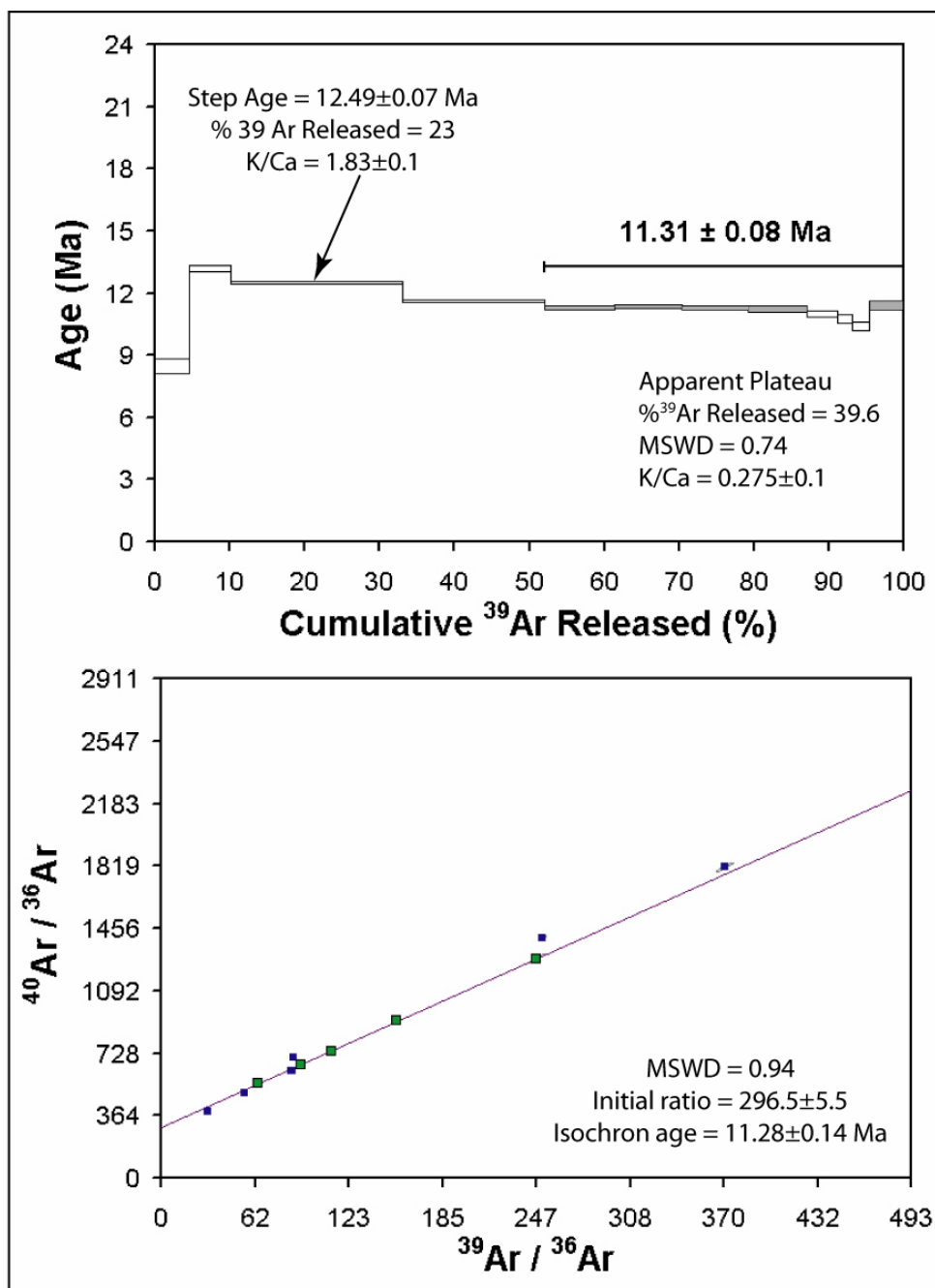
Figure 2.22 Age spectra and inverse isochron plots for the ignimbrite sample SJS-79A 23.4m above the San Jose gold deposit.

The age for the ignimbrite above the San Jose gold deposit is estimated by comparing the "preferred" isochron age of 11.28±0.14 Ma for sample SJS-79A 23.4m (Figure 2.22), and the plateau age for SJS-79A 20.3m at 11.43±0.11 Ma (Figure 2.8; Table 2.1); both are statistically similar within a 2σ error. The two most significant step ages in the sample at 20.3 meters have apparent ages younger than the plateau age and closer to the isochron age of the sample at 23.4 meters. The mean of the two ages is ~11.36±0.11 Ma, and considered the best age estimate for the SJS-79A sample at San Jose.

Problematic Alunite

Sample contamination and analytical error produced poor results for eleven alunite samples, but results met the conditions for an acceptable age. The age spectra display large uncertainties from the effects of increased proportions of atmospheric $^{40}Ar_{(a)}$, Ar-loss, excess Ar, Ar recoil, and coverslip fogging. Release of nonradiogenic $^{40}Ar_{(a)}$ in magmatic-hydrothermal alunite is maximized at temperatures between 400-700°C, but the highest proportions of $^{40}Ar_{(a)}/^{40}Ar_{(r)}$ exist ≤400°C and >750°C (Itaya et al., 1996). Atmospheric $^{40}Ar_{(a)}$ is adsorbed on the mineral surfaces of alunite and impurities, such as illite and kaolinite, and dominates at low temperatures (Itaya et al., 1996). The results are discussed in detail below.

KBr Coverslip Fogging

The K-Br coverslip fogged from releases of SO_2 and SO_3 gas during critical heating steps and compounded problems with four samples (CS-1, QN-1, YN-105, and YO-1); therefore, alunite ages have distinct patterns in their age spectra (Fig. 2.23). Initial heating steps released the most significant amounts of $^{39}Ar_{(K)}$ and $^{40}Ar_r$, at low temperatures from 500° to 600°C. Alunite, as previously discussed, releases Ar and other gases at temperatures from 400° to 750°C. Fogging of the coverslip took place during the 600°C step. After fogging, the $^{39}Ar_K$ and $^{40}Ar_{(r)}$ gases diminished and analytical error increased greatly due an increased proportion of atmospheric $^{40}Ar_{(a)}$ and the inability to adequately heat the sample to the next temperature level. Ages were estimated using
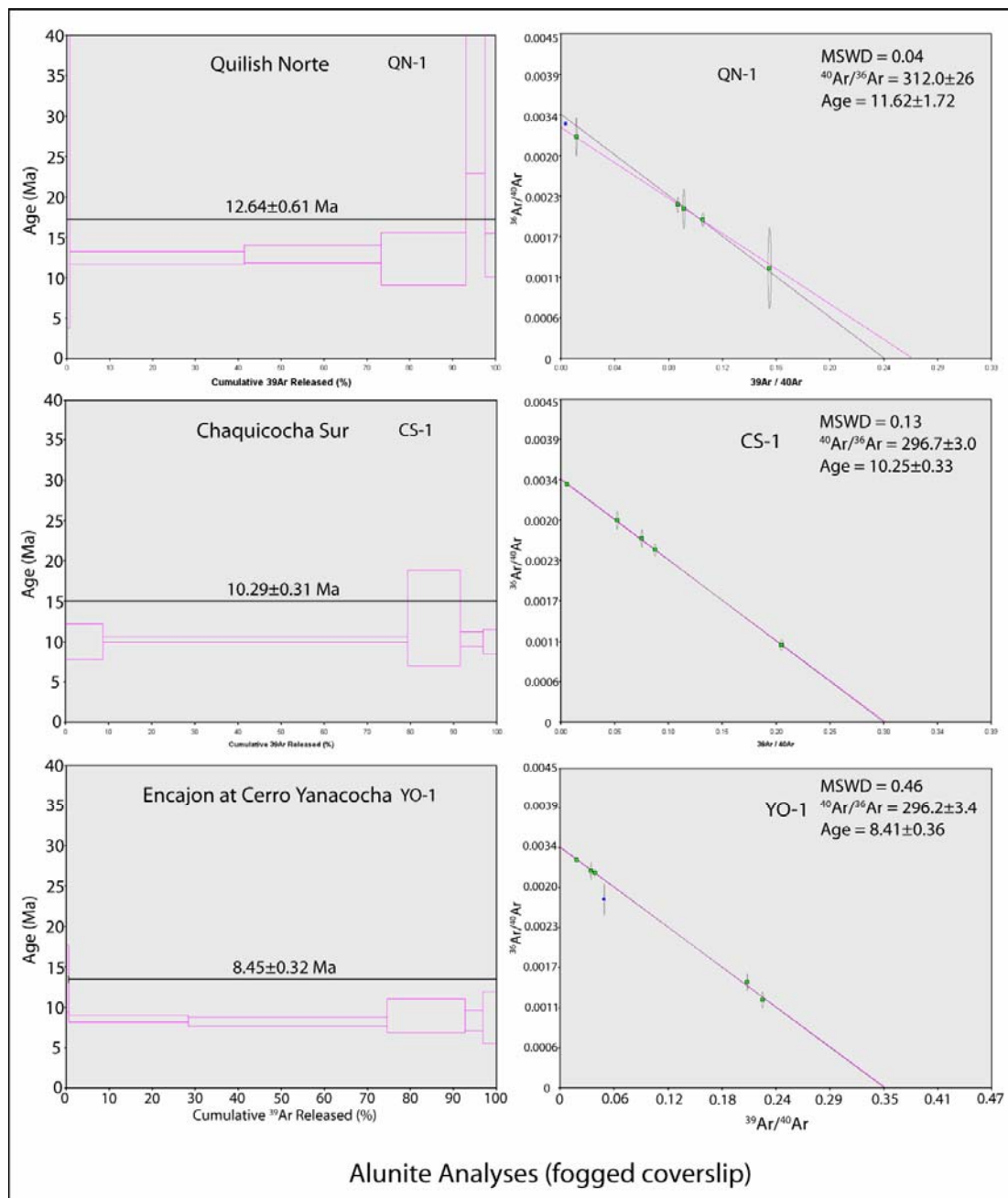
Figure 2.23 Experimental $^{40}Ar/^{39}Ar$ age data for problematic alunite analyses do to fogging. Data are plotted as plateau age spectrum diagrams that produced large analytical error from coverslip fogging. Preferred ages came from the inverse isochron diagrams that are valid and within the limits of the MSWD and initial ratio. Each heating step is represented by a horizontal rectangle whose height is ± 2σ uncertainty of the step age.

all heating steps to secure a statistically valid age, although all were highly influenced by the initial steps. Ages obtained meet the plateau criteria and are considered valid. Errors are $\geq 4\%$ for all samples affected by fogging and primarily related to high proportions of atmospheric $^{40}Ar_{(a)}$ to radiogenic $^{40}Ar_{(r)}$. This assumption is supported by the isotopic ratio $^{36}Ar/^{39}Ar$ near 1 indicating a high atmospheric component and the calculated $^{40}Ar_{(a)} >> ^{40}Ar_{(r)}$ with proportions as high as 50 times more $^{40}Ar_{(a)}$. Nonetheless, isochron ages are concordant and support the plateau age (data tables and plots are in CD Appendix I; see Table 2.1 for sample and experiment numbers).

Problematic alunite not affected by fogging

Six other samples not affected by *fogging* showed unusually high errors related to the high proportion of atmosphereic $^{40}Ar_{(a)}$ to radiogenic $^{40}Ar_{(r)}$. Some error is also related to low K/Ca ratios in some of the alunites (eg., CLL-1; K/Ca Table IIc, CD Appendix II). These alunites include CLL-1, CLL-2, CQ-37, LBQ-40, MM-46377, and YS-219 (Figure 2.24). Typically, the plateaus are concordant with over 50% $^{39}Ar_{(K)}$ from three or more steps, but each step displays a high degree of age uncertainty (4 to 8%). A tight clustering of data on the isochrons is distinct to samples in this category and results in large uncertainties of the initial ratio and isochron age. Duncan et al. (1997) attributed larger analytical error to tight clustering of step compositions on the isochron that results in lower precision of the regression analyses and large uncertainties in the $^{40}Ar/^{36}Ar$ intercepts. Isochron ages are in some cases older and in other cases younger than the corresponding plateau age, but are within analytical error (Figure 2.24). Therefore, the isochron ages do not provide much constraint to the crystallization age, and the weighted plateau age is preferred relative to the isochrons for estimating the age of the alunites (data tables and plots are in CD Appendix II).

Summary Discussion

Factors that influence uncertainties in the age and contribute to high analytical error are as follows: (1) high proportions of ^{40}Ar atmospheric, (2) Ar recoil, (3) excess Ar, (4) Ar-loss, (5) tight clustering of data in isochron diagrams producing initial ratios higher or lower than the atmospheric composition.
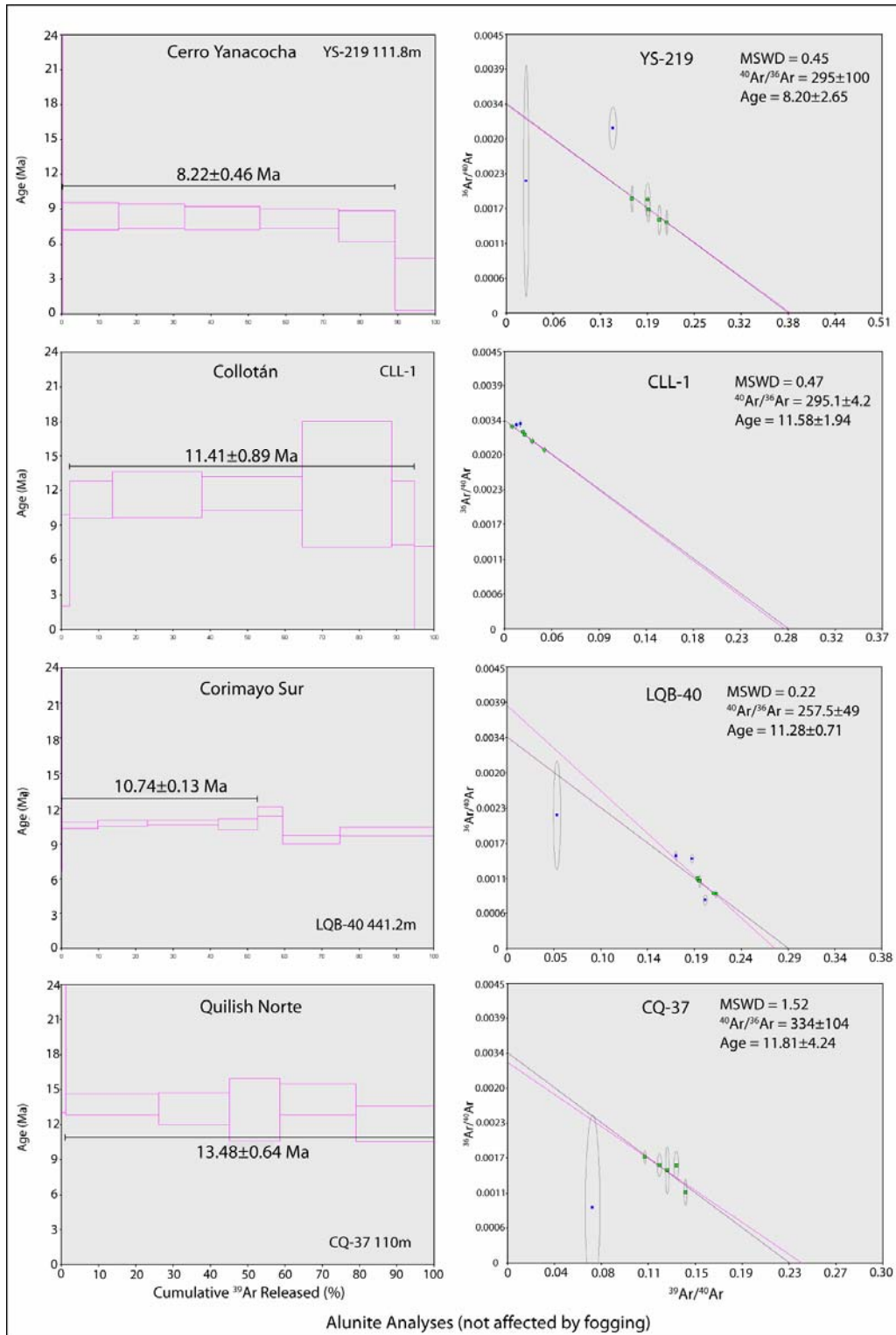
Figure 2.24 Experimental ^{40}Ar/^{39}Ar age data for problematic alunite ages not affected by fogging. Data are plotted as plateau age spectrum diagrams and inverse isochron diagrams for comparison. Each heating step is represented by a horizontal rectangle whose height is ± 2σ uncertainty of the step age.

Alunite samples are contaminated by impurities of quartz, pyrophyllite, diaspore, and sanidine sometimes leaving only 25% alunite in the sample. Sample impurity results in contamination with nonradiogenic argon (eg. atmospheric argon $^{40}Ar_{(a)}$) that can have a significant effect on the reliability of alunite ages resulting in poor analytical precision (Itaya et al., 1996). Unusually high error in the alunites of this study are attributed to high proportions of nonradiogenic $^{40}Ar_{(a)}$ relative to low amounts of radiogenic $^{39}Ar_k$ and $^{40}Ar_{(r)}$ gas, and coverslip fogging.

Patterns of Ar-loss and Ar recoil in the initial low temperature steps are related to low temperature alteration and the presence of fine-grained clay minerals. Effects of alteration are referenced in anomalously high and low $^{39}Ar/^{37}Ar$ ratios (K/Ca ratios) in the initial steps and the equivalent K/Ca plots (Figures 2.6-2.9; Table IIc, CD Appendix II) suggesting low temperature Ca-clay minerals, calcite, or fine-grained K-rich phases may be present that produce younger ages and the effect of Ar-loss and Ar recoil. The inverse staircase pattern in low temperature heating steps results from Ar recoil, or $^{39}Ar_{(K)}$ loss, from fine-grained potassium-bearing alteration minerals. This results in a subsequent decrease in step ages with increased temperature, and imparts a pattern that suggests alteration contributed to ^{39}Ar loss in the low temperature steps leaving the higher temperature steps more reliable indicators of the crystallization age.

Excess Ar in some dated Yanacocha rocks are in part the result of hydrothermal alteration of samples that, in some cases, were colleted from areas affected by hydrothermal solutions. The presence of excess Ar in the Yanacocha samples may be attributed to processes as follows: (1) diffusion of Ar from hydrothermal fluids into the low temperature alteration minerals that coat the primary mineral and fill fractures and veinlets that crosscut the phenocryst, (2) diffusion of Ar from the magmatic fluids trapped in melt inclusions within the phenocryst, and (3) excess Ar trapped at the time of crystallization reflecting compositions in the magma. Significant excess Ar may be related to the presence of melt inclusions, fluid inclusions, and mineral inclusions in low potassium minerals such as plagioclase. Diffusion of Ar from the hydrothermal fluid into outer margins of a phenocryst during alteration may explain the excess Ar in the low temperature steps. Larson et al. (2004) indicate that during the hydrothermal alteration diffusion rates are very slow in feldspar. Dilles (pers comm., March 2005) suggests that

these diffusions rates are negligible in feldspar and not an important process for the diffusion of Ar from the hydrothermal fluids into feldspar, but may be an effect that can cause excess-Ar in biotite. Kelly (2002) points out that argon solubility is higher in hydrous and silicate fluids relative to the mineral phase, and excess Ar is released at both low and high temperatures from fluid inclusions (representative of the hydrothermal fluids) and melt inclusions (representative of the primary magmatic fluids). In contrast to affects from hydrothermal alteration, Duncan (pers comm., March 2005) offers the hypothesis that excess Ar is trapped at the time of crystallization and reflects the magma composition.

Geologic Discussion

The $^{40}Ar/^{39}Ar$ age determinations presented above firmly established the timing of the Miocene volcanic stratigraphy at Yanacocha, and results are summarized in Figures 2.25 and 2.26. The rock sequences include three pre-Yanacocha volcanic units and five volcanic units that represent rocks of the Yanacocha Volcanic Field (Figure 2.2 and 2.26). Pre-Yanacocha rocks were erupted before 15.0 Ma, and include: (1) the Huambo Cancha andesite that is older then 19.5 Ma, (2) the Tual and Chaupiloma lower andesite lahar sequences that range from 19.5 to 15.9 Ma, and (3) the Cerro Frailes dacite pyroclastic sequence that erupted from vents outside the Yanacocha district from 15.5 to 15.2 Ma. Eruptions of Yanacocha Volcanic Field began after 15.0 Ma and consist of (1) the lower Yanacocha volcanic sequence (14.5 to 13.3 Ma), (2) the Maqui Maqui pyroclastic sequence (12.6 to 12.4 Ma), (3) the upper Yanacocha volcanic sequence (12.4 to 11.7 Ma), (4) the San Jose ignimbrite (11.5 to 11.2 Ma), and (5) the late dacite (10.8 to 8.4 Ma). Details are discussed below in stratigraphic order.

Pre-Yanacocha Volcanic Rocks

Huambo Cancha Andesite

The Huambo Cancha andesite is typically altered to clay with disseminated limonite and pyrite and was not dated. The Huambo Cancha andesite overlies Cretaceous quartzite and is overlain by unaltered pumice-rich andesite lahars of the Tual sequence

dated at 19.53±0.13 Ma, therefore, the age of the Huambo Cancha andesite is between late Cretaceous to early Miocene.

Tual and Chaupiloma Lahar Sequences

Three samples produced acceptable plateau ages for the lower andesite lahar sequences (Table 2.1a). Ages in the lahar sequences could range from 19.53±0.13 Ma (CC-18) for the plagioclase in pumice of the Tual andesite lahar sequence, to 15.90±0.18 Ma (DN-84) for plagioclase in a lava flow from the Chaupiloma andesite lahar sequence at Maqui Maqui Norte to 15.41±0.36 Ma (DE-18) for the hornblende in an andesite lahar at Cerro Collotan. However, these sequences are extensive and quite thick up to 400 meters. Only three samples represent the entire range of time. Present age data are not sufficient to define the Tual and Chaupiloma sequences as two separate sequences with a large time gap of 2.5 m.y. or cessation of volcanism. It is possible they represent one continuous 5 m.y. sequence that overlap in time with out a volcanic gap.

Sample DE-18 provides an age that indicates a upper age limit for the lahar sequences and the error overlaps with ages for the Cerro Frailes dacite sequence. The two sequences were not observed intercalated in the field. The sample was affected by weak intermediate argillic alteration and the analyses may represent effects of Ar recoil in the initial steps and Ar-loss in subsequent steps providing an age slightly younger than the actual age. Therefore, caution is advised when using DE-18 to bracket the upper age limit, and the age from DN-84 is more reliable. For this reason DE-18 was not reported in the stratigraphic interpretation presented in Figure 2.26.

Cerro Frailes Dacite Pyroclastic Sequence

Five age spectra were obtained, and all but one sample (Chaupiloma, DN-12) produced undisturbed and acceptable plateau ages that range from 15.51±0.05 Ma at Cerro El Fraile, to 15.15±0.06 Ma at Maqui Maqui Norte. Samples were collected from different stratigraphic levels within the Cerro Frailes pyroclastic sequence. The pyroclastic flow at Cerro El Fraile is directly above a contact to the Chaupiloma lower andesite lahars and has an age of 15.51±0.05 Ma; it represents the base of the sequence. Another flow sampled below pyroxene-hornblende andesite lavas of the Lower

Yanacocha volcanic sequence at Maqui Maqui Norte has an age of 15.15±0.06 Ma, and represents the top of the sequence. One $^{40}Ar/^{39}Ar$ age from Turner (1997) of biotite in a Cerro Frailes dacite tuff yielded an age (15.78±0.17 Ma) older than the basal unit in this study (Figure 2.25). The preferred age for the Cerro Frailes biotite dacite tuff at Chaupiloma is 15.18±0.14 Ma and represents the plagioclase plateau age from sample DN-12 (Figure 2.17).

Rocks of the Yanacocha Volcanic Field

Lower Yanacocha volcanic sequence

Six samples analyzed in the lower Yanacocha volcanic sequence of pyroxene-hornblende andesite domes, lava flows and tuff yielded undisturbed age spectra with acceptable plateau ages that range from 14.52±0.13 to 13.85±0.09 Ma in the west district (n = 4), and 13.72±0.17 to 13.31±0.08 Ma in the east district (n = 2) (Figure 2.25). In the west district, the older ages represent pyroxene andesite lavas that have dates of 14.52±0.13, 14.27±0.16, and 14.21±0.16 Ma. They are intruded by later pyroxene-hornblende-quartz andesite domes one dated at 13.85±0.09 Ma (CR-4). The oldest age in east district of 13.76±0.17 Ma represents the plateau age from a whole rock sample of CB-5. This sample is a monolithic andesite tuff interpreted in the field as lower in the stratigraphic section than a lava flow dated at 13.31±0.08 Ma south of Arnacocha. These data suggest that Lower Yanacocha andesite sequence is older in the west district by ~1 million years, compared to the east district.

Early Dacite Intrusions

No radiometric age determinations are available for the early dacites and age relationships are based on field geology. Early dacite intrudes Cretaceous quartzite, Tual and Chaupiloma lower andesite lahars, Cerro Frailes tuff and Lower Yanacocha andesite volcanic rocks (Lpha). Dacite has not been observed to intrude Upper Yanacocha andesite volcanic rocks (Upha) in the west district north of Quilish, therefore, these rocks are bracketed as younger than Lpha (14.5-14.2 Ma), and older than Upha (12.1 Ma). The early dacites may possibly be older than the Maqui Maqui ignimbrite (12.6-12.4 Ma).

Field evidence exists adjacent the Quilish Norte Au deposit where quartz-eye porphyritic rocks with similar textures to early dacite intrusions are spatially associated with fine-grained fragmental and laminated rocks interpreted as part of the Maqui Maqui pyroclastic sequence. These rocks are intensely altered to vuggy silica and alunite, but original textures remain. Early dacites have an inferred age of Middle Miocene between 14 and 12 Ma.

A gap in time is indicated in Figure 2.25 from 13.31±0.08 Ma (age of the youngest Lpha lava) to 12.63±0.05 Ma (age of the oldest Maqui Maqui ash flow tuff). The age determinations suggest a cessation of volcanism for ~ 680,000 years, but early dacites could fall in this interval. This volcanic gap is also supported in the field with the presence of laminated rocks and fine tuffs that overlie the Lpha, termed *laminated 1* in Figure 2.24. This period is represented in Figure 2.26 as a stage of porphyritic and porphyry intrusive activity with early dacite and feldspar porphyry plugs and diatremes.

Maqui Maqui Pyroclastic Sequence

Explosive eruptions of the Maqui Maqui pyroclastic sequence spanned at least 230,000 years based on $^{40}Ar/^{39}Ar$ ages from three samples of ignimbrite that range from 12.63±0.05 to 12.40±0.10 Ma (Table 2.1, Figures 2.25 and 2.26). Out of the four samples analyzed for the Maqui Maqui ignimbrite only one failed to produce an acceptable age (DN-52), and it is discussed above under *discordant ages* and is not presented in the age summary in Figure 2.25. The ignimbrite sequence is separated into two members based on field relationships, phenocryst mineralogy and composition. The lower member is named the Cori Cashpa ash-flow tuff and is a non-welded tuff that contains distinct biotite phenocrysts and white pumice fragments with SiO_2-total alkali compositions near trachyandesite. The ash-flow tuff overlies thin bedded altered tuff and siliceous laminated rocks at its base, and overlies the Cerro Frailes dacite tuff. It also is intruded by Upper Yanacocha pyroxene-hornblende andesite. The Cori Cashpa ash-flow tuff yielded an age of 12.63±0.05 Ma and represents the base of the Maqui Maqui pyroclastic sequence. The upper member is called the Maqui Maqui ignimbrite and is a welded tuff that commonly displays eutaxitic textures. In contrast to the Cori Coshpa tuff, it contains rare biotite with SiO_2-total alkali compositions from andesite to dacite. The Maqui Maqui ignimbrite

yielded two age determinations that are the same within error with ages of 12.49±0.08 Ma and 12.40±0.10 Ma. The younger age is considered the top of the Maqui Maqui pyroclastic sequence and was collected from a eutaxitic textured tuff ~90 meters below the contact to Upper Yanacocha pyroxene-hornblende andesite lava flows in the Colorado graben near Maqui Maqui.

Two samples were analyzed of porphyritic rocks considered part of the Maqui Maqui eruptive sequence that display undisturbed age spectra and yielded plateau ages of 12.39±0.12 Ma and 12.13±0.10 Ma (Table 2.1). They have mineral assemblages similar to the Maqui Maqui pyroclastic sequence. Both samples lack pyroxene, and therefore, they are different from the typical pyroxene-bearing Lower and Upper Yanacocha porphyritic rocks. One sample (DN-77) was collected from a coarse porphyritic hornblende andesite plug with abundant hornblende phenocrysts (>12 vol.%; 2 to +10mm) and intrudes the upper member Maqui Maqui ignimbrite at Maqui Maqui Norte. This intrusion has textures similar to altered intrusions called Yp at Cerro Yanacocha. Sample DN-77 yielded an age of 12.13±0.10 Ma and may represent intrusions associated to a stage of effusive volcanism after the eruption of the Maqui Maqui ignimbrite and before the episode of effusive eruptions from the Upper Yanacocha pyroxene-hornblende andesite. Sample YS-370 was collected from ~47 meters depth from drill core at Cerro Yanacocha of fresh trachytic-texture andesite called a Yp sill. The textures resemble similar trachytic-textures observed in the lava flows from the Lower and Upper Yanacocha andesite sequence. The sample returned an age of 12.39±0.12 Ma and may represent an effusive stage at Cerro Yanacocha that may have coexisted or immediately preceeded the final explosive eruptions of the Maqui Maqui ignimbrite.

Two age determinations on unaltered porphyritic rocks at Cerros Yanacocha place temporal constraints on the Maqui Maqui volcanic sequence and suggest a similar age for rocks that host ore in the Cerro Yanacocha Complex. These include a black andesite dike (YSBD) that intruded fragmental and porphyritic rocks that host ore and yielded a date of 12.11±0.08 Ma. The dike was collected from a bench at the 4080 meter level of the Yanacocha Sur deposit near the original summit elevation for Cerro Yanacocha. The YSBD dike represents an intrusion in the upper levels of the Cerro Yanacocha volcanic system. A second sample (YS-370; 12.39±0.12 Ma) represents fresh to weakly clay-

calcite-pyrite altered trachytic-textured hornblende andesite to dacite lava that cropped out on the surface on south of Cerro Yanacocha. Ignimbrites that underlie the trachytic hornblende andestite (Loayza, 2002) would be older than 12.39±0.12 Ma. Therefore, volcanic rocks at Cerro Yanacocha are older than the 12.1 Ma YSBD andesite dike and may have an upper age limit of ~12.4 Ma similar to the upper age of the Maqui Maqui pyroclastic sequence.

Upper Yanacocha Volcanic Sequence

Eruptions of the Upper Yanacocha volcanic field (Upha) are geologically bracketed by the Maqui Maqui ignimbrite dated at 12.40±0.10 Ma and the San Jose ignimbrite dated at 11.54±0.09 Ma. Age spectra for eight samples of Upha were undisturbed and produced robust plateau ages. Ages for the lava flows range from 12.09±0.10 to 11.91±0.08 Ma, and ages for the domes range from 12.01±0.10 to 11.68±0.09 Ma (Table 2.1f, Figures 2.25 and 2.26). The age determinations suggest that by ~12 Ma Upha volcanism ranged district-wide from Cerro Negro to the Machay dome near Arnacocha (Figure 2.26; Plate 1).

Upha rocks were dated in several areas across the district. Samples were collected from rocks that represent lava flows and domes in the sequence. Pyroxene-hornblende andesite lava flows were dated in the west district at Cerro Negro Este (DO-60) where an erosional remnant covers a 1 square kilometer with thicknesses estimated at 50 meters. The sample returned an age of 12.09±0.10 Ma. Upha lava flows were also found below gravels northwest of Corimayo in drill holes COR-7, PAB-19, and PAB-25. These rocks are interpreted to belong to the Upha rock sequence that crops out in the west district from Pampa Corimayo to Pabellon and northwest below the La Quinua-Cerro Negro Leach Facility to the bypass road and entrance gate (Plate 1), and may extend below the gravels for 1.5 km south to Quebrada Encajon and 4 km north to Shoclla (CD Plates 1 and 2). A sample from Corimayo drill hole COR-7 was collected from a trachytic-textured pyroxene-hornblende andesite at 178 meters below the la Quinua gravels and yielded an age of 11.91±0.08 Ma. The sample is interpreted to be a lava flow because the trachytic textures display near horizontal foliations relative to the core orientation. A third sample was dated from a dike with contacts to altered porphyritic rocks and breccia.

The dike rock is a strongly trachytic-textured hornblende dacite that lacks pyroxene but yielded an age of 11.90±0.11 Ma from hornblende. The lack of pyroxene suggests a genetic difference from the typical UPHA rocks that is similar to the older intrusives discussed for the Maqui Maqui sequence.

In the east district, Upper Yanacocha pyroxene-hornblende andesite and dacite rocks (Upha) were dated from the YSBD pyroxene-hornblende dike at Cerro Yanacocha (discussed above), lava flows south of Cerro Baul, domes in the Ocucho complex and Machay, and a lapilli tuff intruded by a Upha dome in the Colorado graben west of Maqui Maqui. These data imply effusive eruptions of the Upper Yanacocha volcanic rocks spanned over ~410,000 years from 12.09±0.08 Ma to 11.68±0.07 Ma. Lava flows south of Cerro Baul and San Jose (CHQS-2) represent a thick sequence of fresh pyroxene-hornblende andesite and dacite rocks that host ore in the adjacent Chaquicocha Sur Au deposit. The Upper Yanacocha (Upha) lavas are intruded by a late pyroxene-hornblende dacite dome called the San Jose Sur or Montura dome (CHQS-1) temporally associated with the San Jose ignimbrite. Hornblende from the dacite lava in sample CHQS-2 returned an age of 12.05±0.15 Ma, and the dome sample CHQS-1 yielded a plagioclase age of 11.28±0.09 Ma (discussed below in domes related to the San Jose ignimbrite). Domes are clustered in a northeast trend and approximately 5 km northeast the Ocucho (AZU-2) and Machay (CB-65) pyroxene-hornblende andesite and dacite domes were dated (Plate 1 and 4). Plagioclase samples from these domes returned ages of 11.68±0.07 Ma and 12.01±0.10 Ma., respectively. Approximately 5 kilometers north of the domes, thick sequences of UPHA are preserved in the Colorado graben and overlie the Maqui Maqui ignimbrite (12.40±0.10 Ma). Pyroxene-hornblende monolithic andesite lapilli tuff (DN-83) was dated that crops out below Upper Yanacocha (Upha) lavas from a nearby dome. The sample yielded an age of 12.05±0.11 Ma and the age is complemented by a nearby sample from Turner (1997) that returned an age of ~12.3 Ma.

Age determintions from eight samples in both east and west portions of Yanacocha district bracket effusive eruptions of the Upper Yanacocha volcanic sequence within a relatively short span of time from ~12.09 to 11.68 Ma over an area that covered 60 km^2. All ages are younger than the Maqui Maqui pyroclastic sequence and therefore distinct from the Lower Yanacocha volcanic sequence whose ages are older than the

Maqui Maqui sequence and >13.3 Ma. The oldest ages for Upper Yanacocha pyroxene-hornblende andesite volcanic rocks (Upha) are in the west district at Cerro Negro and at Cerro Yanacocha, and the youngest ages were found in the east district and part of the Ocucho dome complex. Ages in the east district span ~370,000 years from ~12.05 to 11.68 Ma, and in the west district ages span ~180,000 years from 12.09 to 11.91 Ma (the SLT-02 dike lacks pyroxene and does not represent rocks with Upha compositions). Age determinations imply an eastward migration of effusive volcanism related to the Upper Yanacocha volcanic sequence (Upha) from Cerro Negro for nearly 10 km that centered in the east district.

San Jose Ignimbrite Sequence

Age spectra for twelve samples of ash-flow tuffs of the San Jose ignimbrite were undisturbed and produced robust plateau ages (Table 2.1). One whole rock sample from the eutaxitic ignimbrite above the San Jose gold deposit (SJS-79A 23.4m) displayed a combination of Ar recoil and Ar-loss, and the isochron age was preferred over the plateau age. The $^{40}Ar/^{39}Ar$ age determinations indicate eruptions of the San Jose ignimbrite span a period of ~300,000 years from 11.54±0.09 to 11.22±0.08 Ma. The sequence was divided into three ash-flow tuff members based on field relationships, phenocryst mineralogy, and composition. The Lower San Jose and Upper San Jose members contain 1.5 to 7 vol.% pyroxene phenocrysts, whereas pyroxene in the Middle San Jose member is absent or in trace amounts. The Middle San Jose ash-flow tuffs are typically more alkaline than the Lower and Upper members and plot in the trachyandesite and trachydacite fields in the SiO_2-Total alkali diagram (discussed in Chapter 4). Upper San Jose spatter ignimbrite contains the most mafic phenocryst assemblage with pyroxene abundances as high as 7 vol.%. Their ages are as follows (Figure 2.25 and 2.26):

(1) the lower San Jose ash-flow tuff has 6 dates of 11.54±0.09, 11.53±0.13, 11.50±0.09, 11.43±0.11, 11.43±0.06, and 11.34±0.16 Ma all within error and essentially the same age,

(2) the middle San Jose white ash-flow tuff has five dates of 11.30±0.06, 11.29±0.15, 11.29±0.08, 11,28±0.22, and 11.24±0.10 Ma,

(3) the upper San Jose spatter ignimbrite has two dates of 11.25±0.07 and

11.24±0.10 Ma.

The middle and upper San Jose ignimbrites are all essentially the same age within error. However, they are significantly younger than the lower San Jose ignimbrite. Therefore, $^{40}Ar/^{39}Ar$ dates identify two temporally distinct events in the San Jose ignimbrite. Eruptions of the Lower San Jose ignimbrite member preceded eruptions of middle San Jose *white tuff* and upper San Jose *spatter ignimbrite*. The white tuff and spatter ignimbrite are compositionally distinct but their eruptive episodes coexisted in time.

Domes associated with the San Jose Ignimbrite

Three dome complexes are spatially associated with the San Jose ignimbrite, and have $^{40}Ar/^{39}Ar$ ages identical to the ages of the San Jose ignimbrite (Figure 2.25 and 2.26, Table 2.1). Age spectra for all three samples were undisturbed and produced robust plateau ages. They include an endogenous lobe in the Ocucho dome complex (sample DE-2, 11.36±0.09 Ma), that is within error and identical to all ages for the San Jose ignimbrite. The ages of the Chaquicocha Sur dome (sample CHQS-1, 11.28±0.09 Ma), and the Alto Machay dome (sample CB-3, 11.23±0.07 Ma) are identical to the ages of the Middle San Jose *white ash-flow tuff* and the Upper San Jose *spatter ignimbrite*. Differences in phenocryst mineralogy and composition distinguish the Alto Machay dome from the Ocucho and Chaquicocha Sur dome (discussed in Chapters 3 and 4). The Alto Machay dome lacks pyroxene and has higher alkaline contents typical of the white ash-flow tuff.
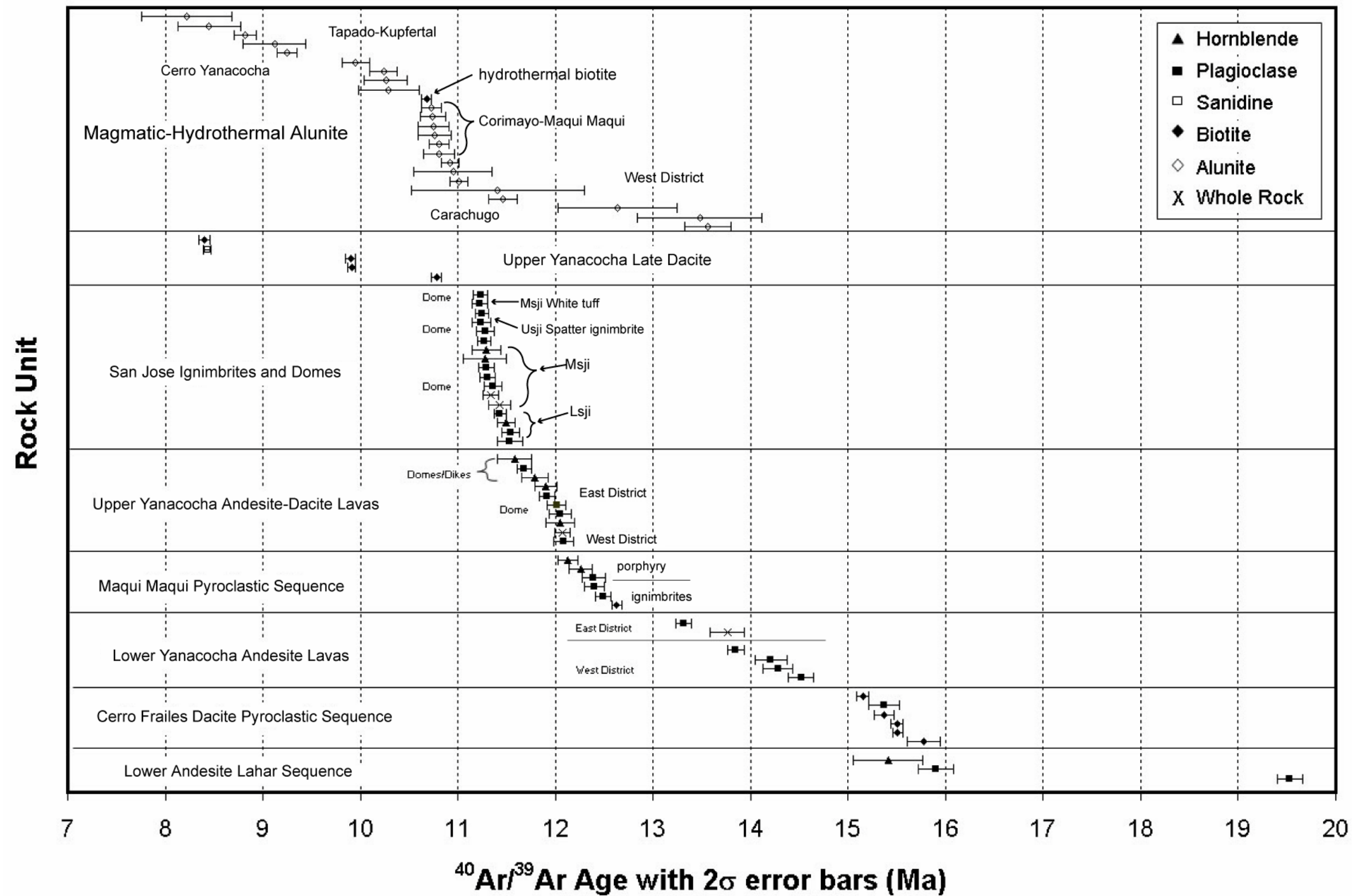
Figure 2.25 Diagram of the geochronologic history of the Cenozoic events at Yanacocha. The preferred ages are plotted for all samples analyzed in this study.
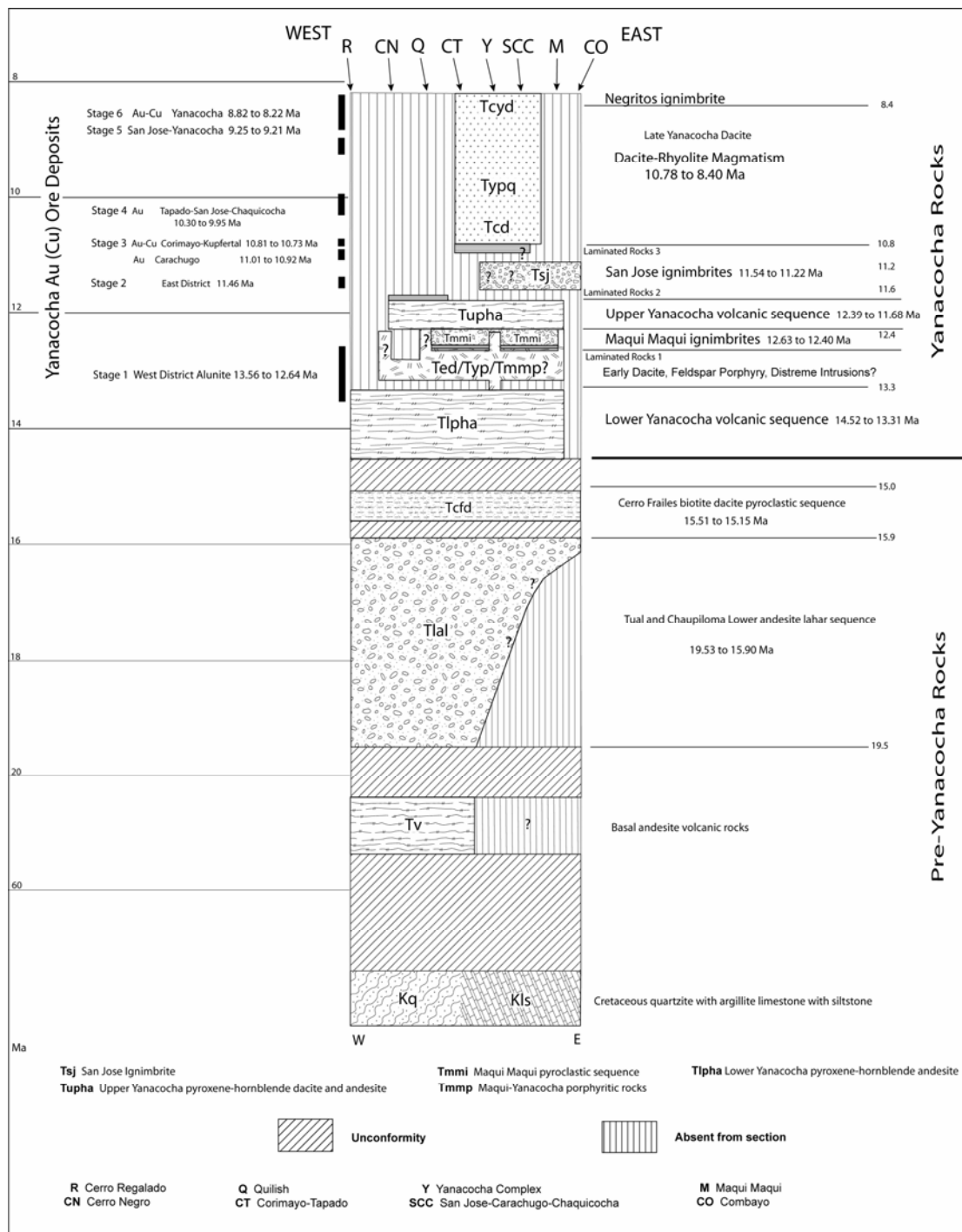
Figure 2.26 A composite chronostratigraphic summary showing the temporal and spatial relationships of the volcanic stratigraphy, intrusions and gold ore at Yanacocha. The section approximates a west to east slice through the district and the unit rectangles represent time and not stratigraphic thicknesses. Ages of mineralization are from radiometric ^{40}Ar/^{39}Ar age determinations on alunite and secondary biotite (Kupfertal). Ages of volcanic rocks and intrusions are from radiometric ^{40}Ar/^{39}Ar age determinations on plagioclase, biotite and hornblende.

Late Dacite and the Negritos Ignimbrite

Age spectra from two samples of the late dacite domes-intrusions and one sample of the Negritos ignimbrite are undisturbed and produced robust plateau ages. These rocks represent three igneous events with compositions from dacite and rhyolite. The $^{40}Ar/^{39}Ar$ plateau ages from this study are10.78±0.05 from the Corimayo dacite dome, 9.91±0.04 Ma from the Yanacocha dacite porphyry, and 8.43±0.04 Ma from the Negritos ignimbrite (Table 2.1H; Figures 2.25 and 2.26). Two additional $^{40}Ar/^{39}Ar$ age determinations are available from the work of Turner (1997) and include 9.90±0.05 Ma on biotite from the Yanacocha dacite porphyry at Yanacocha Norte and 8.40±0.06 on biotite from a Yanacocha Lake rhyodacite dike. These dates support the late dacite ages reported in this study.

The $^{40}Ar/^{39}Ar$ age from the Corimayo dome of 10.78±0.05 Ma has the same age within error as the alunite alteration that crosscuts it. Alunite ages from Corimayo are 10.76±0.17 and 10.74±0.13 Ma (Table 2.1I, figure 2.25 and 2.26). Porphyry dacite intrusions at Cerro Yanacocha are spatially associated with a northwest trend of gold ore, and at Yanacocha Norte they are fresh. At least two dacite intrusions are present at Cerro Yanacocha. One at Yanacocha Norte has an age of 9.91±0.04 Ma, and the other at Punta Negra is similar to the Corimayo dacite and older than 10.81±0.16 Ma. Both dacites are bracketed by alunite alteration from the Cerro Yanacocha area (Table 2.1J). The Punta Negra dacite plug is altered to quartz-alunite and the alunite has an age of 10.81±0.16 Ma. This dacite has identical amounts of quartz as found in the Corimayo dacite (3 vol.% quartz) and may be related to it, and is older than the Yanacocha dacite porphyry. At Kupfertal, hydrothermal biotite was found at depths of over a half kilometer (Plate 1, cross section N-S) and has an age of 10.73±0.05 Ma. Close by at San Jose (<1 km south) alunite from a porphytic rock has an age of 9.95±0.14 Ma, and is the same age as the Yanacocha dacite porphyry within analytical error. The Yanacocha dacite porphyry is crosscut by late alunite-matrix breccia and patchy quartz-alunite and quartz-pyrophyllite alteration in the Cerro Yanacocha deposit. Alunite thought to be associated with Kupfertal was dated from quartz-alunite alteration 500 meters south below Punto Negro and Yanacocha Sur (Plate 4 and CD Plate IV; location map for alunite alteration) and has

an age of 9.25±0.10 Ma. Other dates include alunite that crosscuts altered Yanacocha dacite porphyry. These alunite dates are 9.12±0.32, 8.82±0.11, 8.45±0.32, and 8.22±0.46 Ma (Table 2.1j). Like the Kupfertal alunite, all are significantly younger than the Yanacocha dacite porphyry from Yanacocha Norte.

Late dacite dikes and plugs of the Chaupiloma and Yanacocha Lake dacites have a ^{40}Ar/^{39}Ar age of 8.40±0.06 Ma determined on biotite by Turner (1997). They are confined to a northwest trend through the Cerros Yanacocha deposits. The Negritos rhyolite ignimbrite has an identical ^{40}Ar/^{39}Ar age of 8.43±0.04 Ma and may have vented during a fissure eruption of the Chaupiloma-Yanacocha Lake rhyodacite.

Age determinations available for the Late Dacite episode at Yanacocha imply that this late felsic phase of magmatism at Yanacocha was spatially associated with alunite and hydrothermal biotite alteration. Late Dacite was first present in the Corimayo and Cerro Yanacocha area at ~ 10.8 Ma. A second pulse of dacite at ~9.9 Ma postdates early alunite and hydrothermal biotite but predates and is crosscut by late alunite. A final pulse of rhyodacite at ~8.4 Ma followed a northwest trend that crosscut the Cerro Yanacocha deposit and Yp diatreme, and may have erupted the Negritos ignimbrite. All three events took place within a period of ~ 2.4 million years.

Alteration

Twenty-one ^{40}Ar/^{39}Ar age determinations on hydrothermal alteration establish that the hydrothermal activity in the Yanacocha district occurred at distinct intervals within a period of ~ 5.3 m.y. from 13.56±0.24 to 8.22±0.46 Ma. Alteration appears to be episodic and can be separated into discrete pulses of hydrothermal activity (Figure 2.16). Hydrothermal alunite alteration began at Cerro Negro at 13.56±0.24 Ma then migrated eastward to Quilish by 13.48±0.64 to 12.64±0.61 Ma. The younger ages from Quilish are analytical distinct, but potentially only slightly younger (~0.1 m.y.) than Cerro Negro.

Hydrothermal activity then migrated eastward and became widespread in the east district at ~ 11.5 Ma. This hypothesis is supported by the following facts and include: (1) the presence of extensive and barren massive silica and vuggy silica crosscut by later stages of mineralization, heterolithic breccia, and alunite (Harvey et al., 1999; Longo, 2000), (2) the presence of abundant previously altered accidental fragments of massive

and vuggy silica in the lower and middle San Jose ignimbrite, and (3) one alunite sampled from a zone barren acid-sulfate alteration at Cerro Azufre that yielded an age of 11.46±0.15 Ma (Turner, 1997).

A third pulse hydrothermal activity then centered on an area that extends nearly 7 km along the Yanacocha northeast trend, from Corimayo to Carachugo. Hydrothermal activity was present at Corimayo-Tapado and Carachugo from ~11.0 to 10.7 Ma for a period of ~300,000 years. The age and duration of this pulse are supported by 8 dates in this study (7 from alunite and 1 from hydrothermal biotite) that include alunites from Corimayo to Carachugo and the Maqui Maqui deep patchy quartz-pyrophyllite-alunite. The alunites yielded ages of 11.01±0.09 at Baul near Carachugo Sur, 10.81±0.10 from patchy alteration at Maqui Maqui deep, 10.81±0.16 Punta Negra at Cerro Yanacocha, 10.76±0.17 at Corimayo, 10.75±0.16 at Collotan immediately west of Punta Negra, 10.74±0.13 at Corimayo Sur, and 10.73±0.10 from deep quartz-alunite altered feldspar porphyry at San Jose, and hydrothermal biotite from 571 meters depth in the Kupfertal porphyry Cu-Au system of 10.73±0.05 Ma. Additional evidence for the timing of alteration comes from alunite at Carachugo Sur with dates of 10.95±0.40 and 10.92±0.09 Ma (Turner, 1997; Noble, 1998).

A fourth pulse hydrothermal remained centered in the east district as discrete pulses at Tapado, San Jose, Chaquicocha and Maqui Maqui from 10.30 to 9.95 Ma for a duration of ~350,000 years. This is supported by four analytically indistinguishable ages on alunite from Tapado, Chaquicocha, Maqui Maqui (surface), and San Jose (surface). Ages include 10.29±0.31 from alunite matrix to vuggy silica breccia at Chaquicocha, 10.26±0.22 from alunite veins at Maqui Maqui, 10.24±0.14 from alunite matrix breccias at Tapado, and 9.95±0.14 from quartz-alunite altered porphyritic rocks on the surface above Kupfertal.

Final pulses of episodic hydrothermal activity became centered only at Cerro Yanacocha from ~ 9.25 to 8.22 Ma. The total duration of this event may be misleading because of the large uncertainties in the ages and many alunites are the same age within analytical error. Alunites are all from the zone of hydrothermal alteration effected by the Cerro Yanacocha Au deposit and dates include 9.25±0.10, 9.12±0.32, 8.82±0.11, 8.45±0.32, and 8.22±0.46 Ma.

The ^{40}Ar/^{39}Ar age determinations on alteration minerals from Yanacocha indicate at least five discrete pulses of hydrothermal activity took place across the district and began in the west then migrated east. The data suggest that hydrothermal activity then became episodic and cyclic in nature as reflected in the alunite dates from the east district. These data imply that four separate pulses of hydrothermal activity in the east district began at ~11.5 Ma and reoccurred after periods of inactivity for ~400,000 to 500,000 years with durations that lasted ~350,000 years. The final episodes of activity then became centered at Cerro Yanacocha until ~8.2 Ma. All hydrothermal activity was spatially and temporally associated with dacite magmatism. Late Dacites in the east district and possible the Early Dacites of the west district.

Temporal Relationship of Porphyry and Epithermal Alteration at Yanacocha

Complex spatial and temporal relationships, and overprinting of high- and low-temperature hydrothermal alteration, have been recognized in hydrothermal systems that evolve from deeper porphyry Cu deposits spatially associated with shallow advanced argillic alteration of the high-sulfidation epithermal environment (Sillitoe, 1973; Gustafson and Hunt, 1975; Einuadi, 1977; Sillitoe, 1983; Dilles and Einuadi, 1992; Hedenquist et al., 1998; Muntean, 1998; Dilles, 2002). The evolution of hydrothermal alteration in the Yerington district resulted from a complex thermal history with fluid flow paths attributed to separate pulses of magmatic-hydrothermal activity associated with multiple porphyry dike emplacement through time (Dilles and Einuadi, 1992). Advanced argillic alteration above Yerington porphyry Cu±Mo deposits may be time-equivalent to the deep K-silicate alteration, and related to the upward ascent of magmatic-hydrothermal fluids along permeable porphyry dike margins (Dilles, 2002). The upward and lateral transition of hydrothermal alteration from the Far Southwest porphyry Cu-Au deposit to the adjacent Lepanto high-sulfidation Au-Cu deposit demonstrates the link between the porphyry and epithermal environments (Hedenquist et al., 1998). Spatial and temporal relationships that suggest a transition from porphyry Cu deposits to high-sulfidation epithermal deposits have been proposed for Refugio, Aldebaran, and La Pepi in the Maricunga Belt, Chile (Muntean, 1998).

Pinto (2002) and Gustafson et al. (2004) documented the spatial relationship of porphyry- and epithermal-style alteration at Kupfertal, Yanacocha Norte, Maqui Maqui, La Zanja, Tantahuatay, Perol and Hualamachay, and suggested that magmatic-hydrothermal advanced argillic alteration associated with the high-sulfidation gold deposits is gradational at depth and in transition with the deeper porphyry-style hydrothermal biotite alteration. Alteration at Cerro Yanacocha and Kupfertal is interpreted to grade downward from high-sulfidation style vuggy and massive quartz to advanced argillic gusano (patchy) and wormy textures with white irregular clots of alunite and pyrophyllite surrounded by gray quartz (Klein and Pinto, 1999; Pinto, 2002). Below the advanced argillic alteration is a halo of sericite that appears to grade into intermediate argillic alteration and downward to potassic alteration dominated by hydrothermal biotite (Pinto, 2002; Gustafson et al., 2004). A transition from patchy to wormy quartz-pyrophyllite-alunite alteration at Kupfertal was recognized near ~150 meter depth (Klein and Pinto, 1999; Sillitoe, 2000). Advanced argillic wormy alteration, termed "pseudo-A" veins, is gradational with depth into sinuous and then planar quartz veins with potassic alteration (Pinto, 2002). Quartz veining with potassic alteration was recognized at the El Salvador porphyry Cu deposit in Chile and classified as A-veins by Gustafson and Hunt (1975).

The ^{40}Ar/^{39}Ar age determinations from the present study indicate the deep porphyry-style hydrothermal biotite at Kupfertal (10.73±0.05 Ma) is statistically similar (within a 2σ error) to the magmatic-hydrothermal alunites from Corimayo, Punto Negro at Encajon above Kupfertal, and deep San Jose adjacent Kupfertal (see the section on alteration above; Table 2.1 I; Plate 4). This suggests a temporal and spatial relationship of the high-sulfidation quartz-alunite alteration to the porphyry Cu-Au mineralization at Kupfertal.

The age of the gusano (patchy) quartz-alunite-pyrophyllite alteration above the porphyry-style hydrothermal biotite is 9.25±0.10 Ma (Table 2.1). The sample was collected at 94 meters in drill hole KUP-3, and is ~500 meters above the hydrothermal biotite in the same drill hole. The age of the deep porphyry-style hydrothermal biotite is ~1.5 m.y. older than the overlying advanced argillic alteration, or gusano-textured quartz-alunite-pyrophyllite. This implies the hydrothermal alteration at Kupfertal, and possibly

Cerro Yanacocha, evolved along complex fluid flow paths as separate pulses of hydrothermal activity associated with multiple intrusions of porphyry plugs through time. The proposed porphyry-epithermal transition at Kupfertal is complex and may be overprinted by the younger mineral systems at Cerro Yanacocha.

Spatial and Temporal Variations in the Ag/Au ratio and Alunite Alteration

Hydrothermal processes that led to the deposition of gold ore at Yanacocha developed as discrete hydrothermal cells that migrated across the district through time. The $^{40}Ar/^{39}Ar$ age determinations from alunites and one hydrothermal biotite define six pulses of hydrothermal activity that spanned 5.4 million years from 13.6 Ma to 8.2 Ma. Hydrothermal quartz-alunite alteration of the Yanacocha rocks is closely spatially and temporally associated with the main high-sulfidation sulfide event and gold ore. Age determinations for hydrothermal alteration, summarized in figures 2.25, 2.26 and 2.27, indicate that multiple stages of hydrothermal activity in the Yanacocha district developed through spatial and temporal variations (discussed above under Alteration). The $^{40}Ar/^{39}Ar$ age determinations from 21 samples of hydrothermal alteration are plotted versus distance and covers a range of >15 kilometers across the Yanacocha district from Cerro Negro Oeste in the southwest to Cerro Sugares at Maqui Maqui in the northeast (Figure 2.27). These data indicate hydrothermal activity migrated from southwest to northeast across the district through time and by ~ 9.25 Ma became centered exclusively at Cerro Yanacocha.

Stage 1 hydrothermal activity began in the west district 13.56±0.24 Ma at Cerro Negro Oeste and migrated eastward to Quilish by 12.64±0.61 Ma. Hydrothermal activity continued its eastward migration, and by 11.46±0.15 Ma (Turner, 1997) Stage 2 became widespread in the east district from Cerro Yanacocha (CLL-1, 11.41±0.89 Ma) to Maqui Maqui. Stage 2 is supported by the presence of hydrothermally altered accidental fragments found in the San Jose ignimbrite sequence (Longo, 2000). After ~500,000 years of inactivity, Stage 3 began in the east district and progressed for ~330,000 years between 11.01±0.09 to 10.73±0.05 Ma along eight kilometers from Corimayo to Maqui Maqui. Stage 4 began at ~10.3 Ma following a second period of inactivity for ~400,000 years and continued for another ~350,000 years between 10.29±0.31 to 9.95±0.14 Ma at
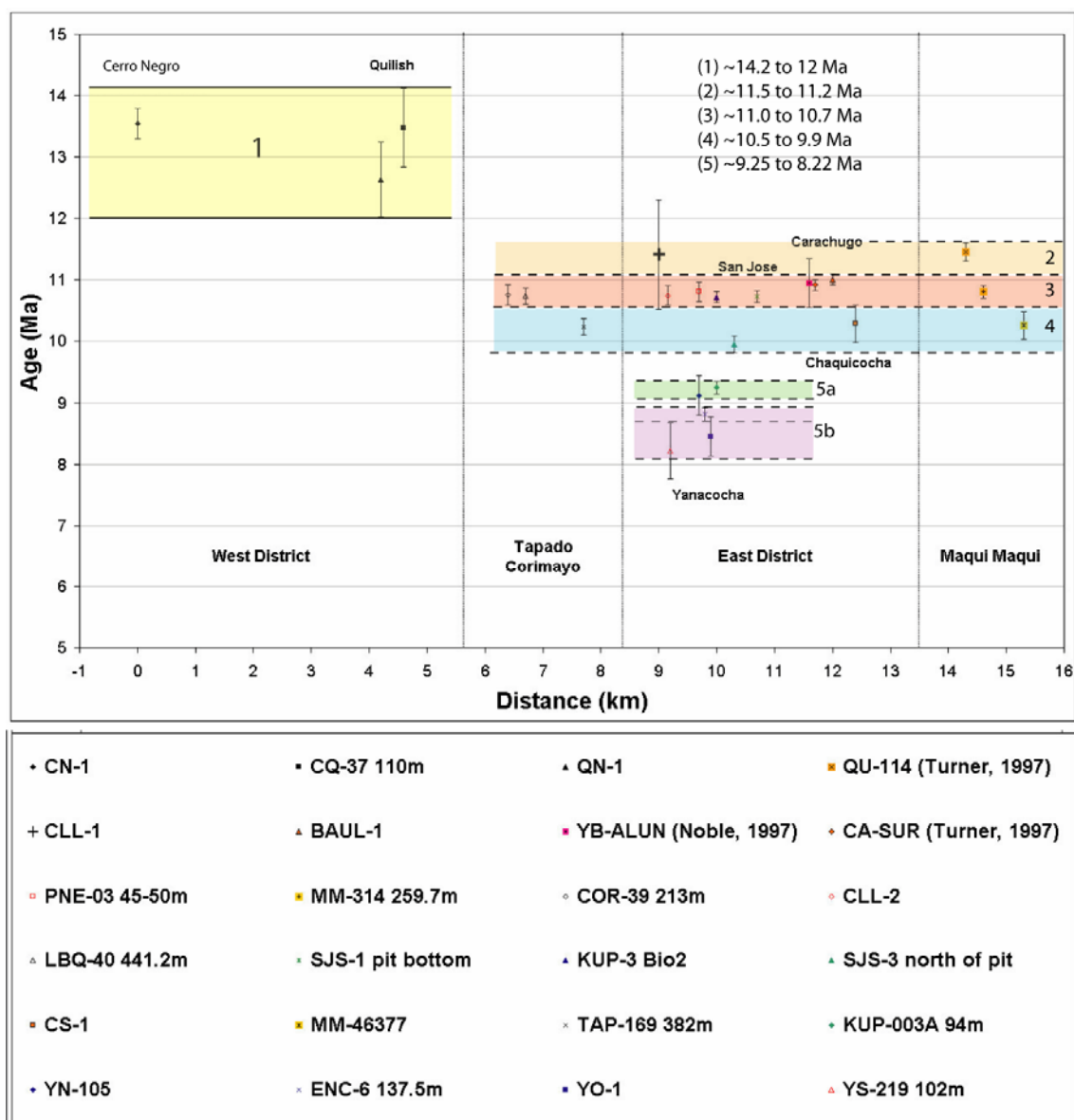
Figure 2.27 Spatial and temporal variation of $^{40}Ar/^{39}Ar$ ages of alunite alteration (and KUP-3 hydrothermal biotite) across the Yanacocha District. The plot reflects a southwest to northeast transect from Cerro Negro to Maqui Maqui.

Tapado, Chaquicocha and Cerro Sugares at Maqui Maqui. Stage 5 followed a third period of inactivity for ~ 700,000 years and is bracketed between alunite ages from ~ 9.25 to 8.22 Ma. The $^{40}Ar/^{39}Ar$ age determinations summarized in Figure 2.25 suggest that Stage 5 could be divided into two sub-stages. Stage 5A began by ~9.3 Ma when hydrothermal activity became centered at Cerro Yanacocha for a duration of 1.1 million years and may have ended before 9.0 Ma, as suggested by the alunite age 9.12±0.32 Ma. Stage 5B began

shortly after at 8.82±0.11 Ma and ended by ~8.22 Ma. This interpretation is supported by geologic evidence from the Cerro Yanacocha deposit that indicates episodic hydrothermal activity (crosscutting veins and breccias with fragments of breccia and veins within later fragments).

Metal ratios for Ag/Au and Cu/Au from the dated alteration are plotted versus time (Figures 2.28 and 2.29). Metal ratios from dated samples also display spatial and temporal variations across the district. These data are preliminary and based on only 21 samples, but suggest that metal ratio values range from 0.30 to 51.7 for Ag/Au and 4.6 to >12,000 for Cu/Au (Table 2.2). Metal ratios from Stage 1 in the west district range from 0.3-0.6 for Ag/Au and 9.5 to 309 for Cu/Au and suggest that early Stage 1 mineralization may have been gold dominant. Stage 2 is relatively barren of mineralization and may have only contained trace Au and Cu as evidenced by the bulk rock geochemical analyses from the altered accidental fragments in the San Jose ignimbrite (Appendix VII: altered fragment geochemistry). Harvey et al. (1999) also report that this stage was responsible for the extensive barren massive and vuggy silica present throughout the east district that lacked a major period of ore deposition. During Stage 3, Yanacocha experienced a wide diversity in style of mineralization with metal ratio values ranging from 0.3 to 52 for Ag/Au and 4.6 to over 6,300 for the Cu/Au ratio. By Stage 4 metal ratios were moderate to low ranging from 1.4 to 30 for Ag/Au and 106 to 1,300 for Cu/Au. Two distinct groups of Cu/Au ratios support the addition of Stage 5B (Figure 2.19). Alunites associated with high ratios of Cu/Au > 8,000 are older than 9.0 Ma and represent Stage 5A, whereas alunites associated with low ratios of Cu/Au, ranging from 82 to 160, are younger than 9.0 Ma and represent Stage 5B. Ag/Au ratios display values in the moderate range (9.4 to 21) for both Stage 5 groups.

On a smaller scale, Figure 2.27 suggests that hydrothermal activity at each deposit also migrated eastward through time. This is apparent for gold deposits at Tapado-Corimayo, Carachugo-Chaquicocha, and Maqui Maqui. At Cerros Yanacocha, hydrothermal alteration tends to become younger from southeast to northwest, from the San Jose deposit (SJS-1) to the northwest end of the Cerros Yanacocha complex (YS-219).
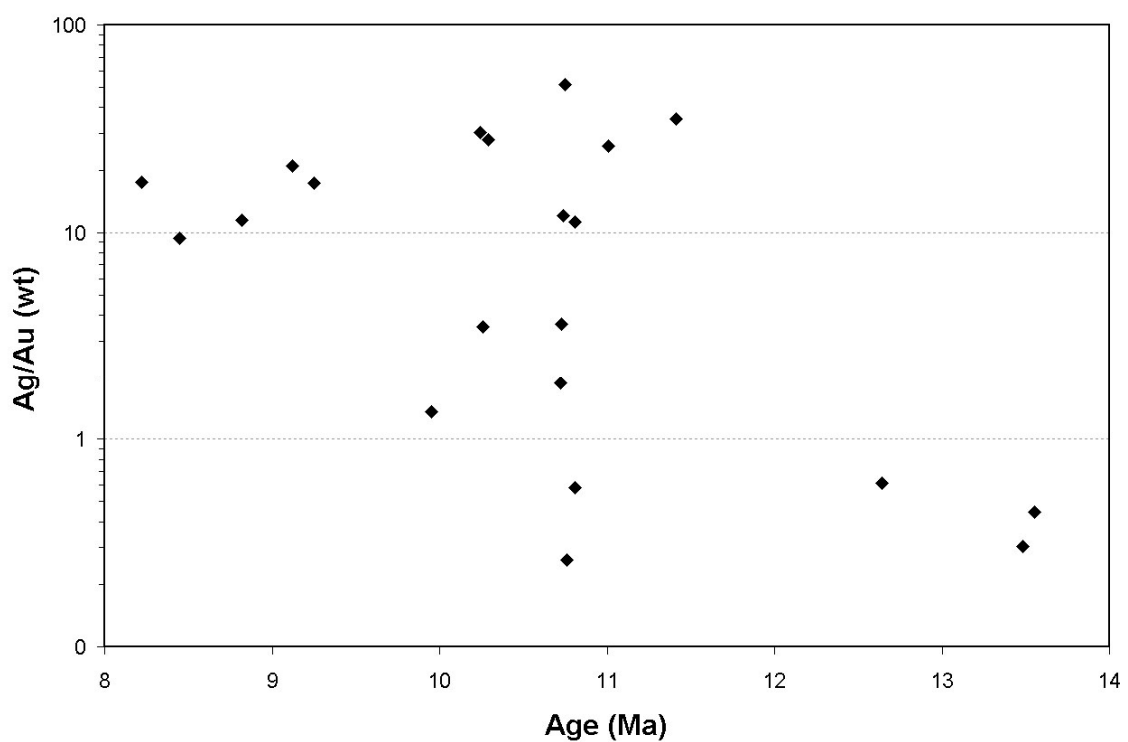
Figure 2.28 Temporal variation in the Ag/Au ratio in rocks from which alunites and hydrothermal biotite were the same samples dated in this study.
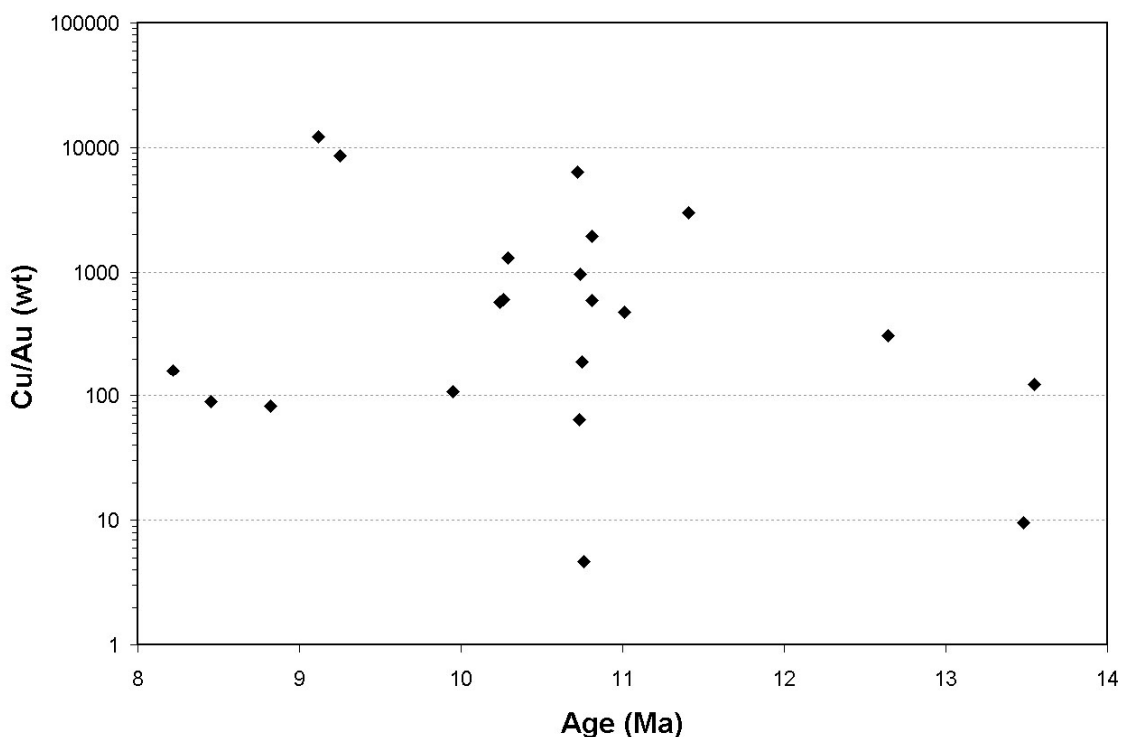
Figure 2.29 Temporal variation in the Cu/Au ratio in rocks from which alunites and hydrothermal biotite were from the same samples dated in this study.

District Model for the Yanacocha Volcanic Field

Rock packages that belong to the Yanacocha Volcanic Field represent volcanic and intrusive rocks from five episodes of andesite to rhyolite magmatism centered in the Yanacocha district. These rocks evolved from spatially and temporally distinct centers and developed a northeast-trending corridor of Middle Miocene volcanism 25 km long that covered an area more than 500 km^2 with lava flows and pyroclastic rocks. The volcano-tectonic-alteration history can be described by distinct phases and styles of volcanism, stages of hydrothermal activity, and the episodes of evolving magmatism through time across Yanacocha.

Effusive Phase I

The lower Yanacocha Volcanic Field (or Lpha) developed from effusive eruptions of pyroxene andesite from numerous monogenetic volcanoes and small composite cones

such as Cerro Atazaico (Figure 2.30A). Effusive eruptions were followed by dome-building and minor pyroclastic eruptions with block and ash flows of quartz-bearing pyroxene andesite. These included the Cerro Regalado dome complex and domes at Quilish and Cerro Negro Oeste. Quilish domes include the sub-vertical, flow-foliated, quartz-bearing andesite at Antibuyoc and acid-sufate altered remnants of the Cerro Quilish dome cross cut with hydrothermal breccia.

Effusive activity and subsequent dome-building progressed from west to east across the district and was centered along three separate north-northwest trending vent areas for ~1.2 million years. An andesite volcanic field developed with an areal expanse of ~340 square kilometers with an estimated average thickness of 80 meters. Effusive pyroxene andesite volcanism was centered in the west district over Cerro Negro from 14.5 to 14.2 Ma followed by quartz-pyroxene andesite domes at 13.9 Ma. Volcanism progressed eastward to the Chaupiloma trend and on to the Chugares volcano in the west by 13.3 Ma.

Stage 1 West District Alunite and Early Dacite

Stage I alunite resulted during hydrothermal activity associated with gold ore in the west district at Cerro Negro Oeste and Quilish between 13.56±0.24 and 12.64±0.61 Ma (Figure 2.30B). This period corresponds to a cessation of volcanism for ~ 700,000 years after effusive phase I from 13.3 to 12.6 Ma. During stage I dacite and feldspar porphyry plugs, and related diatremes, intruded the lower Yanacocha andesite volcanic rocks (Figures 2.30 B and C). Intrusions of early hornblende-biotite dacite porphyry plugs and dikes crop out along a northwest trend for 13.5 kilometers spatially associated with centers of hydrothermal activity. These rocks include the dacite intrusions of Los Pinos, Exaltado, Quilish and Rio Grande in the west district. The Tatiana dacite is similar in composition and intruded limestone and pre-Yanacocha lower andesite lahars within the Chaupiloma Trend. To the far northeast, dacite dikes with quartz-kaolinite-K feldspar alteration intruded limestone, pre-Yanacocha rocks, and Lower Yanacocha pyroxene-hornblende andesite volcanic rocks (Lpha) at Sorpresa, Yutucmana and Misacocha.

Explosive Phase I (Maqui Maqui ignimbrite)

The Maqui Maqui pyroclastic sequence represents an early period of explosive volcanism (Figure 2.30C) with eruptions of hornblende ±biotite trachyandesite to dacite ignimbrites between 12.6 to 12.4 Ma. The sequence is centered on the proposed Yanacocha composite volcano, a center of magmatic activity for ~ 4 million years from 12.4 to 8.4 Ma, at Cerro Yanacocha. Exposures of pyroclastic rocks crop out as an erosional remnant that covers ~90 square kilometers with an estimated thickness that averages 100 meters. These rocks post-date early dacite and feldspar porphyries in the west district, but are temporally related to domes, porphyritic intrusions, and feldspar porphyry plugs and diatremes with the same composition as the Maqui Maqui ignimbrite (Figure 2.30C). Maqui Maqui porphyritic rocks range in age from 12.4 to 11.9 Ma and are the textural equivalents to the hydrothermally altered Yp porphyries at Yanacocha. Laminated rocks and fine tuffs occasionally crop out at the base of the Maqui Maqui ignimbrite representing an erosional hiatus that developed after the pause in Lower Yanacocha andesite (Lpha) volcanism.

Effusive Phase II

The upper Yanacocha Volcanic Field (Upha) developed during a renewal of effusive andesitic volcanism between 12.1 and 11.7 Ma from monogenetic andesite vents and numerous andesite lava domes from west district that include Pampa Cerro Negro, Corra Blanca, Pampa Corimayo, and Shoclla. Andesite lavas may have covered an area of ~ 120 square kilometers centered over the Yanacocha Volcano (Figure 2.30D). These eruptions were followed by coalescing domes of dacitic composition with coulées (thick extrusions of endogenous or exogenous dome growth that erupt on a slope and flow down hill) and tortas (low flat domes with endogenous growth in flat areas) that developed east-west, north- and northeast- trending dome fields in the east district, from San Jose to Machay and north to Colorado. Large coulées, such as the Chao dacite in northern Chile (Guest and Sanchez, 1969), have developed dacite lava flows that cover 90 square kilometers up to 300 meters thick and flow 15 km down slope. At Yanacocha, dacite and andesite lavas erupted from multiple-vent complexes with small coulée-style effusive

eruptions and related pyroclastic eruptions that covered a total area <60 square kilometers.

Stage 2 Alunite and Hypogene Advanced Argillic Alteration

Stage II alunite resulted from hydrothermal activity centered in both the west district at Cerro Negro Este and Pabellon Sur, and the east district (Figure 2.31E). Alunite between the Maqui Maqui and Carachugo deposits has a $^{40}Ar/^{39}Ar$ age of 11.46±0.15 Ma (Turner, 1997). High-sulfidation systems may have produced widespread hypogene advanced argillic alteration and silicification affecting an area of 42 square kilometers in the east district from Carachugo to Maqui Maqui. Large tabular bodies of dense quartz in the east district developed in proximity to the water table as silica-saturated fluids cooled, precipitated amorphous silica that later recrystallized to quartz. Original rock textures were obliterated as passive silicification totally replaced the rock and overprinted residual silica (Longo, 2000). These rocks contain low grade gold with 30 to 400 ppb gold commonly associated with the leaching and alteration by the vapor condensate, and may represent the earliest stage of gold mineralization in the east district (Harvey et al., 1999; Longo, 2000).

Explosive Phase II (San Jose Ignimbrite)

Ash-flow tuffs of the San Jose ignimbrite represent late explosive eruptions of the Upha dacite that post-date early hypogene advanced argillic alteration in the east district. San Jose ignimbrites are pyroxene dacites that typically contain accidental fragments of acid-sulfate altered volcanic rock. $^{40}Ar/^{39}Ar$ age determinations indicate eruptions of the San Jose ignimbrite span a period of ~300,000 years from 11.5 to 11.2 Ma. The sequence erupted in three phases from distinct and separate vent areas, and include the lower San Jose ash-flow tuff from 11.5 to 11.4 Ma (Figure 2.31F), the middle San Jose white ash-flow tuff from 11.3 to 11.2 Ma (Figure 2.31G), and the upper San Jose spatter ignimbrite (11.25±0.07 Ma) and white tuff (11.22±0.08 Ma) (Figure 2.31H). Eruptions of middle member ash-flow tuffs (ie. the white tuff) overlap in time with the upper member spatter ignimbrite. Subsequent post-ignimbrite dome-building produced three vent-filling dome

complexes at Ocucho, Chaquicocha Sur, and Alto Machay whose $^{40}Ar/^{39}Ar$ ages are 11.4 Ma, 11.3 Ma and 11.2 Ma, respectively (Figure 2.31F-H). Ash-flow tuffs filled a topographic depression called the Coso Trough (Longo, 2001) and covered an estimated 175 square kilometers with thicknesses that range from 40 meters north of Ocucho to 350 meters in the Coso Trough.

Upper (Late) Dacite Episode I

Isolated dacite domes were emplaced at ~10.8 Ma and exposures are aligned east-west for 5 km from Chaquicocha Norte to La Quinua dome (Figure 2.32I). The Cori Coshpa dacite intrusion crops out 2.7 km north where it intruded Maqui Maqui ignimbrite and may be of similar age. These dacites have a distinct mineralogy that differs from the Upper Yanacocha and San Jose dacites. They lack pyroxene and apatite, but contain sphene, magnetite, and quartz, and may represent the initial stage of a highly oxidized, magmatic episode spatially and temporally associated with the ore deposits at Yanacocha. This late episode of highly oxidized felsic magmas developed porphyritic domes with minor lavas and pyroclastic aprons, and intrusions of isolated dacite porphyry plugs. Late hydrothermal breccia crosscuts the domes and commonly borders the intrusive margins and contains gold ore (Gomez, 2002b).

Stage 3 East District Hydrothermal Activity

Stage 3 magmatic-hydrothermal alunite alteration corresponds to hypogene advanced argillic alteration related to the high-sulfidation gold systems in the east district for ~300,000 years between 11.0 to 10.7 Ma, and hydrothermal biotite alteration related to the Kupfertal porphyry Cu-Au system developed at 10.73±0.05 Ma (Figure 2.32J). During this period, high-sulfidation hydrothermal activity was widespread for 10 km from Corimayo to Maqui Maqui, and responsible for some of the most productive gold deposits including Maqui Maqui, Carachugo, and Corimayo. Mineralization was controlled primarily along northwest structural zones, and Yanacocha experienced its greatest diversity for style of mineralization with metal ratio values ranging from 0.3 to

51.7 for Ag/Au and 4.6 to over 6,300 for the Cu/Au ratio (Figures 2.28 and 2.29). Metal fractionation at Kupfertal (10.7 Ma) may have occurred during brine-vapor separation.

Stage 4 East District Hydrothermal Activity

Gold ore and associated Stage 4 magmatic-hydrothermal alunite alteration developed along an east-west trend for 3.5 km from Chaquicocha Sur to Tapado (Figure 2.32K). Large veins of natroalunite with trace gold filled a set of radial fractures on Cerro Sugares northeast of Maqui Maqui (Leach, 1999). Hydrothermal activity may have spanned ~300,000 years from 10.3 to 10.0 Ma. Gold deposits at Tapado, San Jose, and Chaquicocha Sur developed during this stage.

Upper (Late) Dacite Episode II and III

Dacite porphyry plugs and rhyodacite domes and dikes are aligned within a northwest trend for 5.7 km from Chaquicocha Sur to Chaupiloma (Figure 2.32L). The Negritos rhyodacite domes are 8 km northwest on the same trend. Dacite porphyry plugs at Yanacocha and Chaquicocha Sur are considered phase II. The Yanacocha dacite porphyry plugs have an age of 9.91±0.04 Ma and intrude early diatremes, Yp porphyry, and altered fragmental rocks and breccia. The altered Chaquicocha dacite porphyry is similar and believed the same age. Episode III is represented by rhyodacite dikes and domes at Chaupiloma and Yanacocha Lake. These rocks have a $^{40}Ar/^{39}Ar$ age of 8.40±0.06 Ma (Turner, 1997). Episode II and III dacites have similar mineralogy to the late dacite I, and represent the final magmatic episode at Yanacocha.

Stage 5 and 6 East District Hydrothermal Activity

Hydrothermal activity spatially associated with the phase II and III dacite intrusions was centered at Cerro Yanacocha and Chaqucocha Sur for ~1 million years (Figure 2.32M). These stages contributed to the largest resource of Au-Cu ore discovered to date in the Yanacocha district. Magmatic-hydrothermal alunite alteration at Cerro Yanacocha may represent multiple stages of hydrothermal activity. At least two stages are present; one is pre-9.0 Ma and the other post-9.0 Ma, as suggested by the $^{40}Ar/^{39}Ar$

dating. Stage 5 alunite ranges from 9.3 to 9.1 Ma and stage 6 alunite has ages that range from 8.8 to 8.2 Ma. Both are found in hydrothermal breccia that crosscut the Yanacocha dacite porphyry. The margins of the Phase III Chaupiloma rhyodacite dome was also overprinted with weak advanced argillic alteration, but has not been dated.

Explosive Phase III Negritos Ignimbrite

Volcanism ended in a final explosive event with the eruption of the Negritos rhyolite ignimbrite at 8.43±0.04 Ma (Figure 2.24N). The ignimbrite is preserved only in distal areas on Cerros de los Negritos 8 km north of the mine site. This eruption was followed by the emplacement of the Chaupiloma and Yanacocha Lake rhyodacite domes at 8.40±0.06 Ma (Turner, 1997). Eruption of the Negritos ignimbrite was followed by a cessation of arc volcanism in the Yanacocha area and the initiation of flat-slab tectonics and associated volcanic gap from 2°S – 15°S in northern Peru (Gutscher et al., 1999).

Conclusions

Field geology integrated with the ^{40}Ar/^{39}Ar dating presented in this study resolved the problems of volcanic stratigraphy in the Yanacocha district. There are no volcanic sequences that can be considered entirely post-mineral and younger than the Yanacocha high-sulfidation systems. Any volcanic rock within the district can host ore. The "Regalado" andesite volcanic rocks are actually the unaltered equivalents of the lower and upper Yanacocha pyroxene andesite volcanic sequence. In some areas, especially the west district, they post-date early hydrothermal activity, whereas, in the east district they host ore and crop out on the fringes of the epithermal systems. Ash-flow tuffs considered "Frialones and Huambos" can also host ore and are not post-mineral Upper Miocene and Pliocene as once proposed. These tuffs actually belong to three Middle Miocene pyroclastic sequences known as the Cerro Frailes dacite tuff that erupted between 15.5 and 15.2 Ma, the Maqui Maqui ignimbrite that erupted between 12.6 and 12.4 Ma, and the San Jose ignimbrite that erupted between 11.5 and 11.2 Ma. They all preceded ~3.2 million years of hydrothermal activity in the central and east portions of the Yanacocha district between 11.0 to 8.2 Ma.

Alunites in this study are magmatic-hydrothermal as indicated by the typical hypogene S isotope systematics. Samples were collected from hypogene advanced argillic alteration halos related to the high-sulfidation gold systems at Yanacocha. Problems with age interpretation were the result of contamination by impurities of quartz, pyrophyllite, diaspore, and sanidine, sometimes leaving <25% alunite in the sample. Atmospheric $^{40}Ar_{(a)}$ is adsorbed on the mineral surfaces of alunite and impurities, such as illite and kaolinite, and dominates at low temperatures (Itaya et al., 1996). Unusually high error in the alunites of this study are attributed to high proportions of nonradiogenic $^{40}Ar_{(a)}$ relative to low amounts of radiogenic $^{39}Ar_k$ and $^{40}Ar_{(r)}$ gas. Problems also resulted with alunite samples from fogging of the coverslip due to a large release of gas during step heating procedures. During these critical steps, fogging was prevented by using smaller incremental heating steps between 400 and 750°C.

$^{40}Ar/^{39}Ar$ incremental heating experiments produced undisturbed age spectra and acceptable plateau ages for 77% of the Yanacocha sample suite, incorporating fresh rock minerals that include plagioclase, hornblende, biotite, and whole rock samples, and hydrothermally altered rocks with magmatic-hydrothermal alunite and hydrothermal biotite. Valid isochron ages and integrated ages were preferred for the remaining 23% of samples whose age spectra were disconcordant. Problematic results displayed extraneous effects of Ar-loss, excess Ar, Ar recoil, or tight data clustering along the isochron. Effects of excess Ar and Ar-loss in Yanacocha rocks are likely a function of the proximity to hydrothermal systems, and excess Ar in low potassium minerals (i.e. plagioclase) may be related to the presence of melt inclusions and mineral inclusions inherited from the magma chamber, or fluid inclusions in secondary hydrothermal minerals related to the high-sulfidation systems.

Cenozoic volcanism at Yanacocha spanned 11.1 million years from 19.5 to 8.4 Ma and hydrothermal alteration continued 5.4 million years from 13.6 to 8.2 Ma. Volcanism in the Yanacocha Volcanic Field was centered at the Yanacocha Mining District for 6.1 million years from 14.5 to 8.4. Five periods of magmatic activity and volcanism and six phases of hydrothermal activity have been interpreted from the volcanic stratigraphy and age determinations. The duration of magmatic and hydrothermal activity was longer and more persistent than previously hypothesized.

Hydrothermal activity began in the west at 13.6 Ma and migrated east. By 10.8 Ma, high-sulfidation gold mineralization became widespread in the east district and continued for 700,000 years until 10.1 Ma. Activity then became centered at Cerro Yanacocha by 9.3 Ma for a duration of 1.1 m.y. and ended by 8.2 Ma. Temporal and spatial variations in Ag/Au and Cu/Au ratios from samples of advanced argillic alteration indicate that Au-dominate systems in the west evolved into more diverse epithermal systems through time producing both Au-dominate and Cu-Ag enriched ore bodies.

The duration of magmatic and hydrothermal activity at Yanacocha was far longer and more persistent than the other mineral districts that lie within a structural corridor defined by the Cajamarca and La Zanja-Tantahuatay Lineaments. Tantahautay is most similar to Yanacocha in magmatic longevity and compositional variation with 4.9 million years of andesite to rhyodacite magmatism; however, the duration of hydrothermal activity at Tantahuatay is 2.3 million years (Prihar, 1998) versus the 5.4 millions years at Yanacocha. Tantahuatay appears to lack the final post-11 Ma ore phases that contributed to making Yanacocha a world class +50 million ounce gold district.

Acknowledgements
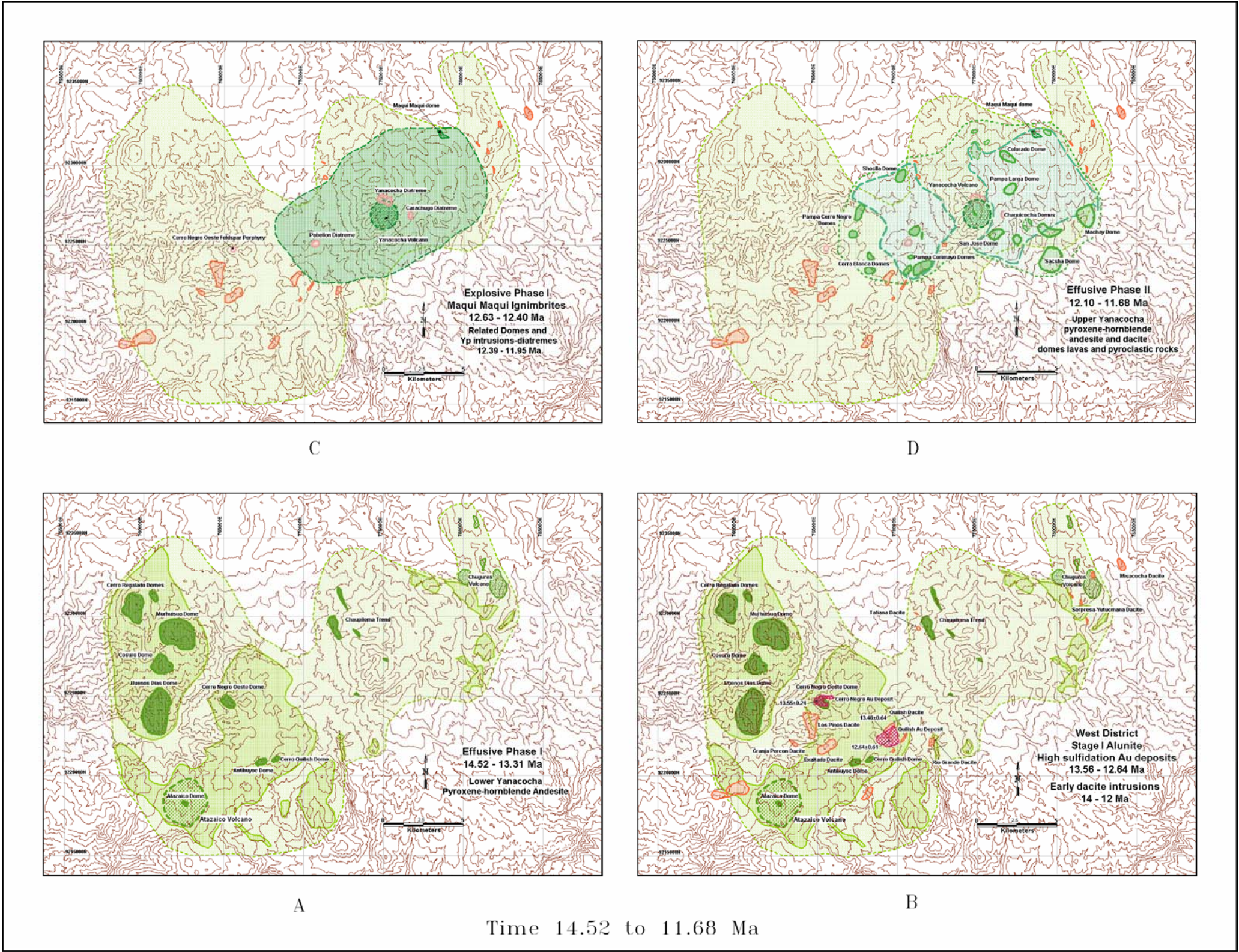
Figure 2.30 Yanacocha Volcanic Field from 14.52 to 11.90 Ma: (A) Effusive phase I 14.52-13.31 Ma, (B) Stage I hydrothermal activity 13.56-12.84 Ma, (C) Explosive phase I 12.63-12.40 Ma, (D) Effusive phase II 12.10-11.68.
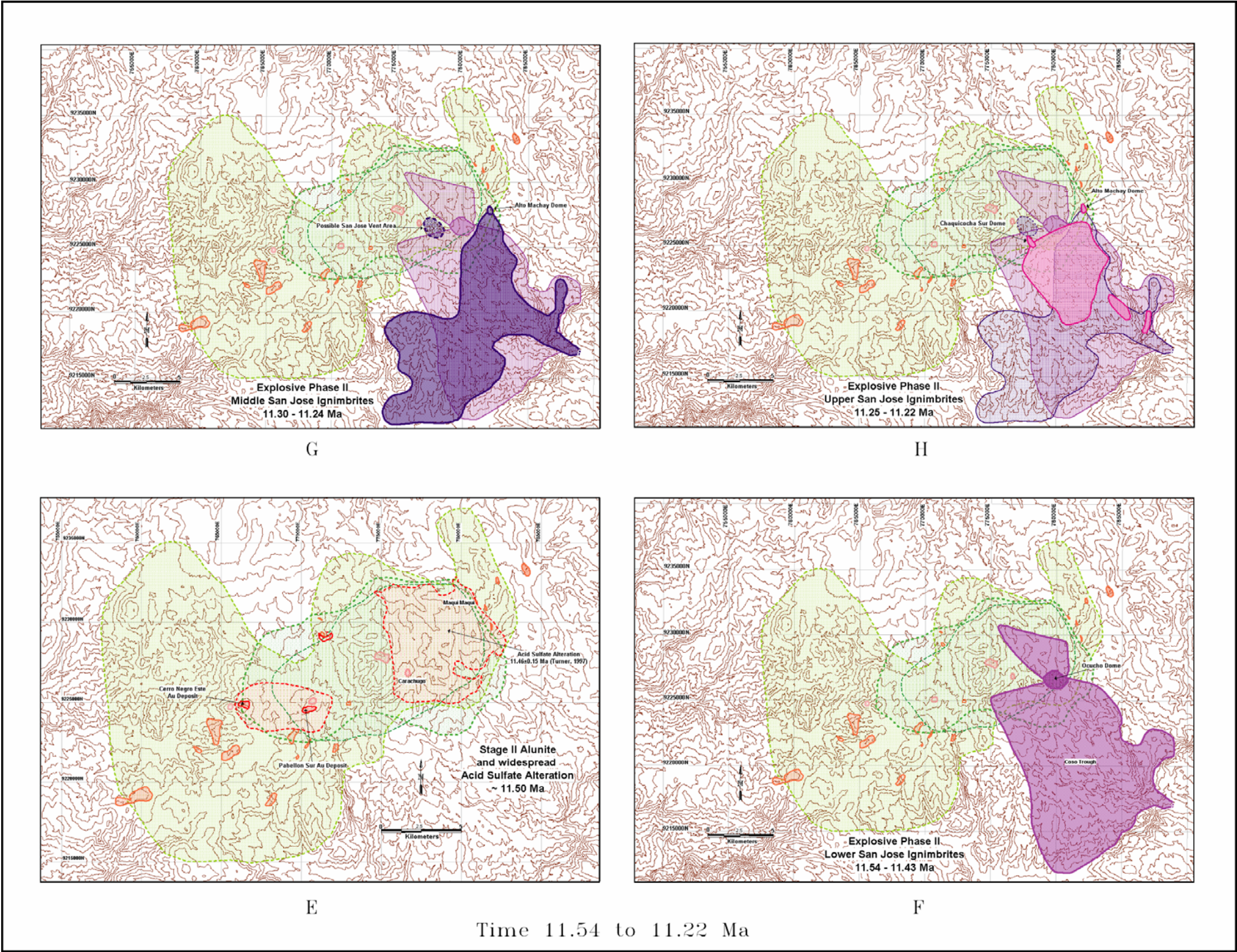
Figure 2.31 Yanacocha Volcanic Field from 11.54 to 11.22 Ma: (E) Stage II hydrothermal activity ~11.50 Ma, (F) Explosive phase II Lower San Jose 11.54-11.43 Ma, (G) Explosive phase II Middle San Jose 11.30-11.24 Ma, (D) Explosive phase II Upper San Jose 11.25 to 11.22 Ma.
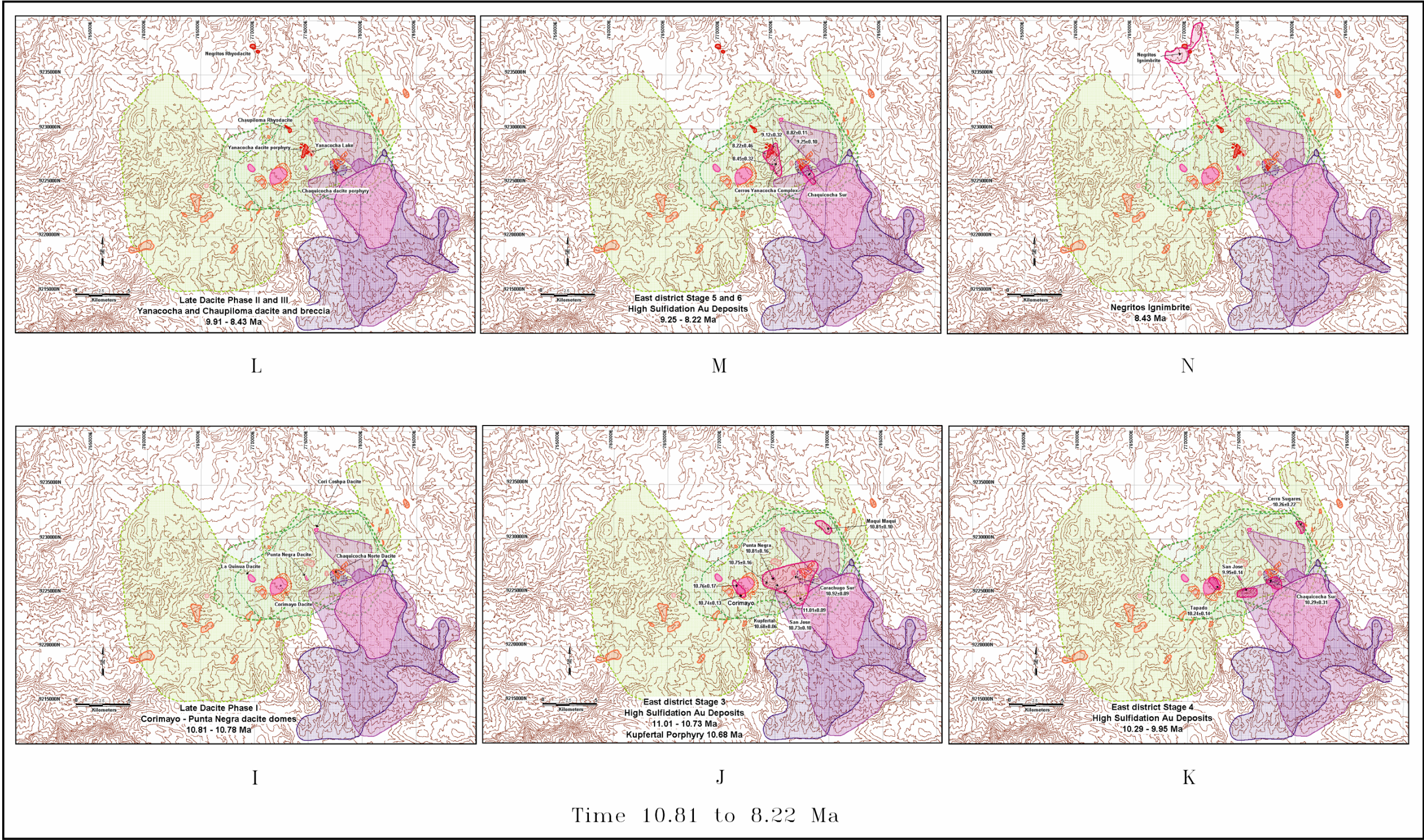
Figure 2.32. Yanacocha Volcanic Field from 10.81 to 8.22 Ma: (I) Late dacite phase I 10.81-10.78 Ma, (J) East district hydrothermal activity stage 3 11.01-10.73 Ma, (K) Stage 5 hydrothermal activity 10.29-9.95 Ma, (L) Late dacite phase II 9.91-8.43 Ma, (M) Stage 5 and 6 hydrothermal activity 9.25-8.22 Ma, (N) Eruption of the Negritos ignimbrite 8.43 Ma..

Table 2.1a. Summary of $^{40}Ar/^{39}Ar$ Age Determinations: Lower Andesite Lahar Sequence

Lower Andesite Lahar Sequence				Plateau Age (Ma)				Isochron Age (Ma)			Ma
Sample & Experiment Number	Name & Location	Material	Total Fusion age (Ma) ±2σ	Plateau Age ±2σ	# of Steps Plateau/ Total	%^{39}Ar in plateau	MSWD	Isochron age ±2σ	Initial $^{40}Ar/^{36}Ar$ ±2σ	MSWD	Preferred age ±2σ
1D28-02 02C951	CC-18 Tual	Plagioclase	19.52±0.16	19.53±0.13	7/9	96.69	0.57	19.64±0.25	288.5±33	0.56	19.53±0.13
2B15-03 03C3724	DN-84 Maqui Norte	Plagioclase	16.41±0.18	15.90±0.18	5/7	79.59	0.33	15.84±0.28	299.14±13	0.34	15.90±0.18
1E03-02 02C1238	DE-18 Cerro Collotan	Hornblende	15.12±0.25	15.41±0.36	4/10	51.76	0.72	15.02±0.76	299.5±6.8	0.34	15.41±0.36
				12.24±0.46	4/10	34.35	2.84	11.76±2.51	302±38.4	4.00	

Table 2.1b. Summary of $^{40}Ar/^{39}Ar$ Age Determinations: Cerro Frailes Dacite Pyroclastic Sequence

Cerro Frailes Dacite Pyroclastic Sequence				Plateau Age (Ma)				Isochron Age (Ma)			Ma
Sample & Experiment Number	Name & Location	Material	Total Fusion age (Ma) ±2σ	Plateau Age ±2σ	# of Steps Plateau/ Total	%^{39}Ar in plateau	MSWD	Isochron age ±2σ	Initial $^{40}Ar/^{36}Ar$ ±2σ	MSWD	Preferred age ±2σ
1E06-02 02C1112	Frail-2 Cerro Frailes	Biotite	15.41±0.06	15.51±0.05	7/10	98.33	0.66	15.51±0.06	294.3±4.4	0.71	15.51±0.05
1E08-02 02C1191	CB-35 Combayo	Biotite	15.51±0.06	15.50±0.06	3/10	82.48	0.14	15.51±0.14	293.1±46	0.27	15.50±0.06
2B03-03 03C2722	DN-12 Chaupiloma *Error plateau*	Biotite	15.98±0.08	15.45±0.10	5/11	48.71	2.33	15.36±0.10	304.2±7	0.22	15.38±0.09
	Case 2			*15.48±0.10*	*7/11*	*58.27*	*2.65*	15.38±0.09	303.3±4.3	0.47	
2E16-03 03C3672	DN-12	Plagio-clase	15.37±0.16	15.18±0.14	7/8	98.22	0.97	15.02±0.22	305.4±11	0.46	15.18±0.14
2E12-03 03C3654	DN-71 Maqui Norte	Biotite	15.06±0.07	15.15±0.06	7/9	93.53	1.12	15.08±0.09	309.3±14	0.54	15.15±0.06

Table 2.1c. Summary of ^{40}Ar/^{39}Ar Age Determinations: Lower Yanacocha Pyroxene-Hornblende Andesite Sequence

Lower Yanacocha Volcanic Sequence				Plateau Age (Ma)				Isochron Age (Ma)			Ma
Sample & Experiment Number	Name & Location	Material	Total Fusion age (Ma) ±2σ	Plateau Age ±2σ	# of Steps Plateau/ Total	%^{39}Ar in plateau	MSWD	Isochron age ±2σ	Initial ^{40}Ar/^{36}Ar ±2σ	MSWD	Preferred age ±2σ
West District											
2B19-03 03C2388	CNN-1 Lava Pampa Cerro Negro	plagioclase	15.23±0.14	14.52±0.13	5/8	73.57	0.81	14.45±0.17	311.3±25	0.50	14.52±0.13
2B17-03 03C2316	DO-43 Lava Quilish	plagioclase	14.79±0.14	14.27±0.16	5/8	68.16	1.67	14.09±0.21	314.8±18	0.48	14.27±0.16
2B14-03 03C2494	Cerro Atazaico Lava	plagioclase	14.87±0.15	14.21±0.16	6/7	69.31	1.30	14.10±0.20	312.7±29.4	0.88	14.21±0.16
2B11-03 03C3530	CR-4 Cerro Regalado Dome	plagioclase	13.87±0.09	13.85±0.09	7/8	99.29	0.28	13.83±0.13	302.4±29.8	0.25	13.85±0.09
East District											
1C20-02 02C858	CB-5 Tuff Alta Machay	whole rock	13.72±0.17	13.76±0.17	5/7	79.55	1.61	13.63±0.19	300.3±4.4	0.60	13.76±0.17
1D29-02 02C923	AZU-1 Lava Elita/Azufre	plagioclase	13.36±0.08	13.31±0.08	6/9	85.19	1.18	13.21±0.18	311.2±25	0.91	13.31±0.08

Table 2.1d. Summary of ^{40}Ar/^{39}Ar Age Determinations: Maqui Maqui Pyroclastic Sequence

Maqui Maqui Pyroclastic Sequence				Plateau Age (Ma)				Isochron Age (Ma)			Ma
Sample & Experiment Number	Name & Location	Material	Total Fusion age (Ma) ±2σ	Plateau Age ±2σ	# of Steps Plateau/ Total	%^{39}Ar in plateau	MSWD	Isochron age ±2σ	Initial ^{40}Ar/^{36}Ar ±2σ	MSWD	Preferred age ±2σ
1E10-02 02C1227	DN-30 Cori Coshpa ash-flow tuff Hornamo	Biotite	12.59±0.05	12.63±0.05	6/10	96.66	0.57	12.59±0.07	302.9±13.4	0.38	12.63±0.05
1E18-02 02C960	DN-7 Maqui Maqui ignimbrite Barranco	Plagioclase	12.56±0.11	12.49±0.08	7/9	97.30	1.13	12.50±0.10	294.6±4.8	1.25	12.49±0.08
2B16-03 03C2333	MM-342 158meters Maqui Maqui ignimbrite Colorado	Plagioclase	12.71±0.14	12.40±0.10	7/9	90.95	0.73	12.45±0.17	292.98±6.5	0.77	12.40±0.10
2E15-03 03C3641	DN-52 Maqui Maqui ignimbrite Maqui Norte	Plagioclase	35.86±0.19	30.62±11.61	4/7	61.44	>5000	13.12±3.41	1904±278	9.02	13.12±3.41
2B1-03 03C2616	DN-77 Maqui Norte Intrusion	Hornblende	12.19±0.11	12.13±0.10	5/8	95.78	0.94	12.09±0.17	299.6±18	0.82	12.13±0.10
2E23-03 03C3547	YS-370 46-48m Trachytic lava flow from CerroYanacocha	Plagioclase	12.75±0.13	12.39±0.12	5/8	68.10	1.02	12.33±0.14	302.7±10	0.65	12.39±0.12
			12.50±0.13	12.05±0.12	5/8	68.93	0.28	12.01±0.14	299±9	0.17	

Table 2.1e. Summary of $^{40}Ar/^{39}Ar$ Age Determinations: Upper Yanacocha Volcanic Sequence and SJI domes DE-2, CHQS-1, CB-3.

Upper Yanacocha Volcanic Sequence				Plateau Age (Ma)				Isochron Age (Ma)			Ma
Sample & Experiment Number	Name & Location	Material	Total Fusion age (Ma) ±2σ	Plateau Age ±2σ	# of Steps Plateau/ Total	%^{39}Ar in plateau	MSWD	Isochron age ±2σ	Initial ^{40}Ar/^{36}Ar ±2σ	MSWD	Preferred age ±2σ
West District											
2E20-03 03C3585	DO-60 Cerro Negro Este	Plagioclase	12.30±0.11	12.09±0.10	5/8	73.81	0.34	12.04±0.17	306.1±31	0.25	12.09±0.10
2B07-03 03C2370	COR-7 178 meters Corimayo Lava	Plagioclase	12.16±0.07	11.91±0.08	6/8	78.11	1.24	11.86±0.10	301.9±8	0.84	11.91±0.08
2B02-03 03C2704	SLT-2 Corimayo Dike	Horn-blende	11.95±0.13	11.90±0.11	8/8	100.00	0.63	11.84±0.13	302.5±11	0.46	11.90±0.11
East District											
1C17-02 02C1087	YSBD Yanacocha Sur Black Dike	Whole rock	12.11±0.08	12.09±0.08	4/7	84.04	0.51	12.04±0.54	298.9±32	0.74	12.09±0.08
1E01-02 02C969	CHQS-2 Chaq Sur Montura Lava	Horn-blende	12.45±0.14	12.05±0.15	3/9	80.20	0.81	12.12±0.92	291.2±54	0.88	12.05±0.15
2E21-03 03C3610	DN-83 Upha tuff Colorado Graben	Plagioclase	12.54±0.13	12.05±0.11	5/8	61.26	1.01	12.01±0.16	299.9±13	1.20	12.05±0.11
2B05-03 03C2526	CB-65 Machay Dome	Plagioclase	12.52±0.10	12.01±0.10	6/8	66.15	1.25	11.83±0.24	303.3±10	0.88	12.01±0.10
1D27-02 02C932	AZU-2 Ocucho Dome	Plagioclase	11.71±0.08	11.68±0.07	6/8	94.71	0.97	11.65±0.07	301.7±6	0.16	11.68±0.07
2B18-03 03C2297	DE-2 Ocucho Dome Sur - SJI	Plagioclase	11.73±0.09	11.36±0.09	5/8	75.98	1.13	11.30±0.11	315.7±20	0.00	11.36±0.09
2E22-03 03C3576	CHQS-1 Chaquicocha Sur Dome - SJI	Plagioclase	11.30±0.09	11.28±0.09	6/8	89.59	1.14	11.22±0.11	297.9±21	0.54	11.28±0.09
2E14-03 03C3561	CB-3 Alta Machay Dome - SJI	Plagioclase	11.39±0.08	11.23±0.07	4/8	71.72	1.09	11.15±0.13	314.5±24	0.29	11.23±0.07

Table 2.1f. Summary of ^{40}Ar/^{39}Ar Age Determinations: San Jose Ignimbrite Sequence

San Jose Ignimbrite Sequence				Plateau Age (Ma)				Isochron Age (Ma)			Ma
Sample & Experiment Number	Name & Location	Material	Total Fusion age (Ma) ±2σ	Plateau Age ±2σ	# of Steps Plateau/ Total	%^{39}Ar in plateau	MSWD	Isochron age ±2σ	Initial ^{40}Ar/^{36}Ar ±2σ	MSWD	Preferred age ±2σ
2B10-03 03C2405	CB-44 Arnacocha	Plagioclase	11.86±0.09	11.54±0.09	5/8	72.53	0.86	11.51±0.12	297.5±6	0.95	11.54±0.09
2E24-03 03C3624	VC-4 Basal SJI Combayo	Plagioclase	12.66±0.42	11.53±0.13	4/8	60.60	0.44	11.47±0.22	300.9±18	0.45	11.53±0.13
1E02-02 02C1098	BS-3 Sacsha Breccia	Horn-blende	11.46±0.12	11.50±0.09	9/12	99.27	0.73	11.30±0.25	314.7±22.5	0.40	11.50±0.09
2B09-03 03C2423	CB-56 Que Azufre Combayo	Plagioclase	11.55±0.06	11.43±0.06	6/9	78.69	1.54	11.37±0.10	307.3±16	1.22	11.43±0.06
1C14-02 02C1009	SJS-79A 20.3 meters San Jose	Whole rock	11.67±0.12	11.43±0.11	7/10	72.81	1.50	11.51±0.23	294±4	1.62	11.43±0.11
1C15-02 02C1020	SJS-79A 23.4 meters San Jose	Whole rock	11.57±0.07	11.30±0.08	4/12	35.05	0.48	11.34±0.16	293.2±7.3	0.51	11.28±0.14
			11.57±0.07	11.31±0.08	5/12	39.60	0.74	11.28±0.14	296.5±5.5	0.94	
2B06-03 03C2580	CB-74 Machay - contact to Machay dome	Plagioclase	11.58±0.11	11.30±0.09	5/8	73.41	0.81	11.14±0.24	319±33	0.28	11.30±0.09
1D26-02 02C896	CB-38 La Masma	Plagioclase	11.45±0.07	11.27±0.07	5/9	59.57	0.83	11.15±0.19	345.1±76	0.30	11.29±0.15
1E22-02 02C1249		Horn-blende	11.19±0.17	11.29±0.15	5/9	97.88	0.24	11.29±0.44	295.6±18	0.36	
2E19-03 03C3664	CB-59 Ventanillas Combayo	Plagioclase	11.27±0.09	11.29±0.08	7/7	100.00	0.74	11.39±0.17	269.3±38	0.52	11.29±0.08
1E04-02 02C1180	RC-6 Rio Chonta	Horn-blende	11.51±0.27	11.28±0.22	4/11	95.70	0.52	11.26±0.40	295.5±6.5	0.46	11.28±0.22

Table 2.1g. Summary of ^{40}Ar/^{39}Ar Age Determinations: San Jose Ignimbrite Sequence (continued)

San Jose Ignimbrite Sequence				Plateau Age (Ma)				Isochron Age (Ma)			Ma
Sample & Experiment Number	Name & Location	Material	Total Fusion age (Ma) ±2σ	Plateau Age ±2σ	# of Steps Plateau/ Total	%^{39}Ar in plateau	MSWD	Isochron age ±2σ	Initial ^{40}Ar/^{36}Ar ±2σ	MSWD	Preferred age ±2σ
2B08-03 03C2598	DE-36 south of Paquerumi	Plagioclase	11.33±0.07	11.25±0.07	6/8	80.70	0.49	11.23±0.11	302.1±57	0.52	11.25±0.07
2E17-03 03C3594	SJS-78A 5.0 meters San Jose	Plagioclase	11.41±0.09	11.24±0.10	6/8	93.52	1.57	11.11±0.14	318.3±21	0.70	11.24±0.10
2B13-03 03C2476	VC-1 Ventanillas Combayo	Plagioclase	11.55±0.07	11.22±0.08	5/8	71.78	0.68	11.22±0.12	326.1±137	0.49	11.22±0.08

Table 2.1h. Summary of ^{40}Ar/^{39}Ar Age Determinations: Upper (Late) Yanacocha Dacite Intrusions, Domes, and Pyroclastic Rocks

Late Yanacocha Dacite Intrusions, Domes, and Pyroclastic Rocks				Plateau Age (Ma)				Isochron age (Ma)			Ma
Sample & Experiment Number	Name & Location	Material	Total Fusion age (Ma) ±2σ	Plateau Age ±2σ	# of Steps Plateau/ Total	%^{39}Ar in plateau	MSWD	Isochron age ±2σ	Initial ^{40}Ar/^{36}Ar ±2σ	MSWD	Preferred age ±2σ
1E07-02 02C1170	COR-1 Corimayo dacite dome	Biotite	10.74±0.04	10.78±0.05	6/10	97.63	1.63	10.74±0.05	303.1±6	0.34	10.78±0.05
1E09-02 02C1216	YN-1A	Biotite	10.06±0.05	9.91±0.04	5/10	82.70	0.35	9.92±0.18	294.0±23	0.47	9.91±0.04
2B04-03 03C2279	NG-5 Negritos	Sanidine	8.48±0.04	8.43±0.04	6/8	93.93	2.00	8.48±0.04	338.5±33.4	0.49	8.43±0.04

Table 2.1i. Summary of ^{40}Ar/^{39}Ar Age Determinations: Magmatic-hydrothermal Alunite Alteration

Alunite and Secondary Biotite Alteration				Plateau Age (Ma)				Isochron age (Ma)			Ma
Sample & Experiment Number	Name & Location	Material	Total Fusion age (Ma) ±2σ	Plateau Age ±2σ	# of Steps Plateau/ Total	%^{39}Ar in plateau	MSWD	Isochron age ±2σ	Initial ^{40}Ar/^{36}Ar ±2σ	MSWD	Preferred age ±2σ
1E12-02 02C1300	CN-1 Cerro Negro Oeste	Alunite	13.32±0.28	13.56±0.24	5/10	93.71	0.02	13.56±0.41	295.5±8.2	0.02	13.56±0.24
2E09-03 03C2998	CQ-37 110 meters Quilish Norte	Alunite	13.55±0.69	13.48±0.64	5/6	98.91	1.19	11.81±4.24	334±104	1.52	13.48±0.64
1E13-02 02C1358	QN-1 Quilish	Alunite	13.63±0.95	12.64±0.61	5/6	95.65	0.48	11.62±1.72	312.0±26	0.04	12.64±0.61
1E11-02 02C1373	CLL-1 Collotan Angelita	Alunite	11.18±1.49	11.41±0.89	5/7	92.50	0.36	11.58±1.94	295.1±4.2	0.47	11.41±0.89
1C18-02 02C1033	Baul-1 Cerro Baul	Alunite vein	11.03±0.14	11.01±0.09	3/4	99.95	0.20	11.02±0.11	295.3±10.4	0.40	11.01±0.09
1C19-02 02C1312	MM-314 259.7 meters Maqui Maqui	Alunite	10.73±0.11	10.81±0.10	4/6	98.12	0.44	10.94±0.49	283.2±46	0.52	10.81±0.10
2E01-03 03C3466	PNE-3 45-50 meters Punta Negra	Alunite	9.94±0.29	10.81±0.16	8/9	83.09	0.81	11.16±0.76	282±28	0.85	10.81±0.16
2D22-03 03C3490	COR-39 213 meters Corimayo	Alunite	10.44±0.24	10.76±0.17	5/8	89.21	1.12	11.01±0.67	290.5±13.5	1.27	10.76±0.17
2E10-03 03C2976	CLL-2 Collotan Angelita	Alunite vein	9.88±0.14	10.75±0.16	5/7	47.10	0.43	10.73±0.17	297.4±10	0.48	10.75±0.16
2E07-03 03C2965	LBQ-40 441.2 meters Corimayo Sur	Alunite vein	10.43±0.14	10.74±0.13	4/8	52.47	0.80	11.28±0.71	257.5±49	0.22	10.74±0.13

Table 2.1j. Summary of $^{40}Ar/^{39}Ar$ Age Determinations: Magmatic-hydrothermal Alunite and Hydrothermal Biotite Alteration

Alunite and Secondary Biotite Alteration				Plateau Age (Ma)				Isochron age (Ma)			Ma
Sample & Experiment Number	Name & Location	Material	Total Fusion age (Ma) ±2σ	Plateau Age ±2σ	# of Steps Plateau/ Total	%^{39}Ar in plateau	MSWD	Isochron age ±2σ	Initial $^{40}Ar/^{36}Ar$ ±2σ	MSWD	Preferred age ±2σ
2E3-03 03C3478	SJS-1 San Jose Pit	Alunite	10.67±0.14	10.73±0.10	4/7	83.28	0.93	10.61±0.75	305.4±61.3	1.33	10.73±0.10
1E05-02 02C1203	KUP-3 571meters Kupfertal	Hydrothermal Biotite	10.70±0.04	10.73±0.05	6/11	85.16	2.23	10.68±0.06	327.6±31.0	1.11	10.73±0.05
1E15-02 02C1363	CS-1 Chaqui- cocha Sur	Alunite	10.59±0.79	10.29±0.31	5/5	100.00	0.25	10.25±0.33	296.7±3.0	0.13	10.29±0.31
1E14-02 02C1330	MM-46377 Cerro Sugares	Alunite vein	9.99±0.31	10.26±0.22	4/6	97.87	0.94	10.29±0.53	294.5±12.8	1.56	10.26±0.22
2E04-03 03C3512	TAP-169 382 meters Tapado	Alunite	10.23±0.19	10.24±0.14	6/7	98.83	1.16	10.78±0.60	271.1±26.3	0.69	10.24±0.14
2E05-03 03C2954	SJS-3 San Jose above Kupfertal	Alunite	9.96±0.14	9.95±0.14	6/7	99.37	1.26	9.95±0.30	294.8±16.7	1.47	9.95±0.14
2E11-03 03C2987	KUP-3 94 meters Kupfertal	Alunite Patchy(gusano) qt-al-pyr	8.93±0.15	9.25±0.10	5/7	83.61	1.20	9.70±0.45	248.3±46	0.59	9.25±0.10
1E16-02 02C1339	YN-105 88.7meters Yanacocha Norte	Alunite (Recalc with 3 steps don't use 400)	9.18±0.32	9.12±0.32	4/4	100.00	0.96	9.18±2.85	287.2±273	0.21	9.12±0.32
2E08-03 03C3502	ENC-6 137.5 meters Encajon Yanacocha	Alunite	8.21±0.15	8.82±0.11	4/7	74.74	1.06	8.23±0.89	341.8±69	0.49	8.82±0.11
1E17-02 02C1368	YO-1Encajon Yanacocha	Alunite	8.51±0.48	8.45±0.32	5/6	99.46	0.37	8.41±0.36	296.2±3.4	0.46	8.45±0.32
2E06-03 03C2944	YS-219 111.8 meters Yanacocha	Alunite	7.67±0.51	8.22±0.46	5/7	88.92	0.31	8.20±2.65	295.1±100	0.45	8.22±0.46

Table 2.2a. Alteration, Ag/Au and Cu/Au ratios, and age determined from magmatic-hydrothermal alunites and hydrothermal biotite in Au deposits at Yanacocha.

Deposit (# samp)	Alunite	Pyrophyllite	Jarosite	Diaspore	Rutile/ zircon	Quartz	Sulfur/ sulfide	Ag/Au	Cu/Au	Age	Comments
Cerro Negro Oeste (1)	A 0.5-2.0 e Na	N	N	N	T rutile	>80% mosaic texture	N	0.45	123.4	13.55±0.24	Vuggy silica with coarse alunite crystals in vugs of a porphyryitic andesite
Quilish (2)	A 0.15 e – s Ka	N to C	N	N	T rutile	70% mosaic and granular textured gm	N	0.3 0.6(1)	9.5 309.4	13.48±0.64 12.64±0.61	Quartz-alunite altered porphyritic andesite. Rare hydrothermal sanidine(1).
Tapado/ Corimayo (4)	A <0.05 C 0.1-0.3 s – a Ka (2,4) Na (3)	N	R to C	N	T to R C rutile in SM(2)	65-70% granular to mosaic textured gm	C dis pyrite	0.3 (2) 30.3(3) 12.0(4)	4.6 572.9 960	10.76±0.17 10.24±0.14 10.74±0.13	Fine-grained white alunite matrix to stage 2 SM fragments crosscut by later SM with rutile (2). Pink alunite veins crosscut Yp hornblende-feldspar porphyry (3) . Matrix supported heterolithic breccia (4).

The relative abundances are reported for each alteration mineral and the maximum size in mm is reported for the alunites. A abundant, C common, R rare, T trace; e euhedral, s shubhedral, a anhedral, sh shreddy, dis disseminated, Pt patchy-wormy alteration. Ypq Yanacocha quartz porphyry, SJI San Jose ignimbrite, SA quartz-alunite, SM massive silica, SV vuggy silica, Ka alunite, Na natroalunite.

(1) Quilish Norte SA with 3.2g Au, (2) Corimayo, (3) Tapado hydrothermal breccia, (4) La Quinua Basin feldspar porphyry, (5) Maqui Maqui tuff at Cerro Collotan, (6) Late alunite crosscuts SM altered rock with embayed quartz eyes at Cerro Collotan, (7) Punta Negra dacite, (8) Kupfertal patchy quartz-alunite, (9) hydrothermal biotite of Kupfertal deep porphyry.

Table 2.2b. Alteration, Ag/Au and Cu/Au ratios and age determined from alunites in Au deposits at Yanacocha.

Deposit (# samp)	Alunite	Pyrophyllite	Jarosite	Diaspore	Rutile/ zircon	Quartz	Sulfur/ sulfide	Ag/Au	Cu/Au	Age	Comments
Cerro Collotan (3)	A .05-0.5 sh to e Na (5) Ka (6)	R mixed with alunite in Pt	C	N	N	Up to 70%	N	35.2(5) 51.7(6)	3012 191.3	11.41±0.89 10.75±0.16	SA with coarse alunite in vugs in a quartz-bearing lapilli tuff (5). Alunite-coated fractures and pink alunite veins crosscut SM with 1-3% primary embayed quartz phenocrysts (6).
Kupfertal Punto Negro (3)	A 0.02 C .25-0.5 Ka Na w/ Pt	R 50m w/ Pt C w/ Pt at +300m	N	C w/ Pt at depth +300m	N	50-85%	T to C dis	11.2(7) 17.3(8) 1.9(9)	589.5 8509 271.5	10.81±0.16 9.25±0.10 10.72±0.09	Hydrothermal biotite >60% (sh <0.1mm) in one sample from 570m depth at Kupfertal (9).
San Jose (2)	A 0.3-1.2 Ka (10) Na (11)	N	T	N	T	50-75%	N	1.4 (10) 3.6 (11)	63.8 106.8	9.95±0.14 10.73±0.10	Porphyritic andesite altered to SV w/ alunite in vugs (10), and SA porphyritic quartz andesite with round feldspar porphyry frgs (11).
Cerro Yanacocha (5)	A <.05 C .08-0.1 Ka Na (12) R 1.0	R	R	T	T-C rutile T zircon	60-90%	R to C enargite pyrite	9.4 (12) 11.4(13) 17.5(14) 21(15)	88.9 82.6 160.2 12190	8.45±0.32 8.82±0.11 8.22±0.46 9.12±0.32	Samples include SA Ypq, SM breccia healed with alunite, stage 2 breccia healed with alunite, and Pt

The relative abundances are reported for each alteration mineral and the maximum size in mm is reported for the alunites. A abundant, C common, R rare, T trace; e euhedral, s shubhedral, a anhedral, sh shreddy, dis disseminated, Pt patchy-wormy alteration. Ypq Yanacocha quartz porphyry, SJI San Jose ignimbrite, SA quartz-alunite, SM massive silica, SV vuggy silica, Ka alunite, Na natroalunite.

(5) Maqui Maqui tuff at Cerro Collotan, (6) Late alunite crosscuts SM altered rock with embayed quartz eyes at Cerro Collotan, (7) Punta Negra dacite, (8) Kupfertal patchy quartz-alunite, (9) hydrothermal biotite of Kupfertal deep porphyry, (10) San Jose surface exposure and vuggy silica with alunite, (11) San Jose porphyry breccia on pit bottom, (12) 2 stage alunite-healed breccia at Encajon, (13) Encajon stage 2 breccia, (14) alunite-matrix heterolithic breccia Yanacocha NW, (15) Massive silica breccia healed with alunite,.

Table 2.2c. Alteration, Ag/Au ratios and age determined from alunites in Au deposits at Yanacocha.

Deposit (# samp)	Alunite	Pyrophyllite	Jarosite	Diaspore	Rutile/ zircon	Quartz	Sulfur/ sulfide	Ag/Au	Cu/Au	Age	Comments
Chaq. Sur / Cerro Baul (2)	A 0.5 Na (16) Ka (17)	N	N	N	C rutile	10-75% 10% in alunite veins	N	26(16) 28(17)	480 1300	11.01±0.09 10.29±0.31	Pink alunite in veins crosscut the SJI at Baul (16) and matrix of a brecciated quartz-bearing tuff at Chaquicocha Sur (17).
Maqui Maqui (3)	A <0.2 C.25-.45 R 2.5 Na	N	T	N	C	50-80% (15) Absent in veins (16)	R to C sulfur enargite pyrite	0.58(18) 3.5(19)	1947 605	10.81±0.10 10.26±0.22	Coarse blades of natroalunite in veins at Cerro Sugares (18)

The relative abundance are reported for each alteration mineral and the maximum size in mm is reported for the alunites. A abundant, C common, R rare, T trace; e euhedral s shubhedral a anhedral sh shreddy, dis disseminated, Pt patchy-wormy alteration. Ypq Yanacocha quartz porphyry, SJI San Jose ignimbrite, SA quartz-alunite, SM massive silica, SV vuggy silica, Ka alunite, Na natroalunite.

(16) Cerro Baul, (17) Chaquicocha Sur, (18) Maqui Maqui deep, (19) large alunite vein at Cerro Sugares east of Maqui Maqui.

Table 2.3. Sulfur Isotope Data

ID	Sample	Weight (ug)	$\delta^{34}S_{cdt}$	%S	Age (Ma)	Comment
26	YN-105 Py	0.193	-2.4	46.88	9.15	Pyrite; α = 1.0185
25	TAP-169 Py	0.222	-14.5	42.00	10.24	Pyrite; α = 1.0312
24	YS-219	0.633	No data	No data	8.22	111.8m, small peak below 300mV
23	YO-1	0.642	18.5	13.02	8.45	
22	ENC-6	0.663	19.0	11.64	8.82	137.5m
21	YN-105	0.625	16.0	9.63	9.12	
20	KUP-3	0.678	15.9	13.85	9.25	94m
19	TAP-169-2A	0.625	15.8	14.43	10.24	382.0m depth
18	TAP 169-1	0.671	16.8	13.09	10.24	376.8m depth w/ py
17	MM-46377	0.669	15.9	14.34	10.26	
16	CS-1	0.725	15.9	10.67	10.29	
15	SJS-3	0.613	20.0	11.49	10.31	
14	SJS-1	0.631	16.4	12.82	10.73	
13	LBQ-40	0.716	16.5	13.89	10.74	441.2m
12	CLL-2	0.663	19.0	14.11	10.75	
11	COR-39	0.646	14.5	5.61	10.76	213m
10	MM-314	0.652	11.4	13.83	10.81	259.4m
9	PNE-3	0.637	16.8	8.82	10.81	45-50m
8	Baul-1	0.708	17.9	13.59	11.01	
7	CLL-1	0.715	18.8	12.43	11.41	
6	QN-2	0.703	21.3	6.74	12.64	duplicate
5	QN-1	0.693	21.8	3.36	12.64	
4	CQ-37	0.604	25.3	3.73	13.48	110m
3	CQ-37A	0.685	25.9	2.95	13.48	duplicate
2	CN-2	0.616	20.4	9.77	13.55	duplicate
1	CN-1	0.709	20.8	12.86	13.55	

$\alpha_{SO4-H2S}$ = equilibrium fractionation factor for the $SO_4^{-2} - H_2S$ pair

YANACOCHA STRATIGRAPHY

Anthony A. Longo

Introduction

District-scale geologic mapping over an area of more than 1000 km^2 and detailed core logging of geology from the Yanacocha ore deposits summarized below have resulted in major revisions to the Tertiary volcanic stratigraphy. New stratigraphic relationships at Yanacocha, and ^{40}Ar/^{39}Ar dates reported in Chapter 2 (Longo et al., 2005), define eight rock packages that include three pre-Yanacocha volcanic sequences and five local volcanic sequences that represent the Yanacocha Volcanic Field. Rock packages considered pre-Yanacocha rocks were erupted before 15.0 Ma. They include the following in stratigraphic order (Figure 3.1):

(1) Pre-20 Ma Huambo Cancha andesite lavas and pyroclastic rocks (Tv) referred to as basal andesite unconformably overlie the Cretaceous basement and early unconformity in the Rio Porcon Valley (Figure 3.3). These rocks may belong to the Llama (55-44 Ma) or Huambos (39-36 Ma) volcanic sequences as discussed by Noble et al. (1990). The time of the uncomformity at the base of the Huambo Cancha andesite is unknown, but resulted during the Cretaceous-Paleocene Peruvian Orogeny (90-60? Ma) and the Paleocene-Eocene Inciac I Orogeny (59-55 Ma) (Cobbing, 1981; Megard, 1984 and 1987; Noble et al., 1985 and 1990).

(2) The Tual and Chaupiloma lower andesite lahar sequence (Tlal) of pumice-rich lahars, debris flows, volcaniclastic sediment, and andesite lava flows range from ~19.5 to 15.9 Ma and filled paleo-channels in the Huambo Cancha andesite. An unconformity after the Huambo Cancha andesite is contemporaneous with the Eocene Inciac II or Oligocene Quechua I Orogenies of McKee and Noble (1982), Noble et al. (1985), and Noble et al. (1990).

(3) The Cerro Frailes dacite pyroclastic sequence (Tcfd) with coarse biotite-rich dacite lithic ash-flow tuffs and debris flows was erupted from 15.5 to 15.2 Ma and deposited over an erosional hiatus marked by stream channels cut into the andesite laha sequence (>15.5 Ma). After eruptions of the Cerro Frailes ash-

flow tuff the Yanacocha area experienced gentle folding and an erosional hiatus from 15.2 to 14.5 Ma.

Rock sequences that belong to the Yanacocha Volcanic Field (YVF) represent volcanic and intrusive rocks from five contiguous episodes of magmatism centered at Yanacocha. Compositional variations are typical of a calc-alkaline rock suite with a complex magmatic system that progressed from andesite to rhyolite. These rocks evolved from spatially and temporally distinct centers and developed a northeast-trending corridor of Middle Miocene volcanism 25 km long that covered an area more than 500 km^2 with lava flows and pyroclastic rocks. These relationships genetically link five episodes of volcanism and associated rocks at Yanacocha to the Yanacocha Volcanic Field.

Volcanism began with two periods of dominantly effusive eruptions of andesite compositions that culminated in two periods of dominantly explosive eruptions of dacitic composition over an interval of 3.3 million years from 14.5 to 11.2 Ma. The early styles of YVF volcanism were followed by 2.4 million years of magmatism from 10.8 to 8.4 Ma with compositional variations from dacite to rhyolite. These rocks are distinct from older ones and contain the mineral assemblage of sphene + magnetite + quartz implying relatively high oxygen fugacities (Wones, 1989). This late episode of highly oxidized felsic magmas developed porphyritic domes with minor lavas and pyroclastic aprons, and intrusions of isolated dacite porphyry plugs. Volcanism ended in a final explosive event with the eruption of the Negritos rhyolite ignimbrite at 8.40±0.06 Ma. Eruption of the Negritos ignimbrite was followed by a cessation of arc volcanism in the Yanacocha area and the initiation of flat-slab tectonics and associated volcanic gap from 2°S – 15°S in northern Peru (Gutscher et al., 1999).

Laminated rocks are present at three levels in the volcanic stratigraphy. Some are distinctly pyroclastic, whereas others have thin and planar laminations of dense silica. They are interpreted as laminated water-lain tuffs and surge deposits within a package of pyroclastic rocks (Edwards, 2000) and accumulations of colloidal silica that deposited in acid lakes associated with hydrothermal and volcanic vent areas (Longo, 2000).

Rocks of the YVF are as follows in stratigraphic order (Figure 3.2):

(1) The Lower Yanacocha pyroxene-hornblende andesite volcanic sequence (Tlpha) with lavas and minor pyroclastic rocks from an early period of effusive volcanism and dome building called *effusive stage 1*.

(2) The middle Yanacocha Maqui Maqui pyroclastic sequence with laminated rocks (Tml), the lower and upper Maqui-Maqui ignimbrite sequence (Tmmi), and early hornblende andesite and dacite porphyry intrusions (Tmmp, Typ, and Ted). The Maqui Maqui ignimbrite sequence consisted of hornblende ± biotite andesite, trachyandesite, and dacite ignimbrites that represent an early period of explosive volcanism called *explosive stage 1*. These rocks post date and are temporally related to porphyritic intrusions, feldspar porphyry plugs and diatremes with the similar mineral assemblages to the Maqui Maqui ignimbrite. A period of early dacite intrusions with quartz + hornblende + biotite phenocrysts intruded the lower Yanacocha volcanic sequence in the west district.

(3) The Upper Yanacocha volcanic sequence (Tupha) with porphyrotic pyroxene-hornblende andesite and dacite lavas and a variety of pyroclastic rocks from a second period of effusive volcanism associated with numerous andesite dome related systems called *effusive stage 2*

(4) The upper San Jose ignimbrite sequence (Tsj) with hornblende ± pyroxene ± biotite dacite ignimbrites from a second period of explosive volcanism called *explosive stage 2*. Endogenous pyroxene-hornblende dacite domes with compositions similar to the Upper Yanacocha volcanic sequence followed the explosive eruptions and may correspond to ignimbrite vent areas.

(5) Upper hornblende-biotite dacite domes and pyroclastic rocks of Corimayo-Tapado (Tcd), the quartz porphyry dacite plugs of Yanacocha (Typq), and the rhyodacite dikes and domes of Chaupiloma-Yanacocha Lake (Tcyd) represent the final, highly oxidized, magmatic phase spatially and temporally associated with the ore deposits at Yanacocha.

(6) Volcanism ended in a final explosive event with the eruption of the Negritos rhyolite ignimbrite at 8.4 Ma that may have vented from a fissure near the

location of the Chaupiloma and Yanacocha lake rhyodacite dikes (*explosive stage 3*).

Five unconformities, three intervals of erosion or disconformities, and three brief cessations of volcanism were recognized in the field and listed below as follows:

(1) A late Cretaceous - early Cenozoic angular uncomformity resulted during the Cretaceous-Paleocene Peruvian Orogeny (90-60? Ma) and the Paleocene-Eocene Inciac I Orogeny (59-55 Ma) (Cobbing, 1981; Megard, 1984 and 1987; Noble et al., 1985 and 1990). All pre-Yanacocha rock packages the Humabo Cancha volcanics, Tual and Chuapiloma lahars, and Cerro Frailes dacite tuffs have been observed to overlie Cretaceous limestone and quartzite with angular unconformity.

(2) An unconformity after the Huambo Cancha volcanic rocks and before the Tual lahar sequence may be contemporaneous with the late Eocene Inciac II or early Oligocene to Lower Miocene Quechua I Orogenies (McKee and Noble, 1982; Noble et al., 1985; and Noble et al., 1990) where andesite lahars of the Tual sequence filled channels from a drainage system that incised the Tv,

(3) *Erosional hiatus 1* may represent a temporal gap and interval of erosion between the Tual member and the Chaupiloma member of the lower andesite lahar sequence. The gap may correspond to a Lower Miocene disconformity that represents up to ~3.5 m.y. of before the deposition of the Chaupiloma member. Lahars, volcaniclastic sediments and lava flows of the Chaupiloma member have been observed to fill channels that down cut into the Tual member.

(4) *Erosional hiatus 2* represents a second interval of erosion marked by a disconformity between the Tual and Chaupiloma lahar sequences and the overlying Cerro Frailes dacite tuffs. Lahars and tuffs of Cerro Frailes dacite were deposited and filled channels carved into Tual and Chaupiloma lahar sequence. This hiatus is early mid-Miocene and is bracketed between about 15.9 Ma and 15.5 Ma and may correspond to a second disconformity.

(5) *Erosional hiatus 3* marks a gap in the stratigraphy and distinct change in the composition of the volcanic rocks at Yanacocha from biotite dacite to pyroxene

andesite. After eruptions of the Cerro Frailes pyroclastic rocks (Tcfd), the Yanacocha area experienced gentle folding with an erosional hiatus from about 15.2 to 14.5 Ma that may represent a gentle angular unconformity of Middle Miocene. Andesite lava flows of the Lower Yanacocha volcanic sequence were channeled into a drainage system that cut canyons into the Cerro Frailes tuffs and Tual-Chaupiloma lahars.

In the Yanacocha Volcanic Field, laminated rocks mark gaps in the volcanic stratigraphy. Laminated rocks consist of a sequence of thinly laminated siliceous rocks interpreted as accumulations of colloidal silica that were deposited in acid lakes intercalated with thin bedded, fine-grained tuffs. These volcanic gaps are as follows:

(1) *Volcanic gap 1* is bracketed by Lower Yanacocha andesite lava at ~13.3 Ma and a lower Maqui Maqui ash-flow tuff at ~12.6 Ma. The gap contains thin laminated siliceous rocks and thin ash layers that lie below the Maqui Maqui pyroclastic sequence.

(2) *Volcanic gap 2* is bracketed by lava flows of the Upper Yanacocha volcanic rocks at ~11.9 Ma and the oldest known ignimbrite of the San Jose sequence at ~11.5 Ma. Youngest domes of the Upper Yanacocha sequence have an age of ~11.7 Ma but lack any outcrop evidence of overlying laminated rocks. The hiatus is marked in some areas by siliceous and opaline laminated rocks below the San Jose ignimbrite sequence. These rocks crop out north of Cerro Paquerumi on the west slope of Quebrada Chaquicocha, below the ignimbrite on Cerro Baul, and at Cerro Chaquicocha. They also were found in drill holes at Huacataz and San Jose Sur.

(3) *Volcanic gap 3* represents a time interval after a cessation of San Jose ignimbrite volcanism and is bracketed by the age for an upper San Jose ash-flow tuff at 11.2 Ma and the earliest known dacite dome at Corimayo with an age of ~10.8 Ma. At Corimayo and Rosas, siliceous laminated rocks, tuffaceous lacustrine sediments, and thin bedded tuffs lie below dacite lavas from the Corimayo dome.

All Yanacocha rock sequences are discussed below in detail and summarized in Figures 3.1 and 3.2.
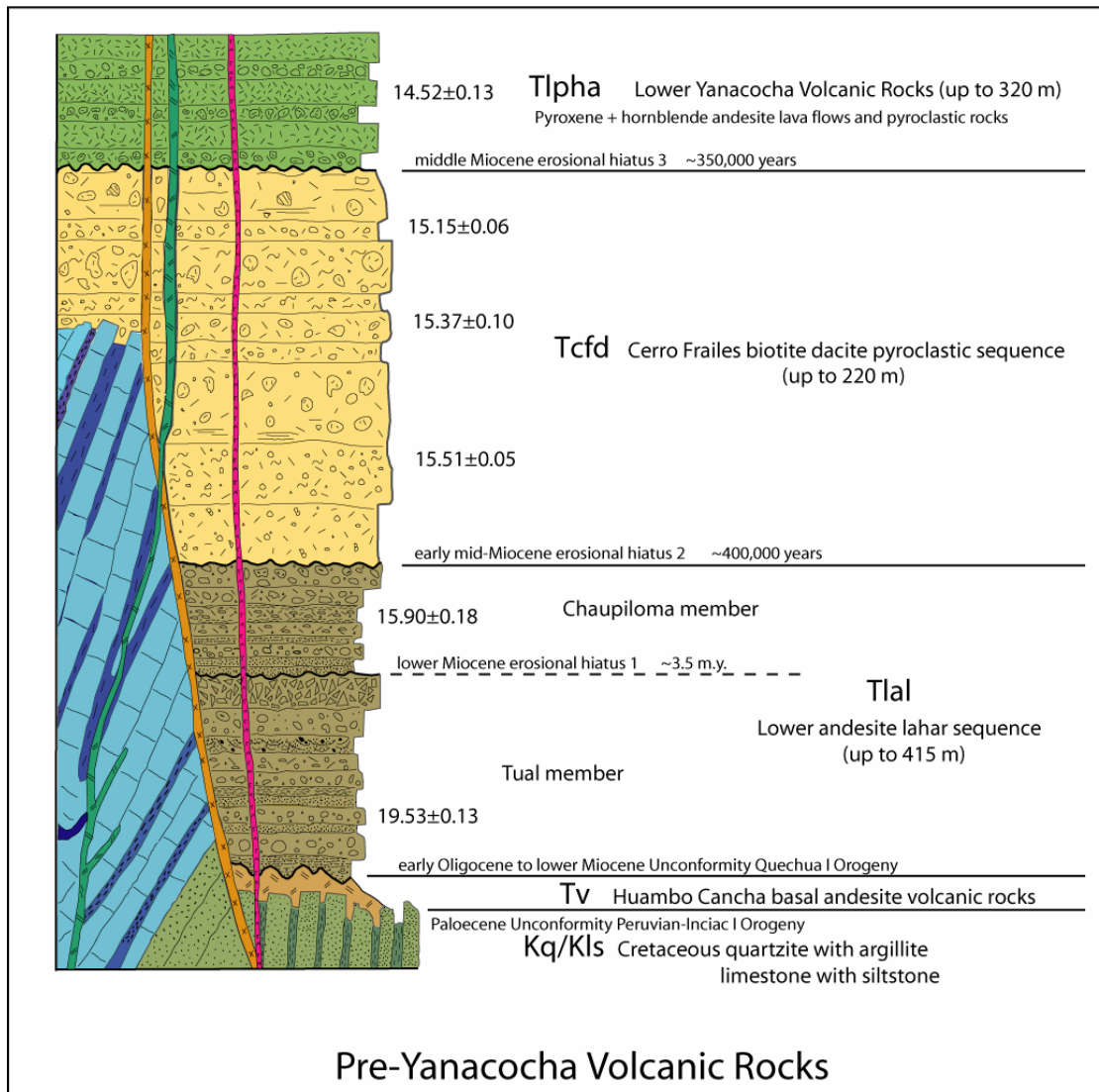
Figure 3.1. Stratigraphic section for the pre-Yanacocha volcanic rocks including the Middle Miocene Lower Yanacocha andesite volcanic sequence. Thicknesses in the section are schematic and do not represent true stratigraphic thicknesses. Unconformities and erosional gaps are included in the diagram based on field relationships and $^{40}Ar/^{39}Ar$ data shown (Longo et al., 2005; Chapter 2).
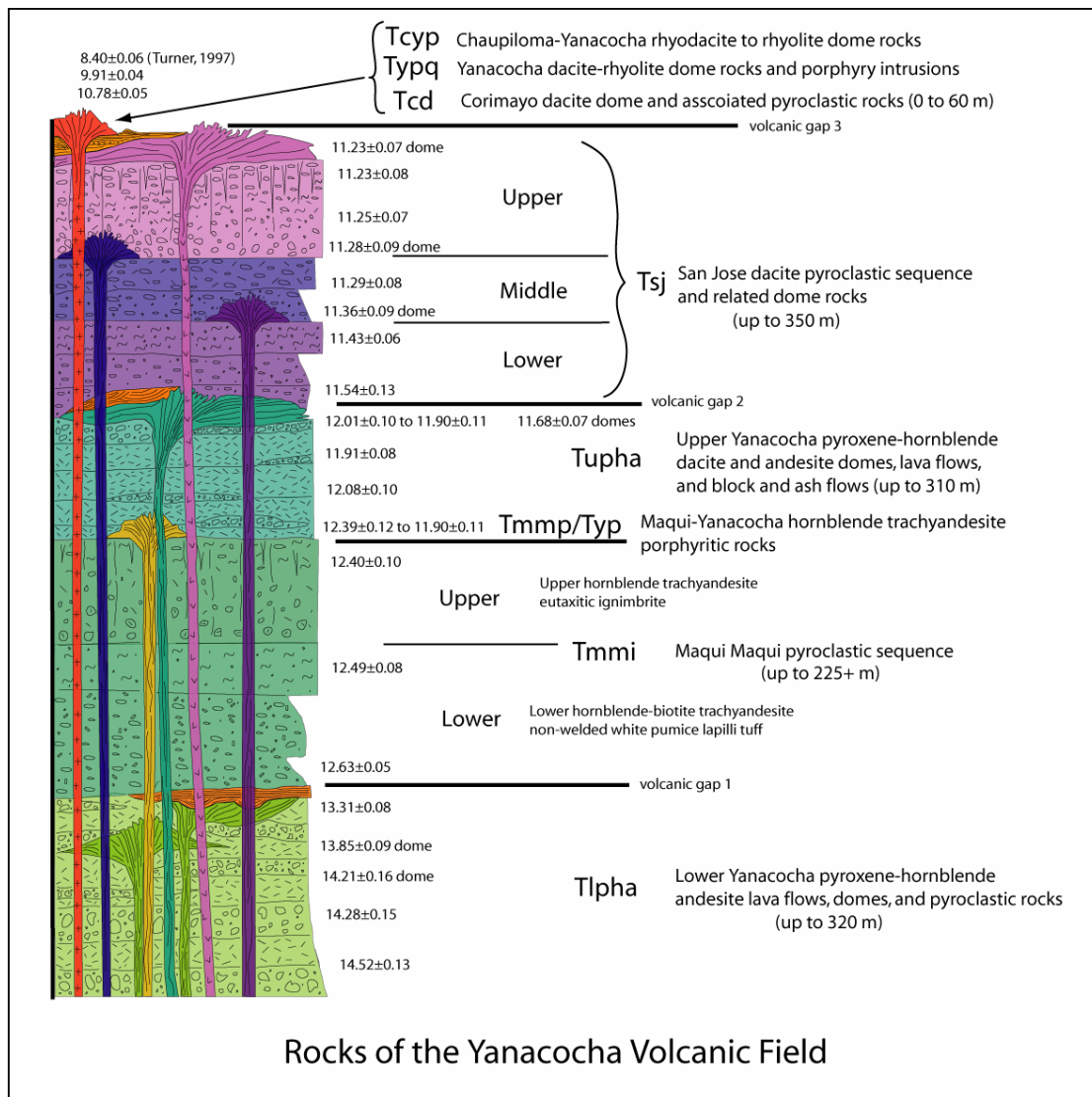
Figure 3.2. Stratigraphic section for the Middle Miocene Yanacocha Volcanic Field including the Upper Miocene late Yanacocha dacite domes and intrusions. Thicknesses in the section do not represent true stratigraphic thicknesses. Unconformities and erosional gaps are included in the diagram (Longo et al., 2005; Chapter 2).
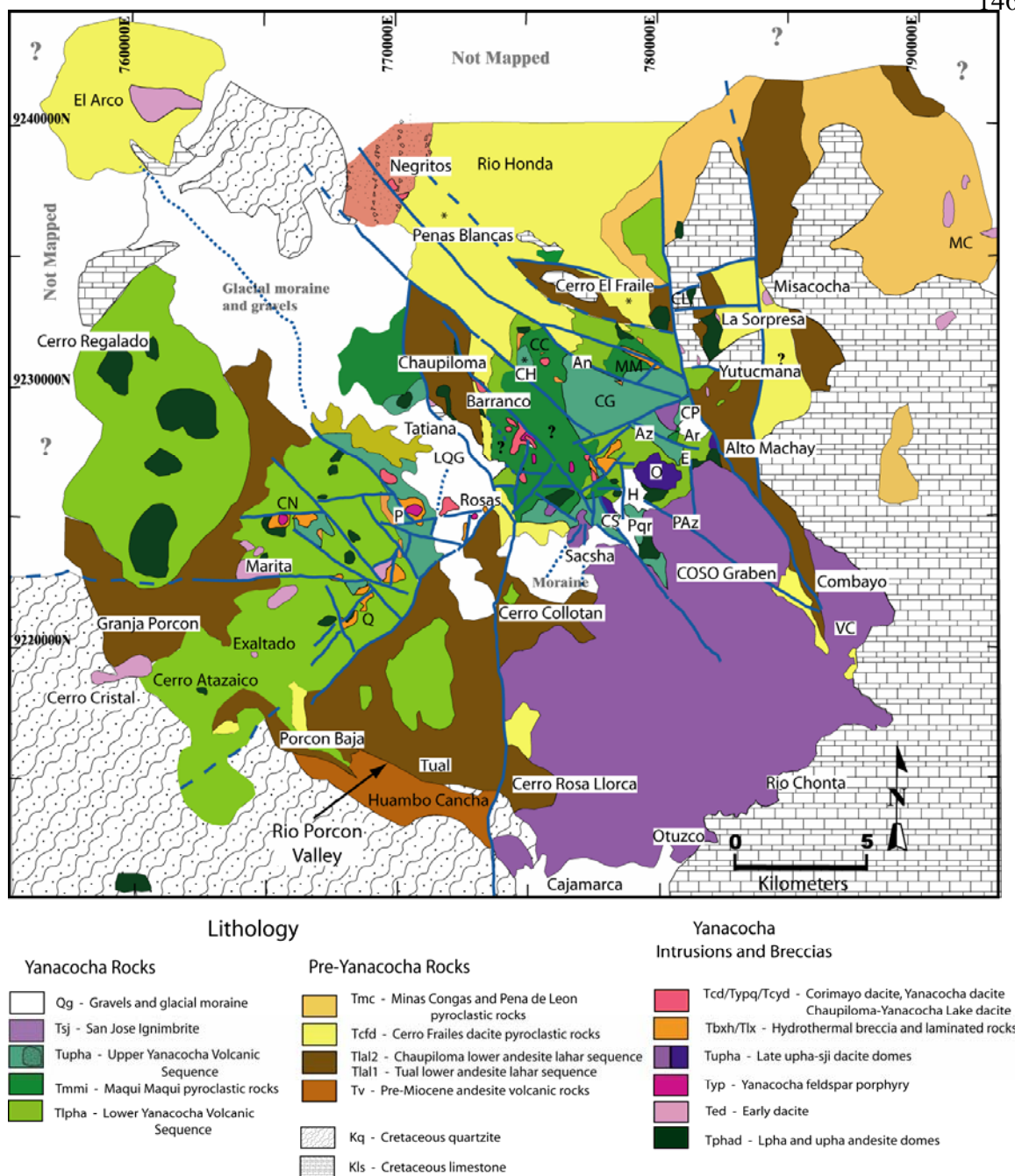
Figure 3.3. Generalized geology map of the Yanacocha district with locations discussed in the text. The geology is based on the 1:50,000 scale geologic mapping by A. Longo (Plate 1). CN Cerro Negro, Q Quilish, P Pabellon, LQG La Quinua Graben, CS Chaquicocha Sur dome, O Ocucho dome complex, Pqr Paquerumi, H Huacataz moraine, PAz Pozo de Azufre, E Elita, Ar Arnacocha, CP Cerro Pachanes, Az Azufre, An Antonio, CH Cerro Hornamo, CC Cori Cospha, CG Colorado Graben, MM Maqui Maqui, MC Minas Congas, VC Ventanillas de Combayo.

Pre-Yanacocha Volcanic Rocks

Three volcanic rock sequences in the study area were erupted and deposited before 15.0 Ma before the Yanacocha Volcanic Field and are considered pre-Yanacocha. These rocks consist of the following and are discussed below in detail: (1) the Huambo Cancha and Rio Porcon basal andesite volcanic rocks, (2) the Tual lower andesite lahar sequence and Chaupiloma lower andesite lahar sequence, and (3) the Cerro Frailes biotite dacite pyroclastic sequence.

Basal Andesite of Huambo Cancha and Rio Porcon

Porphyritic andesite and volcaniclastic rocks at Huambo Cancha and Rio Porcon overlie intensely deformed Cretaceous basement quartzite with angular unconformity. Volcaniclastic rocks are thin-bedded and fine-grained siltstones interbedded with pilotaxitic to coarsely porphyritic andesite lavas (Figure 3.3; Plate 1). These rocks crop out in the Rio Porcon Valley from Tual to Porcon Baja and cover an area of 10.5 km^2 in the study area. These rocks were not dated and are typically altered to clay with disseminated limonite and pyrite. They are considered pre-20 Ma since at Huambo Cancha they underlie an erosional disconformity overlain by debris flows and a pumice-rich andesite lahar of the Tual lahar sequence dated herein by ^{40}Ar/^{39}Ar at 19.5 Ma.

Reyes (1980) named these rocks, and most volcanic rocks at Yanacocha, as the San Pablo volcanic sequence of the upper Calipuy Group that overlie rocks of the lower Calipuy Chilete and Tembladera volcanics with a slight erosional disconformity. Volcanic rocks of the Calipuy Group have ages >43 Ma (Noble et al., 1990; and Benavides-Cacéres, 1999) and are also considered the Llama Volcanics by Wilson (1984) and Noble et al. (1990). Calipuy Group rocks display folding from deformation caused by orogenies younger than the Inciac I orogenic pulse in northern Perú (59-55 Ma; Noble et al., 1990; and Benavides-Cacéres, 1999). Deformation in the Huambo Cancha andesite sequence can be observed in road cuts below Huambo Cancha where folded volcaniclastic sediments are tilted up to 55° southwest. Reyes (1980) also described folds in volcanic sequences of the Calipuy Group at San Pablo, Chilete, and Tembladera.

Lower Andesite Lahar Sequence

Volcanic rocks of the Lower Andesite Lahar Sequence (LAL) overlie the Cretaceous basement with an angular unconformity and the basal andesite at Huambo Cancha with an erosional disconformity and slight angular unconformity (Figure 3.1 and 3.3). Lahars filled paleo-channels that down-cut the basal andesite and Cretaceous basement. This erosional disconformity can be observed in road cuts along the Cajamarca-Yanacocha-Bambamarca road below Porcon Baja. Thicknesses range from <100 to 430 meters (Figures 3.1 and 3.2, the fence diagrams in Figures 3.18 and 3.19; Table 3.1) across the district dependant on the paleo-topography. Typical outcrops are stratified thin- to thick-bedded, poorly-sorted, matrix-supported, and heterolithic hornblende andesite conglomerates with a variety of basement and andesite fragments. The sequence consists of two distinct packages of rocks designated the Tual lahar sequence (LAL-1) and the Chaupiloma lahar sequence (LAL-2). LAL-1 beds are tilted 10°-25° northeast in the Tual area and on Cerro Rosa Llorca above Cajamarca. LAL-2 beds are tilted 12°-35° northeast at Chaupiloma, 8°-20° northeast at Alto Machay-Yutucmana, and 5°-15° east southeast at Cerro Collotan east of Quebrada Rio Grande (Figure 3.3; Plate 1). LAL is regionally extensive and covers an area >420 km^2 (Table 3.1).

Mineralogy

Mineralogy of the sequence is typical of andesites in the Andean region (Tables 3.2 and 3.3; Figures 3.21-3.26 and A5.1c and d). Phenocrysts consist of plagioclase > amphibole > pyroxene > Fe-Ti oxides, and percent total phenocrysts vary between 14 vol.% in lava flows to 60 vol.% in the lahar matrix. Clinopyroxene is more abundant than orthopyroxene, and amphiboles are both green pleochroic with opacite rims and oxy-hornblende totally replaced with Fe-Ti oxides. Percent total mafics vary between 6 vol.% and 13 vol.%. Detrital quartz and alkali feldspar are present in debris flows at Chaupiloma. Opaque minerals are also quite variable from 2 to 10 vol.%, and up to 20 vol.% when the mafics are oxidized to opaques.

Age

The ^{40}Ar/^{39}Ar ages for LAL-1 and LAL-2 are 19.53 Ma and 15.90 Ma, respectively. Ages were determined on plagioclase from pumice in a basal LAL-1 lahar at Tual, and a glomeroporphyritic andesite lava flow near the top of the LAL-2 section north of Maqui Maqui.

Tual lahar sequence

The best exposures of the Tual andesite lahar sequence (LAL-1) crop out north of Cajamarca where numerous stratified debris flows form small cliffs and steep slopes with little vegetation in the hills east and north of Rio Porcon Valley and on Cerro Rosa Llorca above Hacienda Puruay, and covers an area of over 25.5 km^2 with thicknesses >230 meters (Figure 3.3 and 3.4; Plate 1). Rocks are distinctly stratified with a yellow-brown hue from yellow clay matrix-supported andesite conglomerates and debris flows, pumice-rich lahars, and volcaniclastic sediments. The base of the sequence is typically a yellow clay matrix-supported coarse boulder-rich heterolithic and bi-lithic hornblende-pyroxene andesite debris flows interbedded with channels of volcaniclastic sandstone, siltstone and pebbly conglomerates. Boulders are commonly flow-banded hornblende-pyroxene andesites that are rounded to sub-rounded which suggest extended transport and deposition distal from the source. Debris flows grade upward into numerous white pumice-rich heterolithic lahars separated by channeled and regularly bedded volcaniclastic siltstone. Toward the top of the sequence are resistant cliff-forming units consisting of nearly clast-supported angular to sub-angular andesite blocks with a sandy yellow clay matrix. East of Huambo Cancha is a white pumice-rich andesite lahar that lies above andesite debris flows and volcaniclastic sediments. This lahar is near the base of the sequence and has a ^{40}Ar/^{39}Ar age of 19.53 Ma.

Other exposures include a thick sequence (~250m) of andesite conglomerates that cover an area of <9 km^2 in Quebrada Rio Tinte north of Cerro Negro dominated by well stratified, medium- and thin- bedded andesite conglomerates that vary from matrix-supported to nearly clast-supported and suggest a transition between the lahar en masse flow regime of Smith and Lowe (1991) to the more turbulent stream flow regime (Figure A3.1). At least four types of sub-rounded fragments were identified in the conglomerates

and include a red "melaphyre-like" fine-grained hornblende andesite, a coarsely
porphyritic hornblende andesite, a black fine-grained basaltic-andesite, and rare quartzite.
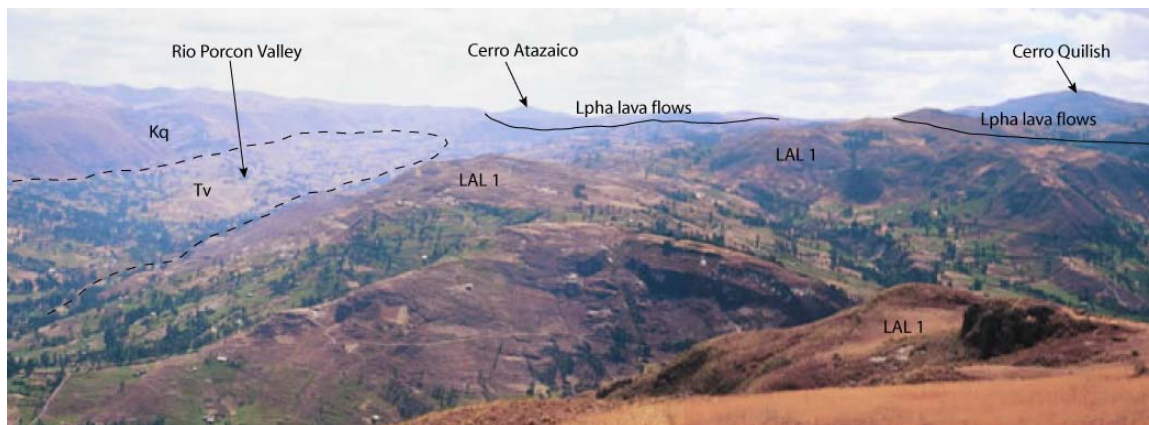
Figure 3.4. Photograph of the Tual lahar sequence (LAL-1) from Cerro Rosa Llorca
looking north to Cerro Quilish and Cerro Atazaico. The Huambo Cancha volcanic rocks
(Tv) underlie the LAL-1 and crop out in the Rio Porcon Valley. Cretaceous quartzite
forms the cliffs in the upper left of the photo. LAL-2 fill channels in the Tv below Lower
Yanacocha andesite lava flows (Lpha) lava flows at Cerro Atazaico. Cajamarca City lies
below and behind the observer.

Chaupiloma lahar sequence

The Chaupiloma andesite lahar sequence (LAL-2) consists of thick- to medium-
bedded hornblende-pyroxene (opx-dominant) andesite lahars, debris flows and
volcaniclastic sediments that are distinguished in the field from LAL-1 by color, outcrop
pattern and 1 to 3 meter thick, massive beds of poorly sorted volcaniclastic debris (Figure
3.4 and A3.2). Thick bedded and massive debris flows and lahars are characteristic of "en
masse" flow regime and deposition of gravity induced viscous mass flow breccia (Smith
and Lowe, 1991). Outcrops of LAL-2 are light gray to gray with maroon patches and
sometimes weather into columns called "Frailones" by locals at Alto Machay (Figure
A4.2, appendix IV; Figure 3.5). LAL-2 overlies the Cretaceous limestone in the east
district with angular unconformity and disconformably overlies LAL-1 and Huambo
Cancha volcanics in the west district. The best exposures of LAL-2 within the study area
include the following sites (Plate 1):

(1) Below Cerro Chaupiloma the LAL-2 crops out in some of the best exposures
along a 5.5 km strike length from Tatiana northwest to Cerro Cardón (Figure 3.5).

North of Tatiana the basal LAL-2 is intruded by pyroxene andesite dikes and a sill.

(2) Excellent exposures crop out above Combayo at Yutucmano and Alto Machay and overlie massive thick-bedded limestone (Figure A4.2, appendix IV). These outcrops are exposed over an area of ~10 km² from Combayo to Yutucmano.

(3) LAL-2 is exposed in stream channels below Marita at Granja Porcon and Exaltado, and west of Cerro Negro Oeste in Rio Tinte, and crop out over an area of ~6.5 km².

(4) East of Quebrada Rio Grande outcrops of LAL-2 are exposed over an area of ~9.5 km² centered over Cerro Collotan.

(5) North of Cerro Maqui Maqui in Quebrada La Viscacha and at Cerro El Fraile, exposures of the LAL-2 crop out below the Cerro Fraile dacite tuffs. A rare glomeorporphyritic andesite lava flow was dated at this site and has a ^{40}Ar/^{39}Ar age of 15.90 Ma.

(6) Minor LAL-2 lahar flows are also found channeled into the upper portions of LAL-1 and Huambo Cancha volcanics at Porcon Baja. These are exposed in the road cut along the Cajamarca-Yanacocha road.

Lahars of LAL-2 are poorly-sorted and heterolithic matrix-supported hornblende-pyroxene andesite interbedded with volcaniclastic sediments from pebble conglomerates to siltstone, and ash fallout that weathered to a claystone. Occasional hornblende andesite lava flows and flow breccia were observed in the sections at Cerro Collotan, Chaupiloma, and north of Cerro Maqui Maqui. Typically the lahars are matrix-supported and heterolithic debris flows with large sub-rounded maroon to blue-gray porphyritic andesite boulders up to +2m in diameter. Some boulders are flow-banded as in the LAL-1. In many areas thick-bedded andesite debris flows grade upward to hyperconcentrated mudflows intercalated with matrix-supported lithic tuffs with white pumice or primarily small ≤ 1cm-size fragments of coarsely porphyritic hornblende andesite and trachytic hornblende-pyroxene andesite. A generalized section of LAL-2 is best observed below Cerro Chuapiloma (Section F; Figure 3.18). Cretaceous limestone and red mudstone crop out north of Tatiana on the hanging wall to the northern splay of the La Quinua fault.

LAL-2 unconformably overlies the Cretaceous sediments with a basal sequence of ~80m with thick and massive beds of matrix-supported and poorly-sorted lahar flows. Beds are 1 to 3 meters thick with sub-rounded maroon to blue-gray and green-gray porphyritic andesite boulders up to +2m in diameter and occasional basement fragment. These are interbedded with 1-2 meter thick gray beds of matrix-supported and massive lahars with 0.5 to 3.0 cm-size pebbles of coarse porphyritic andesite, andesite porphyry, trachytic andesite lava, and volcaniclastic sediments. Similar fragmental textures have been found at the base of drill holes in Chaquicocha Sur (CHQ-97, ~475m) and Barranco (BS-27, ~500m) (Figure A 5.1, Appendix V). Above the basal lahars are a series of thin beds (thicknesses <1 meter) for over 20 meters in section of intercalated fine-grained white pumice-bearing and massive hyperconcentrated mudflows with 1-4% small (1-9mm) fragments of porphyritic andesite. The upper portion of the LAL-2 sequence (40 to 80 meters thick) is dominated by thick and poorly-sorted andesite lahars with rare interbedded laminated silts and porphyritic andesite lava flows.
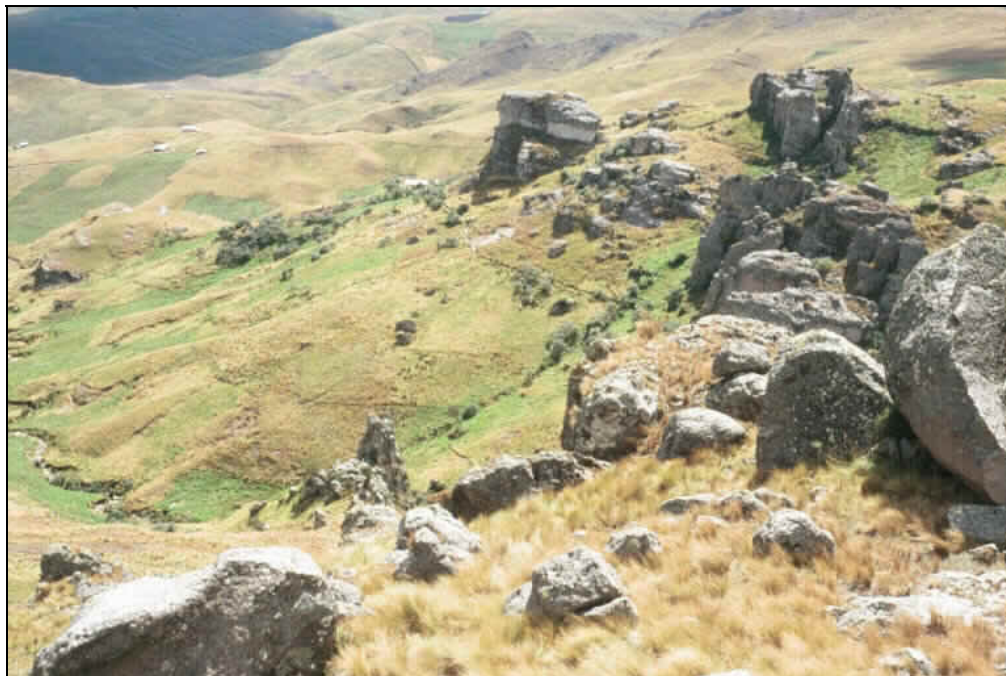
Figure 3.5. Photograph of typical outcrops of the Chaupiloma andesite lahar sequence below Cerro Chaupiloma looking northwest.

Cerro Frailes Dacite Pyroclastic Sequence

The Cerro Frailes dacite pyroclastic sequence (CFD) are biotite-rich dacite ash-flows and lahars with abundant coarse euhedral biotite crystals up to 0.5 cm in size. These rocks were previously classified Huambos Formation by Wilson (1984) and Turner (1997), or the Frailones Member of the Huambos Formation by the local geologists. Cerro Frailes dacite (CFD) rocks crop out regionally and cover an area of >300 km^2 from 5 km north of Cajamarca at Lluscapampa-Puruay, northeast 12 km to Quebrada Rio Azufre near Combayo, northwest 20 km in Quebrada Rio Honda to Cerro de los Negritos, and west 10 km to El Arco (Figure 3.3, Plate 1, Table 3.1). Thicknesses and areal distribution are strongly dependent on the paleo-topography. These rocks are most prominent in the northeast portion of the study area where they filled a north to northwest-trending paleo-basin that extends southeast into the Rio Colorado Graben (10 by 20 km). They overlie both the LAL-2 with an erosional disconformity and limestone basement rocks with an angular unconformity. In the south and west the CFD is confined to paleochannels and drainages. Thicknesses range from >200 meters in the large paleo-basin (Figures 3.1, 3.18 and 3.19 , sections F, G and H) to the northeast to <50 meters from flows in paleo-channels that cut into the LAL in the west district above Porcon Baja (Figure 3.18, section C) and in the southeast at Combayo (Figure 3.19, section J). The sequence is gently folded with regional inclinations in the flow units that vary from 12-40° north northeast to 8-25° east. Outcrops in Quebrada Rio Honda at El Camparario have near horizontal bedding (Figure 3.3, Plate 1).

Rocks consist of tuff, tuff breccia and pyroclastic breccia from both ash-flow tuffs and lahars (Figures A4.3, A4.4, A4.5; Appendix IV). The basal unit at Lluscapampa is a lithic-poor biotite tuff that overlies the LAL-1 of Cerro Rosa Llorca with an erosional disconformity. The biotite tuff is overlain by poorly welded, white pumice, biotite-rich ash-flow tuff rich in accidental fragments of basement rocks and porphyritic dacite. Other exposures of biotite-rich ash-flow tuff with white pumice crop out throughout the study area. These exposures were found near Combayo in Quebrada Azufre and Quebrada Rio Chonta below the Ventanillas de Combayo, ~12 km northwest at Maqui Maqui Norte, 3 km northwest of Maqui Maqui at Cerro El Fraile near the contact to LAL-2, ~5 km

northwest of Maqui Maqui in the bottom of Quebrada Honda, and at El Arco 18 km north west of Cerro Negro. Above the white pumice ash-flow tuff is a package of rocks found exposed only northwest of Maqui Maqui and at El Arco (Plate 1b). These rocks consist of a thick interbedded sequence of ash-flow tuffs and lahars with fragments of hornblende dacite porphyry, dacite tuff, trachytic andesite, basement quartzite and black argillite. The pyroclastic rocks are matrix-supported and poorly-sorted tuffs and lahars that display a crudely normally graded sequence. Lower flow units are pyroclastic breccia with a coarse heterolithic texture and fragment sizes that range from 1 cm to 3m. These crudely grade upward to lithic-rich tuff breccia with 1 to 10cm sized fragments. Some outcrops display a crude jointing pattern reminiscent of columnar jointing that weathered to large irregular free-standing columns the locals call "Frailones" (Figure A4.4b and c, Appendix IV). Lahars tend to be more prominent toward the base of the sequence and typically are matrix-supported with abundant sub-rounded fragments of porphyritic bioite-hornblende dacite and rare fragments of charred wood (Figure A4.3; Appendix IV). Ash-flow tuffs separated by surge deposits increase in frequency upward in the sequence, some surge layers also have remnants of charred wood (Figure A4.15; Appendix IV). Layered pyroclastic sequences with as many as seven to ten flow units of greenish-gray and pinkish-white pumice tuff are interbedded with lithic-rich pumice tuff. This sequence forms large cliffs with several ash-flows and surge units in one cooling unit at El Camparario in Quebrada Honda (Figure 3.3; Figure A4.4d, Appendix IV), and smaller cliffs with many separate and distinct flow units 2-8 meters thick that are partially welded and devitrified with remnant elutriation pipes and irregular columns at Peñas Blancas and Cerro Agua Blanca (Figure 3.3; Figure A4.5, Appendix IV).

Mineralogy

Mineralogy of the Cerro Frailes pyroclastic sequence is distinct and can be readily distinguished from all other rock packages in the Yanacocha district (Figures 3.21-3.26; Table 3.2a and 3.3a). Phenocrysts consist of plagioclase > biotite > quartz > hornblende > Fe-Ti oxides > alkali feldspar. Pyroxene, apatite and sphene are absent. Percent total phenocrystscan range from 20-50 vol.% and typically are ~30 vol.% of the total sample. Percent total mafic minerals range from 4 vol.% to 18 vol.% and typically are 11 vol.%

with abundant (up to 10 vol.%) coarse biotite (0.5 cm across when looking down the C-axis). Percent total biotite is generally higher than the percent total hornblende by four to one in a typical sample. Quartz is also diagnostic with total quartz phenocryst content that varies between 1 vol.% and 9 vol.%, but commonly is estimated at 6 vol.% in hand specimens from most ash-flows tuffs.

Age

Five $^{40}Ar/^{39}Ar$ ages determined from biotite and plagioclase are available for the Cerro Frailes pyroclastic sequence from Chaupiloma, Combayo, Maqui Maqui Norte and Cerro El Fraile. Ages range from 15.5 at Cerro El Fraile to 15.2 Ma at Maqui Maqui Norte.

Figure 3.6. Photograph of the eastern portion of the Yanacocha Volcanic Field from La Quinua to Carachugo from the Cumbe Mayo road west of Cajamarca. The San Jose ignimbrites unconformably overlie LAL-1 and Cretaceous quartzite and extend from Carachugo to Cajamarca City is an area called the COSO basin.

Yanacocha Volcanic Field

The volcanic rocks of the Yanacocha Volcanic Field (YVF) may be distinguished from the older Tertiary volcanic rocks in the area on the basis of grain size and phenocryst types and abundance. Rocks of the YVF are typically coarse-grained and phenocryst-rich (Tables 3.2 and 3.3; Figure 3.21) relative to pre-Yanacocha rocks (Figures A6.1 and A6.2; Appendix VI). The maximum dimensions of phenocrysts in YVF are frequently 2.5 to >5mm, and phenocryst abundances commonly total 50% or more. In contrast, percent total phenocrysts in pre-Yanacocha rocks are generally <40% and the maximum dimension of the largest phenocrysts are ≤3mm (Figure 3.21 and Table 3.3).

Phenocryst percents based on petrographic estimates of the modal mineralogy for each rock package in the YVF fluctuate with decreasing age (Figure 3.21). Percent total phenocrysts in lavas and domes of the Lower Yanacocha andesite sequence (Lpha) are similar to the Upper Yanacocha andesite-dacite volcanic sequence (Upha) and may represent true magma chamber abundances, but vary over wide ranges from 25 to 55 vol.%. Phenocryst abundances are less for rocks from the early dacite (~18 to 44 vol.%), Maqui Maqui intrusive rocks (~10 to 40 vol.%), and the late dacite (~24 to 43 vol.%) (Table 3.2 and Figure 3.21). Total phenocryst abundances increase in the pyroclastic rocks to >70 vol.% due to fines-depletion, and abundances are typically higher than and not representative of the magma chamber. Phenocryst abundances increase from the Maqui Maqui ignimbrite (~55%) through the middle San Jose ignimbrite (~65%), then decrease in the upper San Jose *spatter* ignimbrite (54%). Late dacite intrusions display low total phenocryst abundances similar to the Maqui Maqui porphyritic rocks and early dacite with ~30 vol% (Table 3.2; Figure 3.21). Overall, mafic minerals are most abundant in the Lpha and Upha rocks and decrease in abundance in the Maqui Maqui and San Jose ignimbrites (Figure 3.21). Pyroxene tends to decrease with decreasing age from the Lpha to the Maqui Maqui rocks (MMI) and again from the Upha to the late dacite. Pyroxene and hornblende are common in the Lpha, Upha, Lower San Jose ignimbrites and the Upper San Jose spatter ignimbrite, whereas pyroxene is absent to trace in abundance in the Maqui Maqui ignimbrite, Middle San Jose ignimbrites and white tuff, and the Upper

(late) Dacite (Table 3.2 and 3.3, Figure 3.21). Plagioclase is the most abundant mineral in all the rocks studied at Yanacocha. Quartz, sanidine and biotite are present in abundance only in the Upper (late) Dacite, common in the early dacite, and rare in the Middle San Jose ignimbrite and Maqu Maqui ignimbrite. In summary, the ranges of modal mineralogy and mafic versus felsic abundances fluctuate through time and mimick a pattern recorded by the successive and alternating effusive and explosive stages of volcanism.

Lower Yanacocha Volcanic Sequence

Volcanic rocks of the lower Yanacocha volcanic sequence include lava flows, flow breccias, and pyroclastic flows of pyroxene-hornblende andesite (Lpha) from an early stage of effusive eruptions that developed a large andesitic volcanic field across the district termed *effusive stage 1*. Present exposures of the Lpha volcanic field are scattered over an area of 340 km^2 from Cerro Regalado to La Sorpresa (Figure 3.3, Plate 1). The thickness of the Lpha varies considerably across the district from 200 and 300 meter sections of compound and multiple flows near vent areas at Cerro Atazaico, the Cerro Regalado dome complex, Cerro Quilish and Cerro Negro, and Cerro Pachanes-Arnacocha-Alto Machay to more distal sections with a lava flow only several meters thick (fence diagrams; Figures 3.18 and 3.19). Single lava flows filled paleo-channels from an erosional disconformity that downcut the pre-Yanacocha volcanic sequences (Figure A 4.7e, Appendix IV) at Porcon Baja, Porcon Alta, and northwest of Maqui Maqui, and represent distal expressions of the Lpha volcanic field. Lpha is absent in most areas outside of the district (Figure 3.19, section J). Effusive eruptions were followed by dome-building and minor pyroclastic eruptions of block and ash flows of quartz-bearing pyroxene andesite. These included the Cerro Regalado dome complex and domes at Quilish and Cerro Negro Oeste. Quilish domes include the sub vertical flow-foliated quartz-bearing andesite at Antibuyoc and hypogene advanced argillic altered remnants of the Cerro Quilish dome cross cut with hydrothermal breccia. Pyroclastic rocks are monolithic, poorly-sorted and clast-supported block and ash flows of porphyritic and trachytic pyroxene-hornblende andesite.

Two texturally distinct types of trachytic-textured pyroxene-hornblende andesite lavas crop out in the district. One flow type is fine- to medium-grained (phenocyrsts <2.5mm long) and dark gray with fine-grained pilotaxitic-textures in the ground mass, and the second type is medium-grained (phenocrysts from 1.0 to 5.0 mm long) with large plagioclase and hornblende phenocyrsts. Distinct flow foliations observed in the outcrop developed from the alignment of both phenocrysts and ground mass microlites. These foliations are not always obvious in outcrop and may reflect the more random orientation of phenocrysts characteristic of some lava flows. Edwards (2000) similarly reported two types of flow-banded andesites that he mapped as separate units in the west district based on phenocryst grain size.

In the west district, the Lpha volcanic sequence was tilted 20-48° to the northeast from Pampa de Cerro Negro to Quilish and Cerro Pabellon. Inclinations of flow foliations were measured in andesite lava flows throughout the west district (Plate 1). Over 60 measurements were collected from Lpha and Upha lavas and the strike directions vary from 50º west to 20º west with northeast dip directions. Laminated rocks interbedded between Lpha and Upha also strike northwest and dip northeast. Bedding in the LAL below the Lpha northwest and west of Cerro Negro strike northwest and dip northeast, and the lacustrine sediments below the La Quinua gravels also have bedding that strikes northwest and dips northeast similar to the lavas. The present inclination observed in the foliations from these areas is attributed to normal faulting that down dropped the section to the east into the La Quinua Graben (Plate 3; E-W cross section). Flow-banded Lpha lava flows are inclined 10-20° north northwest on the south flanks of Cerro Quilish, in Chilinpampa, and at Exaltado. In the east district, flow-banded lava flows dip 20-30° southwest at Pachanes and 14-25° south southeast along the ridge west of Elita where the San Jose pyroclastic rocks overlie the Lpha with an angular unconformity (Figure 3.20).

Mineralogy

Mineralogy of the Lower Yanacocha volcanic sequence is distinctive by the presence of abundant green clinopyroxene and acicular hornblende (Tables 3.2 and 3.3). These lavas are commonly flow-foliated with phenocrysts aligned in a trachytic texture with pilotaxitic-textured groundmass microlites (Figures A6.2, Appendix VI). This

texture can be readily distinguished from the pyroclastic sequences at Yanacocha that lack the pilotaxitic groundmass and distinct phenocryst foliation found in the lava flows (Figure A5.3 and A5.5; Appendix V). Rocks are phenocryst-rich (~50 vol.%; but ranges from 26 to 58 vol.%), and phenocrysts consist of plagioclase > pyroxene > hornblende > Fe-Ti oxides. Quartz, alkali feldspar, biotite, and sphene are absent. Accessory apatite is present in many samples examined petrographically. Percent total mafic minerals typically are 15 vol.% and range from 6% to 29 vol.%. In a typical sample, pyroxene is more abundant than hornblende. Quartz is rare but characteristic of the andesite domes in the west district. The Lower Yanacocha volcanic sequence is can be distinguished from the pyroclastic sequences in the Yanacocha district (Figure 3.21; Table 3.2) by its lower overall phenocryst abundance and lack of broken phenocrysts.

Age

It is my hypothesis that the Lpha volcanic field developed from effusive eruptions of numerous monogenetic volcanoes and small composite cones such as Cerro Atazaico (Figure A4.7a; Appendix IV). Effusive activity and subsequent dome-building progressed from west to east across the district as demonstrated by $^{40}Ar/^{39}Ar$ ages that span 1.2 Ma from 14.52±0.13 Ma in the west to 13.31±0.08 Ma in the east. Volcanism from effusive stage 1 was centered along three separate northwest trending linear vent areas from west to east as follows (Figure 3.3, Plate 1):

(1) The Quilish-Negro-Regalado trend of stratocones and dome complexes with $^{40}Ar/^{39}Ar$ ages that range from 14.52±0.13 to 13.85±0.09 Ma;

(2) The Chaupiloma trend defined by dikes and sills of fine-grained pyroxene andesite (no radiometric ages) at Cerro Yanacocha, Barranco, and Tatiana;

(3) The Sugares trend from Alto Machay, Cerro Pachanes to China Linda trend that includes erosional remnants of an Lpha stratocone and dikes at La Sorpresa and north at China Linda.

Lpha rocks in the east district at Cerro Pachanes, Arnacocha and Alto Machay may be remnants from a stratocone at Surprisa that existed as a topographic high during the explosive eruptions of the Maqui Maqui and San Jose Pyroclastic ignimbrite sequences. Presently the flow-banded lava flows dip 20-30° southwest at Pachanes and 14-25°

south-southeast along the ridge west of Elita where the San Jose pyroclastic rocks overlie the Lpha with an angular unconformity (Figure 3.11 and 3.20). These rocks have $^{40}Ar/^{39}Ar$ ages ranging from 13.72±0.17 Ma from a block and ash flow at Alto Machay to 13.31±0.08 Ma from pyroxene-hornblende andesite lava higher in the section east of Ocucho dome at Elita.
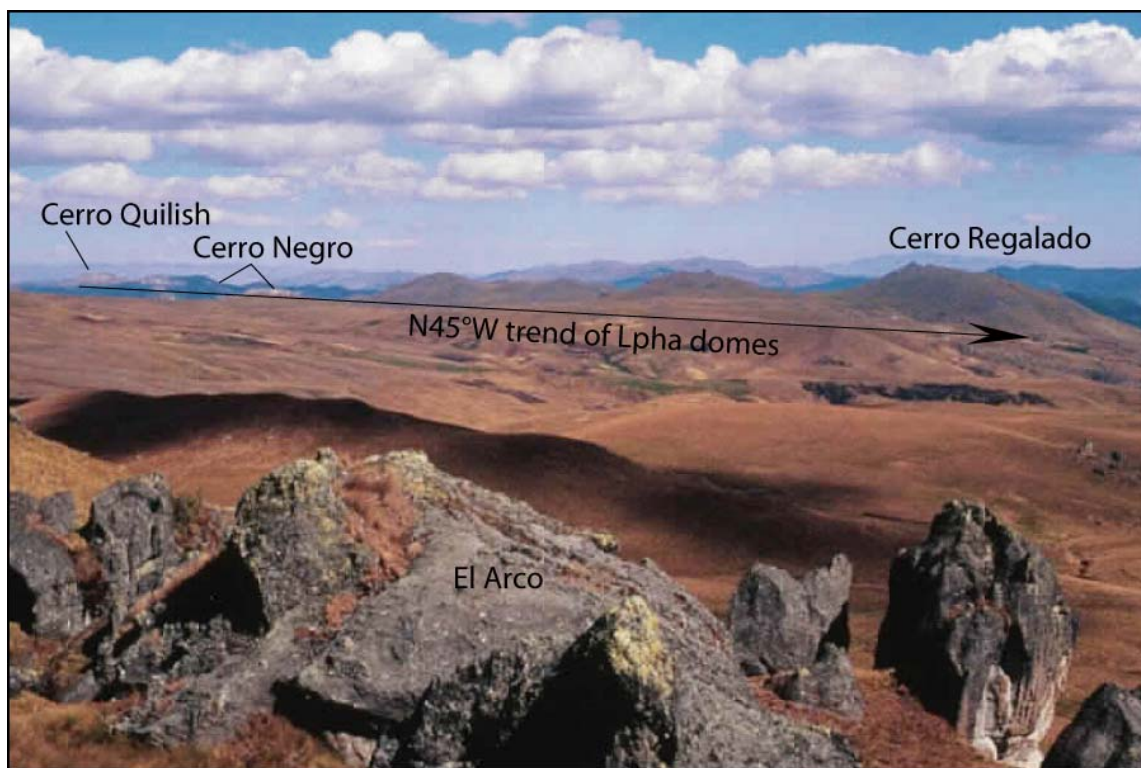
Figure 3.7. Photograph looking south of the Quilish-Negro-Regalado trend in the west district, the best preserved cluster of stratocones and dome complexes in the district. Effusive eruptions from monogenetic and small composite volcanoes were followed by later dome complexes that developed along a north and northwest trend from Cerro Regalado to Cerro Quilish (above). Effusive volcanism dominated and developed stratocones such as Cerro Atazaico from 14.5 to 14.2 Ma (Figures A3.7 and A3.15, Appendix III). By 13.85 Ma quartz-bearing andesite domes were extruded and dome complexes developed at Cerro Quilish, Cerro Negro and Cerro Regalado.
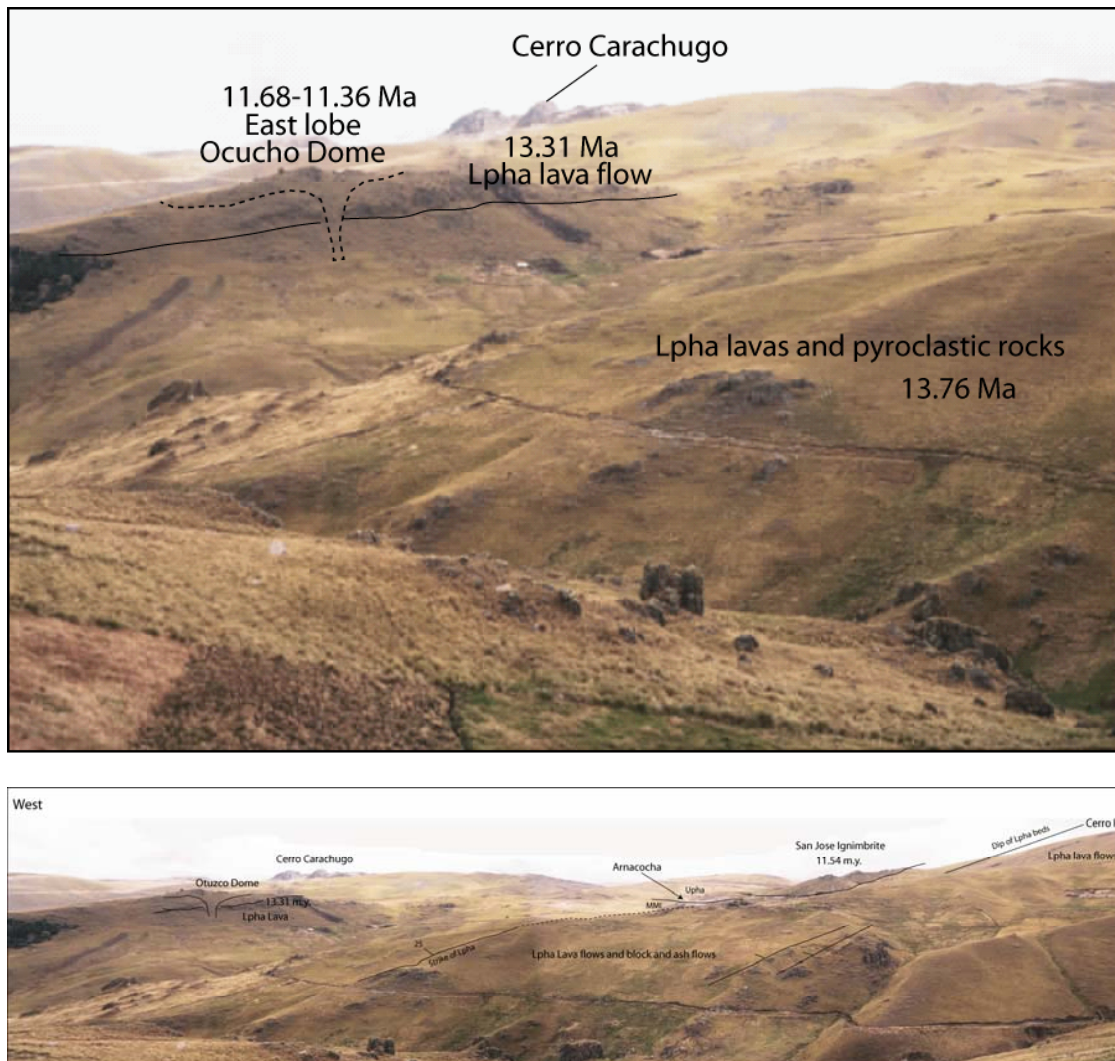
Figure 3.8. Both photographs are taken looking north-northwest from Alto Machay: (a) Photograph of the LPHA volcanic sequence in the east district from Machay dome looking northwest to Cerro Carachugo. The east lobe of the Ocucho dome (11.68±0.07 Ma) overlies and intrudes an andesite lava flow from the Lpha (13.31±0.08 Ma). Ages for the Ocucho dome complex range from 11.68±0.07 Ma to 11.36±0.09 Ma.
(b) Composite photograph of the Lpha volcanic sequence looking northwest from Machay. The view is an east to west section of the westerly-tilted Lpha volcanic rocks from Cerro Pachances through Arnacocha and the Ocucho dome. At Arnacocha the San Jose ignimbrite overlies the Lpha with an angular unconformity. Lava flows of the Lpha at Cerro Pachanes and east of Ocucho are tilted ~25° WNW.

Lower (Early) Dacite Intrusions

Overview and Age

Intrusions of porphyry dikes and plugs considered an early dacite are common in the west district and crop out along a northeast trend parallel to the Yanacocha trend for over 14 km from Cerro Cristal to Rosas. Lower (early) Dacite crops out 3.5 km west of Cerro Atazaico at Cerro Cristal and includes dacite intrusions at Mairita, Exaltado, Quilish, Rosas and a dacite porphyry plug in Quebrada Rio Grande (Figures 3.3; Plate 1). Dacite porphyry intrusions crop out at the Tatiana prospect 8 km north of the Rio Grande and Rosas dacite and intruded limestone and Lpha. Early dacite intrudes basement quartzite and LAL west of Atazaico; LAL and Lpha at Mairita; LAL, Cerro Frailes and Lpha at Exaltado; LAL and Lpha at Quilish; and LAL and Lpha in Quebrada Rio Grande. It does not appear to intrude Upha in the north Quilish area. Therefore, these rocks are younger than west district Lpha (14.5-14.2 Ma) but older than Upha (12.1 Ma) and possibly the Maqui Maqui Ignimbrite (12.6-12.4 Ma), and therefore have an inferred age between 14 and 12 Ma. No radiometric dates are available for early dacite intrusions and age relationships are based on field geology. Intrusive fragmental rocks called diatreme and feldspar porphyry rocks (Yp) that lack quartz eyes are spatially associated with the early dacite dikes and found along dike margins.

Mineralogy

Mineralogy consists of a phenocyrst suite with plagioclase > hornblende > quartz > sanidine > biotite > opaque oxides. Clinopyroxene, apatite and sphene are absent (Tables 3.2b and 3.3a). Phenocrysts typically are 34 vol.%, but vary between 19 and 44 vol.%. Percent total mafics vary between 5% and 12%. Quartz phenocyrsts are rounded and slightly embayed and range in size from 0.2-2.5mm. Overgrowth rims are common around quartz and alkali feldspar phenocrysts. Textures are typical of porphyry intrusions in that 30-40% phenocyrsts are surrounded by an aplitic groundmass (Figure A6.6; Appendix VI).

Sanidine-andalusite altered early dacite dikes also crop out at Yutucmana and La Sorpresa in the east district and intrude Cretaceous limestone and LAL-2. Outcrops of

intrusions are aligned northwest for 2.25 km from Yutucmana, but their occurance outline a continuation of the larger Yanacocha northeast trend for an additional 4 km to the Misacocha porphyry (Figure 3.3, Plate 1).

Maqui Maqui Pyroclastic Sequence

The Maqui Maqui pyroclastic sequence (MMI) was separated into three members known as the basal laminated rocks, the Cori Coshpa ash-flow tuff, and the Maqui Maqui ignimbrite (Figure 3.2). Ash-flow tuffs represent early explosive eruptions classified *explosive stage 1* that post-date the Lower Yanacocha volcanic sequence and overlie laminated rocks that include a variety of thin-bedded, hydrothermally-altered, tuff-like deposits and thinly laminated, very fine-grained, accumulations of chalcedonic silica (Figure A6.8; Appendix VI). Intrusions of porphyritic hornblende trachyandesite and dacite porphyry were emplaced into the ignimbrites Figure A6.4c and d; Appendix VI). Most of the sequence crops out in the Colorado graben from Maqui Maqui southwest across Cerro Rumi Guachac to Cerro Barranco (Plate 1), but is probably an erosional remnant that presently covers an area of 90 km^2 in the east district. Isolated outcrops of quartz-alunite altered, eutaxitic-textured rock with accidental fragments of massive silica overlie the coarse biotite-bearing Cerro Frailes dacite tuff (Plate 1; Figure 3.19, section K) and cap Cerro Collotan at Angelita, and are likely parts of Maqui Maqui. Other rocks related to the MMI include quartz-bearing tuffs, thin-bedded tuffaceous rocks, and tuffaceous lacustrine sediments that overlie the Lpha west of Cerro Pabellon, below Cerro Canta, and above Quebrada Corimayo at Quilish Norte. MMI was not observed west of Cerro Canta. MMI at Cerro Hornamo, Barranco, and in the Colorado Graben dip 10-30° southeast and those at Cerro Pabellon and north of Quilish dip 13-45° east northeast similar to the underlying Lpha lavas.

Thicknesses of the MMI are strongly controlled by the paleo-topography and range from ~90 meters from eroded sections at Chaupiloma and Angelita (Figures 3.18 and 3.19, sections F and K) to a complete section of 230 meters in the Colorado graben (Figure 3.18, section I). I propose thicknesses of ~ 220 meters at Cerro Yanacocha, over 160 meters at Chaquicocha, and 100 meters at Arnacocha where the MMI thins over a paleo-topographic high from an Lpha stratocone (Figures 3.18 and 3.19; Table 3.1).

Hydrothermal alteration of the volcanic rocks is intense in these three areas and the recognition of specific volcanic units is based on surrounding field geology and textural relationships of the rock packages in core from various drill holes (CD Plate 1, drill section map). MMI rocks may also lie at depth in the Corimayo-Tapado section (Figure 3.18, section E); however, these too are hydrothermally altered with intense hypogene advanced argillic and intermediate argillic alteration.

Mineralogy

Mineralogy and textures of MMI rocks are distinct from pyroxene-hornblende andesite lavas and can be distinguished in the field by the lack of pyroxene, the presence of occasional biotite, lack of pilotaxitic textures, and abundant broken phenocrysts. Eutaxitic texture is common but not always present. Phenocrysts consist of plagioclase > amphibole > opaque oxides > biotite with rare quartz and alkali feldspar. Pyroxene is generally absent or present in trace amounts. Apatite is commonly large, striated and cloudy (Table 3.2a). Total percent phenocryst abundance is generally higher and commonly 55 vol.% but ranges from 40 to 68%. In thin section it is common that the plagioclase phenocrysts are shock fractured (Figure A6.3e and f , Appendix VI; Table 3.2a). MMI intrusions frequently have abundant coarse hornblende with phencyrst to >10mm (Table 3.2a; Figure A6.4c, Appendix VI). The maximum dimensions of hornblende phenocrysts in MMI ash-flow tuffs are smaller than hornblende in the San Jose ignimbrite (Table 3.2a).

Age

Explosive eruptions of the Maqui Maqui pyroclastic sequence (MMI) spanned at least 230,000 years based on radiometric $^{40}Ar/^{39}Ar$ ages from three ash-flow tuffs that range from the Cori Coshpa tuff with an age of 12.63±0.05 Ma to the Maqui Maqui ignimbrite with ages of 12.49±0.08 Ma and 12.40±0.10 Ma. Two additional dates on unaltered rocks at the Cerro Yanacocha Au deposit place temporal constraints on the volcanic rock package that hosts ore, and implies an age similar to the Maqui Maqui sequence for rocks at Cerro Yanacocha. A fine-grained trachytic andesite dike (YSBD; known as Yanacocha black dike; Figure A5.4a) intruded fragmental rocks that host ore at at Cerro Yanacocha in the Yanacocha Sur sub-deposit area and has a $^{40}Ar/^{39}Ar$ age of

12.09±0.08 Ma. Fresh porphyritic hornblende andesite lavas (known as the Yp sill at Yanacocha Sur) cropped out on the surface above 4050 meter elevation on Cerro Yanacocha (now mined below the origin surface elevations) and have a $^{40}Ar/^{39}Ar$ age of 12.39±0.12 Ma. These rocks lay adjacent intense alteration and are underlain by ore of the Cerro Yanacocha deposit. Therefore, volcanic rocks at Cerro Yanacocha are older than ~12.1 Ma and may have an upper age of ~12.4 Ma similar to the youngest age of the Maqui Maqui pyroclastic sequence. This suggests that andesite effusive activity at Cerro Yanacocha may have coexisted with the final explosive eruptions of the Maqui Maqui ignimbrite.

Laminated Rocks

Siliceous laminated rocks lie at the base of the Maqui Maqui pyroclastic sequence (MMI) and are intercalated with fine-grained tuff and volcaniclastc sediments related to the Maqui-Maqui pyroclastic sequence (Figure 3.2). These rocks are distinctly laminated to thin-bedded and from range from 0-20m thick at the base of the MMI sequence at Cori Cospha, Maqui Maqui, and Arnacocha (Figure 3.3; Plate 1; Figure 3.18, sections G, H, and I). Kaolinite- and opal-altered thin-bedded to laminated tuff and tuffaceous sediments crop out at the base of the Cori Cospha ash-flow tuff north of Cerro Hornamo at Cerro Las Viejas. Siliceous and chalcedonic laminated rocks and thin-bedded tuff also crop out at the base of the Maqui Maqui ignimbrite east of the Maqui Maqui Norte deposit and at Arnacocha. Outcrops of thin-bedded tuff and lithic tuff with accidental quartzite fragments overlie porphyritic rocks interpreted as Lpha at Ocucho Machay (Figure 3.3, Plate 1). Localized outcrops of siliceous laminated rocks are scattered over a distance of 2.5 km within altered rocks interpreted as Maqui Maqui ignimbrite and stratigraphically above the Cori Coshpa ash-flow tuff. These rocks crop out southwest of Antonio across Cerro Rumi Guachac to Yanacocha Norte. Longo (2000) interpreted the thinly laminated chalcedonic rocks as accumulations of colloidal silica that were deposited in acid lakes associated with hydrothermal and volcanic vent areas.

Edwards (2000) reported a basal sequence of laminated water-lain tuffs and planar-laminated, massive, and cross-bedded surge deposits below quartz-bearing pyroclastic rocks at Cerro Pabellon, and considered it as one rock package underlain by

the porphyritic andesite. This andesite may be Lpha and is overlain by quartz-bearing tuff and other porphyritic andesite. The entire sequence is tilted 15 to 45° east northeast (similar to the underlying Lpha that is tilted 25-48° east northeast) and has a strike length of 2.6 km that extends south to Quilish Norte (Figure 3.9; Plate 1). At Quilish Norte, the
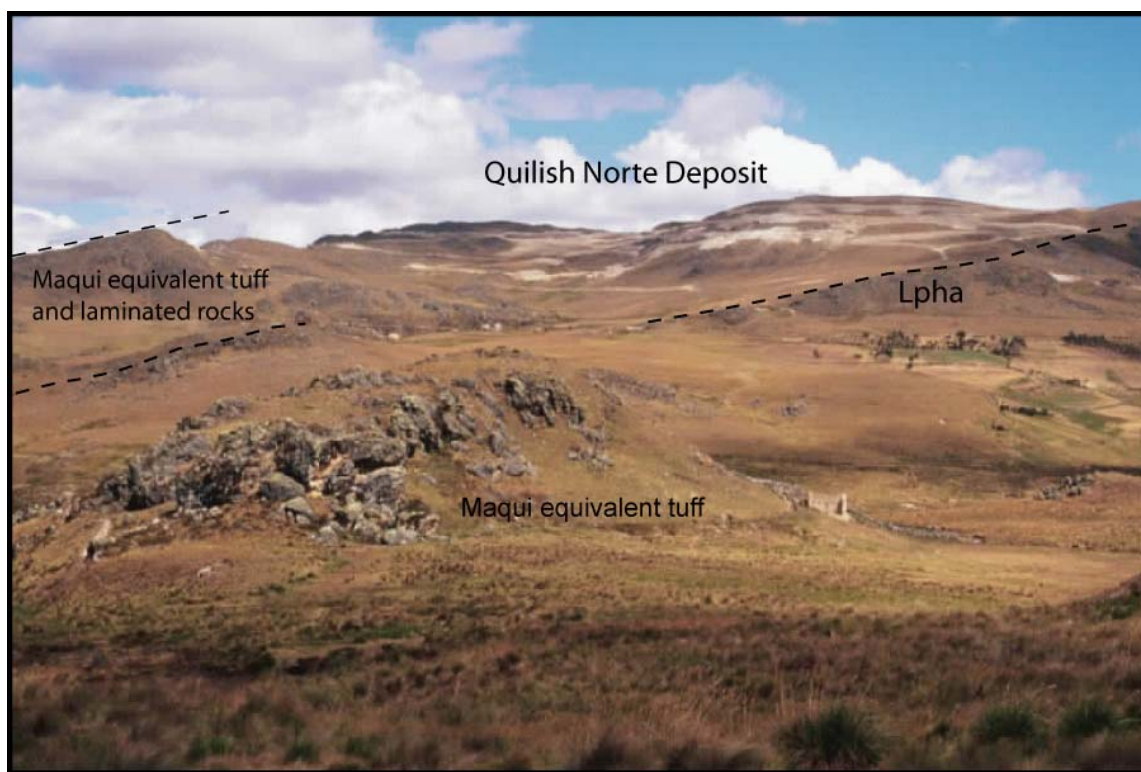
Figure 3.9 Photograph looking south to Quilish Norte from Cerro Canta of the Lpha lava flows overlain by a quartz-bearing pyroclastic sequence. The pyroclastic rocks are quartz-bearing tuffs intercalated with laminated rocks interpreted as temporally equivalent to the Maqui Maqui pyroclastioc sequence. These rocks are hydrothermally altered to assemblages that vary from argillic to advanced argillic quartz-alunite and varieties of residual quartz from massive to granular. The stratigraphic section is tilted east as indicated by the dashed lines along bedding.

laminated rocks are interbedded with quartz-bearing tuffs and overlie porphyritic andesites of the Lpha. The sequence thickens to the north where Edwards (2000) estimated a thickness of up to 200 meters for the entire laminated and quartz-bearing sequence. This study estimated thicknesses that range from 22 meters at Quilish Norte to 130 meters at Cerro Pabellon, and these rocks represent the western-most extent of the MMI in the Yanacocha Volcanic Field. Laminated rocks with interbedded quartz-bearing

tuffs are here interpreted to represent the base of the Maqui Maqui pyroclastic sequence, and can be a useful stratigraphic marker.

Cori Coshpa ash-flow tuff (Lower MMI)

The Cori Cospha trachyandesite tuff is the lower of the two ash-flow tuffs of the Maqui Maqui pyroclastic sequence (MMI). It crops out at Cerro Las Viejas and Cori Cospha where it overlies laminated rocks. Mafic minerals are hornblende and biotite, and pyroxene is absent. Biotite phenocrysts are prominent in hand sample and consistute 1.5 to 2 vol.% with phenocrysts sizes that range from 0.8 to 1.5mm (Tables 3.2 and 3.3). The flow is 40-60 meters thick and inclined 15-25° southeast at Cori Cospha (Figure 3.10). It is a light grey to white, non-welded and fines-depleted tuff with 20-25% white pumice fragments that have 25-30% phenocrysts versus 40-50 vol.% crystals in the ashy groundmass matrix (Table 3.2a). Accidental fragments include dark grey laminated and
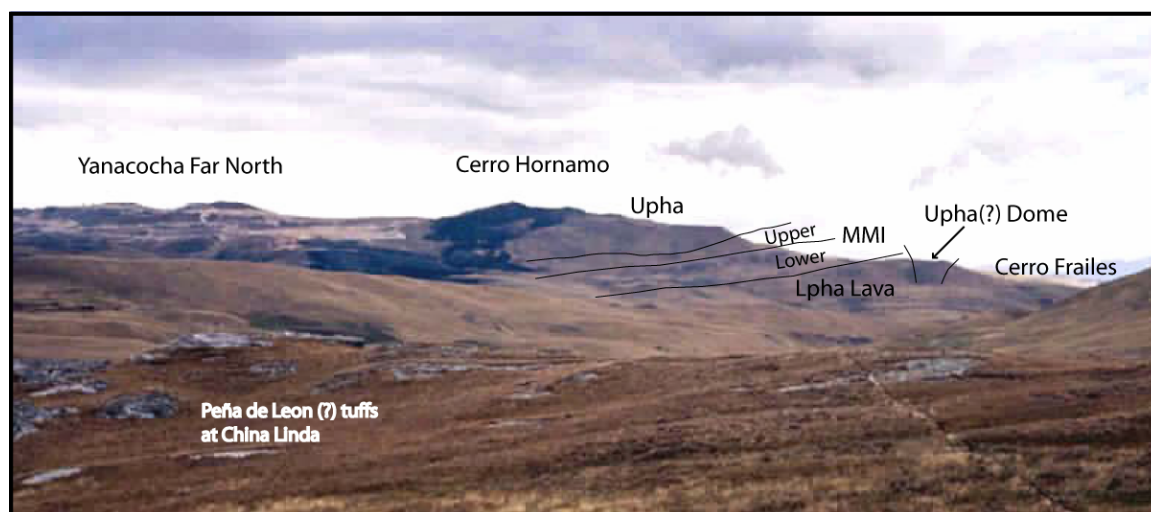
Figure 3.10 Photograph looking west from China Linda to a north-south view of the stratigraphic section from La Cospha through Cerro Hornamo. The Maqui Maqui pyroclastic sequence (MMI) overlies laminated and thin-bedded tuffaceous rocks that are underlain by lavas of Lpha intruded by Upha domes. The entire MMI section is tilted south below the Upha at Cerro Hornamo as indicated by the black lines.

massive argillite and quartzite from the Cretaceous basement, and fragments of porphyritic andesite (Figure A4.8; Appendix IV). The Cori Cospha ash-flow overlies "laminated rocks" including thin-bedded tuffaceous rocks (1-6cm thick beds) interbedded

with thin laminated chalcedonic rocks. The base of the flow is locally altered to quartz-alunite. An $^{40}Ar/^{39}Ar$ age determined on biotite is 12.63±0.05 Ma.

Maqui Maqui Ignimbrite (Upper MMI)

Ash-flow tuffs classified the Maqui Maqui ignimbrite belong to a single cooling unit whose thicknesses were highly dependant on the pre-eruption paleo-topographic setting and late Cenozoic erosion. These tuffs are the upper member of the Maqui Maqui pyroclastic sequence and the final eruptive sequence from explosive stage 1; they overlie the Cori Coshpa ash-flow tuff. The stratigraphic field relationships with the lower Cori Coshpa tuff are covered by talus from the Upha of Cerro Hornamo and alluvium with ichu grass. A series of faults bound the Colorado Graben and complicates the section.

Distinctions between the upper and lower members can be observed in the field by walking from Cori Cospha tuff (DN-30) to the fresh Maqui Maqui ignimbrite (DN-7) at a hill east of Chaupiloma and Barranco adjacent the main assess road. Charateristics observable in the field include mineralology, color, lithic abundance, and degree of welding. Typically, the Maqui Maqui ignimbrite is a dark grey to grey-brown, welded, eutaxitic-textured, crystal-rich hornblende±biotite dacite ignimbrite with minor <1-2% accidental fragments of black argillite, quartzite, and porphyritic rocks that are <1-5 cm in size (Figures A5.2, A 5.3, A 5.5; Appendix V). In contrast to the lower member Cori Cospha ash-flow tuff, the Maqui Maqui ignimbrite has only trace biotite. Some flows within the cooling unit lack distinct eutaxitic texture and are distinguished from lavas flows by the presence of abundant broken phenocyrsts and no distinct trachytic textures (Figure A6.3, Appendix VI). Ignimbrite thicknesses range from >80m at Angelita, to ~100 meters at Arnacocha, and up to 200 meters in the Colorado graben (Figures 3.18 and 3.19; sections H, I and K). Eutaxitic textures are coarse and distinct with flattened pumice that range from <1 to 10 cm in length with aspect ratios (L/W) from 3/1 to 4/1 (Figure A5.3; Appendix V). The ignimbrite crops out at Maqui Maqui, Arnacocha, north of Yanacocha Norte between Cerro Barranco and Cerro Rimi Guachac, and south of Cerro Collotan at Angelita. It hosts Au-ore at Maqui Maqui, Arnacocha, and possibly, Carachugo and Chaquicocha Sur.

Two ^{40}Ar/^{39}Ar dates (Table 2.1) were obtained from plagioclase separates in samples collected at separte sites, and yield ages from 12.49±0.08 to 12.40±0.10 Ma.

Upper Yanacocha Volcanic Sequence

Lava flows of the upper Yanacocha volcanic sequence represent late effusive eruptions of pyroxene-hornblende andesite and dacite (Upha) called *effusive stage 2*. Rocks are primarily porphyritic and trachytic-textured andesite and dacite lava flow, domes and pyroclastic flows. Typically the lavas are flow-banded and intercalated with discontinuous beds of monolithic pyroclastic breccia and autobrecciated blocky lava flows (Figure A4.10: Appendix IV). Mafic minerals are clinopyroxene, orthopyroxene, and hornblende with a distinct lack of biotite. Texturally and mineralogically, the Upha lavas are very similar to Lpha lavas and difficult to distinguish in the field. Differences are found in the geochemical composition, mafic mineral abundances, ^{40}Ar/^{39}Ar age, and stratigraphic position, most of which are not discernable in the field. The chief distinction is that Upha lavas are have less pyroxene and less total mafic minerals than Lpha lavas (Figure 3.21; Tables 3.2 and 3.3). Furthermore, the Upha compositions are commonly dacitic, or in the high silica and high potassium range of the andesite field, whereas, the Lpha rocks always have andesite compositions. In general, pyroclastic deposits are more abundant in the Upha than in the Lpha. These rocks erupted district-wide over an area of 60 square kilometers from Pampa Cerro Negro in the west to Alto Machay in the east (Figure 3.3, Plate 1).

Upper Yanacocha volcanic rocks (Upha) were recognized in several areas scattered across the district, and they are absent from some sections (Figures 3.18 and 3.19; fence diagrams) due to late Cenozoic erosion and pre-eruption paleo-topographic highs. Porphyritic rocks interpreted as Upha are preserved in the la Quinua graben below the gravels where thicknesses range from 100 to 280 meters (Figures 3.18 and 3.19; fence diagram; CD Plate1; drill hole map). Lava flows crop out from Pampa Corimayo to Pabellon and northwest below the La Quinua-Cerro Negro Leach Facility to the bypass road and entrance gate. Lava flows were found below gravels northwest of Corimayo in diamond drill holes COR-7, PAB-19, and PAB-25 (CD Plate 1, map of drill hole sections in the CD appendix) and may extend below the gravels for 1.5 km south to Quebrada

Encajon and 4 km north to Shoclla. Upha rocks of the La Quinua graben crop out within an area of 5.5 km^2, but may extend over greater distances below La Quinua gravels.

Lava flows classified as Upha also crop out at Cerro Negro Este where an erosional remnant covers a 1 square kilometer with thicknesses estimated at 50 meters. In the Colorado graben west of Maqui Maqui, outcrops of Upha cover an area of 8.8 square kilometers with thicknesses that range from 50 to 110 meters (Figures 3.18 and 3.19, . fence diagram; Plate 1; CD Plates 1 and 2, drill hole map and stratigraphic section map). At Chaquicocha, Baul, and San Jose thicknesses range from 100 to >110 meters over an area of 2.8 km^2 (Figures 3.18 and 3.19, fence diagrams).

Remnants of eroded domes are clustered along a westerly trend for 3.5 km from Pampa Corimayo to Cerro Negro Este and northerly for 4.0 km into Pampa Cerro Negro (Figure 3.3, Plate 1). These domes intruded Lpha lava flows, and Upha lavas and pyroclastic rocks directly overlie Lpha lava flows (Figure 3.18, section C; Plate 3, E-W cross section). Domes are clustered in a northeast trend for 6.5 km from San Jose and Quebrada Sacsha to Machay and include the San Jose dome, the Montura dome, the Sacsha Dome, the Chaquicocha domes, the early Ocucho dome, and Machay dome. Domes with Upha conpostions predate the ignimbrites of the San Jose ignimbrite sequence. A disconformable contact can be observed where a San Jose basal ground layer breccia ignimbrite overlies and preserved the Machay dome (Figure A4.13; Appendix IV) in the southeast portion of the district. Several eruptive episodes are represented in younger domes at Alto Machay, Chaquicocha Sur and Ocucho that post-date and intrude older altered domes. An example is best observed in the Ocucho dome complex where a younger fresh dacite dome complex intruded an earlier advanced argillic altered porphyritic dome rock (Figure A 6.7a; Appendix VI).

Mineralogy

The mineralogy and textures of the Upper Yanacocha volcanic sequence (Upha) are similar to the Lower Yanacocha volcanic sequence (Lpha) which causes a problem distinguishing the two in the field. Subtle differences that may assist in field identification include the following criteria (Tables 3.2b and 3.3a): (1) maximum

dimensions in phenocrysts are distinctly larger in the Upha (2.5-5mm) versus Lpha (1-3mm), (2) hornblende phenocrysts are bimodal in Upha with small acicular laths (<0.75mm) and prominent prismatic crystals (>1mm), and (3) generally hornblende abundances in Upha are greater than the overall pyroxene abundance (Table 3.2b, Figure A6.2, Appendix VI). Phenocrysts consist of plagioclase > hornblende > pyroxene > Fe-Ti oxides. Quartz, alkali feldspar, biotite, and sphene are absent. Apatite and zircon are present and more common than observed in the Lpha.

Age and Interpretations

Eruptions of the Upper Yanacocha volcanic field are bracketed stratigraphically by the Maqui Maqui ignimbrite dated at 12.49±0.08 to 12.40±0.10 Ma and the lower age for the San Jose ignimbrite dated at 11.54±0.09 Ma. A total of six samples were dated that represent the Upha (Plates 4 and 5). Three $^{40}Ar/^{39}Ar$ dates came from andesite lavas and tuffs from the west district and east district, and all have similar ages from 12.09±0.10 to 12.05±0.11 Ma. Three other samples from the east district, dacite and andesite lavas and domes in the sequence range from 12.01±0.10 to 11.68±0.07 Ma. The Upha volcanic field developed by effusive eruptions from monogentic andesite vents and numerous andesite lava domes. These eruptions were followed by coalescing domes of dacitic composition with coulées (thick extrusions of endogenous or exogenous dome growth that erupt on a slope and flow down hill) and tortas (low flat domes with endogenous growth in flat areas) that developed east-west, north and northeast trending dome fields as described above. Large coulées, such as the Chao dacite in northern Chile (Guest and Sanchez, 1969), have developed dacite lava flows that cover 90 square kilometers up to 300 meters thick and flow 15 km down slope. At Yanacocha, dacite lavas erupted from multiple-vent complexes with small coulée-style effusive eruptions overprinted by small pyroclastic eruptions and successive flows of dacite lava that covered a total area <60 square kilometers.
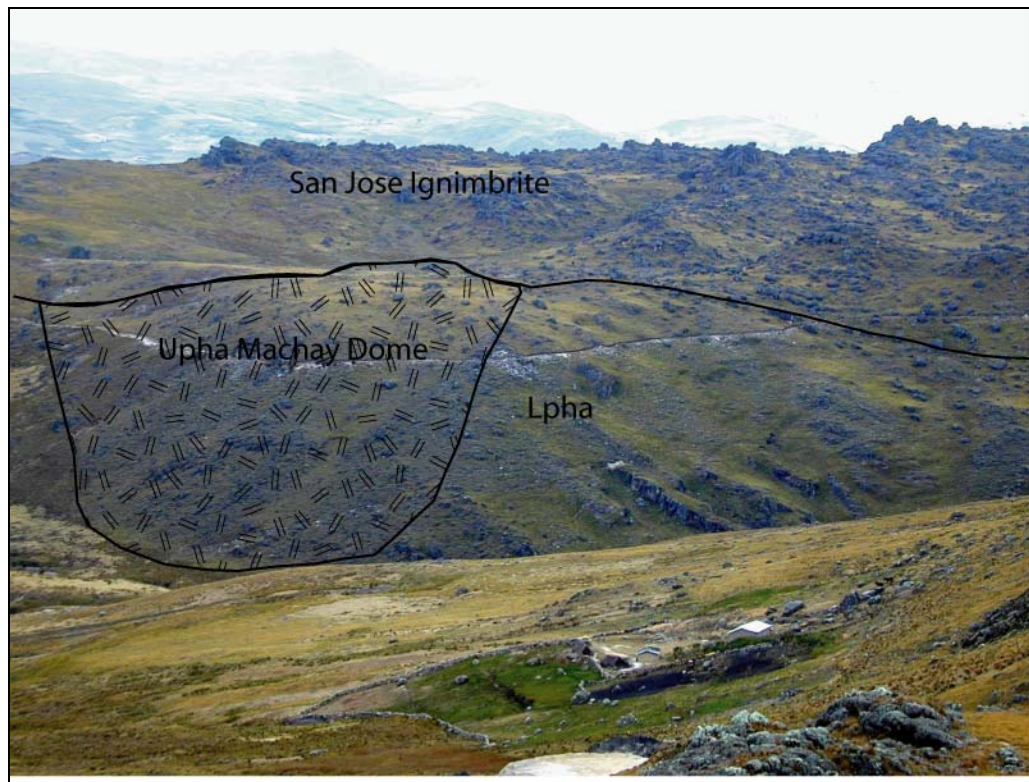
Figure 3.11 Photograph of the middle and upper members of the San Jose ignimbrite sequence (SJI) overlie the Lpha with angular unconformity and the Machay Dome with a disconformity. The Machay dome intruded the Lpha and bedding is truncated. The SJI was tilted 10-15° SW and the Lpha 25-30° WSW.

San Jose Ignimbrite Sequence

Ash-flow tuffs of the San Jose ignimbrite sequence (SJI) represent late explosive eruptions of dacite that post-date the Upper Yanacocha volcanic sequence (Upha). In many exposures, the rock package resembles a compound cooling unit, but consists of a number of cooling units from separate eruptive events significantly separated in time. $^{40}Ar/^{39}Ar$ age determinations indicate eruptions of the San Jose ignimbrite span a period of 300,000 years from 11.5 to 11.2 Ma. The sequence is divided into three ash-flow tuff members that are mineralogically and texturally distinct, and correspond to separate eruptive events from multiple vents. They include the following members: the lower San Jose ash-flow tuff (Lsji), the middle San Jose white ash-flow tuff (Msji), and the upper San Jose spatter ignimbrite (Usji) (Figures 3.12, 3.13 and 3.14). Each ash-flow member records several flows and one or more cooling units. Intramember contacts are rarely marked by obvious depositional features such as surge layers, or co-ignimbrite fallout

layers. More detailed fieldwork is required to accurately define the volcanic stratigraphy of this eruptive phase.

Explosive ignimbrite-forming eruptions were followed by dome-building that developed at least three dome complexes aligned in a northeast trend for 5.7 km from Cerro Baul to Alto Machay (Figure 3.3). Ash-flows filled a topographic depression south of the minesite called the Combayo-Ocucho-Sacsha-Otuzco (COSO) Trough (Figure 3.16; Longo, 2001) that extends from Cerro Baul and Sacsha south to Cajamarca and Otuzco then northeast along Rio Chonta to Combayo and northwest to Ocucho (Figure 3.5, Plate 1). Figure 3.12 shows the prominent contact of San Jose ignimbrite to older rocks south of the minesite that extends 5.5 km from Machay to Bosque de Piedra. Erosional remnants of welded ignimbrite crop out at San Jose, Arnacocha, and a small outcrop at Cori Cospha (Figure 3.3, Plate 1). The San Jose ignimbrite is absent from the other sections in the Yanacocha district (Figures 3.18 and 3.19; Table 3.1) due to Late Cenozoic erosion and possible non-deposition on paleo-topographic highs. The total areal expanse for the San Jose ignimbrite is estimated as 175 km^2 (Table 3.1) with thicknesses that range from 40 meters at Arnacocha to 350 meters in the COSO Trough west of Combayo (Figures 3.18 and 3.19; Table 3.1). Eruptions of the San Jose ignimbrite post-date early hypogene advanced argillic alteration in the east district and typically contain accidental fragments of acid-sulfate altered volcanic rock (this study and Longo, 2000).

Mineralogy

Two compositionally distinct ash-flow tuffs are recognized in the San Jose ignimbrite sequence by phenocryst type and modal% (Tables 3.2 and 3.3). The Lower and Upper San Jose ignimbrite (Lsji and Usji) consist of plagioclase > amphibole > pyroxene > Fe-Ti oxides > biotite and accessory apatite and zircon, whereas the Middle San Jose ignimbrite (Msji) consists of plagioclase > amphibole > Fe-Ti oxides > biotite and accessory sphene, apatite and zircon, pyroxene is absent. Pyroxene > amphibole is common in some flows of the Usji spatter ignimbrite. Single apatites as large as 0.3 to 0.75mm are common in the groundmass of the Lsji and the Usji spatter ignimbrite (Table 3.2b), and typically are striated with clouded cores similar to apatites in the Maqui Maqui ignimbrites. Apatite in the Middle San Jose white tuff is rare, and typically small and

colorless. Composition and phenocryst assemblages of the Lsji and the Usji are similar to Upper Yanacocha pyroxene-hornblende andesite domes and lavas. Compositional and textural distinctions are most pronounced between the Upper San Jose spatter ignimbrite and the Middle San Jose white tuff (discussed below in detail).
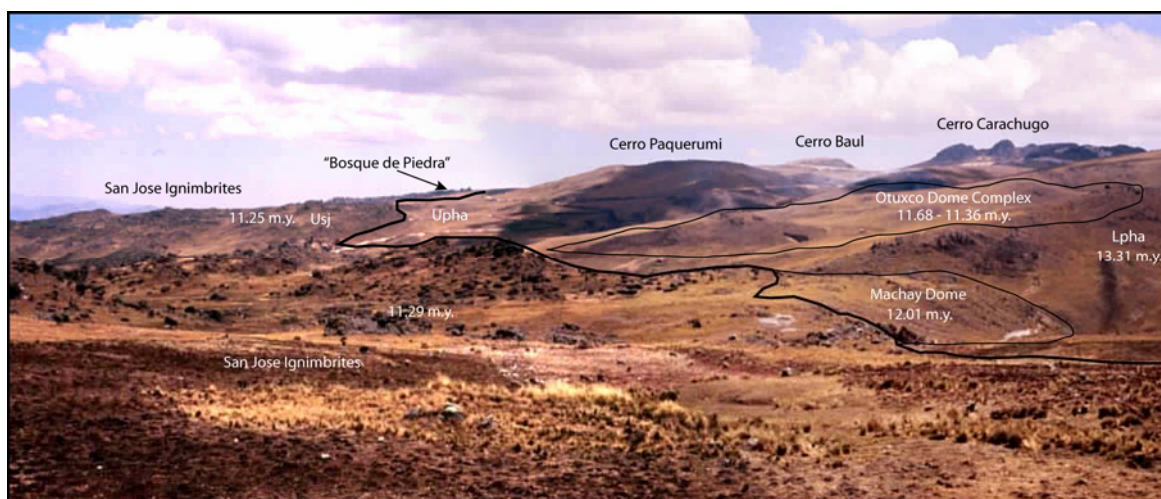
Figure 3.12 Photograph of the San Jose ignimbrite (11.3 Ma) contact to older rocks from Machay to Bosque de Piedra (5.5 km). Older rocks below the contact include Lpha (13.3 Ma), Upha, the Machay dome (12.0 Ma), and the Ocucho dome (11.7 to 11.4 Ma).

Lower San Jose Ash-flow Tuff

The lower San Jose member (Lsji) is a compound cooling unit that combines at least three hornblende-pyroxene-biotite dacite ash-flow tuffs. These include two early poorly-sorted and non-welded lapilli pumice ash-flow tuffs and an upper densely welded eutaxitic ignimbrite. The ash-flow tuffs were elutriated and fines-depleted with up to 63 vol.% broken phenocrysts in the ground mass (Figure A6.5; Appendix VI). Juvenile non-welded pumice lapilli typically contain 5-20 vol.% phenocrysts of plagioclase, amphibole, clinopyroxene, biotite, Fe-Ti oxides and apatite (Figure A6.5a and b; Appendix VI). Large poikilitic hornblende phenocrysts to >5.0 mm long are common. Groundmass glass and pumice display incipient to weak devitrification. These flows unconformably overlie Cretaceous basement at Ventanillas de Combayo, the 15.5 Ma Cerro Frailes dacite ash-flow tuff near Combayo and 13.8 Ma Lower Yanacocha andesite lavas at Pachanes and Arnacocha (Figure 3.3; Plate 1 and 3). Welded units form the cliff faces, whereas the nonwelded cooling units crop out below and overlie Cerro Frailes tuff.

The age of the lower member is 11.54±0.09 to 11.43±0.06 Ma, and the Lsji is the most extensive and voluminous member in the sequence with an areal extent of 134.3 km^2 (Plate 1). Patchy- and wormy-textured quartz-alunite and massive silica rocks are present as accidental fragments in the eutaxitic ignimbrite at Cerro Baul.

Middle San Jose White Ash-flow Tuff

Pyroclastic flows of the Middle San Jose member (Msji) are white hornblende-biotite andesite to trachyandesite, and rare dacite ash-flow tuffs with poorly-sorted, generally non-welded, lapilli-sized pumice fragments. The middle member records several flows and cooling units (Figures 3.18 and 3.19) from non-welded lapilli pumice ash-flow tuffs to densely welded and eutaxitic ash-flow tuffs. As in the lower member, these ash-flow tuffs are also fines-depleted with up to 71 vol.% broken phenocrysts versus 5-15 vol.% phenocrysts in the juvenile pumice lapilli. Mineralogy is distinct and phenocrysts consist of plagioclase > amphibole > opaque oxides > biotite (Table 3.3b). Pyroxene is generally absent, but trace amounts have been observed <1 vol.%. Hornblendes are smaller (0.2-2.5 mm) than the Lsji and generally lack opacite rims, and oxyhornblendes are rare. Apatite is rare and generally <0.1mm, but can be as large as 0.4 mm long. Devitrification of the groundmass glass is generally stronger in the Middle member than the Lower and Upper members displaying both spheriolitic and axiolitic textures.

The Msji white tuff member crops out from Alto Machay (Figures 3.3 and 3.13) to Cajamarca and may have an areal expanse of ~99.6 km^2 (Plate 1). $^{40}Ar/^{39}Ar$ ages (n = 7) range from 11.30±0.09 to 11.22±0.08 Ma and overlap with the age determined for the Upper San Jose spatter ignimbrite. Three cooling units of the white tuff crop out on Cerro Pabellon ridge south of the Ventanillas de Combayo and yield an age of 11.22±0.08 Ma (Figure A4.14b, VC-1; Appendix IV). The age is within a 2σ error of the Upper San Jose spatter ignimbrite suggesting eruptions of the Middle San Jose white tuff coexisted during eruptions of the Upper San Jose spatter ignimbrite.

Coarse lithic concentrations are common at the base of some flows and can be observed in Quebrada Azufre near Pozo de Azufre and along the unconformity over the Machay dome (Figures 3.11, 3.12, and A 4.13. Appendix IV). A pyroclastic flow (CB-

74) dated at 11.30±0.09 Ma unconformably overlies the Machay dome (12.01±0.10 Ma) and contains abundant boulder-sized quartz-sanidine-andalusite altered fragments along the basal contact to the Machay dome (Figure A4.13; Table A2.1 Appendix II XRD methods; samples CB-64 and -68 A and B). These flows unconformably overlie Lpha lava flows in Quebrada Azufre and contain abundant accidental fragments of hypogene advanced argillc alteration and higher temperature sanidine-andalusite alteration. Grey massive silica fragments are common to flows in Quebrada Azufre. Middle member ash-flows below the upper member in Quebrada Azufre, at Alto Machay, and at Sacsha have a weak to intense advance argillic alteration.

Figure 3.13 Photograph looking west at Fieracocha below Alto Machay showing the typical outcrop pattern for the lower, middle and upper members of the San Jose Ignimbrite sequence. The lower eutaxitic ignimbrite in the photograph represents the upper welded unit of the lower member dated nearer to Combayo (CB-56) and has an age of 11.43±0.06 Ma. The middle sequence froms the grassy slope and consists of several ash-flow units that are kaolinite and opal altered in this section. These flows contain previously altered accidental fragments and a middle member flow with altered fragments to the north overlying the Machay dome (12.01±0.10 Ma) has an age of 11.30±0.09 Ma. The upper spatter ignimbrite member is ~ 10 meters thick and appears draped over paleotopography of the middle member. The upper member flow has an age of 11.25±0.07 Ma and thickens to the west of the photo
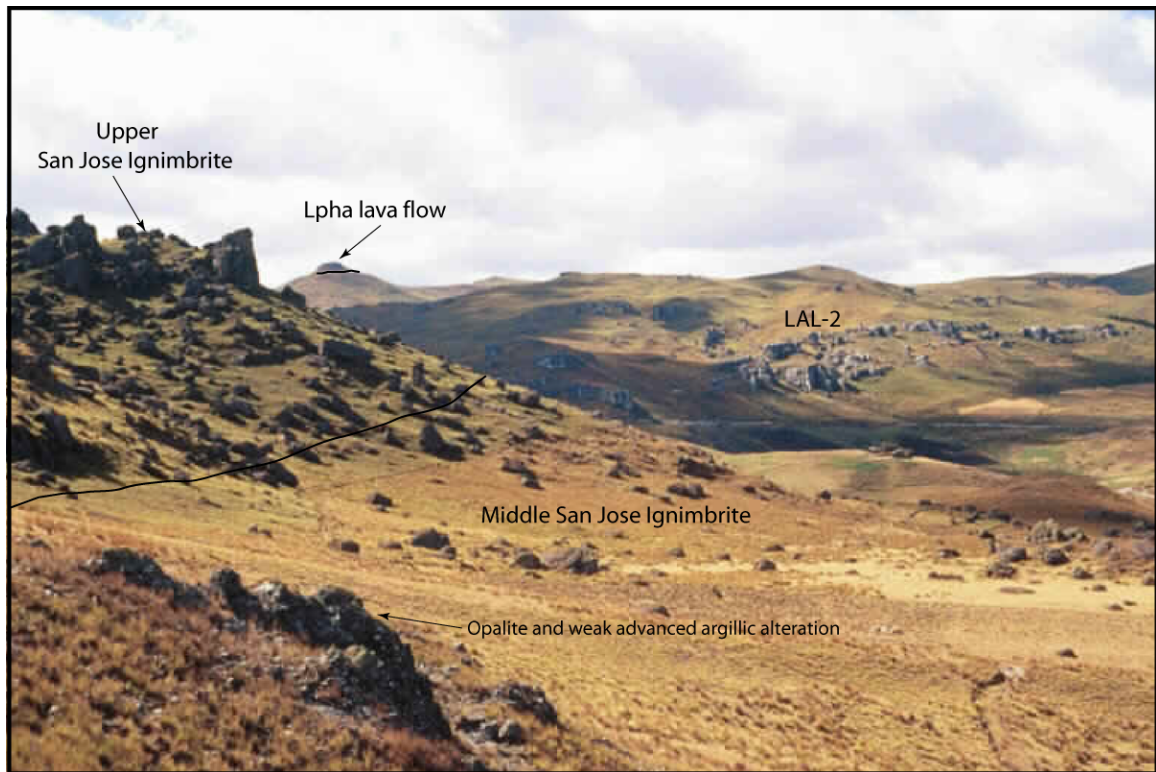
Figure 3.14 Photograph from the kaolinite-opalite altered middle San Jose member near the contact to the upper member in Figure 3.12, looking NNE across a major normal fault to the LAL-2 (gray outcrops in the background). The Lpha lava flow caps Cerro Condor south of Yutucmana and overlies the LAL-2.

Upper San Jose Spatter Ignimbrite

The upper member *spatter* ignimbrite (Usji) is the smallest and most distinct of the pyroclastic flow deposits in the San Jose ignimbrite with an areal expanse of 16.5 km^2, and thicknesses that range from 10 to 100 meters (Figure 3.3, Plate 1, Figures 3.18 and 3.19, Table 3.1). It is a simple cooling unit that is densely welded and contains abundant (20 to 50%) juvenile blobs and blocks that resemble flattened and stretched spatter (Figures A4.11 and A4.12, Appendix IV), and here on is termed *spatter ignimbrite*. The spatter ignimbrite has the following textural characteristics:

(1) The deposit is matrix-supported and must have entrained large amounts of ash from a collapsing plinian plume during lava fountaining (discussed below). The

spatter blobs and blocks are resistive relative to the surrounding matrix and weather as collapsed lapilli to block-sized blobs with positive relief.

(2) The deposit is poorly-sorted and displays a crude reverse grading of spatter blobs and blocks that coarsen upward from <1 to 5cm sized at the base and 1 to 50 cm size at the top.

(3) Spatter blobs range from 1-2 cm size flattened lapilli to bomb-sized blobs that are >10 cm and up to 40-50 cm in length.

(4) Occasionally, the spatter lapilli constitute >50% by volume and appear in contact to one another, however, on fractured weathered outcrop surfaces, eutaxitic textures with pale to dark grey fiamme are separated by ground mass matrix common around larger fragments. The deposit was welded and lacks vesiculated pumice.

(5) In cross sectional view the aspect ratios (length/width) range from 1:7, whereas in planar view the blobs have an oval to rounded pancake-shape with 1:1 and 2:1 aspect ratios (Figure A4.12; Appendix IV). Such variability in the aspect ratios suggests some blobs were hotter than others upon emplacement in the flow (Moore, 2002), or maybe there was a rheological contrast of the matrix versus spatter blobs.

(6) Some fragments are sub-angular blocks and lapilli oriented parallel to the flattened blobs (Figure A4.12 and A4.13; Appendix IV) suggesting the fragment was cooled prior to emplacement and aligned to the plane of compaction. The matrix of these fragments is commonly fine-grained relative to the spatter blobs and groundmass, and some display distinct banding from alternating laminae of fine- and coarse- crystals. The fine-grained angular blocks and lapilli may represent accidental fragments ripped up from vent facies deposits during eruption.

(7) Overall the deposit displays a mixed compaction profile of flattened blobs and lapilli mixed with the sub-angular fragments (Figures A4.11 and A4.12; Appendix IV). Locally it shows a uniform compaction profile.

(8) The spatter ignimbrite grades downward to a grey tuff with similar mineralogy and small 1-5cm size fiamme that resemble spatter blobs. This lower section may

represent the pyroclastic flow that resulted from the initial eruption before lava fountaining (CB-37 abd 38; Figure A5.5b, Appendix V).

(9) The deposit displays a crude columnar jointed pattern, has a regional dip of 10-15° southeast, and is draped over weakly altered middle member ash-flow tuffs that are occasionally eutaxitic with 20% accidental fragments of previously altered rocks.

(10) The deposit has a regional 10-15° inclination that appears draped over the topography and conformable with the middle and lower members of the San Jose ignimbrite sequence.

(11) Outcrops weather with a fluted appearance reminiscent of elutriation pipes (Figure A4.11, Appendix IV).

The spatter ignimbrite represents the final eruption of the late *explosive stage 2* at Yanacocha and has $^{40}Ar/^{39}Ar$ dates of 11.25 Ma.

The unit has the most mafic mineralogy of the San Jose sequence with large poikilitic hornblende 2.0 to >5.0 mm long and green augite (up to 7 vol.%) similar to the lavas and pyroclastic rocks of the Upha, but it is fines-depleted and full of broken phenocyrsts. Mineralogy of the spatter blobs and blocks is the same as the groundmass with oxyhornblende, clinopyroxene, biotite, Fe-Ti oxides, and apatite. The difference between blob and groundmass is in the total phenocryst content, the groundmass is extremely phenocryst-rich and fines-depleted with 50 to 74 vol.% broken crystals, and the spatter blobs have 40 to 45% phenocrysts representative of a crystal-rich magma. Phenocrysts are also broken in the blobs, but textures in the spatter blobs are seriate, porphyritic-like, and much coarser than the groundmass (spatter blob 0.05-4.5mm versus ground mass 0.05-2.5mm). This is because the degree of fracturing is much greater in the groundmass and less in the blobs. Phenocrysts in the fine-grained banded accidental fragments are also broken and display a foliation that developed from alternating laminae of moderately-sorted, size-graded fine to coarse broken crystals (0.05-1.2mm). These accidental fragments resemble vent facies base surge deposits that were ripped up and incorporated in the spatter ignimbrite during the eruption.

Spatter Interpretation

Spatter-rich pyroclastic flows and clastogenic lava flows, with textural characteristics similar to the spatter ignimbrite in the San Jose ignimbrite sequence, have been documented in the literature (Trigila and Walker, 1986, Cas and Wright, 1988; Branney and Kokelaar, 1992; Turbeville, 1992; Sumner, 1998; and Yasui and Koyaguchi, 2004). These flows are described as lava-like, high-grade ignimbrites and clastogenic lava flows. Textures in clastogenic lavas or spatter-rich ignimbrites include the following features: (1) phenocrysts are mechanically broken, (2) flows have zones of dense welding, (3) eutaxitic textures are present in densely welded zones and (4) the areal extents are of similar magnitude to the San Jose spatter ignimbrite (ie., Asama flows covered an area of 7 km^2 with thicknesses of 10m to 65m) (Yasui and Koyaguchi, 2004). Clastogenic andesite lava flows at Izu-Oshima and Asama Volcanoes in Japan were generated by lava fountaining coeval with a plinian eruption and pyroclastic flows (Yasui and Koyaguchi, 2004), and during the 1986 eruption of Izu-Oshima extraordinarily high lava fountaining of 1600 meters was observed associated with a sub-plinian plume that reached 16 km (Sumner, 1998). Turbeville (1992) described a welded pyroclastic deposit of the Pitigliano Tuffs, Italy as a spatter-bearing ignimbrite and proposed coeval emplacement of fountain-fed fall and pyroclastic flows during an eruption of a convecting ash-laden plume synchronous with steady-state fountaining. Trigila and Walker (1986) described the Onano spatter flow at Vulsini Volcano, Italy as a spatter ignimbrite that was deposits by similar mechanisms. Soriano et al. (2002) proposed that the extensive welded phonolites up to 80m thick around the Las Canadas Caldera, Canary Islands formed during coeval evolution from plinian fallout and fountain-fed spatter at the caldera rim. Pyroclastic fall of phonolite spatter and ash accumulated, agglutinated and welded at the vent then flowed down slope and away from the vent similar to lava (rheomorphic flowage). Las Canadas rheomorphic flows display reverse grading similar to the San Jose spatter ignimbrite. Soriano et al. (2002) suggested the upward increase in pumice and lithic grain size and flattening was attributed to an increase in the eruption temperatures and decreasing explosivity as the eruption progressed.

The spatter ignimbrite displays some characteristics similar to welded air-fall deposits. These include internal stratification and reverse grading, an overall uneven or

mixed compaction profile, an appearance of draping topography, and a thin (8-10 meter) and even distribution (Moore, 2002). However, the spatter ignimbrite is also matrix-supported, poorly-sorted and massive to crudely stratified, and also displays a uniform compaction profiles of spatter blobs more typical in ignimbrite deposits (Figures A4.11c and e and A4.12; Appendix IV). The internal stratification is reflected in a crude reverse size grading throughout the deposit and not from abrupt changes in grain size or the compaction profile. The uneven and mixed compaction profile reflects the mixture and uneven distribution of the cooled lithic fragments and the molten spatter blobs (Figure A4.11e). In contrast, tuffs classified as welded air-fall deposits are well sorted, well stratified (medium to thinly laminated beds), mantle topography (a welded air-fall tuff will mantle highly irregular topography from flat surfaces, high ridges to steep slopes up to 30°), and show abrupt variations in grain size and the compaction profile (Sparks and Wright 1979, Turbeville, 1992). In view of the similarities and differences discussed above, the San Jose spatter ignimbrite is not a welded air-fall deposit.

The spatter ignimbrite at Yanacocha is interpreted as a lava-like, high-grade ignimbrite that may have formed from the coeval emplacement of fountain-fed fall and pyroclastic flows at 11.25 Ma. These are different from conventional low-grade ignimbrites in that the cuspate shards and vesicular pumice are reheated during transport and revert to glass droplets and non-vesicular spatter-like blobs (Branney and Kokelaar, 1992); therefore, vesicular pumice is absent. The spatter ignimbrite deposit did not flow en masse but rather developed from a sustained current during continuous column collapse and lava fountaining. Branney and Kokelaar (1992) contend that ignimbrites are not formed by en masse deposition of a pyroclastic flow but by progressive aggradation from a sustained current during continuous column collapse. This style of deposition may explain the internal stratification present in many ignimbrites. The eruption may have started as a plinian eruption that developed an inflated and fines-depleted pyroclastic flow from an initial column collapse. The degree of fracturing in the broken phenocrysts attests to the high explosivity index of the initial eruption. The magma degassed and the style of eruption changed from dominantly Plinian to a coeval lava fountain with a sub-Plinian plume. Pyroclastic flows deflated toward the end of the eruption and coarse

juvenile fountain-fed spatter blobs became incorporated into the top of the flow at the vent and flowed outward as a series of closely spaced flows.
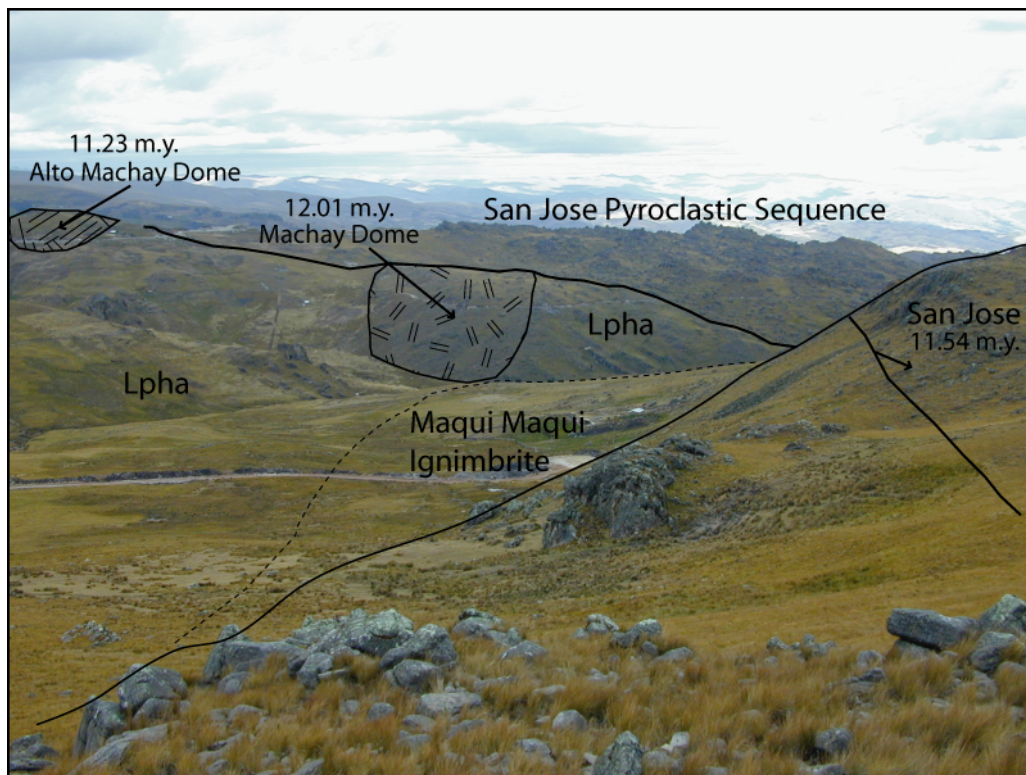
Figure 3.15 Photograph looking south from San Jose ignimbrite at Arnacoha (foreground). These flows overlie a thin section of Upha lava flows and the Maqui Maqui ignimbrite (refer to figure section I). The entire section at Arnacocha was tilted 10-20° west. In the background, the San Jose ignimbrite sequence (11.30-11.25 Ma) unconformably overlies the Lpha (13.76-13.31 Ma) and Machay dome (12.01 Ma) and thins to the east. Domes at Alto Machay and Machay intrude the Lpha volcanic sequence.

Domes associated with the San Jose Ignimbrite

At least three dome complexes were closely associated in time with the San Jose ignimbrite sequence and include the Ocucho dome (11.7-11.4 Ma), the Chaquicocha Sur dome (11.3 Ma), and the Alto Machay dome (11.2 Ma). Domes are here defined as a zone of several closely-spaced sub-vertically flow-banded porphyritic outcrops. All three areas have field evidence for multiple dome-building events from internal growth as fan-shaped endogenous domes or via trapping in the vent. No extensive lava flows are found associated with these domes. Instead the domes intruded lavas and pyroclastic rocks of

Lpha and Upha. Ocucho dome complex (1.58 km^2) shared an older vent and truncated an early Upha or Lpha dome that was altered to kaolinite and opalite (Figure A6.7a; Appendix VI). Each outcrop is strongly flow-banded with near vertical flow foliations that strike northeast at Ocucho and Alto Machay, and northwest at Chaquicocha Sur (Figure A4.9; Appendix IV). Outcrops of the Chaquicocha Sur dome (0.20 km^2) are found in a glaciated valley surrounded by moraine and are the roots of a larger eroded dome complex. The Ocucho domes were also glaciated and crop out between the margins of the Huacataz and Ocucho Machay moraines (Figure A4.15).

Mineralogy of the dome rocks is similar to the pyroclastic flows (Table 3.3c). The Ocucho and Chaquicocha Sur domes contain green augite/cpx pyroxene and hornblende similar to the lower and upper members of the San Jose ignimbrites, whereas, the Alto Machay dome is a hornblende dacite that lacks pyroxene similar to the middle member. Textures are porphyritic to seriate with a pilotaxitic groundmass, and phenocrysts are strongly flow foliated and oriented near vertical.

Figure 3.16 Photograph looking south from the Pachanes moraine showing a view of the Alto Machay dacite dome complex (11.23 Ma) and the location of the co-ignimbrite lag-fall deposit adjacent the Alto Machay vent area for hornblende dacite ash-flows of the middle member. Domes intrude volcanic rocks that represent an Lpha paleotopographic high. In the background, the San Jose ignimbrite crops out in the COSO basin. The road connects China Linda and Chota to Combayo and Cajamarca City.

Least eroded was the Alto Machay dome complex (0.14 km^2) located along the hanging wall of the Sugares fault in contact to Lpha and LAL-2 (Figure 3.16). Remnants of an eroded co-ignimbrite lag-fall deposit (Figure A4.15, Appendix IV) crop out on the south margins of the dome complex and cover an area of 0.13 square kilometers over 10

meters thick. This deposit represents a lithic-rich lag breccia that formed in the deflation zone at the site of a column collapse during an explosive eruption (Wright and Walker, 1977; Walker, 1985), for example, perhaps related to a San Jose pyroclastic flow. The deposit is fines-depleted, crudely stratified, poorly-sorted and lithic-rich with large blocks up to 50 cm of hornblende dacite and pyroxene-hornblende andesite.

Upper (Late) Dacite and the Negritos Ignimbrite

There are at least three types of late dacite at Yanacocha that represent three distinct intrusive events that spanned ~2.4 m.y. from 10.8 to 8.4 Ma and crop out northeast of Cerro Pabellon (Figure 3.3; Plate 1; Figure A5.6, Appendix VI). These include the Corimayo dacite (Cd), the Yanacocha dacite porphyry (Ypq), and the Chaupiloma-Yanacocha Lake dacite (CYd). There is also one rhyolite ash-flow tuff that may be an outflow sheet equivalent to the CYd dikes called the Negritos ignimbrite. Main stage gold ore and Au-Cu-Ag ore in the east district is spatially and temporally associated with the late dacites. This study collected only minimal data on these rocks and additional work is required to better understand the petrogenesis on this late stage of felsic magmatic activity and its relationship to ore.

Corimayo Dacite

Dome rocks and intrusions named the Corimayo dacite dome (Gomez, 2002) are buried beneath the La Quinua gravel deposits in the La Quinua Graben at Corimayo and Tapado. They trend easterly for 7.8 km from the La Quinua dacite (now below the La Quinua Leach Facility) to Chaquicocha where a dacite dome cropped out at Chaquicocha Norte (now part of the Carachugo pit). Corimayo dacites have a distinct mineralogy (Table 3.2c and 3.3c) with 3 vol.% quartz (0.1-2.0mm anhedral rounded to embayed phenocrysts), 10-15% total mafics as 5% biotite (0.2-1.5mm euhedral phenocrysts) and 5-10% hornblende, and accessory sphene phenocrysts (0.5-1.0mm). Textures are porphyritic to seriate with a glassy to aplitic groundmass and 30-43 vol.% phenocrysts. Domes at Corimayo, La Quinua and Chaquicocha Norte have distinct flow foliations. The Corimayo dome was well-preserved below the La Quinua gravels spatially associated with "laminated rocks" interpreted as base surge deposits and tuffaceous lacustrine

sediments (Gomez, 2002). Laminated rocks may have filled a maar-hosted lake that preceded dome building (Gomez, 2002). Dacite tuffs associated with eruptions of the Corimayo dome are not extensive and found only in drill core at Corimayo (COR-47 173.5m; Figure A6.6e, Appendix VI; CD Plate 1, drill hole sections). The $^{40}Ar/^{39}Ar$ age of biotite from the dome at Corimayo is 10.78±0.05 Ma, and the age is also bracketed by $^{40}Ar/^{39}Ar$ ages of 10.75±0.16 Ma on alunite veins and breccia that crosscut the dacite at Corimayo and 10.81±0.16 Ma on alunite in the Punta Negra dacite at Yanacocha Sur.

Yanacocha Dacite Porphyry

Intrusions of Yanacocha dacite porphyry (Ypq) crop out at Yanacocha Norte and Chaquicocha spatially associated with a northwest trend of gold ore (Plate 5). At Yanacocha Norte they are generally fresh but in a few locations are crosscut by late alunite-matrix breccia. Ypq porphyry plugs assume a northerly trend through the Cerro Yanacocha deposit (Plate 1). Mineralogy is distinct with 5-9 vol.% quartz (0.5-3.5mm subhedral to embayed), 6% total mafics as 3% biotite and 3% hornblende, and accessory sphene. Quartz phenocrysts are larger (up to 3.5mm) than the quartz-eyes in the Corimayo dacite, and textures are reminiscent of porphyry intrusions in that the total phenocryst content of ~30 vol.% is enveloped in an altered groundmass with granular textures 0.025-0.05mm that resemble aplitic-textured groundmass observed in porphyry plugs. All Ypq at Chaquicocha was altered to vuggy quartz with well-preserved quartz-eyes. Ypq rocks are common in the Yanacocha Complex at Cerro Yanacocha and are unaltered, advance argillic altered, and vuggy quartz altered, and crosscut by quartz-alunite-pyrophyllite matrix breccia that contains covellite-enargite-pyrite-chalcopyrite (Williams et al., 2001). An age of 9.91±0.04 Ma for the Ypq at Yanacocha Oeste is supported by a $^{40}Ar/^{39}Ar$ date on from Yanacocha Norte (9.90±0.05 Ma; Turner, 1997).

Chaupiloma-Yanacocha Lake Dacite

Late dacite dikes and plugs of the Chaupiloma and Yanacocha Lake dacites (Tcyd) are confined to a northwest trend through Yanacocha Lake and have a combined strike distance of over 3.8 km to Cerro Chaupiloma. These intrusions were called rhyodacite by Turner (1997) or Ybp, and previously believed to be unaltered in all cases by Yanacocha geologists. The Chaupiloma-Yanacocha Lake dacite rocks are part of the

greater group of late dacite domes and intrusions that assume a northwest trend and crop out for over 14 km from Chaquicocha to Negritos. Prominent outcrops at Yanacocha Lake (now part of the greater Yanacocha open pit) and Cerro Chaupiloma are dike-like, strongly flow-foliated, and trend northwest, but have contorted flow banding with foliations from N30°W to N25°E. Weak alteration and limonite oxides were observed on a dike margin at Cerro Chaupiloma where the dike intrudes the lower andesite lahar sequence (LAL-2) and the Cerro Frailes dacite tuffs and surge deposits. A roadcut at Cerro Chaupiloma exposed the N60°W/75°SW (120/75) contact of the Chaupiloma dacite with angular and contorted fragments of the flow-foliated dacite incorporated within a diatreme-like andesite breccia (Figure A 3.16; Appendix III). Mineralogy of this group of dacite rocks consists of 4-5 vol.% quartz (0.2-0.8mm), 10 vol.% total mafics as 3% biotite and 7% hornblende, and sphene. One $^{40}Ar/^{39}Ar$ age of 8.4 Ma is available for the Yanacocha Lake dacite determined on biotite by Turner (1997).

Negritos Ignimbrite

The Negritos ignimbrite crops out at Cerros de los Negritos and may represent an ash-flow sheet that vented during a fissure eruption of the Chaupiloma and Yanacocha Lake dacite. The tuff is an erosional remnant of a single cooling unit of rhyolite composition about 8 km north of Cerro Chaupiloma that covers an area of over 4 square kilometers ~ 50 meters thick. The ignimbrite is a pinkish-tan to light brown, partially welded and vapor phase altered ash-flow tuff that displays eutaxitic textures from the partial compaction of pumice lapilli. Fiamme are foliated and display vapor phase cristobilite and feldspar. Outcrops of the Negritos ignimbrite are columnar jointed and appear to have elutriation pipes in the upper part that have been accentuated by weathering (Figure A4.16, Appendix IV). The ignimbrite is crystal-rich ash-flow tuff with abundant quartz and biotite phenocrysts, and accessory sphene similar to all late dacites in the Yanacocha district. Nearly all phenocrysts are broken, and the quartz phenocrysts are shattered to conchoidal-shaped shards with rare euhedral and embayed phenocrysts (Figure A6.6f, Appendix VI). The flow contains 7-10 vol.% accidental fragments (1 to 20cm in size) of argillite, quartzite, porphyritic dacite, and fragments of granular-textured quartz that may be massive silica altered rock fragments from

Yanacocha. One ^{40}Ar/^{39}Ar date determined on biotite is available for the Negritos ignimbrite with an age of 8.4 Ma.

Lacustrine Sediments of La Quinua Basin

Tuffaceous lacustrine sediments crop out in quebradas and road cuts below the La Quinua gravels north and northeast of the La Quinua dacite (Figure 3.3, Plate 1). They are white to tan and brown colored, thin bedded and laminated rocks interbedded with black peat and carbon-rich shale beds up to 10 cm thick. Some of the lacustrine sediments were silicified to opaline silica and chalcedony similar to the laminated rocks at Corimayo and Quilish Norte, and border intense hypogene advanced argillic alteration alteration in La Pajuela project area (Aguirre, 1998) east of the La Quinua dacite (now completely covered by the La Quinua Leach Facility). Weak Au and Hg anomalies are associated with the alteration (Aguirre, 1998). This study suggests that these rocks represent lacustrine sediments deposited in a late Miocene to Pliocene shallow lake present during phreatic eruptions of the Corimayo dacite dome. Carbon-14 dating was attempted on a single sample from a large wood fragment found at the base of the La Quinua gravels above the lacustrine sediments. One age is reported as >44710 BP and the sample is said to have contained sufficient carbon for an accurate age (Mallette, 2001). If the sediments below the gravels are late Miocene-Pliocene, than chronostratographic dating on microflora in the peat beds could be used to determine an age.

Glacial Moraines and Associated Gravel Deposits

Late Cenozoic glaciers scoured and reshaped the volcanic geomorphology in the east district at Yanacocha, and the present topography reflects the glacial terrane with U-shaped valleys, numerous moraines, and polished and striated massive silica altered rocks about 4100 meters elevation (Figures A4.15d, A4.16e, and A4.17; Appendix IV). Glaciers also polished Cretaceous quartzite basement rocks in higher elevations to the north by Cerros de los Negritos. Moraines in the Yanacocha district are present above 3800 meters elevation and exclusively contain clasts derived from acid-sulfate altered volcanic rocks. Boulders of massive silica and intense quartz-alunite altered volcanics are common. Glaciers preferentially eroded the argillic and granular silica altered rocks

leaving mountains of massive and vuggy quartz-rich rock (Longo, 2000). Moraines include Huacataz-Paquerumi, Sacsha, Ocucho Machay, Maqui Maqui, West Yanacocha, and the quartzite boulder moraines of the Lake District north of the Yanacocha district (Figure 3.3, Plate 1).

The west district is below 3800 meters and does not show the classic erosional characteristics of the Late Cenozoic glaciation. The original volcanic geomorphology is preserved in areas such as the Cerro Atazaico area, and large deposits of gravel with thicknesses of 100 to 200 meters filled tectono-topographic basins such as La Quinua. These gravels represent deposits of braided glacial outwash from the higher elevations that are preserved in small basins as La Quinua. Thin remnants of outwash gravels can be found scattered around the west district the largest being the La Quinua gravel deposit that hosts +10 million ounces of alluvial Au (Mallette et al., 2004) eroded from the deposits of the Cerros Yanacocha Complex.
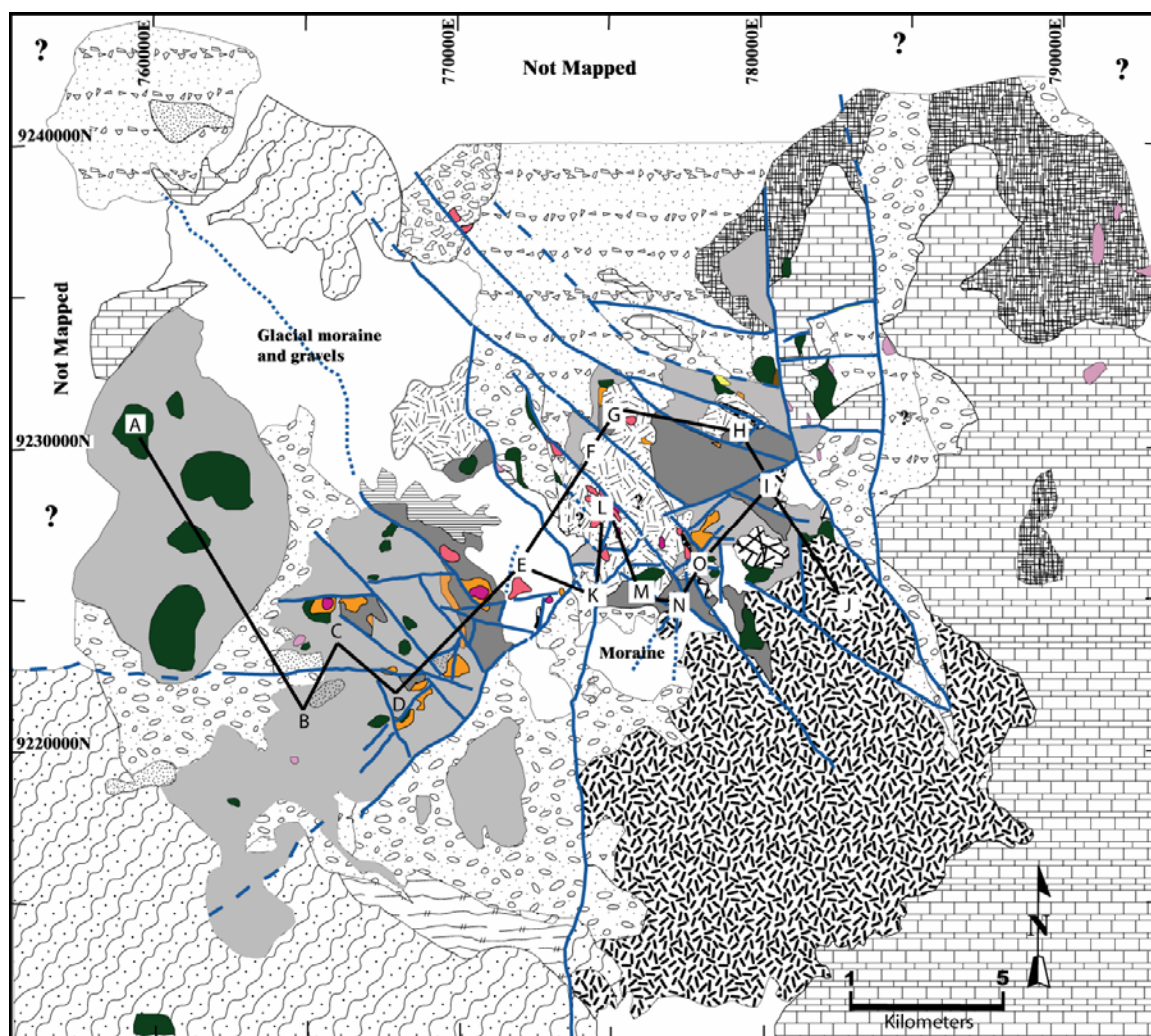
Figure 3.17. Location of the stratigraphic sections in the fence diagrams presented in Figures 3.18 and 3.19.

Figure 3.18. Stratigraphic fence diagram from west (section A) to east (section J) across the Yanacocha district. See the map in figure for the location of the sections. Section A Cerro Regalado, Section B Granja Porcon, Section C Cerro Negro, Section D Cerro Quilish, Section E Corimayo-Tapado, Section F Chaupiloma, Section G Cerro Hornamo, Section H Colorado Graben, Section I Arnacocha, Section J Combayo area. Actual stratigraphic thickinesses and distances are shown.

Upha dike
12.07±0.08 Ma

Tmmp lava?
12.39±0.12 Ma

11.24±0.10 Ma
11.41±0.11 Ma

11.54±0.09 Ma

Tbxh

Tlsj

Tupha

12.05±0.15 Ma
quartzite fragments

N

Tlsj

Tupha

Tmmi

Qg

Tcd

Tlx

Tbxh

Iupha

Tmmi?

10.78±0.05 Ma

11.90±0.11 Ma

11.91±0.08 Ma

E

Tmmi

Tcfd

Tlal2

K

Baul Fault

Tlpha

Tcfd

Iyp

Typq

M

12.01±0.10
11.68±0.07
11.36±0.09 Ma
11.28±0.09

Tmmi?

Tlpha

Tlpha?

Tcfd?

Typq

O

9.91±0.04 Ma

Tlsj

Tupha

Tmmi

Tlpha

I

Tusj

Tmsj

Tlsj

J

11.25±0.07 Ma
11.29±0.08 Ma
11.29±0.08 Ma
11.43±0.06 Ma
11.56±0.13 Ma
15.50±0.05 Ma

0   1000m

0   2500m

Lithology

Yanacocha Intrusions and Breccias

Yanacocha Rocks

Qg - Gravels and glacial moraine

Tusj - Upper San Jose spatter ignimbrite

Tmsj - Middle San Jose ignimbrite

Tlsj - Lower San Jose Ignimbrite

Tupha - Upper pyx-hb dacite and andesite

Tmmi - Maqui Maqui pyroclastic rocks

Tlx - Laminated rocks

Tlpha - Lower pyx-hb andesite rocks

Pre-Yanacocha Rocks

Tcfd - Cerro Frailes dacite pyroclastic rocks

Tlal2 - Chaupiloma lower andesite lahar sequence

Tlal1 - Tual lower andesite lahar sequence

Tv - Pre-Miocene andesite volcanic rocks

Kq - Cretaceous quartzite

Kls - Cretaceous limestone

Tcd/Typq - Corimayo and Yanacocha dacite

Tbxh - Hydrothermal breccia

Ted - Early dacite

Typ - Yanacocha feldspar porphyry

Tupha - Upha domes

Tlpha - Lpha quartz andesite domes

Tlpha - Lpha domes and intrusions

Figure 3.19. Stratigraphic fence diagram from west (section E) to east (section O) across the center and most productive portion of the east Yanacocha district (includes I and J from previous section). See the map in figure for the location of the sections. Section E Corimayo-Tapado, Section K South of Quebrada Encajon at Rosas, Section L Cerros Yanacocha, Section M Cerro San Jose and Piratacocha, Section N Cerro Baul, Section O Chaquicocha Sur. Actual stratigraphic thicknesses and distances are represented.
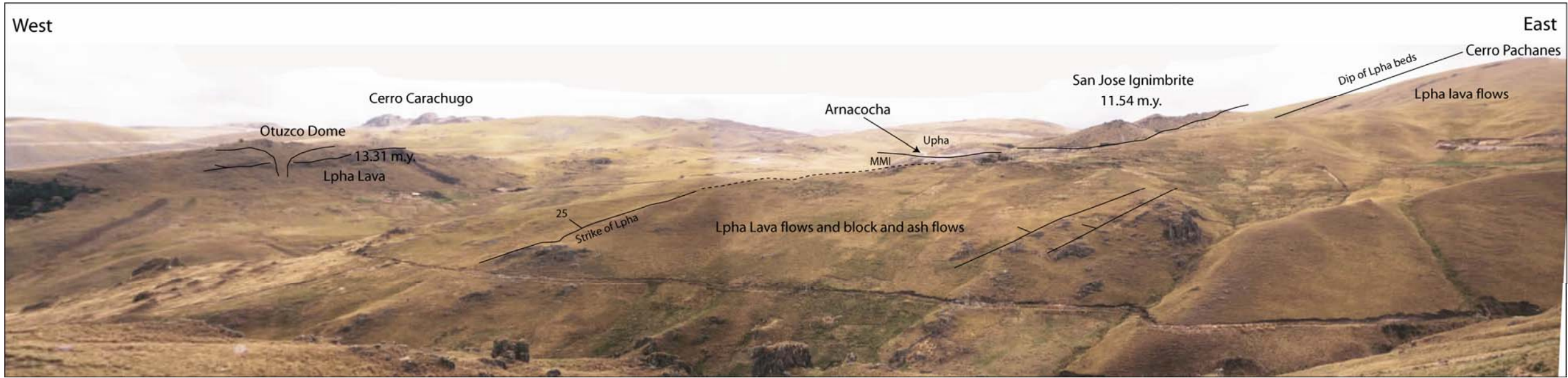
Figure 3.20. Composite photograph of the LPHA volcanic sequence looking north from Machay. The view is an east to west section of the westerly-tilted LPHA volcanic rocks from Cerro Pachances through Arnacocha and figure a east of Ocucho dome. At Arnacocha the San Jose ignimbrite overlies the LPHA with an angular unconformity. Lava flows of the LPHA at Cerro Pachanes and east of Ocucho are tilted ~25° WNW.
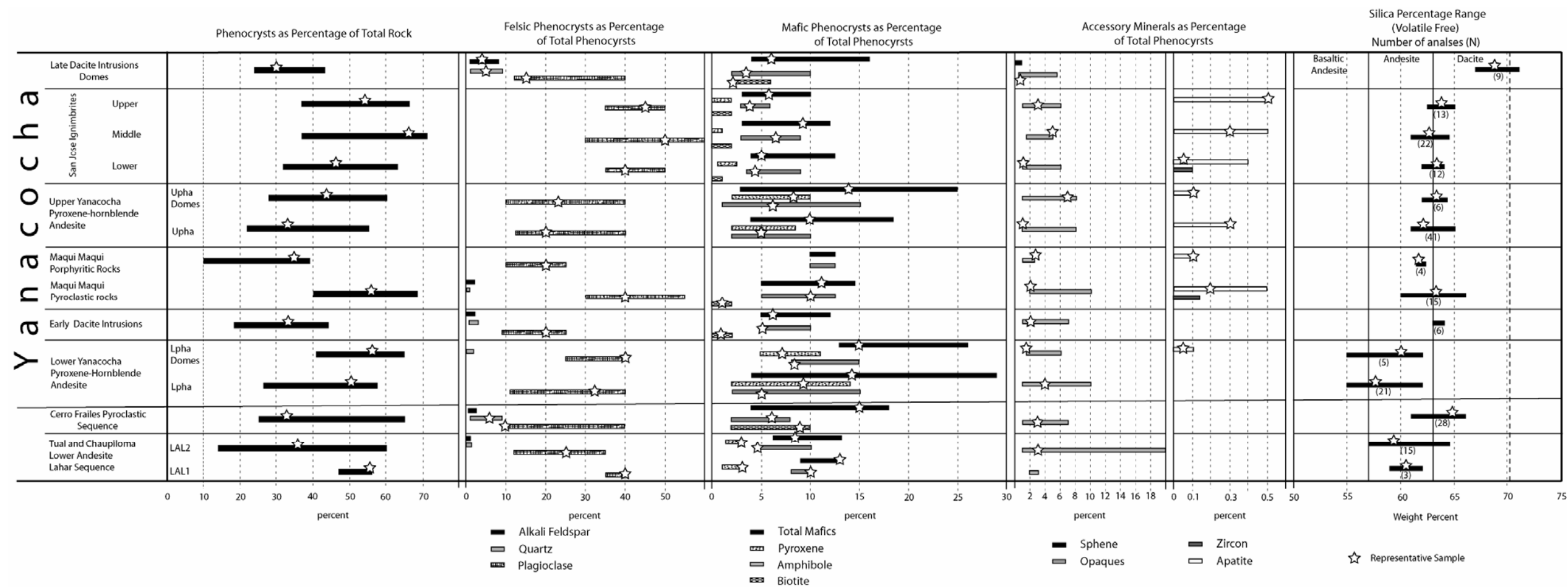
Figure 3.21. Chart showing the ranges of the modal mineralogy estimated from thin sections and silica content for each volcanic rock package at Yanacocha. The rock packages are organized in ascending order by their relative age and oldest is at the bottom.
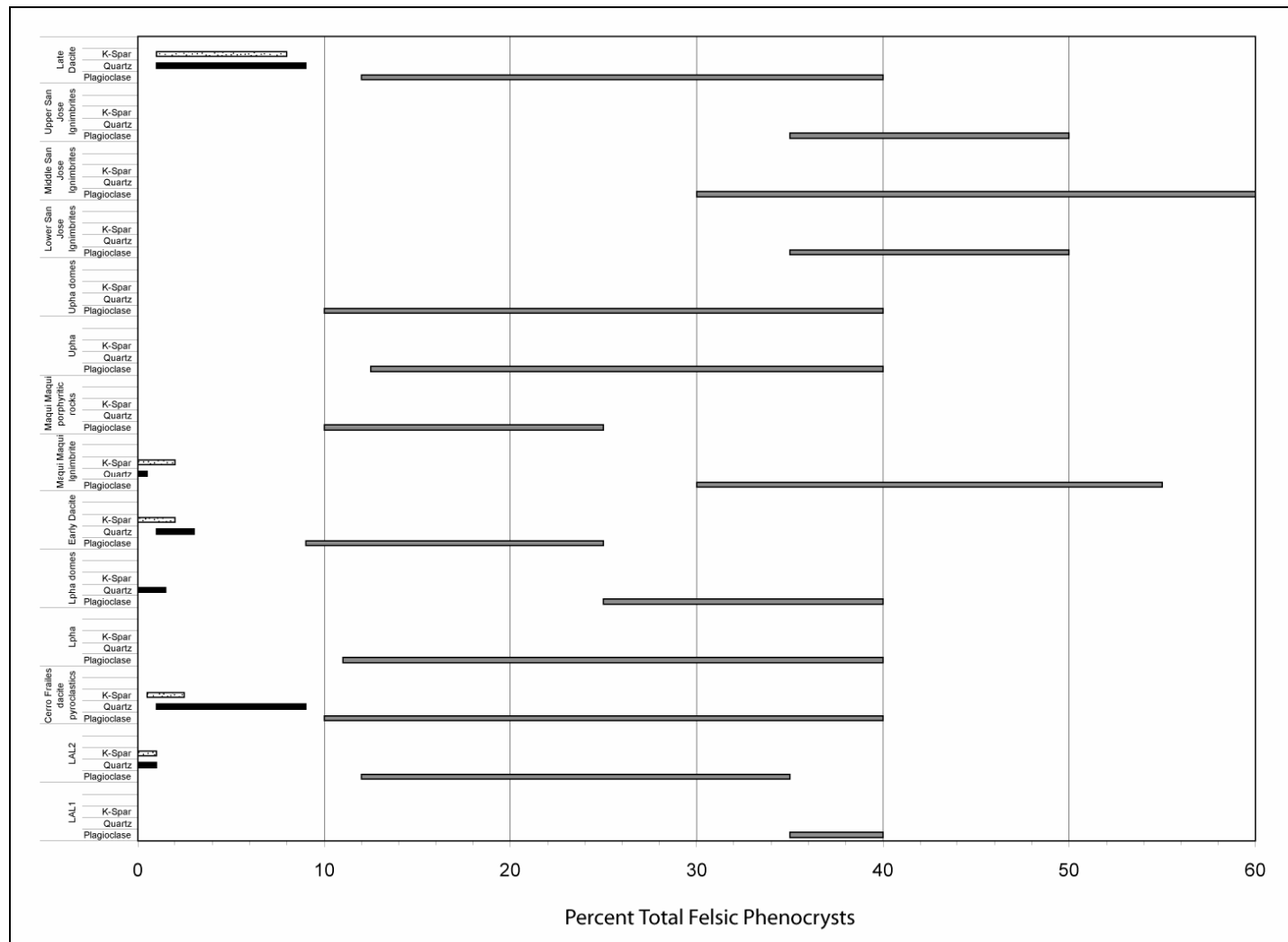
Figure 3.22. Chart showing the range in modal percent of total felsic mineral percent in the rocks at Yanacocha.
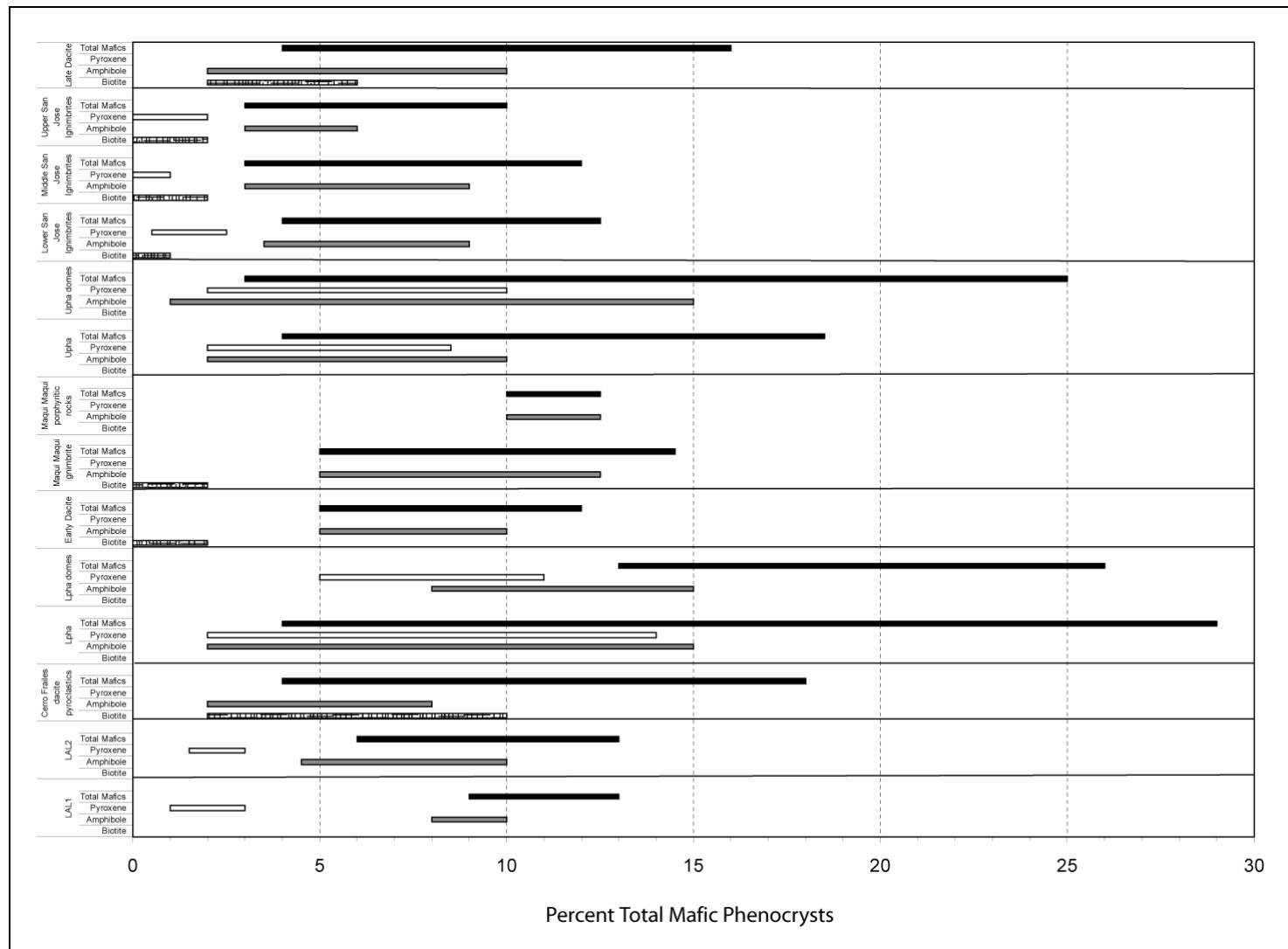
Figure 3.23. Chart showing the range in modal percent of total mafic minerals in the rocks at Yanacocha.
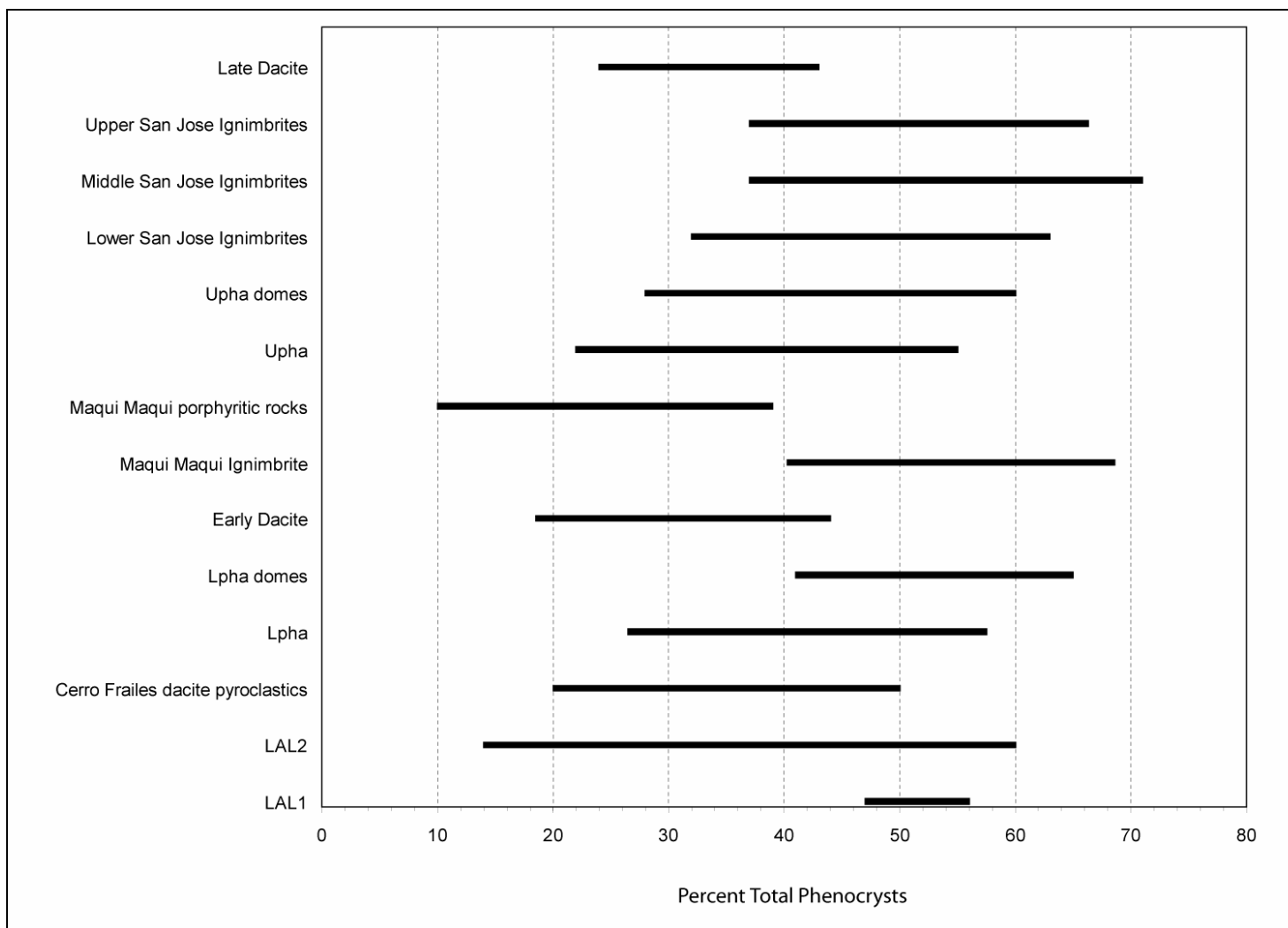
Figure 3.24. Chart showing the range in modal percent of total phenocrysts in the rocks at Yanacocha.
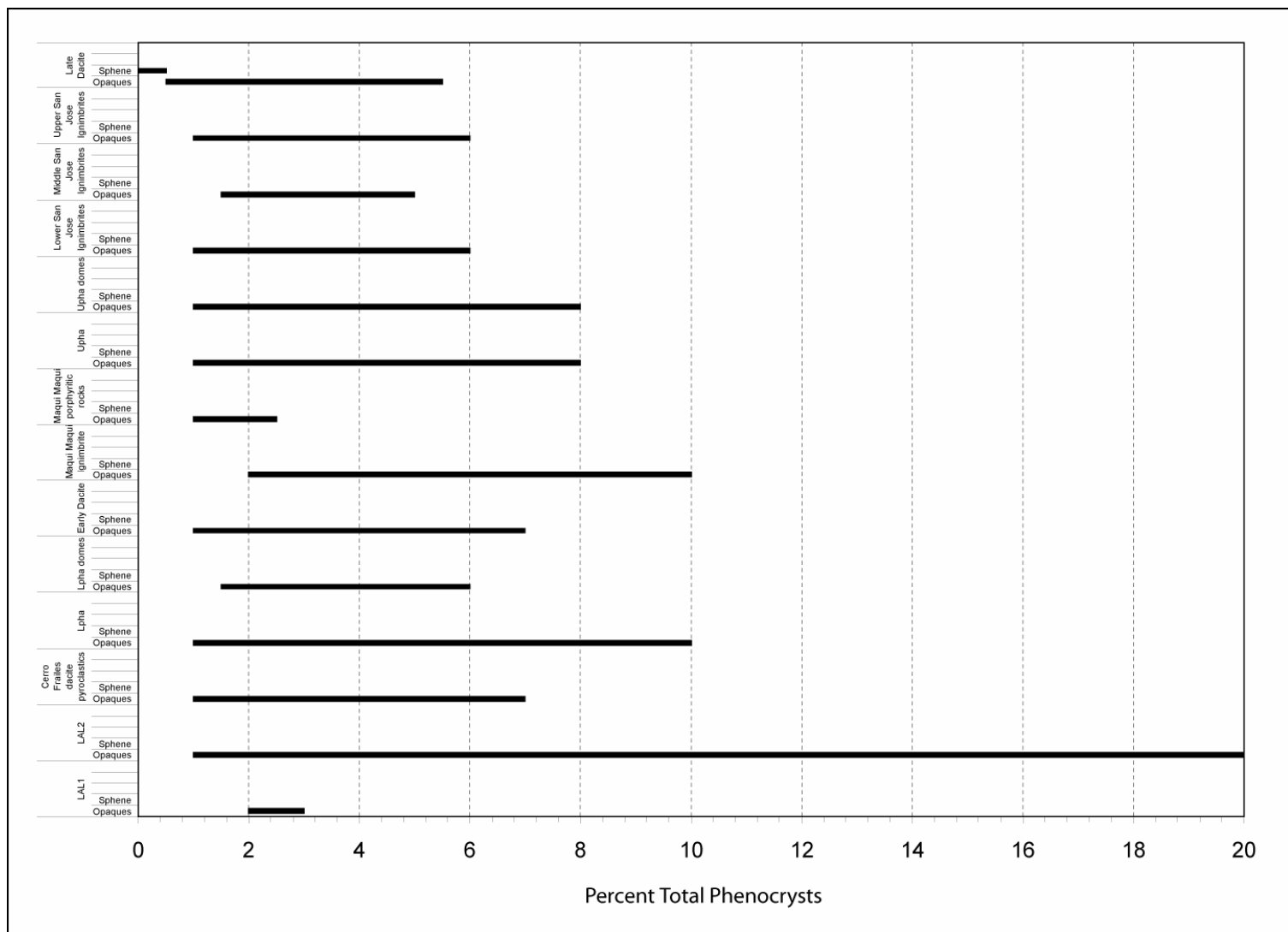
Figure 3.25. Chart showing the range in modal percent for sphene and opaque oxide amounts in the rocks at Yanacocha.
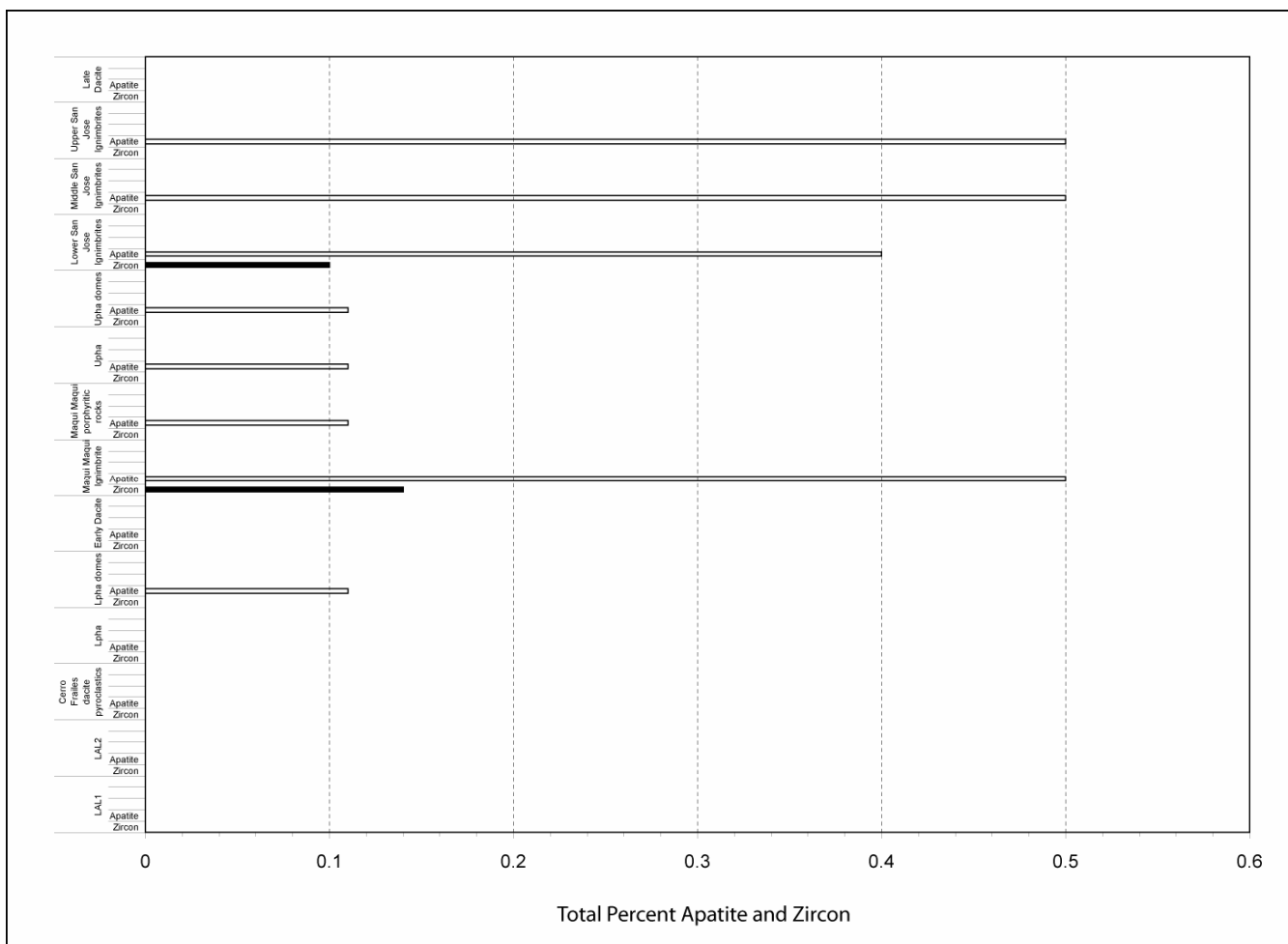
Figure 3.26. Chart showing the range in modal percent of accessory apatite and zircon in the rocks at Yanacocha.

Table 3.1. Thicknesses and Areal Expanse of the volcanic rocks in the Yanacocha district.

Age / Area / Section / Unit			LAL	Cerro Frailes	Lpha	Maqui Ignimbrite	Upha	San Jose Ignimbrite	Late Dacite
Age (Ma)			19.5 - 15.9	15.5 - 15.2	14.5 - 13.3	12.6 - 12.4	12.1 - 11.7	11.6 - 11.2	10.8 - 8.4
Outcrop Area / Areal Expanse (km²)			88 / 430	66.3 / 340+	102.5 / 340	9.8 / 89	22 / 121	136 / 175	1.2 / 4.7
Thickness (m)		Locations	Thickness (m)						
	West District	Regalado	140	?	180	a	a	a	a
		Granja Porcon	230+	?	310	a	a	a	a
		Cerro Negro	415	0-55	320	a	45	a	a
		Quilish	315	?	250	Northeast Quilish	a	a	a
		Corimayo	?	?	45+	90+	±310	?	0-60 domes
		Rosas / Angelita	>250	~210	?	>80	a	a	a
	East District	Yanacocha	?	>125	>40	~220	a	a	intrusions
		Chaupiloma	130+	130	0-20	50-90	a	a	intrusions
		San Jose	?	>90	110	?	80	100+	intrusions
		Baul	?	?	?	?	≥110	≥60	a
		Chaquicocha	?	>190	170	160	?	?	intrusions
		Hornamo	?	>135	40	115	125	a	intrusions
		Maqui Maqui	110+	220	±200	225+	70+	a	a
		Arnacocha	?	?	>50	80+	50	40	a
		Combayo	0-40+	0-50+	a	a	a	350	a

a = absent from the section
? = possibly present

Table 3.2 a. Characteristic mineralogy of the volcanic rocks at Yanacocha.

| Rock Unit (# samples) | Characteristic Mineralogy | | | | | | SiO$_2$ (weight %) | Age (Ma) |
| | Mineral | Phenocryst Percentage Range | Phenocryst Percentage Representative Sample | Total Mafic Minerals | Percentage of total phenocrysts | | | |
					Range	Select		
Tual lower andesite lahar sequence (3)	Plagioclase Amphibole Pyroxene Opaques	35-40 5-10 02-03 02-03	40 10 3 3	9-13	26-56	56	59-62	19.53±0.13
Chaupiloma lower andesite lahar sequence (11)	Plagioclase Alkali feldspar Detrital Quartz Amphibole Pyroxene Opaques	12-34.5 0-0.5 0-0.5 4.5-10 1.5-3 2.5-20	25 4.5 3 3	6-13	14-60	35.5	57-64.5	15.90±0.18 to 15.41±0.36
Cerro Frailes dacite pyroclastic sequence (23)	Plagioclase Alkali feldspar Quartz Amphibole Biotite Opaques	10-40 0.5-2.5 1-9 2-8 2-10 0.5-7	10 2 6 2 9 3	4-18	20-50	32	61-66	15.51±0.05 to 15.15±0.06
Lower Yanacocha pyroxene-hornblende andesite (19)	Plagioclase Amphibole Pyroxene Opaques	10.5-40 2-15 2-14 1-10	32.5 5 9 4	6-29	26-58	50.5	55-62	14.52±0.13 to 13.31±0.08
Lower Yanacocha pyroxene-hornblende andesite domes and intrusions (9)	Plagioclase Quartz Amphibole Pyroxene Opaques Apatite	9-26 0-2 8-15 5-11 1.5-6 0.11	40 1 8 7 1.5 trace	13-26	41-65	57.5	55-62	14.21±0.16 to 13.85±0.09

Table 3.2 b. Characteristic mineralogy of the volcanic rocks at Yanacocha (continued)

Rock Unit (# samples)	Characteristic Mineralogy						SiO$_2$ (weight %)	Age (Ma)
	Mineral	Phenocryst Percentage Range	Phenocryst Percentage Representative Sample	Total Mafic Minerals	Percentage of total phenocrysts			
					Range	Select		
Early dacite intrusions (8)	Plagioclase	9-25	20	5-12	18.5-44	33.8	63-64	?
	Alkali feldspar	0-2	3					
	Quartz	1-3	5					
	Amphibole	5-10	5					
	Biotite	0-2	0.8					
	Opaques	1-7	1					
Maqui Maqui pyroclastic sequence (15)	Plagioclase	30-55	40	5-14.5	40.3-68.3	55.2	60-66	12.63±0.05 to 12.40±0.10
	Alkali feldspar	0-2	2					
	Quartz	0-0.5						
	Amphibole	5-12.5	10					
	Biotite	0-2	1					
	Opaques	2-10	2					
	Apatite	0-0.5	0.2					
Maqui Maqui Porphyritic rocks (7)	Plagioclase	10-25	20	10-13	10-39	35.5	61.5-62.3	12.39±0.12 to 12.13±0.10 to 11.90±0.11
	Alkali feldspar	trace	0.5?					
	Amphibole	10-13	12.5					
	Opaques	1-2.5	2.5					
	Apatite	0-0.10	trace					
Upper Yanacocha pyroxene-hornblende andesite (26)	Plagioclase	12-40	20	4-18.5	22-55	31.3	61-65	12.08±0.10 to 11.91±0.08
	Amphibole	2-10	5					
	Pyroxene	2-8.5	5					
	Opaques	1.5-8	1					
	Apatite	0-0.1	0.3					
	Zircon	trace	trace					
Upper Yanacocha pyroxene-hornblende andesite domes and intrusions (13)	Plagioclase	10-40	23	3-25	28-60	44	62-64.3	12.01±0.10 to 11.28±0.09
	Amphibole	1-15	6					
	Pyroxene	2-10	8					
	Opaques	1.5-8	7					
	Apatite	0-0.10	trace					

Table 3.2 c. Characteristic mineralogy of the volcanic rocks at Yanacocha (continued)

Rock Unit (# samples)	Characteristic Mineralogy						SiO₂ (weight %)	Age (Ma)
	Mineral	Phenocryst Percentage Range	Phenocryst Percentage Representative Sample	Total Percent Mafic Minerals	Percentage of total phenocrysts			
					Range	Select		
Lower San Jose ignimbrites (19)	Plagioclase	35-50	40	4-12.5	32-63	46	62-64	11.56±0.13 to 11.43±0.06
	Amphibole	3.5-9	3.5					
	Pyroxene	0.5-2.5	0.5					
	Biotite	0-1	1					
	Opaques	1-6	1					
	Zircon	0-0.1	trace					
	Apatite	0-0.4	trace					
Middle San Jose ignimbrites (17) White tuff	Plagioclase	30-60	50	3-12	37-71	66.3	61-64.5	11.41±0.11 to 11.22±0.08
	Alkali feldspar	Trace	2					
	Amphibole	3-9	6					
	Pyroxene	0-1	1					
	Biotite	0-2	2					
	Opaques	1.5-5	5					
	Apatite	0-0.5	0.3					
Upper San Jose spatter ignimbrites (18)	Plagioclase	35-50	45	3-10	37-66.3	54	62.5-65	11.25±0.07 and 11.24±0.10
	Amphibole	3-6	4					
	Pyroxene	1.5 -7	1.5					
	Biotite	0-1	0.5					
	Opaques	1-6	3					
	Apatite	0-0.5	0.5					
Late dacite intrusions (19)	Plagioclase	12-40	15	4-16	24-43	30	67-71	10.78±0.05 to 8.40±0.06 (Turner, 1997)
	Alkali feldspar	1-8	4					
	Quartz	1-9	5					
	Amphibole	2-10	3.5					
	Biotite	2-6	2					
	Opaques	0.5-5.5	0.5					
	Sphene	0-0.5	0.5					

Table 3.3a Phenocyrst size and textural descriptions: the pre-Yanacocha and Yanacocha volcanic rocks.

Rock Package	Plagioclase	Amphibole	Pyroxene	Biotite	Quartz	Alkali Feldspar	Opaque oxides	Accessory Minerals	Texture	Lithic & Pumice	#	Comments
LAL	A 0.75 - 2	A 0.75 - 3 rare +3 - 5	C 0.5-1.5	N	R 0.65 detrital	N	C 0.25-1	T Ap 0.1	PBX BP Tlava Clastic	HL, bL, pL, tL, bL, whitePm	14	Tual lahars commonly are pumice-rich.
CFD	A 1 - 2.5	C 0.7 - 2.5	N	A 2 to 5	C 0.7-2.7	C 0.6-1.5	C 0.75	T Ap Zr	Eut NW PBX TBX BP	HL bL pLdacite whitePm 2-5mm	23	Rare fines-depleted tuffs, Amphiboles are commonly green pleochroic
Lpha	A 1 - 3 intrusions up to 6	C 1 - 2.5 domes/int up to 5	C 0.5 - 2 cpx>opx twin cpx common	N	N	N	C 0.5-0.75 Martite	T Ap 0.1	Tr PT P FF	Rare mafic enclaves of diorite	28	Slight resorbtion and ON zoning of plagioclase common. Melt inclusions abundant in outer rims. Hb are oxyhb decomposed w/ rims of FeOx common and red- to orange-brown and brown to yellow pleochroic, rare opacite rims of plg-pyx (dehydration rims). G plg in enclaves. Bimodal P in Plg and Hb is rare.
MMI	A 1.5 - 3.5 Intrusions 2.5 - 6	A 0.75 - 3 Intrusions 2 to +10	T 0.75	R 0.8 to 1.5 rare 4	R 0.5 Int 1.5 Em	R 0.75	C 1.0 Mt-IlmSS Martite	C Ap 0.7 Zr 0.15	BP Eut FD / S plg w/ Int	bL qtz arg common pL rare NWwhite Pm 5-10cm	15 v 7p	ON zoning of plg common, Hb with rims of FeOx and red- to orange-brown and brown to yellow pleochroic, Hb with abundant inclusions of plag, decomposed Hb common. Lower MMP has bio up to 4.0mm. Eut can be very faint to strong and fines-depleted. Fiamme common L/W 6-1. Shock frac Plg. WhitePm 20-25%
ED	A 3 - 6	A 2 - 5	N	R 1-2	C Em 1.5-2.5	R	C 0.8 Martite	T Ap 0.2 Zr 0.2	PPY G ONplg	N	8	Glomeroporphyritic plag and large plg w/ quartz inclusions. Rare convolute zoning. Hb gren pleochroic with rare opacite rims. Rare oxyhb. Slight resorption of bio with FeOx rims.
Upha	A 2.5 - 5 Domes to 6.5	C 1 - 2.5 R 3 - 5 Int to 10	C 1-2.5 cpx>opx	N	R Em 0.8	N	C 1.25 Martite ilmenite Mt-UspSS	R Ap 0.2 T Zr 0.05	Tr PT P bimodal FF rare G	Rare mafic enclaves of diorite	33	Mostly CPX. Bimodal Hb >1mm prismatic and <0.75 acicular phenocrysts. Opacite rims, Oxyhb and dehydrated Hb to plg-cpx. Pleochroic red-brown to yellow-tan. ONplg.

The relative abundance and maximum size in mm are reported for each mineral: A abundant, C common, R rare, T trace, N none, Plg plagioclase, Hb hornblende, Bio biotite, Qt quartz, cpx Clinopyroxene, opx orthopyroxene, Ap apatite, Zr zircon, Sp Sphene. # number of samples

LAL Tual and Chaupiloma lahar sequence, CFD Cerro Frailes dacite pyroclastic sequence, Lpha lower Yanacocha pyroxene andesite lavas, MMI Maqui Maqui pyroclastic sequence, ED early dacite intrusions, Upha upper Yanacocha pyroxene andesite-dacite lavas, Lsji lower San Jose ignimbrite, Msji middle San Jose ignimbrites, Usji upper San Jose ignimbrites, LD late dacite intrusions-domes, v volcanic, p porphyritic.

Textures: PT pilotaxitic, Tr trachytic, S seriate, BP broken phenocrysts, P porphyritic, PPY porphyry, Int intrusions, FF flow foliated, Eut eutaxitic, FD fines-depleted, NW non welded, PBX pyroclastic breccia, TBX tuff breccia, Pm pumice, L lithic, aL previously altered lithic, pL porphyry lithic, tL trachytic lithic, bL basement lithic, ML monolithic, HL heterolithic, ON oscillatory normal zoned, OR oscillatory reverse zoned, Em embayed, G glomeroporphyritic

204

Table 3.3 b. Phenocyrst size and textural descriptions for the San Jose ignimbrite.

Rock Package	Plagioclase	Amphibole	Pyroxene	Biotite	Quartz	Alkali Feldspar	Opaque oxides	Accessory Minerals	Texture	Lithic & Pumice	#	Comments
Lsji	A 1.5 - 4	A 1.5 – 5 +1mm are Poikilitic inc of plg	C rare 2 0.5-0.75 rare opx	R 0.6-2	T 0.15	N	C 0.5-1 Ilmenite and Mt to martite	C Ap 0.3 R Ap 0.75 T Zr 0.2	Eut BP NW FD ONplg	Rare HL and ML w/ tL and bL arg Rare aL of SM Pm 1-4cm	19	Rare large melt inclusions in Plg fragments(VC-4). Hb are dk brown to tan and red-brown to yellow-brown pleochroic. Hb have no opacite rims and rare oxidized rims, and are only slightly resorbed. Rare +1cm Hb megacrysts w/ concentric layering. Bio are partially resorbed w/ inclusions of feldspar and as inclusions in Hb. Ap are typically in the groundmass as large striated crystals with dark clouded cores. Glassy groundmass typically incipient to spheriodal devitrification. Welded flows with fiamme and NW w/ yellow billowy Pm. Rare spatter blobs.
Msji	A 1.5 - 3.5	C 1 - 2.5 R 3.5 T +1cm	T 0.3-0.7	R 0.25-1.5	T 0.5	T 0.5	C 0.25-0.75 Mt to martite w/ Ap inc	R Ap 0.1 T Zr 0.15 T Sp 0.1	BP FD Eut to NW D ONplg	C to R L HL pL bL C aL Pm lapilli ar-2/1 fiamme ar-10/1	17	Hb no opacite rims, rare decomposed w/ FeOx rims, rare resorbed rims, grn-brw to yel-tan and red-brw to yel-brw pleochrioc. Bio partially resorbed, inclusions of feldspar, replaces Hb. Ap are colorless w/ rare clouding. Bulldozed xtal frgs aL abundant in some flows with SM, BXH
Msji *white*	A 1.5 - 2	A 1.25 - 4	R 0.5 -1 Cpx	R 0.75-2.5	T 0.8	N	C 0.5 - 1 Mt to martite	R Ap 0.25 T Zr 0.2	BP FD Eut to NW D	Rare pL and aL C Pm fiamme	7	Plg no overgrowths or resorption. Hb dk brw to lt brw to tan pleochroic, resorbed rims, rare bio inc, large Hb w/ inc of opaque and Plg. Ap rare striated and clouded variety in some flows, colorless common. Flows vary from welded with abundant fiamme to rare fiamme and NW with minor lapilli-sized Pm in glassy gm w/ spheriodal devitrification.
Usji *Spatter*	A 1 - 3	A 1 – 5 oxyhb	A 0.5 - 3	T 1.3	N	N	C 0.5 -0.75 Mt to martite, ilmenite	C Ap T Zr	BP FD Eut ONplg	R fiamme ar 10/1 rare L rare aL	11	Abundant juvenile spatter blobs w/ flattened spatter texture. Hb red-brw to tan pleochroic w/ rims of FeOx, resorbed and decomposed rims. Rare opal altered lithics

The relative abundance and maximum size in mm are reported for each mineral: A abundant, C common, R rare, T trace, N none, Plg plagioclase, Hb hornblende, Bio biotite, Qt quartz, CPX Clinopyroxene, OPX orthopyroxene, Ap apatite, Zr zircon, R rutile, Sp Sphene. # number of samples

LAL Tual and Chaupiloma lahar sequence, CFD Cerro Frailes dacite pyroclastic sequence, Lpha lower Yanacocha pyroxene andesite lavas, MMP Maqui Maqui pyroclastic sequence, ED early dacite intrusions, Upha upper Yanacocha pyroxene andesite-dacite lavas, Lsji lower San Jose ignimbrite, Msji middle San Jose ignimbrites, Usji upper San Jose ignimbrites, LD late dacite intrusions-domes, v volcanic, p porphyritic.

Textures: PT pilotaxitic, Tr trachytic, S seriate, BP broken phenocrysts, P porphyritic, PPY porphyry, Int intrusions, FF flow foliated, Eut eutaxitic, FD fines-depleted, NW non welded, D devitrified, PBX pyroclastic breccia, TBX tuff breccia, Pm pumice, L lithic, aL previously altered lithic, pL porphyry lithic, tL trachytic lithic, bL basement lithic, ML monolithic, HL heterolithic, ON oscillatory normal zoned, OR oscillatory reverse zoned, Em embayed, G glomeroporphyritic.

Table 3.3c Phenocryst size and textural descriptions for the domes of the San Jose ignimbrite and the Upper (late) Dacite.

Rock Package	Plagioclase	Amphibole	Pyroxene	Biotite	Quartz	Alkali Feldspar	Opaque oxides	Accessory Minerals	Texture	Lithic & Pumice	#	Comments
SJI-related domes	A 2 - 3	A 2.5	A0.5-1.5 cpx>opx T 0.1	N	T 0.1	T 0.5	C 0.3-0.5 Mt to martite, ilmenite	R Ap 0.1	P PT S Plg FF	Rare mafic enclaves of Plg-cpx	6	Porphyritic Plg, Hb, Cpx. Seriate Plg in CB-3. Ap rare clouded and striated variety, yellow to colorless common, inc in Hb. Two types domes (1) A cpx, Tr PT (2) T cpx, S plg
LD	A 2.5 - 7	A 0.75-2.5	N	C 0.8-2	C Em 0.8-3.5	R 0.5-1.5	C 0.5-1 Mt Rare He	C Sp 0.3-1.2 T Zr 0.1 T Ap 0.2 T R 0.08	PPY rare FF BP w/ tuff S plg w/ Int	N	19	2 are tuff samples, one has Hb overgrowths around biotite (COR-47 173.5m). 17 are domes and porphyry plugs. One sample has Mt rimmed w/ py and Mt w/ cv inc (COR-47 173.5m). Hb distinct w/ green-tan-brw pleochroism.

The relative abundance and maximum size in mm are reported for each mineral: A abundant, C common, R rare, T trace, N none, Plg plagioclase, Hb hornblende, Bio biotite, Qt quartz, cpx Clinopyroxene, opx orthopyroxene, Ap apatite, Zr zircon, R rutile, Sp Sphene. v volcanic, p porphyritic, # number of samples

SJI-related domes - Domes spatially and temporally associated with the San Jose ignimbrite (SJI), LD - late dacite intrusions-domes.

Textures: PT pilotaxitic, Tr trachytic, S seriate, BP broken phenocrysts, P porphyritic, PPY porphyry, Int intrusions, FF flow foliated, Eut eutaxitic, FD fines-depleted, NW non welded, D devitrified, PBX pyroclastic breccia, TBX tuff breccia, Pm pumice, L lithic, aL previously altered lithic, pL porphyry lithic, tL trachytic lithic, bL basement lithic, ML monolithic, HL heterolithic, ON oscillatory normal zoned, OR oscillatory reverse zoned, Em embayed, G glomeroporphyritic.

Geochemical Variations with Time in the Cenozoic Yanacocha Volcanic Field, Cajamarca Province, Northern Perú

Anthony A. Longo

Anita Grunder

Abstract

Cenozoic volcanism in the Yanacocha study area spanned 11.2 million years from 19.5 to 8.4 Ma and hydrothermal activity continued for 5.4 million years from 13.5 to 8.2 Ma. Volcanism in the Yanacocha Volcanic Field (YVF) was centered at the Yanacocha Mining District for 6.1 million years from 14.5 to 8.4 Ma and the magma evolved from andesite to rhyolite with compositional variations in the geochemical data that typify a calc-alkaline rock suite. Five periods of magmatic activity and volcanism and six discrete pulses of hydrothermal activity have been interpreted from the volcanic stratigraphy and age data. Two episodic effusive to explosive eruptive events are recorded in YVF stratigraphy and include the Lower Yanacocha lavas (effusive stage 1; Tlpha) and Maqui Maqui Ignimbrite (explosive stage 1; Tmmi) followed by the Upper Yanacocha lavas (effusive stage 2; Tupha) and the San Jose Ignimbrite (explosive stage 2; Tsj).

YVF effusive-style eruptions were generated from deep crustal magma reservoirs of ~20 km depth in a crust with thicknesses estimated at 35 km. Magma from the earlier effusive event was stored in the upper crustal reservoirs as shallow as 3 km and later erupted explosively as ignimbrites. YVF melts may have fractionated and assimilated crust over a span of 6 million years. Late magmas were dacite and rhyolite that carry an adakite-like signature as displayed by the Sr/Y ratio whose compositional variations are part of the larger calc-alkaline suite. This latest felsic episode contains the mineral assemblage quartz-magnetite-sphene characteristic of highly oxidized magmas and developed porphyritic domes and intrusions of isolated dacite porphyry plugs spatially and temporally associated with the largest ore deposits at Yanacocha. Volcanism at Yanacocha ended in a final explosive event with the eruption of the Negritos rhyolite ignimbrite at 8.4 Ma (explosive stage 3).

Distinct geochemistry and mineralogy characterize each volcanic sequence and support the stratigraphy as outlined in the study. Phenocryst assemblages are distinct for each rock sequence. The pre-Yanacocha Tual and Chaupiloma andesite lahar sequences contain plagioclase, clinopyroxene, orthopyroxene and hornblende with 36 to 56% phenocrysts, whereas the Cerro Frailes dacite pyroclastic rocks contain coarse biotite, plagioclase, sanidine, quartz and hornblende with about 32% phenocrysts. In contrast,

Yanacocha rocks from the YVF are typically phenocryst-rich and range from 25-55% total phenocrysts in lavas, 30-60% phenocyrsts in dome rocks, and 40% to over 70% phenocrysts in the ignimbrites. Lower Yanacocha pyroxene-hornblende andesite lavas and Upper Yanacocha pyroxene-hornblende andesite to dacite lavas contain abundant plagioclase with clinopyroxene + orthopyroxene + hornblende, whereas ash-flow tuffs of the Maqui Maqui pyroclastic sequence and San Jose ignimbrite sequence contain abundant broken plagioclase with hornblende + biotite ± clinopyroxene. Late dacites and rhyolites at Yanacocha have quartz + biotite + hornblende + magnetite + sphene implying relatively high oxygen fugacities.

Compositional variations of the YVF rocks are typical of a subduction-related calc-alkaline rock suite that evolved by crustal contamination and fractional crystallization. The major element oxide data form a coherent trend from older medium-K andesite to younger high-K andesite, high-K dacite, and rhyolite, and display lower MgO content with increased SiO_2 through time. Trace elements display enrichments in the large ion lithophile elements (e.g., K, Rb, and Ba) and depletions in the heavy rare earth elements with increased SiO_2 content and support the hypothesis that Yanacocha evolved as part of a greater calc-alkaline rock suite.

Eruptive-styles of the YVF fluctuated from effusive stage clinopyroxene + orthopyroxene + hornblende bearing lavas to explosive stage hornblende + biotite ± clinopyroxene bearing ignimbrites. Combined processes of crystal-liquid fractionation, magma mixing, and muticomponent crustal assimilation are suggested for the evolution of the Yanacocha rock suite, and YVF melts evolved in the crust over a span of 6 million years. Patterns can be recognized in the data that imply that discrete magma batches coexisted and evolved separately. These compositions may have followed different evolutionary trends that involved crustal assimilation and mixing of end member deep mafic magmas with shallow crustal, pre-existing andesite and dacite magma. Yanacocha may have evolved from discrete magma batches at different levels and sites in the crust. These magmas erupted rock sequences with different mineral and chemical compositions periodically through time as outlined in this study.

Stratigraphy and Geochronology of the Yanacocha Volcanic Field

The Tertiary volcanic stratigraphy at Yanacocha consists of eight sequences of igneous rocks that include three distally derived pre-Yanacocha volcanic sequences and five locally derived volcanic sequences that comprise the Yanacocha Volcanic Field and covered an area of over 500 km^2 (Plates 1, 2 and 3). Volcanic rocks overlie folded Cretaceous sediments in the Yanacocha district and range in age from ~19.5 to 11.2 Ma with compositions from andesite to dacite. At least three pulses of late dacite intrusions and domes from ~10.8 to 9.9 Ma led to the formation of the largest high-sulfidation Au deposits at Yanacocha and were followed by the emplacement of rhyodacite to rhyolite intrusions and domes. By ~8.4 Ma, a final explosive eruption released a rhyolite ignimbrite after which volcanism and magmatic activity ended.

Pre-Yanacocha Volcanic Rock Sequences

Rock packages considered pre-Yanacocha were erupted from volcanic centers outside Yanacocha and deposited before 15.0 Ma. They are as follows in stratigraphic order (Figure 4.1a):

(1) Pre-20 Ma Huambo Cancha andesite lavas and pyroclastic rocks (Tv), informally referred to as basal andesite, overlie the Cretaceous basement and an early Tertiary unconformity. These rocks may belong to the Llama (55-44 Ma) or Huambos (39-36 Ma) volcanic sequences as discussed by Noble et al. (1990). The Late Cretaceous - early Tertiary uncomformity resulted from uplift related to the Cretaceous-Paleocene Peruvian Orogeny (90-60? Ma) and the Paleocene-Eocene Inciac I Orogeny (59-55 Ma) (Cobbing, 1981; Megard, 1984, 1987; Noble et al., 1985, 1990).

(2) Lower andesite lahar sequences comprise pumice-rich lahars, debris flows, volcaniclastic sedimentary rocks, and andesite lava flows filled paleo-channels in the Huambo Cancha andesite. Two distinct members were defined and include the Tual lahar sequence (~19.5 Ma; Tlal 1) and Chaupiloma lahar sequence (~15.9 Ma; Tlal 2). An unconformity after the Huambo Cancha andesite is

contemporaneous with the Eocene Inciac II or Oligocene Quechua I Orogenies of McKee and Noble (1982), Noble et al. (1985), and Noble et al. (1990).

(3) The Cerro Frailes dacite pyroclastic sequence (Tcfd) consists of coarse biotite-rich dacite lithic ash-flow tuffs and debris flows that yield ages of 15.5 to 15.2 Ma. These rocks were deposited over an erosional hiatus marked by stream channels cut into the lower andesite lahar sequence after ~15.9 Ma. After eruptions of the Cerro Frailes volcanic rocks, Yanacocha experienced gentle folding and an erosional hiatus from 15.2 – 14.5 Ma.

Yanacocha Volcanic Field

Rock sequences that belong to the Yanacocha Volcanic Field (YVF) represent volcanic and intrusive rocks from five contiguous centers of andesite to rhyolite magmatism centered at Yanacocha. These rocks evolved from spatially and temporally distinct eruptive centers in a northeast-trending corridor of middle Miocene volcanism 25 km long that covered more than 500 km^2 with lava flows and pyroclastic rocks. Andesite and dacite volcanism began with two periods of dominantly effusive eruptions that culminated in two periods of dominantly explosive eruptions over an interval of 3.3 million years from 14.5 - 11.2 Ma. These early styles of YVF volcanism were followed by 2.4 million years of magmatism from 10.8 – 8.4 Ma that compositionally varied from dacite to rhyolite. These rocks are distinctive, containing the phenocryst assemblage of sphene + magnetite + quartz that implies high magmatic oxygen fugacities (Wones, 1989). This late episode of highly oxidized felsic magmas developed porphyritic domes with minor lavas and pyroclastic aprons, and intrusions of isolated dacite porphyry plugs. Volcanism ended in a final explosive event with the eruption of the Negritos rhyolite ignimbrite at 8.40±0.06 Ma. Eruption of the Negritos ignimbrite was followed by a cessation of arc volcanism in the Yanacocha area and the initiation of flat-slab tectonics and associated volcanic gap from 2°S – 15°S in northern Peru (Gutscher et al., 1999).

Laminated rocks are present at three levels in the volcanic stratigraphy. Some are distinctly pyroclastic, whereas others have thin and planar laminations of dense silica. They are interpreted as laminated water-lain tuffs and surge deposits within a package of

pyroclastic rocks (Edwards, 2000) and accumulations of colloidal silica that deposited
in acid lakes associated with hydrothermal and volcanic vent areas (Longo, 2000).

Rocks of the YVF are as follows in stratigraphic order (Figures 4.1a and b):

(1) The lower Yanacocha porphyritic sequence (Tlpha) consists of pyroxene-
hornblende andesite lavas and minor pyroclastic rocks from an early period of
effusive volcanism and dome building called *effusive stage 1*.

(2) The middle Yanacocha laminated rocks, Maqui-Maqui ignimbrite sequence
(Tmmi), and early hornblende andesite and dacite porphyry intrusions (Tmmp,
Typ, and Ted). The Maqui Maqui ignimbrite sequence is comprised of hornblende
± biotite trachyandesite to dacite ignimbrites that represent an early period of
explosive volcanism called *explosive stage 1*. These rocks postdate, and are
temporally related to porphyritic intrusions, feldspar porphyry plugs, and
diatremes (Typ and Tmmp) with the same phenocryst assemblages as Tmmi. A
period of early dacite intrusions (Ted) with quartz + hornblende + biotite
phenocrysts intruded the Tlpha in the west district. Laminated rocks occasionally
crop out at the base of the Maqui Maqui ignimbrite.

(3) The upper Yanacocha porphyritic sequence (Tupha) consists of pyroxene-
hornblende andesite and dacite lavas and pyroclastic rocks from a second period
of effusive volcanism associated with numerous andesite dome related systems
called *effusive stage 2*.

(4) The San Jose ignimbrite sequence (Tsj) is comprised of hornblende ± pyroxene ±
biotite dacite ignimbrites from a second period of explosive volcanism called
explosive stage 2. Late upper Yanacocha Tupha pyroxene-hornblende endogenous
dacite domes followed the explosive eruptions and correspond to ignimbrite vent
areas.

(5) Late hornblende-biotite dacite domes and pyroclastic rocks of Corimayo-Tapado
(Tcd), quartz porphyry dacite plugs of Yanacocha (Typq), and rhyodacite dikes
and domes of Chaupiloma-Yanacocha Lake (Tcyd) represent the final, highly
oxidized, magmatic phase spatially and temporally associated with the ore

deposits at Yanacocha. Laminated rocks are also found spatially associated with the Corimayo dacite dome.

(6) Volcanism ended in a final explosive event with the eruption of the Negritos rhyolite ignimbrite at 8.4 Ma that may have vented from a fissure near the location of the Chaupiloma and Yanacocha lake rhyodacite dikes (*explosive stage 3*).
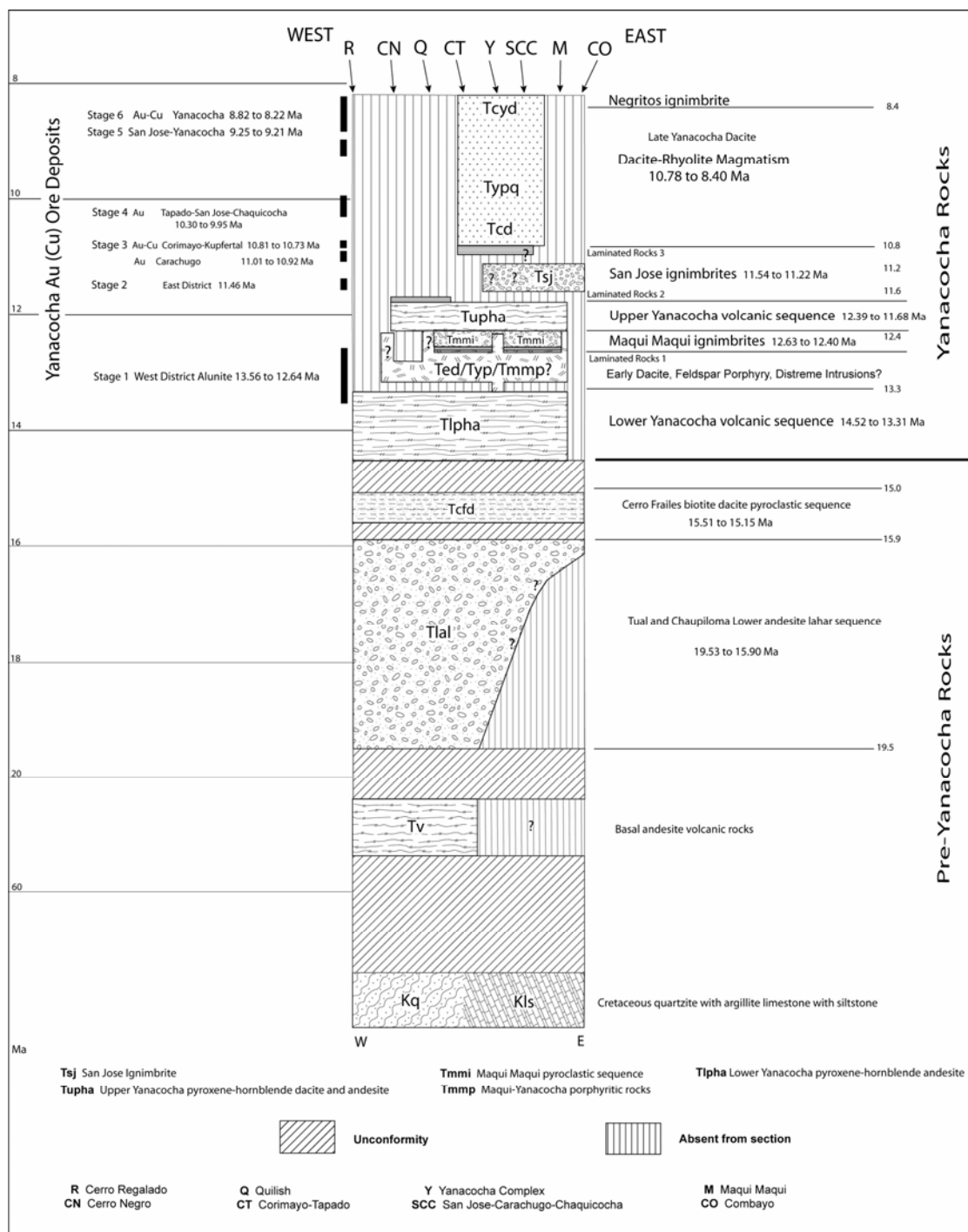
Figure 4.1a. A composite chronostratigraphic summary that shows temporal and spatial relationships of the volcanic stratigraphy, intrusions and gold-copper ore at Yanacocha. The section approximates a west to east slice through the district and the unit rectangles represent time and not stratigraphic thicknesses. Ages of mineralization are from radiometric $^{40}Ar/^{39}Ar$ age determinations on alunite and hydrothermal biotite (Kupfertal). Ages of volcanic rocks and intrusions are from radiometric $^{40}Ar/^{39}Ar$ age determinations on plagioclase, biotite and hornblende. Locations are displayed in Chapter 1 Figure 1.2
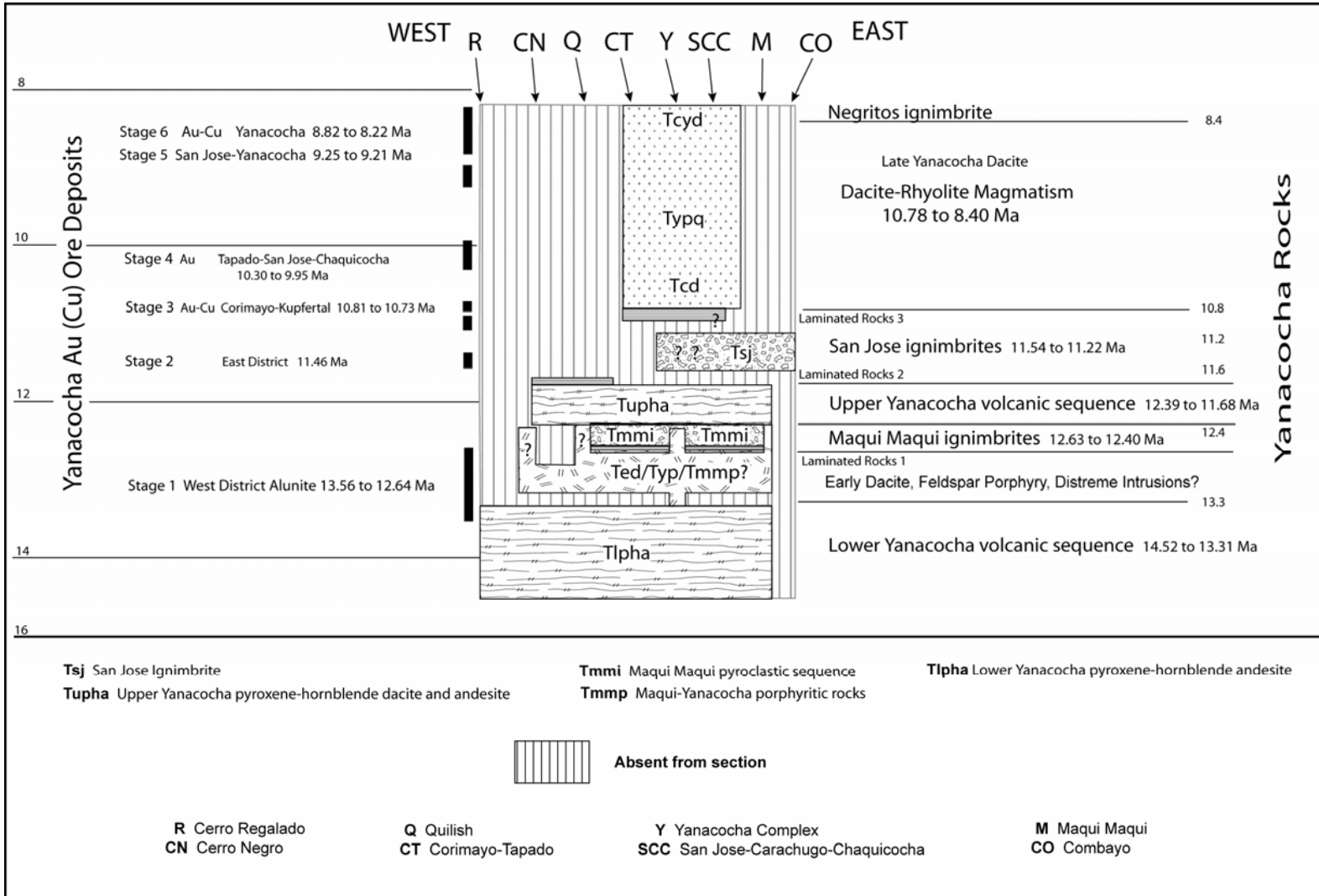
Figure 4.1b A composite chronostratigraphic summary that shows temporal and spatial relationships of the volcanic stratigraphy, intrusions and Au (Cu) ore in the Yanacocha Volcanic Field

Sequence of Events

The sequence of magmatic and hydrothermal events that shaped Yanacocha is as follows from oldest to youngest (Figures 4.1a and b):

(1) Effusive stage 1 volcanism began in the west at approximately 14.5 Ma with eruptions of the lower Yanacocha andesite lavas from small stratocones followed by dome-building and minor pyroclastic eruptions at 13.8 Ma. This style of volcanism migrated northeast and continued to 13.3 Ma. Lower Yanacocha porphyritic rocks (Tlpha) cover an area of 340 km^2 from Cerro Regalado to zones east of Maqui Maqui.

(2) Phase 1 hypogene advanced argillic alteration associated with gold and copper ore began in the west at Cerro Negro Oeste 13.6 Ma and migrated east to Quilish by 12.6 Ma and is spatially associated with early Yanacocha dacite dikes (Ted) and Yanacocha feldspar porphyry plugs (Typ) that intruded the Lower Yanacocha porphyritic rocks (Tlpha).

(3) Explosive stage 1 volcanism was centered in the east district and began with eruptions of the Maqui Maqui ignimbrite (Tmmi) at 12.6 Ma. Explosive activity continued to 12.4 Ma, and ignimbrites were followed by porphyritc lavas, dikes and porphyry plugs with similar mineral assemblages and composition until 12.1 Ma. These rocks covered an area of over 89 km^2.

(4) Effusive stage 2 volcanism extended 16.5 km from Pampa Cerro Negro in the west to Maqui Maqui in the northeast over an area of 121 km^2. Ages range from 12.1 to 11.9 Ma with eruptions of upper Yanacocha andesite and dacite lavas and pyroclastic rocks (Tupha) from numerous lava dome-related systems.

(5) Phase 2 hypogene advanced argillic alteration migrated northeast from Quilish and was centered in the east district near Carachugo and Maqui Maqui by 11.5 Ma (Turner, 1997).

(6) Explosive stage 2 volcanism began with eruptions of the San Jose ignimbrite (Tsj) at 11.6 Ma and spanned 400,000 years until 11.2 Ma. The sequence is divided into three ash-flow members that are mineralogically and texturally distinct and cover an area of 165 km^2. Ash-flow tuffs from the three members

correspond to separate eruptive events from a multiple vent complex. Acidic-altered accidental fragments (fragments of massive silica, and alunite and pyrophyllite-bearing fragments with residual quartz) found in ash-flow tuffs of the lower and middle members in the sequence suggest that the acid-sulfate hydrothermal alteration in the east part of the Yanacocha district preceded the earliest ash-flow (Longo, 2000). Explosive ignimbrite-forming eruptions were followed by dome-building that developed at least three dome complexes aligned in a northeast trend for 5.7 km from San Jose to Alto Machay (2 km east of Arnacocha).

(7) Phase 3a hypogene advanced argillic alteration haloed the high-sulfidation epithermal systems centered at Carachugo from 11.0 to 10.9 Ma in the east district, and was a precursor to the gold ore. Phase 3b from 10.8 to 10.7 Ma included hypogene advanced argillic alteration centered at Corimayo associated with Au mineralization. Hydrothermal biotite alteration at the Kupfertal Au and Cu porphyry system has a similar age.

(8) The Corimayo dacite dome was extruded at 10.8 Ma in a shallow Miocene-age lake and was preceded by local phreatic and phreato-magmatic eruptions. Siliceous laminated rocks, surge deposits, and tuff breccia were deposited prior to the extrusion of the dome.

(9) Phase 4 hypogene advanced argillic alteration was centered at Tapado, San Jose and Chaquicocha from 10.3 to 10.2 Ma with associated Au ore.

(10) At 9.9 Ma the Typq Yanacocha quartz porphyry plugs were intruded at Cerro Yanacocha centered in the Yanacocha Complex.

(11) Phase 5 hypogene advanced argillic alteration was centered at Cerro Yanacocha and San Jose from 9.95 to 9.2 Ma was a precursor to Au and Cu ore.

(12) Phase 6 hypogene advanced argillic alteration was centered at Cerro Yanacocha and Yanacocha Norte from 8.8 to 8.2 Ma with associated of Au ore, and also a precursor to Au and Cu ore.

(13) Domes and dikes of the Chaupiloma rhyodacite intruded a northwest fault zone from Cerro Chaupiloma to Yanacocha Lake at 8.4 Ma, and the Negritos rhyolite

erupted depositing an ignimbrite 10 km north of the Yanacocha Complex at Cerros de Los Negritos in a final explosive stage 3 eruption.

The duration of magmatic and hydrothermal activity was much longer than previously hypothesized. Hydrothermal activity began in the west at Cerro Negro Oeste at 13.6 Ma and migrated east to Quilish by 12.6 Ma, and then moved to Carachugo and Maqui Maqui. By 10.8 Ma, formation of high-sulfidation gold deposits became widespread in the east district spanning >8 km from Corimayo to Maqui-Maqui. This hydrothermal activity continued for about 700,000 years until 10.1 Ma. By 9.3 Ma, magmatic-hydrothermal activity was centered at Cerro Yanacocha for about 1.1 m.y., ending at about 8.2 Ma.

Hydrothermal processes that led to the deposition of gold ore at Yanacocha developed as discrete hydrothermal cells that migrated across the district through time. $^{40}Ar/^{39}Ar$ ages from magmatic-hydrothermal alunites and one hydrothermal biotite define six pulses of hydrothermal activity that spanned 5.4 million years from 13.6 Ma to 8.2 Ma. Hydrothermal quartz-alunite alteration of the Yanacocha rocks is closely spatially and temporally associated with the main high-sulfidation sulfide event and gold ore. Late dacite-rhyolite intrusions and domes are spatially and temporally associated with ore phases 4 through 7 and the largest gold deposits. Early dacite intrusions (Ted) and feldspar porphyry intrusions (Typ) are spatially associated with ore at Quilish and Cerro Negro (the oldest Au-Cu systems) in the west district.

Purpose and Methodology

The purpose of the study was to describe the spatial and temporal variations of geochemistry and phenocryst mineralogy in the Yanacocha Volcanic Field using the new revised volcanic stratigraphy based on the extensive $^{40}Ar/^{39}Ar$ geochronology and field geology described in Chapters 2 and 3. The mineral assemblage in each volcanic rock sequence was characterized by petrography. Rocks were analyzed for major element oxides and trace elements, and results are presented as major element oxide and trace element variation diagrams, and normalized rare earth element diagrams that compare each rock package at Yanacocha. Electron microprobe analyses of hornblende, pyroxene

and minor apatite were completed on 18 samples that represent a stratigraphic suite through the volcanic section. These results suggest different petrogenetic processes were involved that distinguish pre-Yanacocha rocks from Yanacocha rocks, and Yanacocha domes and lavas from Yanacocha ignimbrites.

Petrography

Petrography was done on 250 thin sections of samples collected from rocks in each volcanic package. Studies in transmitted light identified the basic mineralogy and textures characteristic to each volcanic package. Minor ore microscopy was done to verify the presence and types of Fe-Ti oxides in a select group of Yanacocha rocks.

Rock Geochemistry

Major and trace element analyses were done on 184 rocks from the Yanacocha area. Sample were prepared and analyzed by ALS Chemex (ALS). Two analytical methods were employed for geochemical analysis and include the following: (1) Samples for whole rock oxide analysis were analysed by X-ray fluorescence (ME-XRF06), (2) ALS method ME-MS81 was used for trace element determination with inductively coupled plasma mass spectroscopy (ICP-MS) (Appendix IIc). A lithium metaborate fusion was used to ensure total destruction of the rock forming minerals to provide total elemental concentration for the REE's and other resistate elements (Highsmith, 2001) followed by dissolution in a solution of four acids (HF-HNO3-HClO4 digestion and a HCl leach). Elements and ranges of detection for each package are listed in appendix Ic2. Samples AZU-1 and CHQS-2, two unaltered pyroxene andesite lava flows at Yanacocha, were used as internal standards. They were analyzed at regular intervals throughout the analyses to test reproducibility. Range of reproducibility for the major element oxide analyses varied from 0.10 to 3.4 % and was highest for MgO (1.9 and 3.4% in AZU-1 and CHQS-2 respectively) and TiO2 (2.2 and 2.8% in AZU-1 and CHQS-2 respectively) with 1σ (one standard deviation of the mean) values that ranged from 0.00 to 0.13 wt% (Appendix VII1.9 and 3.4% in AZU-1 and CHQS-2 respectively)). Trace element reproducibility show 1.5% to 5 % variability for most elements analyzed and higher

variability of >10% from elements such as Lu, Cs, Th, U, Mo, and W whose values closely approach detection limits (Appendix IIc, CD Appendix V).

Electron Microprobe Analyses

Amphibole, pyroxene, and apatite analyses were carried out on a Cameca SX-50 electron microprobe at Oregon State University (Appendix IId, CD Appendix VI). Samples included 18 polished thin sections of andesite and dacite volcanic and dome rocks from throughout the volcanic section at Yanacocha. Elements analyzed included the following:

Amphibole: Si, Al, Mg, Ca, Na, K, Fe, Ti, Cr, Mn, F, Cl.

Pyroxene: Si, Al, Mg, Ca, Na, K, Fe, Ti, Cr, Mn.

Apatite: P, Mg, Ca, Na, Fe, F, Cl, S.

Oxide weight percent and atomic proportions per formula unit were calculated by computer using Cameca software (Appendix VIII). Amphibole formulas were calculated on the basis of 23 oxygens after Leake (1997). Fe^{+2} and Fe^{+3} were calculated from the total oxide Fe as FeO* for all amphiboles using a general equation for estimating Fe^{3+} where $F = 2X(1-T/S)$ after Droop (1987) on the basis of 23 oxygens (anhydrous) assuming 13 cations ($\sum Mn = Si+Al+Ti+Fe*+Cr+Mg+Mn$) exclusive of Ca, Na and K for calcic-amphiboles. The equation is as follows: $F = 46(1-13/\sum(Mn)$; $T = 13$ (ideal number cations/formula), S = observed cation total/X oxygens calculated assuming all iron is ferrous. The calculations for the amphibole formula are presented for a worked example in Appendix III.

Total volatile concentrations as H_2O wt%, and oxygen equivalents for Cl and F were also calculated for the amphiboles. H_2O is estimated by assuming 2 (OH) groups are present in the formula where 1 oxygen is balanced by 2 H (H_2O) and 1 oxygen is balanced by F and Cl. After normalizing the entire formula (inc. F and Cl) with the O factor, F + Cl are subtracted from 2 to estimate the assumed OH^- ions in the formula. Weight percent H_2O is calculated as follows: (1) OH ions in the formula are divided by 2, (2) ($H_2O = 2(HO_{0.5})$).

Molecular Al^{IV} and Al^{IV} were calculated from total Al_2O_3 for all amphiboles on the basis of both 23 oxygens after Leake (1997) and 24 oxygens after Deer et al. (1993)

220

applying the estimated H_2O content. The aluminum in hornblende model after
Johnson and Rutherford (1989) was then used to calculate the amphibole barometer.

Results

Distinct composition and phenocryst assemblages characterize each volcanic
sequence and support the stratigraphy as outlined in the study. Compositional variations
are typical of subduction-related calc-alkaline rock suites that evolved by crustal
contamination and fractional crystallization (e.g., Thorpe et al., 1980; Rogers and
Hawkesworth, 1989).

Phenocryst mineralogy of rocks in the Yanacocha volcanic sequences is typical of
hydrous calc-alkaline rock suites. Plagioclase is the most abundant phenocryst mineral
with average abundances that range from 16 to 41 modal% (Figure 4.2). All Yanacocha
rocks contain amphibole in abundances that average between 4 to 9 modal % coexisting
with combinations of clinopyroxene, orthopyroxene, biotite, Fe-Ti oxides, plagioclase,
alkali feldspar, and quartz. Least abundant primary phases are orthopyroxene and alkali
feldspar. Accessory minerals include apatite, zircon, rutile, and titanite. Titanite is present
in the late dacite and rhyolite intrusions, the Negritos ignimbrite, and is rare in
ignimbrites of the middle San Jose sequence.

Textural differences between the pre-Yanacocha volcanic rocks and volcanic rocks of
the YVF are distinguishable in the field and include grain size and phenocryst abundance.
Rocks of the YVF are typically coarse grained and phenocryst-rich (Tables 2 and 3)
relative to pre-Yanacocha rocks. The maximum dimensions of YVF phenocrysts are
typically 2.5 to >5mm and phenocryst abundances commonly total 50% or more. In
contrast, percent total phenocrysts in pre-Yanacocha rocks are generally <40% and the
maximum dimension of the largest phenocrysts are ≤3mm.

Mineralogy of the Rock Sequences

Pre-Yanacocha Rock Sequences

Tual and Chaupiloma lower andesite lahar sequence (LAL)

Mineralogy of the sequence is typical of andesites in the Andean region (Figure 4.2; Tables 3.2 and 3.3). Phenocrysts consist of plagioclase > amphibole > pyroxene > Fe-Ti oxides, and percent total phenocrysts vary between 14% in lava flows to 60% in lahars. Clinopyroxene is more abundant than orthopyroxene, and amphiboles are both green pleochroic with opacite rims and oxy-hornblende totally replaced with Fe-Ti oxides. Percent total mafics vary between 6% and 13%. Detrital quartz and alkali feldspar are present in debris flows at Chaupiloma. Opaque minerals are also quite variable from 2% to 20%.

Cerro Frailes dacite pyroclastic sequence (Cfd)

Mineralogy of the Cerro Frailes pyroclastic sequence is distinct and can be readily distinguished from all other rock sequences in the Yanacocha district by the presence of abundant coarse biotite (Figure 4.2; Tables 3.2 and 3.3). Phenocrysts consist of plagioclase > biotite > quartz > hornblende > Fe-Ti oxides > alkali feldspar, and pyroxene, apatite and sphene are absent. Percent total phenocrysts can range from 20-50% and typically are ~30% of the total sample. Percent total mafic minerals range from 4% to 18% and typically are 11% with abundant (up to 10%) coarse biotite (0.5 cm across when looking down the C-axis). Percent total biotite is generally higher than the percent total hornblende by four to one in a typical sample. Quartz is also diagnostic with total quartz phenocryst content that varies between 1% and 9%, but commonly is estimated at 6% in hand specimens from most ash-flows tuffs.

Yanacocha Volcanic Field

Lower Yanacocha pyroxene-hornblende andesite (Lpha)

Mineralogy of the Lower Yanacocha volcanic sequence is distinct with the presence of abundant green pyroxene and acicular hornblende (Figure 4.2; Tables 3.2 and

3.3). These rocks are always flow-foliated and all the phenocrysts are aligned in a flow foliation with a pilotaxitic texture (Figure A6.2, Appendix VI) and can be readily distinguished from the pyroclastic sequences in the Yanacocha district. Phenocrysts consist of plagioclase > pyroxene > hornblende > Fe-Ti oxides, and quartz, alkali feldspar, biotite, and sphene are absent. Accessory apatite is present in many samples examined petrographically. Phenocrysts typically make up ~50% of the total sample, but the percent total phenocrysts ranges from 26-58 modal%. Percent total mafic minerals usually are 15% and range from 6% to 29 modal%. In a typical sample, pyroxene is more abundant than hornblende. Plagioclase is commonly porphyritic with a bimodal size distribution. Quartz is rare, but characteristic of the andesite domes in the west district. The Lower Yanacocha volcanic sequence can be distinguished from the pyroclastic sequences in the Yanacocha district (Figure 4.2; Table 3.2a and 3.3a) by its lower overall phenocryst abundance and lack of broken phenocrysts.

Early dacite intrusions (Ed)

The modal assemblage consists of a phenocryst suite of plagioclase > hornblende > quartz > alkali feldspar > biotite > opaque oxides, and clinopyroxene, apatite and sphene are absent (Figure 4.2, Tables 3.2b and 3.3a). Total phenocryst percent in a typical sample is 34%, but varies between 19 to 44%. Percent total mafics varies between 5% and 12%. Quartz phenocrysts are rounded and slightly embayed and range in size from 0.2-2.5mm. Overgrowth rims of quartz are rare around quartz and alkali feldspar phenocrysts. Textures are typical of porphyry intrusions in that 30-40% phenocyrsts are surrounded by an aplitic groundmass (Table 3.3a).

Maqui Maqui pyroclastic sequence (MMP)

Mineralogy and textures of the Maqui Maqui pyroclastic rocks are distinct from pyroxene-hornblende andesite lavas and can be distinguished in the field by the lack of pyroxene, the lack of pilotaxitic textures, the presence of occasional biotite, and abundant broken phenocrysts. The eutaxitic-textured Maqui Maqui ignimbrite (MMI) is the most prominent member. Eutaxitic textures are common, but not always present.

Phenocrysts consist of plagioclase > amphibole > opaque oxides > biotite with rare quartz and alkali feldspar. Pyroxene is generally absent, or present in trace amounts. Apatite is commonly large (>0.5mm), striated and cloudy (Table 3.2a). Total percent phenocryst abundance is generally higher and commonly 55% but ranges from 40-68%. In thin section it is common that the plagioclase phenocrysts are shock fractured (Figure A6.3e and f , Appendix VI , and Table 3.2a). Sparse intrusions are included in the rock sequence and have abundant coarse hornblende with phenocryst to +10mm (Table 3.2a). The maximum dimensions of hornblende phenocrysts in MMP ash-flow tuffs are smaller than hornblende in the San Jose ignimbrite (Table 3.2a).

Upper Yanacocha pyroxene-hornblende andesite and dacite lavas (Upha)

The mineralogy and textures of the Upper Yanacocha lavas are similar to Lower Yanacocha lavas (Figure 4.2), and distinguishing the two in the field is a problem. Subtle differences, however, will assist field identification and include the following criteria (Table 3.2b and 3.3a): (1) maximum dimensions in phenocrysts are distinctly larger in the Upper Yanacocha (2.5-5mm) versus Lower Yanacocha (1-3mm), (2) hornblende is more commonly porphyritic in the Upper Yanacocha and bimodal with small acicular laths (<0.75mm) and prominent prismatic crystals (>1mm), and (3) generally abundances of hornblende are greater than the overall pyroxene abundance for Upper Yanacocha rocks (Table 3.2b and Figure 4.2). Phenocrysts consist of plagioclase > hornblende > pyroxene > Fe-Ti oxides, and quartz, alkali feldspar, biotite, and titanite are absent. Apatite and zircon are more common in the Upper Yanacocha lavas relative to Lower Yanacocha lavas.

San Jose ignimbrite sequence (SJI)

Phenocryst content and type varies between the lower, middle, and upper members of the San Jose ignimbrite (Figure 4.2, Table 3.2). The Lower San Jose consists of plagioclase > amphibole > pyroxene > Fe-Ti oxides > biotite and accessory apatite and zircon, whereas, the Middle San Jose consists of plagioclase > amphibole > Fe-Ti oxides > biotite with trace pyroxene and accessory titanite, apatite and zircon. Two compositionally and texturally distinct ash-flow tuffs were recognized in the San Jose

ignimbrite (Table 3.3b); these are the Upper San Jose *spatter ignimbrite* and the Middle San Jose *white tuff* (see chapter 3). Phenocrysts in the spatter ignimbrite consist of plagioclase > amphibole > pyroxene > Fe-Ti oxides with trace biotite and accessory apatite and zircon. Pyroxene > amphibole is common in many *spatter* flows. Single apatites as large as 0.3 to 0.75mm are common in the groundmass of the Lower San Jose ignimbrite and the Upper San Jose *spatter ignimbrite* (Table 3.2b), and typically are striated with clouded cores similar to apatites in the Maqui Maqui ignimbrites. Apatite in the Middle San Jose ignimbrite is rare and typically a smaller colorless variety is present.

Upper (Late) dacite intrusions (Ud)

Late dacite intrusions are divided into three groups on the basis of location and age. *Corimayo dacites* (Tcd) have a distinct mineralogy (Figure 4.2, Table 3.2c and 3.3c) with 3% quartz (0.1-2.0mm anhedral rounded to embayed phenocrysts), 10-15% total mafics as 5% biotite (0.2-1.5mm euhedral phenocrysts) and 5-10% hornblende, and accessory titanite phenocrysts (0.5-1.0mm). Textures are porphyritic to seriate with a glassy to aplitic groundmass and 30-43% phenocrysts.

Intrusions of *Yanacocha dacite* porphyry (Ypq) crop out at Yanacocha Norte and Chaquicocha spatially associated with northwest trend of gold ore. Mineralogy is distinct with 5-9% quartz (0.5-3.5mm subhedral to embayed), 6% total mafics as 3% biotite and 3% hornblende, and accessory titanite. Quartz phenocrysts are larger (up to 3.5mm) than the quartz-eyes in the *Corimayo dacite*, and textures are typical of porphyry intrusions with a total phenocryst content of 30% and aplitic-textured groundmass.

Late dacite dikes and plugs of the *Chaupiloma and Yanacocha Lake dacites* (Tcyd) are confined to a northwest trend through the central part of the east district and the outcrop pattern has a combined strike length of ~4 km. Mineralogy of these dacites consists of 4-5% quartz (0.2-0.8mm), 10% total mafic minerals with 3% biotite and 7% hornblende, and accessory titanite.
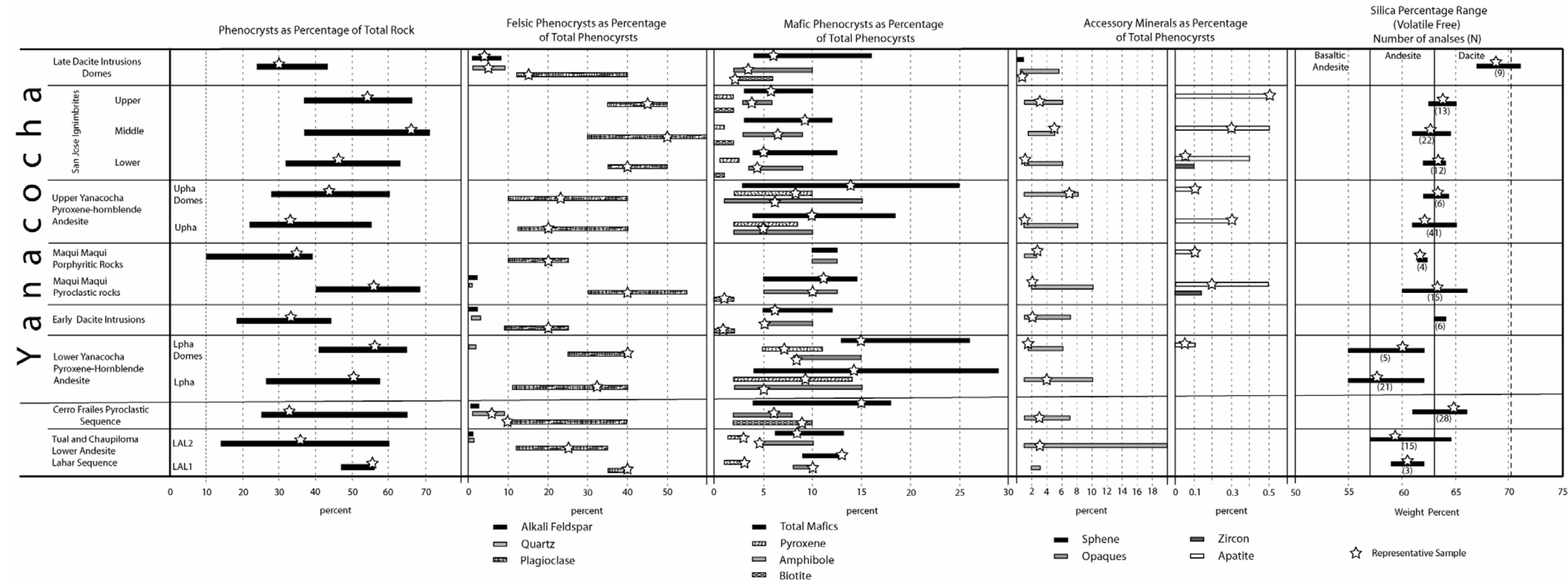
Figure 4.2. Chart of the modal ranges for the phenocryst mineralogy in samples of the Yanacocha rock sequences compared to the range in SiO$_2$ content.

Results of the Petrographic and Microprobe Analyses

Plagioclase

Plagioclase is the most abundant phenocryst in the Yanacocha rocks and typically constitutes 56 to 81% of the phenocrysts by volume. It is commonly pilotaxitic and porphyritic in lavas and rarely glomeroporphyritic (Appendix VI). Varying degrees of fracturing and shattering of phenocrysts are common in the pyroclastic rocks (Appendix VI). Phenocrysts are not resorbed and only slight resorption was observed in the Late Dacite (Figure 4.3). Phenocrysts typically display concentric normal zoning and some display convolute zoning. Carlsbad-albite twinning is common to all the YVF rocks, and also display strong concentric zoning. Plagioclase compositions were not analyzed by microprobe, and due to the intense oscillatory and concentric zoning, optical estimates on composition were difficult to impossible. Optical estimates using Michel-Levy techniques were only completed on selected samples and range from andesine to oligoclase. These estimates indicate compositions range from An_{22} to An_{62} overall with An_{28-53} in pyroxene-hornblende andesites, An_{30-36} in the Maqui Maqui ignimbrite, and An_{22-54} in late dacite. Melt inclusions of glass are common along the outer margins of plagioclase in most rocks of this study. Multiple concentric rings of inclusions were observed in concentrically zoned plagioclase of the pyroxene-hornblende andesite and pre-Yanacocha rocks.

Plagioclase in most Yanacocha rocks show evidence for multiple periods of resorption from dissolution by heating and crystal growth by cooling. Textural criteria observed in the plagioclase at Yanacocha include the following (after Coombs et al., 2000): (1) unsieved and unresorbed phenocrysts, (2) resorbed rims and no sieve textures, (3) sieved cores mantled by unsieved rims, and (4) finely sieved rims with unsieved cores mantled by unresorbed rims. Sieve-textured and resorbed plagioclase are common in the Lower Yanacocha and Upper Yanacocha andesite sequences, and rare in the ignimbrites. Sieved cores display irregular melt inclusions in the An-rich core of the plagioclase (Figure 4.5, Figure A6.2b). Sieve rimmed textures display rims of trapped melt inclusions due to dissolution by heating of the An-poor rims (Figures A6.2c, A6.4a, A6.6d). Sieved

core and rims are commonly mantled by unsieved rims. More work is needed to adequately classify the resorption textures and the compositional variations in plagioclase at Yanacocha. (after Coombs et al., 2000)

Plagioclase phenocryst size and abundance are variable throughout the volcanic stratigraphy. Attributes typical for each rock sequence are presented in Tables 3.2 and 3.3 and summarized as follows:

(1) Plagioclase in the pre-Yanacocha rocks is glomeroporphyritic and trachytic in the Chaupiloma lower andesite lahar sequence lava flows and broken in the pyroclastic rocks. Phenocryst sizes range from 0.75 to 2.5mm and modal phenocryst abundances range from 10 to 40% relative to the groundmass.

(2) Overall size ranges indicate plagioclase phenocrysts in pyroxene-hornblende andesite lavas of the Yanacocha Volcanic Field are smaller in Lower Yanacocha lavas relative to Upper Yanacocha lavas. Phenocryst sizes in the Lower Yanacocha lavas range from 1 to 3mm, whereas they range from 2.5 to 5mm in the Upper Yanacocha lavas. The range of plagioclase abundance in pyroxene-hornblende andesite lavas ranges from 10-40% in both Upper Yanacocha and Lower Yanacocha, although, Lower Yanacocha intrusions were found to contain less plagioclase (9-26%) than Upper Yanacocha intrusions (10-40%).

(3) Broken plagioclase phenocrysts in the ignimbrites of the Yanacocha Volcanic Field (both Maqui Maqui and San Jose ignimbrites) are similar in size and range from 1.5 to 3mm, and abundances range from 30 to 60%.

(4) Plagioclase in most Yanacocha intrusive rocks is porphyritic in pyroxene-hornblende andesite and seriate with rare glomeroporiphyritic clots in the late dacite. Phenocrysts are large and vary in size from 2.5 to 7mm. Abundances are generally less in early dacite and Lower Yanacocha intrusions with 9 to 26% phenocrysts of plagioclase, whereas abundances in the Upper Yanacocha domes range from 10-40% and late dacite intrusions 12-30%.

Quartz

Quartz is common to the Cerro Frailes dacite pyroclastic sequence (Cfd), the early dacite intrusions (Ed), and the late dacite intrusions and pyroclastic rocks (Ld) and ranges from 1 to 9 modal % (Table 3.2). Rare quartz is present in lower Yanacocha andesite

(Lpha) domes, the Yanacocha Sur andesite dike "Black Dike" (YSBD), the ignimbrite of Piedras Gachas, and trace quartz has been observed in the Maqui Maqui ignimbrite (MMI) and middle San Jose ignimbrite (Msji). Phenocrysts are broken in pyroclastic rocks and range in size from 0.15 to 0.5mm in the ignimbrites of the Yanacocha Volcanic Field and 0.7-2.7mm in the Cerro Frailes dacite pyroclastic rocks. Sizes of quartz phenocrysts found in the intrusions range from 1.5 to 2.5mm in the early dacite and 0.8 to 3.5mm in the late dacite. Phenocrysts in the early dacite are subhedral, rounded to slightly embayed (resorbed), whereas, they are rounded to strongly resorbed and anhedral in the late dacite rocks (Figure 4.3).
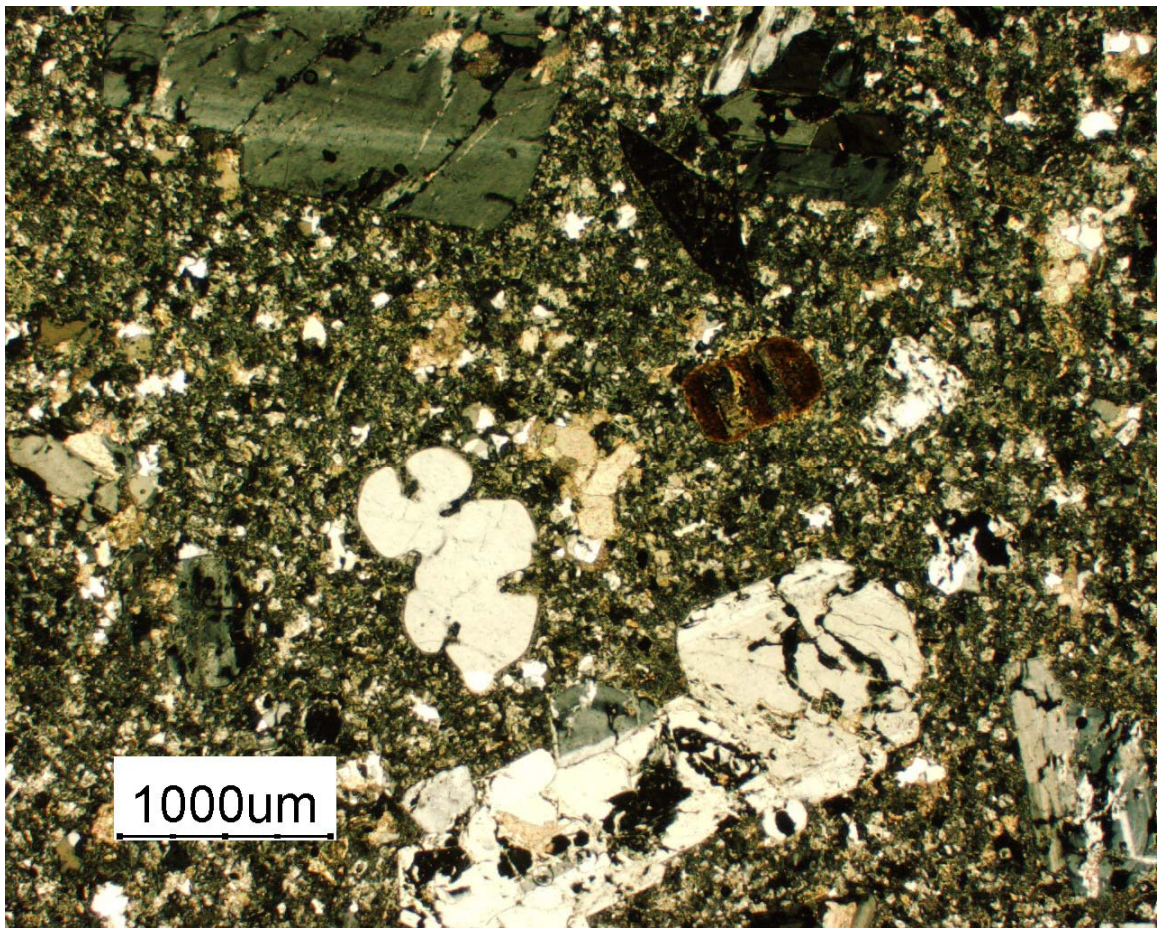
Figure 4.3. Photomicrograph of resorbed quartz and plagioclase in the Yanacocha dacite porphyry (YN-1A). The rounded dark brown phenocryst is biotite and the pinkish-tan mineral in the groundmass is calcite. Plagioclase display resorbed cores.

Alkali Feldspar

Optical estimations for the presence and amounts of alkali feldspar were difficult due to the rarity and small sizes present in the Yanacocha rocks. Further work is required to adequately assess abundances. Alkali feldspar was identified by its optical properties of biaxial (-) and the absence of lamellar twinning slightly lower birefringence relative to plagioclase. It is present in small amounts (1 to 4 modal %) in the Cerro Frailes tuffs, Lower (early) Dacite, Upper (late) Dacite, Negritos ignimbrite, and the middle San Jose ingimbrite. Trace alkali feldspar has been observed in the MMI. Phenocrysts are subhedral (rarely euhedral) and slightly resorbed along the rims, and sizes range from 0.5 to 1.5mm.

Biotite

Biotite is common to rocks in Yanacocha that lack pyroxene and have dacite compositions of > 63 wt.% SiO_2. This includes the Cerro Frailes dacite pyroclastic rocks, the early dacite, and the late dacite. Coarse biotite is ubiquitous in the Cerro Frailes dacites tuffs (up to 10 modal %) and phenocryst sizes are 2 to 5mm. Trace to rare (0 to 2 modal %) biotite is found in the Maqui Maqui and San Jose ignimbrites with amphibole and sizes range from 0.25 to 2.0mm. Biotite found in the Maqui Maqui ignimbrite has inclusions of quartz, and biotite in the Cerro Frailes dacite and San Jose ignimbrite commonly has inclusions of plagioclase and Fe-Ti oxides. Biotite has been observed as inclusions in hornblende in the Maqui Maqui ignimbrite, San Jose ignimbrite, and late dacite. Growth rims of hornblende are rare and have been observed in biotite from the late dacite at Corimayo (Figure 1.2). It is assumed that biotite precipitated late in the crystallization sequence after the mineral phases plagioclase, quartz, and opaque oxides, but before hornblende in the Maqui Maqui ignimbrite, San Jose ignimbrite, and late dacite. Biotite is generally not found in rocks with < 63 wt.% SiO_2. Exceptions are in the San Jose ignimbrites where a few hornblende phenocyrsts display overgrowth rims of biotite.

Amphibole

Amphibole is common in all igneous rocks at Yanacocha; however, phenocyrst abundance, size, and shape are variable throughout the volcanic stratigraphy and distinct to each rock sequence. Amphiboles in the pre-Yanacocha lower andesite lahar sequences and Cerro Frailes pyroclastic sequence range in abundance from 5 to 10 modal %, and phenocryst size is generally 0.7 to 3.5mm (Tables 3.2 and 3.3). YVF rocks display a wide range of phenocryst size from 0.75 to 5.0mm, and up to 10mm in the Maqui Maqui intrusions and San Jose ignimbrites (Table 3.3). Abundance also is quite variable from 2 to 15 modal% in the Lower Yanacocha and Upper Yanacocha pyroxene-hornblende andesite lavas and from 3 to 10 modal % in the Maqui Maqui and San Jose ignimbrites (Table 3.2). Generally, amphibole phenocrysts are coarse grained in the Yanacocha intrusions compared to the lavas and pyroclastic rocks; however, large +5mm megacrysts of amphibole can be found in Upper Yanacocha lavas and domes, and ignimbrites of the San Jose. The following types of amphibole were observed at Yanacocha.

Lower Yanacocha Andesite Domes

Amphiboles in the quartz-bearing Lower Yanacocha pyroxene-hornblende domes, such as Cerro Regalado, display multiple opacite rims with phenocryst sizes are typically 1 to 5mm with abundances from 8 to 15 modal %. Multiple opacite rims indicates resorption occurred in the magma chamber (Gill, 1981; p. 180). Degree of resorption is dependant on temperature and the rate of ascent. The amphibole stability curve has a low and positive dP/dT slope at low temperature (<900ºC) and low pressure (<1.5kb); therefore, resorption will occur at a shallow depth (Gill, 1981; p. 194-196). In this sample (Figure 4.4), opacite rims of Fe-oxide were preserved and developed during the initial stages of decompression. Continuous decompression during ascent resulted in complete dehydration and replacement of the hornblende by pyroxene and plagioclase.
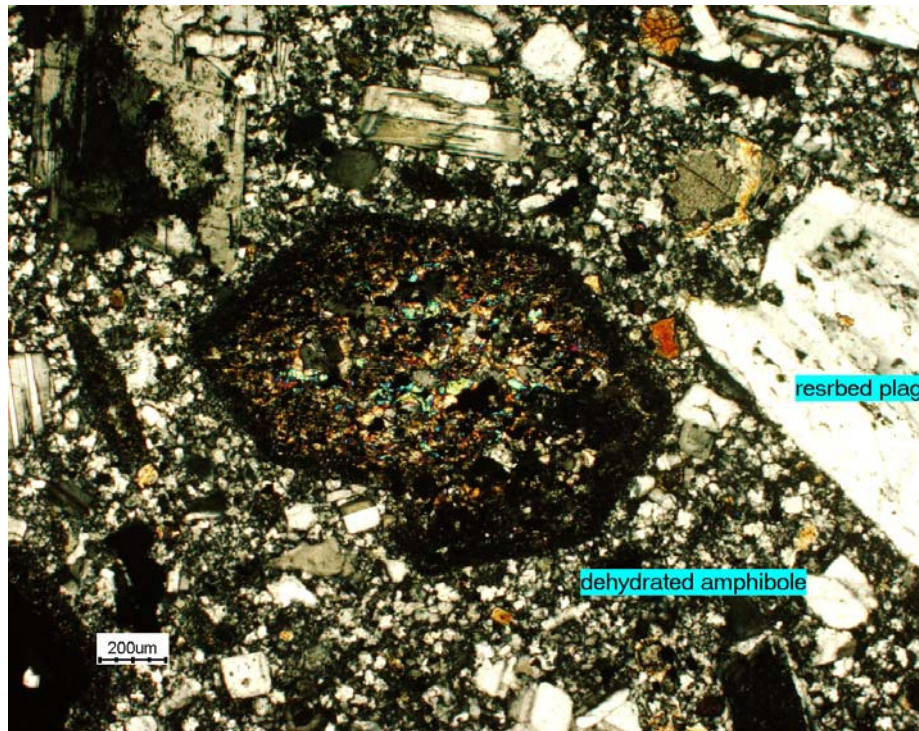
Figure 4.4. Photomicrograph of amphiboles in the quartz-bearing Lpha andesite dome at Cerro Regalado (CR-4). The hornblende in this sample shows dehydration and complete replacement of the amphibole by pyroxene, plagioclase and Fe-oxides. Plagioclase shows resorption textures with occasional sieve-cored textures (large phenocryst in right half).

Lower Yanacocha Andesite Lavas

Amphibole phenocrysts in Lower Yanacocha andesite lavas range in size from 1 to 2.5mm and are resorbed prismatic phenocyrsts and acicular groundmass crystals with opacite rims of magnetite, plagioclase and pyroxene, or phenocrysts are completely replaced with opaque oxides (Figure 4.5, 4.6 and 4.7). Larger phenocrysts typically have inclusions of plagioclase or Fe-Ti oxide, and the cores are not altered (Figure 4.8). Amphibole abundances range from 2 to 15 modal %. Phenocyrsts are small and range from 0.2 to 3mm.
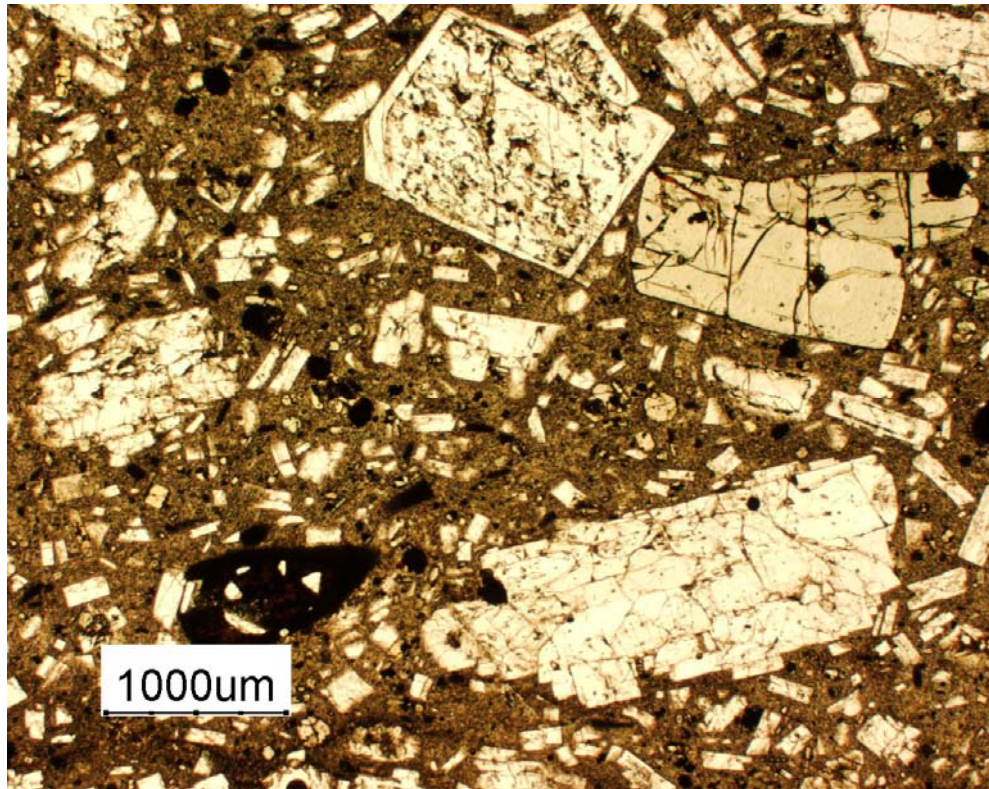
Figure 4.5. Photomicrograph of an Lpha lava flow (CNN-1). The sample shows acicular hornblende in the groundmass and small prismatic hornblende phenocrysts with feldspar inclusions. Hornblende is replaced with Fe oxides and smaller than the clinopyroxene phenocrysts. Some plagioclase are resorbed or show sieve textures as the plagioclase phenocryst (central top adjacent the pyroxene). This phenocryst displays slight sieve-cored and sieve-ringed textures mantled by unresorbed rims as discussed by Coombs et al. (2000) implying resorption and magma mixing.
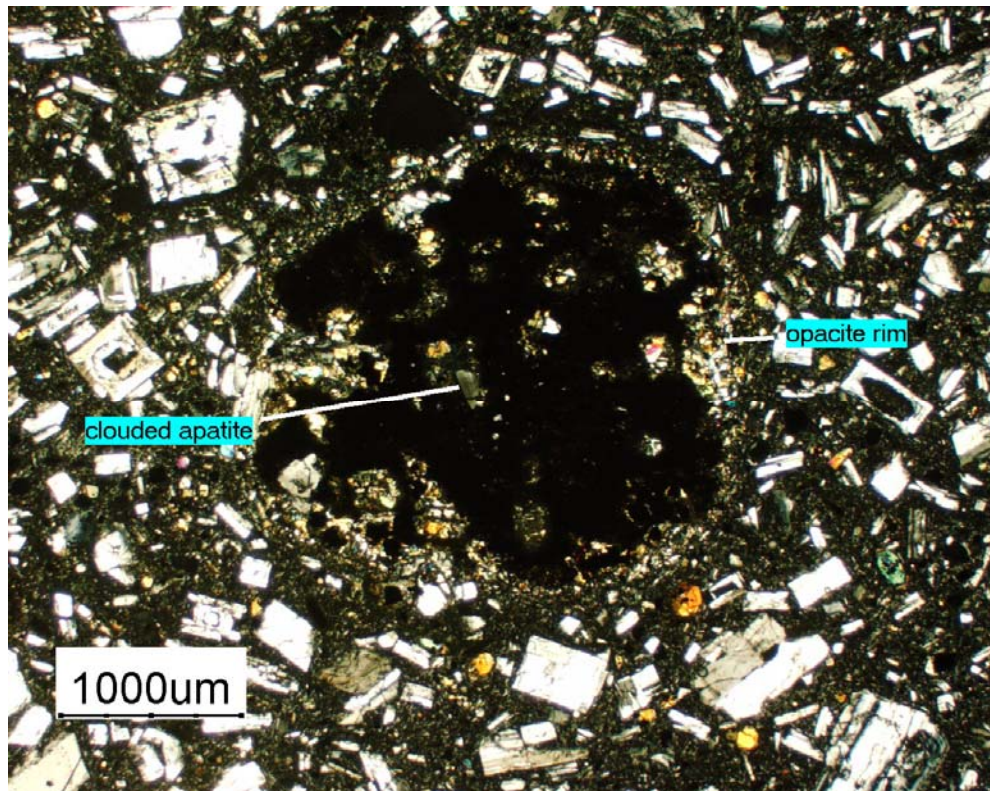
Figure 4.6. Photomicrograph of a completely oxidized and decomposed amphibole from a west district (CNN-1A). Inclusions of pyroxene, plagioclase, and striated "clouded" apatite are enclosed and an opacite rim of plagioclase and pyroxene surrounds the phenocryst. Plagioclase display resorbed rims and slight sieve-cored textures.
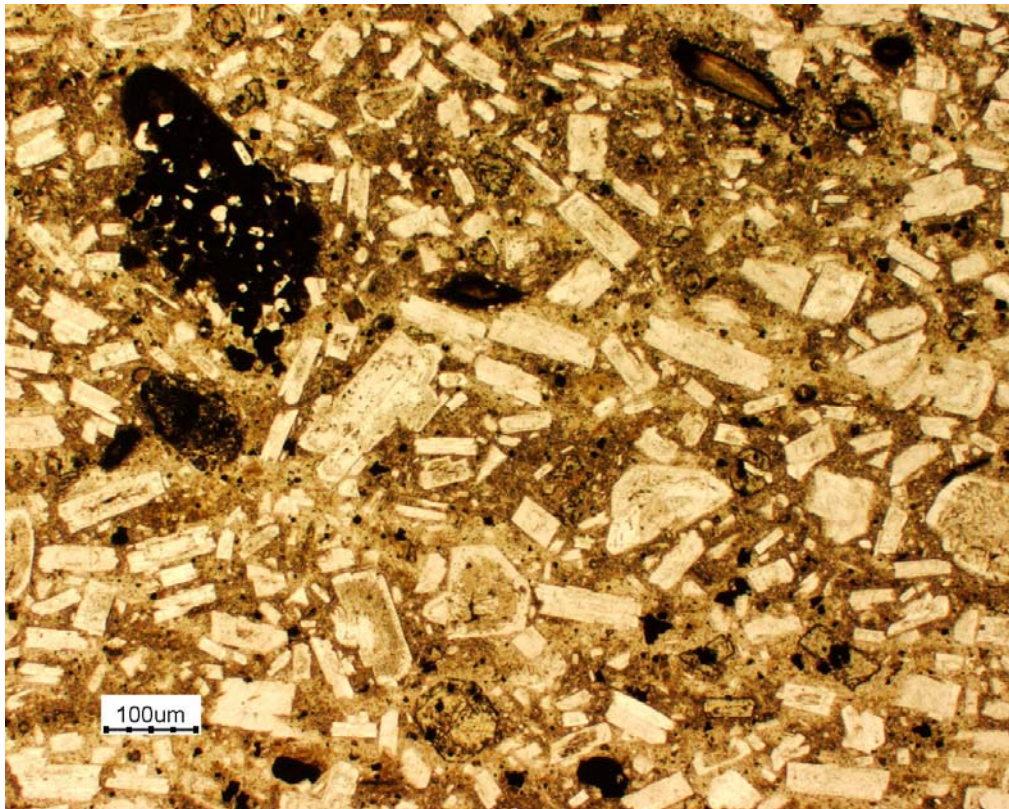
Figure 4.7. Photomicrograph of Lpha lava (DO-43) with small prismatic phenocrysts of amphibole with opacite rims of Fe oxides. Others are completely replaced with Fe oxide. Pyroxene is typically more abundant than hornblende. Plagioclase have sieved textures and resorbed cores that suggest magma mixing.
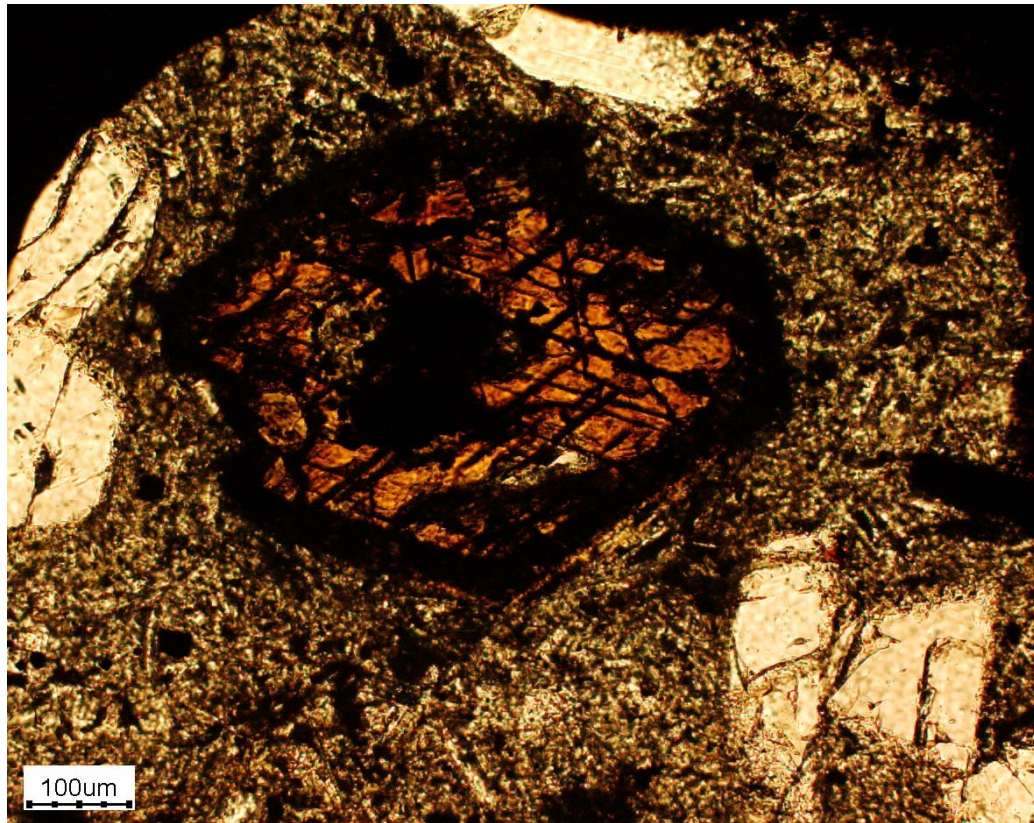
Figure 4.8. Photomicrograph of decomposed amphibole with the rim and cleavage planes replaced by Fe-Ti oxides. The sample (AZU-1A) is from an andesite lava flow in the Lower Yanacocha andesite sequence that forms the cliffs west of Elita in the East District.

Maqui Maqui Ignimbrite

Amphiboles in the Maqui Maqui ignimbrite generally display narrow opacite rims of Fe-Ti oxide and plagioclase (Figure 4.9, 4.10, 4.11, 4.13). Small laths are completely replaced with fine-grained Fe-Ti oxides (Figure 4.12). Phenocryst sizes range from 0.75 to 3.0mm and abundances are 5 to 12.5 modal %.
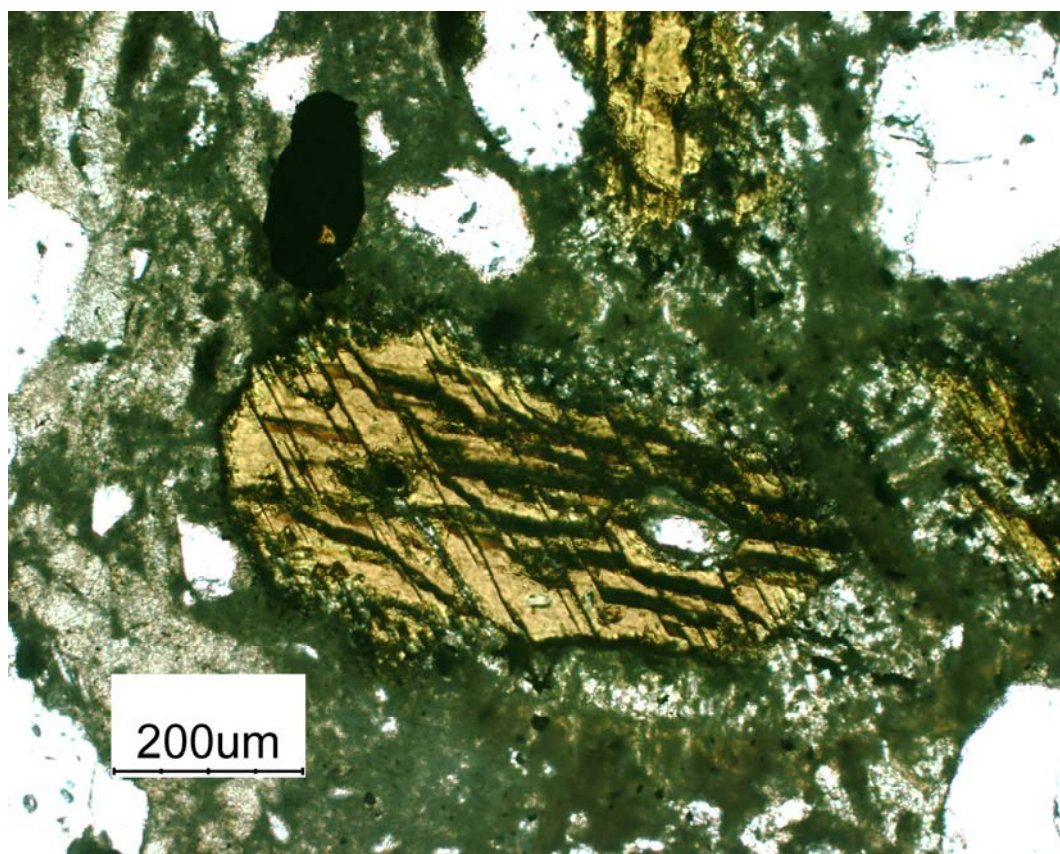
Figure 4.9. Photomicrograph of small partially resorbed and decomposed amphibole in the ground mass of the Maqui Maqui ignimbrite (DN-7). Small amphiboles have uniform compositons with low-Al from core to rim.
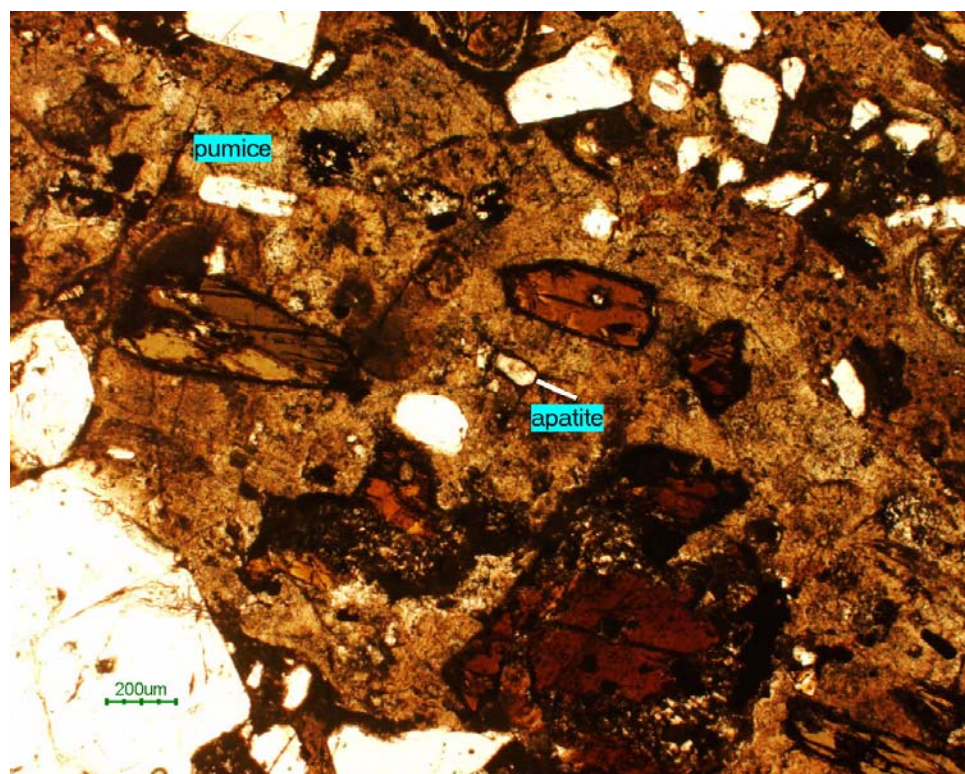
Figure 4.10. Photomicrograph of the small low Al amphibole within a welded pumice clast or fiamme from the Maqui Maqui ignimbrite (DN-7).
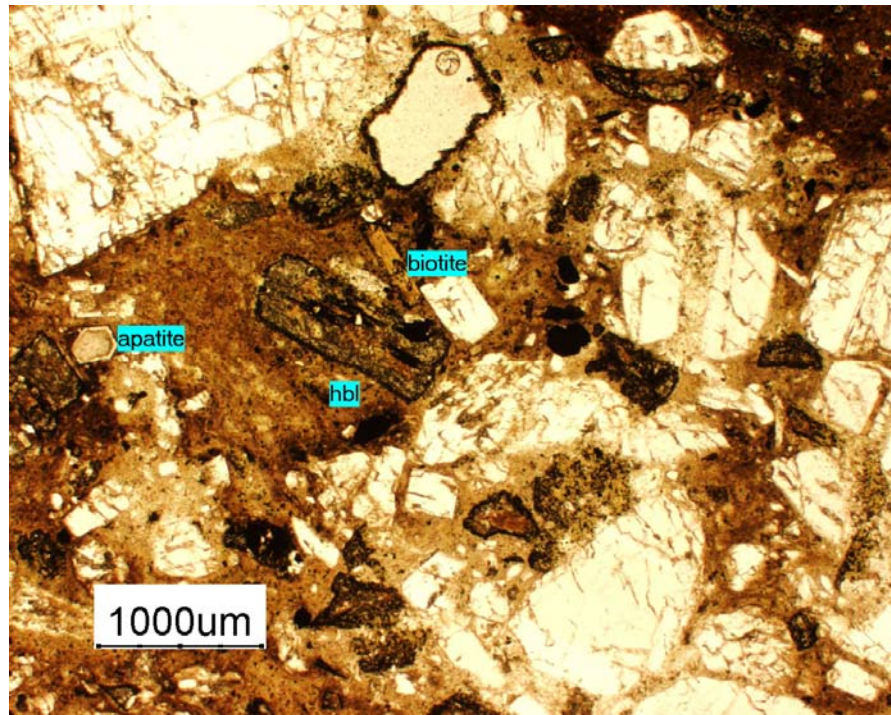
Figure 4.11. Photomicrograph of the Maqui Maqui ignimbrite in BS-27. The characteristic phenocryst assemblage consists of broken plagioclase, hornblende with narrow opacite rims of Fe oxide, small biotite, and apatite.
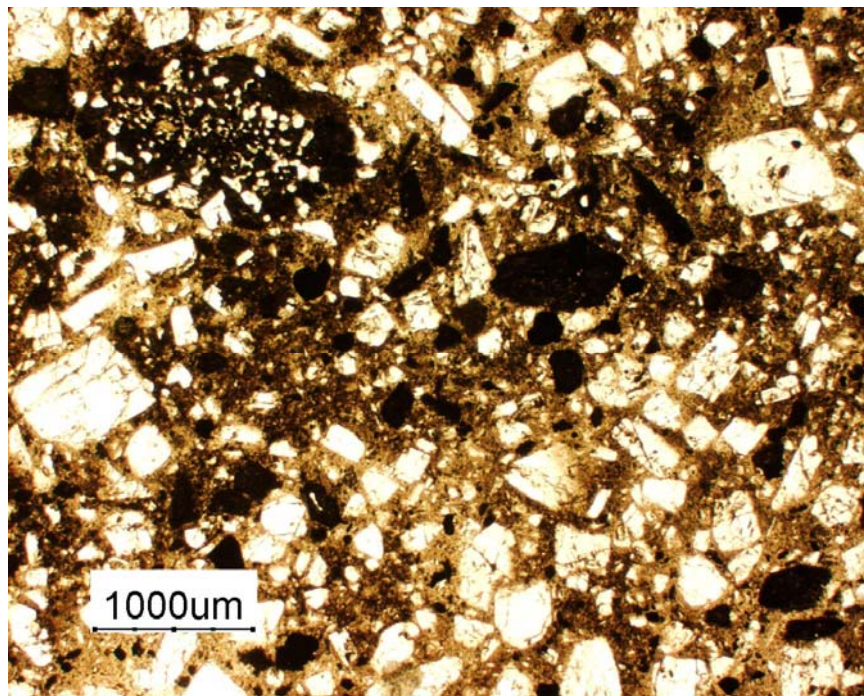
Figure 4.12. Sample of the Maqui Maqui ignimbrite from MM-342 at 170m depth showing broken crystals of plagioclase and hornblende. Hornblende is replaced with Fe oxides and occurs as small prismatic phenocrysts, some with abundant inclusions of feldspar, and others with an acicular habit.
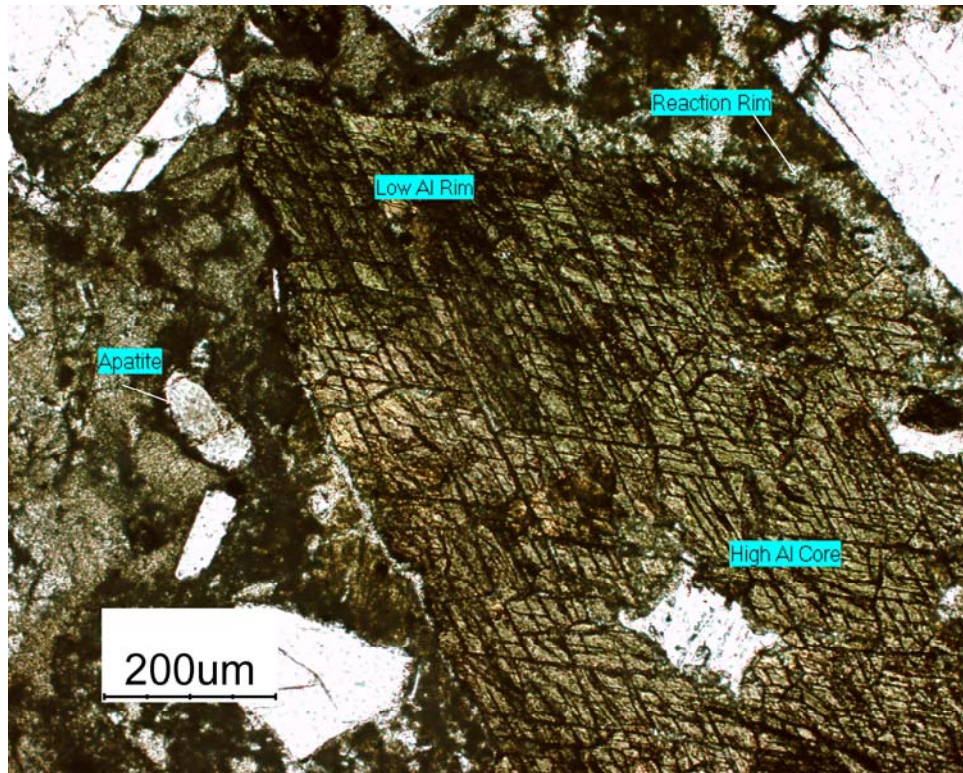
Figure 4.13. Photomicrograph from the upper half of a large >2mm sized amphibole phenocryst in the Maqui Maqui ignimbrite (DN-7 Hb#10). A narrow opacite rim with fine-grained plagioclase and Fe-Ti oxide is noticeable in the upper right. This amphibole has a high Al core and low Al rim. Apatite common to the ignimbrite is to the left.

Upper Yanacocha Andesite lavas and Domes

Amphiboles in the Upper Yanacocha andesite lavas are typically small, resorbed and oxidized similar to amphibole in Lower Yanacocha lavas. Large phenocrysts >1mm are present in greater abundance than the Lower Yanacocha rocks. Many amphiboles from the Upper Yanacocha sequence are strongly decomposed with rims of opaque oxides (Figure 4.14). Reddish oxy-hornblendes that display slight resorption textures and narrow opacite rims of Fe-oxide are common in the Upper Yanacocha lavas (Figure 4.15). The resorbed oxy-hornblendes coexist with resorbed plagioclase that also display sieve-rimmed textures mantled by clear, unresorbed rims (Figure 4.14). Sieved rims in plagioclase consist of a ring of fine melt inclusions that result from dissolution and outline the rim from an earlier stage of crystal growth. These textures suggest melting and dissolution of the plagioclase rim occurred during a heating event followed by

cooling and crystal growth (Coombs et al., 2000). Amphiboles with "opacite" rims of plagioclase and pyroxene are found in some lava flows and domes indicating decompression and dehydration (Gill, 1981; Rutherford and Hill, 1993). Phenocryst sizes are typically 1 to 2.5mm with rare large crystals up to 5mm.
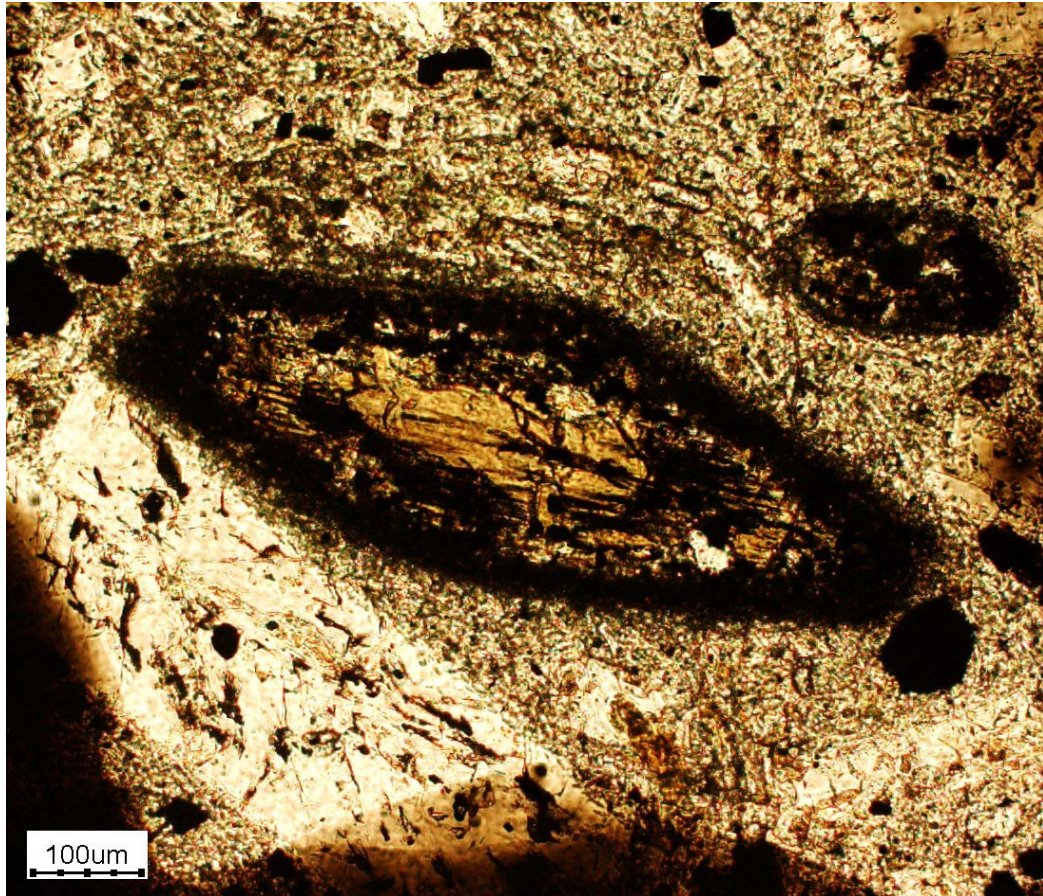
Figure 4.14 Photomicrograph of a decomposed amphibole with rims of Fe-Ti oxides from an andesite lava flow in the Upper Yanacocha andesite-dacite sequence (CHQS-2). Cores of these amphiboles are high in total Al.
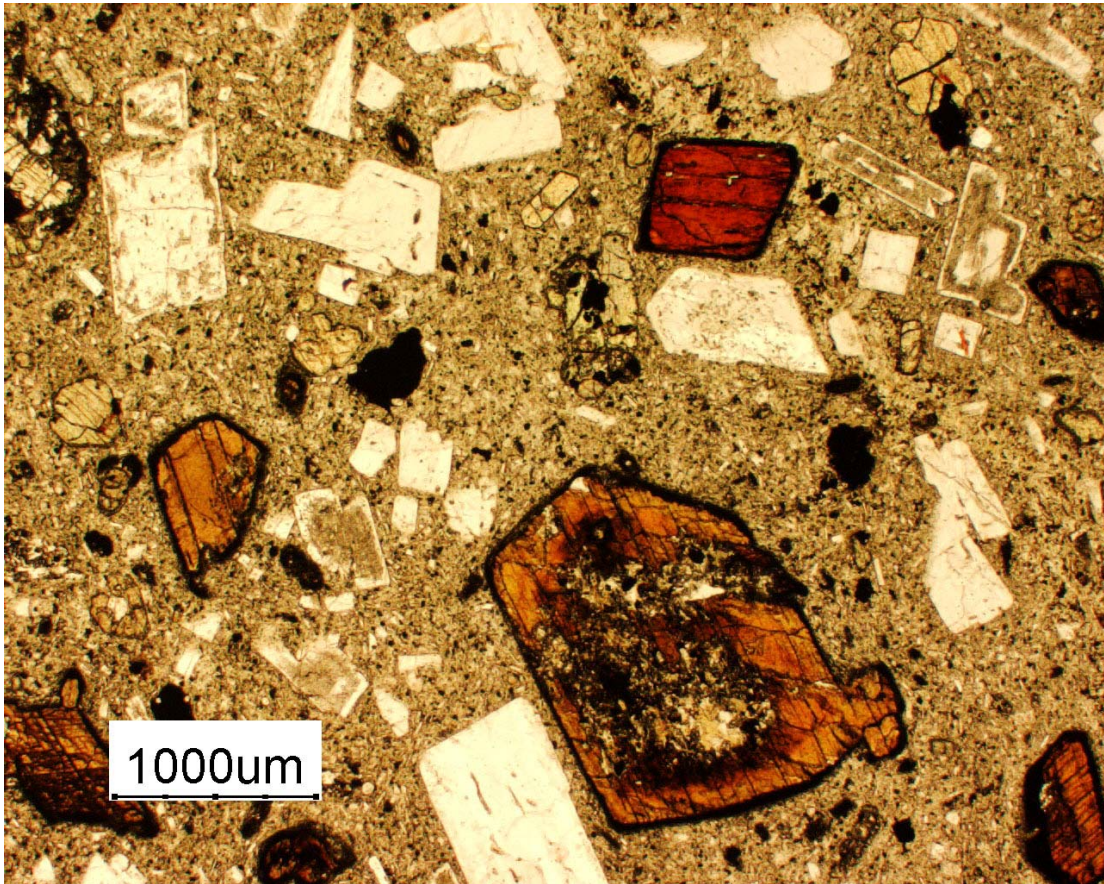
Figure 4.15 Photomicrograph of Upper Yanacocha pyroxene-hornblende andesite (Upha) lava in the west district (DO-60). Oxy-amphiboles have narrow opacite rims and coexist with plagioclase and pyroxene. Hornblende phenocrysts display resorption along rims and more severe resorption to the cores of larger phenocrysts. Some plagioclase display a distinct rim of sieve textures mantled by unresorbed rims (upper right corner) suggestive of magma mixing (Coombs et al., 2000). The fined-grained sieve-rimmed textures sometimes reach to the core. Other plagioclase display slightly resorbed cores and rims. Pyroxene also display slight resorption along the rims. Rare mafic enclaves have also been observe in these Upha lavas.

San Jose Ignimbrite

The San Jose ignimbrites have a variety of amphibole textures that vary from the Lower, Middle and Upper members. Amphiboles in the Lower member are typically not resorbed or decomposed (Figures 4.16 and 4.17). The rims are fresh and do not have the fine-grained Fe-Ti oxide from decomposition, or dehydration and oxidation, as observed in the Upper Yanacocha lavas. Middle member amphiboles also lack opacite rims and are not decomposed or resorbed, but display rare embayments in the rims filled with

groundmass glass (Figure 4.18). Similar rim embayments were observed in an ignimbrite flow from the Lower member (Figure 4.19B) and may imply slight disequilibrium and resorption with the melt.

Two varieties of amphiboles are present in the Upper San Jose spatter ignimbrite. One type is irregularly shaped and resorbed with rims of fine-grained opaque oxides (Figures 4.20, 4.21, 4.22, and 4.23). Some are strongly resorbed reddish-brown oxy-hornblendes with opaque rims as in Figure 4.21. In rare cases, the rims are preserved and oxidized, outlined by opaque oxides as in Figure 4.23. Opaque oxides also outline the cleavage planes. Phenocryst size varies from <0.5 to 1.0mm in the spatter ignimbrite. A second variety of amphibole is represented by large phenocrysts typically ≥1mm with distinct opacite rims of plagioclase and Fe-Ti oxides (Figure 4.24). This type may be similar to the large +1cm-size amphibole megacrysts commonly observed in these ignimbrites.

Figure 4.22 shows a resorbed amphibole with an opacite rim of fine-grained opaque oxides in contact with groundmass glass, whereas, the opaque rim is absent along the amphibole in direct contact with plagioclase. This suggests that post-eruption subsolidus decomposition and increased fo_2 caused the resorption to an amphibole that crystallized in a stable hydrous pre-eruptive magma chamber; however, other mafic minerals in the Upper San Jose ignimbrite are fresh and not oxidized such as the augite phenocryst in Figure 4.21. Subsolidus decomposition would not be confined only to the amphibole, but would also involve the oxidation of other mafic minerals. Resorbed amphiboles coexist with resorbed plagioclase (Figure 4.22) and plagioclase that display sieve-rimmed textures of fine melt inclusions mantled by clear unresorbed rims (Figure 4.17 and 4.21). Therefore, resorption of the amphiboles in Figures 4.20 to 4.23 may have resulted from processes that include magma mixing causing renewed heating, disequilibrium and resorption. Heating may have been combined with later decompression resulting in the opacite rim of fine-grained opaque oxides (Gill, 1981, p. 180).

Amphiboles with opacite rims of plagioclase and opaque oxides are also found in the Upper San Jose spatter ignimbrite flow (DE-36; Figure 4.24). Rutherford and Hill (1993) describe amphiboles from post-1980 eruptions of Mount Saint Helens dacite that have opacite rims of pyroxene in contact with melt, but lack the opacite rim in tight contact

with plagioclase implying amphibole stability at depth in a magma coexisting with plagioclase. Experimental studies indicate that instability in amphibole occurs during a slow ascent (<0.2 m/s), decompression and loss of H_2O initiating stability of anhydrous phases with the melt. The rim of the amphibole not shielded by plagioclase is replaced with pyroxene, plagioclase and Fe-Ti oxides during decompression and dehydration. An average ascent rate >0.2 m/s allows amphibole to erupt free of decompression-induced opacite rims (Rutherford and Devine, 2003).
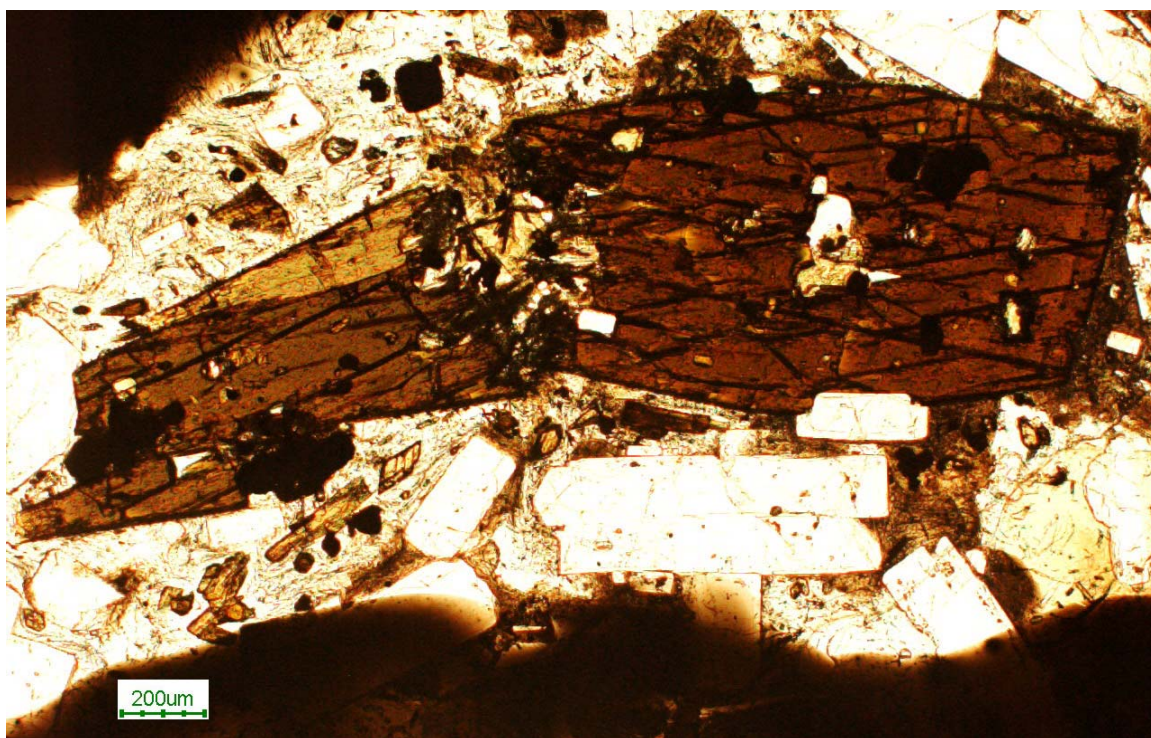
Figure 4.16 Photomicrograph of a large broken amphibole phenocryst in the Lower San Jose ignimbrite at Arnacocha (CB-44). The amphibole has a uniform composition with low Al contents from core to rim. These low-Al amphiboles do not display reaction textures and are not resorbed or decomposed. They are also free of opacite rims that indicates rapid ascent during eruption (Rutherford and Devine, 2003). Plagioclases are unresorbed and clear, and display only minor sieve-rimmed textures mantled by thin unresorbed rims (see Figure 4.17).
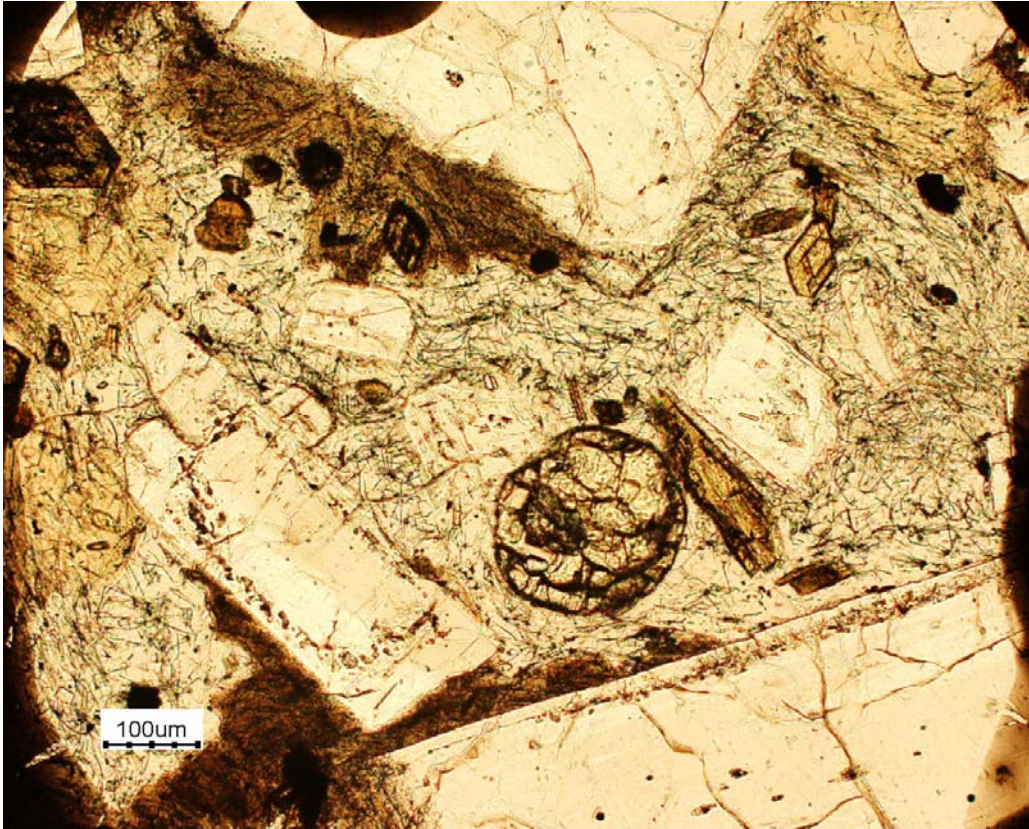
Figure 4.17 Photomicrograph of small euhedral groundmass amphibole (~0.1mm) trapped in glass with incipient divitrification. The sample is from a spatter blob in the Lower San Jose ignimbrite at Arnacocha (CB-44). These small amphiboles have high-Al contents relative to the larger broken hornblende in figure 4.23. The central round phenocryst is clinopyroxene and the large phenocrysts are plagioclase with rims containing melt inclusions. Plagioclase have minor sieve-rimmed textures mantled by unresorbed rims.
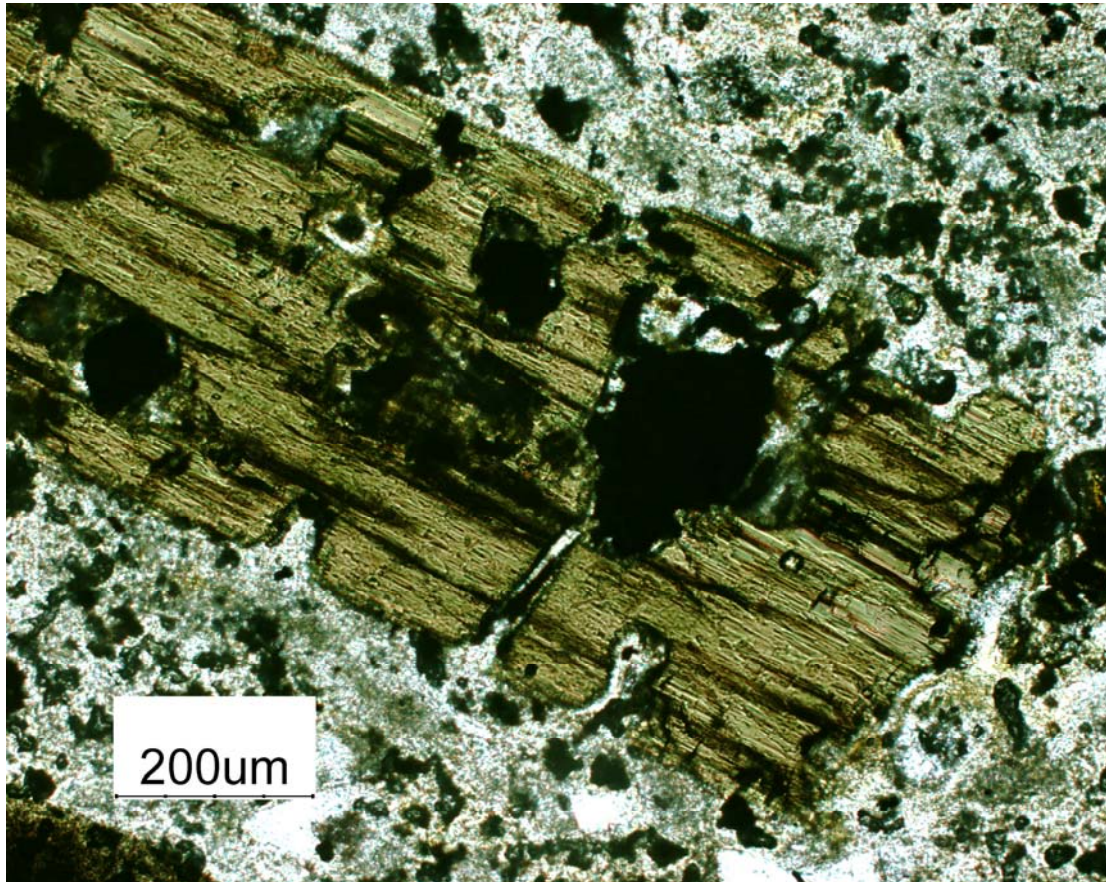
Figure 4.18 Photomicrograph of an amphibole from the Middle San Jose ignimbrite (VC-1 Hb#1). Amphiboles in the Middle member are typically lack opacite rims and strong resorption. This phenocryst displays a rare embayment texture also found in CB-56 Figure 4.19. The embayment areas are filled with groundmass glass and may represent a slight resorption and disequilibrium with the melt.
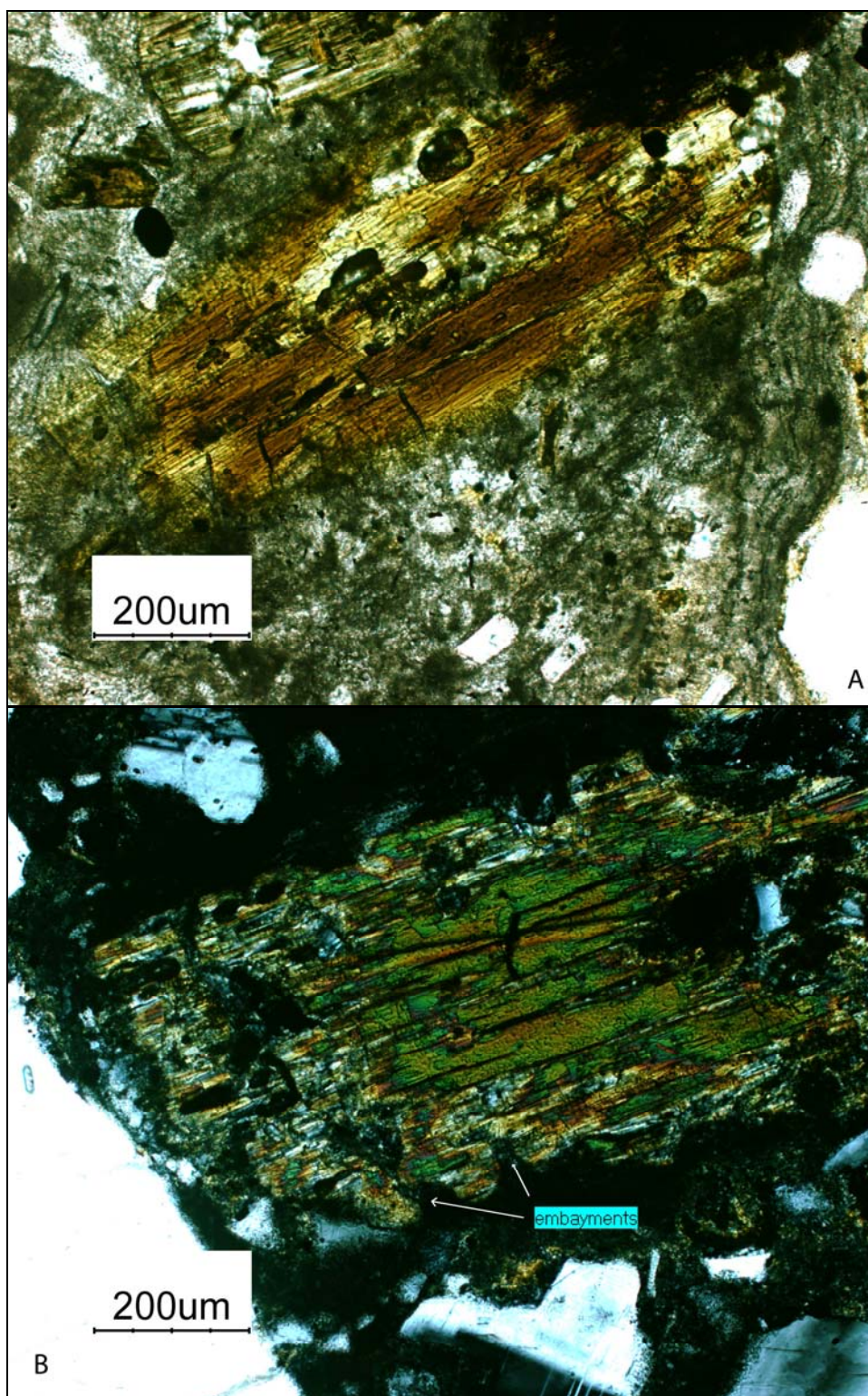
Figure 4.19 Photomicrograph of amphiboles from an ignimbrite (CB-56) at the top of the Lower member directly below the Middle member white tuff. A) Typical amphibole in transmitted light that lack opacite rims and resorption texturtes. B) Rare case of an amphibole with embayed resorption textures filled with groundmass glass.
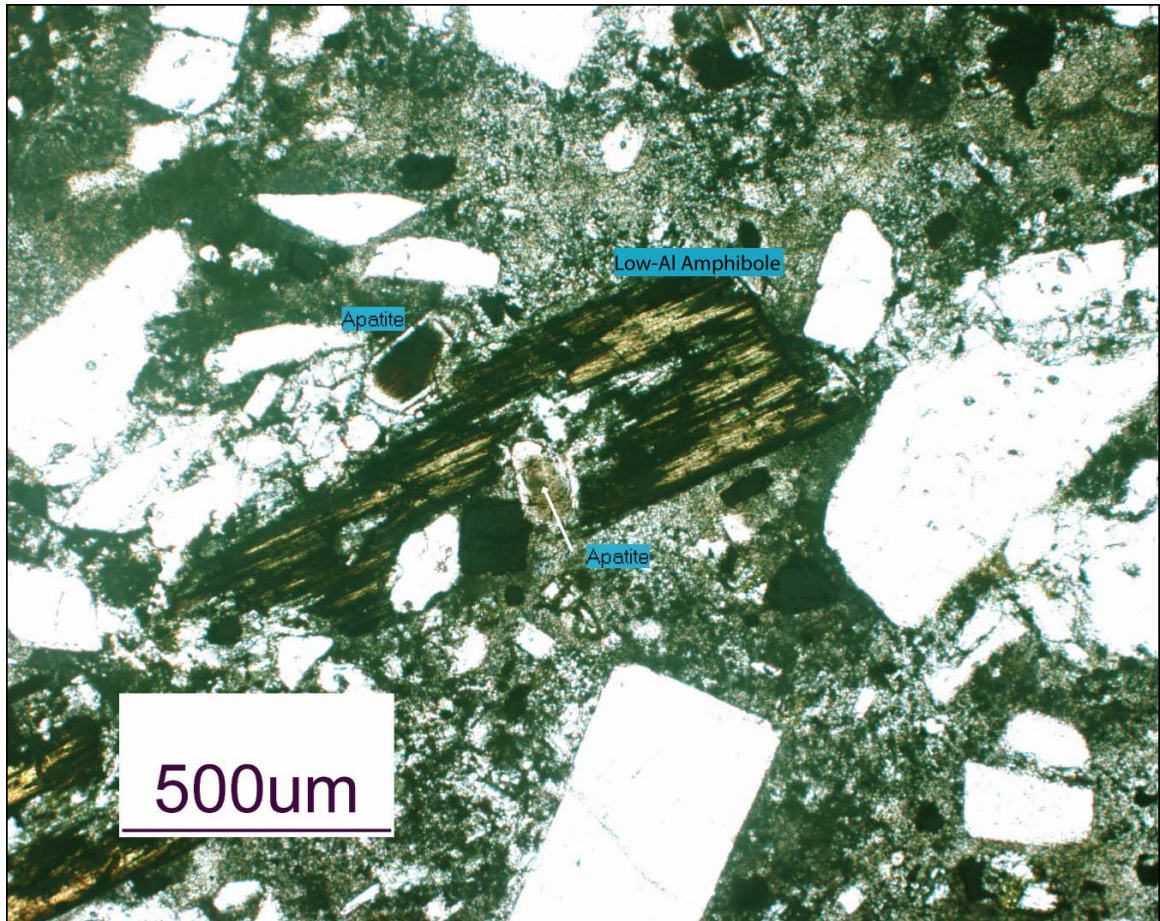
Figure 4.20 Photomicrograph a resorbed amphibole in the San Jose spatter ignimbrite (BS-2B) with the rim and parts of the core resorbed. Fine-grained opaque oxides form the opacite rim that outlines the remaining phenocryst margins. This variety typically has low-Al contents. Apatite occurs in the groundmass and as inclusions in the resorbed amphibole.
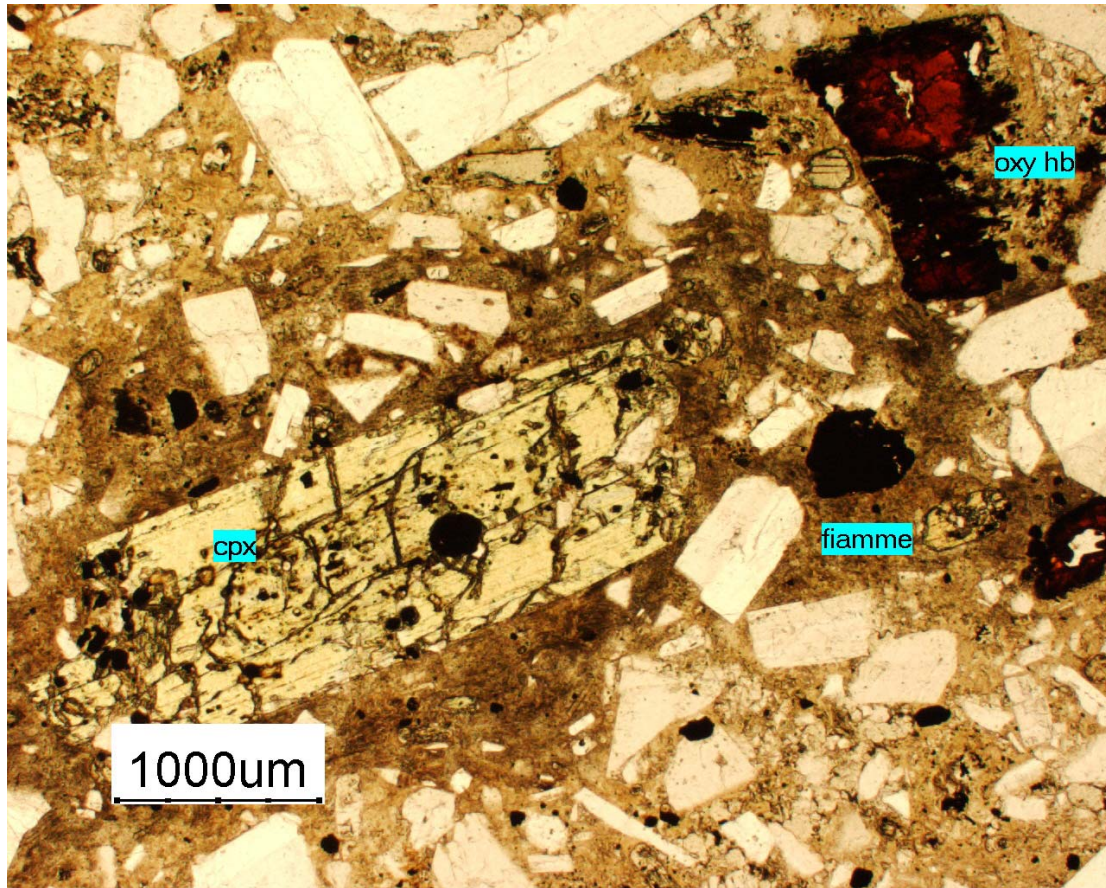
Figure 4.21 Photomicrograph of a strongly resorbed amphibole or oxy-hornblende (oxy hb) in the San Jose spatter ignimbrite (BS-5B). The amphiboles in this sample have opacite rims of fine-grained opaque oxide. A large greenish and fractured phenocryst of augite is fresh and lacks oxidation. The darker groundmass is part of a larger flattened pumice fragment 15mm in length. Rare small fiamme are present in the spatter ignimbrite and have width/length ratios of 1/7. Some plagioclases have thin sieve-rimmed textures mantled by unresorbed rims.
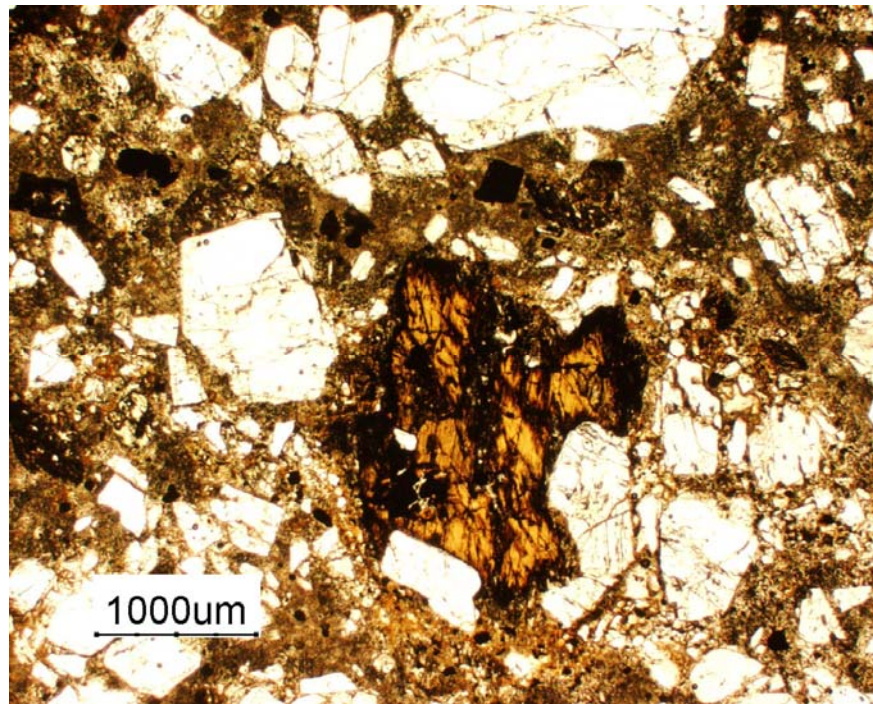
Figure 4.22 Photomicrograph of the upper San Jose spatter ignimbrite (PRI-1). A resorbed amphibole with rims of opaque oxides is in contact with glass, but lacks an opaque rim in contact with a plagioclase phenocryst.
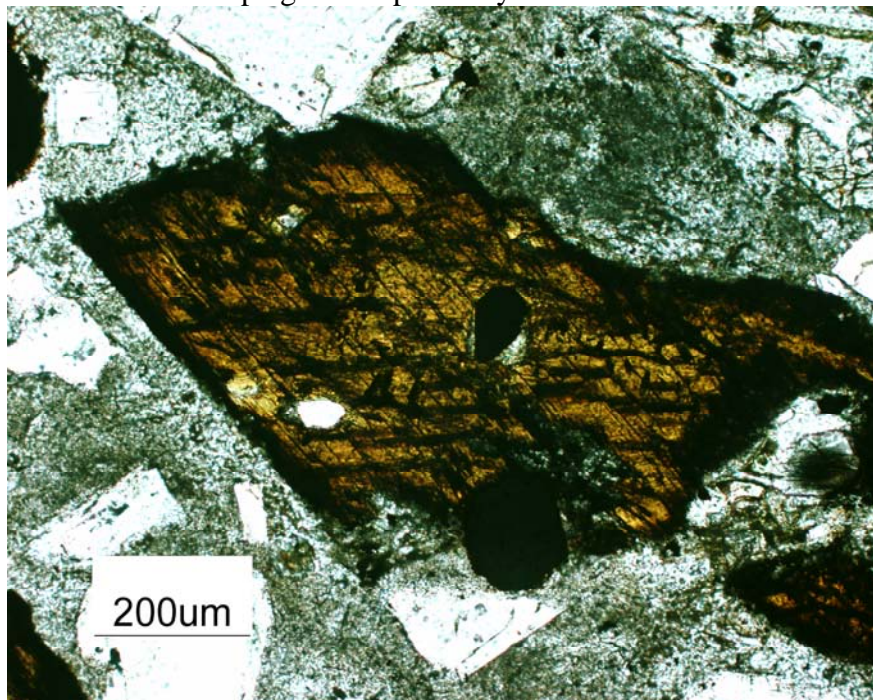
Figure 4.23 Photomicrograph of an amphibole in the San Jose spatter ignimbrite (BS-2B) with uniform low-Al content. Low-Al core (Al_{total} = 1.15 atoms pfu) and low-Al near the rim (Al_{total} = 1.13 atoms pfu). The rim on the left is not resorbed, but is replaced with a narrow opacite rim of opaque oxide. These amphiboles typically lack an opacite rim of plagioclase.
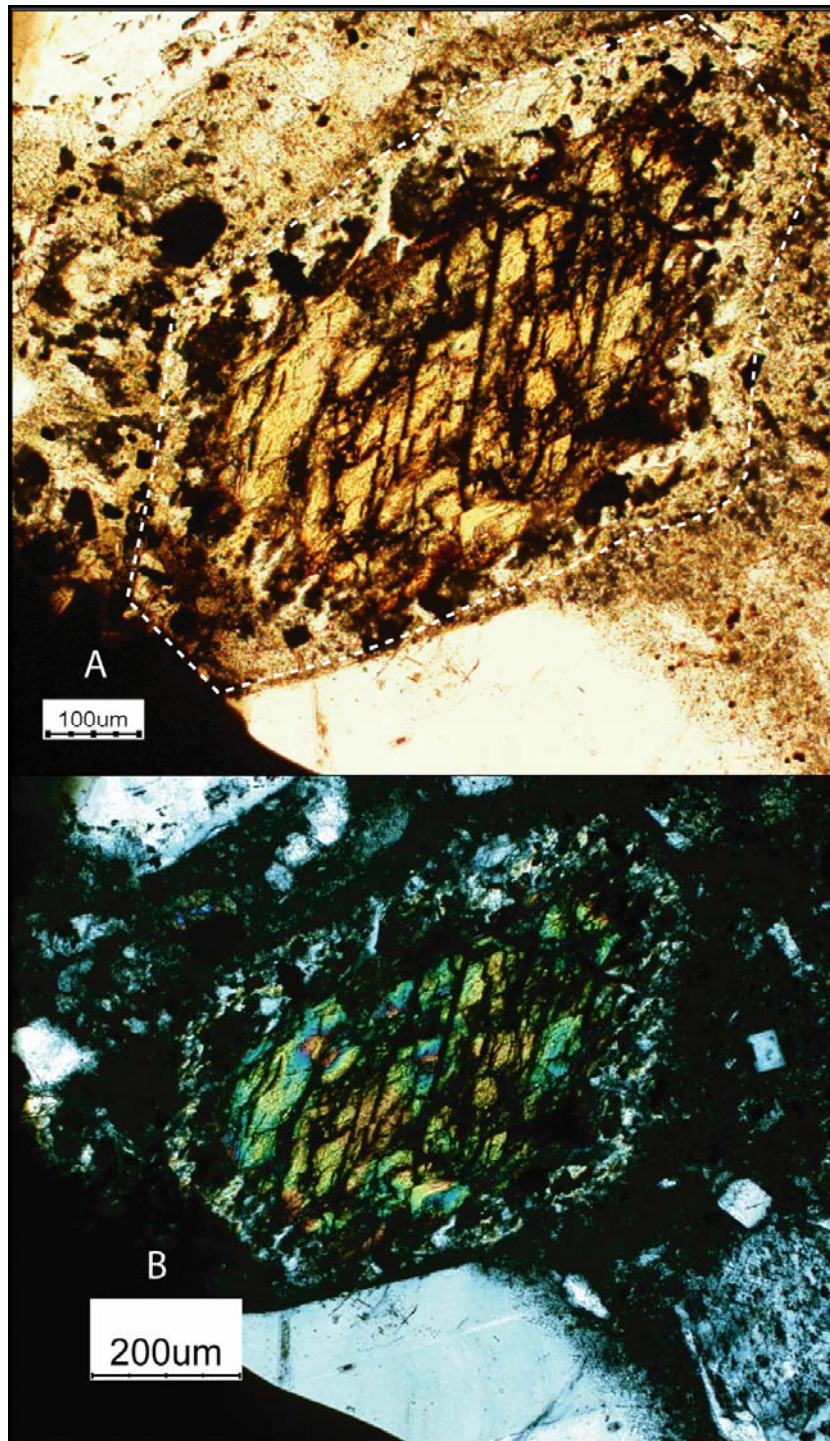
Figure 4.24 Photomicrograph a high-Al amphibole from the Upper San Jose spatter ignimbrite (DE-36 Hb#5). High-Al amphiboles are generally larger than low-Al amphiboles in the ignimbrite, and the high-Al amphibole in the pyroxene andesite lavas, They contain opacite rims with plagioclase and Fe-Ti oxides. Cleavage planes are decomposed with slight replacement by Fe-Ti oxides. The white dashed line approximates the original amphibole shape and outlines the boundary of the feldspar reaction rim. $Al_{total} = 2.15$ atoms pfu near resorbed rim and 2.22 atoms pfu in core.

Two varieties of amphiboles are found in the andesite and dacite domes that are temporally and spatially related to the San Jose ignimbrite. Small oxidized and decomposed amphiboles are common in rocks from the Ocucho and Chaquicocha Sur dome complexes and phenocrysts are commonly <1mm in the elongate direction (Figure 4.25). The core of the amphibole is generally preserved and surrounded by a distinct rim of opaque oxides similar to the decomposed amphiboles observed in the Upper and Lower Yanacocha andesite lavas. Amphiboles in the dacite dome at Alto Machay dome (CB-3) have no opacite rims and lack resorption textures (Figure 4.26). The Alto Machay dome is compositionally similar and temporally related to the Middle San Jose ignimbrite. Phenocrysts are commonly euhedral prisms that range in size from 1 to 2.5 but can be as large as +1cm.
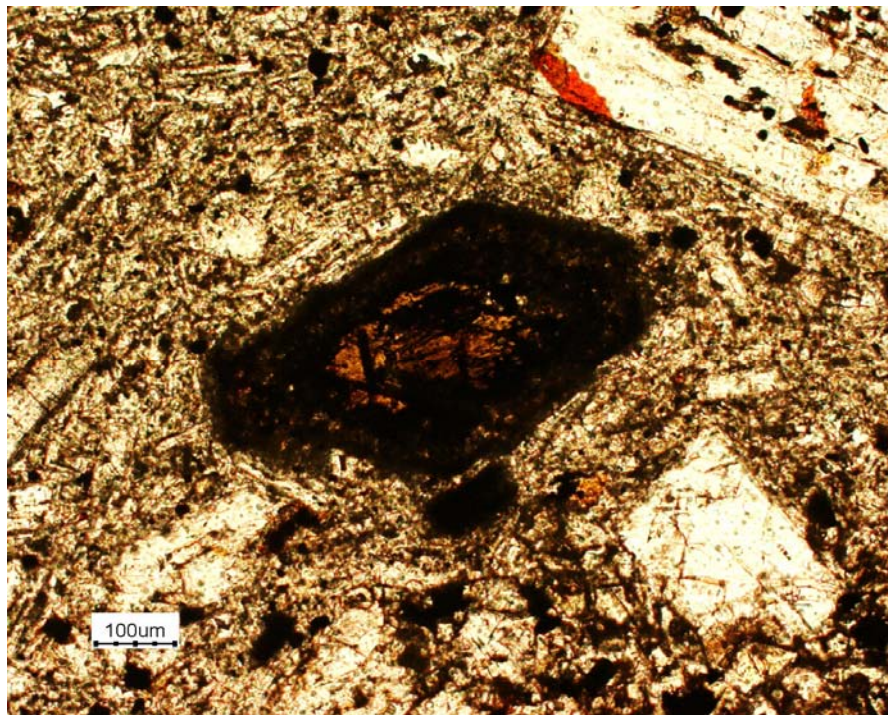
Figure 4.25 Photomicrograph a decomposed amphibole in a San Jose dacite dome at Otuzco (DE-2). Only the core of the amphibole phenocryst was analyzed and the rim is replaced with Fe-Ti oxide. The plagioclase in the upper right corner has a sieved core and an unresorbed rim.
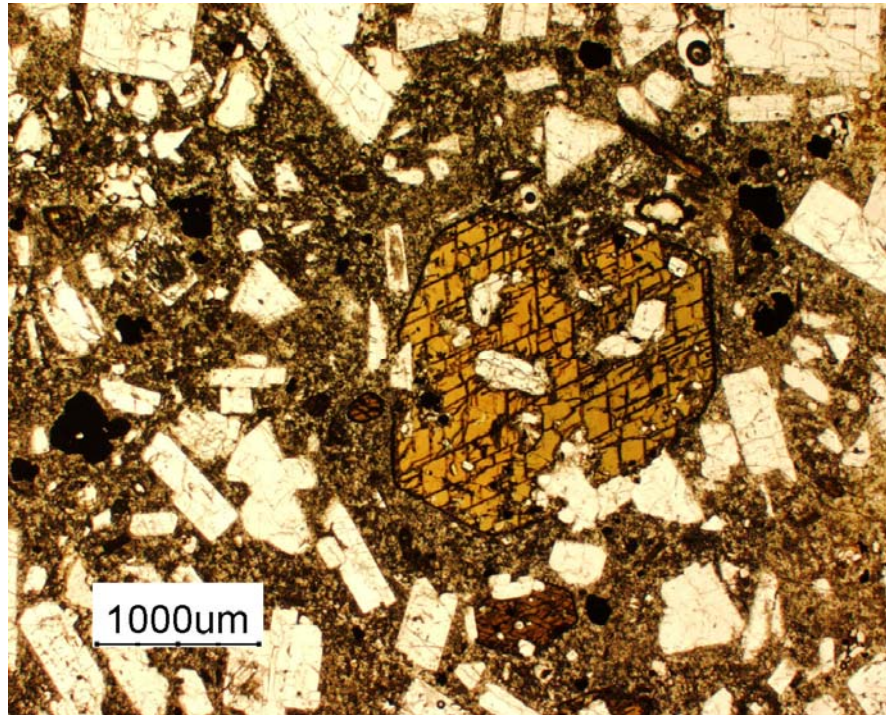
Figure 4.26. Photomicrograph of CB-3. Characteristic mineral assemblages in the Alto Machay dome with plagioclase, hornblende and opaque oxides. The hornblendes lack opacite rims and resorption but have abundant inclusions of plagioclase. These characteristics also are common in the middle San Jose ignimbrites. Plagioclase are mostly unsieved with rare sieve-rimmed phenocrysts and fine-grained sieve textures extending into the core. Other plagioclase are resorbed and lack sieve textures.

Dacite Intrusions

Amphiboles in the dacite and rhyodacite intrusions at Yanacocha are euhedral to subhedral, and lack resorption textures and opacite rims. Characteristics of color, shape, size, and types of inclusions distinguish these amphiboles between the lower dacite intrusions in the west district to the upper rhyodacite dome at Chaupiloma. Amphibole characteristics are discussed for each type of dacite intrusion at Yanacocha as follows from oldest to youngest.

1. Most amphiboles in the oldest lower dacite intrusions (early dacite) are euhedral to subhedral and completely replaced with fine-grained opaque oxides, and they rarely are found fresh (Figure 4.27A). When fresh, as in the Tatiana dacite, they display green to pale green pleochroism and lack resorption textures and opacite rims (Figure 4.27B).

2. Amphiboles in the Corimayo and La Quinua dacites are euhedral prisms that range in size from 0.2 to >5mm. Similarities include the brown color, tan to brown pleochroism, abundant inclusions of euhedral biotite and anhedral plagioclase, and they lack resorption textures and opacite rims (Figure 4.28 and 4.29).

3. Amphiboles in the Yanacocha dacite porphyry plugs are typically small (~0.5mm) euhedral prisms that are altered to chlorite and calcite (Figure 4.30).

4. Rhyodacite domes and dikes at Chaupiloma and Yanacocha Lake may have two varieties of groundmass amphibole, and large phenocrysts are absent.One type include small green subhedral prisms of that display green to pale green pleochroism and resorption textures into the groundmass, but no opacite rims. A second type includes brown acicular crystals and no obvious resorption textures (Figure 4.31).

Field relationships indicate that the four types of dacite discussed above have intruded the rocks of the Yanacocha Volcanic Field. The early dacite crosscuts the Lower Yanacocha andesite lavas and is bracketed between 14 and 12 Ma. The Corimayo and La Quinua dacite domes intruded the Upper Yanacocha andesite lavas and have an age of ~10.78 Ma. The Yanacocha dacite porphyry has an age of ~9.9 Ma, and it intruded trachytic-textured andesite lavas and dikes that range in age from ~12.4 to12.1 Ma. Finally, the Chaupiloma and Yanacocha Lake rhyodacite domes and dikes crosscut the ~12.4 Ma andesite lavas, pyroclastic rocks, and the Yanacocha dacite porphyry at Cerro Yanacocha (Loayza, 2002), and they have an age of ~ 8.4 Ma (Turner, 1997). Resorption textures and the presence of a bimodal population of amphibole imply magma mixing as a process in the evolution of the Chaupiloma rhyodacite. Amphiboles in the other dacites lack of opacite rims and resorption textures and indicate the absence of decompression and non-equilibrium processes. The amphiboles in these dacite intrusions did not ascend from deeper magma reservoirs, but crystallized in equilibrium with the melt at shallow levels within the Yanacocha Volcanic Field. The lack of decompression and dehydration textures implies that these dacites did not erupt, and further supported by the near absence of temporally related dacite to rhyolite volcanic rocks.
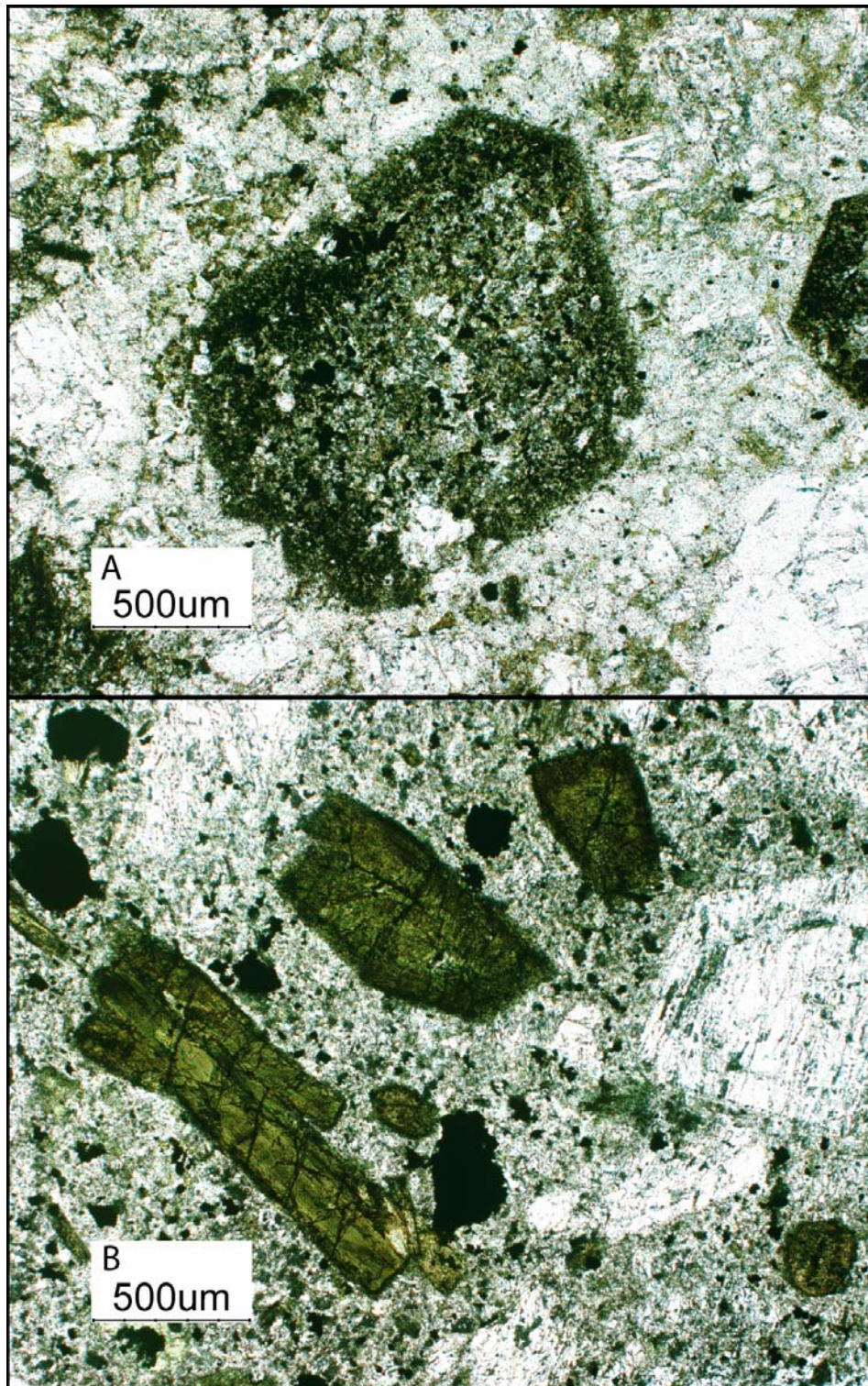
Figure 4.27 Photomicrograph of the amphibole in the early dacite intrusions. Generally the amphiboles lack resorption textures and opacite rims. A) This sample from the Exaltado dacite (DO-5) in the west district is typical of these amphiboles and completely replaced with fine-grained opaque oxides. B) These fresh amphiboles are less common and found in the Tatiana dacite (TAT-02).
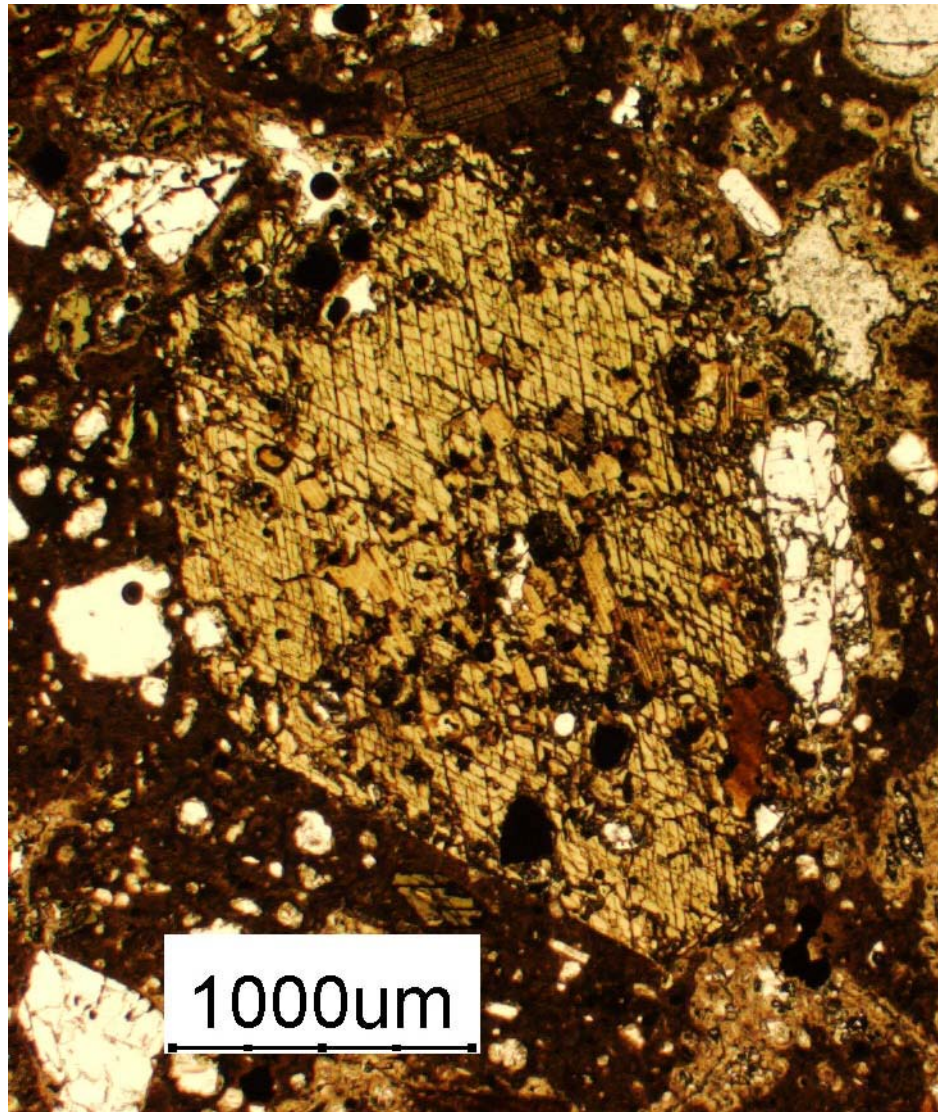
Figure 4.28 Photomicrograph of the amphibole in the Corimayo dacite (COR-1). The amphiboles contain abundant inclusions of biotite, anhedral plagioclase, and opaque oxides, and they lack opacite rims.
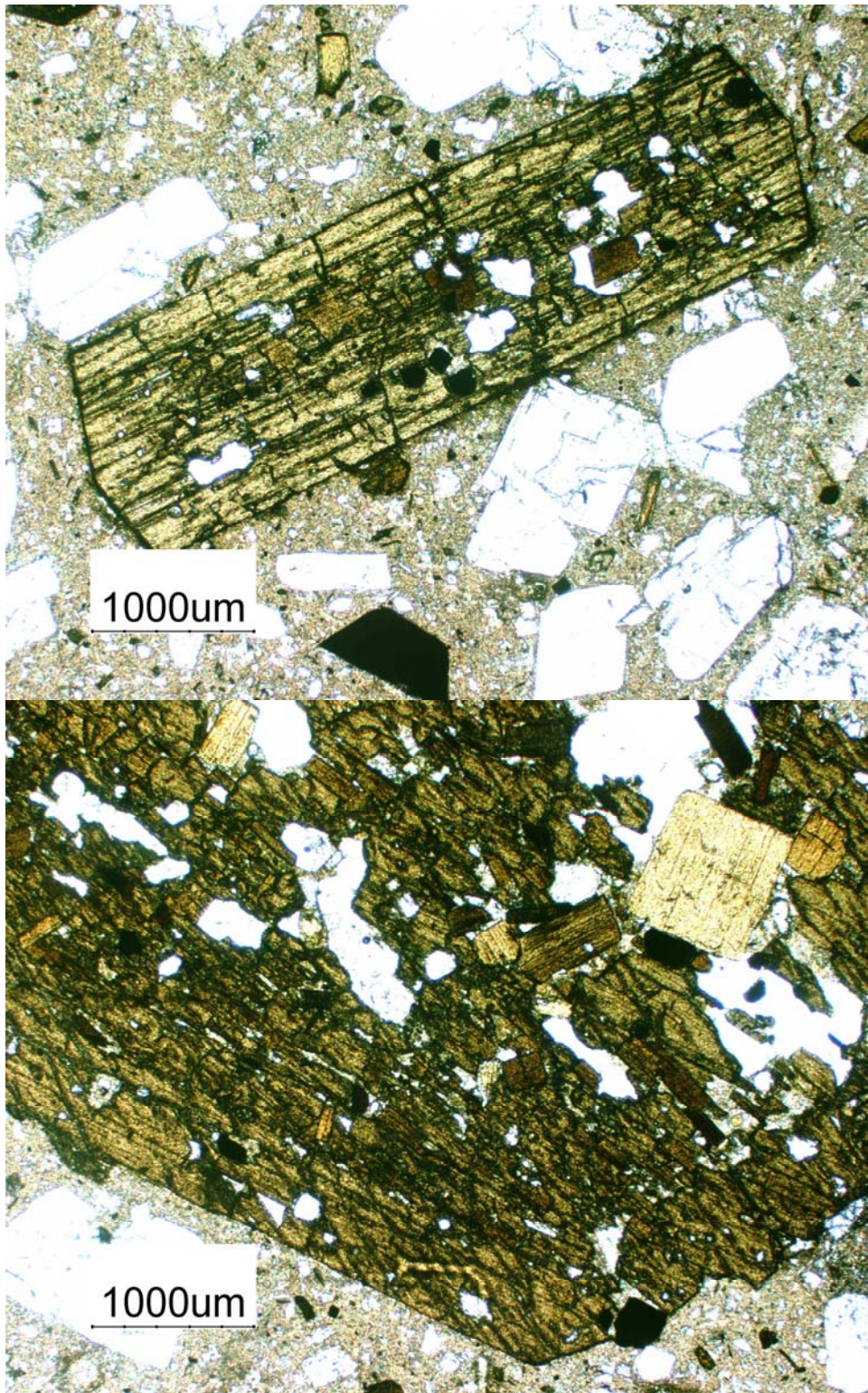
Firure 4.29 Photomicrograph of coarse amphibole phenocrysts in the La Quinua dacite dome. The dome now lies below the La Quinua leach pad facilties (QNQ-3A) and is similar to amphiboles in the Corimayo dacite. Inclusions of euhedral biotite and anhedral plagioclase are common, and the phencrysts lack opacite rims and resorption textures.
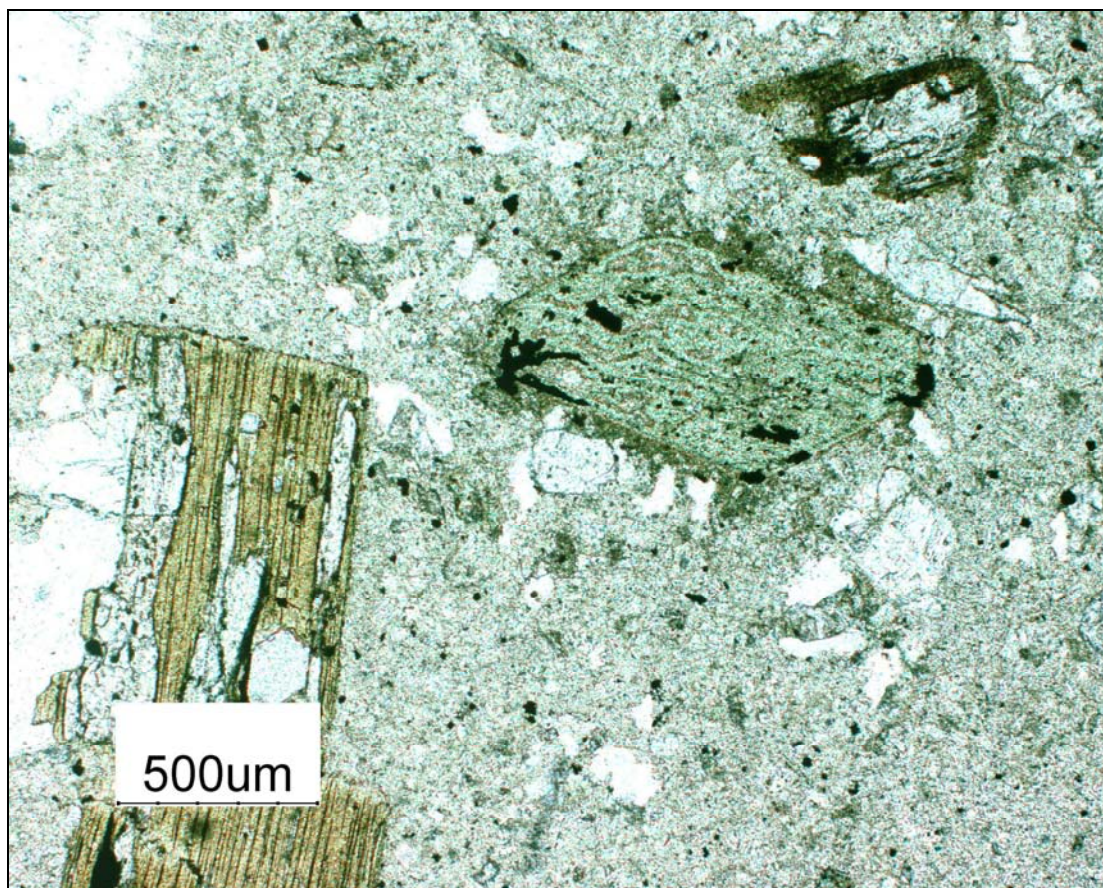
Figure 4.30 Photomicrograph of the altered hornblende typical of the Yanacocha dacite porphyry (Ypq; sample YN-1). Amphiboles are complete altered to chlorite and calcite, and some biotites have laminae with calcite alteration.
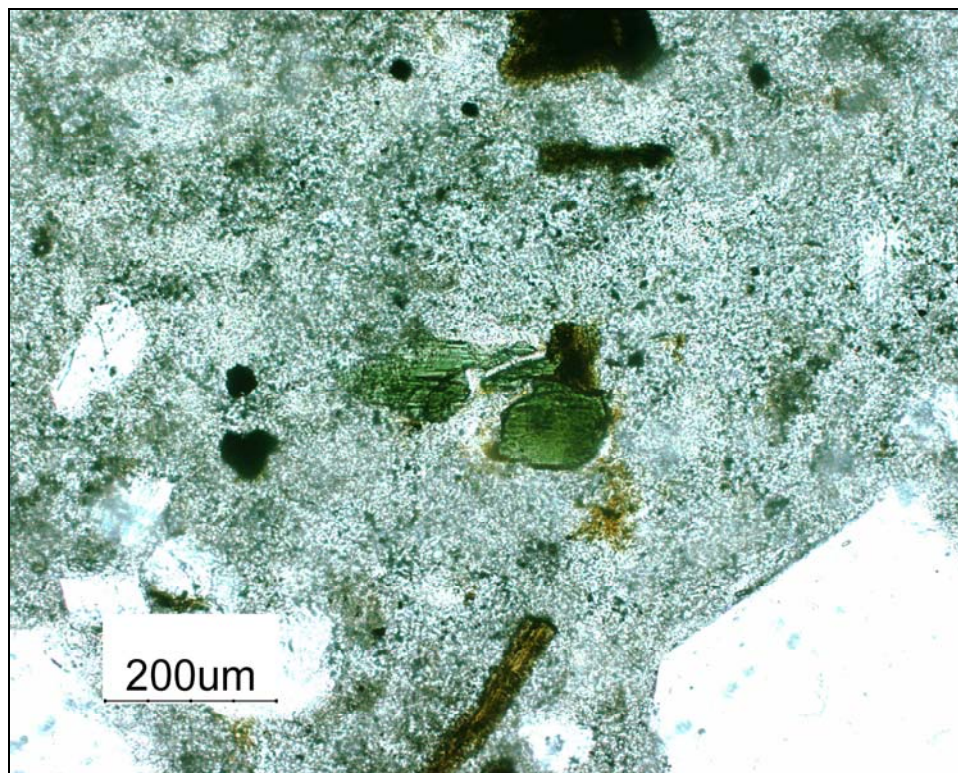
Figure 4.31 Photomicrograph of the amphibole in the Chaupiloma rhyodacite dome (DNS-1). Two types of amphibole may exist a green prismatic variety and an acicular brown variety. Green amphiboles in these late intrusions are resorbed small groundmass amphiboles, and no large phenocrysts have been observed.

Microprobe analyses of the Amphiboles

Microprobe analyses of the amphiboles have relatively narrow but distinct compositional ranges. Nearly all amphiboles at Yanacocha are calcic-amphiboles as defined by Leake (1978) with $(Ca+Na)_B > 1.34$ and $Na_B < 0.67$ in the standard amphibole formula on the basis of 23 oxygen (Tables 4.3). Rims and cores of some amphiboles from the Lower Yanacocha and Upper Yanacocha andesite lavas and domes have compositions that could be classified as sodic-calcic with Na >0.67 but < 1.00; however, these rims are resorbed and are not be representative of the true amphibole composition (Tables 4.3).

Compositional varieties in the YVF are typical of hornblende that trend toward pargasite (Leake, 1978) with higher Al^{IV} and $(Na+K)_A$ cations in the A site (Figure 4.31). Pre-Yanacocha rocks are distinct and have hornblende that trends toward tschermakite compositions with higher Al^{IV} and lower $(Na+K)_A$ (Figure 4.31). Amphiboles from the

Lower Yanacocha andesites (Lpha) have compositions that trend toward pargasite. San Jose ignimbrites (SJI) have amphiboles with lower Al^{IV} and $(Na+K)_A$ than the other rock sequences that trend away from pargasite and lie in the hornblende field. Maqui Maqui ignimbrites have amphiboles that also trend away from pargasite, but trend toward tschermakite with higher $(Na+K)_A$ compositions and away from the San Jose ignimbrite and the dacite domes related to the San Jose ignimbrite (SJI Domes).

Amphibole analyses plotted on both the total aluminum content (Al^{IV} and Al^{VI}) and Al^{IV} diagrams (Figure 4.32 and 4.33) display similar patterns and indicate that more than one compositional variety of amphibole is present in the San Jose and Maqui Maqui ignimbrites, and the San Jose dacite domes. Total molar Al (Al_{TOT}) versus molar $(Na+K)_A$ plots in Figure 4.33 display the differences more dramatically. The pre-Yanacocha amphiboles are clearly separated from the YVF amphiboles and restricted to a field defined by $Al_{TOT} = 1.4$-2.0 atoms pfu and $(Na+K)_A = 0.4$-0.6 atoms in the A site. Lower and Upper Yanacocha pyroxene andesites have high Al_{TOT} that range from 1.7 to 2.5 atoms pfu and high $(Na+K)_A$ from ~0.65 to 1.0 atoms in the A site. The Maqui Maqui and San Jose ignimbrites, and the San Jose dacite domes have more than one compositional variety with amphibole compositions from high Al_{TOT} from ~1.75 to 2.5 atoms pfu to low Al_{TOT} at ~1.0 to 1.5 atoms pfu and low $(Na+K)_A$ at ~0.5 to 0.7 atoms in the A site.

Porphyritic pyroxene-bearing rocks from the Lower and Upper Yanacocha andesite lavas contain amphiboles with high-Al (Al^{IV}>1.5 atoms pfu) that are decomposed and partially to completely replaced with fine-grained Fe-Ti oxides (Figures 4.4 to 4.7 and 4.13 to 4.15). Microprobe analyses represent the unaltered cores of prismatic euhedral phenocrysts from 0.2 to 1.0mm in length with opacite rims of fine-grained opaque oxides. High-Al amphibole cores are also found in pyroxene-bearing andesite to dacite domes spatially and temporally related to the Lower San Jose ignimbrite. These amphiboles are strongly decomposed with rims of opaque oxides similar to the Lower and Upper Yanacocha rocks (Figure 4.25), and due to opaque oxide replacement, only the cores were analyzed and all contain high-Al contents. High-Al amphiboles are also found in the pyroxene-bearing Upper San Jose spatter ignimbrite. The rims of these amphiboles have experienced varying degrees of dehydration due to

decompression. Opacite rims of plagioclase and Fe-Ti oxide are commonly observed in the largest phenocrysts (Figures 4.24).

The San Jose ignimbrite and related dacite domes display two populations of amphibole compositions that represent different domes and ash flow tuffs. Only rarely, in Lower and Upper San Jose ignimbrite, are two compositional varieties found in a single flow unit. One population is represented by amphibole with high-Al content (Al^{IV} 1.5 to 2.4 atoms pfu; Figure 4.31) in pyroxene-bearing rocks from the Upper San Jose spatter ignimbrite and the San Jose pyroxene dacite domes. Edge analyses along the phenocryst margins are lacking since the rims in these amphiboles are decomposed and replaced with Fe-Ti oxides (Figures 4.20 to 4.23), or they have opacite rims with plagioclase and Fe-Ti oxide (Figure 4.24).

The second population of amphiboles is represented by low Al compositions (Al^{IV} 1.1 to 1.5 atoms pfu; Figure 4.31) found in the rocks that lack pyroxene and include the Alto Machay dacite dome, the Maqui Maqui ignimbrite, and the middle San Jose ignimbrites. Low-Al amphiboles have fresh phenocryst margins and lack opacite rims. The rims are not resorbed and only slightly decomposed. The Al contents are uniform from core to rim and may vary by 0.2 atoms pfu. The dacite dome at Alto Machay (CB-3) has large euhedral amphibole phenocrysts 2.0–4.0mm in diameter that have minor rims of Fe-Ti oxide and abundant inclusions of plagioclase, but are not resorbed (Figure 4.26). The Lower San Jose ignimbrite at Arnacocha (CB-44) also has large amphiboles that are not resorbed or decomposed, but have inclusions of plagioclase and pyroxene (Figure 4.16). In another flow from the lower San Jose (CB-56), the amphiboles are broken and mantled by groundmass glass, but not resorbed (Figure 4.19A). Amphiboles in the Middle San Jose ignimbrite are not decomposed, and the rims of some phenocrysts are only slightly resorbed by the groundmass glass (Figure 4.18). All Middle San Jose amphiboles in sample VC-1 have low Al contents and contain inclusions of Fe-Ti oxides. Both core and rim analyses for the amphiboles in these rocks are low in total Al (1.1 to 1.5 pfu).

Low Al amphiboles are also present in pyroxene-bearing Lower and Upper San Jose ignimbrite. Lower San Jose ignimbrites have amphiboles with both high and low Al compositions; however, high Al compositions are rare and found only in small (<0.1mm)

groundmass amphiboles (Figure 4.17). Low-Al amphiboles from the Upper San Jose are strongly resorbed oxy-hornblende as the amphibole in Figure 4.19. Rims in most crystals are resorbed into the groundmass glass and typically rimmed with opaque oxides. In rare cases, the rims of amphiboles are preserved (Figure 4.18) and the Al content is low (Al^{IV}<1.5) and uniform from core to rim.

Different amphibole compositions are also present in the Maqui Maqui ignimbrite. Large amphibole phenocrysts ≥1mm have high-Al cores with overgrowths of low-Al rims (Figure 4.12). Small phenocrysts generally <0.5mm have low-Al contents throughout similar to the rims of large phenocrysts (Figure 4.8 and 4.9). The small
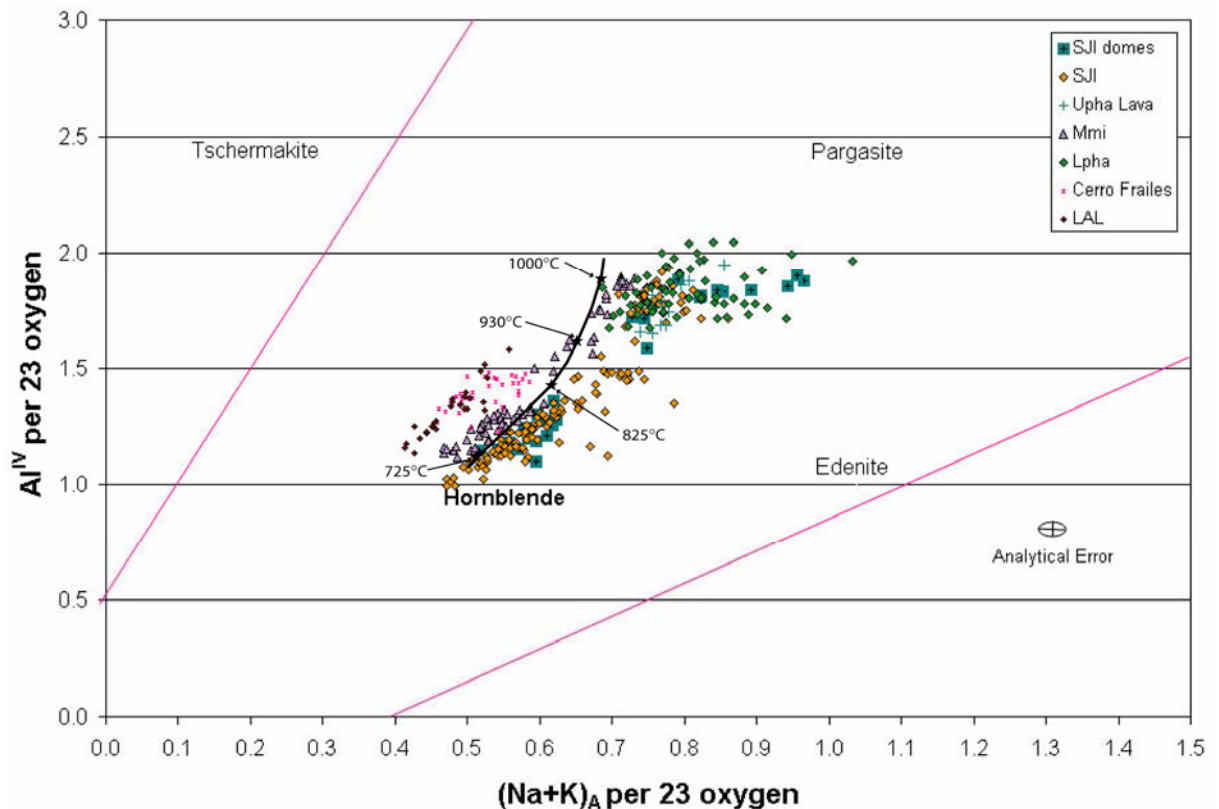
Figure 4.32. Al^{IV} versus $(Na+K)_A$ diagram that plots cations Al^{IV} vs. cations $(Na+K)_A$ in the A site on the basis of 23 oxygen for all amphibole microprobe analyses. The legend is organized oldest to youngest as LAL to SJI and Upha domes. The compositional trend with temperatures for amphiboles at the QMF buffer is shown for reference and was experimentally derived by Helz (1973). The curve is plotted from Feeley and Davidson (1994).
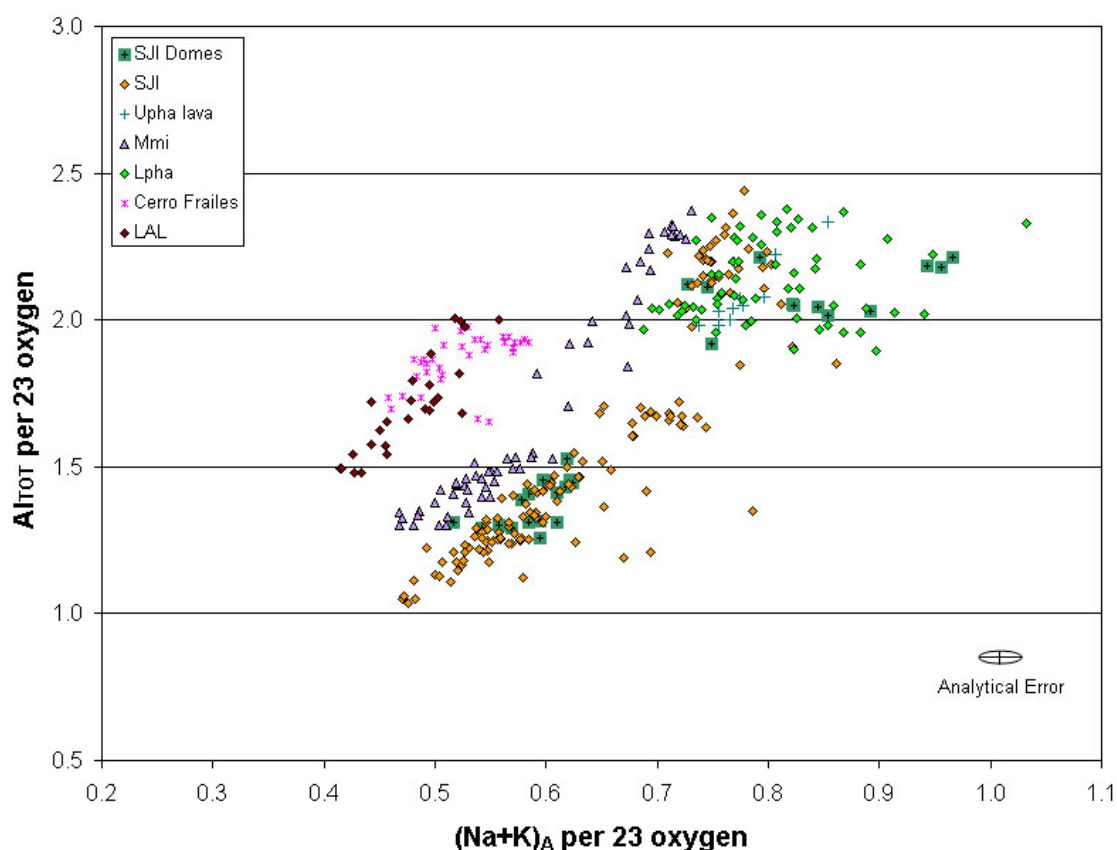
Figure 4.33. Total Al versus (Na+K)$_A$ diagram that plots total cations (Al^{IV} + Al^{VI}) vs. cations (Na+K) in the A site. Calculations are on the basis of 23 oxygen for all hornblende microprobe analyses. The legend is organized oldest to youngest as LAL to SJI and Upha domes.

amphibole phenocrysts in the Maqui Maqui ignimbrite are decomposed with narrow rims of Fe-Ti oxides (Figure 4.9 and 4.10) and slightly resorbed into the groundmass; they are best preserved in eutaxitic pumice fragments (Figure 4.9). Large phenocrysts are also only slightly resorbed with narrow opacite rims of plagioclase and Fe-Ti oxide.

Feeley and Davidson (1994) indicate that increases in Al^{IV} and (Na+K)$_A$ are correlated with increased crystallization temperatures consistent with the less differentiated magmatic inclusions versus the eruptive sequences at Ollague volcanic complex. This is also consistent with differentiation and SiO$_2$ contents of the Yanacocha rocks. Amphibole compositions in YVF rocks with lower SiO$_2$ contents in the less differentiated Lpha trend toward pargasite, whereas, in the more differentiated SJI with higher SiO2 contents are hornblende with lower Al^{IV} and (Na+K)$_A$.

Amphibole compositions outline two separate arrays with decreasing $Fe_{tot}/(Fe_{tot}+Mg)$ that correspond to decreasing values for $(Na+K+Al)/4$ and increasing values of SiO_2 in hornblende (Figures 4.34 and 4.35). These patterns are consistent with the aluminum versus $(Na+K)_A$ plots in Figures 4.32 and 4.33 in that hornblendes from specific rock sequences are restricted to distinct fields defined by the mole fractions and SiO_2 content. Rocks with high $(Na+K+Al)/4$ ratios >0.71 are Lower and Upper pyroxene-hornblende andesite lavas and domes, whereas, pyroxene-hornblende dacites from the San Jose ignimbrite and hornblende dacites and trachyandesites of the Maqui Maqui ignimbrite have lower $(Na+K+Al)/4$ ratios <0.70. Rocks with high $(Na+K+Al)/4$ ratios > 0.71 include the anhydrous, high temperature Lower and Upper Yanacocha pyroxene-hornblende andesite lavas and domes. Lower $Na+K+Al/4$ ratios <0.70 are characteristic of the hydrous, low temperature pyroxene-hornblende-biotite San Jose dacite ignimbrites and hornblende dacite and trachyandesite Maqui Maqui ignimbrite.

The mole fraction $Fe_{tot}/(Fe_{tot}+Mg)$ in amphibole decreases from the pre-Yanacocha rocks to the YVF rocks and implies increased fo_2 within magmas of the Yanacocha magmatic system. Pre-Yanacocha rocks have amphibole with $Fe/(Fe+Mg)$ ratios between ~0.35 and 0.46. Amphibole in the YVF rocks have $Fe/(Fe+Mg)$ ratios ranging from 0.20 to 0.40. Decreased values in $Fe/(Fe+Mg)$ ratios in Ca-amphiboles imply increased fo_2 and lower equilibration temperatures (Czamanske and Wones, 1973; Helz, 1973; Dilles, 1987; Anderson and Smith, 1995).

Amphibole analyses indicate that more than one compositional variety is present in the ignimbrites. Figure 4.36 displays amphibole analyses from one sample of Maqui Maqui ignimbrite (DN-7) plotted on a Al^{IV} vs. $(Na+K)_A$ diagram. The compositional-temperature trend for hornblende, experimentally derived by Helz (1973; 1979), also is referenced with increased crystallization temperature corresponding to increased Al^{IV} and $(Na+K)_A$ contents. These results indicate two distinct compositional varieties of amphibole in the Maqui Maqui ignimbrite that range from low $Al^{IV} < 1.4$ and $(Na+K)_A < 0.6$ to high $Al^{IV} > 1.5$ and $(Na+K)_A$ contents > 0.6. Amphibole compositions with low Al are found in small phenocrysts $<0.5mm$ measured parallel to the C-axis (Figures 4.8 and 4.9). Small amphiboles have uniform compositions with low-Al from core to rim. High
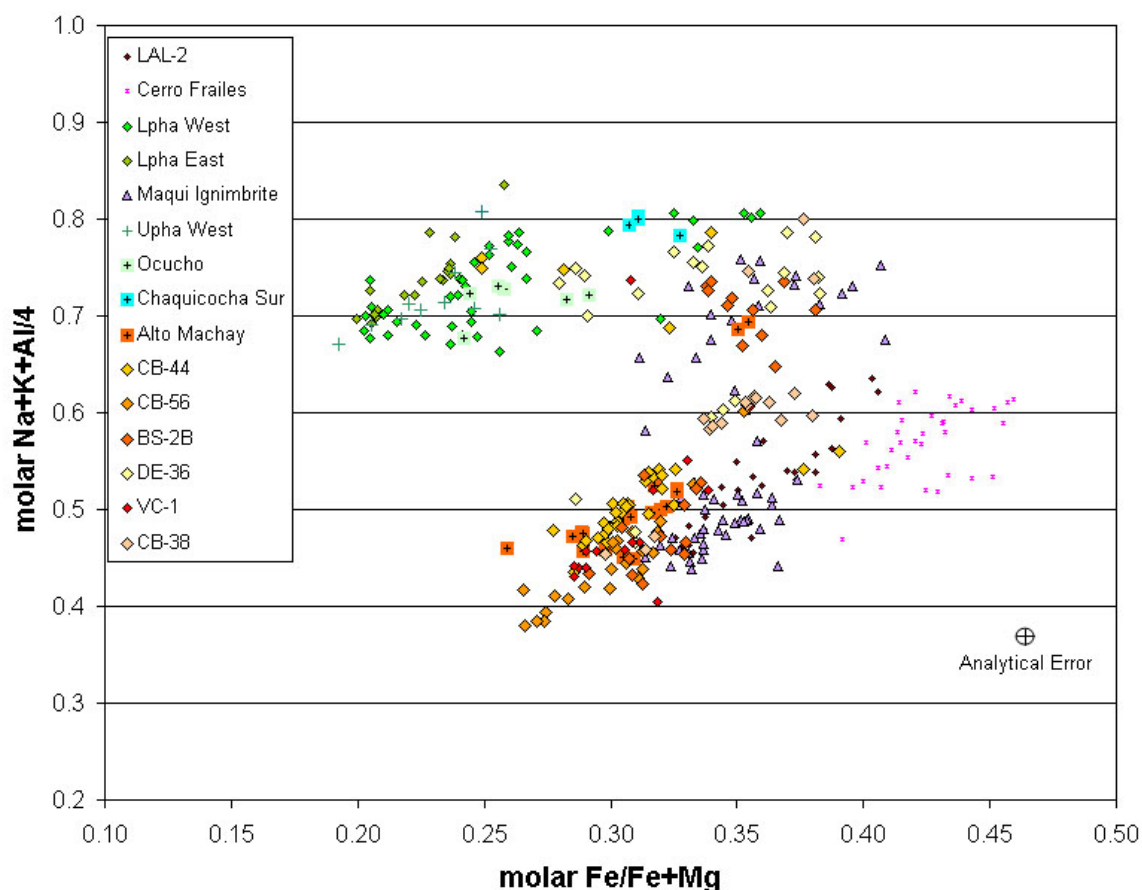
Figure 4.34. Plot of atomic (Na+K+Al)/4 versus $Fe_{tot}/(Fe_{tot}+Mg)$ for all the amphibole analyses. All rock sequences from the Yanacocha study area are represented and listed in the legend as oldest pre-Yanacocha on top and youngest at the bottom. Ocucho, Chaquicocha Sur, and Alto Machay domes are presented separately, as are six samples that represent the San Jose ignimbrite sequence from oldest Lsji (CB-44) to the youngest Usji "white tuff" (VC-1) and spatter ignimbrite (CB-36).
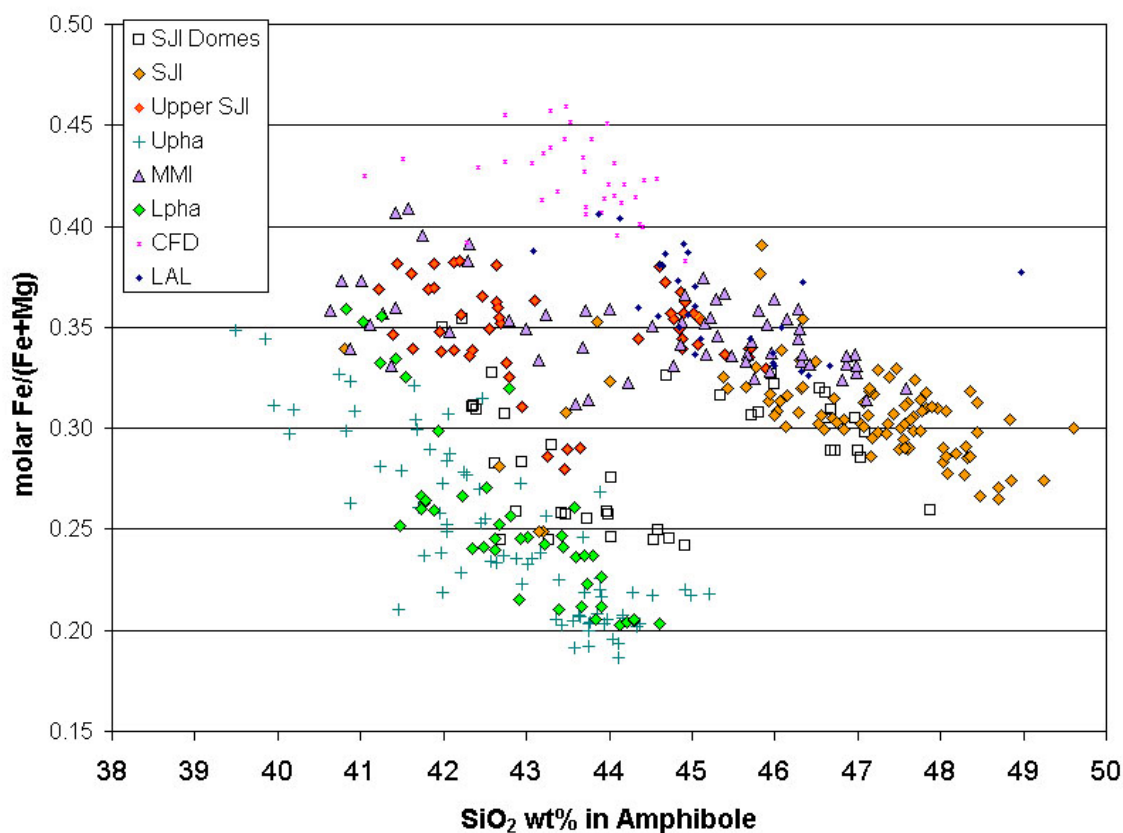
Figure 4.35. Plot of molar $Fe_{tot}/(Fe_{tot}+Mg)$ versus SiO_2 in amphobole on a basis of 23 oxygens. These data display two separate trends that imply two separate evolving magma systems. San Jose and Maqui Maqui ignimbrites display mixed populations that represent less oxidized and lower SiO_2 varieties from the Upper San Jose spatter ignimbrite and the core analyses of amphiboles in the Maqui Maqui ignimbrite.
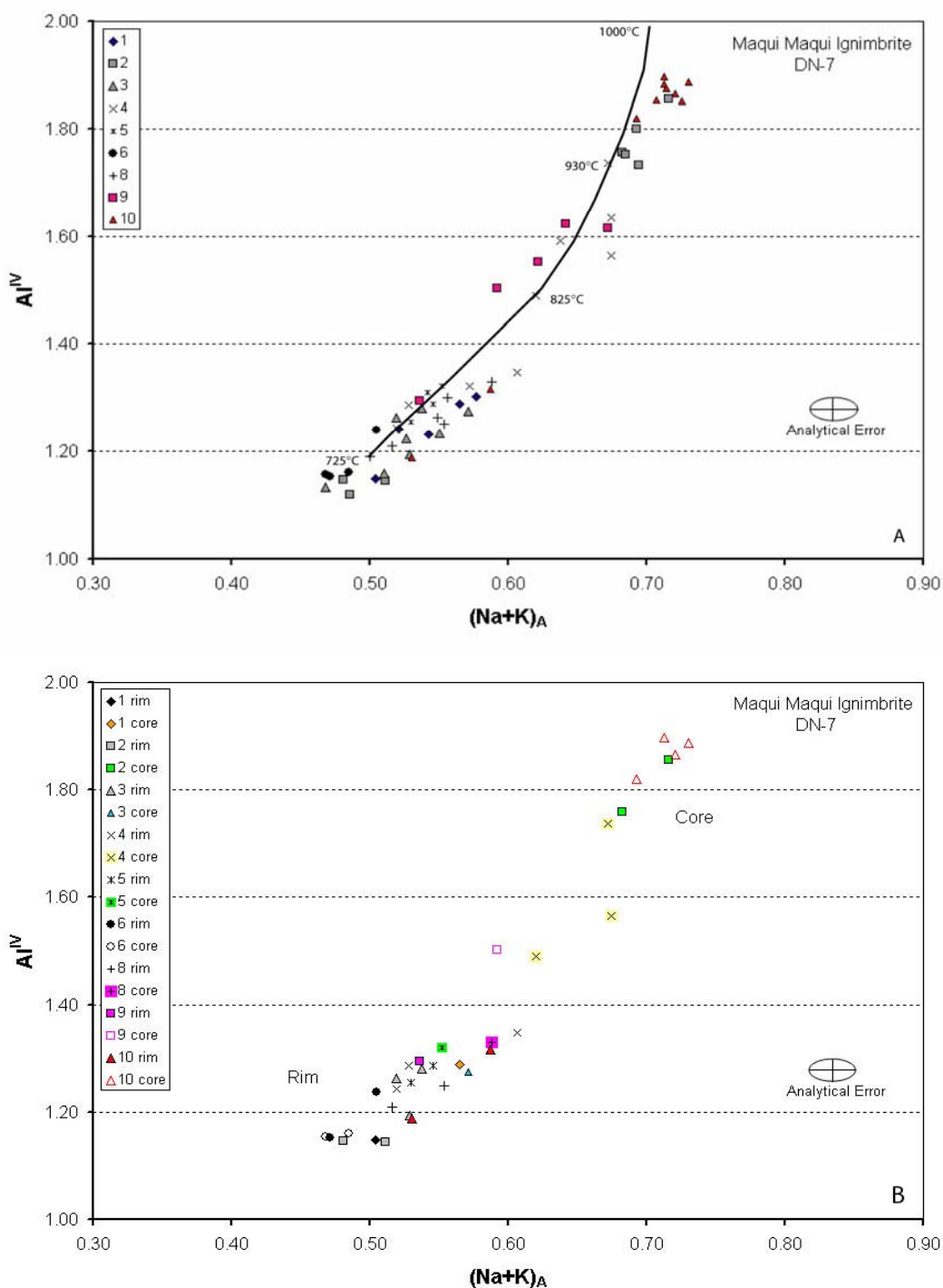
Figure 4.36. Compositional variations for amphiboles in the Maqui Maqui ignimbrite (DN-7). Al^{IV} vs. $(Na+K)_A$ per 24 oxygens are plotted for eight different amphibole phenocrysts in sample DN-7. The compositional trend with temperatures for amphiboles at the QMF buffer is shown for reference and was experimentally derived by Helz (1973). The curve is plotted from Feeley and Davidson (1994), and is intended as a qualitative comparison.

Al contents (Al^{IV} >1.80) are found in the cores of large amphibole phenocrysts >1mm, and the Al content decreases from the core to the rim where the Al^{IV} content is ~1.20. Phenocrysts are slightly resorbed and have narrow opacite rims of Fe-Ti oxides and plagioclase. Crystallization temperatures can be estimated from Figure 4.35A from ~725°C to < 825°C for the low Al^{IV} compositions and >825°C to <1000°C for the high Al^{IV} compositions. These results suggest mixing of high temperature magma containing high Al amphibole phenocrysts and a mafic component with shallow low temperature magma with a felsic component. Prior to eruption, the resulting composition re-equilibrated and the early high Al cores remained stable in the melt. Low Al amphiboles crystallized as rims to the high Al cores developing large compositionally and concentrically zoned phenocrysts, and small amphiboles with a uniform low Al content crystallized similar to the edge composition of the large zoned amphiboles.

Amphiboles in the San Jose ignimbrites (SJI) display similar compositional patterns as displayed in Figure 4.36 with the Maqui Maqui ignimbrite (DN-7). However, in contrast to DN-7, amphibole compositions in the SJI characterize the compositional variations between separate flow units from distinct eruptive phases in the San Jose sequence (Figure 4.37). Unimodal amphibole compositions with uniform low Al^{IV} and (Na+K)$_A$ compositions from core to edge represent ignimbrites of the Lower San Jose ignimbrites (CB-44 and CB-56), and the Middle San Jose "white" tuff (VC-1). Referencing the estimated temperature curve in Figure 4.36, these amphibole compositions imply lower crystallization temperatures and more evolved bulk rock compositions (Tables 4.3 and 4.6). Amphibole compositions with uniform high contents of Al^{IV} and (Na+K)$_A$ are characteristic in the Upper San Jose spatter ignimbrite (DE-36 and BS-2B) and imply higher crystallization temperatures and less evolved bulk chemistry (Tables 4.3 and 4.6). These data support the presence of a compositional variety of amphibole with a high molar content of Al^{IV} and (Na+K)$_A$, similar to the Lower and Upper Yanacocha andesite sequences, characteristic to the Upper San Jose spatter ignimbrite. Therefore, amphiboles with low Al and low A-site cation contents are common to the Lower and Middle San Jose ignimbrites, whereas, amphiboles with high Al and high A-site cation contents are common to the Upper San Jose spatter ignimbrite

and represent the final eruption of the San Jose ignimbrite sequence with compositional similarities to the earlier lavas from the Lower and Upper Yanacocha andesites.

Figure 4.38 displays results from amphibole core-edge analyses in the San Jose ignimbrite. These analyses indicate that core-edge compositional variations are present in individual amphibole phenocrysts, but this variation does not explain the full compositional range for the San Jose amphiboles. Compositional variations from core to edge are rare to absent in amphiboles from single flow units. High Al core to low Al edge variations within single flows in San Jose amphiboles are only present in one or two phenocrysts out of several analyzed, and most display uniform compositions (DE-36 and BS-2B; Figure 4.38). Instead, these data indicate the presence of a bimodal amphibole population in that two compositional varieties of amphibole are present in single flow unit. Bimodal compositions include one compositional variety with uniform high Al and A-site cation contents and another type with uniform low Al and A-site cation contents common only to the pyroxene-bearing Lower and Upper San Jose ignimbrite (Tables ; Figure 4.38; samples CB-44, DE-36, BS-2B, and CB-38). Bimodal populations of amphibole in the Lower San Jose are represented by rare high Al groundmass amphibole (Figure), and in the Upper San Jose spatter ignimbrite with rare phenocrysts (<1mm) containing uniform low Al contents. Large high Al amphibole phenocrysts (≥1mm) in the Upper San Jose have distinct opacite rims of plagioclase (Figure 4.24), whereas the low Al amphiboles are resorbed and typically smaller, but do not have the rims of plagioclase (Figure 4.23). Distinct plagioclase rims on the high-Al amphibole imply decompression and dehydration during ascent from a deeper magma reservoir, whereas the low-Al amphiboles display rims of fine-grained opaque oxide with resorption that represents disequilbrium and a different path of decompression after mixing with the deeper magma. The presence of this bimodal population and lack of compositional zoning implies mixing of deep high temperature andesite magma with shallow low temperature dacite magma concurrent with eruption leaving no repose time for crystallization after mixing. Mixing of the high temperature magma into a shallow reservoir initiated a rapid cataclysmic eruption.
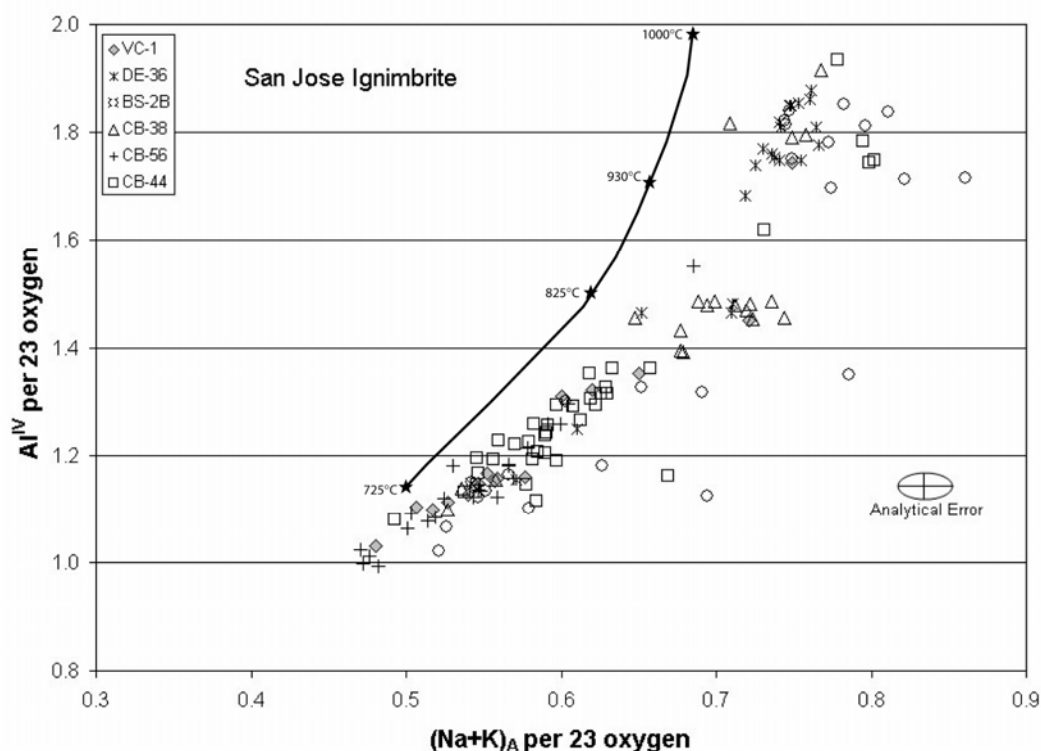
Figure 4.37. Amphibole microprobe analyses from five separate ash-flow tuffs throughout the San Jose ignimbrite sequence. The oldest flow units are CB-44 and CB-56 from the lower San Jose, and upper flows include the spatter ignimbrite represented by DE-36 and BS-2B, and white tuff (VC-1). These flows represent two separate late eruptions and the culmination of the San Jose eruptive sequence. Amphiboles in the ash-flow tuff (CB-38) directly below the spatter ignimbrite (DE-36) display compositional similarities to amphiboles in the spatter ignimbrite. These flows are the same age within a 2σ error and may be related (DE-36 is 11.25±0.07 and CB-38 is 11.29±0.15 Ma). The temperature curve is plotted from Feeley and Davidson (1994), and is intended as a qualitative comparison as in Figure 4.36.
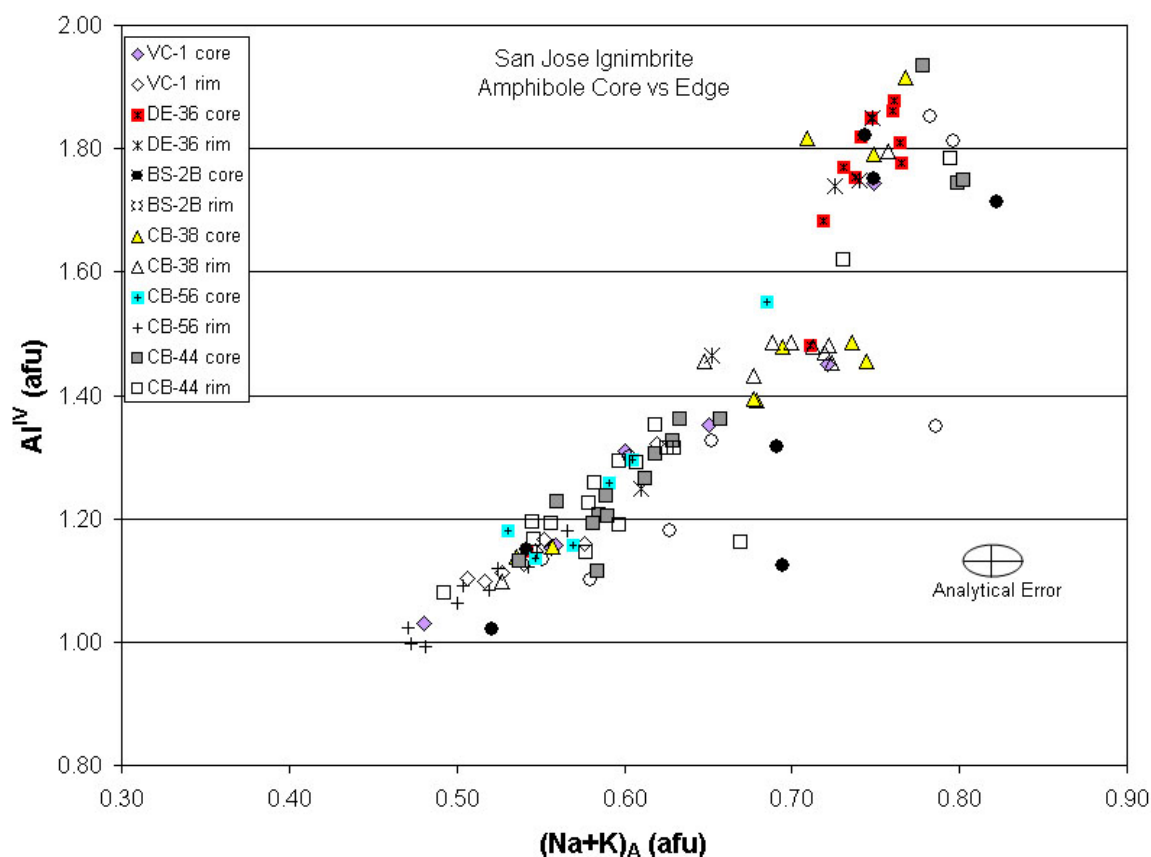
Figure 4.38. Plot of molar contents in atoms per formula unit (afu) of Al^{IV} vs. $(Na+K)_A$ for core-edge analyses of selected individual amphibole phenocrysts throughout the San Jose sequence. VC-1 – Middle San Jose white tuff, DE-36 – Upper San Jose Spatter ignimbrite, BS-2B – Upper? San Jose Spatter ignimbrite, CB-38 – Middle or Upper San Jose ignimbrite flow unit below DE-36, CB-56 – Lower San Jose eutaxitic ignimbrite, CB-44 – Lower San Jose ignimbrite below CB-56.

Pyroxene

Clinopyroxene is common in the lower Yanacocha andesite (Lpha), the upper Yanacocha andesite and dacite (Upha), and the upper and lower San Jose ignimbrite (Usji and Lsji). It is rare to absent in the Maqui Maqui ignimbrite (MMI) and the middle San Jose ignimbrite (Msji), and it is absent in the Lower (early) and Upper (late) Dacite intrusions. Pyroxene is also absent in the pre-Yanacocha Cerro Frailes dacite pyroclastic sequence (CFD). Orthopyroxene is rare, always smaller (0.05-1.25mm), and less abundant than clinopyroxene. Most pyroxene is euhedral to subhedral phenocrysts of the clinopyroxene augite and ferrian-augite. The clinopyroxene is optically (+) and displays weak pale green to pink pleochroism. Inclusions of Fe-Ti oxides and plagioclase are

common and simple twins, or sector zoning, are rare, occurring in only about 1 to 2% of the crystals. Phenocrysts are small and range in size from 0.5-2.0mm in the Lower Yanacocha andesites, 1.0-2.5mm in the Upper Yanacocha andesites, 0.5-1.0mm in the Lower San Jose and Middle San Jose ignimbrites, 0.5 to 3.0mm in the Upper San Jose ignimbrites, and 0.5-1.5mm in the pyroxene dacite domes related to the San Jose ignimbrites (SJI domes). Phenocryst abundances are variable from up to 14 modal% in the pyroxene-hornblende andesites to 1 modal% in the San Jose ignimbrite (Table 3.2). Lower Yanacocha andesite lavas typically have more pyroxene than Upper Yanacocha lavas. Pyroxene identification is still possible in rocks affected by advanced argillic when textures are preserved, and the characteristic monoclinic six-sided clinopyroxene crystal shape is apparent perpendicular to the C-axis.

Microprobe analyses (Figure 4.39. Tables 4.4) indicate the range of composition in the clinopyroxenes is restricted to Wo 43-45 En 40-44 Fs 12-16, and orthopyroxene composition is restricted to Wo 1-2 En 65-71 Fs 27-33. The pyroxene structural formula, or atoms per formula unit (afu), were calculated on a 6 oxygen basis and normalized to 4 cations. The pyroxene nomenclature and Wo-En-Fs components presented for these data are based on Morimoto et al. (1988). Estimations of Fe^{3+} from the FeO* total are based on Lindsley (1983). Clinopyroxenes are classified as augite and ferrian augite, orhtopyroxenes are classified as (clino)enstatite and ferrian (clino)enstatite (Morimoto et al., 1988). Orthopyroxene phenocrysts have Fe/(Fe+Mg) and Mg/(Mg+Fe+Ca) ratios that are more variable and higher than in the coexisting augites. Orthopyroxene components plotted on the pyroxene quadrilateral fall in two distinct fields. Lower Yanacocha andesite plots nearer the enstatite end-member at En 69-71 and Fs 27-29, whereas the San Jose ignimbrites (SJI) and SJI dome plots toward the ferrosalite end-member with En 65-68 and Fs 31-33 (Figure 4.39). Augite do not vary significantly and the compositions are similar throughout the sequences analyzed; however, the Lower Yanacocha andesites tend towards lower Wo and Fs and higher En, whereas the San Jose ignimbrites tend toward slightly higher Wo and Fs. This relationship indicates that with increasing SiO_2 content through time the orthopyroxene compositions trend to higher Fe and lower Mg, whereas the clinopyroxene compositions remain same (Figure 4.39).
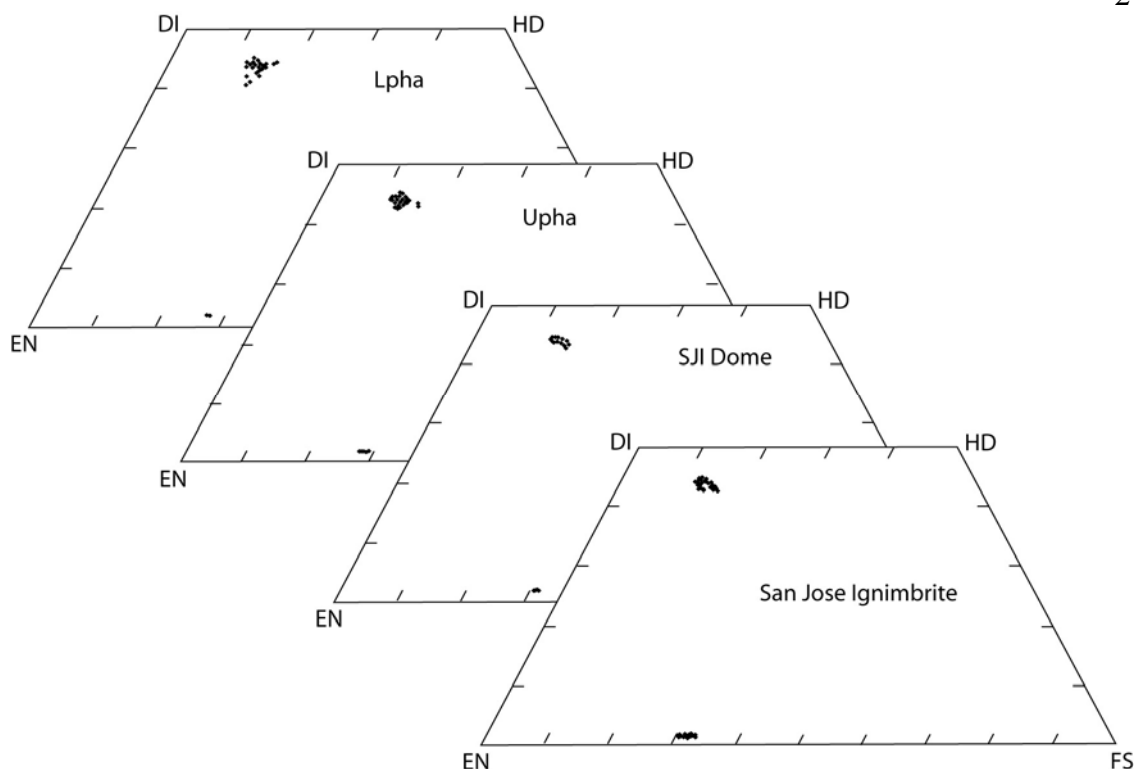
Figure 4.39. Pyroxene microprobe analyses plotted on Di-En-Hd-Fs pyroxene quadrilateral diagrams. The diagram displays the pyroxene compositions for the Lower Yanacocha andesite (Lpha) 13.3 Ma, Upper Yanacocha andesite (Upha) 12.1 Ma, pyroxene-hornblende andesite dome temporally and spatially related to the San Jose ignimbrite (SJI Dome) 11.4 Ma, and the San Jose ignimbrite (SJI) 11.6-11.2 Ma. Each point represents an analysis. Whole rock SiO_2 content increases from Lpha (55-62 wt%) to the San Jose ignimbrite (62-65 wt%).

Fe-Ti Oxides

Opaque oxides are present as subhedral to anhedral phenocrysts in all the Yanacocha rocks in this study. They also occur as inclusions in many mafic phases. Grain sizes range from 0.20 to 1.25mm and constitute approximately 2 to 4 modal % of the total phenocrysts. Apatite is commonly present as inclusions with lesser zircon. Inclusions of plagioclase, biotite, and hornblende are rare, and trace sulfide inclusions (Cpy and Cv?) were found in magnetite from sample MM-342 (169.5m). No microprobe analyses of Fe-Ti oxides were done for this study.

Optical identification of Fe-Ti oxides was performed on a select group of samples throughout the stratigraphic section. Within this group, the primary oxides are titanomagnetite and ilmenite, but these are commonly preserved as magnetite with partial

replacement by martite (hematite develops along crystallographically preferred planes in magnetite). Grains of ilmenite and magnetite solid solution are present, but in less abundance than magnetite replaced by martite. Ilmenite with hematite exsolution laminae was observed in one sample.

Accessory Minerals

Apatite

Apatite is present in all Yanacocha rocks but the late dacite. It is common as separate euhedral crystals within the groundmass in the Maqui Maqui and San Jose ignimbrites, and rare in the Lower and Upper Yanacocha andesites as inclusions in hornblende and opaque oxides (Figure 4.40). Optical properties and the habit of apatites are very similar in the two ignimbrites. Apatite in both ignimbrites is large with clouded and striated cores. At high power (40X), it is possible to recognize minute opaque inclusions (<1 μm) parallel to the elongated C-axis section (Figure 4.9, 4.12, 4.20 and 4.41). Sizes range from 0.05 to 0.75mm, and crystals are length fast with a slight gray-brown pleochroism. Apatites in the Lower and Upper Yanacocha andesites are small, colorless, and generally lack the striated or clouded appearance found in apatites from the ignimbrites. Sizes range from <0.05-0.20mm.

Microprobe analyses were carried out on several apatites from samples of the Maqui Maqui and San Jose ignimbrites. Results show distinct differences in the Cl and F contents between apatites of the two ignimbrites (Table 4.3c; Figure 4.42). Apatites in the Maqui Maqui ignimbrite have no fluorine (F = 0.0006 wt% and near detection limits) and the mole fraction $Cl/(Cl+F+OH)$ ranges from 0.08 to 0.16, whereas the $Cl/(Cl+F) = 1.0$ (Table 4.3c). In the San Jose ignimbrites, the apatite has increased F and decreased Cl relative to the Maqui Maqui ignimbrite, and the $Cl/(Cl+F+OH)$ ratios range from 0.09 to 0.10 (Table 4.5). Also, SO_3 contents are lower for apatites in the Maqui Maqui ignimbrite. The relationship of these differences is presented in Figure 4.41 plotted as molar $Cl/(Cl+F+P)$ as a function of molar $P/(P+S)$.
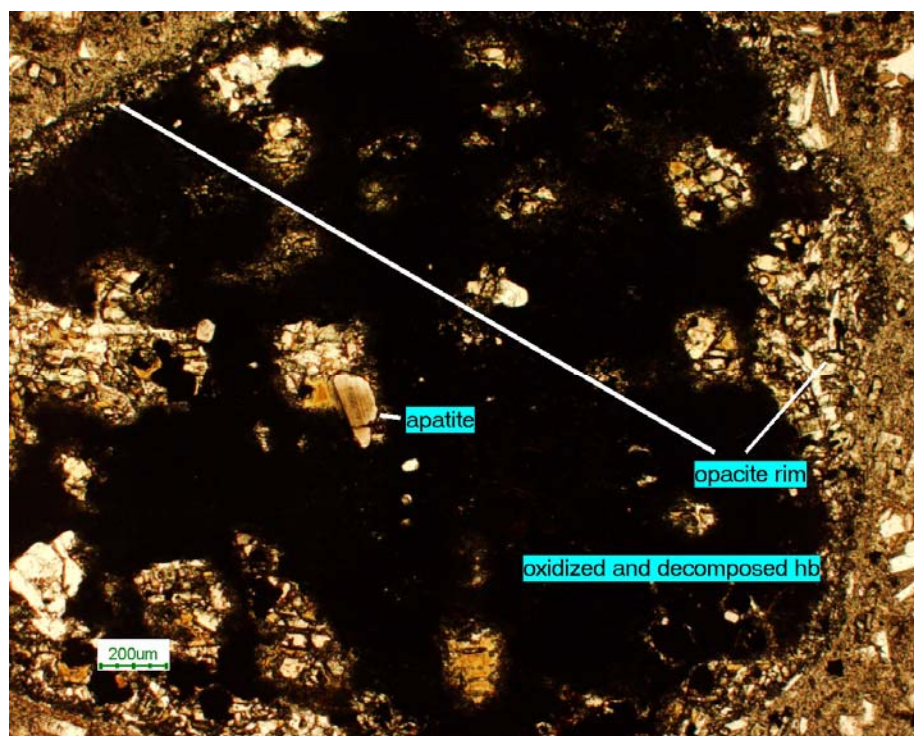
Figure 4.40 Photomicrograph a clouded and striated apatite inclusion in an amphibole from the Lower Yanacocha andesite lava (CNN-1A). The amphibole is a hornblende replaced with opaque oxides and the opacite rim is plagioclase and Fe-Ti oxide.
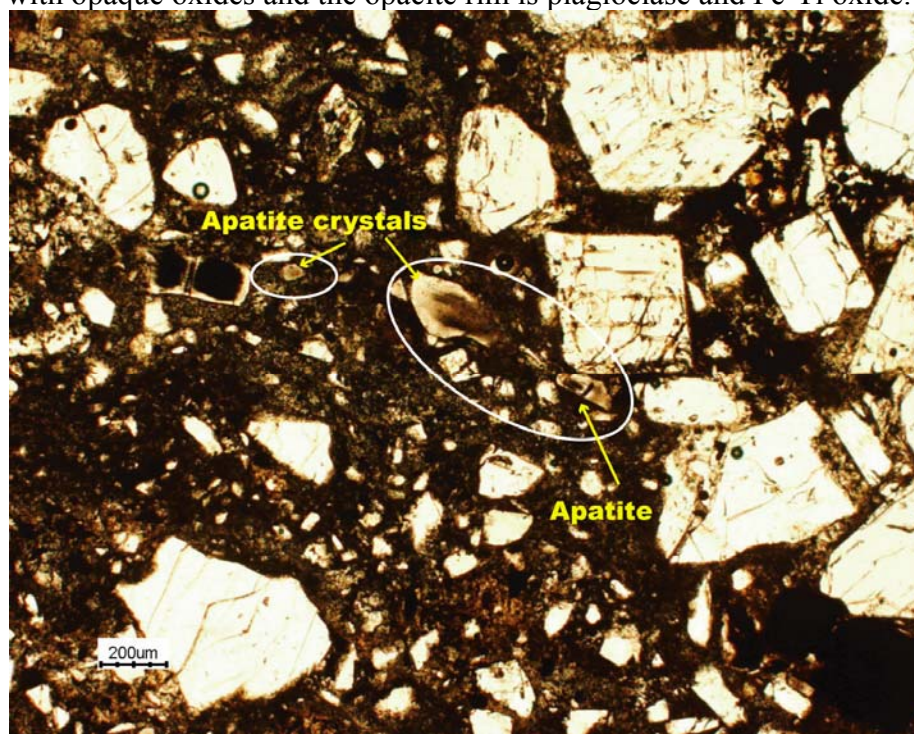
Figure 4.41. Photomicrograph of clouded-striated apatite in the upper San Jose spatter ignimbrite (BS-4).
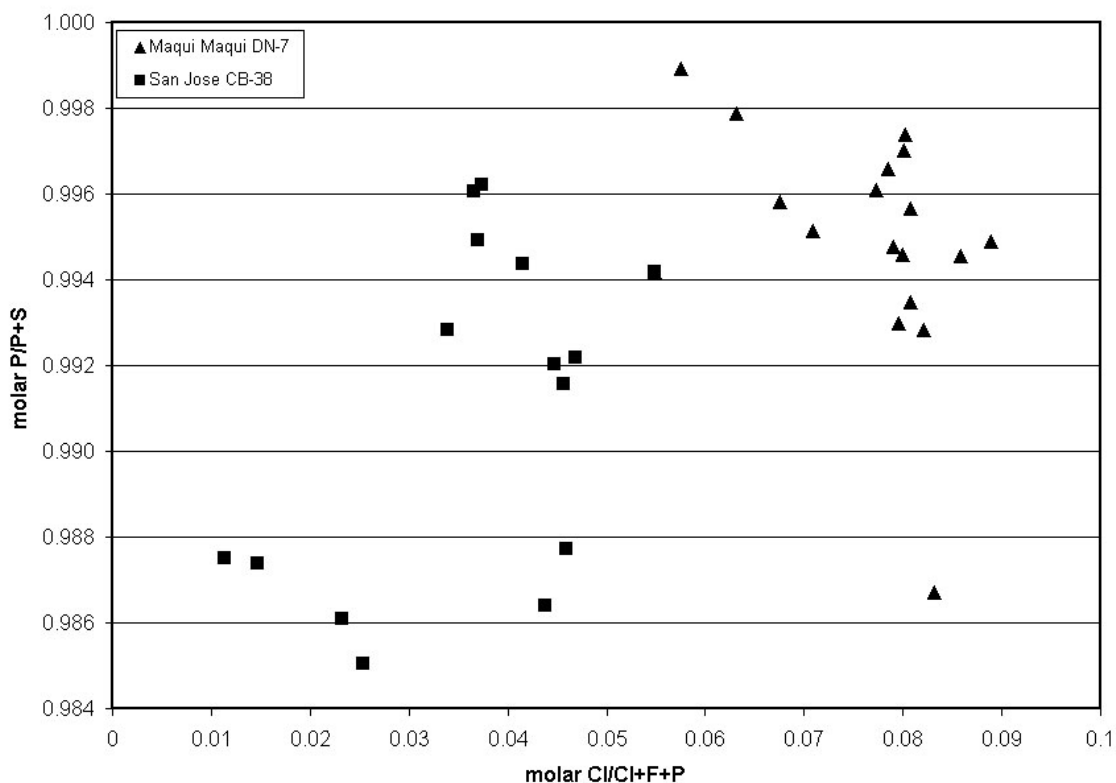
Figure 4.42. Plot of molar fractions P/(P+S) versus Cl/(Cl+F+P) for apatites from the San Jose and Maqui Maqui ignimbrites. Maqui Maqui apatites have virtually no fluorine (0.0006 wt%) and somewhat lower sulfur contents relative to the San Jose apatites (see Table 4.3c).

Zircon

Zircon is found as colorless and euhedral crystals enclosed in the later minerals plagioclase, alkali feldspar, hornblende, and the Fe-Ti oxides. It was found as an accessory mineral in nearly all rocks with apatite. Zircon is commonly euhedral and ranges in size from ≤0.05 to 0.20mm.

Titanite

Titanite is common only to the late dacite sequence and rarely occurs in the Middle San Jose ignimbrites. It was not observed in any other rock sequence at Yanacocha. It is present as euhedral and subhedral phenocrysts, and crystals range in size from 0.2 to 1.2mm in length. Some titanite crystals contain small inclusions of quartz

(Figure 4.43). Dacite porphyry intrusions at Cerro Yanacocha and below the La Quinua leach pad contain the largest crystals of titanite observed in the district (see geologic map for locations; Plate 1 and Figure 4.43).
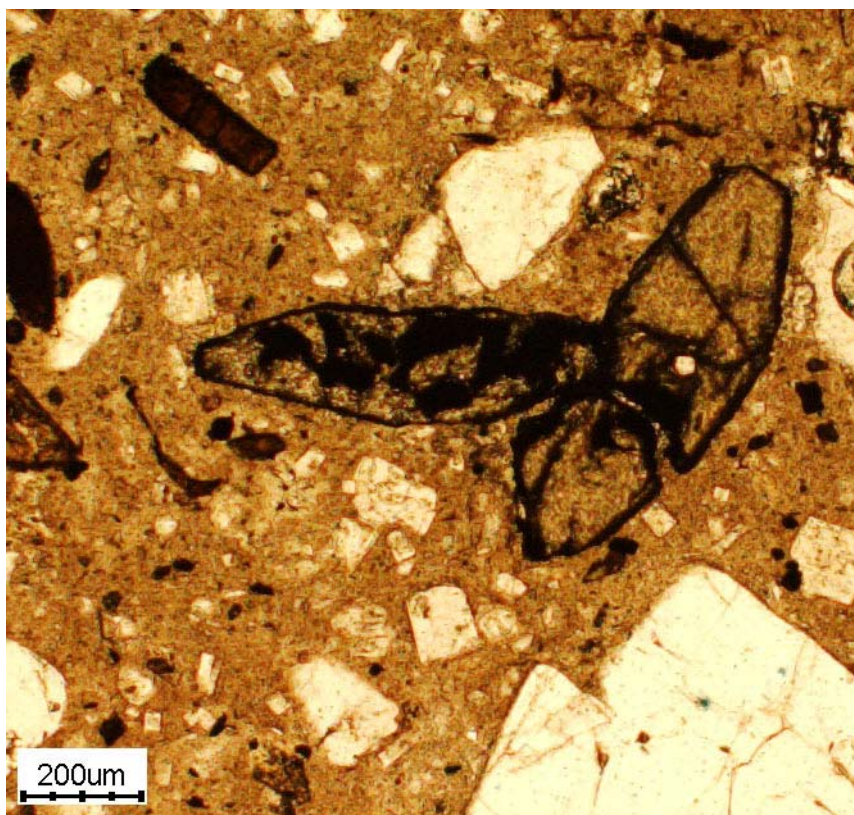
Figure 4.43 Photomicrograph of titanite from the La Quinua dacite (QNQ-3A). A small inclusion of quartz is present in the phenocryst on the right. Biotite is in the upper left corner.

Estimation of Pressure, Temperature, Oxygen Fugacity, and Volatile and Halogen contents in Pre-eruption Magmas

Pyroxene thermometry

The two pyroxene thermometer of Lindsley and Anderson (1983) is applied to the Yanacocha volcanic rocks with coexisting augite-orthopyroxene. The Ca-Mg-Fe distribution between coexisting clinopyroxene and orthopyroxene as applied to the two pyroxene thermometer is a pressure and temperature dependant variable. Accurate temperatures (±30ºC) require precise microprobe analyses, low contents of nonquadrilateral components <2 mole% with Wo-En-Fs ≥98%, and low Al contents <8

wt%. Pyroxene compositions are recalculated to the Wo-En-Fs pyroxene components after Lindsley (1983) and plotted on the pyroxene quadrilateral in Figure 4.44 with isotherms accurate to approximately 20-30ºC from Lindsley and Andersen (1983). Rim temperatures are reported as the equilibrium temperature in the analysis since the cores would potentially represent higher temperatures before the final pre-eruptive equilibration temperature. Rim temperatures are indicated on the diagram and listed below. Pre-eruptive equilibration temperatures estimated from the diagram in Figure 4.44 and range as follows (Table 4.6):

(1) Lower Yanacocha andesite lava AZU-1A (13.31 Ma) has clinopyroxenes in near equilibrium with orthopyroxene, and the core equilibration temperatures are estimated at ~1000±30°C. Clinopyroxene temperatures range from ~925 to 1050±30°C, and rim temperatures range from 975 to 1020±30ºC. No rim analyses are available for the orthopyroxene, but the core temperatures range from ~950-1000±30ºC.

(2) Upper Yanacocha andesite dome DO-60 in the west district has clinopyroxenes in equilibrium with orthopyroxene, and the equilibration temperatures for the rims are estimated at ~950 to 980±30ºC with core temperatures at ~1000±30ºC. Core temperatures range from ~980 to 1020±30ºC.

(3) The San Jose dacite dome DE-2 in the east district has clinopyroxenes in equilibrium with orthopyroxene, and the equilibration temperatures for the rims are estimated at ~910 to 950±30ºC. Core temperatures range from ~925 to 1025±30ºC.

(4) Pyroxenes in the Middle or Upper San Jose dacite ignimbrite CB-38 are nearly in equilibrium. Clinopyroxenes are ~975 to 1075°±30C and rims are ~980±30°C. Orthopyroxenes are ~875 to 910±30°C and rims are ~900±30°C.

(5) Pyroxenes in the Upper San Jose dacite ignimbrite DE-36 are not in equilibrium. Clinopyroxene core temperatures are ~1115 to 1150±30°C and rims are ~1090 to 1110±30°C. Orthopyroxene temperatures range from ~ 875 to 925±30°C and rims are ~900±30°C representing ~100°C difference from clinopyroxene.

(6) Clinopyroxene and orthopyroxene in the Lower San Jose ignimbrite sample CB-44 are not in equilibrium. Clinopyroxene temperatures range from ~1000 to 1100±30°C, and the rim temperatures are ~1000±30°C. Orthopyroxene temperatures range from

~850 to 950±30°C, and rim temperatures are ~900±30°C representing ~100°C difference from clinopyroxene.

Results from two pyroxene thermometry (Figure 4.44) indicate that the Lower and Upper Yanacocha pyroxene andesites have temperatures 950 to 1000°C similar to estimated hornblende temperatures (Figure 4.32; Table 4.6). Augite-orthopyroxene cores in the San Jose ignimbrites are not in equilibrium and the temperatures indicate the presence of a high temperature augite (~1050-1150°C). Coexisting augite and orthopyroxene rim temperatures in the San Jose ignimbrite are closer to equilibrium than the core, but also suggest that a higher temperature augite coexists with a lower temperature orthopyroxene. Only sample CB-38 is in near equilibrium within error (Figure 4.44; Table 4.6). The presence of high and low temperature pyroxene coexisting in the same sample of San Jose ignimbrite is supported by the presence of two varieties of amphibole (high-Al and low-Al) coexisting in these same ignimbrites (Figure 4.37 and 4.38; Table 4.6). These data further support mixing of high temperature magma at ~1000°C with lower temperature magma between ~ 800-900 as a process in the evolution of the San Jose ignimbrite.

Amphibole Geobarometry

The aluminum-in-hornblende (amphibole) geobarometer of Johnson and Rutherford (1989) was applied to the chemical results in hornblendes at Yanacocha. The geobarometer applied in this study uses total Al (Al^T), or the $Al^{IV} + Al^{VI}$ cation concentration, on the basis of the standard amphibole formula calculated to 24(O,OH,F,Cl) and assumes equilibrium with the mineral assemblages quartz + plagioclase + hornblende + biotite + titanite + magnetite or ilmenite (Johnson and Rutherford, 1989; Anderson and Smith, 1995). These phase assemblages are required for geobarometry over a pressure range of 2-8 kb; otherwise Al^T contents may be higher than expected for a given pressure resulting in an overestimate of depth. Al content in amphibole is fixed if all seven phases are in equilibrium with melt and fluid. Therefore, results are considered an estimate of pressures when melt and amphibole were in equilibrium and Al^T diffused into the respective phase assemblages.
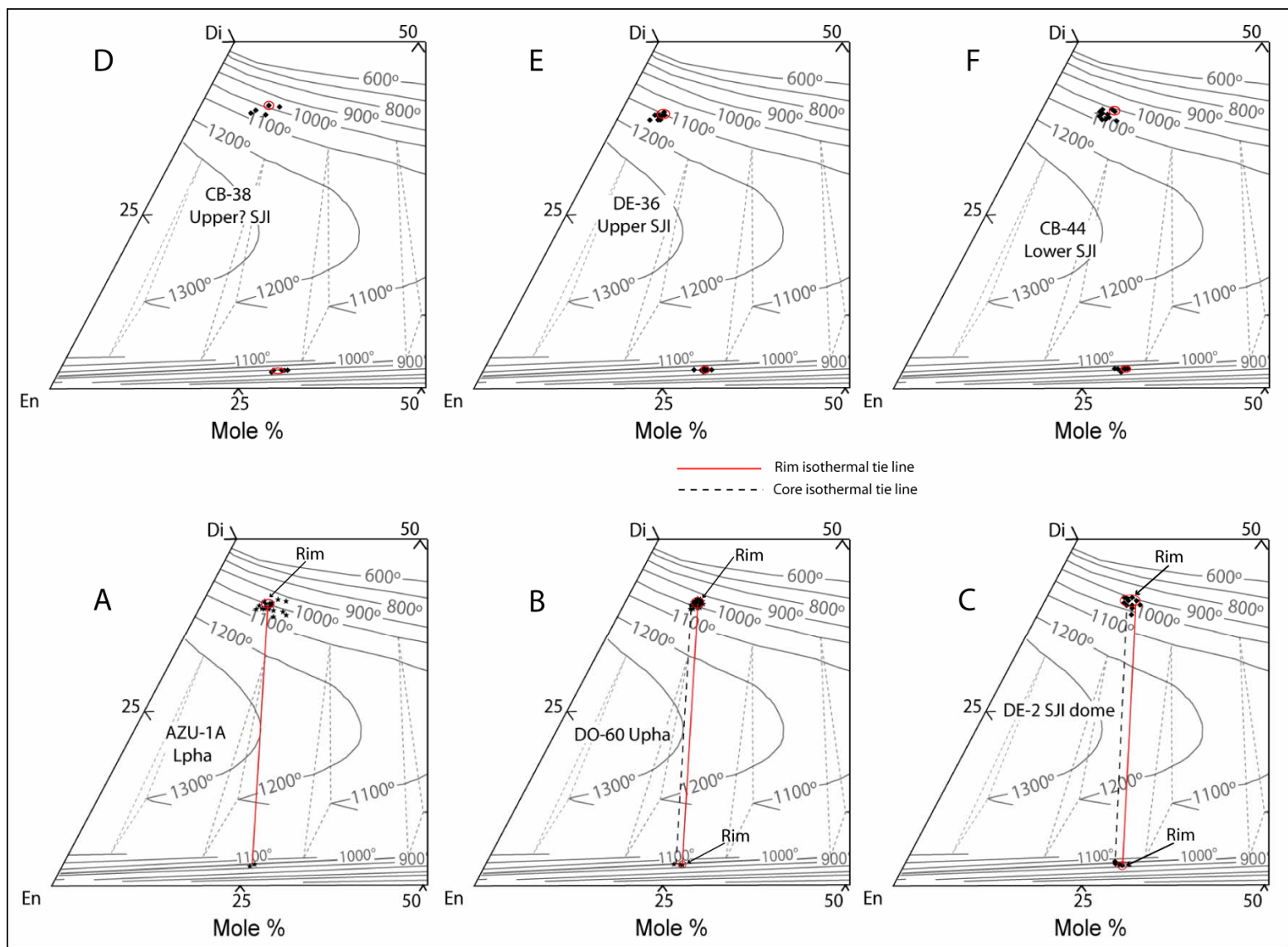
Figure 4.44 The Di-En portion of the Di-En-Hd-Fs pyroxene quadrilateral with isotherms at 5kb after Lindsley and Anderson (1983). The diagrams display microprobe analyses of augite coexisting with orthopyroxene in six samples from the YVF. Each point represents a separate pyroxene analysis, and the tie lines represent equilibrium temperatures for both rim and core analyses. Temperatures estimated with the isotherms from these diagrams are accurate to ±30ºC. A) AZU-1A Lower Yanacocha andesite lavas, B) DO-60 Upper Yanacocha andesite dome, C) DE-2 San Jose dacite dome (11.36 Ma), D) CB-38 Upper or Middle San Jose dacite ignimbrite (11.29 Ma), E) Upper San Jose Spatter dacite ignimbrite (11.23 Ma), F) Lower San Jose dacite ignimbrite (11.56 Ma).

Figure 4.45 displays the Al^T plotted as Al_2O_3 versus pressure in kilobars (kb) for all data, and all rock sequences at Yanacocha are represented in the diagram. Rock sequences without the full range of required mineral assemblages include the Tual and Chaupiloma lower andesite lahars (LAL), the Lower Yanacocha pyroxene andesites (Lpha), and the Upper Yanacocha pyroxene andesite-dacite (Upha). Amphiboles in these rocks have high-Al contents, and pressures are overestimated for these sequences. The required assemblage for Al-in-hornblende barometry is present in the Cerro Frailes dacite (CFD) and the Middle San Jose ignimbrite. Titanite has not been recognized and may be absent in the Lower and Upper San Jose and the Maqui Maqui ignimbrite; however, all other assemblages are present, and both high- and low-Al amphiboles are found in these ignimbrites.

Eruptive-styles of the YVF fluctuated from effusive stage clinopyroxene + orthopyroxene + hornblende bearing Lower and Upper Yanacocha andesite lavas (Lpha and Upha) to explosive stage hornblende + biotite ± clinopyroxene ± sanidine ± titanite bearing ignimbrites of the Maqui Maqui and San Jose (MMI and SJI). The legend in Figure 4.45 displays all rock sequences as outlined in this study. The Tual and Chaupiloma lower andesite lahars (LAL) and the Cerro Frailes dacite (CFD) represent the pre-Yanacocha rocks, and the remaining five sequences from Lower Yanacocha andesites (Lpha) to the San Jose ignimbrite (SJI) represent the Yanacocha Volcanic Field. Three groups of data are represented in the diagram. Low pressure rocks from ~1 to 3.5 kb include the Lower and Middle San Jose ignimbrite (SJI), the Maqui Maqui ignimbrite (MMI), and the San Jose domes (CB-3) spatially and temporally related to the SJI.

Middle pressure rocks from ~3.5 to 5 kb include the pre-Yanacocha Cerro Frailes
pyroclastic rocks and the Middle San Jose ignimbrite (CB-38). Lower and Upper
Yanacocha pyroxene andesite rocks lack the required assemblages for Al-in-hornblende
barometry and pressures are overestimated. These data form a trend with high Al^T and
high pressure of ~5.5 to >7 kb. Amphiboles from the SJI spatter ignimbrite and
amphibole cores from the Maqui Maqui ignimbrite are also represented in this group.
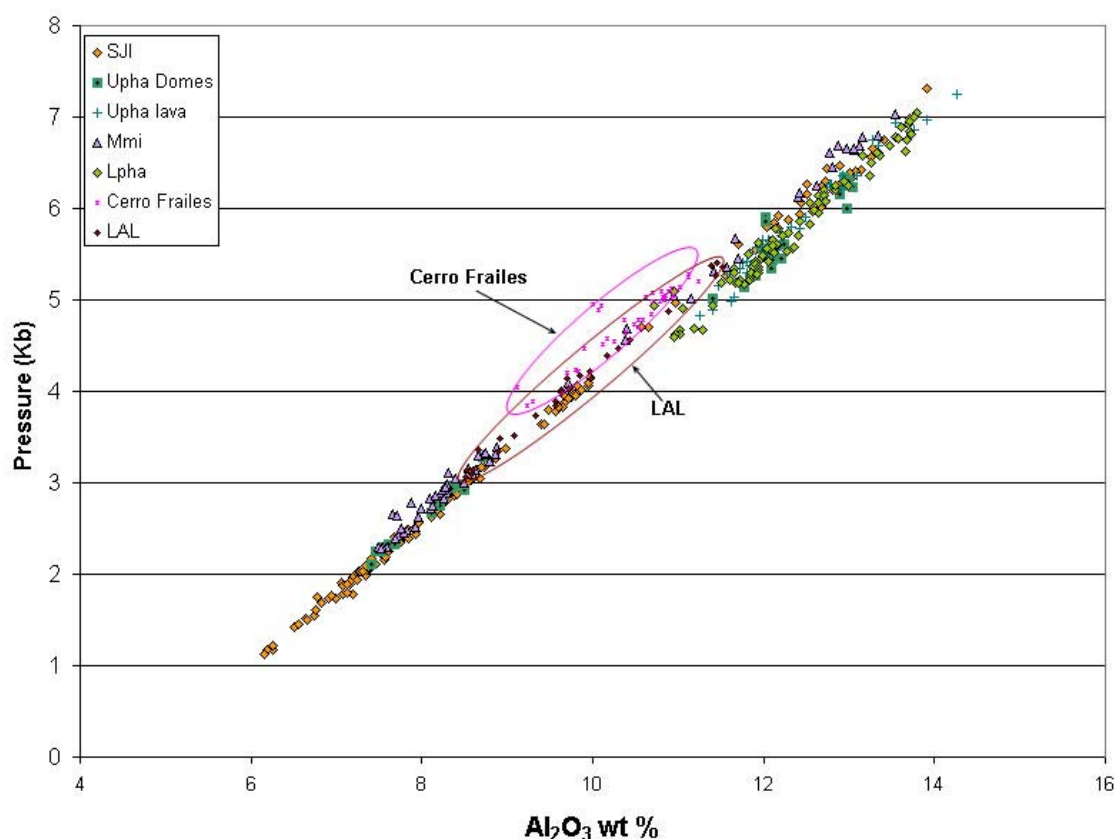
Figure 4.45. Total Al (Al^T) in the Yanacocha amphiboles as Al_2O_3 plotted as a function
of total pressure. Al^T is the sum of the cations $Al^{IV} + Al^{VI}$ that increase in concentration
in the hornblende formula linearly with increasing pressure controlled by Tschermack
substitution (experimentally derived by Johnson and Rutherford, 1989).

Estimates of the magma pressure, using the Al-in-hornblende geobarometer on
the rock sequences with the proper assemblages (pre-Yanacocha Cerro Frailes and low-
Al amphiboles in the Middle San Jose ignimbrite), imply that their amphiboles (Figure
4.46 A and B) equilibrated between ~1 to 5 kb (~3.7 to 18 km) prior to eruption.
Amphiboles of a Cerro Frailes ignimbrite imply pressures of ~3.5 to 5 kb suggesting
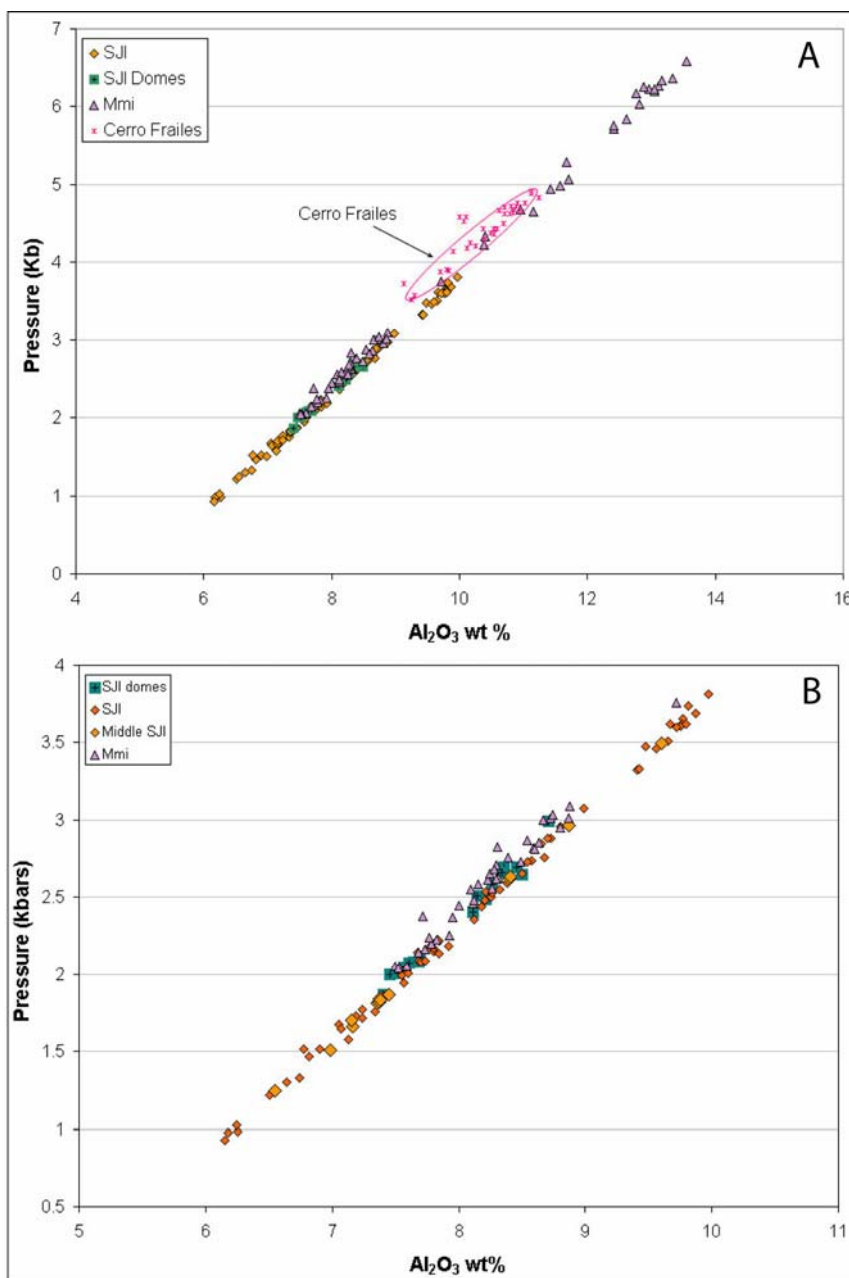
Figure 4.46 A and B. Total Al (Al^T) as Al_2O_3 plotted as a function of total pressure for amphiboles from ignimbrites and domes that have the required mineral assemblage of quartz + alkali feldspar + plagioclase + hornblende + biotite + Fe-Ti oxide + titanite. (A) Plot of the rock sequences with the possibility of having the required mineral assemblage for Al-in-Hb barometry. Titanite was not observed in the Maqui Maqui ignimbrite, and the Lower and Upper San Jose ignimbrite sample from this study. Amphiboles in the Maqui Maqui ignimbrite have high-Al cores and low-Al rims, and the cores represent the high pressure (>3.5kb) portion of the trend. (B) Plot of the low-Al amphiboles in the ignimbrites and related SJI dome. The required assemblage for Al-in-Hb barometry is present in the Middle San Jose ignimbrite (large light orange diamonds) plotted with other sequences with low-Al amphiboles.
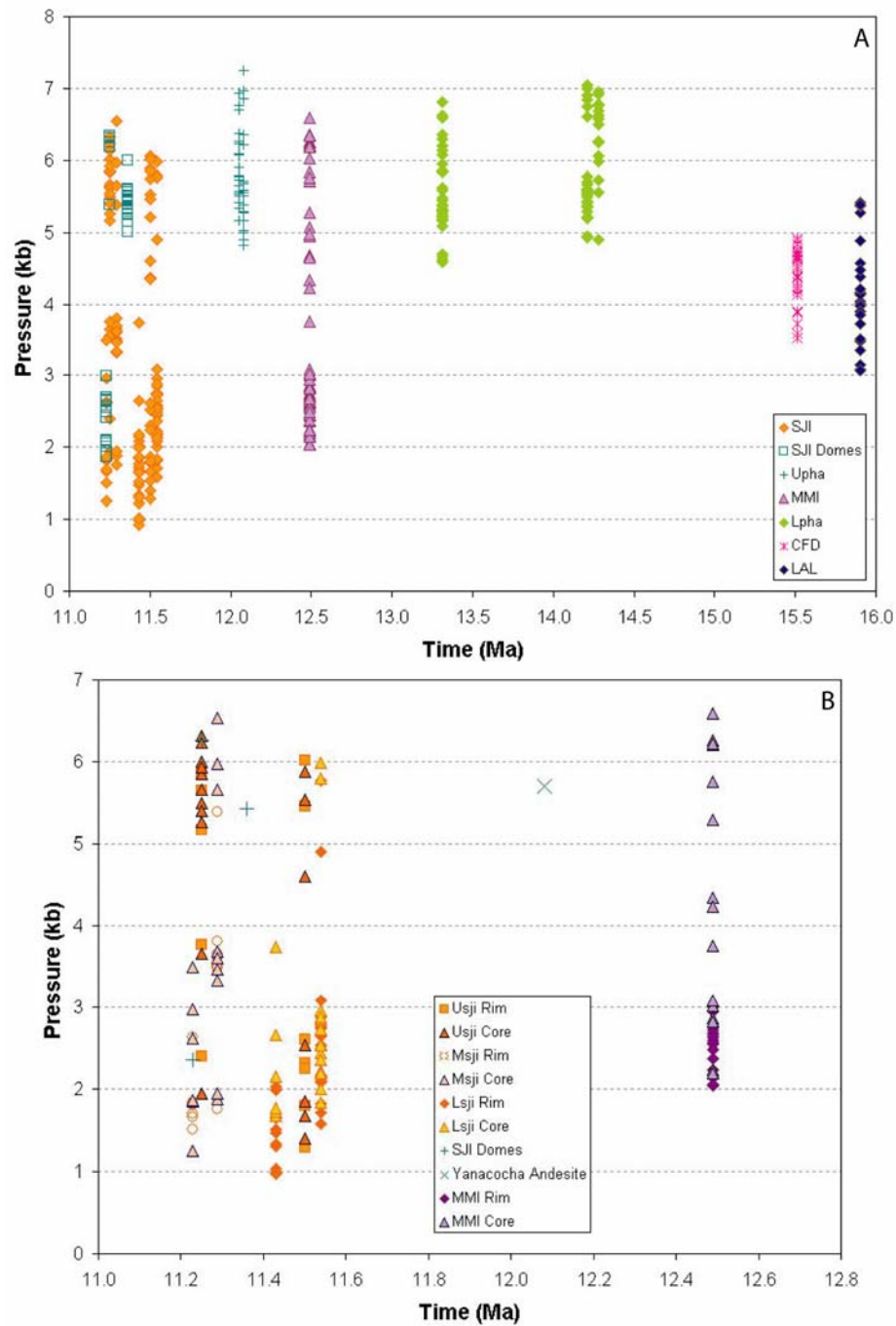
Figure 4.47 Plot of maximum magmatic equilibration pressure in kilobars (kb) versus time based on Al^T in amphiboles of the Yanacocha rock sequences. (A) Plot of all amphiboles analyzed in the Yanacocha rock sequences, and the Cerro Frailes (CFD) and low-Al amphibole in the San Jose have the required assemblages for the Al-in-Hb barometer. (B) Plot of the amphibole core-rim data for rocks <13 Ma that include the Maqui Maqui ignimbrite (MMI), and the San Jose ignimbrite (Lsji, Msji, Usji). Average pressures are plotted for the SJI domes and the Upper Yanacocha pyroxene andesite. Only the Middle San Jose (Msji) has the required mineral assemblages for strict application of the Al-in-hornblende barometer.

equilibration in deep reservoirs with crustal depths of ~11 to 18 km. Low-Al amphiboles in the Middle San Jose ignimbrite indicate pressures of ~1.25 to 3.5 kb (~4.6 to 13 km) (Figure 4.46 B). CB-38 ignimbrite lies directly below the San Jose spatter ignimbrite (CB-36 and BS-2B) and may represent a precursor eruption to the spatter ignimbrite eruption. Pressure estimates for the low-Al amphiboles in the Lower and Upper San Jose ignimbrite are similar to the Middle San Jose ignimbrite and the range of ~ 1 to 4 kb (3.7 to 15 km) assuming titanite is present (Figure 4.46B).

Equivalent depths are estimated on the basis of geobaric and geothermal gradients in continental crust. The geobaric gradient is estimated by assuming crustal densities of 2.2 to 3.0 g/cm3 (average density 2.7 g/cm^3) and a pressure gradient of~270 bars/km or 1 kb = 3.7 km and are considered maximum pressures (Best, 2003; p. 10). The geothermal gradient is estimated at ~25°C/km to crustal depths that represent pressures of ~ 10 kb (Green et al., 1970). In an active magmatic zone the geothermal gradient may be greater. Applying the idea of geothermal gradient to the temperature estimates for the high-Al^T amphiboles (Table 4.6a) suggests that depths of equilibration for amphibole in the Lower and Upper Yanacocha pyroxene andesites and the in the Lower and Upper San Jose ignimbrite (high temperature amphibole (1) in Table 4.6b) are 6 to 8 km deeper (~150 to 200°C hotter; Table 4.6 a and b) than the pressure estimates for low-Al amphiboles (an average pressure for the Middle San Jose of ~2 kb is used as reference). Therefore, estimates for the depth of equilibration for high-Al, high temperature amphibole phenocrysts in the anhydrous pyroxene-bearing YVF rocks may approach ~12 to 14 km, whereas the depth estimate for the low-Al, low temperature amphiboles is ~ 3 to 12 km.

Figure 4.47 displays the estimated pressure data for the amphiboles versus time. The ignimbrites have more than one variety of amphibole and suggest magma mixing of melts that crystallized amphibole at shallow depths with deeper magma containing amphibole that crystallized at higher pressures. This style of mixing occurred during two intervals in time prior to the eruption of the ignimbrites; the Maqui Maqui ignimbrite at 12.4 Ma and again with the San Jose ignimbrite between 11.6 and 11.2 Ma. The high-Al amphiboles from the Lower Yanacocha imply deep magmas existed for ~1.5 m.y. from 14.5 to 13.0 Ma prior to the development of the shallow reservoirs (Figure 4.47). The pyroxene-bearing andesites and dacites of the Upper Yanacocha and SJI domes also have

high-Al amphiboles that suggest deep magma reservoirs coexisted with shallow reservoirs after the eruption of the Maqui Maqui ignimbrite at ~12.1 Ma and during the eruptions of the San Jose ignimbrite (Figure 4.47A).

Volatile Contents and Oxygen Fugacities

Water content and oxygen fugacity in the YVF rocks are constrained by the presence of hydrous minerals and pyroxene as phenocrysts. Calculated H_2O contents are ~2 wt% for the amphiboles in this study and the values range from 1.5 – 1.95 wt%. H_2O is calculated assuming that F+Cl+OH=2 and molar F and Cl are calculated per 23 oxygen basis. Four mineralogically distinct types are present at Yanacocha.

Type 1   Lower and Upper Yanacocha pyroxene andesites (Lpha and Upha) contain hornblende, pyroxene, trace quartz, and trace apatite, but lack biotite and titanite.

Type 2   Upper and Lower San Jose Ignimbrites contain hornblende, rare pyroxene, trace biotite, rare sanidine, apatite, but may lack titanite.

Type 3   The Maqui Maqui ignimbrite and the Middle San Jose Ignimbrite or *white tuff* contain hornblende, trace biotite, trace quartz, apatite, and trace titanite, but lack pyroxene.

Type 4   Upper (late) dacite contains hornblende, biotite, quartz, alkali feldspar, and titanite, but lacks pyroxene and apatite.

Magmatic water contents can be predicted by the presence hydrous minerals such as hornblende and biotite. Hornblende is present in various amounts in all andesite and dacite rocks at Yanacocha, and biotite and hornblende coexist in the San Jose and Maqui Maqui ignimbrites, upper (late) dacites, and the pre-Yanacocha Cerro Frailes dacite. The presence of hornblende in andesite implies magmatic water contents of at least 4 wt% at 2 kb (Naney, 1983) and possibly >4-5 wt.% (Merzbacher and Eggler, 1984; Rutherford et al, 1985; Hammer et al., 2002).

Pyroxene with hornblende indicates less hydrous conditions than rocks with hydrous minerals that lack pyroxene. Pyroxene in Lower and Upper Yanacocha rocks is found as inclusions in the larger hornblende phenocrysts and suggests early crystallization. Early crystallization of pyroxene before hornblende implies lower P_{H_2O}

<1.5 kb (Rutherford et al., 1985; Wallace and Anderson, 2000). Many hornblende phenocrysts in the pyroxene-hornblende andesite of Lower and Upper Yanacocha rocks are affected by opacitization and rimmed with Fe-Ti oxides that reflect decompression and dehydration during ascent (Rutherford and Devine, 2003).

In summary, for the mineral assemblages outlined, pre-eruption water contents range from at least 4 wt% H_2O in Type 1 and Type 2 rocks with amphibole and pyroxene, and >4-5 wt% in Type 3 and 4 rocks that lack pyroxene but have amphibole and biotite.

Oxygen fugacities have been estimated from the mole fraction Fe/(Fe+Mg) in Ca-amphibole (Helz, 1973; Czamanske and Wones; 1973; Dilles, 1997) and from the phase assemblage titanite + magnetite + quartz (Wones, 1989). Amphibole composition is very sensitive to changes in oxygen fugacity (Helz, 1973). Increased f_{O_2} results in decreased Ti^{+4}, decreased Fe/(Fe+Mg), decreased Al^{IV}, and decreased $(Na+K)_A$ with decreasing temperature (Helz, 1973; Czamanske and Wones, 1973). Experimental studies indicate a steady increase in the A-site occupancy (e.g., Na+K) as Al^{IV} increases with temperature (Helz, 1973). Fe/(Fe+Mg) decreased as SiO_2 increased suggesting increased f_{O_2} during differentiation at Finnmarca plutonic complex, Norway (Czamanske and Wones, 1973). Amphiboles analyzed for the Yanacocha volcanic rocks have Fe/(Fe+Mg) that range from 0.17 to 0.39 in the Lower and Upper Yanacocha andesites and the San Jose ignimbrite. The Fe/(Fe+Mg) values in the Maqui Maqui ignimbrite are slightly higher at 0.31 – 0.41 and in pre-Yanacocha rocks from 0.33 to 0.46. Oxidized conditions are reflected in the low Fe/(Fe+Mg) of amphibole at Yanacocha, and petrographic studies of the Yanacocha rocks indicate a greater abundance of magnetite over ilmenite implying increased f_{O_2} during differentiation. Much magnetite is found in the form of martite (hematite pseudomorphs after magnetite). Similar characteristics have been interpreted in the data from the Yerington Batholith and are discussed by Dilles (1997) as indications of magmatc oxidation. Dilles (1997) states high oxidation states were achieved during crystallization and subsolidus cooling.

Upper (late) dacites and rhyolites at Yanacocha have the mineral assemblage quartz + biotite + hornblende + magnetite + titanite implying relatively high oxygen fugacities than in assemblages of coexisting magnetite and ilmenite in the absence of titanite (Lipman, 1971; Wones, 1989). Fe-Ti oxide fractionation causes an increase in

SiO_2 contents and a decrease in Fe/(Fe+Mg) contents by forcing liquid compositions toward SiO_2 and away from FeO* as shown in experimentally derived phase models of the MgO-Fe_3O_4-SiO_2 system (Gill, 1981). This fractionation results in increased fo_2 and decreased TiO_2. Titanite occurs as phenocrysts up to 1.2 mm in the late dacites; therefore, the oxygen fugacities in the upper (late) dacite rocks are relatively high and much greater than the FMQ buffer for temperatures below 1000°C.

Chlorine and Fluorine Content of Hornblende and Apatite

The fluorine and chlorine contents of hornblende in the Yanacocha Volcanic Field are variable throughout the volcanic sequences, but as a general rule, Cl increases and F decreases with increased ignimbrite eruptions through time. These data form a pattern related to their mineral compositions as discussed for compositional types 1 to 3 on the basis of the Al^{IV} and SiO_2 content in the amphibole (Figure 4.48 and 4.49). Type 1 consists of high-Al amphiboles from the pyroxene-hornblende andesites of the Lower and Upper Yanacocha sequences, and the pyroxene dacite San Jose domes, with Al^{IV} contents that approach pargasite compositions (Figure 4.45). Chlorine and fluorine contents expressed as the molar ratio Cl/F per 23 oxygens are <0.05, AlIV contents range from ~1.7 to 2.1, and SiO_2 as wt% in amphibole range from ~40 to 45 wt% (Figures 4.48 and 4.49; Table 4.6). Type 1 high-Al amphiboles represent the andesite mafic input to the magma system at Yanacocha.

Type 2 consists primarily of amphibole from the Maqui Maqui and Upper San Jose spatter ignimbrite that also have high Al contents that approach pargasite compositions (Figure 4.45) with molar Cl/F ratios that range from 0.05 to 0.20, AlIV contents from ~1.6 to 2.0, and SiO_2 from ~41 to 44 wt%. These amphiboles also represent deeper magmas related to the mafic component.

Type 3 are low-Al amphiboles are from the Lower and Middle San Jose ignimbrite (white tuff, CB-38 and CB-44), the Maqui Maqui ignimbrite, and the San Jose dacite dome at Alto Machay (CB-3) associated with the Middle San Jose ignimbrite. These amphiboles have lower contents of tetrahedral Al (Figures 4.32, 4.36, 4.37 and 4.38) typical of oxidized hornblende that lie toward tremolite compositions with Cl/F 0.10-0.35, AlIV contents of ~1.0 to 1.5, and SiO_2 contents from 45 to 50 wt%. The ratio

Cl/F in the type 3 amphiboles tends to decrease with increased SiO_2 and decreased AlIV contents. Type 3 Lower San Jose ignimbrite (CB-44) also has a variety of low-Al amphibole with the highest Cl contents in the study from 0.2 to 0.3 wt% Cl, Cl/F ~0.40 to 0.60, and SiO_2 contents in the hornblende from ~41 to 48 wt%.

      The F and Cl concentrations of amphiboles define two trends (Figure). Amphiboles from the lower and Upper Yanacocha pyroxene-hornblende andesites of (Lpha and Upha), and pyroxene-hornblende dacites from the San Jose spatter ignimbrite have Cl ≤0.01 moles per 23(O) basis and a wide range of F contents that range from 0.02 to 1.4 moles per 23(O) basis. Amphiboles from the Pre-Yanacocha Tual and Chaupiloma lower andesite lahars (LAL), the Cerro Frailes dacite (CFD), and all ignimbrites from the Yanacocha Volcanic Field display a wide range of chlorine concentrations with Cl from 0.01 to 0.08 moles per 23(O) and a restricted range of fluorine concentrations with F <0.30 moles per 23(O).

      Apatites in the ignimbrites contain higher concentrations of chlorine than the coexisting hornblendes. Proportions of chlorine and fluorine in the two coexisting mineral assemblages are represented in figure 4.50 as the molar ratio Cl/F versus the molar fraction Cl/(Cl+F+OH). As a general rule, apatites have higher contents of these ratios relative to their coexisting hornblendes. Fluorine is absent in apatite from the Maqui Maqui ignimbrite (DN-7) and the Cl/F ratios are > 400 and plot off the chart that displays the amphibole results.

      Halogen data combined with the pressure estimates from amphibole barometry suggest the deeper, high temperature magmas were depleted in chlorine and enriched in fluorine relative to the shallow magmas. High-Al amphiboles from the Upper and Lower Yanacocha andesites display unsually high fluorine resulting in low Cl/F ratios. These amphiboles represent the deep, high temperature mafic component to the Yanacocha magma system. Ignimbrites that erupted from shallow magma reservoirs have amphiboles elevated in the Cl/F ratio. The trend toward high Cl and low F is related to shallow, low temperature magma reservoirs and the ignimbrites. Low Cl and high F are related to high-Al amphiboles and the deeper, hotter magmas. Through time, amphiboles fluctuated from low Cl and high F in the early Lower and Upper Yanacocha pyroxene

andesite lavas to high Cl and low F in the later ignimbrites, then back to low Cl and high F in the final eruption of the San Jose spatter ignimbrite.
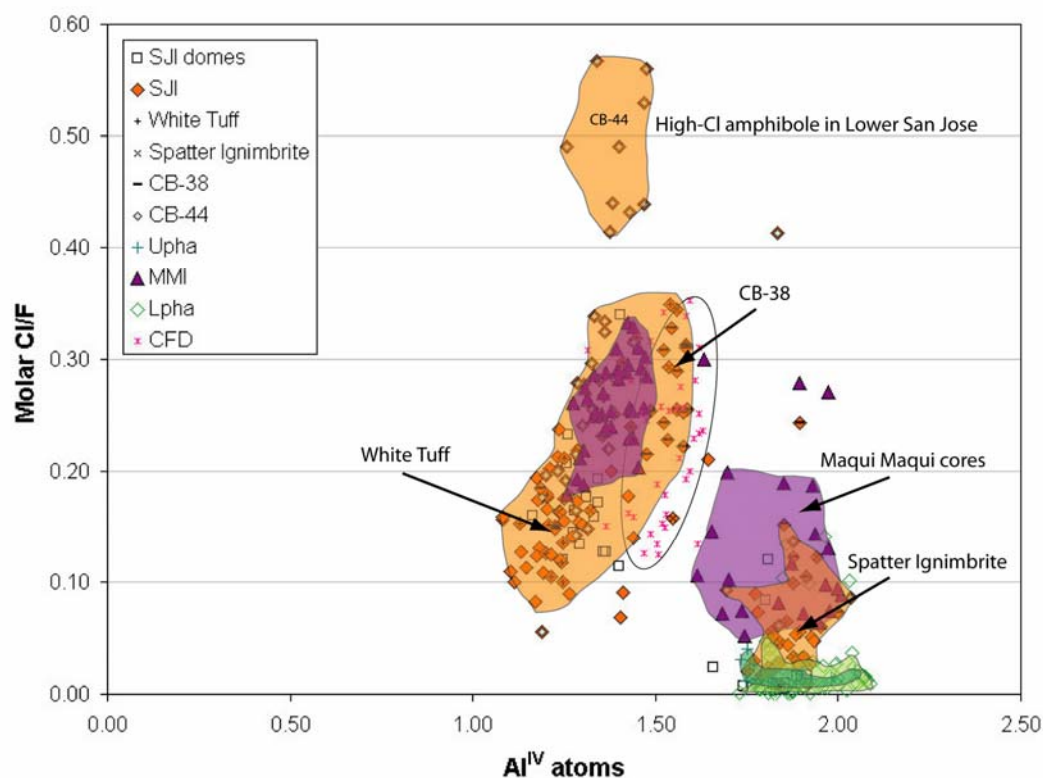
Figure 4.48 A plot of Al^{IV} atoms pfu versus molar Cl/F. The legend is in stratigraphic order with Cerro Frailes dacite (CFD) the oldest and SJI domes the youngest. Molar Cl/F content in the SJI ignimbrite tends to decrease with decreasing Al^{IV} pfu through time (CB-44 11.56 Ma, CB-38 11.29 Ma, white tuff VC-1 11.23 Ma). The spatter ignimbrite erupted amphibole with similar Cl/F ratios as the Yanacocha pyroxene andesite lavas and represent the mafic component. Maqui Maqui amphiboles display two compositions related to the mafic high Al core and felsic lower Al rims. Molar Cl/F and Al^{IV} are calculated per 23 oxygens.
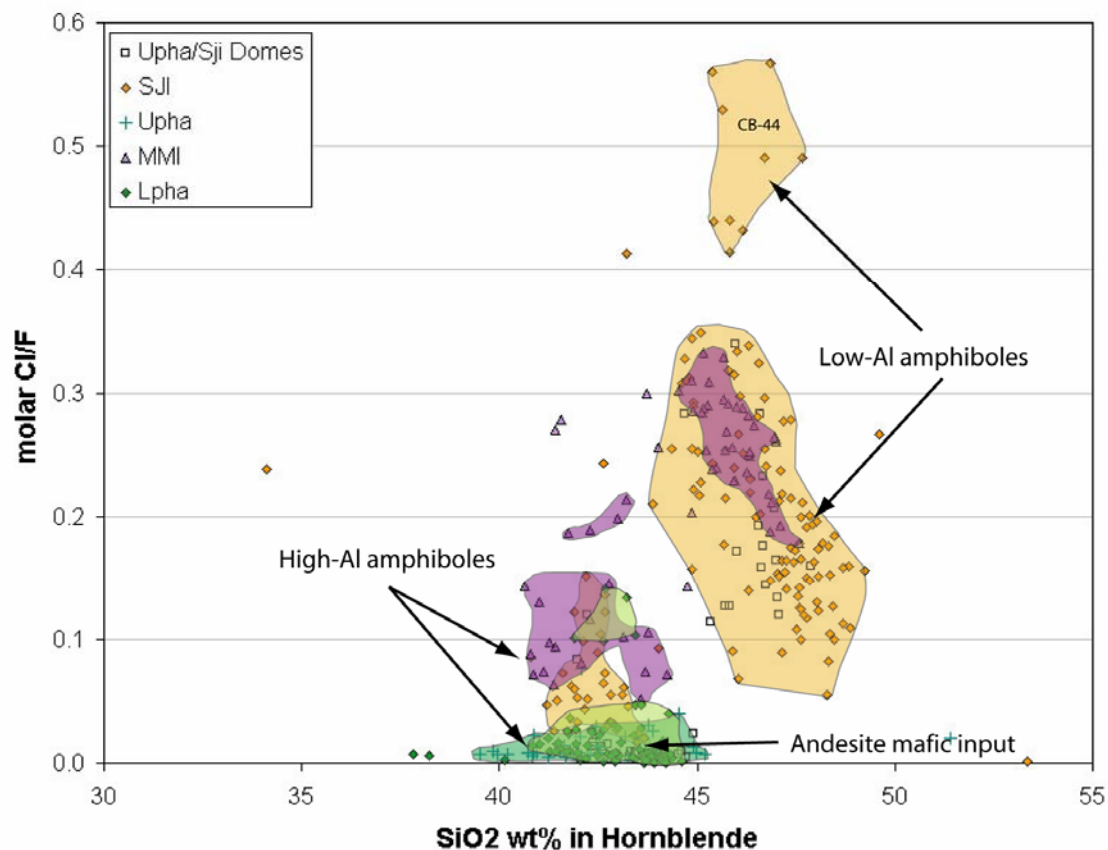
Figure 4.49 Plot of Cl and F contents as molar Cl/F versus SiO_2 in amphibole from volcanic rocks of the Yanacocha Volcanic Field (YVF). Three general clusters of data related to compositional variations discussed in the text are grouped as low SiO_2 and high-Al amphiboles and high SiO_2 and low-Al amphiboles. High-Al amphiboles with the lowest molar Cl/F values represent the mafic component in the Lower and Upper Yanacocha andesites from deep, high temperature magma reservoirs.
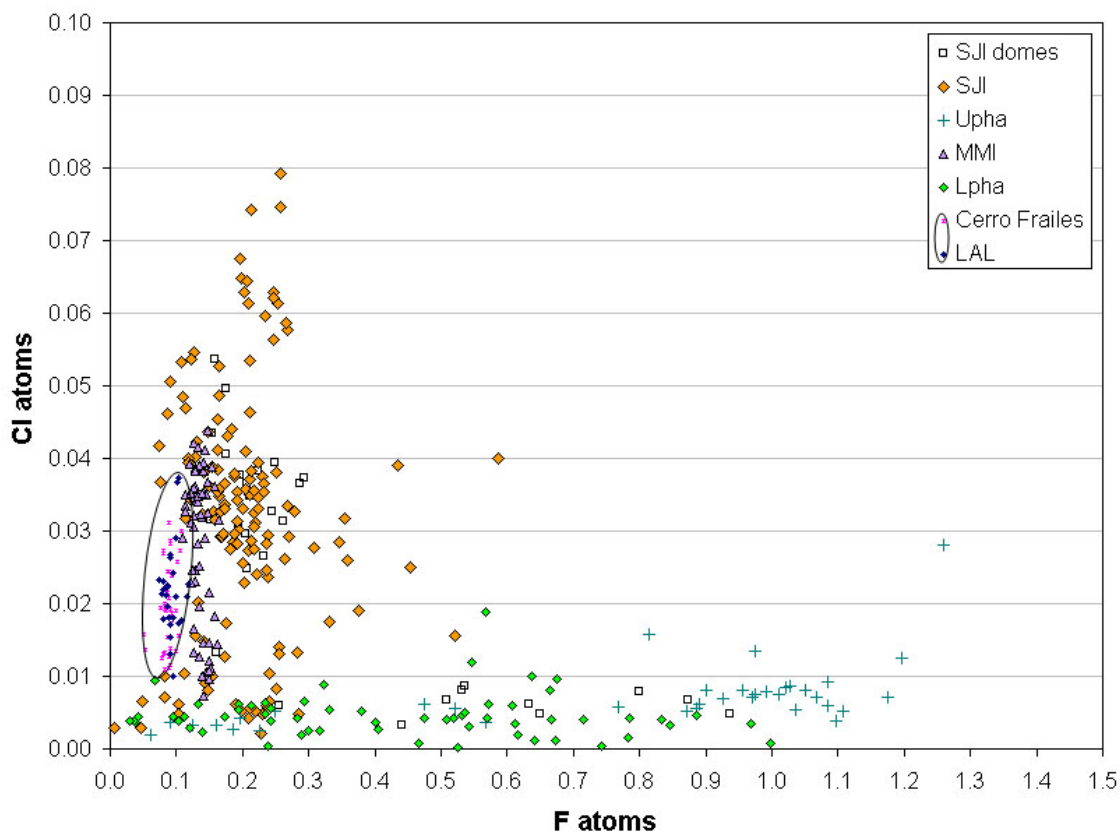
Figure 4.50 F and Cl contents of amphibole in the YVF showing to distinct trends. The trend to high F and low Cl is related to the pyroxene-hornblende andesites and mafic input. Pre-Yanacocha volcanic rocks and dacite ignimbrites have high Cl and low F. Molecular concentrations of the F and Cl anions were calculated as the molecular proportions of each anion from the standard amphibole formula per 23 (O) basis.
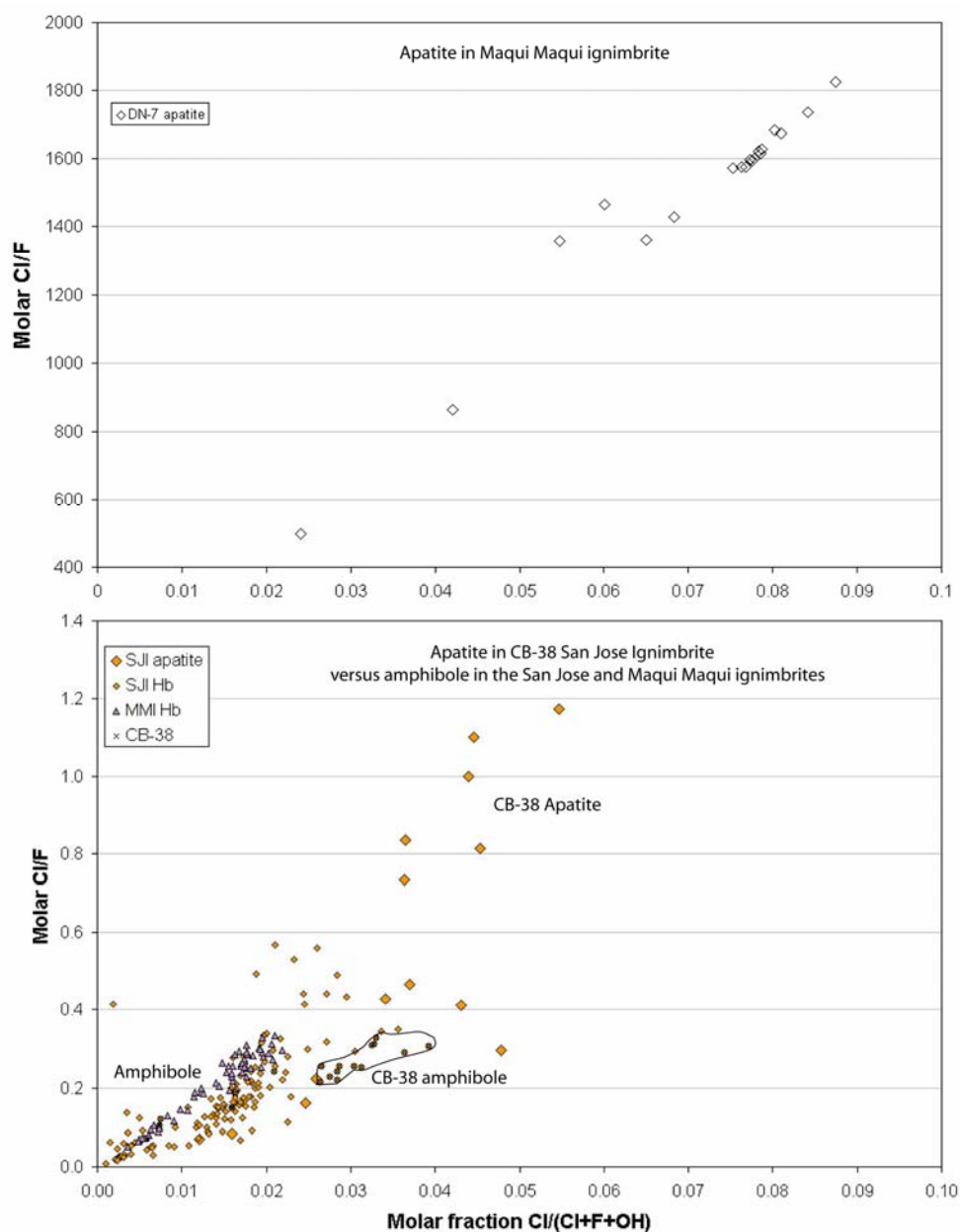
Figure 4.51 Plot of apatite in the DN-7 Maqui Maqui ignimbrite and CB-38 San Jose Ignimbrite as molar Cl/F versus the molar fraction Cl/(Cl+F+OH). The fluorine and chlorine compositions of hornblendes in the two ignimbrites are plotted for comparison. Cl and F in apatite are calculated per 25 (O,OH,F,Cl) basis, and OH is calculated assuming F+Cl+OH=1.

Geochemistry

Major Element Compositions

Major element compositions from rocks at Yanacocha define a medium-K to high-K calc-alkaline rock suite with SiO_2 contents that range from 57 to 71 wt.% in the volcanic rocks and from 55.3 to 70.6 wt.% in the intrusions (Tables 4.1). Contents of K_2O and Na_2O increase (Figure 4.52, Table 4.1), and CaO, Fe_2O_3*, TiO_2, and MgO decrease with increasing SiO_2. Al_2O_3 contents cluster between ~17.5 and 21 wt.% then decrease between ~15.8 and 19.5 wt.% with increasing SiO_2 contents > ~64.5 wt.%.

Volcanic rocks are presented in contrast to intrusive rocks in the SiO_2 versus K_2O diagram and both typify the same suite (Figure 4.53). The bulk of the Yanacocha sample suite ranges from 58 to 66 wt.% SiO_2 and consists dominantly of volcanic rocks. K_2O and SiO_2 compositions of the volcanic rocks are similar to the intrusions between ~58 and 66 wt.% SiO_2, and the compositional trends of both intrusive and volcanic rocks are concordant linking them together. Compositional gaps are indicated with < 58 wt.% SiO_2 and >66% SiO_2 and the K_2O and SiO_2 contents of the intrusive rocks diverge away from the volcanic rocks. SiO_2 contents of the intrusions are as low as ~55% and as high as ~71 wt% SiO_2.

P_2O_5 contents display a similar pattern, but have considerably more scatter in the data between 60 to 65 wt.% SiO_2, and the contents strongly decrease from 65 to 72 wt.% SiO_2 (Figure 4.52). The wide scatter after 60 wt.% SiO_2, and strong decrease in P_2O_5 after 65 wt.% SiO_2 are supported by petrography. Several samples with SiO_2 from 60-65% lack apatite in the Cerro Frailes dacite tuffs and the middle member of the San Jose ignimbrite, and the late dacite intrusions with SiO_2 from 65-72 wt.% lack apatite. Strong enrichments in P_2O_5 result in rocks (e.g., Maqui Maqui ignimbrite) with abundant apatite. Scatter is also partially related to increased analytical error with P_2O_5 results nearer the limit of detection at 0.01% (Appendix IIc and CD Appendix V).
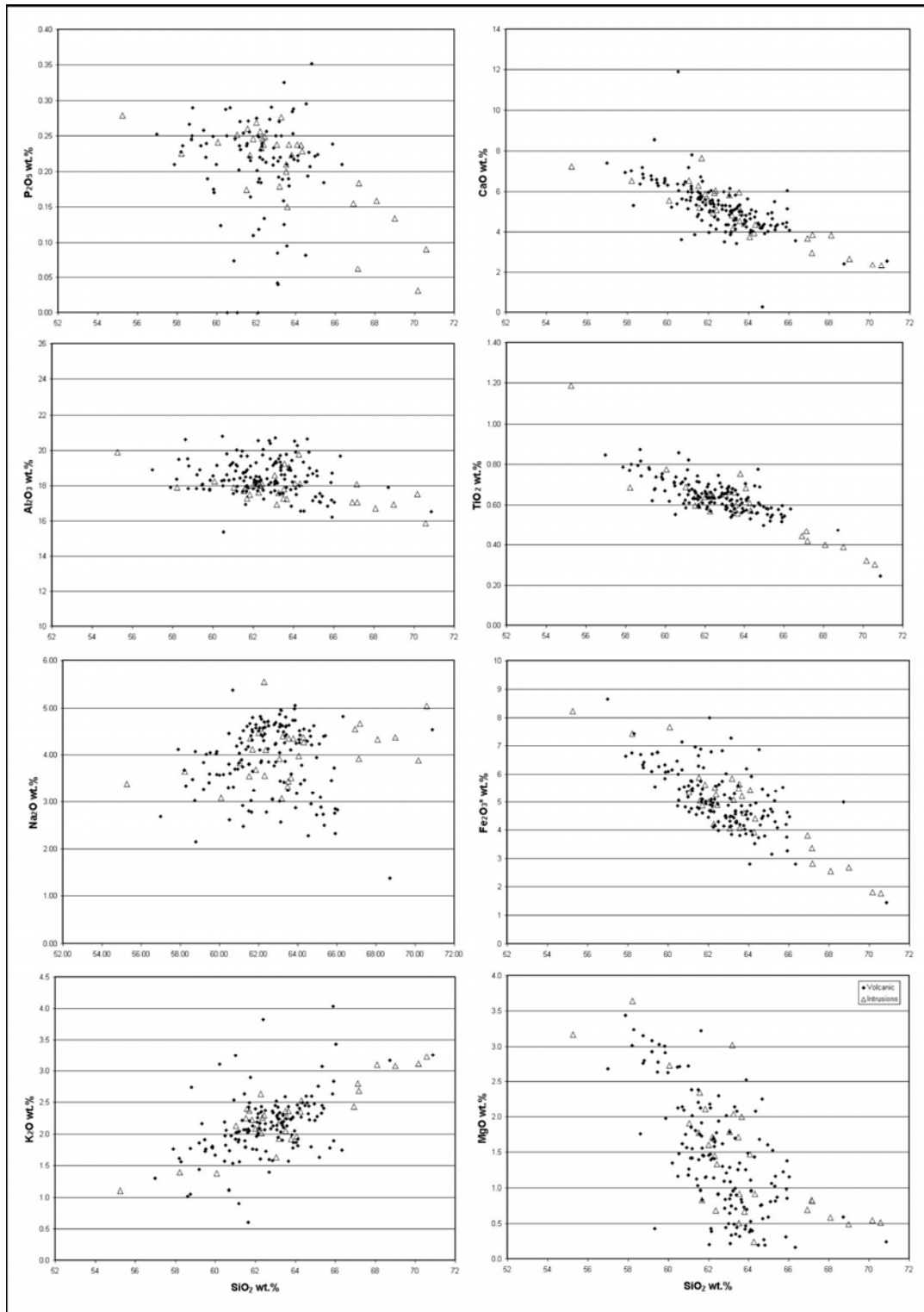
Figure 4.52 Major element oxide variation diagrams versus SiO$_2$ for the Yanacocha rocks. All volcanic rocks are compared to all intrusive rocks. Volcanic rocks form the bulk of the compositions between 58 and 66 wt% SiO$_2$ also represented by intrusions. The lower and upper SiO$_2$ compositional margins of the rock suite are represented by intrusions and minor volcanic rocks.
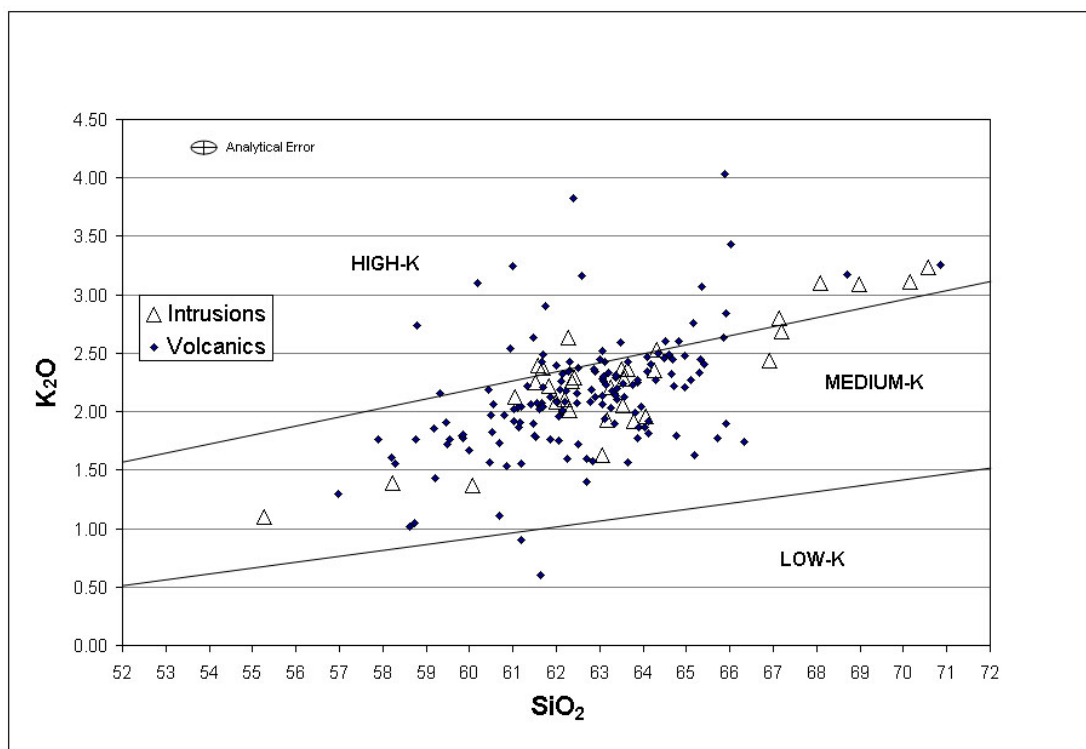
Figure 4.53 SiO$_2$ versus K$_2$O variation diagram that compares intrusions versus volcanics for all Yanacocha rocks in this study. The K$_2$O classification boundaries are from Ewart (1982).

MgO contents in the Yanacocha rocks display two semi-parallel trends (Figure 4.52) and a compositional gap in rocks of the Yanacocha Volcanic Field (YVF) from 63 to 66 wt.% SiO$_2$. The gap is filled by the pre-Yanacocha lower andesite lahar sequence (LAL) and the Cerro Frailes dacite tuffs (CFD). MgO vs. SiO$_2$ contents of the YVF rock sequences Upper Yanacocha volcanic sequence (Upha), the Maqui Maqui ignimbrite (MMI), and the San Jose ignimbrite (SJI) belong to a separate and steeper linear trend with strongly decreasing MgO to <0.5 wt.% and between 60 and 65 wt.% SiO$_2$. A compositional gap is present and MgO content increases at ~65.4 wt.% SiO$_2$ approaching ~1.0 wt.% MgO in the late dacite and then continues in a linear fashion to lower MgO concordant with the pre-Yanacocha trend.

YVF rocks and pre-Yanacocha rocks are plotted together on an MgO-SiO$_2$ variation diagram and a total alkali-SiO$_2$ (TAS) diagram (Figures 4.54 and 4.55). Total alkali contents increase with increasing SiO$_2$ between 55 to 71 wt.% SiO$_2$ and represent compositional variations from basaltic andesite to rhyolite on the TAS diagram (Figure

4.54). Major element oxides in YVF intrusions follow similar trends as observed in the YVF volcanic rocks (Figure 4.56). The MgO vs. SiO$_2$ diagram (Figure 4.54) displays two diverging clusters of data that includes the following: (1) pre-Yanacocha volcanic rocks lower andesite lahars (LAL) and Cerro Frailes dacite tuffs (CFD) with lower total alkali contents well within the andesite and dacite fields, and (2) the YVF rocks with an overall higher total alkali content into the trachyandesite and trachydacite fields and similar ranges in SiO$_2$ to the pre-Yanacocha rocks. In both diagrams, the YVF rocks Maqui Maqui ignimbrite (MMI), Upper Yanacocha volcanic sequence (Upha), and San Jose ignimbrite (SJI) cluster between Upper (late) Dacite and Lower Yanacocha volcanic sequence (Lpha). Compositions range from 60 to 66 wt.% SiO$_2$ and cluster around the upper andesite-dacite compositional boundary into more alkaline rocks at 63 wt.% SiO$_2$ and total alkali content of ~ 6.0 wt.% (Na+K). Compositional gaps are present with the SiO$_2$ and MgO contents of the main YVF cluster and the Upper Dacite that implies the dacite is not part of the YVF fractionation trend defined by rocks from the Lower Yanacocha volcanic sequence (Lpha) to the San Jose ignimbrite (SJI). The YVF clustering and the compositional gaps imply complexities in the evolution of the Yanacocha magmas that may include mixing of the two end-member magma compositions, a deep mafic component with pre-existing andesite and dacite, combined with assimilation and fractional crystallization (AFC).

SiO$_2$, MgO, and total alkali contents vary throughout the stratigraphic package and range as follows (Figures 4.54, 4.55, 4.56, and 4.57; Table 4.2):

(1) Lower andesite lahar sequence (LAL) rocks range 57-64.5 wt.% SiO$_2$, 1.3-3.2 wt% MgO, and 3.4-6.5 wt.% Na$_2$O+K$_2$O.

(2) Cerro Frailes dacite pyroclastic sequence (CFD) rocks range 60.6 to 68.7 wt% SiO$_2$, 0.28 to 2.25 wt.% MgO, and 4.0-6.8 wt.% Na$_2$O+K$_2$O.

(3) Lower Yanacocha andesite volcanic sequence (Lpha) rocks range ~58-62 wt.% SiO$_2$, 1.14 to 3.33 wt.% MgO, and 4.55-6.80 wt% Na$_2$O+K$_2$O.

(4) Maqui Maqui pyroclastic sequence (MMI) rocks range 60.2 to 66.3 wt.% SiO$_2$, 0.81 to 2.12 wt.% MgO, and 5.7-7.1 wt.% Na$_2$O+K$_2$O.

(5) Upper Yanacocha andesite to dacite volcanic sequence (Upha) rocks range 61.1 to 64.8 wt.% SiO$_2$, 0.3 to 2.20 wt.% MgO, and 5.9-7.2 wt.% Na$_2$O+K$_2$O.
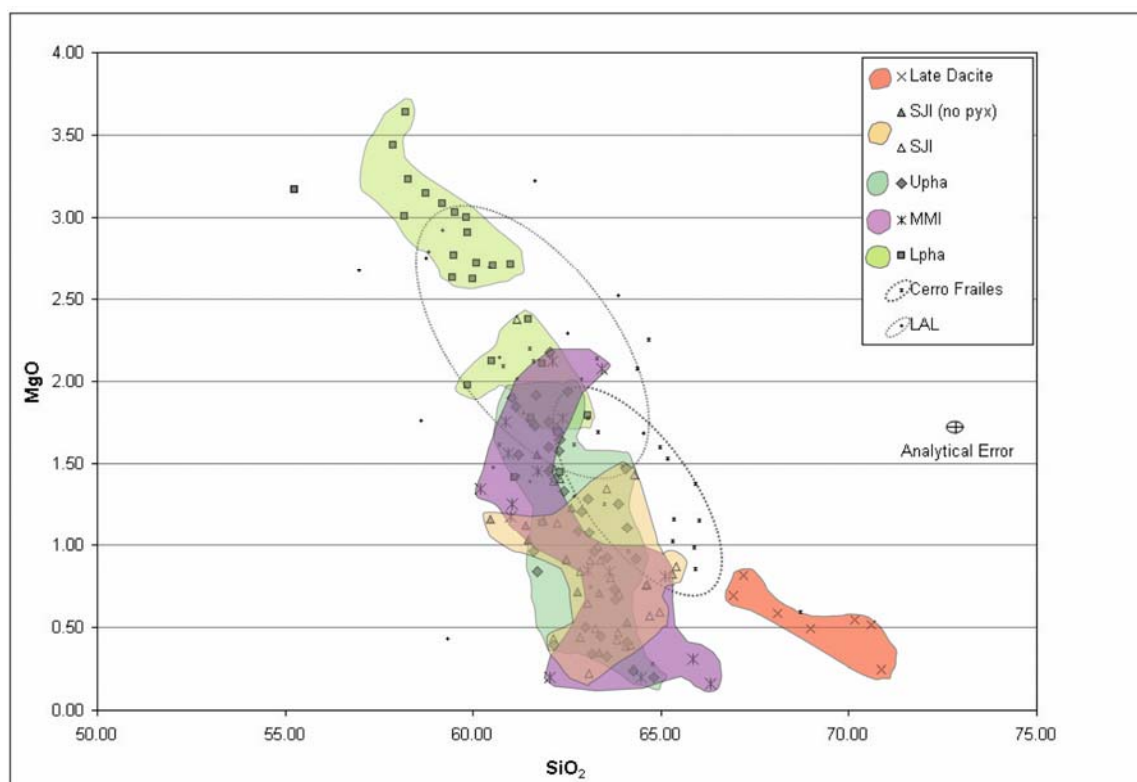
Figure 4.54. MgO versus SiO$_2$ variation diagram showing the variation of MgO and SiO$_2$ through the stratigraphic sequence in the Yanacocha district.
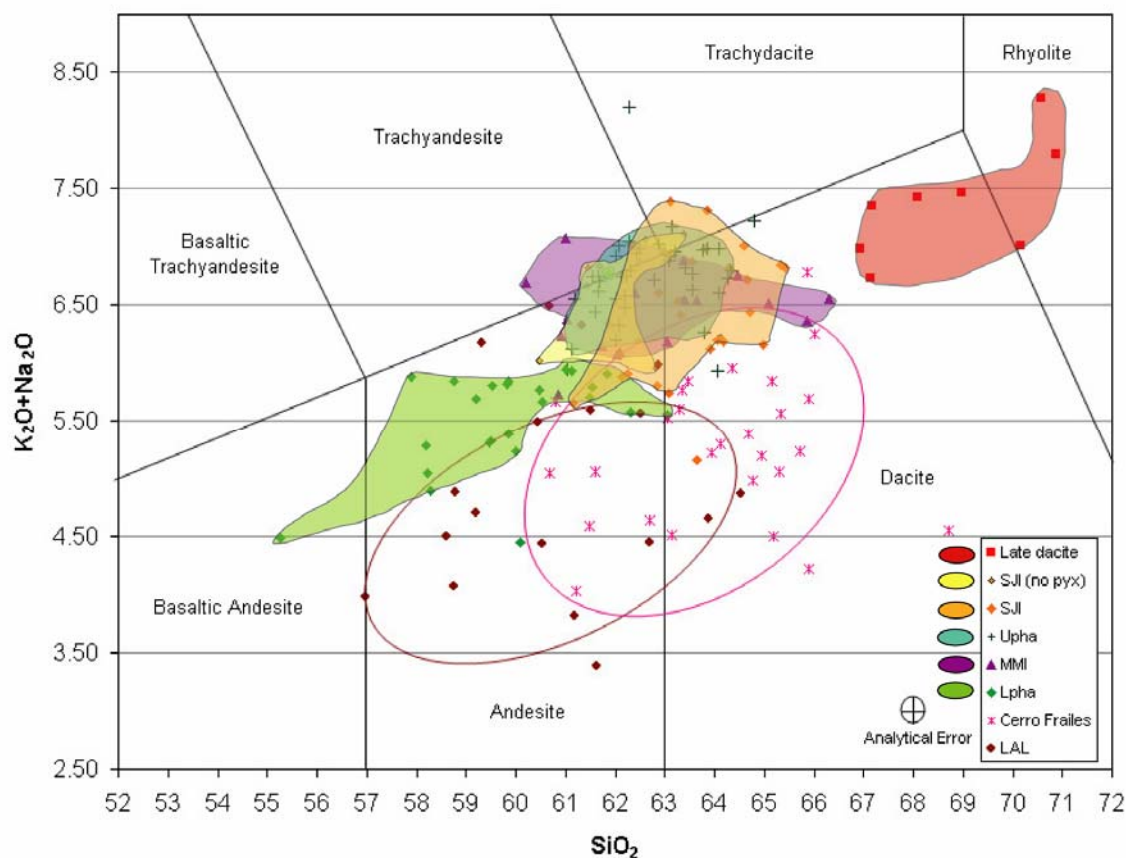
Figure 4.55 Total Alkali Silica (TAS) diagram for all Yanacocha rocks in this study. The TAS diagram is after Le Bas et al. (1986) and Best (2003, p. 32) showing the composition variation in the Yanacocha rock suite through time. Rock sequences are in stratigraphic order with LAL oldest and late dacite youngest.
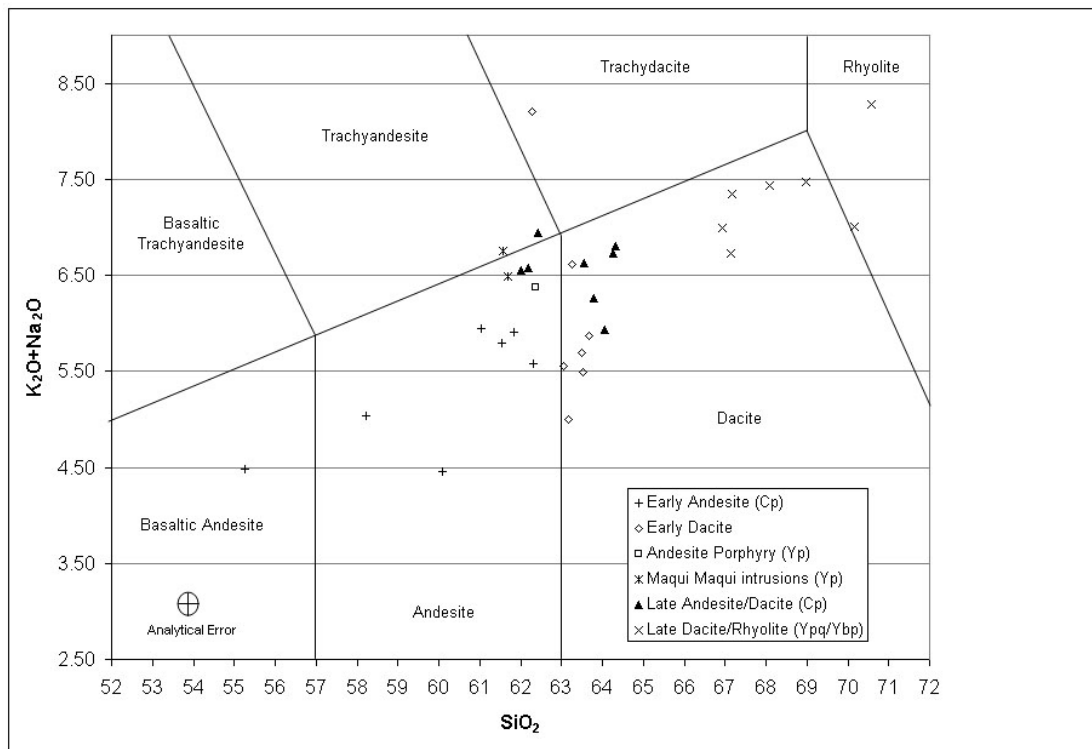
Figure 4.56 Total alkali (K_2O+Na_2O) and SiO_2 variation diagram showing the composition variation in the Yanacocha intrusive rocks through time. The TAS diagram and compositional fields are after Le Bas et al. (1986) and Best (2003, p. 32). Intrusions are in stratigraphic order from top to bottom, and the early andesite is oldest and late dacite/rhyolite is youngest.
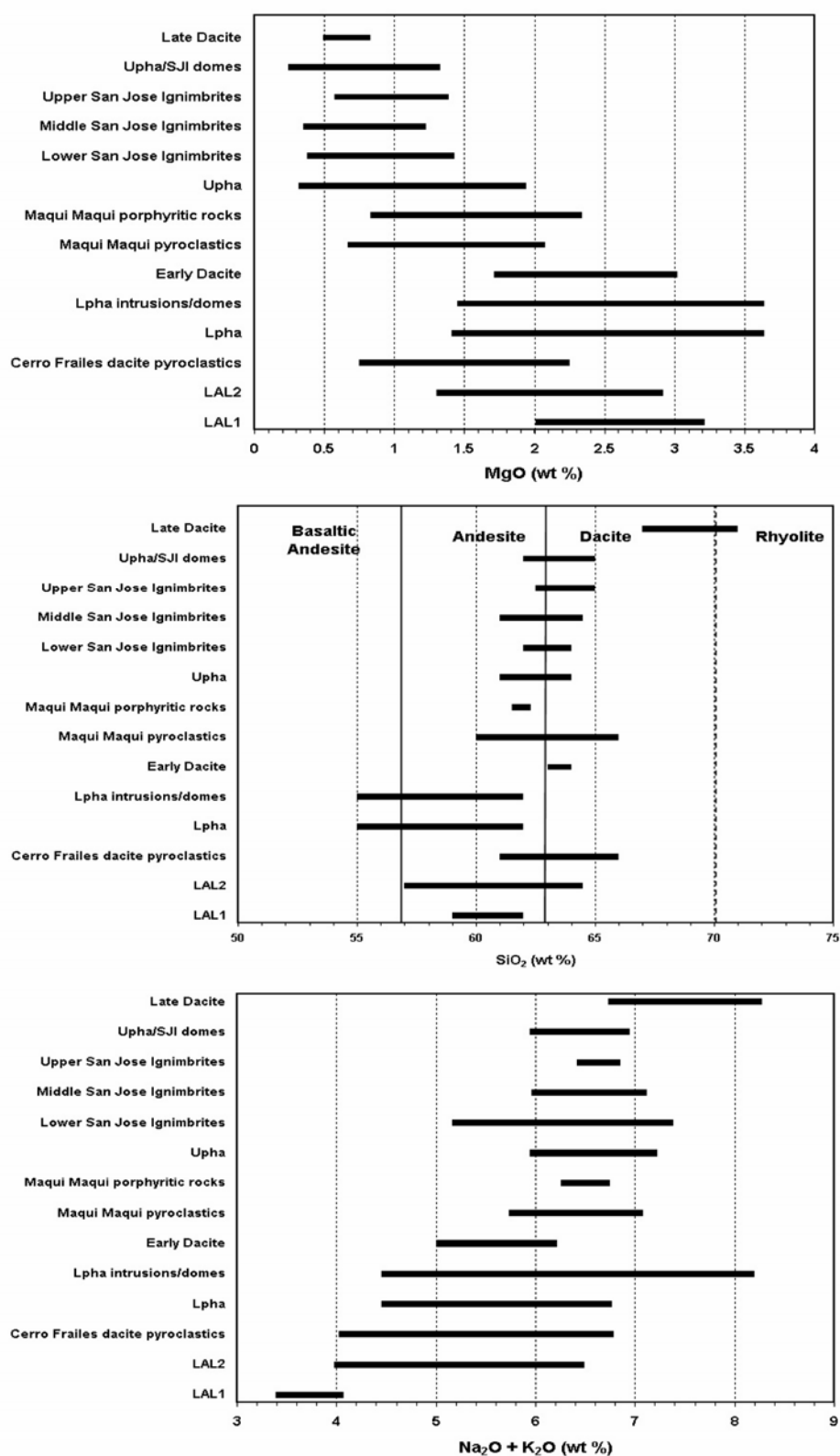
Figure 4.57 Charts that display the range of selected major element oxide data discussed in text and presented in Table 4.2. Age decreases upward in the plots.
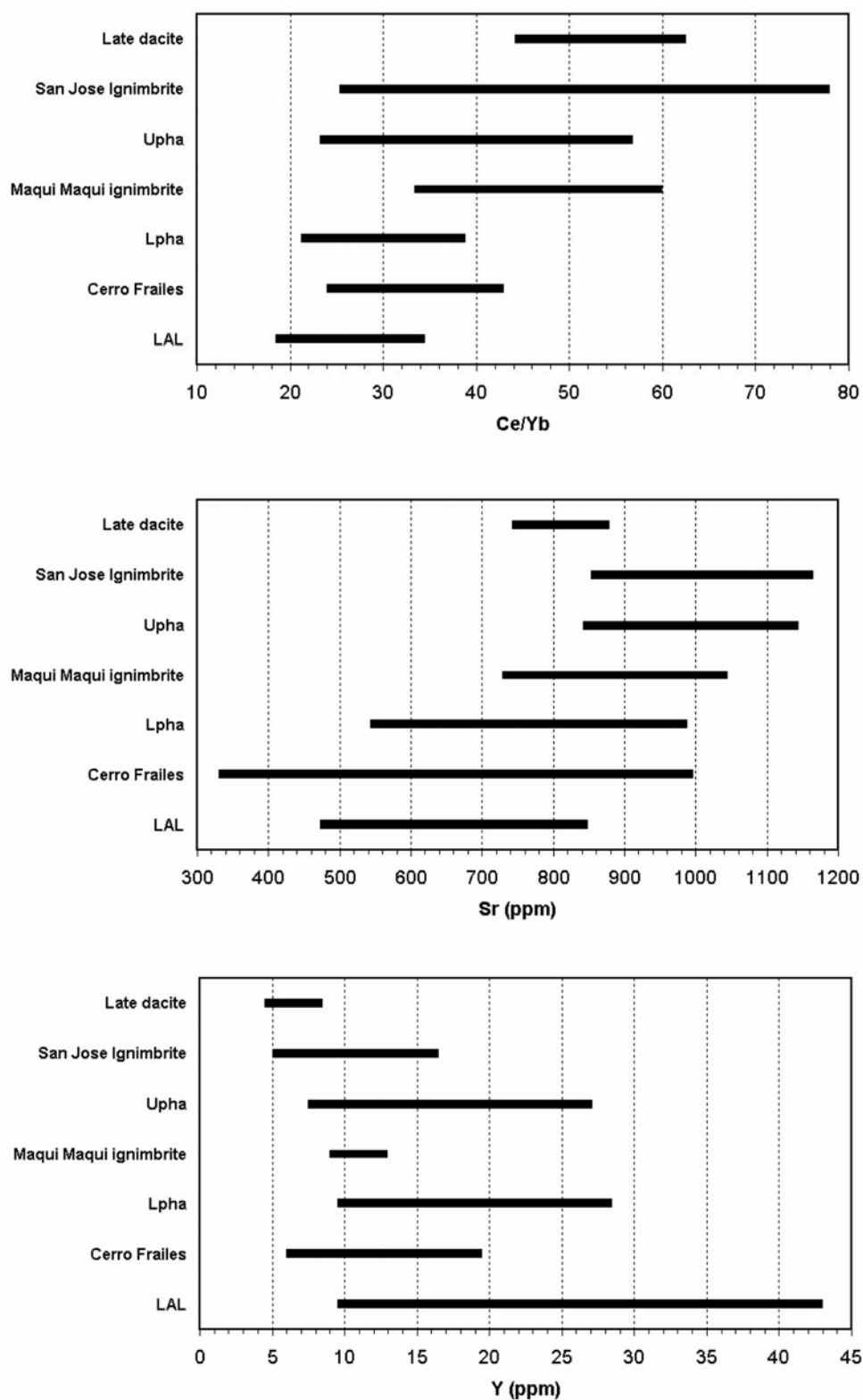
Figure 4.58 Charts that display the range of selected trace element data discussed in text and presented in Table 4.2. Age decreases upward in the plots.

(6) San Jose ignimbrite sequence (SJI) rocks range 61.0-65.4 wt.% SiO_2 and 0.22 to
     1.55 wt% MgO, and 5.2-7.4 wt.% Na_2O+K_2O.

(7) Upper (late) Dacite (Ud) rocks range 66.9 to 70.9 wt.% SiO_2, 0.49 to 0.83 wt.% MgO,
     and 7.35-7.6 wt.% Na_2O+K_2O.

Ranges of these selected major element oxides characterize the rock sequences and support the differences as outlined by the phenocryst mineralogy and field geology.

Trace Element Compositions

Ranges of selected trace elements Sr, Y, and the Ce/Yb ratio in the rocks sequences are presented in Figure 4.58. Trace element compositions versus SiO_2 are presented in variation diagrams with the selected elements Ba, Rb, Sr, and Y (Figure 4.59), Sr and Y versus CaO (Figure 4.60), and trace element ratios of Ce/Yb and Sr/Y are compared to Rb and Y (Figures 4.61 to 4.64). Chondrite-normalized REE diagrams (Figures 4.65, 4.66, and 4.67) are presented for each rock sequence. Trace elements are plotted versus SiO_2 because it is the most abundant major element oxide, and its variability defines the compositional variation within the entire Yanacocha suite. Sr and Y are plotted versus CaO because Ca is also abundant in the Yanacocha rocks. CaO plots add another perspective to the complex evolution of the Yanacocha magmas and support differentiation by plagioclase fractionation. CaO versus SiO_2 displayed excellent analytical reproducibility in the standards (two standards with 30 analyses each scattered throughout the geochemical data set in this study, CD Appendix V). Statistical parameters for SiO_2 and CaO in the standards are well within acceptable limits with very low 2σ <0.10 and mean standard weighted deviate (MSWD) values <2.0. SiO_2 returned 2σ values of ±0.12 and ±0.13 wt.% with MSWD values of 0.94 and 1.11, and CaO gave a 2σ of ±0.05 and ±0.07 wt.% and MSWD values of 0.8 and 0.96.

Ba and Rb increase and Y decreases with increasing SiO_2 contents. The SiO_2 variation diagrams display compositional gaps between the late dacite and the other YVF rock sequences. Sr is variable and increases with SiO_2 content in the pyroxene-bearing rocks from the Lower Yanacocha andesites (Lpha) to Upper Yanacocha andesites (Upha) and the San Jose ignimbrite (SJI) (Figure 4.59), but patterns in the Maqui Maqui
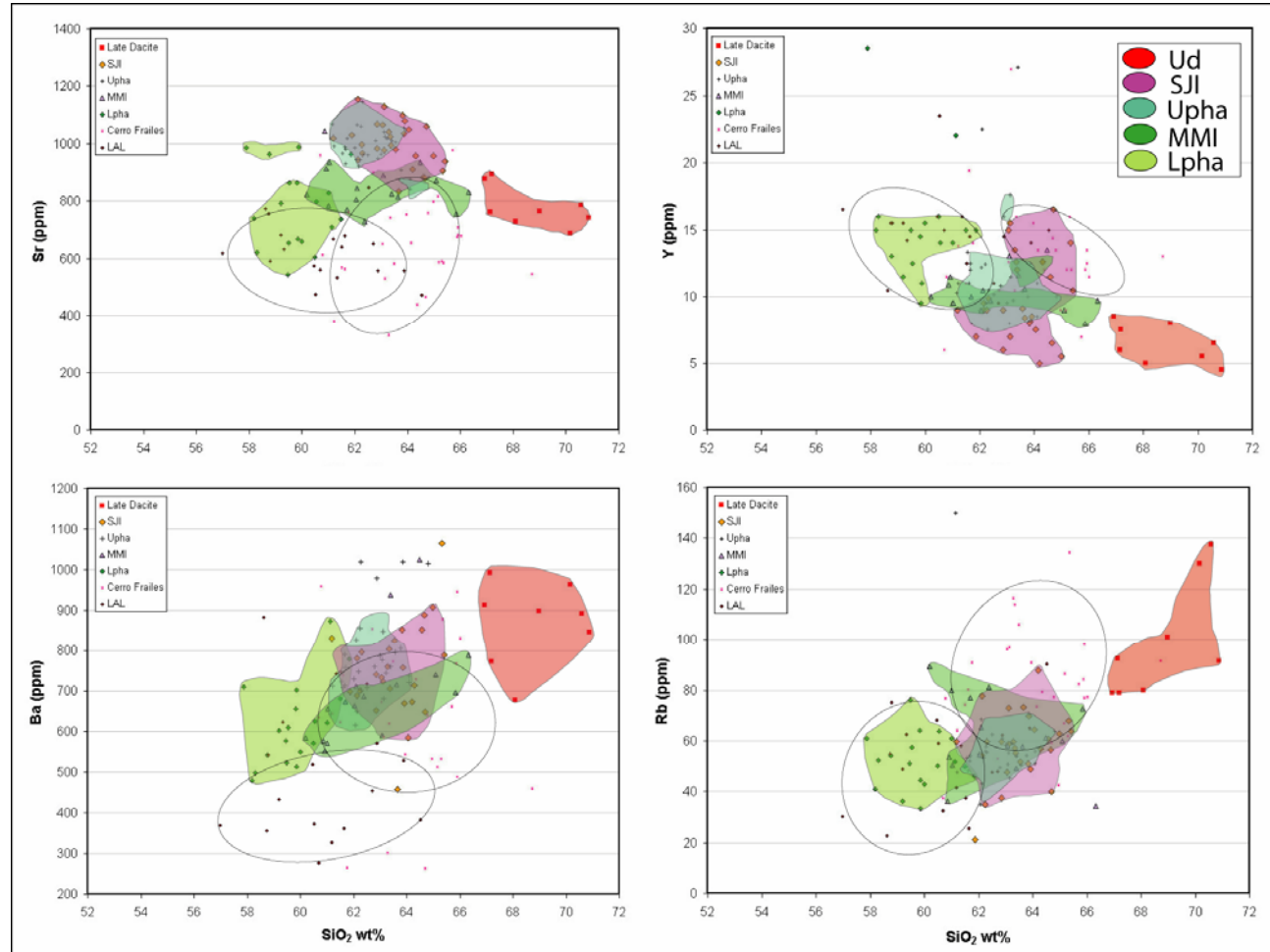
Figure 4.59 Variation diagrams of selected trace elements (Ba, Rb, Sr, and Y) with SiO_2 content through time in the Yanacocha volcanic rocks. Pre-Yanacocha rocks LAL and Cerro Frailes are designated by smaller symbols outlined in black ellipses. Rocks of theYanacocha are shaded was follows: Lower Yanacocha Andesite sequence (Lpha) is light green, the Maqui Maqui pyroclastic sequence (MMI) is purple, the upper Yanacocha Andesite Sequence (Upha) is blue green, the San Jose ignimbrite (SJI) is orange, and the late dacite sequence is red.
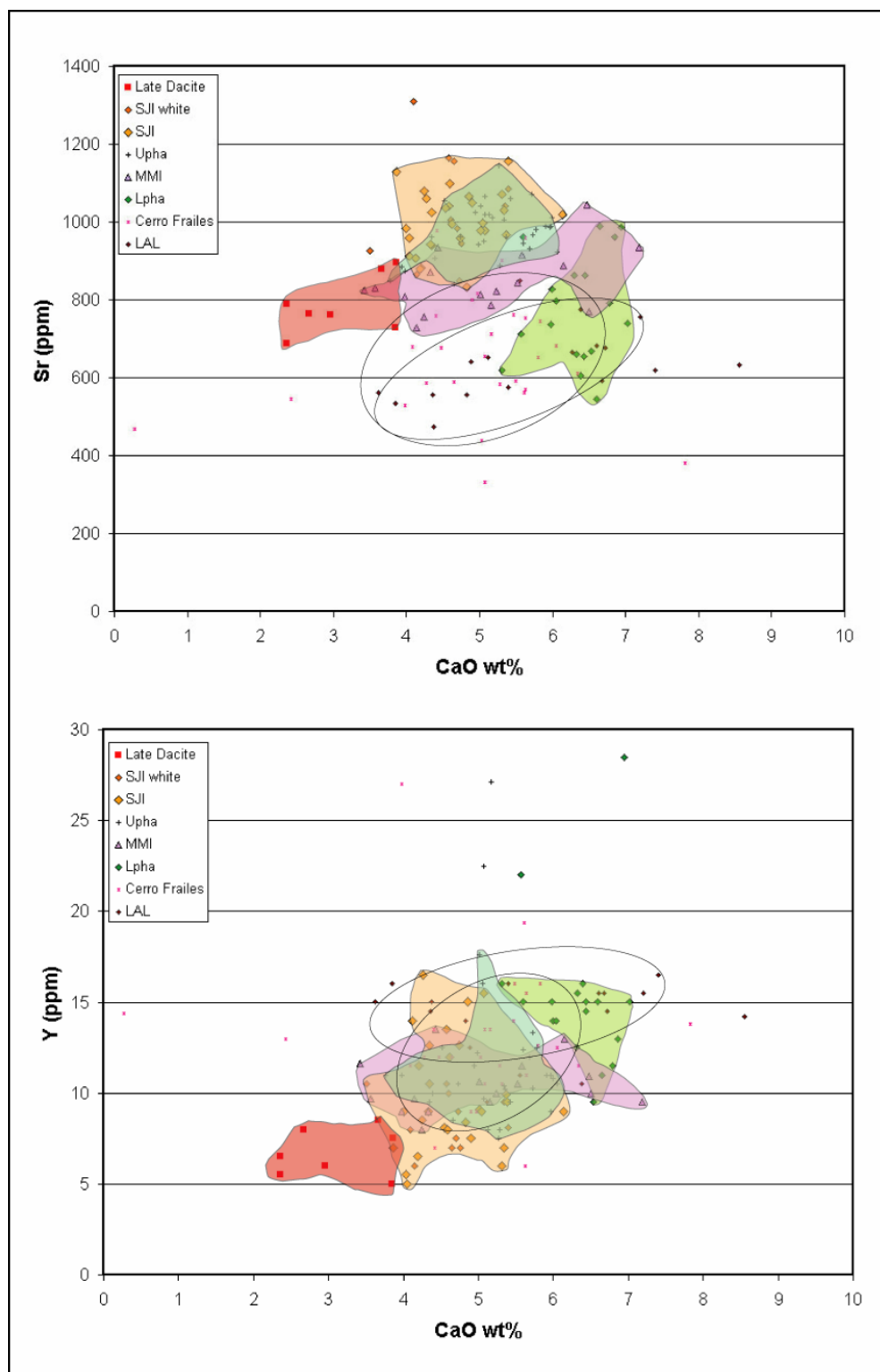
Figure 4.60 Variation diagram of Sr and Y versus CaO. The diagram displays a lack of compositional gaps suggesting differentiation was homogeneous. Compositional gaps are present within the Yanacocha rocks in the SiO2 variation diagrams.

pyroclastic sequence (MMI) and the Upper (late) Dacite are relatively flat and suggest a separate fractionation curve for rocks that lack pyroxene.

Sr and Y decrease with increasing CaO (Figure 4.60) suggesting a decrease with increasing differentiation, and no compositional gaps between any of the Yanacocha rock sequences. Two patterns are presented in the Sr-CaO variation diagram that include: (1) Sr increases with decreasing CaO in the pyroxene-bearing andesite to dacite rock sequences Lpha-Upha-SJI, and (2) Sr decreases with decreasing CaO in rocks that lack pyroxene from the Maqui Maqui sequence (MMI) to the Upper (late) Dacite. Therefore, Sr increases with each successive volcanic sequence from the Lower Yanacocha andesites (Lpha) to the San Jose ignimbrites (SJI) as CaO decreases, Sr decreases in the last magmatic episode represented by the Upper (late) Dacite.

Trace element ranges in Figure 4.58 and Table 4.2 display an overall increase in Sr content with each successive rock package at Yanacocha, and a decrease in Sr in the Upper (late) Dacite. This may be explained by plagioclase fractionation in the YVF magmas and the subsequent abundance of plagioclase in the YVF rocks. Ce/Yb ratio ranges also increase upward throughout the Yanacocha stratigraphy, whereas Y shows an overall decrease.

Ce/Yb ratios display a wide range of variability in the Yanacocha suite when plotted with Rb in Figure 4.61. Intrusions and volcanic rocks have similar compositional variations with Ce/Yb ratios that range from 20 to 60 and Rb contents from 30 to 90 ppm for the main cluster of samples. This variability suggests some uncertainty in the large ion lithiphile (LIL) element, the light rare earth element (LREE) and the heavy rare earth element (HREE) fractionation patterns in the Yanacocha rocks. The same Ce/Yb versus Rb diagram (Figure 4.62), referenced with the specific rock sequences, indicates that the pre-Yanacocha lower andesite lahar sequence (LAL) and the Cerro Frailes dacite tuff (CFD), and the Lower Yanacocha volcanic sequence (Lpha) have Ce/Yb ratios <40, whereas, most rocks of the YVF have Ce/Yb ratios >40 and range from 30 to 80. The degree of fractionation increased in the YVF rocks after the eruption of the Lower Yanacocha pyroxene andesites (Lpha) implying strong HREE fractionation during differentiation of the YVF suite.

Plots of the trace element ratios Sr/Y and Ce/Yb show consistency and variability within the Yanacocha volcanic sequences. Data on the Ce/Yb versus Sr/Y plot increase in a linear fashion with each successive volcanic sequence from the lower andesite lahar sequence (LAL) to the San Jose ignimbrites (SJI) implying increased HREE fractionation (Figure 4.63) through time. Pre-Yanacocha rocks have ratios of Ce/Yb<40 and Sr/Y<60 and overlap with the Lower Yanacocha volcanic sequence (Lpha), but display a compositional gap below the main group of YVF rocks. The San Jose ignimbrites (SJI) show a wide range of results in ratios Sr/Y from 63-182.4 and Ce/Yb from 30-78.9. Rocks from the Upper Yanacocha volcanic sequence (Upha) are tightly clustered with few outliers and results range in Sr/Y from ~60-112 and in Ce/Yb from ~ 35-56 (Table 4.2).

Plots of Sr/Y ratios versus Y (Figure 4.64) display tight clusters for all Yanacocha volcanic sequences and a pattern that is nearly flat in rocks with low Sr/Y ratios. The trends gradient dramatically increases as Y decreases and Sr/Y increases. Pre-Yanacocha rocks fill a compositional gap in the Lower Yanacocha volcanic sequence (Lpha) and develop a low sloping pattern of decreasing Sr/Y with increasing Y typical of "normal" calc-alkaline melts that evolved through plagioclase fractionation (Defant and Drummond, 1990; Feeley and Hacker, 1995). The remaining YVF rocks form the steep portion of the trend clustered together in linear fashion without compositional gaps; a pattern that resembles an adakite-like signature described by Defant and Drummond (1990). Sr and Y contents are similar for the two youngest rock sequences and the patterns of the San Jose ignimbrites (SJI) and Upper (late) Dacite overlap in the adakite-like field.
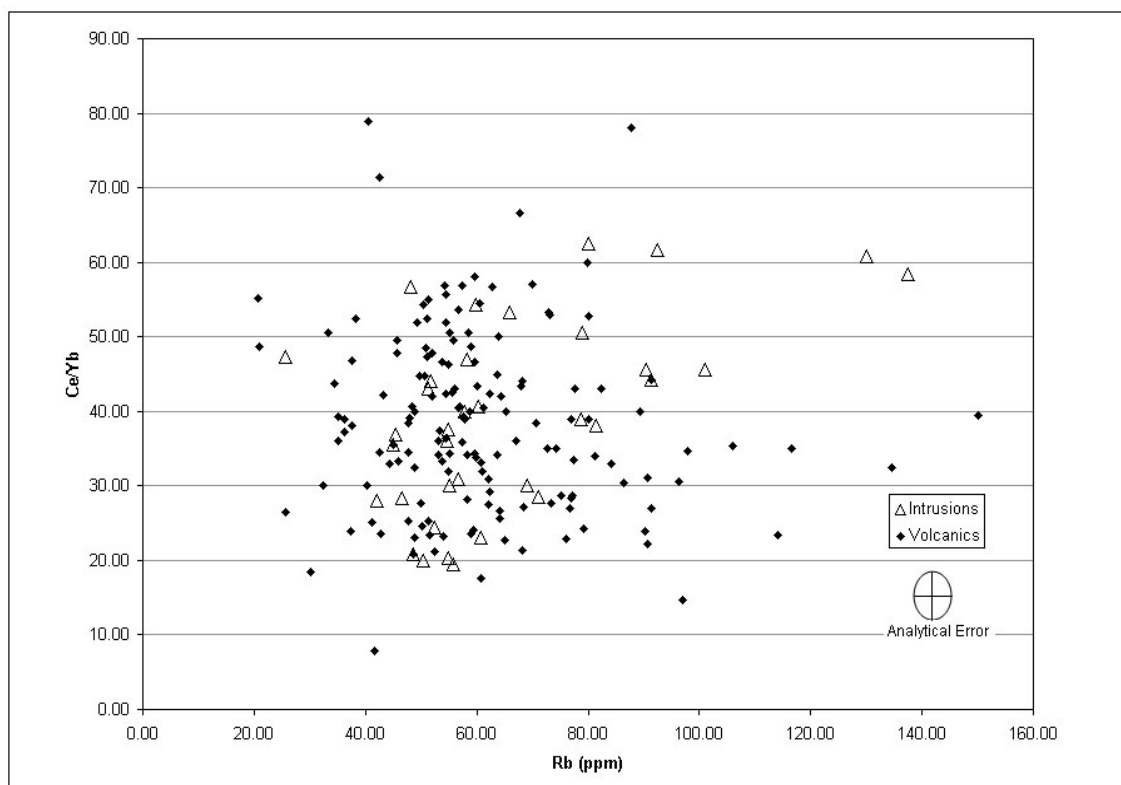
Figure 4.61 Trace element Pearce variation diagram for Ce/Yb versus Rb (ppm) comparing the range of Yanacocha intrusions to Yanacocha volcanic rocks.
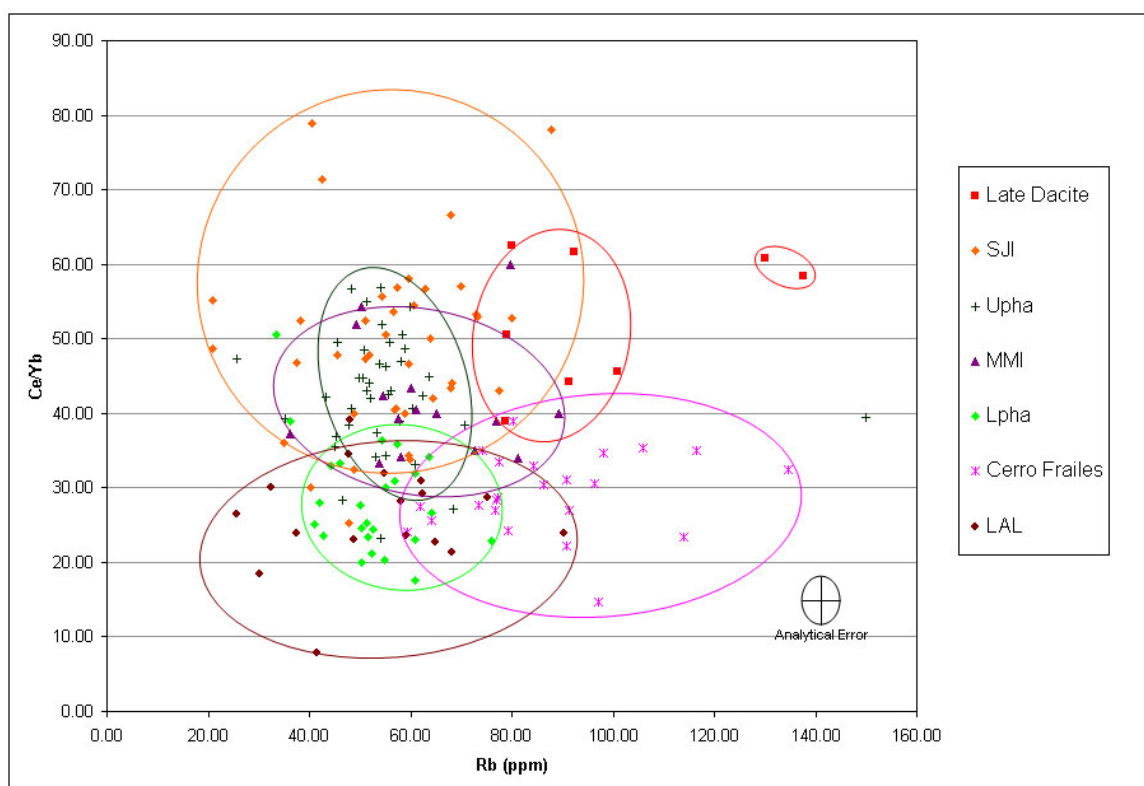
Figure 4.62 Pearce element variation diagram for Ce/Yb versus Rb (ppm) through time at Yanacocha. The symbol key is organized in stratigraphic order with LAL rocks oldest and late dacite youngest.
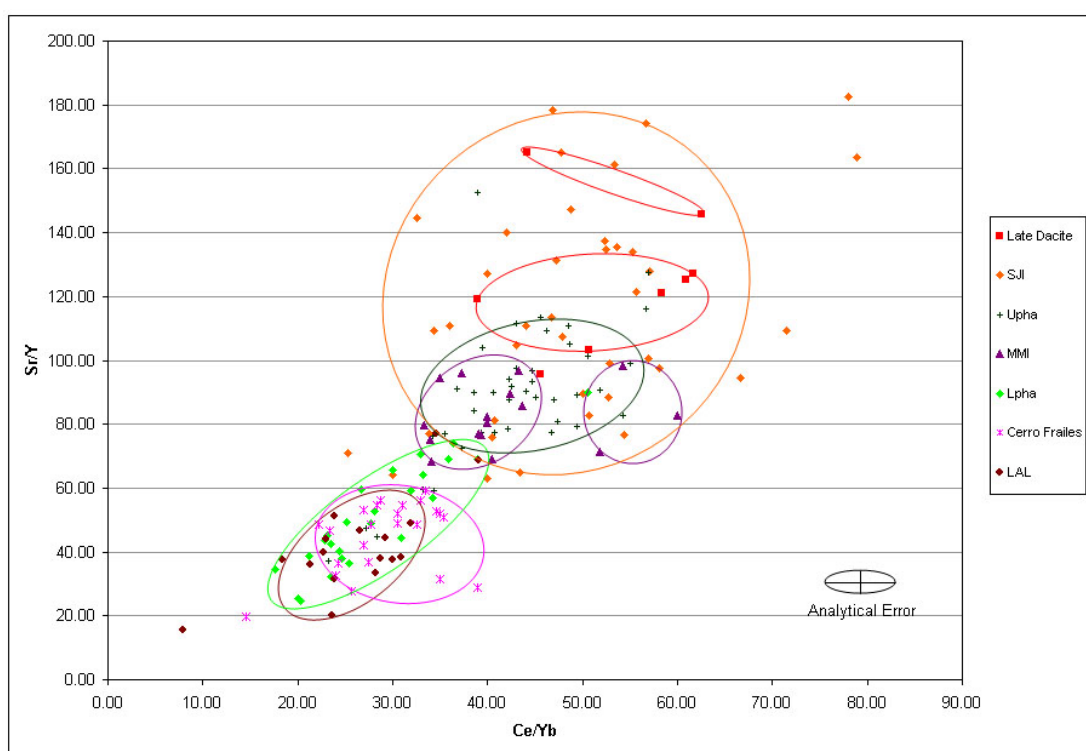
Figure 4.63 Trace element Pearce variation diagram for ratios Sr/Y and Ce/Yb through time at Yanacocha. Pre-Yanacocha rocks are distinct and have Sr/Y ratios < 60 and Ce/Yb ratios < 40, and only the Lpha andesite field overlaps. The symbol key is organized in stratigraphic order with LAL rocks oldest and late dacite youngest
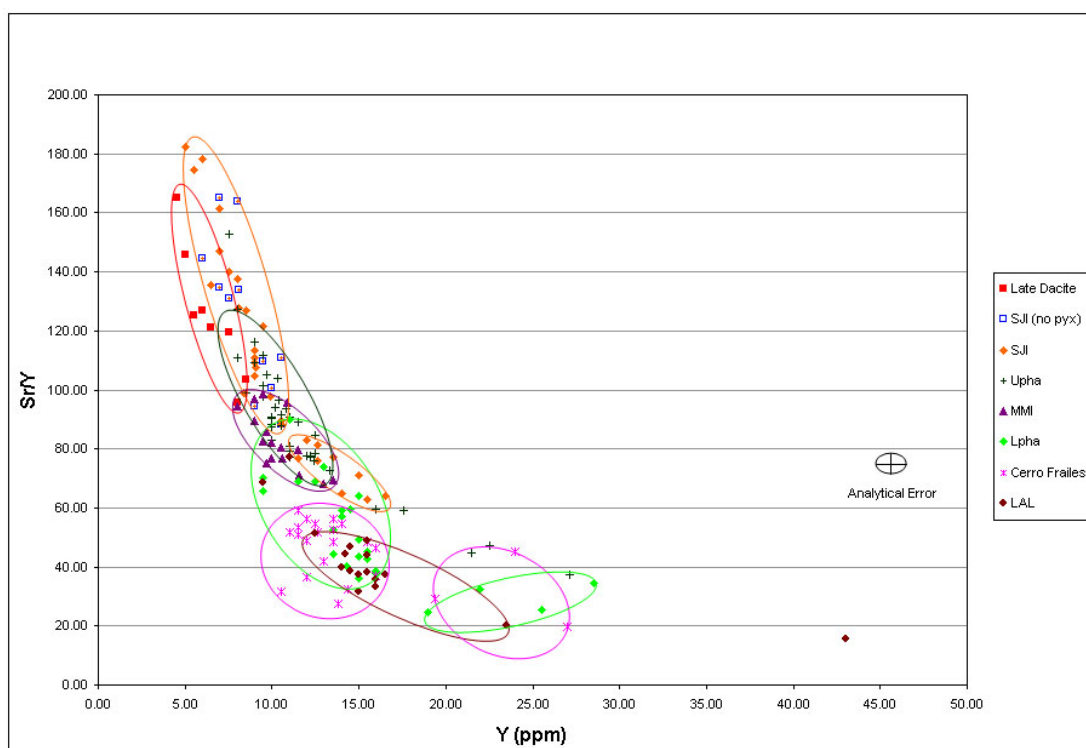
Figure 4.64 Trace element Pearce variation diagram for Sr/Y versus Y through time at Yanacocha. The symbol key is organized in stratigraphic order with LAL rocks oldest and late dacite youngest. An adakite-like signature is displayed in the later volcanic and intrusive rock sequences that are actually a result of fractional crystallization.
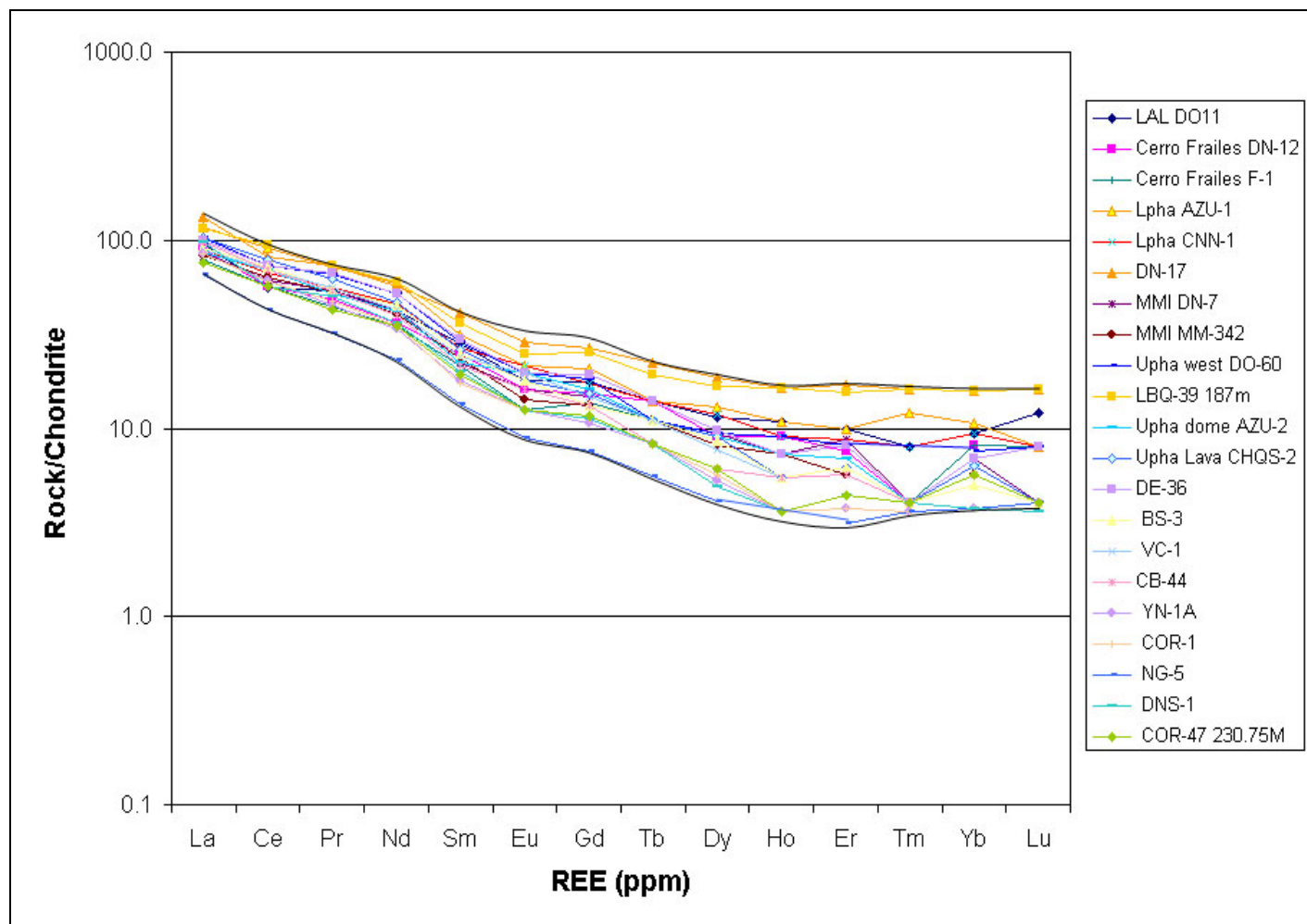
Figure 4.65 REE patterns normalized to chondrite (Sun and McDonough, 1989) for selected samples throughout the volcanic stratigraphy at Yanacocha. These samples define the field for all Yanacocha rocks outlined in black. They are listed in the key oldest to youngest from LAL (1 sample), Cerro Frailes (2 samples), Lpha (3 samples), MMI (2 samples), Upha (4 samples), SJI (4 samples), and late dacite (5 samples).
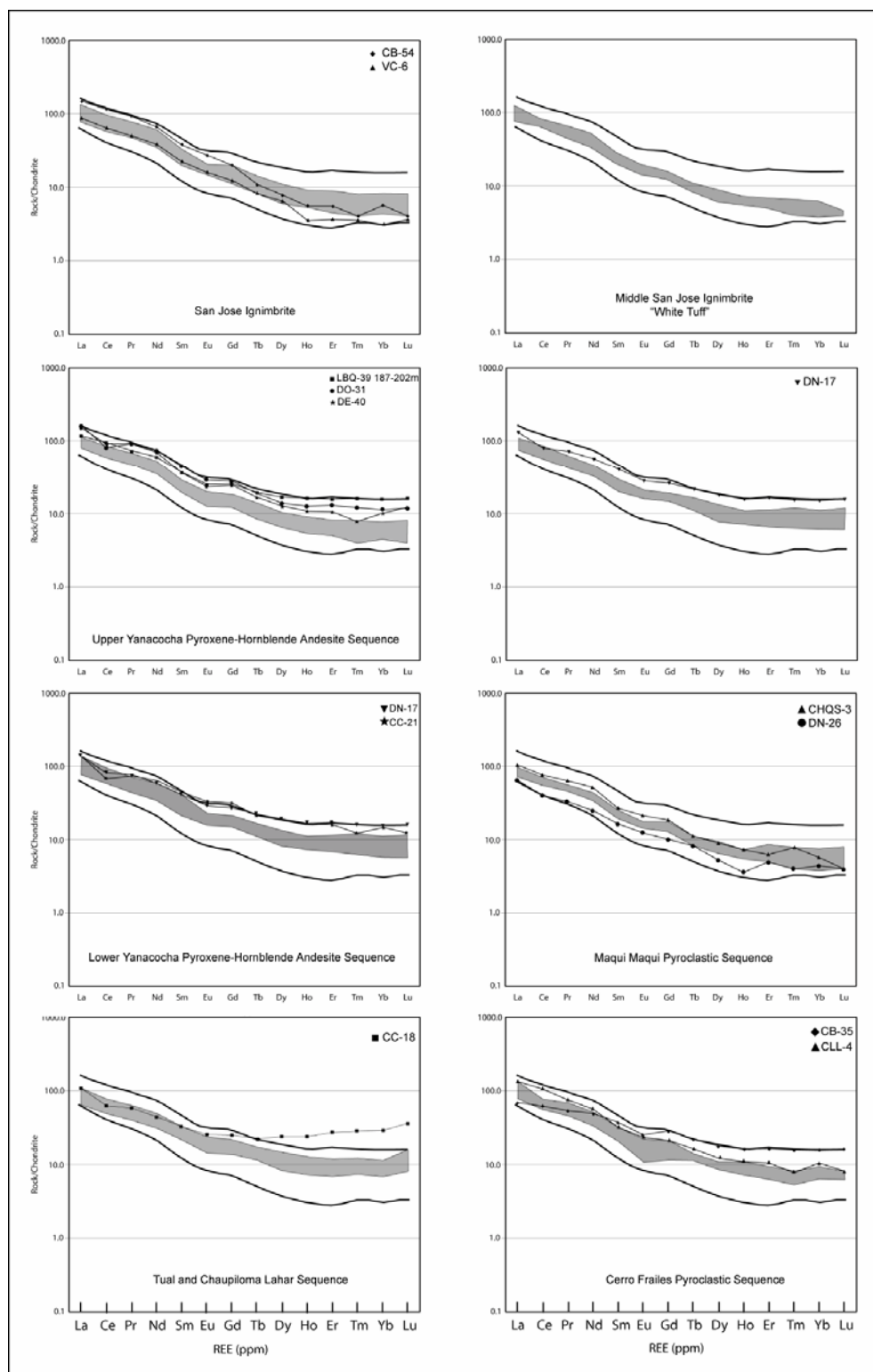
Figure 4.66 REE patterns normalized to chondrite (Sun and McDonough, 1989) for the volcanic rocks at Yanacocha. Oldest rocks are in the bottom left and young upward left to right. The solid black lines outline the entire field for Yanacocha rocks, the grey field represents the individual volcanic sequence, and the single line plots are separate samples in the sequence that deviate from the "ideal" compositions.

Rare earth element (REE) data for selected samples representative of the volcanic sequences at Yanacocha are plotted on a chondrite-normalized diagram and define the range for the Yanacocha sample suite (Figure 4.65). The lower boundary is defined by the 8.4 Ma Negritos rhyolite ignimbrite (NG-5), and the upper boundary by Lower Yanacocha pyroxene-hornblende andesite lava flows (Lpha). Overall REE patterns are somewhat flat with no prominent anomalies that become steeper with each successive rock sequence from the Lower Yanacocha volcanic sequence (Lpha) to Upper (late) Dacite. REE patterns are displayed separately and compared to one another for each volcanic sequence and andesite intrusions (Figures 4.65 and 4.66). These diagrams indicate that the style and degree of LREE/HREE fractionation are similar throughout the Yanacocha rocks. Volcanic rocks from the lower andesite lahar sequence (LAL) show the least dramatic LREE/HREE fractionation, and the San Jose ignimbrites (SJI) show the most fractionation. Volcanic rocks from the Upper Yanacocha pyroxene-hornblende andesite sequence (Upha) have a similar pattern of increased LREE/HREE fractionation to the San Jose ignimbrite (excluding the three outliers; Figure 4.66). Yanacocha andesite intrusions show similar patterns to the Lower Yanacocha pyroxene-hornblende andesite sequence (Lpha), whereas the Maqui Maqui ignimbrites display overall depletions in LREE and HREE relative to the other sequences (Figure 4.66).

Rare earth element (REE) patterns for Yanacocha intrusions are displayed in Figure 4.67. Overall patterns are flat and similar to the volcanic rocks. Subtle differences are found with the early dacite intrusions in the west district that show slight Ce depletions relative to La and a wide range of HREE results relative to the andesite intrusions. The late dacite and rhyodacite intrusions are depleted in both LREE and HREE relative to other YVF rocks especially compared to the Lower and Upper Yanacocha pyroxene-hornblende andesite and dacite volcanic rocks, and Yanacocha andesite intrusions. REE patterns from the Yp and Cp intrusions have strong depletions in the HREE similar to the Maqui Maqui ignimbrites and the Upper Yanacocha andesite-dacite volcanic rocks (Upha).

Degree of REE fractionation in the Yanacocha rocks of this study is displayed in figure 4.68 as chondrite-normalized LREE/HREE, LREE/MREE, and MREE/HREE ratios plotted as a function of Sr. Volcanic rocks are shown with intrusions and the slope
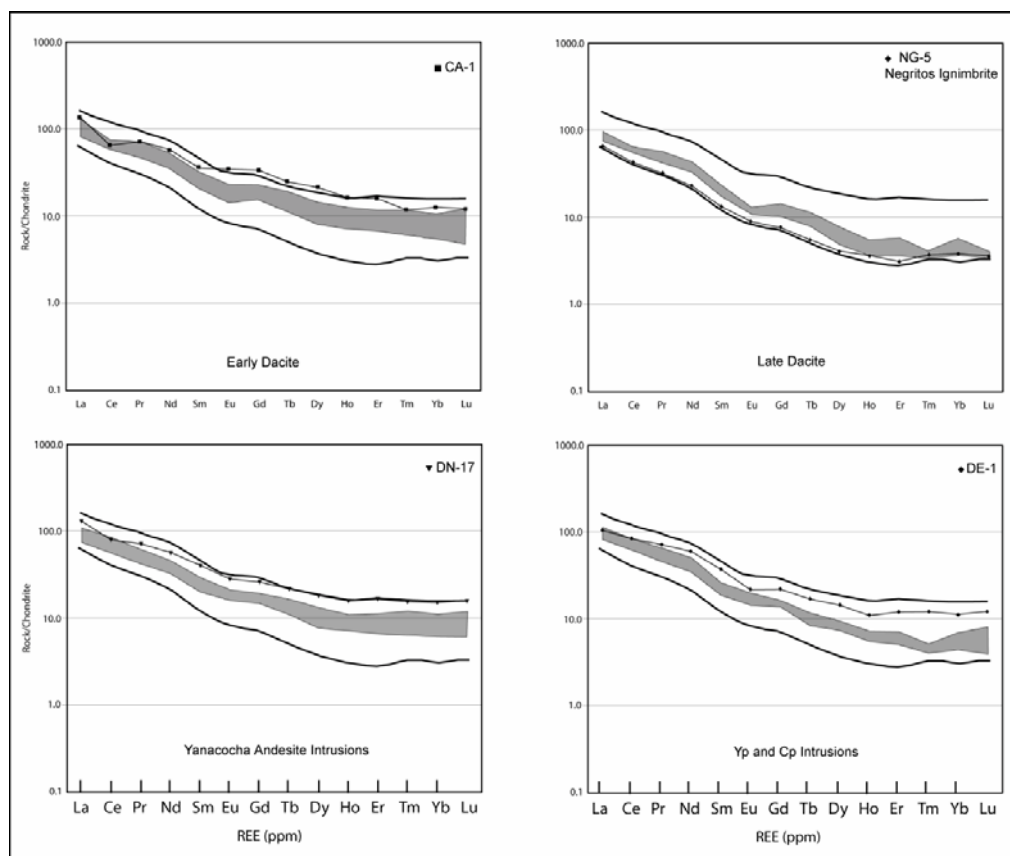
Figure 4.67 REE patterns normalized to chondrite (Sun and McDonough, 1989) for intrusive rocks in the Yanacocha Volcanic Field. The grey shaded fractionation fields represent the selected group of intrusive rocks compared to the general field (black lines) for all rocks at Yanacocha. Samples that fall outside the shaded grey fields for each select group are plotted separate.

of trend lines gives an indication for the degree of fractionation relative to Sr. These data show that the overall chondrite-normalized patterns are similar for all the volcanic sequences at Yanacocha. The data plotted in this fashion indicate stronger LREE/MREE fractionation relative to MREE/HREE fractionation.

The YVF rock sequences are displayed for comparison in each diagram and for each REE ratio. These data suggest that the Lower Yanacocha andesite sequence (Lpha), the Maqui Maqui ignimbrite (MMI), the Upper Yanacocha andesite-dacite sequence (Upha), and the San Jose ignimbrite sequence (SJI) belong to the same differentiation trend. Degrees of $(La/Sm)_N$ and $(Gd/Yb)_N$ fractionation (Figure 4.68b) increase throughout each successive rock sequence from the Lower Yanacocha sequence (Lpha) to the San Jose sequence (SJI). Stronger $(La/Sm)_N$ fractionation versus $(Gd/Yb)_N$
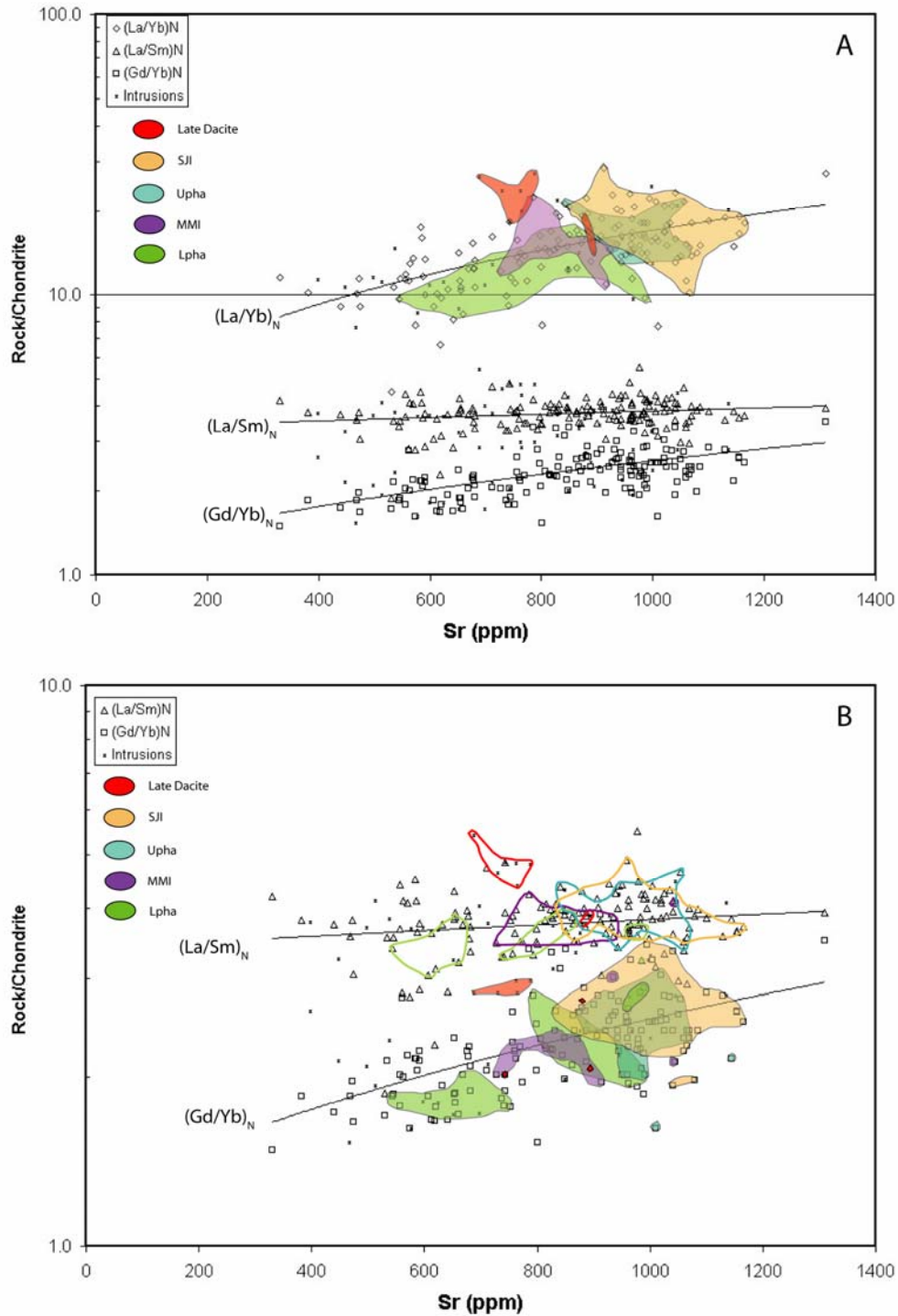
Figure 4.68 Degree of REE fractionation displayed as $(La/Yb)_N$, $(La/Sm)_N$, and $(Gd/Yb)_N$ versus Sr (ppm) for all volcanic rocks at Yanacocha. Ratios are normalized to the chondrite (Sun and McDonough, 1989), and ranges in volcanic rocks for each ratio are as follows: $(La/Yb)_N$ = 7.8 to 27.2, $(La/Sm)_N$ = 1.9 to 5.5, $(Gd/Yb)_N$ = 1.4 to 3.9. Ranges for intrusions include $(La/Yb)_N$ = 3.8 to 28.3, $(La/Sm)_N$ = 2.8 to 5.4, $(Gd/Yb)_N$ = 1.5 to 3.2. Refer to Table 4.2 to reference ranges for all YVF rock sequences.

fractionation is displayed by the Lower Yanacocha sequence (Lpha), and the gap in degree of fractionation merges to overlap in the San jose sequence (SJI) with similar values for $(La/Sm)_N$ and $(Gd/Yb)_N$ fractionation. This reflects increased $(Gd/Yb)_N$ relative to $(La/Sm)_N$ and steep fractionation trends in MREE/HREE for Upha and SJI.

Upper (late) Dacite plots off the main trend with increased REE fractionation relative to the other YVF rocks and may represent a distinct magma batch with different differentiation histories. The patterns for Upper (late) Dacite and the Maqui Maqui ignimbrite (MMI) plotted for $(La/Yb)_N$ display a trend that may indicate a separate differentiation path for these rocks as indicated in the Sr variation diagrams (Figures 4.59 and 4.60). The field for Maqui Maqui ignimbrite (MMI) becomes part of the YVF trend when plotted with the ratios $(La/Sm)_N$ and $(Gd/Yb)_N$ and a compositional gap develops between the YVF trend and the Upper (late) Dacite suggesting a different evolution for the dacite.

Discussion

Evolution and Temporal Variation of the Magma Compositions

Distinct composition and phenocryst mineralogy characterize each rock sequence. The compositional variations displayed in variation diagrams for the major element oxides, selected trace elements, and selected phenocryst chemistry reflect a complex evolution through a combination of processes that took place during magma emplacement and differentiation at relatively shallow crustal levels that can not be explained by crystal fractionation alone. These data support the hypothesis that continental arc magmas follow diverse pathways that include complex thermal-magmatic histories and interactions of multicomponent and multiprocess evolution (Rutherford and Devine, 2003; Dungan and Davidson, 2004). Combined processes of crystal-liquid fractionation, magma mixing, and muticomponent crustal assimilation are implied for the evolution of the Yanacocha rock suite. Separate magma batches below the Yanacocha Volcanic Field (YVF) mixed and differentiated in the crust over a span of 6 million years. Patterns can be recognized in the data that imply separate, and compositionally distinct, magmas coexisted, mixed and then differentiated separately. These compositions may have followed different differentiation trends and involved crustal assimilation and

mixing of a mafic end member such as basalt with andesite and dacite. Separate magma batches likely differentiated at different levels and sites in the crust, and locally mixed to produce periodically the magmas erupted observed rock sequences with characteristic and different mineral and chemical compositions. This proposed origin is supported on the basis of the $^{40}Ar/^{39}Ar$ age determinations and combined with the distinctive phase assemblages and chemical trends for each rock sequence.

Hypotheses from the Results

Evidence for Magma Mixing

Rocks at Yanacocha display textures that indicate a complex thermal and magmatic history. Resorbed amphiboles coexist with resorbed plagioclase and plagioclase that display "sieve-rimmed" textures defined as fine rims of melt inclusions surrounding resorbed An-rich cores mantled by clear unresorbed An-poor rims. Minerals with these textures are found in Lower and Upper Yanacocha andesite lavas and domes, and San Jose ignimbrites and related domes (Figures 4.5 to 4.7, 4.17 and 4.21). Reddish oxy-hornblendes in the Upper Yanacocha andesite lavas display resorption textures and narrow opacite rims of Fe-oxide (Figure 4.15). These resorbed oxy-hornblendes coexist with resorbed plagioclase that also display sieve-rimmed textures mantled by clear, unresorbed rims. Resorption and sieve textures coexist in both amphibole and plagioclase, and suggest melting and dissolution from multiple heating events followed by cooling and growth (Coombs et al., 2000). Plagioclase commonly displays dissolution textures and oscillatory zoning, as shown in the rhyodacite dome at Chuapiloma (Figure 4.45, A6.2f). Some plagioclases also have multiple rims of melt inclusions with successive growth rims (Figure A6.2c, Appendix VI). These textures imply a complex thermal history with multiple processes that may include magma mixing and ponding of hot mafic magmas beneath cooler silicic magma reservoirs causing renewed heating, disequilibrium, resorption, and subsequent cooling and crystal growth.

Amphibole breakdown may follow from decomposition or heating. Textural differences may be used to distinguish P_{H_2O} loss from slow decompression versus heating. Heating causes resorption of more than one phase; for example, plagioclase generally

shows core and rims with sieve textures, caused during dissolution that are mantled with rims that represent subsequent cooling and crystal growth. Decompression causes breakdown of amphibole but crystallization of other phases like plagioclase, pyroxene and Fe-Ti oxides. Heating may have been combined with later decompression and dehydration prior to eruption and this results in the formation of "opacite" rimming amphibole with fine-grained opaque oxides (Gill, 1981, p. 180; Rutherford and Hill, 1993; Rutherford and Devine, 2003).

Amphibole compositions also define a complex thermal history for the evolution of the Yanacocha Volcanic Field (YVF). Four compositional varieties are present and discussed below as follows:

(1) High-Al amphiboles that trend toward pargasite are characteristic of Lower and Upper Yanacocha andesite lavas and domes. These amphiboles all have a uniform composition and distinct Fe-oxide reaction rims that represent disequilibrium reactions. Pargasite is not stable in andesite and may be derived from a mafic magma that mixed with a pre-existing andesite (Rutherford and Devine, 2003). The occurrences of rare mafic enclaves supports this hypothesis.

(2) Amphibole with uniform low-Al compositions (Al^{IV} 1.1 to 1.5 atoms pfu; Figure 4.31) is found in the rocks that lack pyroxene and include the Alto Machay dacite dome, the Maqui Maqui ignimbrite, and the Middle San Jose ignimbrites. Low-Al amphiboles have fresh phenocryst margins and not resorbed by dissolution. Some display slight "opacite" rimming. The Al contents are uniform from core to rim and vary by 0.2 atoms pfu or less.

(3) Core-edge compositional variations from high-Al cores to low-Al edges are observed in individual amphibole phenocrysts within ash-flow tuffs from the San Jose and Maqui Maqui ignimbrite sequences. Crystallization temperatures for such zoned grains are estimated from Figure 4.35A to range from ~725°C to < 825°C for the low Al^{IV} compositions and >825°C to <1000°C for the high Al^{IV} compositions. The data are consistent with an origin by mixing of high temperature magma containing high-Al amphibole phenocrysts with shallow low temperature magma. Prior to eruption, the early high-Al cores were resorbed and

mantled with low-Al amphibole rims to produce the observed

compositionally- and concentrically-zoned large phenocrysts.

Some San Jose ignimbrite samples have two compositionally distinct amphiboles in the matrix of a single flow. These compositions indicate the presence of a bimodal amphibole population. Bimodal compositions include one compositional variety with uniform high-Al and A-site cation contents, and another type with uniform low Al and A-site cation contents, common only to the pyroxene-bearing Lower and Upper San Jose ignimbrite (Figure 4.38; samples CB-44, DE-36, BS-2B, and CB-38). The Lower San Jose ignimbrite contains small high-Al amphibole with larger low-Al amphibole phenocrysts in the groundmass matrix. The Upper San Jose spatter ignimbrite contains amphiboles that display core-edge compositional variations with small amphiboles (<1mm long) that display a uniform low-Al content. Large high Al amphibole phenocrysts (≥1mm long) in the Upper San Jose spatter ignimbrite have distinct rims of plagioclase (Figure 4.24), whereas, the low Al amphiboles are resorbed and typically smaller, but do not have the plagioclase rim (Figure 4.23). Distinct plagioclase rims on the high-Al amphibole indicate decompression and dehydration during ascent from a deeper magma reservoir, whereas the low-Al amphiboles display rims of fine-grained opaque oxide with resorption that represents disequilbrium and dissolution from heating. These bimodal amphibole occurrences may represent crystals from originally distinct levels of the magma chamber that mixed in the eruption column.

The presence of a bimodal population of amphiboles and lack of compositional zoning implies a complex magmatic history that involves mixing of deep high temperature magma with shallow low temperature magma concurrent with eruption leaving no repose time for crystallization after mixing. The lack of decompression-induced rims in the low-Al amphiboles suggests rapid ascent and decompression >0.2 m/s (Rutherford and Devine, 2003). Mixing of the high temperature magma into a shallow reservoir likely initiated a rapid cataclysmic eruption.

The estimated pyroxene thermometry temperatures from the cores of coexisting augite-orthopyroxene in the San Jose ignimbrites indicate the presence of a high temperature augite (~1050-1150°C) with a low temperature orthopyroxene (~ 875 to 925±30°C). The rims of coexisting augite and orthopyroxene also yield a slightly higher

temperature for augite than for coexisting orthopyroxene. The presence of high and low temperature pyroxene coexisting in the same sample of San Jose ignimbrite is supported by the presence of two varieties of amphibole (high-Al and low-Al) in these same ignimbrites (Figure 4.37 and 4.38; Table 4.6).

The San Jose Ignimbrite may have erupted from a thermally zoned magma chamber increasing from ~850 to 1100°C downward and mixed in the eruption column that came from different parts of the magma chamber. The eruption may have been initiated by a heating event from the underplating of a hot mafic magma beneath the San Jose magma chamber. Composition zonations in the minerals suggest that mixing of the high temperature mafic end member with lower temperature the San Jose dacite magma may also have been a process in the evolution of the San Jose ignimbrite.

YVF rocks form a linear trend with pre-Yanacocha rocks on the MgO-SiO$_2$ variation diagram and the Total Alkali-SiO$_2$ (TAS) diagram into rhyolite compositions and imply two end-member compositions that comprise the least evolved Lower Yanacocha andesite (Lpha) and the most evolved Upper (late) Dacite (Figures 4.30 and 4.31). Both diagrams display compositional gaps between the late dacite and a central cluster of YVF volcanic rocks. Lower Yanacocha andesite (Lpha) compositions overlap the central cluster but most lie outside toward less evolved compositions. Clustering is more obvious in the SiO$_2$ range diagram Figure 4.33. Ba and Rb versus SiO$_2$ variation diagrams (Figure 4.35) also display compositional gaps between the late dacite and the other YVF rock sequences. The central cluster of data that lies between the late dacite and the Lower Yanacocha pyroxene andesite (Lpha) has intermediate compositions and represents the bulk of the YVF rock sequences that includes Upper Yanacocha pyroxene andesite (Upha), the Maqui Maqui ignimbrite (MMI), and the San Jose ignimbrite (SJI) (Figures 4.33 and 4.34).

A diversity of mineral assemblages and both normal and reverse zoning of plagioclase is one of the strongest cases for magma mixing (Gill, 1981). Quartz and biotite phenocrysts are rare to absent in the rocks (eg. MMI, Upha, SJI) that may represent mixed compositions of the end member magmas from the Lower Yanacocha andesites and the Upper Dacites. Most plagioclase phenocrysts in the study display

normal and oscillatory zoning. Feldspar in the Upper Dacite (Figure 4.69) are resorbed with later overgrowths of oscillatory zoned feldspar.
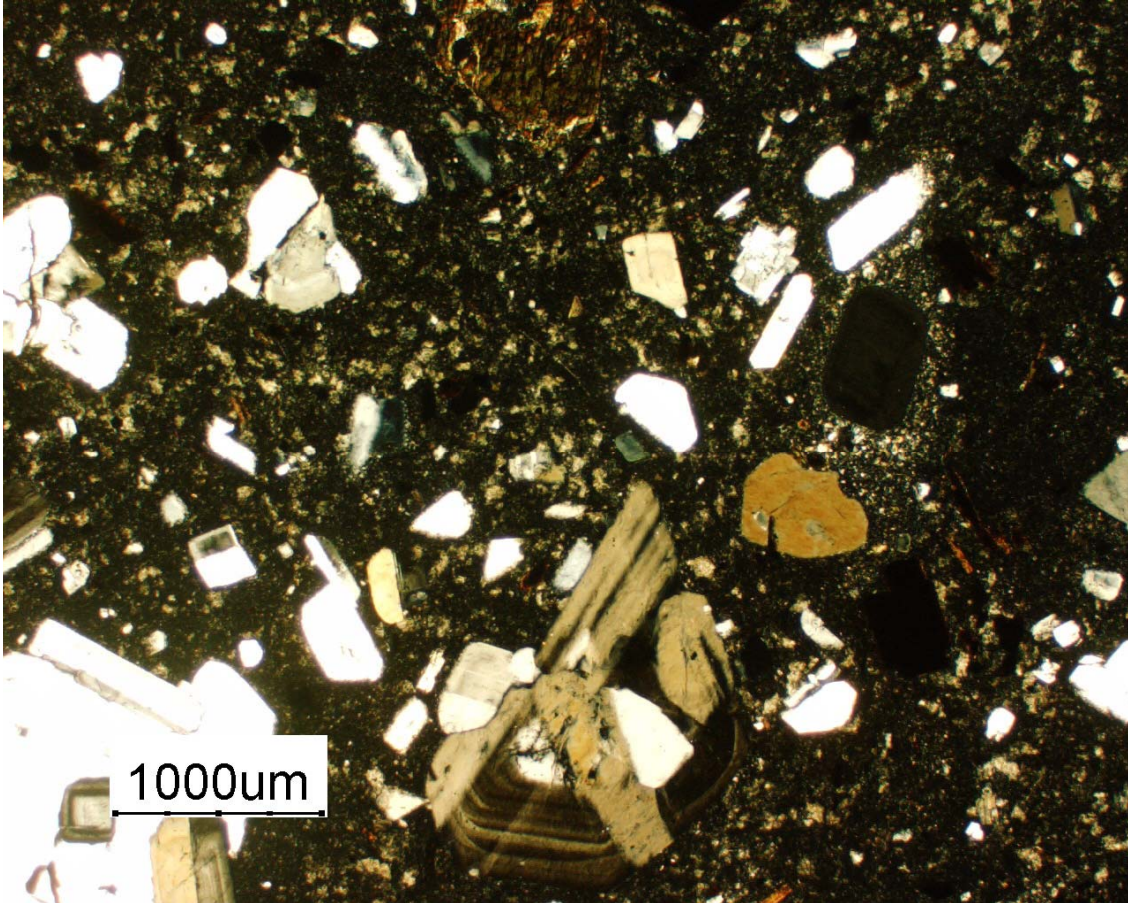
Figure 4.69 Photomicrograph of the Chaupiloma rhyodacite dome. Plagioclase are free of sieve textures, but display dissolution along the rims and concentrically zoned growth around resorbed feldspar with minor sieve-cored textures (bottom center in the above figure). Slightly resorbed plagioclase and quartz, and an oscillatory-zoned growth rim of feldspar around plagioclase phenocrysts with rounded rims. This is another example of textures that may represent dissolution and growth resulting from heating by magma mixing.

Multiple Magma Chambers and Crustal Assimilation

Compositional variations and varieties in amphiboles at Yanacocha (discussed above), and magma pressure estimates using the Al-in-hornblende geobarometer imply that phenocryst assemblages in the YVF rocks equilibrated at different crustal levels with

pressures that may have ranged from ~5 to 7 kb (~15 to 21 km) prior to early effusive eruptions and ~1 to 3.5 kb (~3 to 10 km) prior to the later explosive eruptions (Figure 4.45). These data suggest that amphibole followed different crystallization trends and evolved as separate magma systems. The Lower and Upper Yanacocha andesites were less evolved, hotter, deeper, and the ignimbrites were more evolved, cooler, and shallower. Both were oxidized.

Amphibole with lower Al^{IV} and $(Na+K)_A$ compositions from ignimbrites of the lower and middle San Jose sequence, and the upper San Jose "white" tuff imply lower crystallization temperatures from more evolved bulk rock compositions. Amphibole with high Al^{IV} and $(Na+K)_A$ cation compositions are from the upper San Jose spatter ignimbrite and indicate higher crystallization temperatures and less evolved bulk chemistry. These data imply an increased mafic composition for spatter ignimbrite as supported by its phenocryst assemblage and including high pyroxene content. These compositions may represent the tapping of deeper magmas into a shallow magma reservoir.

Amphibole compositions outline two separate trends with decreasing Fe/(Fe+Mg) that correspond to decreasing values for molar (Na+K+Al)/4 and increasing values of SiO_2 wt.% in amphibole (Figures 4.34 and 4.35). These trends define separate compositional fields; one is characteristic of Lower and Upper Yanacocha andesite sequences and another for the Maqui Maqui and San Jose ignimbrites. They are consistent with the aluminum versus $(Na+K)_A$ plots in Figures 4.32 and 4.33 in that amphiboles from Lower and Upper Yanacocha andesite effusive eruptions are different from the amphiboles of the Maqui Maqui and San Jose explosive eruptions. The patterns cannot be explained by simple fractional crystallization because Fe/(Fe+Mg) increases with an increase in bulk rock SiO_2 contents from the andesite in Lower and Upper Yanacocha rocks to the dacite in Maqui Maqui and San Jose rocks (Figure 4.35) inconsistent with amphibole fractionation.

Compositional variations from the bulk rock geochemistry also suggest separate trends for the evolution of rocks in the Yanacocha Volcanic Field. Two patterns can be recognized from the Sr-SiO_2 and Sr-CaO variation diagrams in Figures 4.59 and 4.60. Sr

increases with increasing SiO_2 and decreasing CaO in the Lower and Upper
Yanacocha pyroxene-bearing andesite (Lpha and Upha) to the pyroxene dacite San Jose
ignimbrite sequence (SJI), whereas, Sr decreases and a flat pattern develops in rocks that
lack pyroxene from the Maqui Maqui ignimbrite to the Upper (late) Dacite. Therefore, Sr
increases with each successive volcanic sequence from the Lower Yanacocha andesites to
San Jose ignimbrites, and decreases in the Maqui Maqui ignimbrite and the final
magmatic episode of Upper Dacite. These patterns suggest separate compositional trends
for rocks with and without pyroxene at Yanacocha.

Depletions in the light rare earth elements (LREE) and heavy rare earth elements
(HREE) within rock sequences in the Yanacocha Volcanic Field (YVF) require
compositional differences that may reflect different source areas for crustal derived melts
or assimilates. Strong LREE/HREE fractionation is typical of crustal compositions
(Petrinovic et al., 2005) and consistent with assimilation of silicic crust. Silicic crustal
melts may reflect the source area for the YVF rocks enriched in LREE. Rare earth
element (REE) normalized patterns in amphiboles display convex upward curves that
characterize depletions in LREE and HREE relative to the middle REE as a result of the
low mineral/melt distribution coefficients (D) for the LREE and high D's for MREE in
amphiboles (Sisson, 1994). Maqui Maqui ignimbrites and the Upper Dacite display
overall depletions in LREE and HREE and a flat sloping pattern that defines the lower
boundary of the field for all Yanacocha rocks in the study. Other YVF rocks display REE
patterns enriched in LREE and HREE relative to the Maqui Maqui ignimbrite, and the
degree of La/Yb fractionation in the younger San Jose ignimbrite is more pronounced
with a steeper pattern (Figures 4.65 to 4.67 and 4.68).

Depleted and somewhat flattened patterns displayed by the normalized REE plots
for the Maqui Maqui and Upper Dacite are inconsistent with fractional crystallization and
assimilation of mature silicic crust. Mafic crustal melts rich in amphibole or pyroxene
may explain the flatter and depleted patterns relative to other YVF rocks. Dungan and
Davidson (2004) discuss a complex multicomponent process by which crustal melts
develop through assimilation of their mafic plutonic roots in long-lived volcanic arcs
leading to melts with trace element covariations much different than expected for melts
contaminated by mature upper crust. Mafic inclusions or enclaves and refractory

xenoliths are rare or have not been recognized in the YVF rocks. Mafic enclaves with 40% pyroxene and 60% Ca-plagioclase were found in an Upper Yanacocha andesite lava flow at Cerro Corra Blanco, and may be remnants of the deep mafic crustal melts. Although no direct evidence is available from is study, contamination of late magmas by assimilation of the old mafic plutonic roots rich in pyroxene or amphibole could help explain the depleted REE signature in the Upper Dacite.

Chemical differences between the Maqui Maqui ignimbrite and the other YVF rocks also are supported by amphibole and apatite microprobe data (Tables 4.3 and 4.5). Apatite microprobe results show distinct differences in the Cl and F contents in apatites between the San Jose and Maqui Maqui ignimbrite. Apatites in the Maqui Maqui ignimbrite have extremely low F (near detection limits) and a mole fraction Cl/(Cl+F) = 1.0. In the San Jose ignimbrites, apatite has increased F and decreased Cl relative to the Maqui Maqui and the Cl/(Cl+F) ratios range from 0.06 to 0.86. Also, SO_3 contents are lower for apatites in the Maqui Maqui ignimbrite. Relationships of these differences are presented in Figures 4.48, 4.49, 4.50, and 4.51.

Crystal-Liquid Fractionation

Amphibole Fractionation

Residual liquids that develop during the fractional crystallization of amphibole are moderately to slightly enriched in large ion lithophile (LIL) elements, high field strength elements (HFSE) and SiO_2, and strongly depleted in light rare earth elements (LREE), heavy rare earth elements (HREE) and Ti (Gill, 1981; Sisson, 1994). Amphibole has high mineral/melt partition coefficients (D) for Y, HREE (D_{HREE}»1), V, and the HFSE. Amphibole also has low SiO_2 contents, high FeO*/MgO ratios, high K/Na ratios, and low D_{Sr} (Gill, 1981, Green, 1994; Sisson, 1994). Rare earth element (REE) and Y patterns in amphibole are shaped convex upward and reflect the low D for the LREE, the high D for the middle rare earth elements (MREE) and Y, and a slight decrease in D for Yb. Partition coefficients increase for the rare earth elements (REE), Y, and Sr in amphibole as the melt becomes more silicic (Green, 1994; Sisson, 1994). Amphibole crystallizing in the initial melt will sequester Ti (D_{Ti}»1) and cause a depletion in the andesite melt that is

three to four times that of the Ti in the amphibole (Sisson, 1994). Consequently, amphibole fractionation could explain enrichment of SiO_2 and LREE, depletions of Fe maintaining higher Mg/Fe ratios and lower Fe/(Fe+Mg) in the residual liquid, depletions in Ti with increasing SiO_2 in the residual melt, depletions in Na, and the negative correlation between HREE + Y and SiO_2. Amphibole fractionation must occur at <30 kb (Gill, 1981), and the high-Al amphiboles in the Lower and Upper Yanacocha pyroxene andesites probably crystallized in deep crustal magma chambers. High-Al amphiboles with pargasite compositions are not stable in andesite and require mixing of a mafic magma with a pre-existing andesite (Rutherford and Devine, 2003). Liquids generated by extreme amphibole fractionation would have concave-upward REE patterns.

Amphibole thermal stability increases with increased temperature and P_{H_2O} so amphibole will crystallize first from a magma with high P_{H_2O} >2 kb and high temperatures > 950°C. Pyroxene, plagioclase and the Fe-Ti oxides will crystallize last (Wallace and Anderson, 2000), and the residual liquids will reflect amphibole fractionation. As the magma cools and P_{H_2O} decreases to <1.5 kb (Wallace and Anderson, 2000) pyroxene, plagioclase and Fe-Ti oxides will crystallize before amphibole. At Yanacocha, high-Al amphiboles from the Lower Yanacocha pyroxene andesite have simple compositions that trend toward paragasite, do not enclose early minerals, and generally have low Fe/(Fe+Mg) ratios. Later amphiboles show textural and compositional variability and are larger with low-Al composition, and typically enclose abundant minerals of plagioclase and Fe-Ti oxides. Their Fe/(Fe+Mg) is higher so they crystallized from a residual liquid less dominated by amphibole fractionation and more by plagioclase, pyroxene fractionation, and crustal assimilation.

Pyroxene Fractionation

Values of distribution coefficients for pyroxene plot to form a convex upward curve with very small mineral/melt distribution coefficients (D«1) for the LREE and LIL elements, increased D for Ti, MREE and Y that approach 1, and slight decreases for HREE with D≤1 (Gallahan and Nielsen, 1992; Green, 1994). The D's increase for MREE, HREE, Y and Ti with increasing Ca in the M2 site and increased Al^{IV} in pyroxene, but remain < 1 (Hack et al., 1994). Mg/(Mg+Fe) content also increases. The

low distribution coefficients (D < 1) for Ca-pyroxene will not effect depletions in the residual liquids as are characteristic for amphibole. Compositions from these melts may result in slight concave upward REE normalized curves from LREE to HREE.

Plagioclase Fractionation

Increased Sr and Ba contents with each successive rock sequence at Yanacocha may have been controlled by plagioclase fractionation. Crystallization of plagioclase typically follows a crystal-liquid path from Ca-rich to Na-rich compositions. The crystallization of anorthite varieties causes an increase in Sr and Ba contents in the residual liquid resulting in increases of these LIL elements in the more Na-rich plagioclase (Korringa and Noble, 1971; Blundy and Wood, 1991). Increases in Sr and Ba contents in the YVF rocks through time and are most pronounced in the Maqui Maqui ignimbrite, Upper Yanacocha volcanic sequence, and the San Jose ignimbrite sequence (Figures 4.35 and 4.36). Modal percent abundance of plagioclase also increases with Sr and Ba contents in the YVF rock sequences. Plagioclase modal percent decreases in the Upper Dacite, but does not adequately explain the sudden and significant decrease in Sr relative to the increase in Ba.

The assumption that the different compositional trends discussed above represent differentiation by plagioclase fractionation in different magma batches is supported by the rare earth element (REE) normalized diagrams in Figures 4.66 and 4.67. The decrease in Al_2O_3 and P_2O_5 in the Yanacocha rocks with >65 wt.% SiO_2 (Figure 4.27) reflects the crystal fractionation of large amounts of plagioclase and minor amounts of apatite common in the early sequences with <65% SiO_2 (e.g., Upper Yanacocha sequence, lower San Jose, and the Maqui Maqui ingnimbrite). Strong enrichments in P_2O_5 result in rocks (e.g., Maqui Maqui ignimbrite) with abundant apatite with up to 0.5 modal %. Later P_2O_5 depletions and the absence of apatite in the late dacite may be explained by the strong apatite fractionation in the SJI.

Biotite Fractionation

The Upper Dacite contains more biotite than the other YVF rocks. Biotite has high mineral/melt partition coefficients (D>1) compatible for Rb, Ba and K, and

moderate and slightly incompatible for Sr and Y (Green, 1994). Ba increases relative to increased Rb content, and decreased Sr and Y contents in the late dacite (Figures 4.35 and 4.36). The Upper Dacite also has less plagioclase than all other YVF rocks and more alkali feldspar. Compositional variations of the late dacite relative to other YVF rock sequences may be a result of the abundant biotite and less plagioclase that crystallized from a fluid depleted in Sr and enriched in other LIL's. Residual fluids depleted in Sr could have resulted after the crystallization of plagioclase in the Sr-enriched Upper Yanacocha volcanic sequence and the San Jose ignimbrite that have very abundant plagioclase.

Summary

Fractional crystallization does not fully explain the compositional variations present in rocks of the Yanacocha Volcanic Field (YVF). Compositions for residual liquids that would have resulted from amphibole and pyroxene fractionation in Lower and Upper Yanacocha volcanic sequences do not match actual patterns in normalized REE plots and the plots of normalized REE fractionation (Figures 4.65 to 4.68). However, fractionation of plagioclase and apatite may explain compositional trends observed in the YVF for Sr, Ba, Al_2O_3 and P_2O_5. Therefore, crystal-liquid fractionation may explain some of the compositional variations in the YVF rocks, but does not provide an adequate model to explain all patterns and trends displayed by the data.

Degrees of $(La/Sm)_N$ and $(Gd/Yb)_N$ fractionation increase throughout each successive rock sequence from Lpha to SJI also inconsistent with amphibole fractionation (Figure 4.43). Moreover, stronger $(La/Sm)_N$ fractionation versus $(Gd/Yb)_N$ fractionation is present in the Lpha, and the gap in degree of fractionation merges to overlap in SJI rocks with more similar values for $(La/Sm)_N$ and $(Gd/Yb)_N$ fractionation. This reflects increased $(Gd/Yb)_N$ relative to $(La/Sm)_N$ and steep fractionation trends in MREE/HREE for Upha and SJI and implies amphibole fractionation may have dominated difeerentiation processes for Lpha melts, whereas through time amphibole fraction can not explain the patterns observed in the Upha and Lpha. Crustal melts must have dominated through AFC processes quite different than that for Lpha.

Adakites vs. Crustal-level Differentiation

Adakites are generally defined by compositional patterns that reflect a chemical signature attributed to melting subducted oceanic crust (slab melting) and the presence of residual garnet ±amphibole that have high mineral/melt partition coefficients for HREE and LIL relative to LREE and Y (Kay, 1977). Partial melts from the subducted slab will have a geochemical signature with SiO_2 >56 wt.%, Al_2O_5 >15 wt.%, low HREE with Yb <1.9 ppm and Y <18 ppm, high Sr >400 ppm and Sr/Y >40, low HFSE, and positive Sr and Eu anomalies (Defant and Drummond, 1993; Stern and Kilian, 1996; Beate et al., 2001; Samaniego et al., 2002). Steep Sr/Y vs Y patterns as in Figure 4.38 reflects a chemical signature attributed to slab melts (Defant and Drummond, 1993; Stern and Kilian, 1996; Beate et al., 2001). These patterns are also characteristic of many crustal melts (Garrison and Davidson, 2003), and typical of convergent plate magmas that have traversed large spans of continental crust and assimilated and fractionated in the crust (Hawkesworth et al., 1979; Thorpe et al., 1979; Frey et al., 1984; Grunder and Mahood, 1988; Feeley and Hacker, 1995; Dungan and Davidson, 2004). In the region of Yanacocha, crustal thicknesses are estimated at 35 km (Gutscher et al., 1999, 2000). These thicknesses allow ample time for ascending magmas to assimilate crust and fractionate (cf., Grunder and Mahood, 1988). Composition variations observed in the YVF rocks and presented in this study show similar patterns to variations described for magma systems in Central Chile and Central Perú (Hawkesworth et al., 1979; Thorpe et al., 1979; Frey et al., 1984; Grunder and Mahood, 1988; Feeley and Hacker, 1995; Petford and Atherton, 1995; Petford et al., 1996).

Evidence that may support an origin by through crustal melt and AFC rather than an origin by direct slab melts is displayed in Figure 4.68. Strong LREE/MREE fractionation relative to MREE/HREE fractionation for all YVF rocks implies crustal compositions and assimilation, and strong decrease in Yb and Y with increasing La/Yb, is typical of parental magmas with crustal compositions that result by crystal fractionation and assimilation of a silicic crustal source (Feeley and Davidson, 1994; Feeley and Hacker, 1995; Petrinovic et al., 2005). Similar characteristics in REE fractionation patterns would be expected from slab melts. HREE's from Dy to Lu are

strongly compatible in garnet and Gd to Lu in amphibole, therefore, slab melts with residual garnet and amphibole would result in very strong enrichments of LREE/MREE fractionation relative to MREE/HREE fractionation. However, intensities of LREE/MREE should approach LREE/HREE and not overlap with the MREE/HREE as in Figure 4.44.
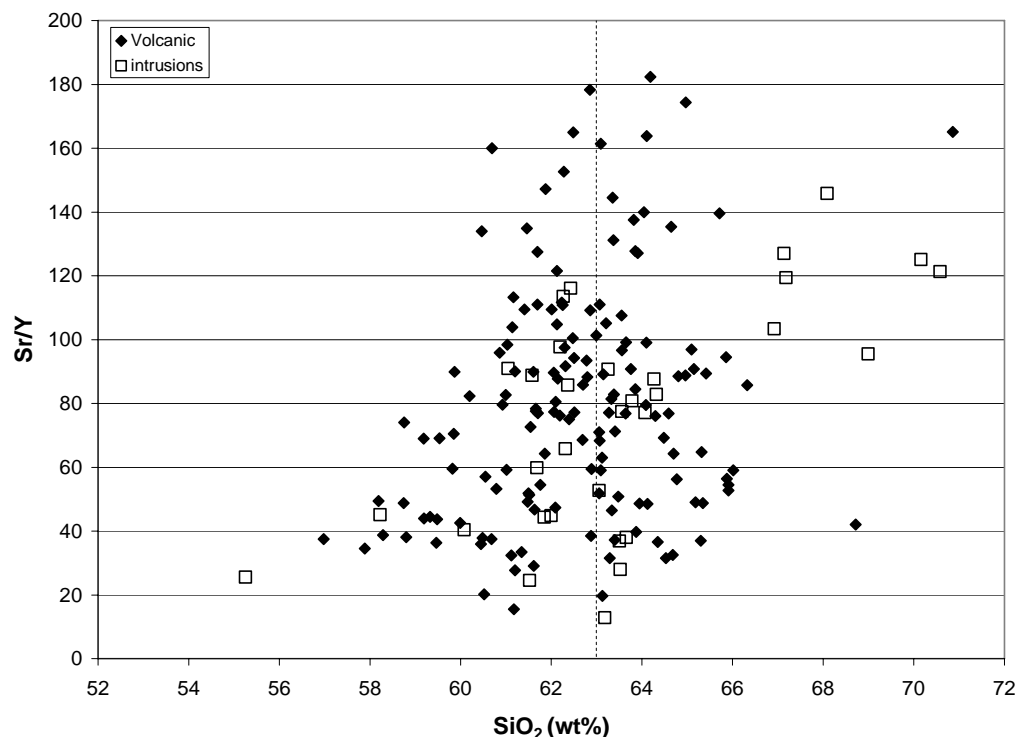
Figure 4.70 Plot of Sr/Y ratios versus SiO_2 showing a wide spread of SiO_2 with anomalous Sr/Y >40. Adakite compositions with Sr/Y >40 are found only in slab melts with SiO_2 wt% from 63-70 (Garrison and Davidson, 2003).

Garrison and Davidson (2003) tested the strength of the adakite geochemical signature in the Northern Volcanic Zone with compositions of known slab melts and found that only slab melts with SiO_2 from 63 to 70% wt.% should have anomalous Sr/Y >40. Figure 4.70 shows a wide spread in SiO_2 contents with anomalous Sr/Y for Yanacocha rocks suggesting that slab melting is not the only process.

Temporal and Spatial Variations of the Magma Composition

Yanacocha experienced a progression of magmatism and hydrothermal activity from southwest to northeast through time across the district. Volcanism began in the west at 14.5 Ma with monogenetic effusive eruptions of pyroxene-hornblende andesite lavas forming a series of stratocones (*effusive stage 1*). Andesite dome-building and minor explosive eruptions followed the early effusive activity, and volcanism migrated to the northeast becoming dominantly explosive and dacitic in composition with eruptions of the Maqui Maqui ignimbrite (*explosive stage 1*). By 12 Ma, a second stage of effusive eruptions began that extended from Cerro Negro to Maqui Maqui associated with numerous andesite dome related systems (*effusive stage 2*). Effusive stage 2 was followed by a second stage of explosive volcanism that concluded at 11.2 Ma with the eruption of the San Jose ignimbrite (*explosive stage 2*). Magmatism then shifted to a stage of highly oxidized dacite to rhyolite magmas with dome building and intrusions of isolated porphyry plugs that spanned 2.4 m.y. from 10.8 – 8.4 Ma. Volcanism ended in a final explosive event with the eruption of the Negritos ignimbrite at 8.4 Ma (*explosive stage 3*).

Compositional variations in the YVF rocks display an overall increase in SiO_2, total alkali, LIL elements, and the LREE's, and a decrease in HREE's and Y through time. Major element oxide compositions display a clustering effect for the rock sequences Maqui Maqui ignimbrite (MMI) through the San Jose ignimbrite (SJI) (Figure 4.55). Trace element compositions tend to display a greater variation (Figures 4.58 to 4.64). Phenocryst type and percent modal abundances increase and fluctuate through time (Figure 4.2). Percent phenocrysts in lavas from the Lower and Upper Yanacocha volcanic sequence (Lpha and Upha) are similar. Phenocryst abundances increase in the pyroclastic rocks as expected due to fines-depletion. Phenocryst abundance increases temporally from the Upper Yanacocha volcanic sequence (Upha) through the middle San Jose ignimbrite (Msji), then decreases in the Upper San Jose spatter ignimbrite (Usji) and again in the Upper (late) Dacites. Mafic minerals are most abundant in the Lower and Upper Yanacocha volcanic sequences (Lpha and Upha) and decrease in abundance in the Maqui Maqui pyroclastic sequence (MMI) and San Jose ignimbrites (SJI) (Figure 4.2).

Pyroxene tends to decrease through time from the Lower Yanacocha volcanic sequence (Lpha) to the Maqui Maqui pyroclastic sequence (MMl) and again from the Upper Yanacocha volcanic sequence (Upha) to the Upper (late) Dacite. Pyroxene and hornblende are common in the Lower Yanacocha volcanic sequence (Lpha), Upper Yanacocha volcanic sequence (Upha), the Lower San Jose ignimbrite (Lsji), and the Upper San Jose (Usji) spatter ignimbrite (Table 3.2 and 3.3, Figures 4.2 and 4.74). Pyroxene is absent to trace in abundance in the Maqui Maqui pyroclastic sequence (MMl), the Middle San Jose ignimbrite (Msji), the Upper San Jose ignimbrite (Usji) white tuff, and the Upper (late) Dacite (Tables 3.2 and 3.3). Quartz, alkali feldspar, and biotite are present in abundance only in the late dacite, common in the early dacite, and rare in the Middle San Jose ignimbrite (Msji) and the Maqui Maqui ignimbrite (MMl). In summary, the ranges of modal mineralogy and mafic versus felsic modal abundances fluctuate through time with successive and alternating effusive and explosive stages of volcanism.

Effusive Phase I

The lower Yanacocha Volcanic Field (Lpha) developed from effusive eruptions of pyroxene-hornblende andesite from numerous monogenetic volcanoes and small composite cones such as Cerro Atazaico (Lpha, Figure 4.71). Effusive eruptions were followed by dome-building and minor pyroclastic eruptions with block and ash flows of quartz-bearing pyroxene andesite. These included the Cerro Regalado dome complex and domes at Quilish and Cerro Negro Oeste. Quilish domes include the sub-vertical, flow-foliated, quartz-bearing andesite at Antibuyoc and acid-sufate altered remnants of the Cerro Quilish dome cross cut with hydrothermal breccia.

Two distinct magma compositions were present during this period and included Lower Yanacocha andesite (Lpha) and an early set of dacite intrusions. Pyroxene with hornblende is common to the Lpha, whereas early dacite lacks pyroxene, but quartz and hornblende are present. Compositions vary from basaltic andesite to dacite and the trace element pattern is similar.

Effusive activity and subsequent dome-building progressed from west to east across the district and was centered along three separate north-northwest trending vent

areas for ~1.2 million years. An andesite volcanic field developed with an areal expanse of ~340 square kilometers with an estimated average thickness of 80 meters. Effusive pyroxene andesite volcanism was centered in the west district over Cerro Negro from 14.5 to 14.2 Ma followed by quartz-pyroxene andesite domes at 13.9 Ma. Volcanism progressed eastward to the Chaupiloma trend and on to the Chugares volcano in the west by 13.3 Ma.

Explosive Phase I (Maqui Maqui ignimbrite)

The Maqui Maqui pyroclastic sequence (MMI and MMP) represents an early period of explosive volcanism (Figure 4.72) with eruptions of hornblende ±biotite andesite, trachyandesite, and dacite ignimbrites between 12.6 to 12.4 Ma. The sequence is centered on the proposed Yanacocha composite volcano, a center of magmatic activity for ~ 4 million years from 12.4 to 8.4 Ma, at Cerro Yanacocha. Exposures of pyroclastic rocks crop out as an erosional remnant that covers ~90 square kilometers with an estimated thickness that averages 100 meters. These rocks post-date early dacite and feldspar porphyries in the west district, but are temporally related to domes, porphyritic intrusions, and feldspar porphyry plugs and diatremes with the same composition as the Maqui Maqui ignimbrite. Maqui Maqui porphyritic rocks range in age from 12.4 to 11.9 Ma and are the textural equivalents to the hydrothermally altered Yp porphyries at Yanacocha.

Compositional variations include a lack of pyroxene and the presence of common apatite phenocrysts, and total alkalis and the Sr/Y and Ce/Yb ratios increased with increased SiO_2. Phenocryst assemblages consist of plagioclase > hornblende > Fe-Ti oxides > biotite > apatite and pyroxene is absent.

Effusive Phase II

The upper Yanacocha Volcanic Field (Upha) developed after a renewal of effusive andesitic volcanism between 12.1 and 11.7 Ma from monogentic andesite vents and numerous andesite lava-domes in the west district that include Pampa Cerro Negro, Corra Blanca, Pampa Corimayo, and Shoclla. Andesite lavas may have covered an area of ~ 120 square kilometers centered over the Yanacocha Volcano (Figure 4.73). These

eruptions were followed by coalescing domes of dacitic composition in the east district with coulées (thick extrusions of endogenous or exogenous dome growth that erupt on a slope and flow down hill) and tortas (low flat domes with endogenous growth in flat areas) that developed east-west, north- and northeast- trending dome fields in the east district, from San Jose to Machay and north to Colorado. Dacite and andesite lavas erupted from multiple-vent complexes with small coulée-style effusive eruptions and related pyroclastic eruptions that covered a total area <60 square kilometers.

Pyroxene is common with hornblende, but apatite and quartz are rare. The compositional ranges for the Maqui Maqui ignimbrite (MMI) and the Upper Yanacocha volcanic sequence (Upha) overlap; however, there is a slight decrease in SiO_2, slight increase in total akali contents, and a slight increase in the Sr/Y ratio that represents a strong increase in Sr contents over the Sr contents of the MMI (Figure 4.58).

Explosive Phase II (San Jose Ignimbrite)

Ash-flow tuffs of the San Jose ignimbrite (SJI) represent late explosive eruptions of the Upha dacite that post-date early acid-sulfate alteration in the east district (Figure 4.74). San Jose ignimbrites are pyroxene dacites that typically contain accidental fragments of acid-sulfate altered volcanic rock. $^{40}Ar/^{39}Ar$ dates indicate eruptions of the San Jose ignimbrite span a period of ~300,000 years from 11.5 to 11.2 Ma. The sequence erupted in three phases from distinct and separate vent areas, and include the lower San Jose ash-flow tuff (Lsji) from 11.5 to 11.4 Ma, the middle San Jose white ash-flow tuff (Msji) from 11.3 to 11.2 Ma, and the upper San Jose (Usji) spatter ignimbrite (11.25±0.07 Ma) and white tuff (11.22±0.08 Ma). Eruptions of middle San Jose ash-flow tuffs (ie. the white tuff) overlap in time with the upper member spatter ignimbrite. Subsequent post-ignimbrite dome-building produced three vent-filling dome complexes at Ocucho, Chaquicocha Sur, and Alto Machay whose $^{40}Ar/^{39}Ar$ ages are 11.36±0.09 Ma, 11.28±0.09 Ma and 11.23±0.07 Ma, respectively. Ash-flow tuffs filled a topographic depression called the Coso Trough (Longo, 2001) and covered an estimated 175 square kilometers with thicknesses that range from 40 meters north of Ocucho to 350 meters in the Coso Trough.

Differences in mineralogy occur within the San Jose iginimbrite (SJI) sequence between the SJI members (Figure 4.74). Pyroxene is present and often quite abundant in the Upper San Jose spatter ignimbrite and common in the Lower San Jose (Lsji), whereas pyroxene is absent to trace in the Middle San Jose (Msji) and Upper San Jose white tuff (Usji). Apatite is quite common and coarse-grained in the Upper San Jose ignimbrite (Usji) and Lower San Jose ignimbrite, but very fine-grained and found in trace amounts in the Middle San Jose ignimbrite and Upper San Jose white tuff. Rare sphene was found in the Middle San Jose ignimbrite but is absent in the other members.

The major element oxide and trace element compositional ranges for the San Jose ignimbrite (SJI) overlap with the Upper Yanacocha volcanic sequence and the Maqui Maqui ignimbrite (Figures 4.54, 4.58, 4.59 and 4.60). Ranges for SiO_2 gradually increase through each successive SJI member over that for the Upper Yanacocha volcanic sequence. Total alkali ranges increase with Lower and Middle San Jose ignimbrites, then decrease for Upper San Jose ignimbrite. Trace element variations show increases in the LREE and LIL relative to Upper Yanacocha volcanic sequence and the Maqui Maqui pyroclastic sequence.

Late Dacite to Rhyolite Episode

Figure 4.75 shows the Upper (late) Dacite (in red) relative to other YVF volcanic and intrusive rocks. Isolated dacite domes were emplaced at ~10.8 Ma, and exposures are aligned east-west for 5 km from Chaquicocha Norte to La Quinua dome. The Cori Cashpa dacite intrusion crops out 2.7 km north where it intruded Maqui Maqui ignimbrite and may be of similar age. These dacites have a distinct mineralogy that differs from dacites in the Upper Yanacocha volcanic sequence and the San Jose dacite domes. They lack pyroxene and apatite, but contain sphene, magnetite, and quartz, and may represent the initial stage of a highly oxidized, magmatic episode spatially and temporally associated with the ore deposits at Yanacocha. This late episode of highly oxidized felsic magmas developed porphyritic domes with minor lavas and pyroclastic aprons, and intrusions of isolated dacite porphyry plugs. Late hydrothermal breccia commonly borders the intrusive margins and contains gold ore.

Dacite porphyry plugs and rhyodacite domes and dikes are aligned within a northwest trend for 5.7 km from Chaquicocha Sur to Chaupiloma. The Negritos rhyodacite domes are 8 km northwest on the same trend. Dacite porphyry plugs at Yanacocha and Chaquicocha Sur are considered phase II. The Yanacocha dacite porphyry plugs have an age of 9.91±0.04 Ma and intrude early diatremes, Yp porphyry, and altered fragmental rocks and breccia. The altered Chaquicocha dacite porphyry is similar and believed the same age. Episode III is represented by rhyodacite dikes and domes at Chaupiloma and Yanacocha Lake. These rocks have a $^{40}Ar/^{39}Ar$ date of 8.40±0.06 Ma (Turner, 1997). Episode II and III dacites have similar mineralogy to the late dacite I, and represent the final magmatic episode at Yanacocha.

Volcanism ended in a final explosive eruption of the Negritos rhyolite ignimbrite at 8.43±0.04 Ma. The ignimbrite is preserved only in distal areas on Cerros de los Negritos 8 km from the mine site (outlined in red with tie lines to proposed source; Figure 4.75). This eruption was followed by the emplacement of the Chaupiloma and Yanacocha Lake rhyodacite domes. Eruption of the Negritos ignimbrite was followed by a cessation of arc volcanism in the Yanacocha area and the initiation of flat-slab tectonics and associated volcanic gap from 2°S – 15°S in northern Peru (Gutscher et al., 1999).

Upper (late) Dacite has the highest SiO_2 and total alkali contents of all YVF rocks, and their compositional ranges lie along a trend that suggests differentiation with total alkali contents increasing with increasing SiO_2. The major element oxide contents of total alkali vs. SiO_2 fall within the dacite and rhyolite compositional fields and show a compositional gap in the SiO_2. Upper (late) Dacite trace element compositions Sr/Y versus Ce/Yb overlap with the San Jose ignimbrites.
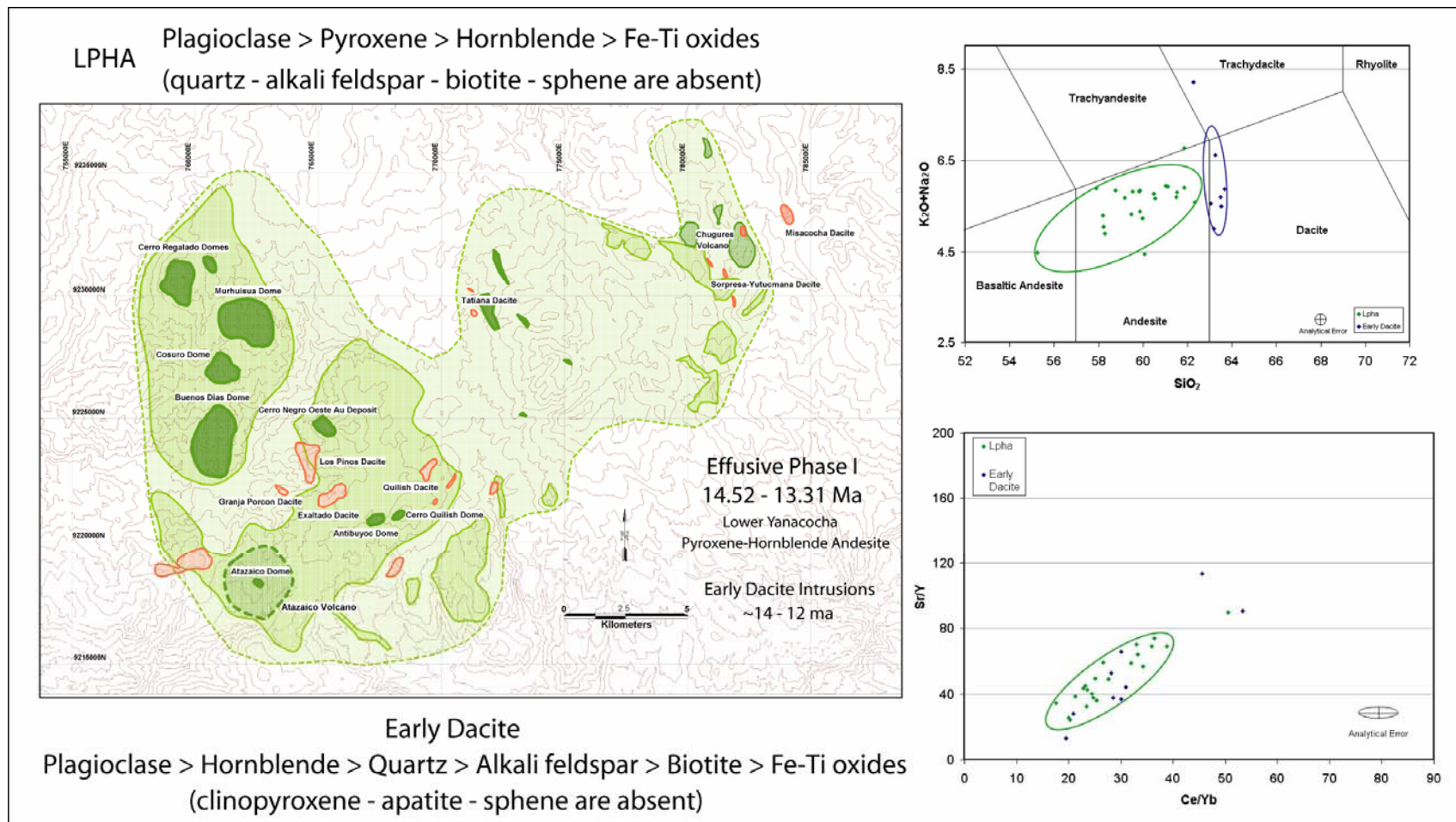
Figure 4.71 Chemical variations and phenocryst mineralogy of Effusive Phase I from 14.5 to 13.3 Ma. Rocks include the Lower Yanacocha pyroxene-hornblende andesite and the Lower (early) Dacite of the Yanacocha Volcanic Field.
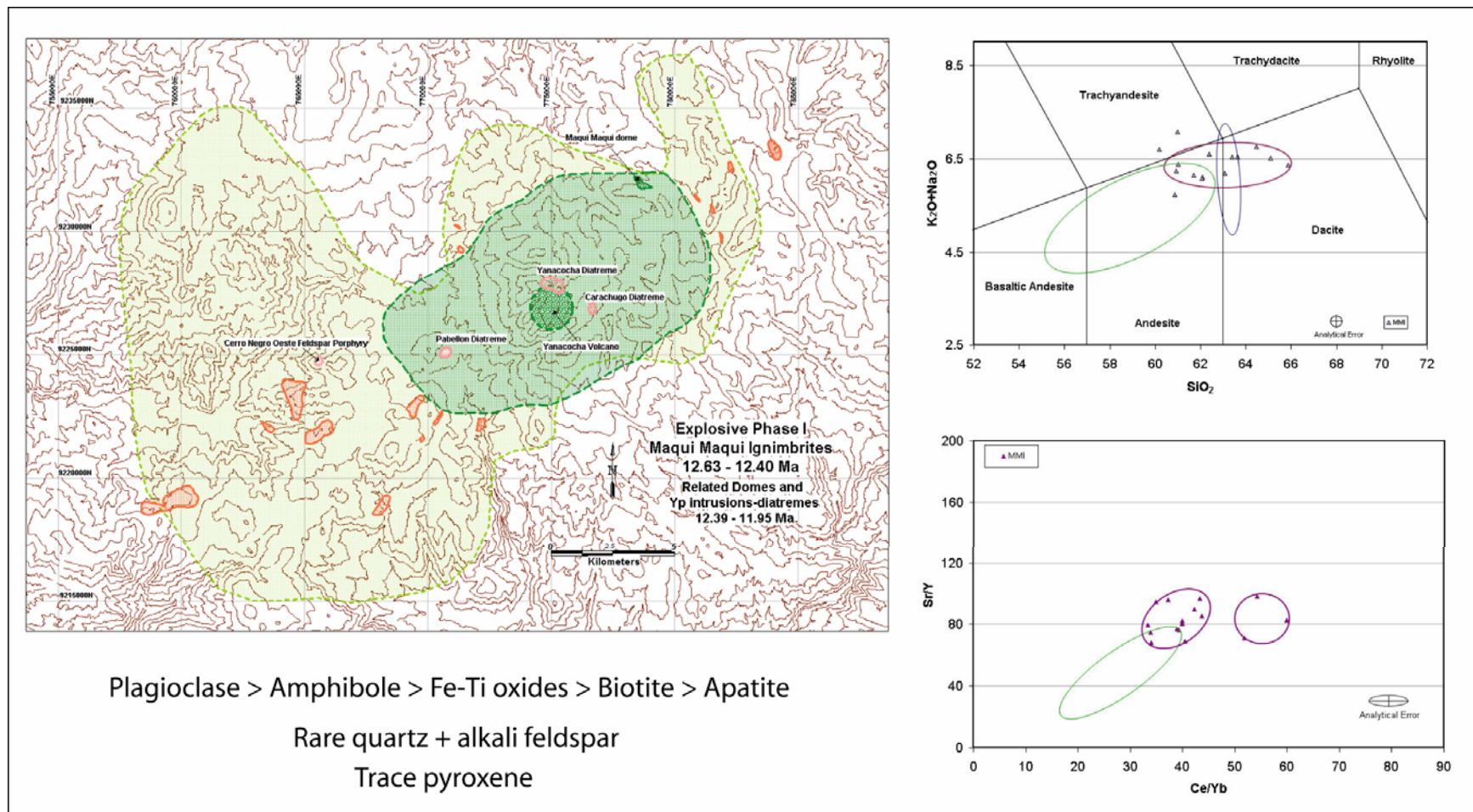
Figure 4.72 Chemical variations and phenocryst mineralogy of Explosive Phase I from 12.6 to 12.4 Ma. Rocks include the Maqui Maqui ignimbrite (green) and related domes and intrusions of the Yanacocha Volcanic Field.
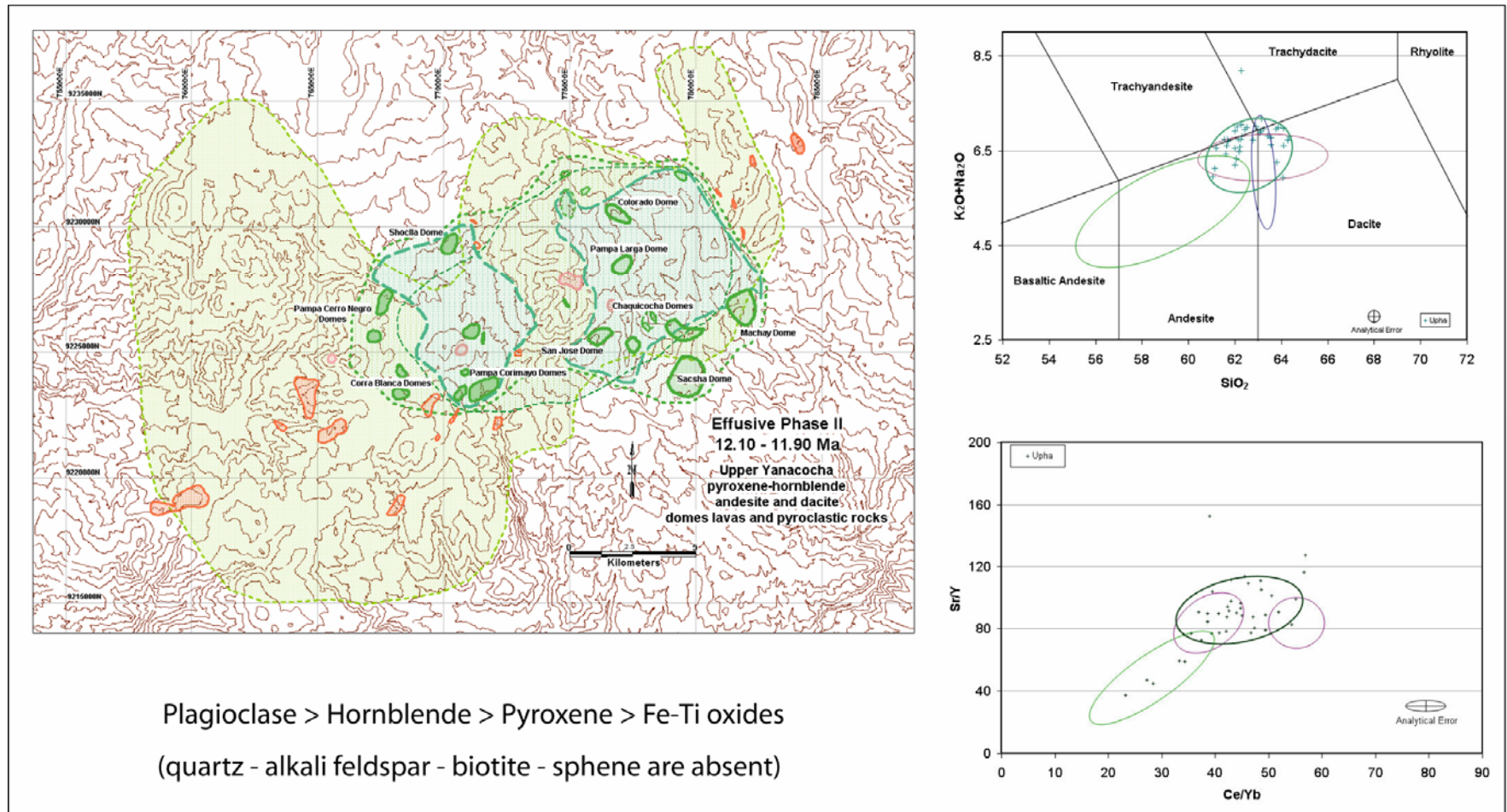
Figure 4.73 Chemical variations and phenocryst mineralogy of Effusive Phase II from 12.1 to 11.9 Ma. Rocks include the Upper Yanacocha pyroxene-hornblende andesite and dacite domes, lavas, and pyroclastic rocks (green) that belong to the Yanacocha Volcanic Field.
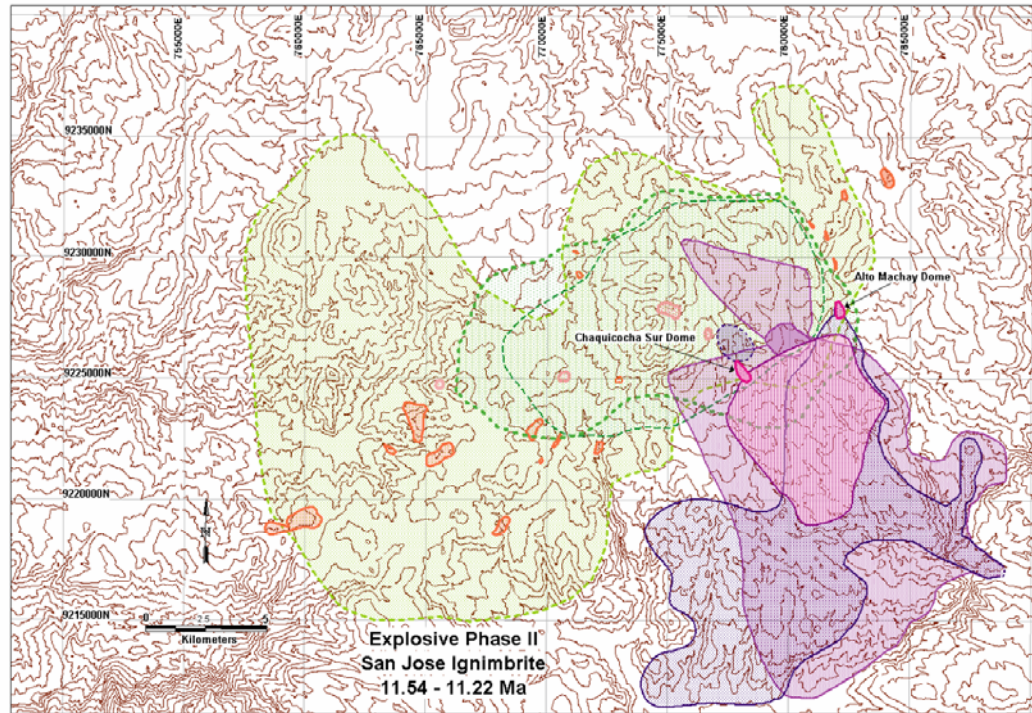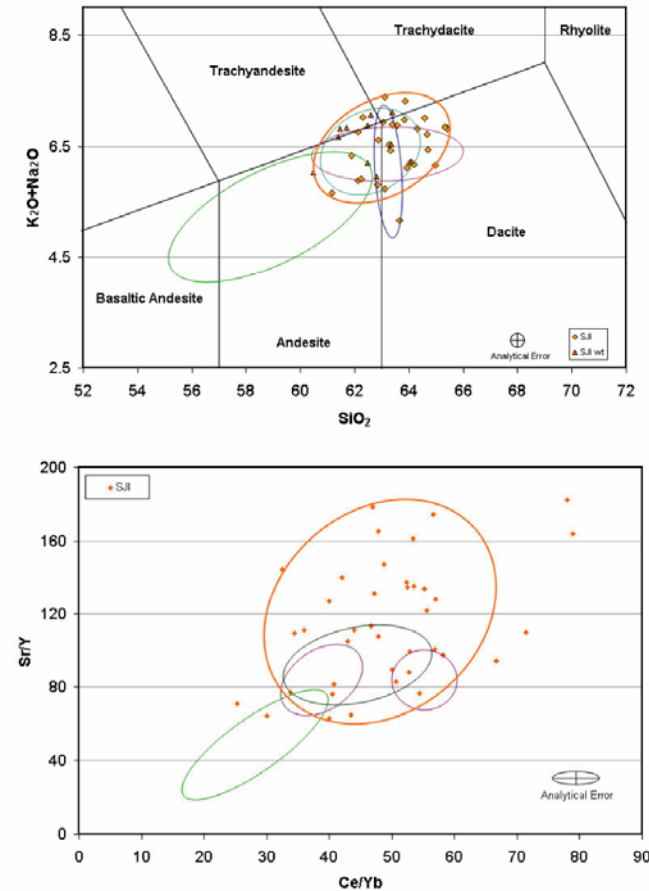
Figure 4.74 Chemical variations and phenocryst mineralogy of Explosive Phase II from 11.5 to 11.2 Ma. Rocks include ash-flow tuffs of the upper member (Usji), the middle member (Msji), and the lower member (Lsji) of the San Jose ignimbrite sequence (various shades of purple) and their location in the Yanacocha Volcanic Field.
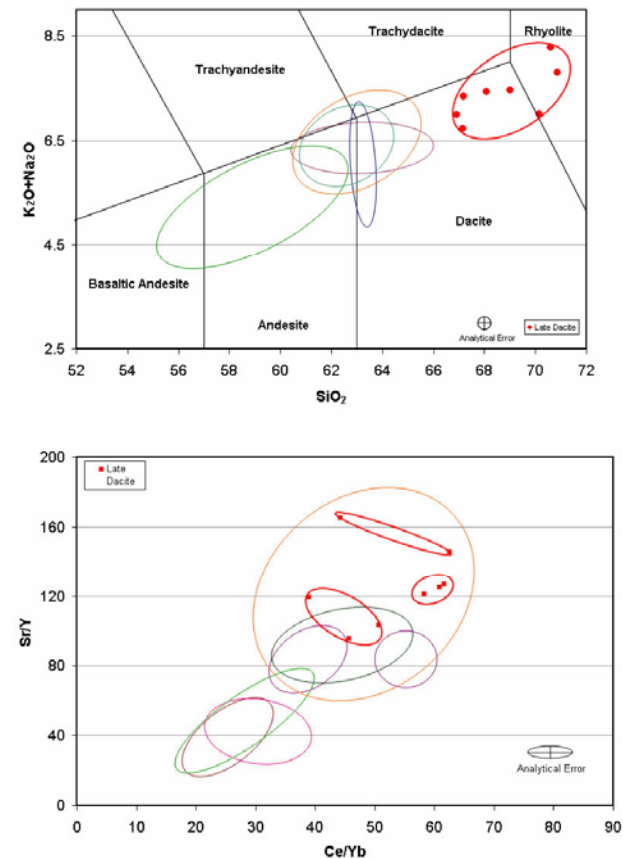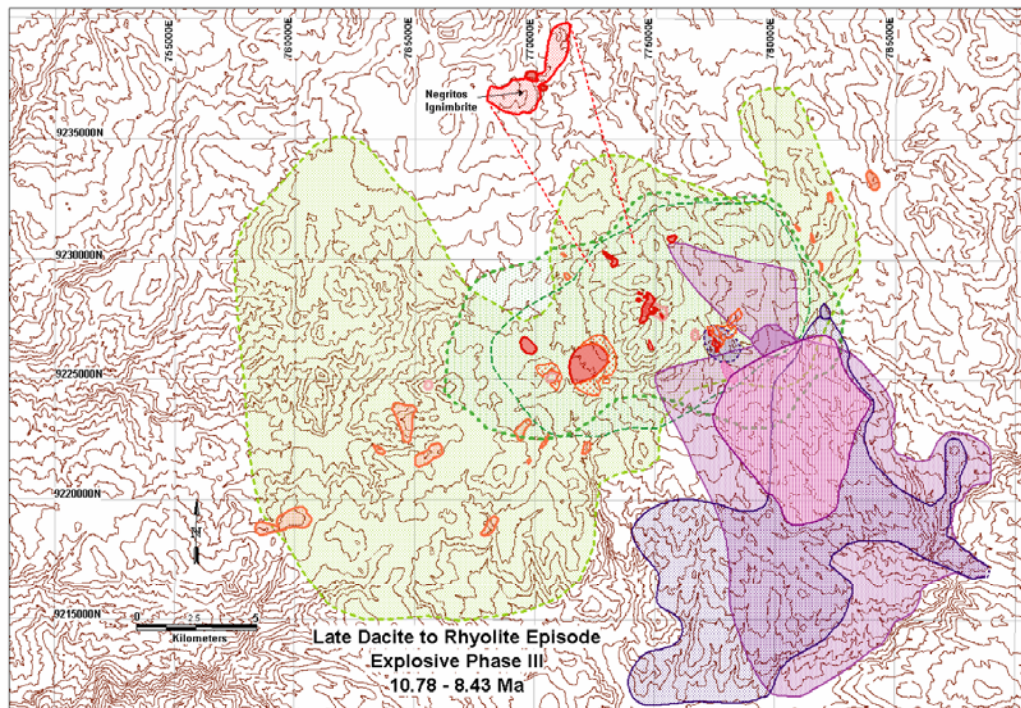
Figure 4.75 Chemical variations and phenocryst mineralogy of the late dacite to rhyolite episode and Explosive Phase III from 10.8 to 8.4 Ma. Rocks include late dacite intrusions (central area in red) from Corimayo, Cerros Yanacocha, Chaquicocha Sur, and Chaupiloma, and the Negritos ignimbrite (Top). Their locations are show in red in the Yanacocha Volcanic Field.

Conclusions

Petrologic Model for the Yanacocha Volcanic Field

Rock sequences at Yanacocha have distinct phenocryst mineralogy and modes, chemical compositions, $^{40}Ar/^{39}Ar$ ages, and field relationships that are characteristic and provide evidence that suggests dynamic multicomponent processes were involved in their evolution. Compositional variations presented in this study distinguish each rock sequence. Yanacocha magmas may have followed diverse pathways that include complex thermal-magmatic histories and interactions that involve a multicomponent and multiprocess evolution. A subvolcanic batholith evolved below Yanacocha from ponding of ascending mafic magmas and assimilation of deep crust (~20 km) within the Yanacocha structural corridor (Figure 4.76A). Dimensions of the batholith may be reflected in the shape of the Lower Yanacocha andesite (Lpha) volcanic field (~15-20 km northeast and ~10 km northwest) (Figure 4.72). Discrete magma batches were intruded at shallow crustal levels and evolved through mixing, crustal assimilation, and fractional crystallization. The resulting subvolcanic and volcanic magmatic system developed a thick and monotonous sequence of pyroxene-hornblende andesite that represent effusive eruptions that spanned 15 km across the Yanacocha district over an area of ~ 340 km^2. Explosive ignimbrite-forming eruptions of the Maqui Maqui ignimbrite (MMI) and the San Jose ignimbrite (SJI) were restricted to the east district and coexisted with effusive volcanism. Late stage dacite intrusions were centrally located and spatially associated with the largest ore bodies centered at Cerro Yanacocha, Corimayo, and Chaquicocha. These spatial, temporal, and compositional differences indicate a complex magma system was present below Yanacocha (Figure 4.76).

Shallow magma batches that ascended from a deeper batholith, possibly located at ~15 to 20 km, evolved via assimilation and fractional crystallization (AFC). By ~14.5 Ma, mafic magma from the batholith mixed with the pre-existing crustal magmas of andesite composition initiating eruptions of the Lower Yanacocha pyroxene andesite (Lpha). High-Al amphiboles, that trend toward pargasite, and plagioclase display textures characteristic of heating and dissolution, and may represent minerals from the deeper

batholith. Magmatism migrated east through time across Yanacocha until ~ 13.3 Ma, and effusive stage I eruptions of the Lpha covered most of the Yanacocha district. Shallow-level dacite intrusions and quartz-bearing andesite domes intruded the Lpha, and have similar trace element compositions. The rare earth element fractionation patterns are typical of crustal compositions. Multicomponent processes attributed to the evolution of these rocks are supported by the amphibole chemistry and phenocryst mineralogy as discussed in this study.

Volcanism ended in the west district and became centered in the east district below Cerro Yanacocha with eruptions of the Maqui Maqui ignimbrite that coexisted with continued effusive eruptions of pyroxene andesite at Cerro Yanacocha. High-level crustal magma chambers developed and mixed with deeper fractionated andesite magmas that lacked pyroxene, but carried high-Al amphiboles. Zoned amphiboles with low-Al rims and high-Al cores crystallized as the magma continued to evolve in the shallow reservoirs. The deeper andesite magmas were recharged by mafic magmas from the deep subvolcanic batholith, and effusive eruptions of andesite with deep Lpha compositions continued at Cerro Yanacocha coexisting with explosive stage I eruptions of the Maqui Maqui ignimbrite (MMI) (Figure 4.76B). Compositions in the batholith may have also evolved by AFC, plutons may have mixed, and portions of the batholith became less mafic through time.

After eruptions of the MMI, district-wide volcanism again flared up with effusive activity of the Upper Yanacocha andesite and dacite sequence (Upha) from Cerro Negro to Sugares. Pre-existing andesite magmas from the Lpha were reheated and mixed with mafic and intermediate magmas containing high-Al amphiboles and pyroxene from the batholith. The reservoir homogenized and first erupted pyroxene-hornblende andesite lavas with increased Sr but similar SiO_2 contents as Lpha. The magma continued to differentiate by plagioclase fractionation, assimilation, and mixing. As activity continued, Upha compositions evolved to dacite, and SiO_2 contents increased with increases in Sr and LREE relative to HREE and Y. Pyroxene-hornblende dacite domes erupted in the east district.

Volcanism ended in the west, and high-level magma reservoirs developed in the east district that erupted the San Jose ignimbrite (explosive stage II) with three distinct compositions from at least two separate magma reservoirs (Figure 4.76D); Lower San Jose (Lsji), Upper San Jose (Usji), and Middle San Jose (Msji). Deeper andesite magmas from the Upha mixed with shallow magma that intruded the volcanic pile. A high-level magma erupted ignimbrites that lack pyroxene (Msji) and contains low-Al amphiboles that display minor dissolution textures and rare sieve-rimmed plagioclase. A second magma composition erupted early ignimbrites (Lsji) with pyroxene, low-Al amphibole, and sieve-rimmed plagioclase, and then erupted later spatter ignimbrites increased pyroxene and two varieties of amphibole phenocrysts (coexisting high-Al and low-Al). Petrologic evidence discussed in thus study suggests that these eruptions were spontaneous as a result of heating by magma mixing. Rutherford and Devine (2003) provide evidence that recent eruptions at Soufrière Hills Volcano in Montserrat occurred within ~30 days of the heating. Amphiboles and plagioclase in the spatter ignimbrite display dissolution textures that suggest heating from magma mixing. The increased mafic component of the spatter ignimbrite may represent mixing with magmas sourced from deeper levels in the Upha plutons versus higher levels as represented by the upper conduit to the Msji reservoir (Figure 4.76D). During this period, shallow magma chambers may have continued to evolve directly below Cerro Yanacocha.

The San Jose phase of volcanism ended and magmatic activity then became centered below Cerro Yanacocha and the isolated intrusions of Late Dacite porphyry plugs evolved at shallow levels in the YVF volcanic pile. Late dacites intruded both the Lpha and MMI at Cerro Yanacocha and Chaquicocha, and domes were extruded atop Upha lava flows at Corimayo. These magmas may have assimilated some early YVF rocks. Compositions are depleted in LREE and HREE relative to other YVF rocks, and LREE/MREE and MREE/HREE fractionation is anomalous and stronger that may reflect melts from mafic source areas (ie. older mafic plutonic roots of the early Yanacocha system containing high-Al amphibole) (Figure 4.67). Late Dacites that intruded Lpha and MMI at Cerro Yanacocha, Chaquicocha, and domes at Corimayo may have assimilated

some early YVF rocks and show compositions similar to the YVF volcanic rocks (three
samples on Figure 4.43b fall in the field for YVF).
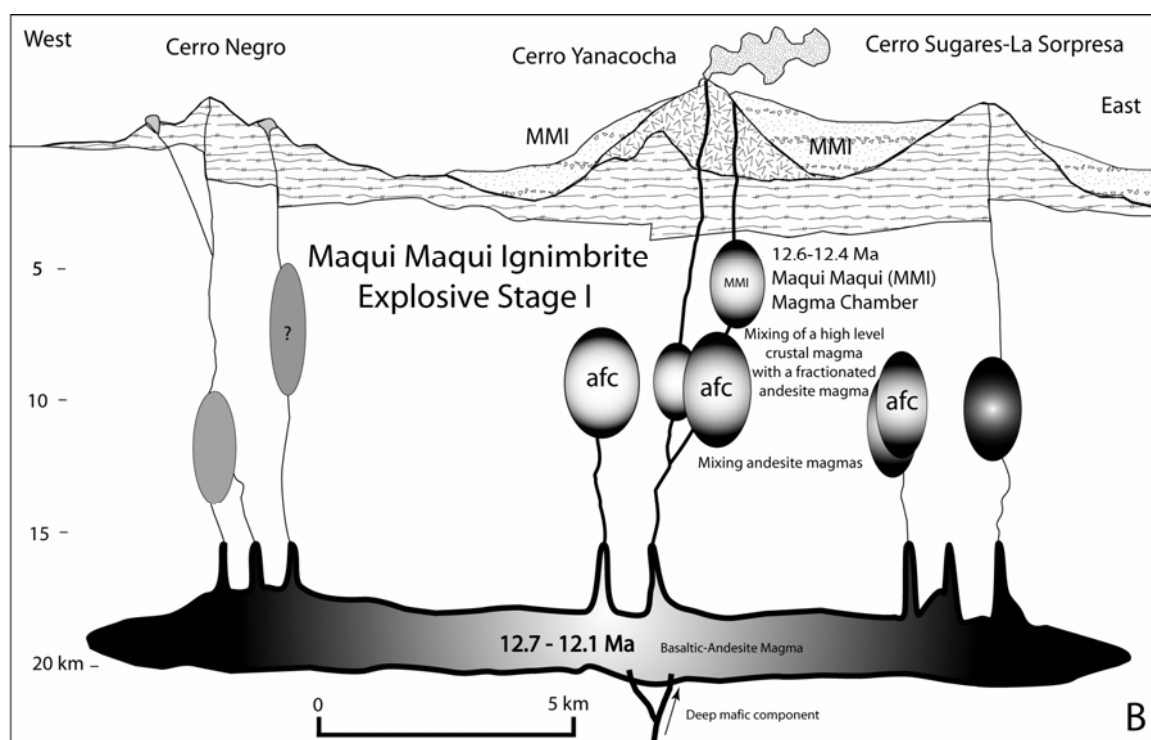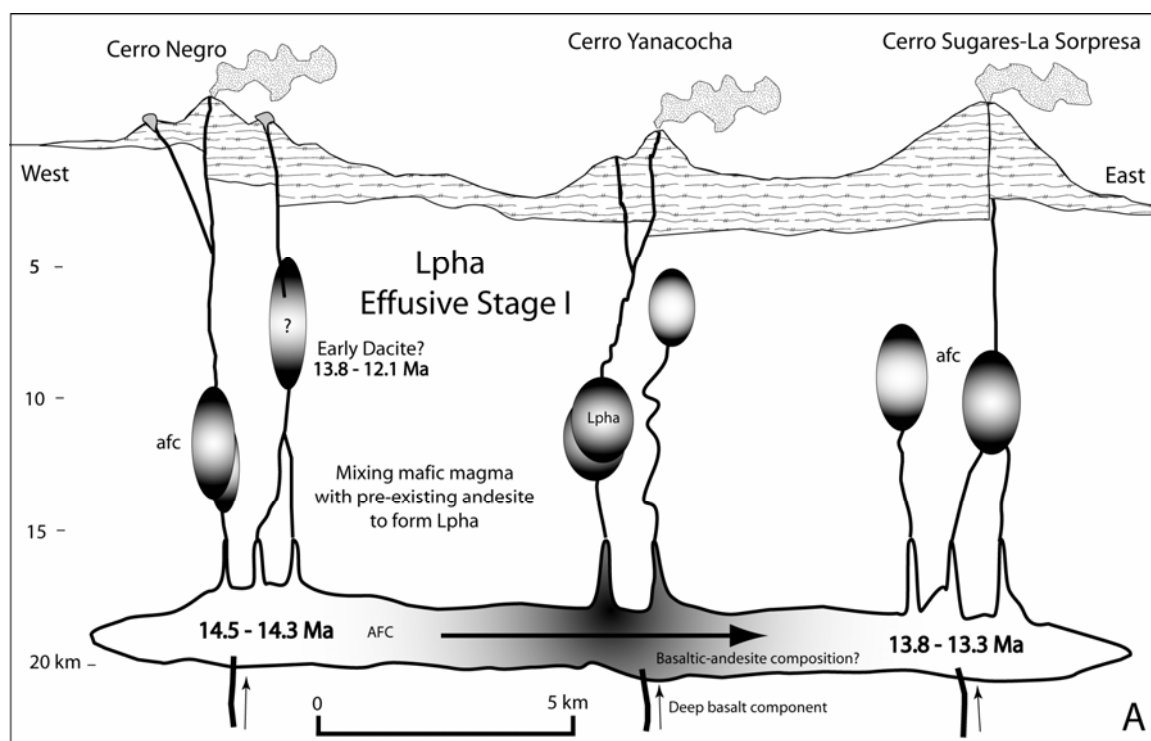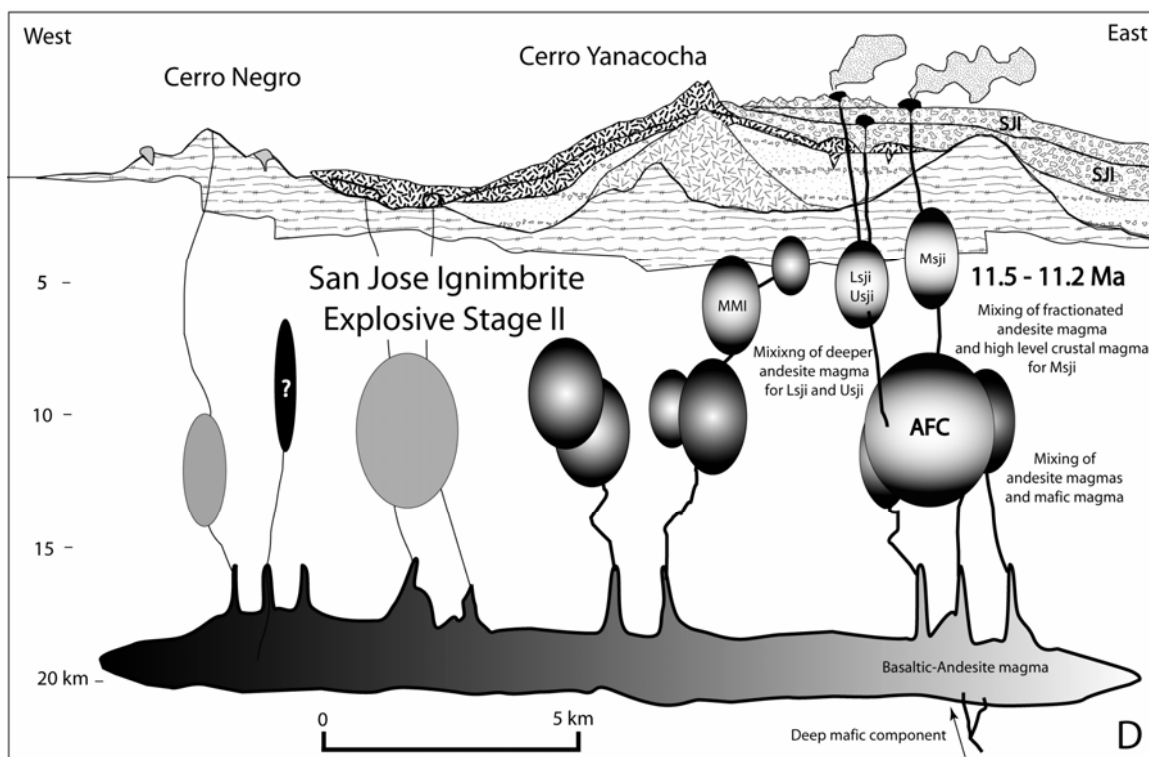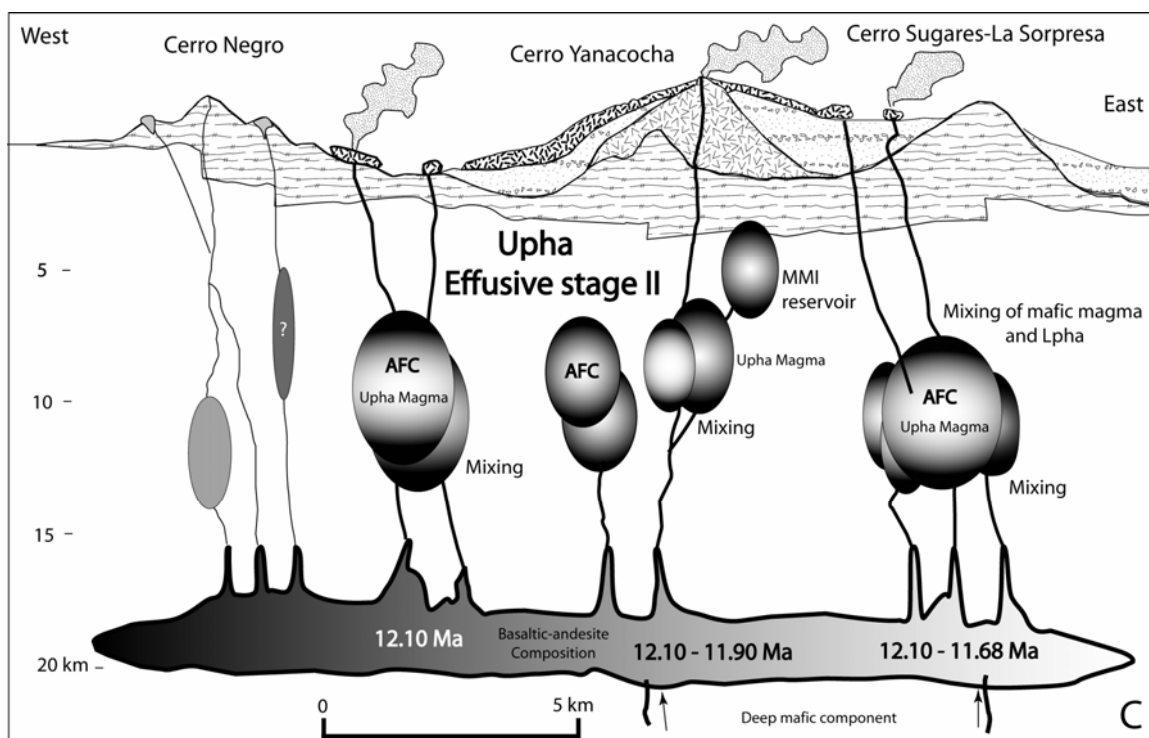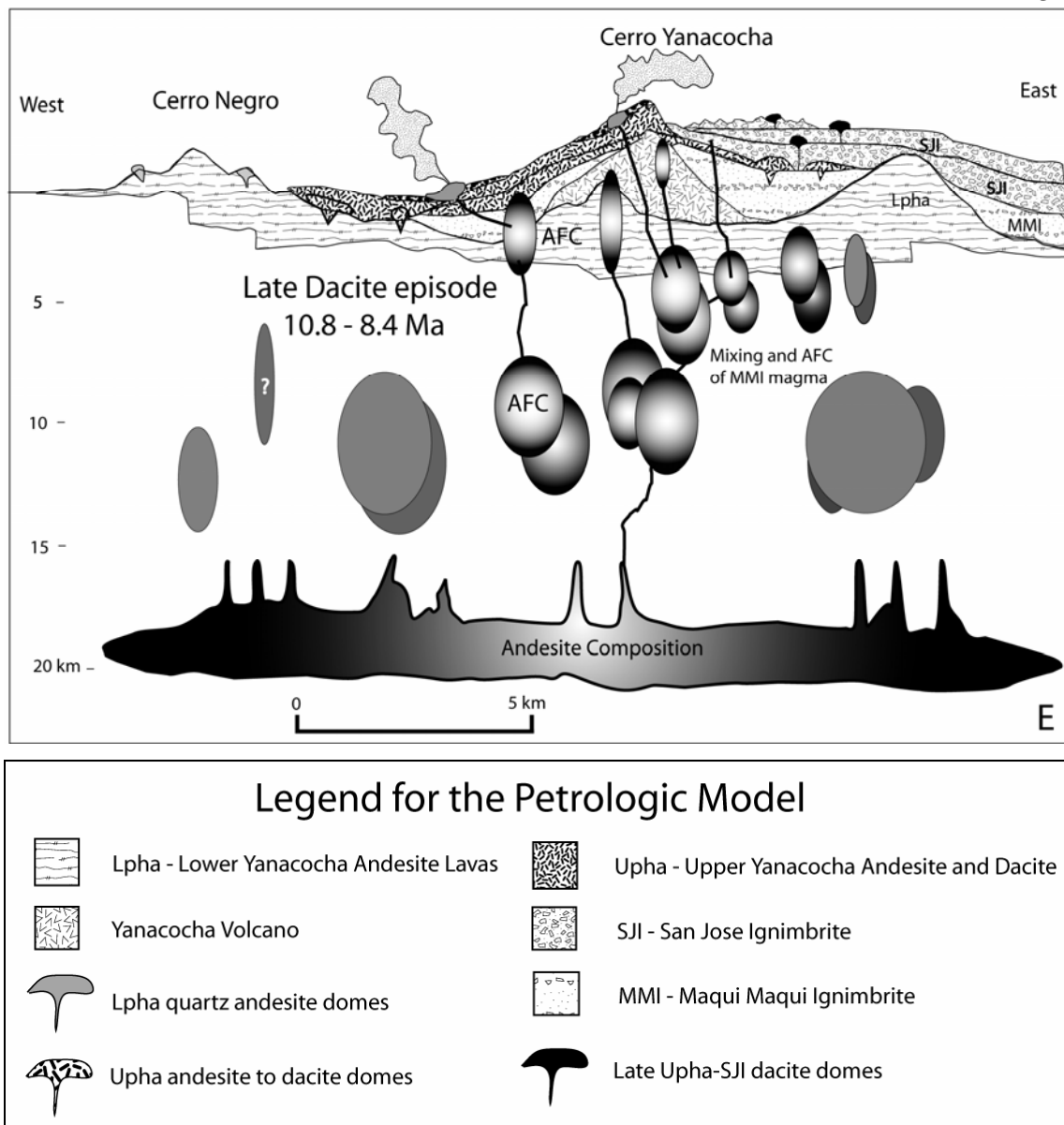
Figure 4.76a-e Petrologic model that describes the temporal and spatial evolution of the Yanacocha magmatic system. Crustal depths below Yanacocha may extend to a maximum depth of 35 km (Gutscher, 1999). Estimated depths in kilometers (km) are referenced on the left margin in figures A-E above, and the vertical scale of the geologic section is highly exaggerated and schematic. (A) Early deep basaltic intrusions ponded and a subvolcanic batholith developed; mafic magmas evolved by AFC and mixing in the deep crust. By ~14.5 Ma, eruptions of the Lpha in the west district from small intrusions of andesite mixing with mafic magma from the batholith. Magmatism migrated east through time across Yanacocha until ~ 13.3 Ma.

Figure 4.76 (continued) (B) Volcanism ended in the west district and became centered in the east district below Cerro Yanacocha. High-level crustal magma chambers developed and mixed with deeper fractionated andesite magmas that are recharged by mafic magmas from the deep subvolcanic batholith. Effusive eruptions of andesite with deep Lpha compositions continued at Cerro Yanacocha and coexisted with explosive stage I eruptions of the MMI from the shallow reservoir. (C) After eruptions of the MMI, district-wide volcanism again flared up with effusive activity of the Upha. Pre-existing andesite magmas from the Lpha mixed with mafic and intermediate magmas from the batholith. (D) Volcanism ended in the west, and high-level magma reservoirs developed in the east district that erupted the San Jose ignimbrite (explosive stage II) in phases from at least two separate reservoirs. Shallow magma was intruded into the volcanic pile and mixed with andesite magmas from different depths and degrees of fractionation. (E) Magmatic activity then became centered below Cerro Yanacocha and the isolated intrusions of Upper (late) Dacite porphyry plugs evolved at shallow levels in the YVF volcanic pile. Late dacites intruded Lpha and MMI at Cerro Yanacocha and Chaquicocha, and domes were extruded atop Upha at Corimayo. These magmas may have assimilated some early YVF rocks.

Summary

Cenozoic volcanism in the Yanacocha study area spanned 11.2 million years from 19.5 to 8.4 Ma and hydrothermal alteration continued 5.4 million years from 13.5 to 8.2 Ma. Volcanism in the Yanacocha Volcanic Field (YVF) was centered at the Yanacocha Mining District for 6.1 million years from 14.5 to 8.4 Ma and the magma evolved from andesite to rhyolite with compositional variations in the geochemical data that typify a calc-alkaline rock suite. Five periods of magmatic activity and volcanism and six discrete pulses of hydrothermal activity have been interpreted from the volcanic stratigraphy and age data. Two episodic effusive to explosive eruptive events are recorded in YVF stratigraphy and include the Lower Yanacocha lavas (effusive stage 1) and Maqui Maqui Ignimbrite (explosive stage 1) followed by the Upper Yanacocha lavas (effusive stage 2) and the San Jose Ignimbrite (explosive stage 2). Volcanism at Yanacocha ended in a final explosive event with the eruption of the Negritos rhyolite ignimbrite at 8.4 Ma (explosive stage 3). Eruptive-styles of the YVF fluctuated from effusive-dominant clinopyroxene + orthopyroxene + hornblende bearing lavas to explosive-dominant hornblende + biotite ± clinopyroxene bearing ignimbrites.

Distinct geochemistry and mineralogy characterize each volcanic sequence and support the stratigraphy as outlined in the study. Mineral assemblages are distinct for

each rock sequence. The pre-Yanacocha andesite lahars contain plagioclase, clinopyroxene, orthopyroxene and hornblende, whereas the the Cerro Frailes dacite pyroclastic rocks contain coarse biotite, plagioclase, sanidine, quartz and hornblende. In contrast, Yanacocha rocks from the YVF are typically phenocryst-rich and range from 25-55% total phenocrysts in lavas, 30-60% phenocyrsts in dome rocks, and 40% to over 70% phenocrysts in the ignimbrites. Lpha and Upha lavas contain abundant plagioclase with clinopyroxene + orthopyroxene + hornblende, whereas ash-flow tuffs of the MMI and SJI contain abundant broken plagioclase with hornblende + biotite ± clinopyroxene. Late dacites and rhyolites at Yanacocha have quartz + biotite + hornblende + magnetite + sphene implying relatively high oxygen fugacities (Wones, 1989).

Compositional variations in the geochemical data typify a subduction-related calc-alkaline rock suite. Melts evolved by crustal contamination and fractional crystallization though time (Thorpe et al., 1980; Rogers and Hawkesworth, 1989). The major element oxide data form a trend from older medium-K andesite to younger high-K andesite, high- K dacite, and rhyolite. Trace elements display enrichments in the LIL's and depletions in the HREE with increased SiO_2 content over time and support the hypothesis that Yanacocha evolved as part of a greater calc-alkaline rock suite.

YVF effusive-style eruptions were generated from crustal magma reservoirs possibly located at ~20 km depth in a crust with thicknesses estimated at 35 km (Gutscher et al., 1999, 2000). Magma from the earlier effusive event was stored in the upper crustal reservoirs as shallow as 3 km and later erupted explosively as ignimbrites. YVF melts may have fractionated and assimilated crust over a span of 6 million years. Late magmas were dacite and rhyolite and carry an adakite-like signature as displayed by the Sr/Y ratio whose compositional variations are part of the larger calc-alkaline suite. This latest felsic episode contains the mineral assemblage quartz-magnetite-sphene characteristic of highly oxidized magmas and developed porphyritic domes and intrusions of isolated dacite porphyry plugs spatially and temporally associated with the largest ore deposits at Yanacocha.

Combined processes of crystal-liquid fractionation, magma mixing, and muticomponent crustal assimilation are suggested for the evolution of the Yanacocha

rock suite, and YVF melts differentiated in the crust over a span of 6 million years. Patterns can be recognized in the data that imply that discrete magma batches coexisted and evolved separately. These compositions may have followed different evolutionary trends that involved crustal assimilation and mixing of end member deep mafic magmas with shallow crustal, pre-existing andesite and dacite magma. Yanacocha may have evolved from discrete magma batches at different levels and sites in the crust. These magmas erupted rock sequences with different mineral and chemical compositions periodically through time as outlined in this study.

Table 4.1 Summary of Geochemical Results: Representative Samples

Weight %	LAL DN-84	Cerro Frailes-1	Lpha CNN-1	Upha CHQS-2	Maqui Maqui DN-7	San Jose Ignimbrite CB-56	Late Dacite YN-1A
SiO_2	59.33	64.96	61.48	63.07	63.07	63.86	68.09
TiO_2	0.62	0.50	0.67	0.59	0.58	0.56	0.40
Al_2O_3	18.90	17.17	17.67	18.09	18.21	18.87	16.72
Fe_2O_3	5.54	5.24	5.61	4.31	4.47	3.88	2.55
MnO	0.08	0.11	0.10	0.06	0.10	0.03	0.05
MgO	0.43	1.60	2.38	1.28	0.85	0.47	0.58
CaO	8.55	4.89	5.98	5.28	6.15	4.54	3.85
Na_2O	4.01	2.72	3.81	4.60	4.05	5.05	4.33
K_2O	2.16	2.48	1.89	2.28	2.14	2.27	3.10
P_2O5	0.26	0.16	0.24	0.23	0.22	0.25	0.16
BaO	0.08	0.10	0.06	0.08	0.05	0.13	0.06
SrO	0.07	0.07	0.09	0.12	0.11	0.09	0.12
Cr_2O_3	<0.01	<0.01	0.01	<0.01	0.01	<0.01	0.00
Total	100.03	100.00	100.00	100.00	100.00	100.00	100.00
Na_2O+K_2O	**6.17**	**5.20**	**5.70**	**6.88**	**6.19**	**7.32**	**7.43**

ppm							
Ba	624	959	681	776	591	758	677
Co	9.3	9.5	13.0	7.5	8.0	6.7	3.5
Cr	70	nd	nd	nd	nd	40.0	nd
Cs	2.8	2.2	0.9	1.0	1.8	10.3	7.6
Cu	17	20	25	<5	20	13	<5
Ga	21	20	21	23	22	25	23
Hf	4	3	3	3	3	3	3
Mo	3	nd	nd	nd	nd	2	nd
Nb	7	7	4	5	6	5	4
Ni	<5	15	15	<5	5	6	<5
Pb	10	20	30	10	5	13	25
Rb	62.4	76.8	50	50.8	58.2	69.9	80
Sn	1	1	<1	<1	1	1	<1
Sr	632	612	737	888	888	1035	729
Ta	0.5	0.5	<0.5	<0.5	<0.5	<0.5	<0.5
Th	6	5	4	6	5	5	7
Tl	<0.5	<0.5	0.5	<0.5	<0.5	<1	<0.5
U	1.6	4	1.5	1.5	1.5	1.8	2.5
V	111	85	135	10	80	107	10
W	1	1	<1	<1	3	1	<1
Y	14.2	11.5	15	8	13	8.1	5
Zn	80	65	70	75	60	99	215
Zr	114	102.5	116.5	126	131.5	112.5	111.5
La	19.2	18.5	21	24.5	20.5	20.7	20
Ce	38	35	41.5	48.5	37.5	39.9	37.5
Pr	4.5	4.1	5.2	5.8	5	4.8	4.2
Nd	17.8	16	21	21.5	19.5	18	15.5
Sm	3.2	3.2	4.0	3.9	3.3	3	2.7
Eu	1.1	0.7	1.2	1	0.9	0.9	0.7
Gd	3.1	2.7	3.4	3.0	2.9	2.4	2.1
Tb	0.5	0.4	0.5	0.4	0.4	0.3	0.3
Dy	2.6	2.3	2.9	2.2	2.3	1.6	1.3
Ho	0.5	0.4	0.5	0.3	0.4	0.3	0.2
Er	1.4	1.3	1.4	1.0	1.4	0.8	0.6
Tm	0.2	0.1	0.2	0.1	0.1	0.1	0.1
Yb	1.3	1.3	1.5	1.0	1.1	0.7	0.6
Lu	0.2	0.2	0.2	0.1	0.1	0.1	0.1
Sr/Y	**44.5**	**53.2**	**49.1**	**111.0**	**68.3**	**127.8**	**145.8**
Ce/Yb	**29.2**	**26.9**	**27.7**	**48.5**	**34.1**	**57.0**	**62.5**

Table 4.1a Geochemistry: Lower Andesite Lahar and Cerro Frailes

Weight %	LAL			Cerro Frailes			
	DE-18	DN-84	CC-18	CB-35	DN-12	DN-71	FRAIL-1
SiO_2	58.80	59.33	61.18	63.13	61.75	65.30	64.96
TiO_2	0.74	0.62	0.82	0.68	0.64	0.52	0.50
Al_2O_3	19.11	18.90	20.02	19.36	17.89	17.10	17.17
Fe_2O_3	6.42	5.54	5.45	7.28	6.22	5.04	5.24
MnO	0.15	0.08	0.08	0.06	0.08	0.15	0.11
MgO	2.79	0.43	2.01	0.75	1.44	1.02	1.60
CaO	6.68	8.55	6.26	3.98	5.46	5.49	4.89
Na_2O	2.15	4.01	2.92	2.57	3.24	2.73	2.72
K_2O	2.74	2.16	0.90	1.94	2.90	2.33	2.48
P_2O_5	0.28	0.26	0.25	0.13	0.23	0.18	0.16
BaO	0.05	0.08	0.04	0.06	0.05	0.08	0.10
SrO	0.08	0.07	0.06	0.07	0.07	0.05	0.07
Cr_2O_3	<0.01	<0.01	<0.01	<0.01	0.01	<0.01	<0.01
Total	100.00	100.03	100.00	100.00	100.00	99.99	100.00
Na_2O+K_2O	4.88	6.17	3.82	4.51	6.14	5.06	5.20
ppm							
Ba	543	624	327	586	460	728	959
Co	11	9.3	6.5	16	9.5	8	9.5
Cr	Nd	70	50	Nd	Nd	90	Nd
Cs	3.2	2.8	1.7	14.8	6.9	3.2	2.2
Cu	<5	17	35	<5	35	15	20
Ga	20	21	22	18	21	18	20
Hf	3	4	3	2	3	3	3
Mo	Nd	3	8	Nd	Nd	4	nd
Nb	3	7	7	5	6	7	7
Ni	<5	<5	10	<5	5	5	15
Pb	<5	10	10	<5	10	10	20
Rb	75.2	62.4	41.6	97	91.4	79.3	76.8
Sn	<1	1	2	<1	1	<1	1
Sr	591	632	667	530	546	439	612
Ta	<0.5	0.5	0.5	<0.5	<0.5	0.6	0.5
Th	5	6	5	6	6	7	5
Tl	<0.5	<0.5	<0.5	<0.5	<0.5	<1	<0.5
U	1	1.6	1.5	2	1.5	3.2	4
V	150	111	160	135	95	83	85
W	<1	1	3	<1	3	1	1
Y	15.5	14.2	43	27	13	12	11.5
Zn	60	80	65	220	70	56	65
Zr	109	114	122	83	96.5	108.5	102.5
La	17	19.2	25	16.5	21	18	18.5
Ce	34.5	38	36.5	38	35	34	35
Pr	4.4	4.5	5.3	5.2	4.5	4	4.1
Nd	17	17.8	20	22.5	16.5	15.3	16
Sm	3.7	3.2	4.8	5.5	3.7	3	3.2
Eu	0.9	1.1	1.4	1.4	0.9	0.9	0.7
Gd	3.3	3.1	4.9	5.5	3	3	2.7
Tb	0.5	0.5	0.8	0.8	0.5	0.4	0.4
Dy	2.6	2.6	5.8	4.4	2.2	2.2	2.3
Ho	0.5	0.5	1.3	0.9	0.5	0.4	0.4
Er	1.5	1.4	4.3	2.6	1.2	1.3	1.3
Tm	0.2	0.2	0.7	0.4	0.1	0.5	0.1
Yb	1.2	1.3	4.6	2.6	1.3	1.4	1.3
Lu	0.2	0.2	0.9	0.4	0.2	0.2	0.2
Sr/Y	38.1	44.5	15.5	19.6	42.0	36.6	53.2
Ce/Yb	28.8	29.2	7.9	14.6	26.9	24.3	26.9

Table 4.1b Geochemistry: Lower Yanacocha Pyroxene-hornblende Andesite

Weight %	Lower Yanacocha Pyroxene-hornblende Andesite (Lpha)						
	Atazaico	DO-43	CNN-1	CR-3	AZU-1	CB-4	CB-5
SiO_2	59.99	58.19	61.48	61.85	61.85	61.34	63.88
TiO_2	0.67	0.77	0.67	0.61	0.66	0.68	0.61
Al_2O_3	18.57	18.38	17.67	17.49	18.47	18.44	16.84
Fe_2O_3	6.08	6.75	5.61	5.62	4.95	6.97	6.19
MnO	0.12	0.17	0.10	0.15	0.07	0.14	0.11
MgO	2.62	3.01	2.38	2.11	1.14	1.81	2.53
CaO	6.32	7.02	5.98	5.88	5.60	3.85	4.83
Na_2O	3.57	3.68	3.81	3.68	4.64	4.12	2.87
K_2O	1.66	1.61	1.89	2.22	2.13	2.21	1.78
P_2O5	0.25	0.27	0.24	0.25	0.29	0.30	0.24
BaO	0.03	0.06	0.06	0.05	0.07	0.07	0.07
SrO	0.08	0.08	0.09	0.08	0.13	0.07	0.06
Cr_2O_3	0.02	<0.01	0.01	<0.01	<0.01	<0.01	<0.01
Total	100.00	99.99	100.00	100.00	100.00	100.00	100.00
Na_2O+K_2O	**5.24**	**5.29**	**5.70**	**5.91**	**6.77**	**6.33**	**4.65**
ppm							
Ba	550	479	681	608	779.0	742.0	528.0
Co	11.5	14.6	13	13	9.0	11.5	10.0
Cr	Nd	30	Nd	Nd	nd	nd	90.0
Cs	1.2	1.6	0.9	2.9	0.8	1.9	1.8
Cu	15	29	25	<5	10.0	<5.0	35.0
Ga	21	22	21	20	23.0	18.0	18.0
Hf	3	3	3	3	4.0	3.0	2.0
Mo	nd	2	nd	nd	nd	nd	6.0
Nb	4	6	4	6	4.0	4.0	6.0
Ni	15	8	15	5	5	<5	10
Pb	20	6	30	10	30	<5	5
Rb	42.8	41.1	50	56.8	46	58.2	65
Sn	1	1	<1	<1	1	<1	1
Sr	660	741	737	598	963	534	557
Ta	<0.5	0.5	<0.5	0.5	<0.5	<0.5	<0.5
Th	4	5	4	7	5	5	3
Tl	<0.5	<1	0.5	<0.5	<0.5	<0.5	<0.5
U	1	1.6	1.5	2	1	0.5	1
V	140	158	135	60	120	145	135
W	<1	<1	<1	<1	1	<1	3
Y	15.5	15	15	13.5	15	16	14
Zn	85	85	70	120	70	50	45
Zr	181	108	116.5	87.5	130.5	101.5	98.5
La	20.5	19.4	21	26	27.5	21	24
Ce	40	37.7	41.5	52.5	56.5	39.5	34
Pr	5	4.8	5.2	5.9	6.7	5.1	4.7
Nd	20.5	18.8	21	21.5	27	19	18
Sm	4	3.7	4	4.4	4.7	3.7	3.4
Eu	1.1	1.1	1.2	1.2	1.2	1	1
Gd	3.6	3.3	3.4	3.8	4.1	3.7	3.3
Tb	0.5	0.5	0.5	0.6	0.5	0.6	0.4
Dy	3.3	2.7	2.9	3.3	3.2	2.6	2.6
Ho	0.6	0.6	0.5	0.6	0.6	0.5	0.5
Er	1.6	1.6	1.4	1.6	1.6	1.7	1.5
Tm	0.3	0.5	0.2	0.2	0.3	0.2	0.2
Yb	1.7	1.5	1.5	1.7	1.7	1.4	1.5
Lu	0.3	0.3	0.2	0.3	0.2	0.2	0.2
Sr/Y	**42.6**	**49.4**	**49.1**	**44.3**	**64.2**	**33.4**	**39.8**
Ce/Yb	**23.5**	**25.1**	**27.7**	**30.9**	**33.2**	**28.2**	**22.7**

Table 4.1c Geochemistry: Upper Yanacocha Pyroxene-hornblende Andesite

Weight%	Upper Yanacocha Pyroxene-hornblende Andesite (Upha)								
	AZU-2	CB-3	CB-65	CHQS-1	CHQS-2	COR-7 178m	DE-2	DO-60	DN-83
SiO_2	62.20	64.32	63.56	64.27	63.07	62.50	62.43	61.54	61.14
TiO_2	0.66	0.57	0.60	0.61	0.59	0.61	0.64	0.66	0.65
Al_2O_3	18.12	18.13	19.23	19.77	18.09	17.75	18.14	18.29	19.17
Fe_2O_3	4.72	4.42	4.08	3.93	4.31	4.29	4.89	4.76	4.77
MnO	0.07	0.05	0.05	0.05	0.06	0.12	0.06	0.07	0.08
MgO	1.71	0.91	0.92	0.24	1.28	1.94	1.33	1.76	1.85
CaO	5.49	4.37	4.56	3.95	5.28	5.36	5.10	5.73	5.72
Na_2O	4.48	4.27	4.35	4.38	4.60	4.62	4.66	4.67	4.26
K_2O	2.10	2.53	2.28	2.35	2.28	2.37	2.29	2.07	1.87
P_2O_5	0.26	0.23	0.15	0.24	0.23	0.24	0.25	0.26	0.27
BaO	0.06	0.08	0.10	0.08	0.08	0.08	0.06	0.09	0.08
SrO	0.12	0.11	0.11	0.11	0.12	0.11	0.15	0.11	0.12
Cr_2O_3	<0.01	<0.01	<0.01	<0.01	<0.01	<0.01	<0.01	<0.01	<0.01
Total	100.00	100.00	99.99	100.00	100.00	99.99	100.00	100.01	99.98
Na_2O+K_2O	6.58	6.80	6.63	6.73	6.88	6.99	6.95	6.74	6.13
ppm									
Ba	792	904	807	830	776	708	808	724	643
Co	8.5	6.5	6.2	5.5	7.5	9.4	10.0	10.9	9.9
Cr	nd	nd	40	nd	nd	50	nd	40	40
Cs	0.7	1.2	4.9	1.2	1.0	1.4	0.5	1.0	7.8
Cu	15	<5	22	5	<5	19	25	26	28
Ga	22	21	25	22	23	23	24	24	23
Hf	4	3	4	4	3	4	3	4	4
Mo	nd	nd	3	nd	nd	2	nd	2	3
Nb	4	3	6	4	5	6	6	5	6
Ni	5	<5	5	5	<5	11	15	9	5
Pb	45	<5	12	15	10	10	15	11	21
Rb	51.4	59.8	60.4	58.2	50.8	62.4	48.2	53.3	150
Sn	1	<1	1	1	<1	1	1	1	1
Sr	928	828	945	876	888	961	1045	966	1070
Ta	<0.5	<0.5	<0.5	<0.5	<0.5	<0.5	<0.5	<0.5	<0.5
Th	5	5	6	5	6	5	4	4	5
Tl	<0.5	<0.5	<1	<0.5	<0.5	<1	<0.5	<1	<1
U	1	1.5	1.7	1.5	1.5	2.2	1.5	1.6	1.6
V	115	125	99	95	10	148	105	128	109
W	1	<1	<1	1	<1	<1	1	1	2
Y	9.5	10	12.2	10	8	10.2	9	13.3	10.3
Zn	60	45	77	60	75	79	95	89	85
Zr	133.5	111.5	141	142.5	126	118	124	128	119
La	20.5	21.5	22.4	22.5	24.5	21.4	26.5	24.5	21.3
Ce	43.0	38	40.7	47	48.5	42.3	51	44.8	43.4
Pr	4.8	5.1	5	5.1	5.8	5.4	6.1	6.1	5.3
Nd	19.0	18.5	18.4	21.0	21.5	21.1	23	23.6	20.3
Sm	3.3	3.6	3.3	3.9	3.9	3.7	3.7	4.3	3.6
Eu	1.1	0.8	0.9	0.9	1	1	0.9	1.1	1.1
Gd	3.2	2.7	2.7	3	3	2.9	3.1	3.6	3.2
Tb	0.4	0.4	0.4	0.4	0.4	0.4	0.4	0.4	0.4
Dy	2.2	1.8	1.8	2.3	2.2	1.9	2	2.3	2
Ho	0.4	0.3	0.4	0.4	0.3	0.4	0.3	0.5	0.4
Er	1.1	0.9	1.1	1.0	1.0	1.1	0.8	1.3	1.1
Tm	0.1	0.1	0.5	0.1	0.1	0.5	0.1	0.5	0.5
Yb	1	0.7	1	1	1	1	0.9	1.2	1.1
Lu	0.1	0.1	0.2	0.1	0.1	0.1	0.1	0.2	0.1
Sr/Y	97.7	82.8	77.5	87.6	111.0	94.2	116.1	72.6	103.9
Ce/Yb	43.0	54.3	40.7	47.0	48.5	42.3	56.7	37.3	39.5

Table 4.1d Geochemistry: Maqui Maqui Rocks

Weight %	Maqui Maqui Rocks							
	Pyroclastic Rocks					Porphyritic Rocks		
	DN-7	DN-30	DN-85*	MM-342 156-170m	DN-52	YS-370 46-48m	DN-77	SLT-02 68.0m
SiO$_2$	63.07	61.00	62.39	65.09	64.48	63.64	61.58	63.79
TiO$_2$	0.58	0.62	0.63	0.58	0.60	0.62	0.65	0.75
Al$_2$O$_3$	18.21	19.29	18.34	17.37	19.33	17.92	17.84	19.05
Fe$_2$O$_3$	4.47	5.17	5.56	4.74	3.74	4.87	5.05	4.61
MnO	0.10	0.06	0.14	0.05	0.02	0.13	0.10	0.04
MgO	0.85	1.18	1.77	0.81	0.20	0.84	2.34	0.67
CaO	6.15	5.15	4.14	4.33	4.43	5.01	5.20	4.40
Na$_2$O	4.05	3.83	2.78	4.24	4.30	4.11	4.35	4.35
K$_2$O	2.14	3.25	3.82	2.27	2.45	2.43	2.40	1.91
P$_2$O$_5$	0.22	0.27	0.27	0.25	0.22	0.25	0.26	0.22
BaO	0.05	0.05	0.10	0.12	0.11	0.09	0.10	0.10
SrO	0.11	0.11	0.06	0.13	0.13	0.09	0.11	0.11
Cr$_2$O$_3$	0.01	<0.01	<0.01	0.01	<0.01	<0.01	<0.01	0.01
Total	100.00	100.00	100.01	100.00	100.00	100.00	99.98	100.02
Na$_2$O+K$_2$O	6.19	7.08	6.60	6.51	6.76	6.54	6.75	6.26
ppm								
Ba	591	572	687	740	1025	715	842	857
Co	8	7.5	9.8	7.5	4	11.2	12.8	7.6
Cr	nd	nd	40	nd	nd	90	60	20
Cs	1.8	0.8	0.8	4.7	1.6	0.9	1.1	0.7
Cu	20	<5	18	25	<5	25	30	16
Ga	22	22	23	22	23	22	23	24
Hf	3	3	3	3	3	4	4	4
Mo	nd	nd	<2	nd	nd	3	2	<2
Nb	6	3	7	5	3	6	6	6
Ni	5	<5	7	15	<5	6	10	10
Pb	5	<5	11	35	<5	12	25	13
Rb	58.2	79.8	81.2	60	61.2	57.7	57.8	25.6
Sn	1	<1	1	1	<1	1	<1	1
Sr	888	785	728	872	935	814	967	888
Ta	<0.5	<0.5	0.5	<0.5	<0.5	<0.5	<0.5	<0.5
Th	5	4	5	3	5	5	5	4
Tl	<0.5	<0.5	<0.5	<0.5	<0.5	<1	<1	<0.5
U	1.5	1.5	2	1.5	1.5	1.8	1.6	1.3
V	80	120	106	85	115	116	124	107
W	3	<1	1	1	<1	3	1	1
Y	13	9.5	9.7	9	13.5	10.6	10.9	11
Zn	60	95	124	115	75	94	79	92
Zr	131.5	94	107	106	127	118	118	120.5
La	20.5	19	17.2	19.5	23.5	21.9	20.2	22.1
Ce	37.5	36	33.9	39	44.5	43.2	39.9	47.3
Pr	5.0	4.3	4.2	4.9	5.4	5.2	4.9	5.4
Nd	19.5	16	16.8	18.5	20.5	19.4	18.2	20.6
Sm	3.3	2.8	3.1	3.5	3.8	3.6	3.4	3.7
Eu	0.9	0.8	0.8	0.8	0.9	1	1	1
Gd	2.9	2.5	2.5	2.6	3.5	3.1	3	3.1
Tb	0.4	0.3	0.3	0.4	0.4	0.4	0.4	0.4
Dy	2.3	1.6	1.7	2	2.2	1.9	1.9	2
Ho	0.4	0.3	0.3	0.4	0.4	0.4	0.4	0.4
Er	1.4	0.8	1	0.9	1.3	1.1	1.1	1.1
Tm	0.1	0.1	0.1	0.1	0.1	0.5	0.1	0.1
Yb	1.1	0.6	1	0.9	1.1	1.1	1	1
Lu	0.1	0.1	0.1	0.1	0.1	0.2	0.1	0.1
Sr/Y	68.3	82.6	75.1	96.9	69.3	76.8	88.7	80.7
Ce/Yb	34.1	60.0	33.9	43.3	40.5	39.3	39.9	47.3

*Pumice of DN-30

Table 4.1e Geochemistry: San Jose Ignimbrite Sequence

Weight %	San Jose Ignimbrite Sequence					
	CB-44	VC-4	BS-3	RC-6	CB-56	CB-38
SiO_2	63.55	64.05	62.13	62.85	63.86	63.27
TiO_2	0.56	0.70	0.59	0.69	0.56	0.62
Al_2O_3	18.38	20.53	18.52	19.54	18.87	19.53
Fe_2O_3	3.81	2.80	4.66	4.51	3.88	4.44
MnO	0.06	0.05	0.09	0.03	0.03	0.06
MgO	1.35	0.38	1.39	0.84	0.47	0.49
CaO	5.01	4.90	5.39	5.31	4.54	4.58
Na_2O	4.63	4.33	4.76	4.23	5.05	4.50
K_2O	2.24	1.87	2.00	1.58	2.27	2.03
P_2O_5	0.19	0.17	0.24	0.19	0.25	0.27
BaO	0.12	0.05	0.07	0.06	0.13	0.08
SrO	0.09	0.16	0.14	0.16	0.09	0.13
Cr_2O_3	<0.01	<0.01	<0.01	<0.01	<0.01	0.01
Total	99.99	100.00	99.98	99.99	100.00	100.01
Na_2O+K_2O	**6.87**	**6.20**	**6.76**	**5.81**	**7.32**	**6.53**
ppm						
Ba	825	585	780	652	758	760
Co	7.8	5	9.5	7	6.7	7.5
Cr	50.0	nd	nd	nd	40.0	nd
Cs	2.8	19.9	1.8	3.9	10.3	2.2
Cu	12	<5	<5	5	13	60
Ga	24	25	24	25	25	26
Hf	4	3	3	3	3	3
Mo	2	nd	nd	nd	2	nd
Nb	6	4	4	4	5	5
Ni	8	<5	20	<5	6	5
Pb	12	5	20	5	13	15
Rb	51.9	64.4	54.4	37.6	69.9	59.8
Sn	1	<1	1	<1	1	1
Sr	979	1050	1155	1070	1035	1040
Ta	<0.5	<0.5	<0.5	<0.5	<0.5	<0.5
Th	6	4	4	4	5	5
Tl	<1	<0.5	<0.5	<0.5	<1	<0.5
U	2.0	1.5	1	1.5	1.8	1.5
V	108	60	110	50	107	85
W	1	<1	<1	<1	1	1
Y	9.1	7.5	9.5	6	8.1	13.5
Zn	82	60	80	65	99	110
Zr	132.5	99.5	216	117.5	112.5	136.5
La	22.9	19.5	21.5	20.5	20.7	24
Ce	43.1	42	44.5	37.5	39.9	44
Pr	5.0	5.1	5.1	4.7	4.8	6
Nd	18.2	20	20.5	18.5	18	23
Sm	3.2	4.1	3.7	3.2	3	3.8
Eu	0.9	1.1	1	1	0.9	1.1
Gd	2.6	3.2	2.6	2.4	2.4	3.1
Tb	0.3	0.4	0.4	0.3	0.3	0.4
Dy	1.5	2.1	2.1	1.6	1.6	2.5
Ho	0.3	0.4	0.3	0.3	0.3	0.5
Er	0.9	1	1	0.8	0.8	1.3
Tm	0.1	0.1	0.1	0.1	0.1	0.1
Yb	0.9	1	0.8	0.8	0.7	1.3
Lu	0.1	0.1	0.1	0.1	0.1	0.1
Sr/Y	**77.0**	**140.0**	**121.6**	**178.3**	**127.8**	**107.6**
Ce/Yb	**33.8**	**42.0**	**55.6**	**46.9**	**57.0**	**47.9**

Table 4.1f Geochemistry: Late Dacite

| Weight % | Late Dacite | | | |
| | Corimayo-Yanacocha Dacite | | | Negritos Ignimbrite |
	COR-1	YN-1A	DNS-1	NG-5
SiO_2	67.14	68.09	70.58	70.86
TiO_2	0.47	0.40	0.30	0.24
Al_2O_3	18.11	16.72	15.89	16.53
Fe_2O_3	3.37	2.55	1.76	1.44
MnO	0.12	0.05	0.04	0.03
MgO	0.83	0.58	0.51	0.24
CaO	2.96	3.85	2.36	2.57
Na_2O	3.92	4.33	5.04	4.54
K_2O	2.80	3.10	3.23	3.26
P_2O_5	0.06	0.16	0.09	0.08
BaO	0.09	0.06	0.10	0.08
SrO	0.10	0.12	0.09	0.11
Cr_2O_3	0.01	0.00	0.00	0.00
Total	100.00	100.00	100.00	100.00
Na_2O+K_2O	**6.73**	**7.43**	**8.28**	**7.80**
ppm				
Ba	992	677	847	892
Co	9.5	3.5	1.5	3
Cr	Nd	Nd	Nd	50
Cs	3.1	7.6	6.3	4.6
Cu	30	<5	<5	345
Ga	24	23	23	22
Hf	3	3	3	3
Mo	nd	Nd	nd	6
Nb	5	4	4	4
Ni	15	<5	<5	5
Pb	25	25	25	20
Rb	92.4	80	91.4	137.5
Sn	1	<1	<1	1
Sr	762	729	743	788
Ta	<0.5	<0.5	<0.5	<0.5
Th	4	7	7	6
Tl	0.5	<0.5	0.5	<0.5
U	2.5	2.5	3	3.5
V	60	10	<5	35
W	1	<1	<1	3
Y	6	5	4.5	6.5
Zn	140	215	40	50
Zr	127	111.5	91.5	118.5
La	20	20	15.5	23
Ce	37	37.5	26.5	35
Pr	4.4	4.2	3	4.7
Nd	16	15.5	10.5	16.5
Sm	2.6	2.7	2	3
Eu	0.7	0.7	0.5	0.7
Gd	2.2	2.1	1.5	2.2
Tb	0.3	0.3	0.2	0.3
Dy	1.4	1.3	1	1.2
Ho	0.2	0.2	0.1	0.2
Er	0.6	0.6	0.5	0.7
Tm	0.1	0.1	0.1	0.1
Yb	0.6	0.6	0.6	0.6
Lu	0.1	0.1	0.1	0.1
Sr/Y	**127.0**	**145.8**	**165.1**	**121.2**
Ce/Yb	**61.7**	**62.5**	**44.2**	**58.3**

Table 4.2 Range of geochemical data discussed in the text for the Yanacocha rocks.

Volcanic Sequences (#samples)	(La/Yb)$_N$	(La/Sm)$_N$	(Gd/Yb)$_N$	Ce/Yb	Sr/Y	Ba (ppm)	Sr (ppm)	Rb (ppm)	Y (ppm)	SiO$_2$ wt%	MgO wt %
LAL (18)	3.9-16.4	2.3-4.1	1.6-2.8	7.9-39.1	15.5-51.3 (2)>68	277-883	473-849	22.8-90.2	9.5-43	57.0-64.5	1.3-3.2
Cerro Frailes (28)	9.1-17.4	3.5-5.1	1.5-2.7	14.6-40	19.6-59.0 (4)>80	264-2090	331-997	37.6-134.5	6-19.5	60.6-68.7	0.28-2.25
Lpha (18)	3.1-18.1	3.0-3.9	1.8-2.9	17.6-50.6	33.3-89.9	479-873	544-989	33.4-76.0	9.5-28.5	58-62	1.14-3.44
MMI (16)	10.9-22.4	3.0-4.2	2.0-3.4	33.3-60.0	68.3-98.4	552-1025	728-1045	34.5-89.4	9.0-13.0	60.2-66.3	0.81-2.12
Upha (31)	12.2-21.6	3.4-4.7	2.0-3.1	23.2-56.9 (7)<40	37.3-152.7 (4)<60 (2)>112	616-1120	842-1145	35.1-150.0	7.5-27.1	61.1-64.8	0.3-2.20
SJI (40)	10.2-28.3	2.9-4.9	1.5-3.9	30.0-78.9 (6)<40	63.0-182.4	457-1050	853-1165	20.8-87.8	5.0-16.5	61.0-65.4	0.22-1.55
Late Dacite (2)	18.3-18.6	3.8-4.8	2.0-2.7	44.2-50.6	103.4-165.1	847.0-914.0	743-879	79-91.4	4.5-8.5	66.9-70.9	0.2-0.7
Intrusions											
Pyroxene Andesites (11)	7.8-20.1	3.3-4.1	1.5-2.8	20.0-45.6	24.5-113.5	486-914	466-1135	45.4-90.4	9.5-19.0	55.3-63.06	1.44-3.63
Early Dacite (5)	10.6-11.1	3.3-4.1	1.9-2.6	19.5-53.3	12.8-90.6	470-998	398-997	48.6-71.2	11.0-31.0	63.2-63.7	1.71-3.02
Yanacocha Yp (1)	12.4	4.3	2.0	36.0	85.6	647.0	848.0	54.6	9.9	62.4	0.7
Late pyroxene andesite/dacite (8)	9.6-21.8	2.8-4.5	1.9-3.1	28.3-56.7	44.8-116.1	792-904	828-1045	45.1-60.4	9.0-21.5	62.0-64.3	0.23-1.71
Late dacite (6)	14.2-27.2	3.9-5.4	2.0-3.2	38.8-62.5	95.5-145.8	677-992	688-895	78.8-137.5	5.0-8.0	66.9-70.6	0.49-0.83

N = chondrite normalized REE fractionation ratios+

Table 4.3a. Representative microprobe analyses: Amphibole from the Upha-SJI domes with comparisons of the rim and the core for each phenocryst.

Label	CB3-1.1	CB3-1.2	DE2-2.1	DE2-2.2	CHQS1-1.6	CHQS1-1.7	AZU1A-3.1	AZU1A-3.2
Position	Rim	Core	Resorbed Rim	Core	Rim	Rim	Rim	Core
Location	Alto Machay	Alto Machay	Ocucho	Ocucho	Chaquicocha Sur	Chaquicocha Sur	Ocucho	Ocucho
SiO_2	47.87	46.67	43.97	44.54	42.36	42.58	43.02	42.88
TiO_2	1.75	1.77	1.94	1.89	1.93	1.97	1.69	1.56
Al_2O_3	7.41	7.64	12.09	11.90	12.99	12.89	12.54	12.83
Cr_2O_3	0.00	0.01	0.00	0.09	0.00	0.03	0.02	0.01
FeO	6.35	5.76	11.07	6.34	9.68	10.42	6.96	2.97
Fe_2O_3	4.25	6.40	-0.97	3.51	2.16	2.28	2.34	6.75
MnO	0.33	0.41	0.08	0.08	0.11	0.12	0.14	0.13
MgO	16.33	15.92	16.41	16.42	14.45	14.36	16.78	16.45
CaO	11.22	11.09	11.45	11.63	11.36	11.48	11.96	11.74
Na_2O	1.73	1.68	2.70	2.41	2.83	2.56	2.63	2.56
K_2O	0.61	0.76	0.69	0.73	0.86	0.85	0.52	0.53
H_2O	1.84	1.81	0.99	1.66	1.52	1.41	1.41	1.87
F	0.43	0.45	2.40	0.96	1.16	1.43	1.47	0.43
Cl	0.13	0.15	0.03	0.01	0.03	0.03	0.02	0.03
O=F	0.18	0.19	1.01	0.40	0.49	0.60	0.62	0.18
O=Cl	0.03	0.03	0.01	0.00	0.01	0.01	0.00	0.01
Total	100.06	100.32	101.84	100.79	100.95	101.83	100.89	100.54
Al-IV	1.16	1.27	1.64	1.53	1.81	1.72	1.82	1.84
Al-VI	0.09	0.03	0.42	0.51	0.43	0.52	0.31	0.34
Al Total	1.25	1.30	2.06	2.04	2.24	2.24	2.12	2.18
(Na+K)a	0.59	0.61	0.88	0.82	0.96	0.89	0.83	0.81
Na+K+Al/4	0.46	0.48	0.74	0.71	0.80	0.78	0.74	0.75
Fe/Fe+Mg	0.26	0.29	0.26	0.24	0.31	0.33	0.23	0.24

Table 4.3b. Representative Microprobe Analyses: Amphibole from the Lpha and Upha lavas with comparisons of the rim and the core for each phenocryst.

	Yanacocha Volcanic Sequence							
Label	Co Atazaico.area 3.1	Co Atazaico.area 3.2	AZU-1A.area 2.1	AZU-1A.area 2.2	DO43-3.2	DO43-3.1	DO60-6.2	DO60-6.3
Position	Core	Rim	Rim	Core	Rim	Core	Rim	Core
Sequence	Lpha west	Lpha west	Lpha east	Lpha east	Lpha west	Lpha west	Upha west	Upha west
SiO$_2$	42.63	43.43	43.64	42.94	42.79	41.94	42.57	43.76
TiO$_2$	1.85	1.90	1.61	1.68	2.43	1.95	1.87	1.50
Al$_2$O$_3$	12.14	11.82	11.83	12.43	11.05	13.47	12.21	11.57
Cr$_2$O$_3$	0.20	0.14	0.32	0.00	0.00	0.03	0.02	0.73
FeO	2.89	2.17	11.87	4.12	10.35	7.29	5.38	2.37
Fe$_2$O$_3$	7.17	8.16	-4.25	5.02	2.11	4.37	4.18	5.52
MnO	0.18	0.08	0.09	0.11	0.19	0.09	0.09	0.10
MgO	16.13	16.26	17.24	16.92	14.64	14.77	16.74	17.28
CaO	11.23	11.23	11.57	11.41	11.33	12.01	11.99	11.77
Na$_2$O	2.34	2.24	2.74	2.57	2.78	2.50	2.46	2.32
K$_2$O	0.56	0.54	0.60	0.55	0.57	0.59	0.58	0.59
H$_2$O	1.80	1.92	0.80	1.55	1.46	1.73	1.58	2.00
F	0.53	0.29	2.76	1.14	1.23	0.70	1.05	0.14
Cl	0.00	0.03	0.02	0.02	0.08	0.04	0.03	0.01
O=F	0.22	0.12	1.16	0.48	0.52	0.29	0.44	0.06
O=Cl	0.00	0.01	0.00	0.00	0.02	0.01	0.01	0.00
Total	99.44	100.11	99.73	99.98	100.48	101.19	100.30	99.71
Al-IV	1.94	1.79	1.87	1.91	1.77	1.86	1.90	1.78
Al-VI	0.09	0.20	0.09	0.17	0.13	0.47	0.17	0.15
Al Total	2.03	1.99	1.96	2.08	1.90	2.33	2.06	1.94
(Na+K)a	0.74	0.72	0.85	0.81	0.89	0.82	0.79	0.75
Na+K+Al/4	0.69	0.68	0.70	0.72	0.70	0.79	0.71	0.67
Fe/Fe+Mg	0.25	0.25	0.21	0.22	0.32	0.30	0.23	0.19

Table 4.3c. Representative microprobe analyses: Amphibole from the San Jose ignimbrite with comparisons of the rim and the core for each phenocryst.

	San Jose Ignimbrite					
Label	**DE36-1.1**	**DE36-1.2**	**BS-28.2.1**	**BS-28.2.2**	**VC1-1.1**	**VC1-1.2**
Position	Rim	Core	Rim	Core	Core	Rim
Type	Upper spatter Ignimbrite	Upper spatter Ignimbrite	Upper spatter Ignimbrite	Upper spatter Ignimbrite	Upper SJI white tuff	Upper SJI white tuff
SiO_2	42.32	41.83	42.65	41.44	48.36	48.18
TiO_2	2.13	2.37	2.16	2.15	1.64	1.55
Al_2O_3	12.84	12.69	10.97	11.70	6.55	7.16
Cr_2O_3	0.00	0.01	0.03	0.00	0.00	0.00
FeO	8.35	9.05	9.57	8.89	7.38	5.68
Fe_2O_3	4.72	5.04	4.49	6.11	6.10	6.73
MnO	0.06	0.13	0.38	0.35	0.48	0.31
MgO	13.97	13.04	13.58	13.11	15.44	16.31
CaO	12.04	11.90	11.22	11.09	11.22	11.38
Na_2O	2.23	2.16	2.39	2.37	1.33	1.43
K_2O	0.67	0.73	0.74	0.70	0.61	0.68
H_2O	1.81	1.88	1.64	1.62	1.81	1.86
F	0.51	0.31	0.77	0.81	0.50	0.42
Cl	0.03	0.04	0.10	0.08	0.14	0.14
O=F	0.22	0.13	0.33	0.34	0.21	0.18
O=Cl	0.01	0.01	0.02	0.02	0.03	0.03
Total	101.48	101.02	100.36	100.06	101.32	101.64
Al-IV	1.74	1.80	1.74	1.93	0.95	0.98
Al-VI	0.50	0.42	0.15	0.09	0.18	0.25
Al Total	2.24	2.22	1.90	2.02	1.13	1.23
(Na+K)a	0.77	0.76	0.82	0.80	0.49	0.53
Na+K+Al/4	0.75	0.74	0.68	0.71	0.40	0.44
Fe/Fe+Mg	0.34	0.37	0.36	0.38	0.32	0.29

Table 4.3d. Representative microprobe analyses: Amphibole from the San Jose and Maqui Maqui ignimbrite with comparisons of the rim and the core for each phenocryst.

	San Jose Ignimbrite					Maqui Maqui Ignimbrite	
Label	CB38-4.4	CB56-1.1	CB56-1.2	CB44-1.1	CB44-1.3	DN-7.1.4	DN-7.1.5
Position	Rim	Rim	Core	Rim	Core	Rim	Core
Type	Middle SJI	Lower SJI	Lower SJI	Lower SJI	Lower SJI	Eutaxitic Ignimbrite Yanacocha Norte	
SiO_2	44.35	47.50	47.08	46.14	45.42	47.11	45.67
TiO_2	1.77	1.70	1.73	1.77	1.84	1.49	1.77
Al_2O_3	9.67	6.82	7.06	8.58	8.65	7.60	8.63
Cr_2O_3	0.00	0.03	0.00	0.01	0.00	0.00	0.00
FeO	7.58	7.55	6.98	6.02	6.39	4.81	6.12
Fe_2O_3	6.46	4.55	6.10	7.36	6.94	8.71	7.85
MnO	0.31	0.36	0.45	0.38	0.38	0.44	0.45
MgO	14.32	16.00	15.39	15.31	15.11	15.51	14.58
CaO	11.10	11.57	11.34	11.28	11.38	10.95	10.97
Na_2O	1.69	1.47	1.54	1.65	1.73	1.45	1.62
K_2O	1.13	0.61	0.63	0.93	0.94	0.56	0.65
H_2O	1.73	1.76	1.85	1.89	1.89	1.86	1.85
F	0.53	0.59	0.36	0.27	0.24	0.36	0.32
Cl	0.25	0.12	0.14	0.22	0.20	0.13	0.18
O=F	0.22	0.25	0.15	0.11	0.10	0.15	0.14
O=Cl	0.06	0.03	0.03	0.05	0.04	0.03	0.04
Total	100.60	100.36	100.46	101.66	100.97	100.78	100.49
Al-IV	1.51	1.15	1.17	1.21	1.34	1.18	1.36
Al-VI	0.16	0.01	0.03	0.28	0.16	0.11	0.12
Al Total	1.67	1.16	1.21	1.49	1.50	1.30	1.48
(Na+K)a	0.69	0.52	0.55	0.65	0.67	0.51	0.58
Na+K+Al/4	0.59	0.42	0.44	0.53	0.54	0.45	0.51
Fe/Fe+Mg	0.34	0.29	0.31	0.32	0.32	0.31	0.34

Table 4.3e. Representative microprobe analyses: Amphibole from the pre-Yanacocha rocks.

Label	DN-16. area 6.2	DN-16. area 6.3	Frial-2B.area 1.1	Frial-2B.area 1.2
Sequence	LAL	LAL	Cerro Frailes	Cerro Frailes
SiO_2	46.40	44.95	44.07	44.31
TiO_2	1.39	1.54	0.95	1.00
Al_2O_3	8.57	9.72	10.84	10.39
Cr_2O_3	0.00	0.00	0.02	0.02
FeO	2.40	4.36	7.91	7.43
Fe_2O_3	11.74	10.32	8.81	8.79
MnO	0.45	0.41	0.49	0.52
MgO	15.06	13.86	11.70	12.16
CaO	10.47	10.61	10.83	10.82
Na_2O	1.35	1.51	1.39	1.35
K_2O	0.33	0.35	0.59	0.62
H_2O	1.92	1.91	1.90	1.89
F	0.23	0.20	0.17	0.20
Cl	0.07	0.06	0.08	0.07
O=F	0.10	0.08	0.07	0.08
O=Cl	0.02	0.01	0.02	0.02
Total	100.27	99.72	99.66	99.49
Al-IV	1.34	1.54	1.58	1.57
Al-VI	0.11	0.11	0.28	0.21
Al Total	1.45	1.65	1.86	1.78
(Na+K)a	0.43	0.49	0.50	0.50
Na+K+Al/4	0.47	0.53	0.59	0.57
Fe/Fe+Mg	0.33	0.36	0.43	0.41

Table 4.4a. Representative microprobe analyses of pyroxene from the Yanacocha rocks with comparisons of the rim and the core for each phenocryst.

Clinopyroxene

Label	Lpha	Lpha	Upha	Upha	Usji Spatter	Lsji	Msji	Ocucho dome	Chaquicocha Sur Dome
Ox wt%	DO43-1.1rim	AZU1A-6.1rim	CHQS2A-2.1rim	DO60-1.2core	DE36-3.1rt core	CB44-3.2core	CB38-2.2core	DE2-6.3midway	CHQS1-3.1core
SiO_2	52.26	52.03	51.48	52.29	50.07	51.90	51.54	53.32	51.39
Al_2O_3	2.06	1.38	1.01	1.11	0.83	1.04	0.81	1.61	1.49
FeO*	8.96	7.91	7.32	7.75	7.98	8.57	7.98	8.87	8.57
MgO	16.08	15.39	15.55	15.76	16.02	15.28	15.98	14.54	15.34
MnO	0.44	0.42	0.42	0.48	0.45	0.61	0.61	0.50	0.60
TiO_2	0.41	0.29	0.22	0.33	0.16	0.16	0.16	0.17	0.22
Cr_2O_3	0.00	0.00	0.00	0.01	0.03	0.00	0.02	0.02	0.03
CaO	20.56	21.73	22.31	21.60	22.71	22.01	22.39	21.54	21.90
Na_2O	0.27	0.44	0.44	0.32	0.38	0.46	0.32	0.54	0.48
K_2O	0.01	0.01	0.00	0.00	0.00	0.00	0.00	0.00	0.00
Total	99.59	98.76	99.64	101.06	98.62	100.02	99.80	101.11	100.02
Ca/Ca+Mg+Fe	0.45	0.48	0.49	0.48	0.49	0.48	0.48	0.48	0.48
Fe/Fe+Mg	0.36	0.34	0.32	0.33	0.33	0.36	0.33	0.38	0.36
WO	40.89	44.82	44.62	43.24	44.04	43.63	43.61	43.88	43.63
EN	44.50	42.41	43.28	43.89	43.20	42.14	43.32	41.21	41.77
FS	14.61	12.78	12.11	12.87	12.76	14.22	13.07	14.91	14.60
Range									
WO	40.6-44.4	43.4-45.5	44-45.4	34.9-45.3	43-7-44.6	42.6-44.2	43.2-44.6	42.3-44.4	42.8-44.4
EN	38.9-45.4	40.4-44.0	41.3-44	40.3-44.4	42-2-43.9	41.2-43.4	39.8-43.9	41.2-43.7	41.8-43.7
FS	13.4-16.8	11.9-15.7	11.6-14.4	12.6-16.3	12.0-13.4	13-16	12.9-15.7	12.2-15.4	21.2-15.4

Wo-En-Fs components calculated after Morimoto et al. (1988)
See CD appendix VI for Wo-En-Fs components calculated after Lindsley (1983)

Table 4.4b. Representative microprobe analyses of pyroxene from the Yanacocha rocks with comparisons of the rim and the core for each phenocryst. (Continued)

Orthopyroxene

Label Ox wt%	CB38-7.2core	CB44-11.4rim	DE36-2.3rim	DE2-9.2	DO60-2.4core	AZU1A-4.3core
SiO_2	52.07	51.51	51.41	51.48	53.67	54.16
Al_2O_3	0.44	0.50	0.46	0.74	0.85	0.56
FeO*	20.02	20.42	20.42	19.61	18.05	17.54
MgO	25.99	25.33	25.50	25.22	25.31	26.59
MnO	1.20	1.45	1.18	0.93	1.01	0.78
TiO2	0.09	0.11	0.12	0.13	0.18	0.09
Cr_2O_3	0.00	0.00	0.01	0.01	0.01	0.00
CaO	0.77	0.82	0.87	1.05	1.01	0.99
Na_2O	0.01	0.01	0.02	0.02	0.03	0.00
K_2O	0.00	0.00	0.00	0.00	0.00	0.00
Total	100.60	100.14	99.98	100.13	100.72	99.20
Ca/Ca+Mg+Fe	0.02	0.02	0.02	0.02	0.02	0.02
Fe/Fe+Mg	0.44	0.45	0.44	0.44	0.42	0.40
WO	1.45	1.54	1.63	1.85	1.98	1.98
EN	67.57	66.31	66.66	67.25	68.88	69.95
FS	30.98	32.15	31.70	30.90	29.14	28.07
			Range			
WO	1.45-1.54	1.2-1.5	1.5-1.8	1.78-1.86	2.00	1.9-2
EN	65.2-67.6	65.8-67.8	65.1-67.9	66.8-67.2	69.2-70.4	69-71
FS	31.0-33.3	30.7-32.2	30.5-33.2	30.9-31.4	27.6-29.1	27.4-29.0

Wo-En-Fs components calculated after Morimoto et al. (1988)
See CD appendix VI for Wo-En-Fs components calculated after Lindsley (1983)

Table 4.5a. Representative microprobe analyses of apatite from the Maqui Maqui ignimbrite with comparative analyses from a traverse across a phenocryst.

Maqui Maqui Ignimbrite - Apatite

Wt %	DN7-1.7	DN7-1.8	DN7-1.9	DN7-1.10	DN7-1.11	DN7-1.12
FeO*	1.48	0.28	0.38	0.24	0.57	0.20
MgO	0.16	0.19	0.20	0.20	0.19	0.16
CaO	54.97	55.96	55.84	56.28	55.20	55.58
Na$_2$O	0.18	0.13	0.17	0.15	0.25	0.14
P$_2$O$_5$	41.18	42.08	41.17	41.97	41.36	41.15
SO$_3$	0.16	0.08	0.10	0.09	0.25	0.10
Cl	0.97	1.52	1.79	1.60	1.88	1.77
F	0.00	0.00	0.00	0.00	0.00	0.00
O=Cl+F	0.22	0.34	0.40	0.36	0.42	0.40
OH	0.9	0.87	0.84	0.86	0.84	0.85
Total	98.88	99.90	99.25	100.18	99.28	98.70
Cl/Cl+F	1.00	1.00	1.00	1.00	1.00	1.00
P/P+S	1.00	0.99	1.00	0.99	0.99	0.99
Cl/Cl+F+OH	0.08	0.13	0.16	0.14	0.16	0.15

Table 4.5b. Representative microprobe analyses of apatite from the San Jose ignimbrite with comparative analyses from a traverse across a phenocryst.

San Jose Ignimbrite - Apatite

Wt %	CB38-1.7	CB38-1.8	CB38-1.9	CB38-1.10	CB38-1.11	CB38-1.12
FeO*	2.73	3.37	0.38	0.59	0.48	0.56
MgO	0.19	0.20	0.14	0.14	0.15	0.17
CaO	54.10	53.95	55.70	55.62	56.05	56.39
Na$_2$O	0.11	0.18	0.13	0.13	0.17	0.15
P$_2$O$_5$	41.44	39.97	41.79	41.26	41.21	40.95
SO$_3$	0.15	0.22	0.15	0.16	0.26	0.23
Cl	1.02	1.01	1.03	1.05	1.12	0.28
F	0.54	0.49	0.09	0.69	2.03	2.16
O=Cl+F	0.46	0.43	0.27	0.53	1.11	0.97
OH	0.82	0.83	0.9	0.8	0.58	0.63
Total	99.82	98.97	99.14	99.11	100.35	99.91
Cl/Cl+F	0.50	0.52	0.86	0.45	0.23	0.06
P/P+S	0.99	0.99	0.99	0.99	0.99	0.99
Cl/Cl+F+OH	0.09	0.09	0.09	0.9	0.1	0.02

Table 4.6a. Select amphibole data including estimated amphibole and pyroxene temperatures.

Unit	Sample	Amphibole Temperature(~°C)	Pyroxene Temperature(±30°C)	Amphibole Pressure (kb)	Fe/(Fe+Mg)	SiO$_2$	Estimated H$_2$O wt%	Age (Ma)	2 σ Error
LAL	DN-16	725-825	nd	4.08	0.36	45.16	1.91	15.90	±0.18
CFD	Frail-2B	750-825	npx	4.42	0.42	43.56	1.87	15.51	±0.05
Lpha east	AZU-1A	950->1000	C ~1000±30	5.54	0.22	43.06	1.48	13.31	±0.08
Lpha west	Atazaico DO-43	950->1000	nd	5.76	0.26	42.76	1.69	14.21	±0.16
Upha	DO-60	950-1000	R ~950-980±30 C ~1000±30	5.70	0.23	43.34	1.81	12.08	±0.10
MMI	DN-7 Core	950.00	npx	4.44	0.36	43.31	1.85	12.49	±0.08
	DN-7 Rim	725-800	npx	2.53	0.34	45.98	1.86	12.49	±0.08

Pre-Yanacocha rocks: LAL – Lower Andesite Lahar Sequence; CFD – Cerro Frailes dacite pyroclastic sequence.   nd – no data   npx – no pyroxene (1) high Al amphibole (2) Low Al amphibole
Yanacocha Volcanic Field: Lpha – Lower Yanacocha px-hb andesite sequence, Upha – Upper Yanacocha px-hb andesite sequence, MMI – Maqui Maqui Ignimbrite, Lsji – Lower San Jose Ignimbrite, Msji – Middle San Jose Ignimbrite, Usji – Upper San Jose Ignimbrite, Lsjd – Lower San Jose domws, Msjd – Middle San Jose domes, Usjd – Upper San Jose domes.

Table 4.6b. Select amphibole data including estimated amphibole and pyroxene temperatures.

Unit		Sample	Amphibole Temperature(~°C)	Pyroxene Temperature(±30°C)	Amphibole Pressure (kb)	Fe/(Fe+Mg)	SiO$_2$ (wt%) average	Estimated H$_2$O wt%	Age (Ma)	2 σ Error
Lsji	CORE	CB-44	(1) 940-1000 (2) 730-800	cpx~1025-1100±30 opx~850-950±30	2.95	0.31	45.78	1.92	11.54	±0.09
		CB-56	725-850	nd	2.29	0.32	46.30	1.85	11.43	±0.06
Msji		CB-38	(1) 950-980 (2) 800-830	cpx~1050-1075±30 opx~875-910±30	3.94	0.35	44.86	1.82	11.29	±0.15
		VC-1	(1) 950 (2)<725-825	npx	2.34	0.32	46.30	1.81	11.23	±0.08
Usji		DE-36	(1) 950-1000 (2) 825	cpx~1115-1150±30 opx~900-925±30	5.25	0.35	43.18	1.89	11.25	±0.07
		BS-2B	(1)930-980 (2) 725-790	nd	3.35	0.33	45.12	1.77	11.50	±0.09
Lsji	RIM	CB-44	(1) 900-950 (2) 725-790	cpx~1000±30 opx~900±30	2.69	0.31	46.50	1.88	11.54	±0.09
		CB-56	<725-750	nd	1.43	0.29	48.05	1.83	11.43	±0.06
Msji		CB-38	(1) 950 (2) 800-830	cpx~980±30 opx~900±30	3.61	0.35	44.97	1.78	11.29	±0.15
		VC-1	(1) 950 (2)<725-780	npx	1.83	0.30	47.62	1.84	11.23	±0.08
Usji		DE-36	(1) 930-940 (2) 775-825	cpx~1090-1110 opx~900±30°C	4.56	0.32	44.18	1.82	11.25	±0.07
		BS-2B	(1) 930-980 (2) 725-790	nd	2.94	0.33	45.57	1.68	11.50	±0.09
Lsjd		DE-2	950-1000	R~910-950±30 C~925-1025±30	5.42	0.26	43.70	1.45	11.36	±0.09
Msjd		CHQS-1	950->1000	nd	2.35	0.31	45.98	1.80	11.23	±0.07
Usjd		CB-3	735-825	npx	6.26	0.31	42.36	1.52	11.25	±0.07

Pre-Yanacocha rocks: LAL – Lower Andesite Lahar Sequence; CFD – Cerro Frailes dacite pyroclastic sequence.   nd – no data   npx – no pyroxene (1) high Al amphibole (2) Low Al amphibole
Yanacocha Volcanic Field: Lpha – Lower Yanacocha px-hb andesite sequence, Upha – Upper Yanacocha px-hb andesite sequence, MMI – Maqui Maqui Ignimbrite, Lsji – Lower San Jose Ignimbrite, Msji – Middle San Jose Ignimbrite, Usji – Upper San Jose Ignimbrite, Lsjd – Lower San Jose domws, Msjd – Middle San Jose domes, Usjd – Upper San Jose domes.

CONCLUSIONS

Miocene volcanism at Yanacocha spanned 11.1 million years from 19.5 to 8.4 Ma and hydrothermal activity continued 5.4 million years from 13.5 to 8.2 Ma as temporally and spatially discrete cells that migrated across the district and led to the deposition of gold ore (Figure 5.1). Eight volcanic sequences are distinguished on the basis of mineralogy, composition, and age. Three rock sequences are older than 15 Ma and erupted from "pre-Yanacocha" volcanic centers outside the district. Volcanism in the Yanacocha Volcanic Field was centered at the Yanacocha Mining District for 6.1 million years from 14.5 to 8.4 Ma and produced a calc-alkaline suite with five rock sequences that evolved from andesite to rhyolite. Magmatism and hydrothermal activity progressed from southwest to northeast through time across the district. Five periods of magmatic activity with volcanism and six stages of hydrothermal activity have been interpreted from the volcanic stratigraphy and age data.

Rock sequences that belong to the Yanacocha Volcanic Field (YVF) represent volcanic and intrusive rocks that evolved from spatially and temporally distinct eruptive centers in a northeast-trending corridor 25 km long covering an area more than 500 km^2 with lava flows and pyroclastic rocks. Volcanism alternated between effusive and explosive stages over an interval of 3.3 million years from 14.5 to 11.2 Ma; an early and a late period of dominantly effusive eruptions each culminated in a period of dominantly explosive eruptions. Effusive eruptions began with pyroxene-hornblende andesite lavas (Lower Yanacocha volcanic sequence, Lpha) in the west and ended with explosive dacite volcanism in the east (San Jose ignimbrite, SJI). Magmatism then shifted to highly oxidized dacite to rhyolite compositions forming domes and intrusions of isolated porphyry plugs, and ended in the final explosive eruption of the Negritos rhyolite ignimbrite at 8.4 Ma.

Each eruptive episode spanned discrete intervals in time separated by periods without volcanism (Figure 5.1). Gaps in time between eruptive episodes apparently correspond to periods of volcanic quiescence with durations ranging from ~680,000 years between the Lower Yanacocha volcanic sequence (Lpha) and the Maqui Maqui ignimbrite (MMI) to ~140,000 years between the Upper Yanacocha volcanic sequence

(Upha) and the San Jose ignimbrite (SJI), and ~440,000 years between the SJI and the Upper (late) Dacite. Early effusive eruptions began at 14.5 Ma with the Lpha and lasted ~1.2 million years. Explosive eruptions began with the MMI and spanned 230,000 years before the second stage of effusive volcanism erupted Upha for ~420,000 years.
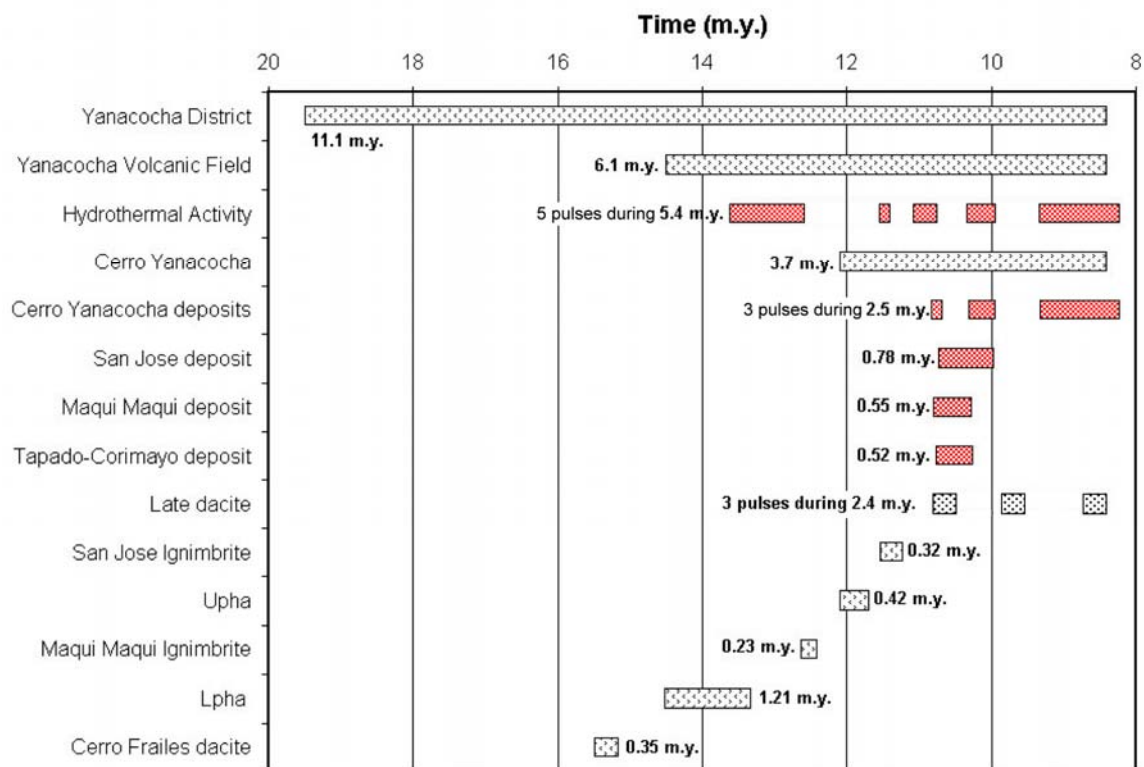
Figure 5.1. Bar chart displaying the time span for events at Yanacocha. Red bars represent the duration of discrete hydrothermal events in the district and individual deposits. White bars with dots represent the duration of discrete magmatic events. Durations for each event are presented adjacent the graphic display.

Following the Upha, the explosive eruptions of the San Jose ignimbrite continued for a duration of ~320,000 years. Early styles of YVF volcanism were followed by three brief episodes of magmatism that compositionally varied from dacite to rhyolite and spanned 2.4 million years from 10.8 to 8.4 Ma. These rocks are distinctive, containing the phenocryst assemblage of sphene + magnetite + quartz that implies high magmatic oxygen fugacities (Wones, 1989). This late episode of highly oxidized felsic magmas developed porphyritic domes with minor lavas and pyroclastic aprons, and intrusions of isolated dacite porphyry plugs. Volcanism ended in a final explosive event with the

eruption of the Negritos rhyolite ignimbrite at 8.40±0.06 Ma. Eruption of the Negritos ignimbrite was followed by a cessation of arc volcanism in the Yanacocha area and the initiation of flat-slab tectonics and associated volcanic gap from 2°S – 15°S in northern Peru (Gutscher et al., 1999).

Distinctive geochemistry and mineralogy characterize each volcanic sequence and support the stratigraphy as documented in the study. Phenocryst assemblages are distinct for each rock sequence. The pre-Yanacocha andesite lahars (LAL) contain plagioclase, clinopyroxene, orthopyroxene and hornblende with 36 to 56 vol.% phenocrysts, whereas, the Cerro Frailes dacite pyroclastics contain coarse biotite, plagioclase, sanidine, quartz and hornblende with about 32 vol.% phenocrysts. In contrast, the younger rocks from the Yanacocha Volcanic Field are typically phenocryst-rich and range from 25 to 55 vol.% phenocrysts in lavas, from 30 to 60 vol.% phenocyrsts in dome rocks, and 40 to 75 vol.% phenocrysts in the ignimbrites. Lower and Upper Yanacocha lavas contain abundant plagioclase with clinopyroxene + orthopyroxene + hornblende, whereas ash-flow tuffs of the Maqui Maqui and San Jose ignimbrites contain abundant broken plagioclase with hornblende + biotite ± clinopyroxene. Late dacites and rhyolites at Yanacocha have quartz + biotite + hornblende + magnetite + sphene implying relatively higher oxygen fugacities compared to earlier units (Wones, 1989).

Compositional variations of rocks in the Yanacocha Volcanic Field (YVF) typify a subduction-related calc-alkaline rock suite. Each period of magmatism displays a distinctive composition produced by varying proportions of mafic magma input, and discrete magma systems evolved by crustal contamination, fractional crystallization, and magma mixing. The major element oxide data form coherent trends from older medium-K andesite to younger high-K andesite, dacite and rhyolite, and display decreased MgO content with increased SiO_2 content through time. Trace elements display enrichments in the light rare earth elements and the large ion lithophile elements, and depletions in the heavy rare earth elements with increased SiO_2 content. Combined processes of crystal-liquid fractionation, magma mixing, and multicomponent crustal assimilation are implied for the evolution of the YVF melts over a span of 6 million years. Patterns recognized in the data with distinct trends imply that discrete magma batches temporally coexisted but

likely were physically separated. These compositions may have followed different differentiation trends that involved crustal assimilation and mixing of end member compositions that include pyroxene andesite and dacite. A deep basaltic to andesitic batholithic magma chamber is inferred as the source to shallow magma reservoirs that locally intruded the base of the eruptive volcanic pile (Figure 4.76).

Hydrothermal activity that produced hypogene advanced argillic alteration began in the west part of the Yanacocha district at 13.6 Ma and migrated east with at least five discrete pulses (Figure 5.1). By 10.8 Ma, high-sulfidation gold mineralization became widespread in the east district and continued for ~700,000 years until 10.1 Ma. Activity then became centered exclusively at Cerro Yanacocha by 9.3 Ma for a duration of 1.1 m.y. and ended by 8.2 Ma. Alunite ages at Cerro Yanacocha define three pulses of magmatic-hydrothermal activity that spanned ~2.6 m.y. from 10.8 to 8.2 Ma (Figure 5.1). Temporal and spatial variations in Ag/Au and Cu/Au ratios from samples with advanced argillic alteration indicate that the Au-dominant systems in the west district evolved into more diverse epithermal systems through time producing both Au-dominant and Cu-Ag-enriched ore bodies. Early dacite intrusions and feldspar porphyry intrusions are spatially associated with ore at Quilish and Cerro Negro (the oldest Au deposits) in the west district. Late dacite to rhyolite intrusions and domes are spatially and temporally associated with the later stages of ore and the largest gold deposits (e.g., Cerro Yanacocha). Hydrothermal and magmatic activity was centered longer at Cerro Yanacocha than any other location in the Yanacocha district (Figure 5.1) and apparently are related to its large size, diverse metal enrichments, and economic importance. Volcanism there had a duration ~3.7 m.y. and hydrothermal activity spanned ~2.6 millon years. In contrast, the duration of hydrothermal activity in other Yanacocha deposits spanned a much shorter time (~0.5 to 0.8 m.y.) that is typical for most high-sulfidation systems worldwide (Figures 5.1 and 5.2).

Contributions of the Study

The data and models presented in this study provides new insights that improves the understanding of the volcanism and volcanic stratigraphy and unravels the temporal relationship of volcanism to acid-sulfate alteration and Au mineralization. Detailed field studies of the unaltered analogs to volcanic rocks at Yanacocha, and geologic mapping of these fresh rocks into the halo of hydrothermal alteration, allowed for petrographic and chemical characterization of each rock sequence that hosts gold ore in the district. In this way, the current study documents the sequence of volcanic events that shaped Yanacocha and establishes the absolute timing of magmatism. This new work combined with the mountains of data already collected and synthesized by Minera Yanacocha S.R.L. provides critical geologic constraints relevant to assessing the remaining mineral potential of the greater Yanacocha District.

This is the first study at Yanacocha that thoroughly documents the composition of volcanic rocks and their variation with stratigraphic position and absolute age. The data cofirm and refine the conclusion that volcanism and mineralization were coeval Miocene events. An important aspect is that this is the first detailed field study of the fresh volcanic rocks beyond the limits of the hydrothermally altered rocks in the district. Detailed field and petrographic descriptions of each rock sequence are outlined and presented in chart and graphical formats that are intened to be useful to future work. A detailed geologic map, that includes the Yanacocha district and surrounding fresh volcanic terrane, can be integrated with existing exploration maps from Minera Yanacocha S.R.L. for improved understanding of the district geology. A generalized stratigraphic section was compiled of the volcanic rocks for the entire district. Stratigraphic columns from specific locations across the district were compiled that detail the volcanic stratigraphy and unit thicknesses. A composite chronostratigraphic summary shows the temporal and spatial relationships of the volcanic stratigraphy, intrusions and gold-copper ore at Yanacocha.

Field geology integrated with the $^{40}Ar/^{39}Ar$ dating, petrography, and geochemistry has resolved many problems of volcanic stratigraphy in the Yanacocha district. An important conclusion is that no volcanic sequences that can be considered entirely post-

mineral and younger than the Yanacocha high-sulfidation gold ore systems. Therefore, any volcanic rock within the district can host ore. The $^{40}Ar/^{39}Ar$ dates presented here confirm that rocks once considered younger than, and covering high-sulfidation ore zones, are actually older than the hydrothermal alteration. Ash-flow tuffs classified *Huambos, Frailones,* and *Otuzco* belong to two separate packages of rocks from the Middle Miocene termed the Cerro Frailes dacite pyroclastic sequence (15.5-15.1 Ma) and the San Jose ignimbrite sequence (11.5-11.2 Ma). Although similar in appearance where unaltered, neither are post-mineral and Pliocene deposits, nor do they correlate with the Oligocene Huambos Formation (35.4 Ma; Noble et al., 1990). This study also verifies that little altered and fresh pyroxene andesite lavas, tuffs and domes at Yanacocha previously classified the *Regalado* volcanic rocks are actually Middle Miocene and an integral part of the Yanacocha Volcanic Field. They are not post-Yanacocha volcanic rocks and should not be considered as younger than the mineral systems they host. This understanding makes Yanacocha even more exciting to the exploration geologist because ore bodies have been discovered below fresh rocks that are not post-mineral.

Intense hydrothermal alteration that was related to and precursor to the high-sulfidation gold deposition at Yanacocha obscures rock classification and geologic-stratigraphic interpretation. As a result, prior to this study, many problems and much confusion existed in the correlation of volcanic rocks across the region. Stratigraphic interpretations within the ore deposits resulted in models for the volcanic stratigraphy largely based on textural characteristics observed in zones of intense hypogene advanced argillic alteration. In many cases, the textures interpreted to be distinct volcanic characteristics may be primary or secondary and induced by the hydrothermal activity. Relative ages were applied to each distinct textural attribute on the basis of superposition. Problems arose in the interpretation of ignimbrites and lavas with similar textures or lithic concentrations and types. For example, within the zone of hypogene advanced argillic alteration it is very difficult to distinguish Maqui Maqui ignimbrites from San Jose ignimbrites; nevertheless, these units have been carried across the district from deposit to deposit and used as marker horizons. Many characteristics critical for modeling

volcanic stratigraphy, such as identification of phenocryst assemblages and composition, isotopic age, and field relationships only observable in fresh volcanic terrane, are simply not obtainable within the realm of Yanacocha gold deposits. Thus there remain many stratigraphic questions in the central part of the district.

The new stratigraphic model presented in this study provides an understanding not recognized in previous studies at Yanacocha. The enormous spans of time associated with the volcanism and hydrothermal activity in large centers such as Yanacocha provide complexities and variables of interest to the explorationist not commonly considered. Any volcanic rock within the Yanacocha district can host ore, and the very same host rock can be found fresh and conceal older ore. The corollary that "no post-Yanacocha volcanic rocks exist younger than the mineral systems they host" is important to recognize at Yanacocha, but is not entirely accurate when applied to an exploration model. Older hydrothermal systems such as Quilish and Cerro Negro could be covered by pyroclastic and lava flows from successive eruptions that post-date an early stage of ore deposition, and also pre-date later hydrothermal activity. These complexities are very exciting to the exploration geologist in areas with low levels of erosion and low relief because ore bodies can be found below fresh rocks that are not post-mineral but belong to the same volcanic center. World-class high-sulfidation epithermal systems can actually be concealed by the volcanic rocks that host them. At Yanacocha, the recent period of glaciation has provided windows into the ore bodies and intense magmatic-hydrothermal acid-sulfate alteration, and without this level of erosion Yanacocha might possibly still be undiscovered. A message to exploration is when exploring large and complex volcanic centers in regions of recent volcanism and little erosion (e.g., the Northern and Central Volcanic Zones in South America) look for the subtle expressions of hydrothermal systems in areas with a complex magmatic history; they could lead to large discoveries.

Duration of Yanacocha Compared to Other Systems

The Yanacocha district and the Yanacocha Volcanic Field are now documented to represent one of the world's longest-lived Cenozoic volcanic centers. Figure 5.2 compares the duration of volcanism and hydrothermal activity from numerous Cenozoic

volcanic centers and related mineral districts worldwide. Yanacocha ranks second and the Yanacocha Volcanic Field ranks eighth within the top ten volcanic centers whose durations of volcanism span 6 to 14 m.y. These include from longest to shortest duration as follows (Figure 5.2): (1) Portrerillos, Chile (Marsh et al., 1997), (2) Yanacocha district including pre-Yanacocha volcanic rocks (this study), (3) Auconquilcha, Chile (Klemetti and Grunder, 2003; Grunder et al., 2004), (4) Nansatsu district, Japan (Hedenquist et al., 1994), (5) Rodalquilar, Spain (Arribas et al., 1995), (6) Toquima Caldera Complex (Henry et al., 1997), (7) the Southwestern Nevada Volcanic Field (Sawyer et al., 1994), (8) the Yanacocha Volcanic Field (this study), (9) the Coromandel Volcanic Zone, New Zealand (Clarke et al., 1990), and (10) the Timok Massif, eastern Serbia (Clark and Ullrich, 2004).

Similar comparisons for duration of hydrothermal activity places Yanacocha (5.4 m.y.) second only to the duration of periods of porphyry copper mineralization in the Potrerillos District (8.5 m.y.) and nearby epithermal precious metal deposits at El Hueso. The Nansatsu epithermal precious metal district in Japan (4.5 m.y.) is a close contender in third place. All three areas had long-lived pulses of hydrothermal activity related to calc-alkaline volcanism and complex magmatic systems associated with ocean slab subduction at convergent plate boundaries. Hydrothermal activity at Nansatsu and Potrerillos were closely spatially and temporally associated with oxidized magnetite-series intrusions. Hydrothermal activity at Yanacocha also was coeval with the magmatic events associated with calc-alkaline volcanism. The main stage of epithermal ore deposition closely followed the eruptions of the San Jose ignimbrite by ~0.4 m.y. and was coeval with highly oxidized dacite to rhyolite magmatism. At Nansatsu, hydrothermal activity also was associated with volcanism and followed the deposition of the andesite host rocks by 0.5 m.y. (Hedenquist et al., 1994). Similar to Yanacocha, both volcanism and hydrothermal activity at Nansatsu shifted from west to east through time and all major Au deposits are spatially associated with oxidized magnetite-series felsic intrusions. Major differences between these centers include a mature, thick continental crust at Yanacocha and Portrerillos versus a somewhat thinner and younger continental crust at Nansatsu.

Duration of magmatism and hydrothermal activity are also compared for single deposits in Figure 5.2. The Cerro Yanacocha Au deposit represents one of the world's longest-lived hydrothermal systems documented, with a hydrothermal duration of ~2.5 m.y. associated with ~3.7 m.y. of magmatism. It is estimated that volcanism preceded gold mineralization at Cerro Yanacocha by 1.2 m.y. and that compositions evolved from calc-alkaline andesite to rhyolite. Other deposits with long-lived hydrothermal systems include: (1) the El Salvador porphyry copper system (~ 0.6 to 1 m.y.; Cornejo et al., 1997; Gustufson et al., 2001), (2) the Chuquicamata porphyry copper system (~ 2.7 m.y.; Zentilli et al., 1994; Reynolds et al., 1998; Ballard et al., 2001), (3) Tantahuatay high-sulfidation Au deposit (~2.3 m.y.; Prihar, 1998), (4) Rodalquilar high-sulfidation Au deposit (~1.7 m.y.; Arribas et al., 1995), and (5) Goldfield high-sulfidation Au deposit (~ 1.5 m.y.; Ashley and Silberman, 1976).

References for the ages presented in figure 5.2 include the following: Potrerillos (Marsh et al., 1997), Auconquilcha Volcanic Complex (Klemetti and Grunder, 2003; Grunder et al., 2004), Nansatsu district, Japan (Hedenquist and Matsuhisa, 1994), Rodalquilar, Spain (Arribas et al., 1995), San Juan Volcanic Field (Lipman, 2000: Barton et a., 2000), Majdanpek, Timok, Serbia (Clark and Ullrich, 2004), Coromandel Volcanic Zone, N.Z. (Clarke et al., 1990), El Salvador (Cornejo et al., 1997), Tantahuatay (Prihar, 1998), Minas Congas(Llosa et al, 1999, Noble et al, 2004, and Thompson, 2003), Chuquicamata (Zentilli et al., 1994; Reynolds et al., 1998; Ballard et al., 2001), Farallon Negro-Bajo de la Alumbrera (Halter et al, 2004; Harris et al., 2004), Long Valley-Mammoth Mtn (Hildreth, 2004), Goldfield, Nevada (Ashley and Silberman, 1976), Julcani, Peru (Dean et al., 1994), Cerro del Pasco and Colquijirca, Peru (Silberman and Noble, 1977; Vidal et al., 1997; Bendezú et al, 2003), Quimsacocha Volcanic Center (Beate et al., 2001), Valles Caldera (Doell et al, 1968), Far Southwest-Lepanto (Hedenquist et al., 1998), La Pepa and Refugio, Chile (Muntean, 1998; Muntean and Einuadi, 2000), Round Mountain and the Toquima Caldera Complex (Henry et al, 1997), Waiotapu, N.Z. (Hedenquist and Henley, 1985), Southwestern Nevada Volcanic Field (Sawyer et al, 1994), Ceboruco-San Pedro volcanic field (Frey et al., 2004), and Mt Adams Volcanic Field (Hildreth and Lanphere,1994).
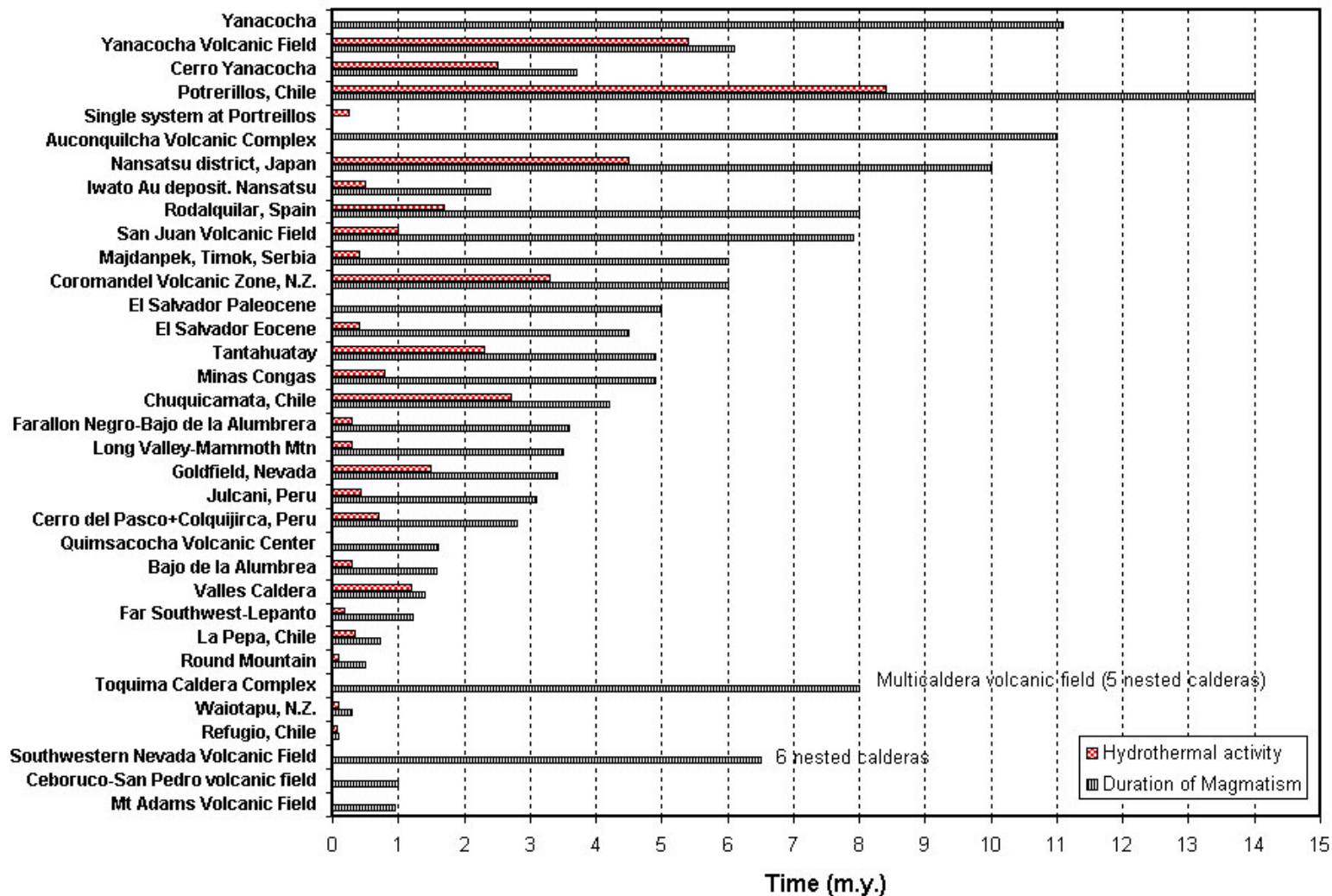
Figure 5.2. Bar chart that compares durations for hydrothermal activity and magmatic activity from volcanic centers and mineral districts worldwide to Yanacocha. References for the range in ages presented above are listed in the text.

Eruptive Volumes, Magmatic Silica Content, and Gold Through Time at Yanacocha

Comparisons are presented for the volume of the eruptive products versus SiO_2 content of the volcanic and subvolcanic rocks and the total accumulated gold resource at Yanacocha through time. Volume calculations are derived from estimated average thicknesses and areal extent for each rock sequence in the Yanacocha Volcanic Field (YVF) as presented in this study (Table 5.1). Average thicknesses are estimated from the stratigraphic fence diagrams presented in Chapter 3 of this study, and the areal extent for each rock sequence is estimated from the known outcrop distribution as presented in the geology map (Plate 1). Thickness and areal extent for the Upper (late) Dacite are estimated from outcrop exposures of the La Quinua dacite dome and from work by Gomez (2002) on the Corimayo dacite dome. Ignimbrites are fines-depleted and amounts of ash dispelled into the atmosphere are not factored in to the calculation. Therefore, volume estimates are constrained to known outcrop exposures affected by erosion and should be considered a minimum eruptive volume. SiO_2 contents in Table 5.1 and plotted on Figure 5.3 are averages for each rock sequence as defined in this study. Gold endowment in million ounces is estimated in Table 5.1 from the past production statistics at Yanacocha from Leng (1999), Hall (2000), and various annual reports (Newmont Mining Corporation, 2002 and 2003) and the global resource calculations acquired for Yanacocha from the recent Newmont Mining Corporation 2004 annual report. Temporal relationships presented for these comparisons include $^{40}Ar/^{39}Ar$ age determinations from this study and Turner (1997).

Estimated erupted volumes of magma during YVF volcanism, as presented in this study, increased to a maximum (>20 km^3; Table 5.1) for the Lower Yanacocha volcanic sequence by ~14.0 Ma and the San Jose ignimbrite sequence by ~11.2 Ma (Table 5.1; Figure 5.3). Moderate erupted volumes (>10 km^3; Table 5.1) were estimated for the Maqui Maqui pyroclastic sequence and the Upper Yanacocha volcanic sequence. Accumulation of gold ore increased when eruptive output decreased and the volumes of erupted products were at a minimum. At least four discrete pulses of hydrothermal
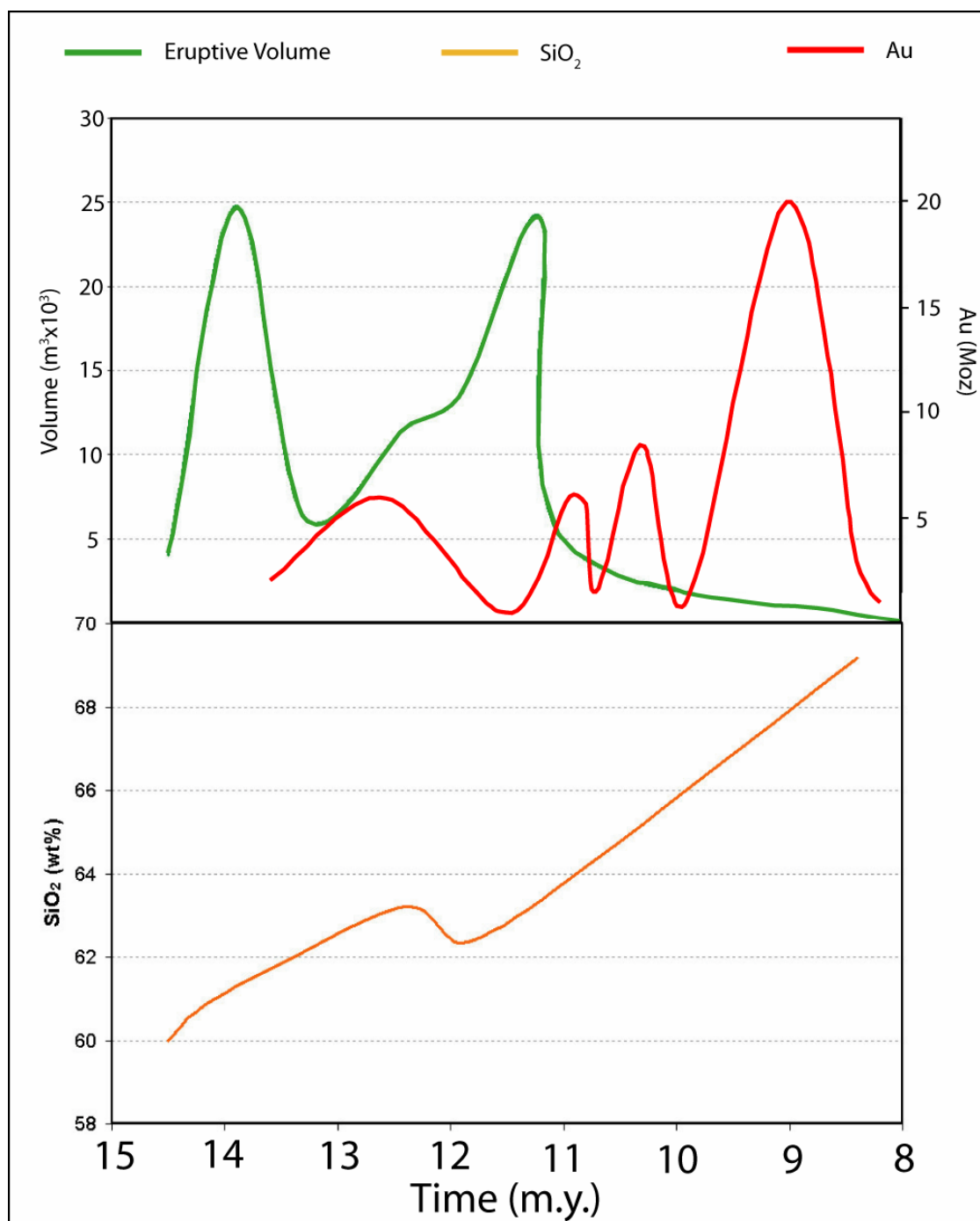
Figure 5.3 Chart showing a comparison of the eruptive volume for the Yanacocha Volcanic Field in km^3, total gold in millions of ounces, and SiO$_2$ content through time at Yanacocha.
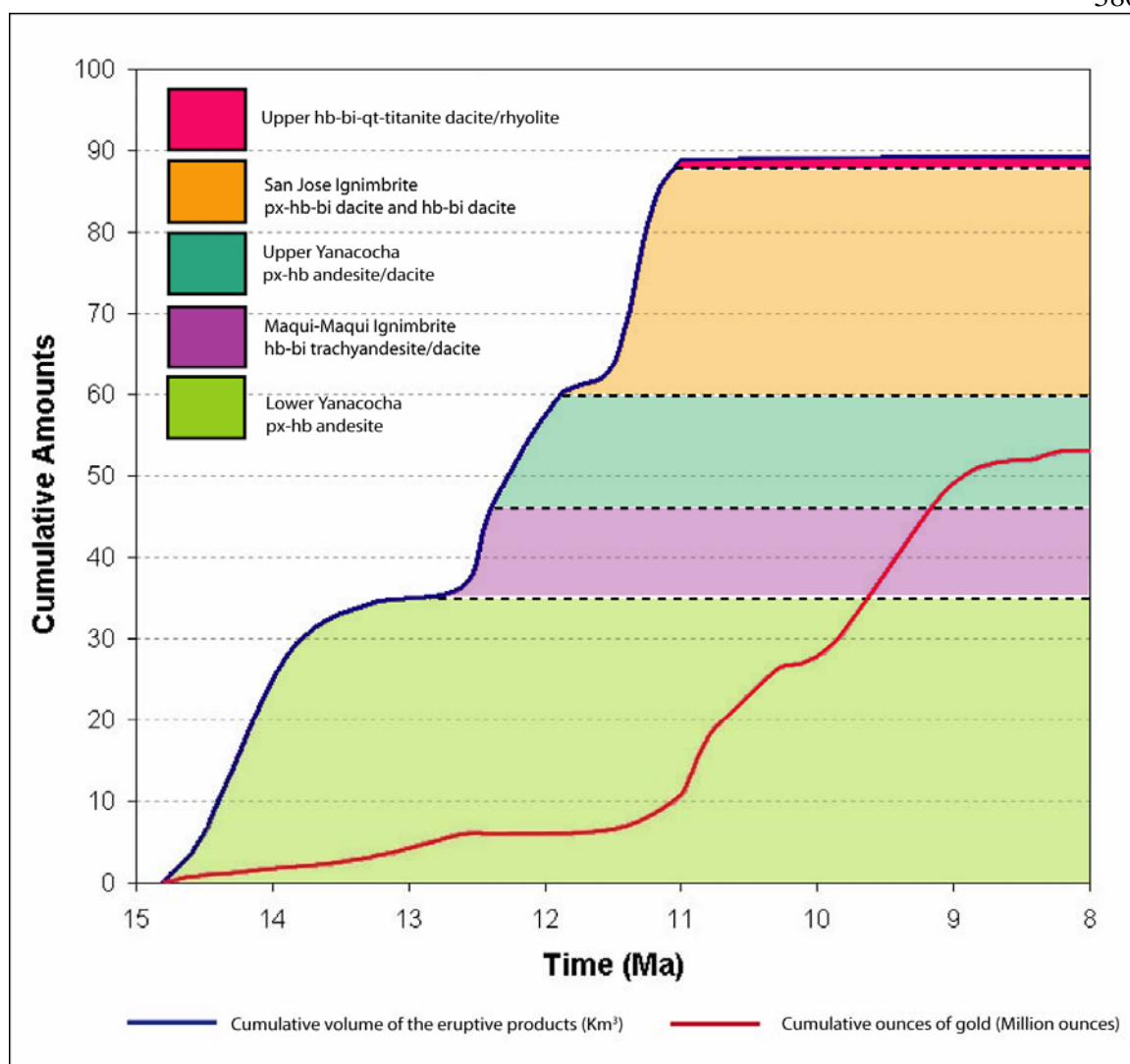
Figure 5.4 Chart showing the cumulative volume (km^3) for the eruptive products in the Yanacocha Volcanic Field compared to the cumulative ounces (million ounces) of gold at Yanacocha.

activity at ~13 Ma and after ~11 Ma are associated with decreased eruption rates (Table 5.1; Figure 5.3). Early gold deposition in the west district declined with renewed volcanism and was at a minimum by ~11.5 Ma during eruptions of the San Jose ignimbrite. Late gold mineralization occurred in three pulses of hydrothermal activity at Cerro Yanacocha, and peaked after the intrusion of the Yanacocha quartz dacite porphyry (Table 5.1: Figure 5.3). Magmatic SiO_2 contents increased through time in the Lower Yanacocha volcanic sequence and peaked by ~12.4 Ma with the Maqui Maqui dacite ignimbrite, then decreased slightly in pyroxene andesites from the initial eruptions of the

Upper Yanacocha volcanic sequence. Magmatic SiO_2 content increased again through time in rocks with dacite compositions and peaked by 8.4 Ma during eruptions of the Chaupiloma and Negritos rhyolite (Table 5.1; Figure 5.3).

A plot of estimated cumulative volumes of erupted magma versus gold indicates that by ~11.2 Ma nearly 10 million ounces (Moz) of gold accumulated during the period of YVF volcanism that deposited ~88 km^3 of volcanic rocks at Yanacocha (Table 5.1; Figure 5.4). Eruptions of the Lower Yanacocha volcanic sequence and the San Jose ignimbrite produced the greatest volume of volcanic rocks during this time. After 11 Ma, eruption rates decreased, and the late dacite produced low volumes and the least amount of volcanic rocks in the YVF, and cumulative gold increased dramatically from ~10 Moz to over 50 Moz gold (Figure 5.4). Rates of gold deposition increased dramatically after ~11 Ma when eruptive output decreased and magmatic SiO_2 content increased.

Multivent volcanic stratocone fields cover wide areas and contain numerous small andesite to dacite stratovolcanoes, stratocones and monogenetic volcanoes. Volumetric eruption rates are well documented and typically range from 0.04 to 0.6 km^3/1000 years (Kudo et al., 2003; Hildrith et al., 2003; Grunder et al., 2004; Siebe et al, 2004). Examples of multivent volcanic fields that have a similar geomorphological volcanic setting to Yanacocha include the following:

(1) A cluster of ten stratovolcanoes called the Aucanquilcha Volcanic Center erupted 340 km^3 of magma for 11 m.y. with compositions from andesite to dacite (Grunder et al., 2004). A volumetric eruption rate at Aucanquilcha is estimated at 0.34 km^3/1000 years (Grunder et al., 2004).

(2) The Mount Baker Volcanic Field represents a multivent cluster of stratocones, and a small caldera, that erupted 161±56 km^3 of volcanic rocks with eruption rates that range from 0.17 to 0.43 km^3/1000 years (Hildreth et al., 2003). The Mount Baker stratovolcano is the most prominent feature. The caldera at Mount Baker produced the largest single eruption with 50 km^3 of rhyodacite ash-flow tuff (Hildrith et al., 2003). Cumulative volumes of erupted magma at Mount Baker are similar to Yanacocha if the caldera is omitted.

(3) An average eruption rate for the Sierra del Chichinautzin Volcanic Field was estimated at 0.6 km^3/1000 years and contains a high concentration of monogenetic volcanoes including ~220 overlapping cinder cones and lava shields. Compositions range from basalt to dacite.

(4) Mount Griggs is a rear-arc stratovolcano in the Aluetian arc that erupted 30-35 km^3 of andesite magma, and has an estimated volumetric eruption rate of 0.10-0.12 km^3/1000 years (Hildreth et al., 2004). Volumes of erupted magma are similar to the Lower Yanacocha volcanic sequence (Figure 5.4).

(5) The Kita-Hokkada volcanic field in northeast Japan is an active group of andesite stratovolcanoes with a low volumetric eruption rate of 0.04-0.06 km^3/1000 years (Kudo et al., 2003).

The estimated cumulative volume of the Yanacocha Volcanic Field (~88 km^3 of erupted magma during 6.1 m.y.) yielded an average volumetric eruption rate of 0.09 km^3/1000 years. The cumulative volume of erupted products and volumetric eruption rates at Yanacocha are small and of similar magnitude to other multivent stratocone volcanic fields.

Calderas that erupt dacite and rhyolite ash-flow tuffs display rapid and high volumetric eruption rates. Caldera complexes have much larger culmulative volumes of erupted magmas than andesite to dacite multivent stratovolcano fields. The central San Juan caldera complex erupted 8800 km^3 of magma (Lipman, 2000), 20,000 km^3 erupted from the central Nevada caldera complex (Best et al. 1995), the Bishop Tuff eruption expelled 600 km^3 of magma and caused collapse of the Long Valley caldera (Hildreth, 2004), and 2500 to 3000 km^3 of magma erupted for the Toba Tuff (Chesner, 1991). Volumes of erupted magma from caldera complexes are generally two magnitudes greater than amounts erupted at Yanacocha.

Remaining Questions and Limitations of the Study

This dissertation was limited to field mapping of geology, ^{40}Ar/^{39}Ar dating, major and trace element geochemistry, optical petrography, and selected microprobe studies. These limitations, along with remaining questions, included the following:

(1) Field geology was confined to a 1000 km^2 area centered on Yanacocha. Pre-Yanacocha vent areas were not identified in the study area. *Where was the eruption site for the ~15 Ma Cerro Frailes dacite pyroclastic rocks? What was the areal extent of the eruptive products?*

(2) Fieldwork occurred over two successive seasons of three months duration. Time constraints necessitated geologic mapping along numerous traverses selected throughout the study area to maximize the geologic understanding. Geologic contacts mapped in the field were interpreted between the traverse sites, and when questionable, additional traverses were added to adequately explain the geology. Not every stone was overturned and important outcrops may have been overlooked. *Are the gaps in time between eruptive events (Figure 5.1) actually related to cessations in volcanism, or will additional work close the time gaps between eruptive events?*

(3) Assumptions for the petrogenesis and evolution of the YVF magmas are made on the basis of extensive isotopic dating, major oxide and trace element geochemistry, and selected microprobe studies on hornblende and pyroxene. No other isotopic analyses were completed on the YVF rocks. Furthermore, limited geochemical data were collected on the late dacite intrusions, partly because they are spatially associated with the ore deposits and hydrothermally altered. Some geochemical evidence as presented in Chapter 4 suggests a different pathway during differentiation for the late dacite versus other YVF rocks. *What is the genetic relationship of these late dacite intrusions to other YVF rocks?*

(4) The microprobe work was a pilot study limited to major element oxides, Cl and F for hornblende from one sample of the Chaupiloma lower andesite lahar sequence, one sample of Cerro Frailes dacite tuff, and several samples from the Yanacocha Volcanic Field (YVF), and major element oxides for pyroxenes from selected YVF rocks. Apatite was analyzed from only two samples of YVF ignimbrite. No plagioclase or biotite was analyzed. These data define separate compositional fields characteristic of Lower and Upper Yanacocha volcanic rock sequences and the Maqui Maqui and San Jose ignimbrites inconsistent with

amphibole fractionation. A more thorough study of the hydrous minerals would add significantly to the petrogenetic hypotheses as modeled in this study. Continued studies will help evaluate the evolution of the ore forming fluids at Yanacocha through a better understanding of the partitioning in Cl, F, and OH through time within YVF magmas.

(5) Questions still remain regarding the age of the hydrothermal alteration and the actual number of magmatic-hydrothermal cells that wandered through Yanacocha. Alunites dated in the west district resulted in uncertainties in the age of over 0.6 Ma for samples at Quilish. Limited analyses were conducted on the Quilish and Cerro Negro deposits, and alunite from Pabellon and Cerro Negro Este was not dated. Two alunites were dated for most deposits in the east district and several analyses were completed for the Cerro Yanacocha Complex and hydrothermal alteration ranges from 10.8 to 8.2 Ma. The oldest alunites age in the east district are ~11.5 and 11.0 Ma. Alunites were not dated at the Arnacocha, Antonio, and Quecher deposits. *Are there other hydrothermal events younger than the Quilish alunite at 12.64±0.61 in the west district? Are there gold deposits in the east district that range in age from 11.5 to 11.0 Ma? Were there cells of hydrothermal activity that fill the time gaps between the known deposits? In addition, was some gold introduction contemporaneous with alunite alteration, or is it slightly younger, as is typical for this type of mineralization?*

Recommendations

The following are recommendations for further research and exploration in northern Perú and the Yanacocha Mining District:

1) Detailed structural analysis and synthesis at Yanacocha has not been fully addressed or studied at an academic level. A better understanding of the structural setting would likely provide answers concerning the tectonic evolution of the district, thereby assisting in target evaluations during step-out exploration drilling.

2) Additional dating of alteration minerals, closely associated with gold ore in the Yanacocha deposits, would improve the resolution for the age of hydrothermal

alteration and may increase the understanding of how these deposits developed through time.

3) Alunite was the only alteration mineral dated. Illite has been described in PIMA studies at Yanacocha and can be dated using K/Ar and ^{40}Ar/^{39}Ar methods; however, its association with the mineralization is poorly understood. The combined use of illite and alunite dating better constrained the age of hydrothermal activity at Rodalquilar (Arribas et al, 1995). However, more PIMA work is necessary to define this style of alteration and the relationship to gold ore at Yanacocha prior to dating. Illite provides excellent K/Ar dates but may experience recoil in ^{40}Ar/^{39}Ar analyses and caution is warranted (A. Arribas, pers comm., 2001).

4) Feldspar (Yp) and late dacite (Ypq and Ybp) intrusions are spatially associated with gold ore. More isotopic dating of the feldspar porphyry and late dacite porphyry intrusions is also required to better constrain their ages and temporal associations. In the La Quinua basin, it is possible to date fresh feldspar porphyry plugs that are have very similar textures to the intrusions called Yp.

5) Microprobe and laser ablation studies on amphibole, apatite, and sulfide inclusions are currently underway at Oregon State University to evaluate the evolution of the ore forming fluids at Yanacocha. These studies will provide a better understanding of the partitioning in Cl, F, and OH through time within YVF magmas. Many questions remain regarding the evolution of the hydrothermal fluids at Yanacocha. *How did YVF magma differentiation and partitioning of Cl, F, and OH contribute to the metal flux and ore fluids at Yanacocha through time? During differentiation of the YVF magmas how did the aqueous phase develop and evolve?* I recommend these studies should include comparisons of hornblende and apatite from throughout the YVF rock sequences and include the Lower and Upper Yanacocha pyroxene andesites, Maqui Maqui intrusions (DN-77), the Maqui Maqui and San Jose ignimbrites, and the Upper (late) Dacites.

6) Core to edge microprobe analyses on the oscillatory zoned sieved and unsieved plagioclases in the YVF is necessary to increase the understanding of the magmatic evolution below Yanacocha.

7) Microprobe analyses are required for Fe-Ti oxide minerals throughout the YVF stratigraphy in order to estimate oxygen fugacities and temperatures during magma evolution.

8) Microprobe analyses on hornblende and biotite have not been done for the late dacite and are recommended to compare with present results from the older rock sequences. This will add important information to the petrogenetic model as hypothesized in this study.

9) Discrete magma batches may have evolved by a combination of complex multiprocess and multicomponent processes that include crustal assimilation, crystal-liquid fractionation, and magma mixing across Yanacocha. Stable isotope analyses of H and O are necessary to characterize each YVF rock sequence. O and H isotopic compositions will reflect the different crustal assimilates and magma signatures, and will better define the evolution of the magmatic system. YVF rocks require both stable O isotope and radiogenic $^{143}Nd/^{144}Nd$ and $^{87}Sr/^{86}Sr$ isotope studies to answer questions about source regions for the parental melts, assimilation processes during their ascent in the crust, and origin of the Yanacocha magma system.

Summary

New $^{40}Ar/^{39}Ar$ dating integrated with field geology, petrography, and compositions in this study have redefined the volcanic stratigraphy, and the duration of volcanism and hydrothermal activity in the Yanacocha Mining District. The new model unravels the spatial and temporal relationship of volcanism and hydrothermal activity at Yanacocha, and has implications that benefit the exploration of epithermal high-sulfidation systems worldwide.

Yanacocha represents one of the longest-lived volcanic centers (6.1 m.y.) and most enduring hydrothermal systems (5.4 m.y.) in the world. World-class gold deposits

develop in large volcanic centers over complex calc-alkaline magma systems with compositions that evolve from andesite to highly oxidized rhyolite. Volcanism is spatially and temporally related to the hydrothermal activity and both evolve together through long durations of time exceeding at least 2 or 3 million years (e.g., the time estimated for the Cerro Yanacocha deposit). The Cerro Yanacocha gold deposit represents one of the longest-lived group of epithermal systems known with a duration that spanned 2.5 m.y. associated with 3.7 m.y. of magmatism. Only a few other mineral deposits, such as the world's largest porphyry copper deposits Chuquicamata, have matched or exceeded the duration of the events at Cerro Yanacocha.

The Yanacocha Volcanic Field has an estimated cumulative eruption volume of ~88 km^3 of magma, and represents a small- to moderate-sized volcanic center similar in size to other multivent stratocone volcanic fields. Figure 5.3 indicates that gold ore at Yanacocha is related to at least five pulses of magmatic-hydrothermal activity (Figure 5.1 and 5.3). Rates of gold deposition increased dramatically after ~11 Ma when eruptive output decreased and magmatic SiO_2 content increased, and decreased during periods of volcanism and higher eruption rates (Figure 5.3).

Yanacocha is a +50 million ounce gold district with gold deposition temporally and spatially associated with a moderate-sized multivent stratocone and dome-related volcanic field that is characterized by low to moderate volumetric eruption rates. Low volumes of erupted magma may suggest that large volumes of subvolcanic magma remained in the crust. The compositional diversity of the subvolcanic rocks and the discrete pulses of hydrothermal activity imply a complex magmatic system existed at depth that evolved through time for more than 6 million years. Discovery of Yanacocha-like systems are less likely in volcanic centers with high volumetric eruption rates, and simple and short-lived magmatic-hydrothermal systems. World-class gold deposits may have increased rates of discovery in volcanic centers with low volumes of erupted magma, compositional diversity and abundance of the subvolcanic intrusive rocks, and complex magmatic-hydrothermal histories that evolve through large spans of time.

Table 5.1 Table that presents the estimated variables used in the calculations for the eruptive volume and total gold endowment at Yanacocha as shown in Figures 5.3 and 5.4.

Rock Sequence	Average Thickness (m)	Areal Extent (km^2)	Volume (km^3)	Age (Ma)	SiO$_2$ (Wt.%)
early Lpha	100	60	6.0	14.5	60.0
Lpha west	140	157	22	13.9	60.8
Lpha east	95	80	7.6	13.3	61.9
MMI	130	95	12.4	12.4	63.2
Upha	115	125	14.4	11.9	62.4
SJI	138	175	24.2	11.2	63.4
Late Dacite	100	15	1.5	8.4	69.2
Totals			88.1		

Gold Deposits	Au (Moz)	Age (Ma)
Cerro Negro deposits	2.0	13.6
Cerro Quilish deposits	6.0	12.6
District-wide acid-sulfate alteration	0.5	11.5
Carachugo-Chaquicocha	6.0	11.0
Chaquicocha-San Jose	5.6	10.8
Maqui Maqui-Corimayo-Tapado	1.5	10.7
San Jose-Tapado	8.5	10.3
Ypq-related at Cerro Yanacocha	1.0	9.9
Cerro Yanacocha Complex	22.0	9.3 to 8.2
Total Gold	53.1	

Abbreviations: Lpha – Lower Yanacocha volcanic sequence, Upha – Upper Yanacocha Volcanic sequence. MMI – Maqui Maqui ignimbrite, SJI – San Jose ignimbrite.

Bibliography

Abarca, D., and Harvey, B., 1997, Modelo geologico del proyecto Encajon: *in* Macharé, J., Cánepa, C., and Injoque, J., eds., IX Congreso Peruano de Geología , Resúmenes Extendidos, Sociedad Geológica del Perú, Vol. Especial 1, p. 3-7.

Aguirre, C., 1998, La Pajuela folio: Unpublished Minera Yanacocha S.R.L. map set, scale 1:5000, folio LP-1.

Anderson, J.L., and Smith, D.R., 1995, The effects of temperature and f_{O_2} on the Al-in-hornblende barometer: American Mineralogist, V. 80, p. 549-559.

Arribas, A., Jr., 1995, Characteristics of high-sulfidation epithermal deposits, and their relation to magmatic fluid: *in* J.F.H. Thompson, ed., Magmas, Fluids, and Ore Deposits: Mineralogical Association of Canada Short Course, v. 23, p. 419-454.

Arribas, A., Jr., Cunningham, C.G., Rytuba, J.J., Rye, R.O., Kelly, W.C., Podwysocki, M.H., McKee, E.H., and Tosdal, R.M., 1995, Geology, geochemistry, fluid inclusions, and isotope geochemistry of the Rodalquilar gold alunite deposit, Spain: Economic Geology, v. 90, no. 4, p. 795-822.

Ashley, R.P., and Silberman, M.L., 1976, Direct dating of mineralization at Goldfield, Nevada, by potassium-argon and fission track methods: Economic Geology, v. 71, p. 904-924.

Ashley, R.P., 1979, Relationship between volcanism and ore deposition at Goldfield Nevada: *in* Papers on mineral deposits of western North America, proceedings of the 5th Quadrennial Syposium of the International Association on the Genesis of Ore Deposits, v. 2, Nevada Bureau of Mines and Geology, no. 33, p. 77-85.

Atherton, M.P., 1990, The Coastal Batholith of Peru: The product of rapid recycling of "new" crust formed within rifted continental margin: Geological Journal, v. 25, p. 337-349.

Atherton, M.P., and Petford, N., 1993, Generation of sodium-rich magmas from newly underplated basaltic crust: Nature, v. 362, p. 144-146.

Atherton, M.P., and Petford, N., 1996, Plutonism and the growth of Andean crust at 9º S from 100 – 3 Ma: Journal of South American Earth Sciences, v. 9, p. 1-9.

Ballard, J.R., Palin, J.M., Williams, I.S., and Campell, I.H., 2001, Two ages of porphyry intrusion resolved for the super-giant Chuquicamata copper deposit of northern Chile by ELA-ICP-MS and SHRIMP: Geology, v. 29, no. 5, p 383-386.

Barton, P.B., Rye, R.O., Bethke, P.M., 2000, Evolution of the Creede Caldera and its relation to mineralization in the Creede Mining District, Colorado: *in* Bethke, P.M., and Hay, R.L. (eds.), Ancient Lake Creede; Its volcanic setting, history of sedimentation, and relation to mineralization in the Creede Mining District: Boulder, Colorado, Geological Society of America, special paper 346, p. 301-326.

Bartra, R., Leach, B., and Longo, A., 1999, Yanacocha district north: Unpublished Minera Yanacocha S.R.L. map set, scale 1:10000, folio YD-17.

Beate, B., Monzier, M., Spikings, R., Cotten, J., Silva, J., Bourdon, E., and Eissen, J.P., 2001, Mio-Pliocene adakite generation related to flat subduction in southern Ecuador: the Quimsacocha volcanic center: Earth and Planetary Science Letters, v. 192, p. 561-570.

Bell, P.D., Gomez, J.G., Loayza, C.E., Pinto, R.M., 2004, Geology of the gold deposits of the Yanacocha district: Pacific Rim Congress, PacRim 2004, Bali, Australia, 10-13 October, Proceedings, 24 p.

Benavides-Cacéres, V., 1999, Orogenic evolution of the Peruvian Andes-The Andean Cycle, *in* Geology and ore deposits of the Central Andes: *in* Skinner B.J., ed., Society of Economic Geologists Special Publication 7, p. 61-108.

Bendezú, R., Fontboté, L., Cosca, M., 2003, Relative age of the Cordilleran base maetal lode replacement deposits, and high sulfidation Au-Ag epithermal mineralization in the Colquijirca mining district, central Perú: Mineralium Deposita, v. 38, p. 683-694.

Bersch, M.G., 2000, Yanacocha high grade study: An optical and SEM-microprobe study of Yanacocha core samples: Newmont Mining Corporation, unpublished company report, 157 p.

Best, M.G., Christiansen, E.H., Dieno, A.L., Gromme, S., and Tingey, D.G., 1995, Correlation and emplacement of a large, zoned, discontinuously exposed ash-flow sheet: The $^{40}Ar/^{39}Ar$ chronology, paleomagnetism, and petrology of the Pahranagat Formation, Nevada: Journal of Geophysical Research, v. 100, no. B-12, p. 24,593-24,609.

Best, M.G., 2003, Igneous and metamorphic petrology: Blackwell Publishing Company, Oxford, U.K., 2nd edition, p.729.

Bethke, P.M., Rye, R.O., Stoffregen, R.E., and Vikre, P.G., 2005, Evolution of the magmatic-hydrothermal acid-sulfate system at Summitville, Colorado: integration of geological, stable isotope, and fluid inclusion evidence: Chemical Geology, v. 215, p.281-315.

391

Blundy, J.D., and Wood, B.J., 1991, Crystal-chemical controls on the partitioning of Sr and Ba between plagioclase feldspar, silicate melts, and hydrothermal solutions: Geochimica et Cosmochimica Acta, v. 35, p. 193-209.

Borredon, E.R., 1982, Etude geologique et metallogenique du district minier de Hualgayoc (Perou septentrional) a plomb-zinc-cuivre-argent: these 3e cycle, University Pierre et Mari Curie, Paris 6, 287p.

Branney, M. and Kokelaar, P., 1998, A reappraisal of ignimbrite emplacement: progressive aggradation and changes from particulate to non-particulate flow during emplacement of high-grade ignimbrite: Bulletin of Volcanology, v. 54, p. 504-520.

Brimhall, G.H., 1979, Lithologic determination of mass transfer mechanisms of multiple-stage porphyry copper mineralization at Butte, Montana: Vein formation by hypogene leaching and enrichment of potassium silicate protore: Economic Geology, v. 74, p. 556-589.

Byers, F.M. Jr., Carr, W.J., Orkild, P.P., Quinlivan, W.D., and Sargent, K.A., 1976, Volcanic suites and related cauldrons of Timber Mountain-Oasis Complex, southern Nevada: U.S.G.S. Professional Paper 919, pp. 70.

Calderón-Myers, E., 1997, Cerro Negro Project: Unpublished Minera Yanacocha S.R.L. memorandum, March 1997, p. 1-11.

Cas, R.A.F. and Wright, J.V., 1988, Volcanic Successions: modern and ancient: Chapman and Hall, London, 528 p.

Chauvet, A. and Bailly, L., 2001, Resultados preliminaries de las observaciones estructurales y mineralogicas realizadas en las muestras del sector de Minas Conga, norte del Peru: Reporte de la mission comun, Universidad de Orléans – Grupo BRGM-GDR – Mayo, 1999, Traducido del original frances por Karina Rosales, 29 p.

Chesner, C.A., Rose, W.I., Drake, A.D.R., Westgate, J.A., 1991, Eruptive history of Earth's largest Quaternary caldera (Toba, Indonesia) clarified: Geology, v.19, p. 200-203.

Clark, A.H., and Ullrich, 2004, $^{40}Ar/^{39}Ar$ age data for andesite magmatism and hydrothermal activity in the Timok Massif, eastern Serbia: implications for metallogenetic relationships in the Bor copper-gold subprovince: Mineralium Deposita, v. 39, p. 259-262.

Clarke, D.S., Sporli, K.B., Smith, I.E.M., Locke, C.A., Kobe, H.W., Black, P.M., and Balance, P.F., 1990, The geologic setting of gold deposits in the Coromandel volcanic zone, New Zealand: Pacific Rim Congress 90, proceedings, 6-12 May 1990, Gold Coast, Queensland, Australia, p. 337-350.

Cobbing, E.J., Pitcher, W.S., Wilson, J.J., Baldock, J.W., Taylor, W.P., McCourt, W.J., and Snelling, N.J., 1981, The Geology of the Western Cordillera of northern Peru: Institute of Geological Sciences, London, Overseas Memoir 5, 143 p.

Cole, Dr., Larson, P.B., Riciputi, L.R., Mora, C.I., 2004, Oxygen isotope zoning profiles in hydrothermally altered feldspars: estimating the duration of water-rock interaction: Gelogy, v. 32, no. 1, p. 29-32.

Coombs, M.L., Eichelberger, J.C., and Rutherford, M.J., 2000, Magma storage and mixing conditions for the 1953-1974 eruptions of Southwest Trident volcano, Katmai National Park, Alaska: Contributions of Mineralogy and Petrology, v. 140, p. 99-114.

Cornejo, P., Tosdal, R.M., Mpodozis, C., Tomlinson, A.J., Rivera, O., Fanning, C.M., 1997, El Salvador, Chile porphyry copper deposit revisited: Geologic and geochronologic framework: International Geology Review, v. 39, p. 22-54.

Dalyrymple, G.B. and Lanphere, M.A., 1974, ^{40}Ar/^{39}Ar age spectra of some undisturbed terrestrial samples: Geochimica et Cosmochimica Atca, v. 38, p. 715-738.

Deen, J.A., Rye, R.O., Munoz, J.L., and Drexler, J.W., 1994, The magmatic hydrothermal system at Julcani, Peru: Evidence from fluid inclusions and hydrogen and oxygen isotopes: Economic Geology, v. 89, p. 1924-1938.

Defant, M.J. and Drummond, M.S., 1990, Subducted lithosphere-derived andesite and dacite rocks in young volcanic arc settings: Nature, v. 347, p. 662-665.

Deyell, C.L., Rye, R.O., Landis, G.P., and Bissig, T., 2005, Alunite and the role of magmatic fluidsin thr Tambo high-sulfidation deposit, El Indio-Pascua belt, Chile: Chemical Geology, v. 215, p. 185-215.

Dilles, J.H., 1987, Petrology of the Yerington Batholith, Nevada: Evidence for evolution of porphyry copper ore fluids: Economic Geology, v. 82, p. 1750-1789.

Dilles, J.H., and Einuadi, M.T., 1992, Wall-rock alteration and hydrothermal flow paths about the Ann Mason porphyry copper deposit, Nevada – A 6-km vertical reconstruction: Economic Geology, v. 87, p. 1963-2001.

Dilles, J.H., 2002, Magmatic-hydrothermal fluids: A summary of temporal and spatial evolution from the 6 km vertical transect of the porphyry copper systems in the Yerington batholith, Nevada: GSA Abstracts, 98th Annual Meeting Corvallis, Oregon, May 13-15, 2002, v.34, no. 5, p.A15.

Doell, R.R., Dalrymple, G.B., Smith, R.L., and Bailey, R.A., 1968, Paleomagnetism, potassium-argon ages and geology of rhyolites and associated rocks of the Valles Caldera, New Mexico: *in* Coates R.R., Hay, R.L., and Anderson, C.A., eds., Studies in Volcanology: Geological Society of America Memoirs No. 116, p. 211-248.

Droop, G.T.R., 1987, A general equation for estimating Fe^{3+} concentrations in ferromagnesian silicates and oxides from microprobe analyses, using stoichiometric criteria: Mineralogical Magazine, v. 51, p. 431-435.

Duncan, R.A., Hooper, P.R., Rehacek, J., Marsh, J.S., and Duncan, A.R., 1997, The timing and duration of the Karoo igneous event, southern Gondwana: Journal of Geophysical Research, v. 102, no. B8, p. 18,127-18,138.

Dungan, M.A. and Davidson, J., 2004, Partial assimilative recycling of the mafic plutonic roots of arc volcanoes: An example from the Chilean Andes: Geology, v. 32, no. 9, p. 773-776.

Einuadi, M.T., 1977, Enviroment of ore deposition at Cerro de Pasco, Peru: Economic Geology, v. 72, p. 893-924.

Edwards, J., 2000, Yanacocha west district geologic interpretation and implications for exploration: Unpublished Minera Yanacocha S.R.L. memorandum, August 5, 2000, p. 1-22.

Edwards, J., and Barreda, J., 2000, Yanacocha district west – 2000: Unpublished Minera Yanacocha S.R.L. map set, scale 1:10000, folio YD-29.

Ewart, E., 1982, The mineralogy and petrology of Tertiary - recent orogenic volcanic rocks with special reference to the andesite-basaltic composition range: *in* Thorpe, R.S., ed., Andesites, John Wiley and Sons, New York, p. 25-87.

Feeley, T.C. and Davidson, J.P., 1994, Petrology of calc-alkaline lavas at Ollagüe and the origin of compositional diversity at central Andean Volcanic stratovolcanoes: Journal of Petrology, v. 35, p. 1295-1340.

Feeley, T.C. and Hacker, M.D., 1995, Intracrustal derivation of Na-rich andesite and dacitic magmas: An example from Ollagüe, Andean Central Volcanic Zone: Journal of Geology, v. 103, p. 213-225.

Field, C.W., and Gustufson, L.B., 1976, Sulfur isotopes in the porphyry copper deposit at El Salvador, Chile: Economic Geology, v. 71, p. 1533-1548.

Field. C.W., Rye, R.O., Dymond, J.R., Whelan, J.F., ands Senechal, R.G., 1983, Metalliferous sediments of the East Pacific, *in* Shanks, W.C., III, ed., Cameron Volume on Unconventional Mineral Deposits: New York, Society of Mining Engineers of A.I.M.E., p. 133-156.

Field, C.W., and Fifarek, R.H., 1986, Light stable-isotope systematics in the epithermal environment, *in* Berger, B.R., and Bethke, P.M., eds., Geology and geochemistry of epithermal systems, Society of Economic Geologists, Reviews in Economic Geology, v. 2, p. 99-128.

Fifarek, R.H., and Rye, R.O., 2005, Stable isotope chemistry of the Pierna high-sulfidation Au-Ag deposit, Peru: influence of hydrodynamics on SO_4^{2-} -H_2S sulfer isotope exchange in magmatic-steam and steam-heated environments: *in* Seal II, R.R., Jambor, J.L., and Alpers, C.N. (eds.), Geochemistry of Sulfate Minerals: A Tribute to Robert O. Rye, Chemical Geology, v. 215, p. 253-279.

Fisher, R.V. and Schmincke, H.U., 1984, Pyroclastic Rocks: Springer-Verlag, Berlin Heidelberg, 472 p.

Flores, E., Terrones, H., and Rogowski, P., 2003, Cerro Quilish project, exploration summary report, December, 2003: Unpublished Minera Yanacocha S.R.L. Report, 24 p.

Frey, H.M., Lange, R.A., Hall, C.M., and Delgado-Granados, H., 2004, Magma eruption rates constrained by $^{40}Ar/^{39}Ar$ chronology and GIS for the Ceboruco-San Pedro volcanic field, western Mexico: Geological Society of America Bulletin, v. 116, p. 259-276.

Gallahan, W.E., and Nielsen, R.L., 1992, The partitioning of Sc, Y, and the rare earth elements between high-Ca pyroxene and natural mafic to intermediate lavas at 1 atmosphere: Geochimica et Cosmochimica Acta, v. 56, p. 2387-2404.

Garrison J.M., and Davidson, J.P., 2003, Dubious case for slab melting in the Northern volcanic zone of the Andes: Geology, v. 31, no. 6, p.565-568.

Gill, J.B., 1981, Orogenic andesite and plate tectonics: Springer and Verlag, Berlin, p. 385.

Goldie, M., 2000, A geophysical case history of the Yanacocha gold district, northern Peru: Society of Exploration Geophysicists, p. 1-4.

Gomez, J.G. and Klein, T., 2000, Corimayo folio: Unpublished Minera Yanacocha S.R.L. map set, scale 1:2,500, folio COR-02.

Gomez, J.G., 2002a, Chaqucocha Alta and Chaquicocha Alta Norte Folios: Unpublished Minera Yanacocha S.R.L. map set, scale 1:500, folio CHQ-09 and 10.

Gomez, J.G., 2002b, Geology and mineralization of the Corimayo gold deposit, Universidad Nacional Mayor de San Marcos: unpublished thesis for the professional title of Ingeniero Geólogo de Perú, 55 p.

Green, T.H., 1994, Experimental studies of trace element partitioning applicable to igneous petrogenesis-Sedona 16 years later: Chemical Geology, v. 117, p.1-36.

Grunder, A.L., and Mahood, G.A., 1988, Physical and chemical models of zoned silicic magmas: the Loma Seca Tuff and Calabozos caldera, southern Andes: Journal of Petrology, v. 29, no. 4, p. 831-867.

Grunder, A.G., Klemetti, E.W. , Feeley, T.C., McKee, C.M. and Knox, K.L., 2004, 11 Million years of arc volcanism at the Aucanquilcha Volcanic Complex, northern Chilean Andes: Implications on the lifespan and emplacement of batholiths in arc settings: Journal of Volcanology and Geothermal Research, *in prep, submitted 12/04.*

Guest, J.E. and Sanchez, R.A., 1969, A large dacitic lava flow in northern Chile: Bulletin of Volcanology, v. 33, p. 778-790.

Gustafson, L.B., and Hunt, J. P., 1975, The porphyry copper deposit at El Salvador, Chile: Economic Geology, v. 70, p. 857-912.

Gustafson, L.B., Orquera, W., McWilliams, M., Castro, M., Olivares, O., Rojas, G., Malvenda, J., Mendez, M., 2001, Multiple centers of mineralization in the Indio Muerto district, El Salvador, Chile: Economic Geology, v. 96, p. 325-350.

Gustafson, L.B., Vidal, C.E., Pinto, R., Noble, D.C., 2004, Porphyry-epithermal transition, Cajamarca Region, northern Perú: *in* R.H. Sillitoe, J. Perello and C.E. Vidal (eds.), Society of Economic Geologists Special Publication 11, Andean Metallogeny: New Discoveries, Concepts and Updates, p. 279-300.

Gutscher, M-A., Olivet, J.L., Aslanian, D., Eissen, J.P., and Maury, R., 1999, The "lost Inca Plateau": cause of flat subduction beneath Perú?: Earth and Planetary Science Letters, v. 171, p. 335-341.

Gutscher, M-A., Sparkman, W., Bijwaard, H., and Engdahl, E.R., 2000, Geodynamics of flat subdustion: Siesmicity and tomographic constraints from the Andean margin: Tectonics, v. 19, no. 5, p. 814-833.

Hall, D., 2000, Chaquicocha Sur and El Tapado reserve and resource information: Unpublished company memorandum, Minera Yanacocha, S.R.L.

Halter, W.E., Bain, N., Becker, K., Heinrich, C.A., Landtwing, M., VonQuadt, A., Clark, A.H., Sasso, A.M., Bissig, T., Tosdal, R.M., 2004, From andesitic volcanism to the formation of a porphyry Cu-Au mineralizing magma chamber: the Farallón Negro Volcanic Complex, northeastern Argentina: Journal of Volcanology and Geothermal Research, v. 136, p. 1-30.

Hammer, J.E., Rutherford, M.J., Hildreth, W., 2002, Magma storage prior to the 1912 eruption at Novarupta, Alaska: Contributions to Mineralogy and Petrology, v. 144, p. 144-162.

Harris, A.C., Allen, C.M., Bryan, S.E., Campbell, I.H., Holcombe, R.J., and Palin, J.M., 2004, ELA-ICP-MS U_Pb zircon geochronology of regional volcanism hosting the Bajo de la Alumbrera Cu-Au deposit; implications for porphyry-related mineralization: Mineralium Deposita, v. 39, p. 46-67.

Harvey, B., Myers, S., and Klein, T., 1999, Yanacocha Gold District, Northern Peru: Australian Institute of Mining and Metallurgy, Pacific Rim Congress, PacRim '99, Bali, Indonesia, 10-13 October, Proceedings, p. 31-?

Hawkesworth, C.J., Norry, M.J., Roddick, J.C., Baker, P.E., Francis, P.W., and Thorpe, R.S., 1979, 143Nd/144Nd, 87Sr/86Sr, and incompatible element variations in calc-alkaline andesites and plateau lavas from South America: Ibid., v. 42, p. 45-57.

Hedenquist, J.W., and Henley, R.W., 1985, Hydrothermal eruptions in the Waiotapu geothermal system, New Zealand: Their origin, associated breccias and relation to precious metal mineralization: Economic Geology, v. 80, p. 1640-1668.

Hedenquist, J.W., Matsuhisa, Y., Izawa, E., White, N.C., Giggenbach, W.F., Aoki, M., 1994, Geology, geochemistry, and origin of high-sulfidation Cu-Au mineralization in the Nansatsu District, Japan: Economic Geology, v. 89, no. 1, p. 1-30.

Hedenquist, J.W., Arribas, A., Jr., and Reynolds, T.J., 1998, Evolution of an intrusive-centered hydrothermal system: Far Southwest-Lepanto Porphyry and epithermal Cu-Au deposits, Philippines: Economic Geology, v. 93, p. 373-404.

Hedenquist, J.W. and Arribas, A., Jr., 1999, Epithermal gold deposits: I Hydrothermal processes in intrusive-related systems, and II. Characteristics, examples and origin of epithermal gold deposits: *in* Molnar, F., Lexa, J., and Hedenquist, J. W., eds., *in* Epithermal Mineralization of the Western Carpathians: Society of Economic Geologists, Guidebook series, vol. 31, p. 13-63.

Hedenquist, J.W., 2000, Observations from the Yanacocha and Minas Conga properties, northern Perú: Relationships between epithermal and porphyry environments: unpublished company report, Minera Yanacocha, S.A., 44 p.

Helz, R.T., 1973, Phase relations of basalts in their melting range at $P_{H_2O} = 5$ kb as a function of oxygen fugacity: Journal of Petrology, V. 14, p. 249-302.

Helz, R.T., 1979, Alkali exchange between hornblende and melt: a temperature sensitive reaction: American Mineralogist, V. 64, p. 953-965.

Henry, C.D., Elson, H.B., McIntosh, W.C., Heizler, M.T., and Castor, S.B., 1997, Brief duration of hydrothermal activity at Round Mountain, Nevada, determined from [40]Ar/[39]Ar geochronology: Economic Geology, v. 92, p. 807-826.

Hildreth, W., 2004, Volcanological perspectives on the Long Valley, Mammoth Mountain, and Mono Craters: several contiguous but discrete systems: Journal of Volcanology and Geothermal Research, v. 136, p. 169-198.

Hildreth, W., Fierstein, J., Lanphere, M., 2003, Eruptive history and geochronology of the Mount Baker volcanic field, Washington: Geological Society of America Bulletin, v. 115, no. 6, p.729-764.

Hildreth, W., Fierstein, J., Siems, D.F., Budhan, J.R., Ruiz, J., 2004, Rear-arc vs. arc-front volcanoes in the Katmai reach of the Alaska Peninsula: a critical appraisal of across-arc compositional variation: Contributions of Mineralogy and Petrology, v. 147, p. 243-275.

Hildreth, W., and Lanphere, M.A., 1994, Potassium-argon geochronology of a basalt-andesite-dacite arc system: The Mount Adams volcanic field, Cascade Range of southern Washington: Geological Society of America Bulletin, v. 106, p. 1413-1429.

Hildreth, W. and Moorbath, S., 1988, Crustal contribution to arc magmatism in the Andes of Central Chile: Contributions Mineralogy and Petrology, v. 98, 455-489.

Huard, J., 2003, Noble gas mass spectrometer lab: Oregon State University Marine Geology, OSU COAS MG Geochronology web site, http://www.coas.oregonstate.edu/mg/chronology.html

Itaya, T., Arribas Jr., A., and Okada, T., 1996, Argon release systematics of hypogene and supergene alunite based on progressive heating experiments from 100 to 1000°C: Geochimica et Cosmochimica Acta, v. 60, no. 22, p. 4525-4535.

Jakes, P. and White, A.J.R., 1972, Hornblendes from calc-alkaline volcanic rocks of island arcs and continental margins: American Mineralogist, v. 57, p. 887-902.

James, J., 1998, Geology, alteration, and mineralization of the Cerro Corona porphyry copper-gold deposit, Cajamarca Province, Peru: Unpublished Masters thesis, University of British Columbia, Vancouver, British Columbia, Canada, 188 p.

Johnson, M.C., and Rutherford, M.J., 1989, Experimental calibration of the aluminum-in-hornblende geobarometer with application to Long Valley Caldera (California) volcanic rocks: Geology, v. 17, p. 837-841.

Kay, R.W., 1977, Geochemical constrants on the origin of Aleutian magmas: *in* Talwani, M., and Pittman III, W.C. (eds.), Island Arcs, Back Arcs Basins, and Deep-sea Trenches, American Geophysical Union, Maurice Ewing Series 1, p. 229-242.

Kelly, S., 2002, Excess argon in K-Ar and Ar-Ar geochronology: Chemical Geology, v. 188, p. 1-22.

Klein, T., Barreda, J., and Harvey, B., 1997, Sur Jose Sur high-sulfidation gold deposit, Yanacocha district, northern Peru: *in* Macharé, J., Cánepa, C., and Injoque, J., eds., IX Congreso Peruano de Geología , Resúmenes Extendidos, Sociedad Geológica del Perú, Vol. Especial 1, p. 57-60.

Klein, T., and Pinto, R., 1999, Yanacocha district south project – Collotan, Kupertal, and San Jose: unpublished Minera Yanacocha S.R.L. map set, scale 1:5000, folio YD-14.

Klein, T., 2000, Yanacocha lithology and gold deposits: unpublished Minera Yanacocha S.R.L. memorandum, November, 2000, p. 1-71.

Klemetti, E.W., and Grunder, A.G., 2003, Longevity and distribution of dacitic magma chambers: A case study of Volcán Aucanquilcha, Central Volcanic Zone of the Andes, northern Chile: SOTA 2003 Meeting Proceeding, http://terra.rice.edu/sota/sotaabstracts.html.

Klemetti, E.W. and Grunder, A.G., 2004, Volcanic Evolution of Volcán Aucanquilcha, a long-lived dacite volcano in the Central Andes of Northern Chile: Bulletin of Volcanology, *in prep. Submitted 12/04.*

Koppers, A.A.P., 2002, ArArCALC – software for $^{40}Ar/^{39}Ar$ age calculations: Computers and Geosciences, v. 7, p. 1-14. (http://earthref.org/tools/ararcalc.htm)

Korringa, M.K., and Noble, D.C., 1971, Distribution of Sr and Ba between natural feldspar and igneous melt: Earth and Planetary Science Letters, v. 11, p. 147-151.

Kudo, T., Okuno, M., and Nakamura, T., 2003, Eruptive history of the Kita-Hakkoda volcanic group during the last 6000 years, northeast Japan: Journal of the Geological Society of Japan, v. 109, no. 3, p. 151-165.

Lanphere, M.A., and Dalrymple, G.B., 1976, Identification of excess 40Ar by the 40Ar/39Ar age spectrum technique: Earth and Planetary Science Letters, v. 32, p. 141-148.

Laughlin, A.W., Damon, P.E., and Watson, B.N., 1968, Potassium – argon data from Toquepala and Michiquillay, Peru: Economic Geology, v. 63, p. 166-168.

Le Bas, M.J., Le Maitre, R.W., Streckeisen, A., Zanettin, B., 1986, A chemical classification of volcanic rocks based on the total alkali-silica diagram: Journal of Petrology, v. 27, no. 3, p. 745-750.

Leach, B.E., 1999, Yanacocha district northeast project: unpublished Minera Yanacocha S.R.L. map set, scale 1:5000, folio YD-12.

Leake, B.E., 1978, Nomenclature of amphiboles: Canadian Mineralogist, V. 16, p. 501-520.

Leake, B.E., Wooley, A.R., Arpa, C.E.S., Birsh, W.D., Gilbert, M.C., Grice, J.D., Hawthrone, F.C., Kato, A., Kisch, H.J., Krivovichev, V.G., Linthout, K., Laird, J., Mandarino, J.A., Maresch, W.V., Nickel, E.H., Rock, N.M.S., Schumacher, J.C., Smith, D.C., Stephenson, N.C.N., Ungaretti, L., Whittaker, E.J.W. and Youzhi, G., 1997, Nomenclature of amphiboles: Report of the Subcommittee on Amphiboles of ther International Mineralogical Association, Commission on New Minerals and Mineral Names: Mineralogical Magazine, v. 61, p. 295-321.

Leng, L, 1999, Minera Yanacocha mining statistics, in Data Estadistica de Minera Yanacocha 1993-2001: Unpublished company report, Minera Yanacocha, S.A.

Lindsley, D.H., 1983, Pyroxene thermometry: American Mineralogist, V. 68, p. 477-493.

Lindsley, D.H. and Andersen, D.J., 1983, A two-pyroxene thermometer, Proceedings of the 13th Lunar and Planetary Science Conference, Part 2: Journal of Geophysical Research, V. 88, p. A887-A906.

Lipske, J.L., Advanced argillic and sericitic alteration in the Buckskin Range, Nevada: a product of ascending magmatic fluids from the deeper Yerington porphyry copper environment: Unpublished Masters thesis, Oregon State University, Corvallis, Oregon, 71 p.

Lipman, P.W., 2000, Central San Juan caldera cluster: regional volcanic framework: *in* Bethke, P.M., and Hay, R.L. (eds.), Ancient Lake Creede; Its volcanic setting, history of sedimentation, and relation to mineralization in the Creede Mining District: Boulder, Colorado, Geological Society of America, special paper 346, p. 9-69.

Llosa, F.T., Lescuyer, J.L., and Milesi, J.P., 1996, Minas Conga: Descubrimiento, exploración y marco geológico de los porfidos Au-Cu en la region de Cajamarca: Segundo Symposium International del Oro, Lima, Peru, p. 275-283.

Llosa, F.T., Veliz, J.M., and Georgel, J.M.P., 1999, Los Porfidos Au-Cu Minas Congas: Historia del descubrimiento y exploracion entre 1992-1998: *in* Primer Volumen de Monografías de Yacimientos Minerales Peruanos, p. 177-195.

Loayza, C.E., 2002, Geologic study of the Cerro Yanacocha gold-silver deposit, Yanacocha district, northern Peru: Unpublished Masters thesis, University of Nevada, Reno, 94 p.

Longo, A.A., 2000, The San Jose-Carachugo-Chaquicocha Gold Trend, Yanacocha District, northern Perú: *in* Geology and Ore Deposits 2000, The Great Basin and Beyond, Proceedings, v. 1, p. 201-220.

Longo, A.A., 2001, Yanacocha study 2001 field season: stratigraphy, exploration targets, and budget, Unpublished company report, Minera Yanacocha, S.A.

Longo, A. A., 2002, El estudio de Yanacocha: Estratigrafia, geoquimica, y dataciones radiometrica de $^{40}Ar/^{39}Ar$, *in* The Yanacocha Study 2nd Quarter Report, Unpublished company report, Minera Yanacocha, S.A.

Longo, A., Escalante, J., Bartra, R., Barreda, J., Velasco, C., Loayza, C., 1999, Yanacocha district east; Unpublished Minera Yanacocha S.R.L. map set, scale 1:10000, folio YD-16.

Longo, A., Velasco, C., Loayza, C., Rutti, M., Bartra, R., and Escalante, J., 2000, The Chaquicocha Project: Surface and subsurface geology, geochemistry, and diamond drill core data from 1997-2000: Unpublished Minera Yanacocha S.R.L. map set, scale 1:2000, folios CHQ-03, CHQ-08, and QUE-01.

Longo, A., Escalante, J., and Bartra, R., 2000, The Arnacocha Project, Surface and subsurface geology, geochemistry, and RVC drill data: Unpublished Minera Yanacocha S.R.L. map set, scale 1:5000, folio ARN-01.

Longo, A., and Escalante, J., 2000, The Cerro Quilish and Antibuyoc project: Unpublished Minera Yanacocha S.R.L. map set, scale 1:5000, folio CQ-09.

Longo, A., Edwards, J., Goldie, M., and Teal, L., 2000, Yanacocha district geology, alteration, geochemistry, geophysics, and targets: Unpublished Minera Yanacocha S.R.L. map set, scale 1:25000, folio YD-26, 28, 40 and 41.

Longo, A.A. and Saderholm, E. 2002, Volcanic stratigraphy and host rocks of gold and copper ore in the Yanacocha Mining District, northern Peru: GSA Abstracts, 98th Annual Meeting Corvallis, Oregon, May 13-15, 2002, v.34, no. 5, p.A15.

Longo, A.A., 2004, The Quilish-Corimayo Connection folio: Unpublished Minera Yanacocha S.R.L. map set and monthly report, August 9, 2004, scale 1:5000.

Lowell, J. D., and Guilbert, J. M., 1970, Lateral and vertical alteration-mineralization zoning in porphyry ore deposits: Economic Geology, v. 65, p. 373-408.

Macfarlane, A.W., and Peterson, U., 1990, Lead Isotope provinces of the Hualgayoc area, northern Peru: Implcations for metal provenance and genesis of a cordilleran polymetallic mining district: Economic Geology, v. 85, p. 1303-1327.

Macfarlane, A.W., Prol-Ledesma, R.M., and Conrad, M.E., 1994, Isotope and fluid inclusion studies of geologicical and hydrothermal processes, northern Peru: International Geology Review, v. 36, p. 645-677.

Mallette, P.M., 2001, Dating of hematized and carbonized wood from the La Quinua gravel deposit, Yanacocha, ^{14}C – Radiocarbon date result for sample LQ-001-C14 from D. Hood: Unpublished Minera Yanacocha S.R.L. memoradum, December 5, 2001.

Mallette, P.M., Rojas, R.E., and Gutierrez, A.R., 2004, Geology, mineralization, and genesis of the La Quinua gold deposit, Yanacocha district, northern Perú, Chapter 16: in R.H. Sillitoe, J. Perello and C.E. Vidal (eds.), Society of Economic Geologists Special Publication 11, Andean Metallogeny: New Discoveries, Concepts and Updates, p. 301-312.

Marquez, E.A., 1997, Porphyry host Cu-Au mineralization Laguna Chamis: in Macharé, J., Cánepa, C., and Injoque, J., eds., IX Congreso Peruano de Geología , Resúmenes Extendidos, Sociedad Geológica del Perú, Vol. Especial 1, p. 101-105.

Marsh, T.M., Einaudi, M.T., and McWilliams, M., 1997, ^{40}Ar/^{39}Ar geochronology of the Cu-Au and Au-Ag mineralization in the Portrerillos District, Chile: Economic Geology, v. 92, p. 784-806.

Martin, M.W., and Dilles, J.H., 2000, Timing and duration of the Butte porphyry Cu-Mo system: GSA Cordilleran Section, 96th annual meeting, Abstracts with programs, v.32, no. 6, p.28.

Masterman, S., 2001, Shoclla and Huangayoc project: Unpublished Minera Yanacocha S.R.L. geology map set, scale 1:5000, folio SHC-02.

Masterman, S., and Bartra, R., 2000, Arnacocha geophysics and geology: Unpublished Minera Yanacocha S.R.L. map set, scale 1:2000, folio ARN-03.

McKee E.H., and Noble, D.C., 1982, Miocene volcanism and deformation in the western Cordillera and high plateaus of south-central Peru: Geological Society of America Bulletin, v. 93, p. 657-662.

Megard F, 1984, The Andean orogenic period and its major structures in central and northern Peru: Geological Society of London Journal, v. 141, p. 893-900.

Megard, F., 1987, Structure and evolution of the Peruvian Andes: *in* Schaer, J.P., and Rogers, J., The Anatomy of Mountain Ranges, Princeton University Press, p. 179-210.

Meldrum, S., 2001, Patterns of geochemical zonation at the Cerro Yanacocha Complex and Corimayo gold deposit: Unpublished Minera Yanacocha S.R.L. report, +350 p.

Merzbacher, C., and Eggler, D.H., 1984, A magmatic geohygrometer: Application to Mount St. Helens and other dacitic magmas: Geology, v. 12, p. 587-590.

Meyer, C., Shea, E.P., and Goddards, C.C., Jr., 1968, Ore deposits at Butte, Montana: *in* Ridge, J.D., ed., Ore Deposits of the United States, 1933-1967, Graton-Sales vol., New York, American Inst. Mining Metall. Petrolium Engineers, p. 1373-1416.

Mitouard, P., Kissel, C., and Laj C., 1990, Post-Oligocene rotations in southern Ecuador and northern Peru and the formation of the Huancabamba deflection in the Andean Cordillera: Earth and Planetary Science Letters , v. 98, p. 329-339.

Moore, S., 2002, Sacsha Breccia: welded pyroclastic fall deposit: Unpublished Minera Yanacocha S.R.L. memorandum, October 13, 2002, p. 1-8.

Moore, S., and Saderholm, E., 2002a, Yanacocha district stratigraphy summary, June 2002: Unpublished Minera Yanacocha S.R.L. Report, 54 p.

Moore, S., and Saderholm, E., 2002b, Yanacocha district stratigraphy summary, December 2002: Unpublished Minera Yanacocha S.R.L. Report, 72 p.

Morimoto, N., Fabries, J., Ferguson, A.K., Ginzburg, I.V., Ross, M., Seifert, F.A., Zussman, J., Aoki, K., Gottardi, G., 1988, Nomenclature of pyroxenes: Mineralogical Magazine, V. 52, P. 535-550.

Myers, S., 1997, Carachugo project: Unpublished Minera Yanacocha S.R.L. map set, scale 1:2000, folio CHG-01.

Myers, S.A., Changanaqui, M., Bond, R.W., Aquirre, C., Mallette, P.M., 1997, Geology of the Carachugo deposits, Yanacocha district, Peru: *in* Macharé, J., Cánepa, C., and Injoque, J., eds., IX Congreso Peruano de Geología , Resúmenes Extendidos, Sociedad Geológica del Perú, Yanacocha Field Trip Guide Book, p. 24-34.

Myers, S. and Williams, C., 2000, Geologic evolution of the Yanacocha district high-sulfidation gold system, northern Peru (abs): *in* Cluer, J.K., Price, J.G., Struhsacker, E.M., Hardyman, R.F., and Morris, C.L., eds., Geology of Ore Deposits 2000 – The Great Basin and Beyond: Geological Society of Nevada Symposium, Reno, Nevada, May 15-18, 2000, p. 235.

Muntean, J.L., 1998, Magmatic-hydrothermal gold deposits of the Maricunga belt, northern Chile: Unpublished Ph.D. thesis, Stanford University, Stanford, CA, 400p.

Muntean, J.L. and Einaudi, M. T., 2000, Porphyry gold deposits of the Refugio district, Maricunga belt, Northern Chile: Economic Geology, v. 95, no. 7, p. 1445-1472.

Naney, M.T., 1983, Phase equilibria of rock-forming ferromagnesian silicates in granitic systems: American Journal of Science, v. 283, p. 933-1033.

Nelson, C.E., 2000, Volcanic domes and gold mineralization in the Pueblo Viejo district, Dominican Republic: Mineralium Deposita, v. 35, p.511-525.

Newmont Mining Corporation, 2002, Newmont - The gold company, Annual Report 2002, Form 10-K, pp. 1-167.

Newmont Mining Corporation, 2003, Newmont - Take stock in gold, 2003 Annual Report, Form 10-K, pp.1-281.

Noble, D.C., 2002, New ^{40}Ar/^{39}Ar age determinations on rocks from Minas Congas and Michiquillay: Unpublished company memo, Minera Buenaventura, S.A.

Noble, D.C., 1997, Yanacocha Ages: Memorandum to Minera Yanacocha: Unpublished company memorandum, Minera Yanacocha, S.A., September, 1997, p. 1.

Noble, D.C., McKee, E.H., Farrar, E., and Petersen, U., 1974, Episodic Cenozoic volcanism and tectonism in the Andes of Peru: Earth and Planetary Science Letters, v. 21, p. 213-220.

Noble, D.C., and McKee, E.H., 1982, Nevado Portugueza Volcanic Center, central Peru: A Pliocene central volcano-collapse caldera complex with associated silver mineralization: Economic Geology, v. 77, p. 1893-1900.

Noble, D.C., Sébrier, M., Megard, F., and McKee, E.H., 1985, Demonstration of two pulses of Paleogene deformation in the Andes of Peru: Earth and Planetary Science Letters, v. 73, p. 345–349.

Noble, D.C., McKee, E.H., Mourier, T., and Megard, F., 1990, Cenozoic stratigraphy, magmatic activity, compressive deformation, and uplift in northern Peru: Geological Society of America Bulletin, v. 102, p. 1105-1113.

Noble, D.C. and Vidal, C.E., 1994, Gold in Peru: SEG Newsletter, Society of Economic Geologists, no. 17, p. 1-13.

Noble, D.C. and McKee, E.H., 1999, The Miocene Belt of Central and Northern Perú: *in* Skinner, B.J. ed., Geology and ore deposits of the Central Andes, Society of Economic Geologists Special Publication 7, p. 155-193.

Noble, D.C., Vidal, C.E., Perelló, J., and Rodríguez, O.P., 2004, Space-time relationships of some porphyry Cu-Au, epithermal Au, and other magmatic-related m9neral deposits in northern Perú, Chapter 17: *in* R.H. Sillitoe, J. Perello and C.E. Vidal (eds.), Society of Economic Geologists Special Publication 11, Andean Metallogeny: New Discoveries, Concepts and Updates, p. 313-318.

Ossandon C., G., Freraut C., R., Gustafson, L.B., Lindsay, D.D., and Zentilli, M., 2001, Geology of the Chuquicamata mine: A progress report: Economic Geology, v. 96, no. 2, p. 249-270.

Palacios M.O., Sanchez F.A., and Herrera R.F., eds., 1995, Geologia del Peru (1st ed.): Carta Geologica Nacional, INGEMET, Lima, Perú, Boletin 55, ser. A, 177 p.

Paredes, J., 1997, Metalogenia del distrito minero de Hualgayoc: *in* Macharé, J., Cánepa, C., and Injoque, J., eds., IX Congreso Peruano de Geología , Resúmenes Extendidos, Sociedad Geológica del Perú, Vol. Especial 1, p. 139-144.

Pavard, A. and Bowerman, A., 1994, Yanacocha project chronology: Unpublished company report, Newmont Mining Corporation, p. 1-15.

Petersen, U., Noble, D.C., Arenas, M.J., and Goodell, P.C., 1977, Geology of the Julcani Mining District, Peru: Economic Geology, v. 72, p. 931-949.

Petersen, G. and Vidal, C., 1983, Tres epocas metalogeneticas evidenciadas en el Cenozoico del Peru: Boletin de Sociedad Geologica del Peru, no. 71, p. 107-112.

Petford, N., and Atherton, M.P., 1995, Cretaceous-Tertiary volcanism and syn-subduction crustal extension in northern central Peru: *in* Snellie J.L., ed., Volcanism ssociated with extension at consuming plate margins, Geological Society of London Special Publication 81, p. 233-248.

Petford, N., Atherton, M.P., and Halliday, A.N., 1996, Rapid magma production rates, underplating, and remelting in the Andes: isotopic evidence from northern-central Perú: Journal of South American Earth Sciences, v. 9, p. 69-78.

Petrinovic, I.A., Riller, U., and Brod, A.J., 2005, The Negro Muerta volcanic complex, southern Central Andes: geochemical characteristics and magmatic evolution of an episodically active volcanic centre: Journal of Volcanology and Geothermal Research, v. 140, p. 295-320.

Pinto, R.M., 2002, Transición de un sistema de alta sulfuración a un sistema porfiritico de alto nivel en Kupfertal, Distrito Minero de Yanacocha, Cajamarca, Perú: Unpublished thesis for the professional title of Ingeniero Geólogo de Perú, Universidad Nacional Mayor de San Marcos, 46 p.

Prihar, D., 1998, Geology map of the Hualgayoc District, Tantahuatay Project: Unpublished company report, CIA. Minera Coimolache, S.A., scale 1:2,500.

Quiroz, A., 1997, Sintesis de la Geologia del Peru y metalogenia del oro: Unpublished company report, Minera Yanacocha, S.A., 35 p.

Quiroz, A., 1997, El corridor estructural Chicama-Yanacocha su importancia en la metalogenia del norte del Peru: *in* Macharé, J., Cánepa, C., and Injoque, J., eds., IX Congreso Peruano de Geología , Resúmenes Extendidos, Sociedad Geológica del Perú, Vol. Especial 1, p. 149-154.

Rehrig, W.A., and Hardy, J.J., 2001, Structural study of the Central Yanacocha District, Peru: Unpublished Minera Yanacocha S.R.L. report, 156 p.

Reynolds, P., Ravenhurst, C., Zentilli, M., and Lindsay, D., 1998, High precision 40Ar/39Ar dating of two consecutive hydrothermal events in the Chuquicamata porphyry system, Chile: Chemical geology, v. 148, p. 45-60.

Renne, P.R., Swisher, C.C., Deino, A.L., Karner, D.B., Owens, T.L., and DePaulo, D.J., 1998, Intercalibration of standards, absolute ages and uncertainties in $^{40}Ar/^{39}Ar$ dating, Chemical Geology, vol. 145, p. 117-152.

Reyes, L.R., 1980, Geología de los cuadrángulos de Cajamarca, San Marcos y Cajabamba: Instituto Geológico Minero y Metalúrgico, Lima, Boletín 31 serie A, 71 p.

Rogers, G. and Hawkesworth, C.J., 1989, A geochemical transverse across the North Chilean Andes: evidence for crust generation from a mantle wedge, Earth and Planetary Science Letters, v. 91, p. 271-285.

Rose, W.I., 1999, Reading volcanic rocks in the field: Minera Yanacocha Volcanic Short Course I, Laguna Seca, Banos del Inca, Peru, p. 1-30.

Ross, C.S. and Smith, R.L., Ash-flow tuffs: Their origin, geologic relations and Identification: USGS Professional Paper 366, p. 1-67.

Rota, J., 1997, Carachugo geologic model March 97: Unpublished Newmont Mining Corporation company report, June 10, 1997.

Rota, J., 1998, Yanacocha geologic model: Unpublished Newmont Mining Corporation company report.

Rutherford, M.J., and Hill, P.M., 1993, Magma ascent rates from amphibole breakdown: and experimental study applied to the 1980-1986 Mount Saint Helens eruptions: Journal of Geophysical Research, v. 98, p. 19,667-19,685.

Rutherford, M.J., and Devine, J.D., 2003, Magmatic conditions and magma ascent as indicated by hornblende phase equilibria and reactions in the 1995-2002 Soufière Hills magma: Journal of Petrology, v. 40, no. 8, p. 1433-1454.

Rutti, M., Teal, L., Quispe, J., Melgar, J., 2000, La Sorpresa project: Unpublished Minera Yanacocha S.R.L. map set, scale 1:2000, folio SOR-02.

Rye, R.O, Bethke, P.M., and Wasserman, M.D., 1992, The stable isoptope geochemistry of acid sulfate alteration: Economic Geology, v. 87, no. 2, p. 225-262.

Rye, R.O., 2005, A review of the stable-isotope geochemistry of sulfate minerals in selected igneous environments and related hydrothermal systems: *in* Seal II, R.R., Jambor, J.L., and Alpers, C.N. (eds.), Geochemistry of Sulfate Minerals: A Tribute to Robert O. Rye, Chemical Geology, v. 215, p. 5-36.

Samaniego, P., Martin, H., Robin, C., and Monzier, M., 2002, Transition from calc-alkalic to adakitic magmatism at Cayambe volcano, Ecuador: Insights into slab melts and mantle wedge interactions: Geology, v. 30, no. 11, p. 967-970.

Sawyer, D.A., Fleck, R.J., Lanphere, M.A., Warren, G.G., Broxton, D.E., and Hudson, M.R., 1994, Episodic caldera volcanism in the Miocene southwestern Nevada volcanic field: Revised stratigraphic framework, 40Ar/39Ar geochronology, and implications for magmatism and extension: Geological Society of America Bulletin, v. 106, p. 1304-1318.

Schnell, C., Williams, C, Teal, L., and Klein, T., 2000, Yanacocha Field Trip Guide Book: ProExplor 2000, Lima, Peru, 34 p.

Snee, L., Miggins, D., Geissman, J.W., Reed, M.H., Dilles, J.H., Zhang, L., 1999, Thermal history of the Butte porphyry system, Montana, Geological Society of America 1999 annual meeting, Abstracts with programs, v. 31, no. 7, p. 380.

Siebe, C., Rodriguez-Lara, V., Schaaf, P., Abrams, M., 2004, Radiocarbon ages of Holocene Pelado, Guespalapa, and Chichinautzin scoria cones, south of Mexico city: implications for archaeology and future hazards: Bulletin of Volcanology, v. 66, p. 203-225.

Sillitoe, R.H., 1973, The tops and bottoms of porphyry copper deposits: Economic Geology, v. 68, p. 799-815.

Sillitoe, R.H., 1983, Enargite-bearing massive sulfide deposits high in porphyry copper systems: Economic Geology, v. 78, p. 348-352.

Sillitoe, R.H., 2000, Comments on geology and exploration of porphyry copper-gold mineralization in the Yanacocha District, Peru: Unpublished company report, Minera Yanacocha, S.A., 11 p.

Sisson, T.W., 1994, Hornblende-Melt Trace-Element Partitioning Measured by Ion Microprobe: Chemical Geology, v. 117, p. 331-344.

Smith, R.L., 1960, Zones and zonal variation in welded ash flows: U.S.G.S. Professional Paper 354-F, p. 149-159.

Smith, G.A. and Lowe, D.R., 1991, Lahars: volcano-hydrologic events and deposition in the debris flow-hyperconcentrated flow continuum, in: Sedimentation in Volcanic Settings: SEPM (Society of Economic Paleontologists and Mineralogists) Special Publication No. 45, eds. Fisher, R.V. and Smith G.A., p. 59-70.

Soriano, C., Zafrilla, S., Marti, J., Bryan, S., Cas, R., and Ablay, G., 2002, Welding and rheomorphism of phonolitic fallout deposits from the las Canadas caldera, Tenerife, Canary Islands: Geologic Society of America Bulletin, v. 114, no. 7, p. 883-895.

Sparks, R.S.J. and Wright, J.V., 1979, Welded air-fall tuffs: *in* C.E. Chapin and W.E. Elston (eds), Ash-Flow Tuffs: Geological Society of America, Special Paper 180, p. 155-166.

Stern, C.R., and Kilian, R., 1996, Role of the subducted slab, mantle wedge and continental crust in the generation of adakites from the Andean Austral Volcanic Zone: Contributions to Mineralogy and Petrology, v. 123, p. 263-281.

Sumner, J.M., 1998, Formation of clastogenic lava flows during fissure eruption and scoria cone collapse: the 1986 eruption of Izu-Oshima volcano, eastern Japan: Bulletin of Volcanology, v. 60, p. 195-212.

Sun, S.S., and McDonough, W.F., 1989, Chemical and isotopic systematics of ocean basalts: implications for mantle composition and process: *in*, Saunders, A.D., Norry, M.J. (eds.), Magmatism in Ocean Basins, Geological Society of London, Special Publication, V. 42, p. 313-345.

Tegner C., and Duncan, R.A., 1999, ^{40}Ar/^{39}Ar chronology for the volcanic history of the southeast Greenland rifted margin: *in* Larsen, H.C., Duncan, R.A., Allan, J.F., Brooks, K. (eds.), Proceedings of the Ocean Drilling Program, Scientific Results, v. 163, p. 53-62.

Thompson, T., 2003, ^{40}Ar-^{39}Ar age dates for northern Minas Congas area: Unpublished company report, Minera Yanacocha, S.A..

Thorpe, R.S., Francis, P.W., Harmon, R.S., 1980, Andean andesites and crustal growth: Revista Geologica de Chile, No. 10, p. 55-73.

Torres, A., Camero, D., Duran, G., 2001, Proyecto Tantahuatay: Informe de actividades geologicas, compeña de exploraciones 2000: Unpublished report, Compania Minera Coimolache, S.A., Lima, 7 de Junio, 2001, p. 54.

Trigila, R., and Walker, G.P.L., 1986, The Onano spatter flow, Italy: evidence for a new ignimbrite depositional mechanism (abs): IAVCEI General Assembly, New Zealnd, p. 81.

Trujillo, J., 2004, Chaupiloma-Shoclla-Huancayoc Folio: Unpublished Minera Yanacocha S.R.L. map set, scale 1:5000.

Turbeville, B.N., 1992, Tephra fountaining, rheomorphism, and spatter flow during emplacement of the Pitigliano Tuffs, Latera caldera, Italy: Journal of Volcanology and Geothermal Research, v. 53, p. 309-327.

Turner, S.J., 1997, The Yanacocha epithermal gold deposits, northern Peru: high-sulfidation mineralization in a flow–dome setting: Unpublished Ph.D. thesis, Colorado School of Mines, 341 p.

Turner, S.J., 1999, Settings and styles of high-sulfidation gold deposits in the Cajamarca region, northern Peru: Australian Institute of Mining and Metallurgy, PacRim '99, Bali, Indonesia, 10-13 October, Proceedings, p. 461–468.

Turner, S.J., 1999, Comments and speculations on Yanacocha: Unpublished Minera Yanacocha S.R.L. memorandum, March 1999, p. 1-15.

Velasco, C., 1999, Yanacocha north project – Far north and Antonio: Unpublished Minera Yanacocha S.R.L. map set, scale 1:5000, folio YD-13.

Vidal, C.E., Proano, J.A., and Noble, D.C., 1997, Geologia y distribucion hidrotermal de menas con Au, Cu, Zn, Pb y Ag en el distrito minero Colquijirca, Pasco: *in* IX Congreso Peruano de Geologia, Resumenes Extendidos, Publicacion Especial no. 1, Sociedad Geologica del Peru, Lima, p. 217-219.

Walker, G.P.L., 1985, Origin of coarse lithic breccias near ignimbrite source vents: Journal of Volcanology and Geothermal Research, v. 25, p.157-171.

Wallace, P., and Anderson, A.T., 1999, Volatiles in Magmas: *in* H. Sigurdsson et al. (eds), Encyclopedia of Volcanoes, Academic Press, p. 149-170.

Williams, C., and Calderón, E., 2000, The La Quinua gold deposit: *in* Cluer, J.K., Price, J.G., Struhsacker, E.M., Hardyman, R.F., and Morris, C.L., eds., Geology of Ore Deposits 2000 – The Great Basin and Beyond: Geological Society of Nevada Symposium, Reno, Nevada, May 15-18, 2000, p. 250-260.

Wilson, 1984, Geología de los cuadrángulos de Jayanca, Incahuasi, Cutervo, Chiclayo, Chongoyape, Chota, Celendín, Pacasmayo y Chepén: Instituto Geológico Minero y Metalúrgico, Lima, Boletín 38 serie A, 104 p

Wones, D.R., 1989, Significance of the assemblage titanite + magnetite + quartz in granitic rocks: American Mineralogist, v. 74, p. 744-749.

Wright, J.V. and Walker, G.P.L., 1977, The ignimbrite source problem: Significance of a co-ignimbrite lag-fall deposit: Geology, v. 5, p. 729-732.

Yasui, M. and Koyaguchi, T., 2004, Sequence and eruptive style of the 1783 eruption of Asama Volcano,central Japan: a case study of an andesitic explosive eruption generating fountain-fed lava flow, pumice fall, scoria flow and forming a cone: Bulletin of Volcanology, v. 66, #3, p. 243-262.

Zeil, W., 1979, The Andes: A geological review: Stuttgart, Gebruder Borntraeger Publishers, 260 p.

Zentilli, M., Krough, T.E., Maksaev, V., and Alpers, C.N., 1994, Uranium-lead dating of zircons from the Chuquicamata and La Escondida porphyry copper deposits, Chile: Inherited zircon cores of Paleozoic age with Tertiary overgrowths: Comunicaciones, no. 45, p, 101-110.

Zhu, C. and Sverjensky, mD.A., 1991, Partitioning of F-Cl-OH between minerals and hydrothermal fluids: Geochimica et Cosmochimica Acta, V. 55, pp. 1837-1858.

APPENDICES

Appendix I Terminology

Pyroclastic Rocks

Ash-flows are mixtures of gas and pyroclastic material of >50% ash with scattered crystals, pumice and accidental lapilli and blocks that were ejected explosively at a high temperature from a crater or fissure and travels down the slopes of a volcano along the ground surface (Ross and Smith, 1960).

Ash flow tuffs are the consolidated deposits of ash flows that may range from non-welded, partially welded to strongly welded.

Block and ash flows are small volume, poorly-sorted, monolithic fragmental or pyroclastic flows that are produced from gravitational or explosive dome collapse, column collapse, and "boiling over" and confined to drainages and canyons. Radial fractured blocks are common (Figure A3.15; Appendix III) due to less transport time than lahars.

Clastogenic lava flows form from the rapid accumulation of spatter that is flattened, stretched and deformed during mass flow down a slope (Cas and Wright, 1988). These "lava" flows are originally formed by rheomorphism of pyroclastic material and are not erupted as a coherent lava (Sumner, 1998).

Cooling Units of Ash Flow Tuff

(1) A simple cooling unit results by rapid emplacement of one or more ash flows with no hiatus in cooling resulting in simple continuous welding variations (Smith, 1960).

(2) Compound cooling units develop from breaks in the cooling history during eruptions of numerous pyroclastic flows and can vary by horizontal gradation from a single simple cooling unit to several separate cooling units (Smith, 1960). Compound cooling units are deposits of multiple ash flows with several zones of dense welding and partial welding that suggest the tops of earlier flows were cooled before the emplacement of later flows over a span of tens of years (Fischer and Schmincke, 1984; Cas and Wright, 1988). Some ignimbrite sequences, such as the San Jose ignimbrite, may resemble compound cooling units, but actually consist of multiple separate cooling units from distinct events related to an eruptive stage that spanned over 300,000 years.

Ignimbrite is a general term applied to the consolidated deposits of numerous sheet-like pyroclastic flows or ash flow tuffs that make up a larger depositional package or sequence of rocks. The term literally means fiery rain cloud.

Pyroclastic flows are volcanically produced accumulations of poorly-sorted juvenile and accidental fragments that range from ash-, lapilli- to block-size and deposited as a hot consolidated or unconsolidated, high-energy, gaseous particulate density current (Fischer and Schmincke, 1984; Rose, 1999) that include topographically controlled block and ash flows to sheet-like ash-flow tuffs. Air mixes with debris and acts as a lubricant along the base at the head of the flow (Rose, 1999).

Pyroclastic surge deposits are any type of surge deposit that formed from an explosive volcanic event from ash-cloud, base, and ground surge. They are fine-grained, moderately sorted, thin-bedded massive, laminated, and cross-bedded deposits associated with ignimbrites or hydrovolcanic eruptions.

Epiclastic Sedimentary Rocks

Lahar and Debris flows are poorly sorted gravity induced viscous mass flow breccia with very coarse to fine sediment debris mobilized by the addition of water. Flows are strongly controlled by topography and the high viscosity enables transport of huge blocks not characteristically found in pyroclastic flows. In contrast to pyroclastic flows, water acts as the lubricant and charred or uncharred fragments are common. Lahars are contemporaneous volcanic debris (i.e., pumice) with volcanic eruptions and difficult to distinguish from non-volcanic debris flows.

Hyperconcentrated flows are high-discharge, granular mass flows with a high ratio of interstitial water to sediment that produces increased turbulence, fluid buoyancy and grain-to-grain deposition that results in lower viscosities, better sorting, and finer grained deposits compared to debris flows (Smith and Lowe, 1991). Deposition does not occur en masse as in debris flows.

Mud flow is a fine-grained viscous mass flow without coarse debris (Cas and Wright, 1988).

Appendix II Methods

Fieldwork

Two field seasons (2001 and 2002) were spent mapping and collecting samples directly related to this study and totaled four months of actual field time. Prior to this study A.A.Longo spent three and a half years working at Yanacocha mapping various areas in the district at 1:2,500 and 1:5,000 scale in areas including Chaquicocha, Quecher, Azufre, Arnacocha, Baul, Sacsha, Paquerumi, Angelita-San Jose Sur, and Quilish. The 2001-2002 field program was designed to include geologic mapping at 1:25,000 scale, sampling, and detailed core logging of the igneous rocks within and around the Yanacocha district.

Fieldwork began by mapping fresh volcanic rocks outside the district. These rocks are the unaltered analogs of the volcanic rocks that host gold, silver, and copper ore within the Yanacocha district and were mapped from outside district boundaries into the core of the district (the "outside-in" mapping concept). Least-altered volcanic and intrusive rocks were sampled from areas within and surrounding the Yanacocha District for radiometric dating and petrologic analysis. Alunite was collected from zones of quartz-alunite alteration within and surrounding the ore zones of each major Yanacocha deposit.

Diamond drill core (DDH) and reverse-circulation rotary drill cuttings (RVC) were selected from key sites throughout the district and their geology of 57 drill holes (3 are the RVC pre-collars to the DDH) was logged at a scale of 1:50 and summarized in plate 5 at a 1:500 vertical scale and 1:50,000 map scale. These data have provided important results critical to the temporal framework and model for the district. Categories recorded during logging include the following: (1) primary mineralogy, (2) percent phenocyrsts, (3) rock textures, (4) alteration mineralogy and texture, (5) vein and breccia mineralogy, types, and general orientations, and (5) interpretive rock units. Rock units and alteration identified in select drill core were sampled for petrographic and geochemical characterization, and $^{40}Ar/^{39}Ar$ geochronology.

$^{40}Ar/^{39}Ar$ Geochronology

Analytical Methods

Ages reported in this study were determined in the noble gas mass spectrometry lab of the College of Oceanic and Atmospheric Sciences at Oregon State University. Two $^{40}Ar/^{39}Ar$ step heating methods were used and discussed below: (1) incremental heating with a furnace for whole rock, plagioclase, hornblende, biotite and one alunite sample, and (2) step heating by laser fusion for 19 alunites.

A total of 69 samples were collected from volcanic and intrusive rocks throughout the Yanacocha region and dated with radiometric $^{40}Ar/^{39}Ar$ analyses (48 of fresh rocks and 21 of hydrothermal alteration). Age of volcanism was dated with 37 samples from a variety of ash-flows and lava flows complimented with 11 samples from domes and intrusions from across the region. The age of mineralization was dated with 20 alunites collected from west to east across the district and represents the following deposits: (1) Cerro Negro Oeste, (2) Cerro Quilish Norte, (3) Corimayo and Tapado, (4) the Yanacocha Complex, (5)

Chaquicocha and Cerro Baul, and (6) Maqui Maqui. Alunite alteration of the Yanacocha rocks is assumed to be associated with the main high-sulfidation event and gold ore (Turner, 1997; Harvey et al., 1999, Prihar, 1999, Hedenquist, 2000). Secondary biotite associated with anomalous gold, copper and molybdenum was collected from a diamond drill hole at Kupfertal and provides an age for the hypothesized porphyry system that lies at depth between the Yanacocha Complex and the San Jose gold deposits.

Sample Preparation

All samples were individually crushed and pulverized to -30+50 mesh, then a hand magnet was stirred through each sample to remove magnetite. Alunite separates TAP-169, ENC-6, PNE-3, and MM-314 were sieved to -80+100 and -120 mesh due to the fine nature of the alunite. All other alunites were sieved to -30+50 mesh and handpicked for purity. Plagioclase and amphibole were separated using a Frantz isodynamic magnetic separator Model L-1, and the vibrator control and sample holder were adjusted to a setting that allowed for a steady stream one to two crystals wide (68-70 on the vibrator control and a couple of turns on the sample cone to loosen the sample holder) for 2 to 4 hours. Plagioclase separation began at 0.15 amps and was increased stepwise by 0.15 to 0.30 amps until a maximum of 1.9 amps was reached, and the nonmagnetic concentrate was nearly all feldspar. During amphibole separation the power was increased stepwise from 0.1 to 0.7 the magnetic separates of the initial steps were discarded until visible amphibole was dropping out. Both plagioclase and amphibole then were handpicked to assure 100% purity. All mineral separates were washed in distilled/de-ionized water with an ultrasonic cleaner for 5 to 10 minutes until clear, then decanted, and finally dried overnight at 70° C. Plagioclase mineral separates were washed in 5% HF for 1 minute, and 5% HNO_3 for 15 minutes, and then washed in de-ionized water as described above.

Biotite was separated using a technique of decantation. The pulverized sample containing biotite was poured into a large +1.0 liter-sized beaker. The beaker was rapidly filled with de-ionized water and decanted halfway into a second large beaker. Biotites momentarily float in the upper portion of the beaker while all other minerals rapidly settle out. The second beaker is allowed to sit until all the sample settles and then was decanted of the water. This procedure was repeated several times, allowing concentration of biotite in the second beaker. Biotite concentrates were dried overnight at 70° C and then handpicked for purity.

Yanacocha mineral separates were weighed and 92-100 mg of plagioclase, 28-43 mg of alunite (the optimum amount of alunite), 20-30 mg of biotite, 30-50 mg of hornblende were each placed in separate copper-foil containers and labeled with a sample ID. All samples were irradiated in the Oregon State University Triga Reactor at 1 megawatt for 6 hours in evacuated quartz vials loaded in Al-Triga tubes. Sample height in millimeters is recorded for each sample. The neutron flux (J) is monitored with several 2.5 to 10 mg samples of Fish Creek Tuff FCT-3 biotite standard with an age of 28.03±0.12 Ma (Renne et al., 1998). The FCT-3 monitor is placed at regular intervals in the quartz vials, monitor height is recorded

as for the samples, the J is calculated for each monitor, and a second-degree polynomial fitted to the measured J's that can be used for each sample distance from the neutron source.

Laboratory Procedures

^{40}Ar/^{39}Ar radiometric ages reported in this study were determined in the noble gas mass spectrometry lab of the College of Oceanic and Atmospheric Sciences at Oregon State University. Two gas extration methods were used and discussed below: (1) incremental heating with a furnace for whole rock, plagioclase, hornblende, biotite and one alunite sample, and (2) step heating by laser fusion for 19 alunites.

Furnace Method

Age analyses on mineral separates of plagioclase, biotite, hornblende, whole rock mini-cores, and one alunite were accomplished using stepwise or incremental heating with a furnace in the noble gas mass spectrometry lab. The system is equipped with a Heine low-blank, double-vacuum resistant furnace with a Mo-lined, Ta-Nb crucible (Huard, 2003). Gas extraction in plagioclase, hornblende, biotite and whole rock samples is achieved by incremental heating in the furnace. Irradiated samples, individually wrapped in Cu foil, and whole rock mini-cores are loaded into a glass sample holder attached to the furnace manifold and an all metal, vacuum sealed extraction line system fixed with Varian valves. At the onset of an incremental heating experiment, samples are separately dropped from the manifold into the furnace crucible. Temperatures in the crucible are controlled by a programmable power supply thermocouple system (Huard, 2003). All samples were degassed at the start of the experiment at 400°C and the end at a ~1500°C final degas between samples. During the degas stage and between heating steps the extraction lines are pumped out with two ion pumps at 150L/s and 200L/s. During a heating step the gas is exposed for 15 minutes to the ST 101 Zr-Al primary getter. On cool down after 2½ minutes the gas is exposed to the ST 172 Zr-V-Fe final getters for approximately 4 minutes. The gas is slowly released through the inlet valve into a Mass Analyser Products model 215-50 rare gas mass spectrometer for ^{40}Ar/^{39}Ar analyses and the age calculations begin for all isotopes of argon (Huard, 2003).

Laser Fusion Method

Incremental heating experiments for 19 alunite mineral separates were conducted by a Merchantek 30 watt CO_2 laser system with a microscopic infrared pyrometer API Micro Probe model MSP-200G that monitors the temperature of a 50 micron spot on the sample over a temperature range of 400-1500°C (Huard, 2003). The system is computer operated and temperatures are controlled with percent laser power by the computer. As with the furnace, gas extractions are cleaned for 15 minutes in a ST 101 Zr-Al primary getter. One minute after heating is complete the gas is exposed to the ST 172 Zr-V-Fe final getters for the remaining 4 minutes before the gas is expanded into the spectrometer. Both the primary and final getters were degassed for one hour after every sample and the extraction line system was vented for an additional hour to prevent contamination.

Alunite $\left((K,Na)Al_3(SO_4)_2(OH)_6\right)$ is a sulfate that will release SO_2, SO_3, and OH radicals into the extraction line system during incremental step heating experiments. The getters are unable to adequately clean these gases before admittance into the spectrometer, and the desulfatization reaction can potentially damage the extraction line system. Release of radiogenic $^{40}Ar_{(r)}$ from alunite occurs during the dehydroxylation reaction associated with the thermal decomposition of alunite to alum $(KAl(SO_4)_2)$ and alumina (Al_2O_3) (Itaya et al., 1996). Incremental heating experiments on alunite from 100 to 1000°C were conducted by Itaya et al. (1996) at intervals of 100°C defining the quantitative release patterns of radiogenic $^{40}Ar_{(r)}$ and nonradiogenic Ar. Optimum release of $^{40}Ar_{(r)}$ exists at temperatures >400°C and <750°C, and minimum release occurs at 400°C and 800°C. Therefore, step heating must be achieved by using small incremental amounts of laser power between the critical temperature range 400-750°C of gas release to minimize contamination. All alunite samples in this study required a three minute period for the final clean up of the gases in the spectrometer getter before starting the timer to record data.

Approximately 10-20 mg of the irradiated alunite sample was loaded into separate pans in a Cu-planchette. Sample sizes >20 mg were problematic due to large amounts of SO_2 and SO_3 gases. The planchette is capped with a coverslip that is transparent to the CO_2 laser wave. Coverslips used in 2002 analyses were KBr, and these easily fogged while alunite was heated during the higher power steps. During the 2003 analyses, smaller samples of 10-15 grams were loaded into the planchette, and a BaF coverslip was employed that did not readily fog. Once fogged, the ability to transmit the CO_2 laser wave was severely diminished and laser power had to be greatly increased to heat the sample. Required temperatures are not reached with fogged coverslips, and therefore, the experiments are terminated and finished at a later date after replacing the coverslip during sample reloads.

Typical incremental heating procedures for alunite began with a 15 minute laser blank for calibration. Thereafter, a 15 minute laser blank was run following two to three heating stages during an experiment. Alunite heating experiments consisted of seven heating increments that began at 400°C, increased to 500°C, and than increased slowly by 50°C until 700°C. The final heating stage used was 800°C, and in a few cases a 900°C step was added to test the potential gas release. Temperatures above 800°C leads to further release of SO_3 and the formation of H_2SO_4 that damage the extraction-line system (Itaya et al., 1996). The temperature range for the optimum release of $^{40}Ar_{(r)}$ and $^{39}Ar_{(K)}$ gas in the alunite from this study was generally from 500°C through 700°C, however, each sample behaved differently and in some samples gas was released over smaller temperature intervals. Optimal temperatures for the release of $^{40}Ar_{(r)}$ in alunite were at 600° and 650°C, however, in some samples the greatest amount of $^{40}Ar_{(r)}$ was released at 550°C and others at 700°C.

Temperatures were controlled by laser power, monitored with an infrared pyrometer, and reported as degrees centigrade. A variation in sample size and size fractions also affects the heating procedures. Smaller size fractions and larger samples generally require more laser power to reach the required temperature, but as a "rule of thumb" the starting temperature of 400°C was reached with 2 – 2.5% laser

power (<0.1 watts), and an increase in laser power of 0.7% and 1% to ~3.0% (0.18 watts) was required to reach the 500°C step. Laser power was increased 0.4% to 0.8% (0.15-0.75 watts) for each consecutive 50°C interval to 700°C and to 9.5% and 10.0% (1.55-1.65 watts) to reach the final 800°C heating stage. A "dual-step" heating procedure was employed after the 400°C heating step. During each consecutive heating increment the laser power was increased in two stages with two separate scans across the sample tray. This technique helped prevent the fogging problem from a single large release of gas that will end the experiment. The dual-step heating procedure is described as follows: (1) a 15 minute timer is started, (2) laser power is increased until half of the temperature required for the heating stage is reached, (3) the sample is scanned and the gas is released to the getters, (4) the power is increased to the total required temperature for the heating increment, and (5) the sample is scanned a second time releasing the remaining gas to the getters. The entire dual-step heating procedure must be no more than 10 minutes and provides for a one minute pause after heating and four minute exposure to the final getters. The final procedure for all alunite samples was to open the inlet valve and wait one minute while the gas expands into the spectrometer. After the inlet valve was closed a period of approximately three minutes was allowed as the peak intensity climbed and stabilized before starting the timer and collecting data at the computer. This is due to SO_2 and SO_3 contaminants and the abundant OH radicals in the alunites and the ineffectiveness of the getters to thoroughly getter these gases.

Rock Geochemistry

A total of 229 samples (184 fresh rocks, 24 advanced argillic altered (alunite) rocks, and 21 miscellaneous acid-sulfate altered rocks) from the Yanacocha area were prepared and analyzed by ALS Chemex in Reno, Nevada and Vancouver, Canada. Three analytical methods were employed for geochemical analysis and include the following: (1) ME-XRF06 for whole rock oxide analysis, (2) ME-MS81for trace element analysis of the fresh rocks, and (3) ME-MS61+Au for trace element analysis of altered and mineralized rocks. Elements and ranges of detection for each package are listed in appendix . Samples AZU-1 and CHQS-2, two unaltered pyroxene andesite lava flows at Yanacocha, were used as internal standards. They were analyzed at regular intervals throughout the analyses to test reproducibility. Geochemical method ME-XRF06 for whole rock oxide analyses used a lithim metaborate fusion technique followed by X-ray fluorescence spectroscopy (XRF) determination from the fused glass disk. Method ME-MS81 also used a lithim metaborate fusion to ensure total destruction of the rock forming minerals to provide total elemental concentration for the REE's and other resistate elements (Highsmith, 2001) followed by dissolution in a solution of four acids (4 acid technique of HF-HNO3-HClO4 digestion and a HCl leach) and trace element determination with inductively coupled plasma mass spectroscopy (ICP-MS). The final method ME-MS61+Au uses a 4-acid digestion technique (appendix Ic2) followed by ICP-MS determination of trace elements more specifically designed for mineralized rocks (ie. Au, Ag, As, Sb, Cu, Pb, Zn, Mo, Te and Bi). Au concentrations were determined by fire assay preconcentration followed by atomic absorption spectroscopy with a 5ppb detection limit.

All samples were dried in ovens at 110-120°C, crushed with an oscillating steel jaw crusher and split into two parts, one for whole rock characterization and another for trace element analyses. The two splits for each sample were than pulverized using a ring mill. Two methods were employed in the pulverization process; (1) one split was pulverized using a zirconia ring to avoid contamination in the ME-XRF06 major element oxide analyses, (2) the second split was pulverized using a Mn-steel jumbo ring for the ME-MS81 trace element analyses. Contamination of Mn, Fe, Cr(?), V(?) is possible, however, Mn and Fe are not analyzed in ME-MS81 only in ME-XRF06. Also, Cr is analyzed in ME-XRD06 and ME-MS81 with no obvious contamination problems from the Mn-steel jumbo ring. Special care was taken to minimize the risk of cross contamination during all preparation processes.

Whole Rock Analysis by X-Ray Fluorescence

Samples for whole rock analysis by XRF are fused using a lithium borate fusion. The melt is then poured into a mould and cooled to yield a solid glass disk. The disks can then be analysed and the elements determined by comparison with standard reference materials.

The ME-XRF06 Basic Whole Rock Package

The ME-XRF06 package offers thirteen major and minor elements (reported as oxides), plus loss on ignition (LOI), and the sum of the elements reported.

Table A1.1 ME-XRF06 detection limits

Method	Description	Elements and Ranges (%)					
ME-XRF06	Whole rock analysis. All elements by lithium meta or tetra borate fusion* and XRF.	Si	SiO_2	(0.01 - 100)	Cr	Cr_2O_3	(0.01 - 100)
		Al	Al_2O_3	(0.01 - 100)	Ti	TiO_2	(0.01 - 100)
		Fe	Fe_2O_3	(0.01 - 100)	Mn	MnO	(0.01 - 100)
		Ca	CaO	(0.01 - 100)	P	P_2O_5	(0.01 - 100)
		Mg	MgO	(0.01 - 100)	Sr	SrO	(0.01 - 100)
		Na	Na_2O	(0.01 - 100)	Ba	BaO	(0.01 - 100)
		K	K_2O	(0.01 - 100)	Loss on Ignition		(0.01 - 100)

The ME-MS81 Fusion Package

This package provides quantitative results for 38 elements, including those encapsulated in resistive materials. A fusion is effective for the dissolution of Tin and Tantalum minerals which are not readily dissolved by acid digestion.

Fusion (Lithium metaborate)

For quantitative results of all elements, including those encapsulated in resistive materials

Table A1.2 ME-MS81 detection limits

Method code ME-MS81	38 elements by lithium meta-borate fusion and ICP-MS.						
Elements and Ranges (ppm)							
Ag	(1 - 1000)	Ga	(1 - 1,000)	Pb	(5 - 10,000)	Tl	(0.5 - 1,000)
Ba	(0.5 - 10,000)	**Gd**	(0.1 - 1,000)	**Pr**	(0.1 - 1,000)	**Tm**	(0.1 - 1,000)
Ce	(0.5 - 10,000)	Hf	(1 - 10,000)	Rb	(0.2 - 10,000)	U	(0.5 - 1,000)
Co	(0.5 - 10,000)	**Ho**	(0.1 - 1,000)	**Sm**	(0.1 - 1,000)	V	(5 - 10,000)
Cr	(10 - 10,000)	**La**	(0.5 - 10,000)	Sn	(1 - 10,000)	W	(1 - 10,000)
Cs	(0.1 - 10,000)	**Lu**	(0.1 - 1,000)	Sr	(0.1 - 10,000)	**Y**	(0.5 - 10,000)
Cu	(5 - 10,000)	Mo	(2 - 10,000)	Ta	(0.5 - 10,000)	**Yb**	(0.1 - 1,000)
Dy	(0.1 - 1,000)	Nb	(1 - 10,000)	**Tb**	(0.1 - 1,000)	Zn	(5 - 10,000)
Er	(0.1 - 1,000)	**Nd**	(0.5 - 10,000)	Th	(1 - 1,000)	Zr	(0.5 - 10,000)
Eu	(0.1 - 1,000)	Ni	(5 - 10,000)				

The ME-MS61 Ultra-Trace Package

A total of 47 elements are reported following 4 acid technique of $HF-HNO_3-HClO_4$ digestion and a HCl leach. Only the most resistive elements, such as Zircons, are incompletely dissolved using this procedure.

Four acid "near-total" digestion

Quantitatively dissolves nearly all elements for the majority of geological materials. Only the most resistive minerals, such as Zircons, are only partially dissolved using this procedure.

Table A1.3 ME-MS61 detection limits

Method code ME-MS61	47 elements by $HF-HNO_3-HClO_4$ acid digestion, HCl leach and a combination of ICP-MS and ICP-AES.						
Elements and Ranges (ppm)							
Ag	(0.02 - 100)	Cu	(0.2 - 10,000)	Na	(0.01% - 10%)	Ta	(0.05 – 100)
Al	(0.01% - 25%)	Fe	(0.01% - 25%)	Nb	(0.1 - 500)	Te	(0.05 - 500)
As	(0.2 - 10,000)	Ga	(0.05 - 500)	Ni	(0.2 - 10,000)	Th	(0.2 - 500)
Ba	(0.5 - 10,000)	Ge	(0.05 - 500)	P	(10 -10,000)	Ti	(0.01% - 10%)
Be	(0.05 - 1000)	Hf	(0.1 - 500)	Pb	(0.5 - 10,000)	Tl	(0.02 - 500)
Bi	(0.01 - 10,000)	In	(0.005 - 500)	Rb	(0.1 - 500)	U	(0.1 - 500)
Ca	(0.01% - 25%)	K	(0.01% - 10%)	Re	(0.002 - 50)	V	(1 - 10,000)
Cd	(0.02 - 500)	La	(0.5 - 500)	S	(0.01% - 10%)	W	(0.1 - 10,000)
Ce	(0.01 - 500)	Li	(0.2 - 500)	Sb	(0.05 - 1,000)	Y	(0.1 - 500)
Co	(0.1 - 10,000)	Mg	(0.01% - 15%)	Se	(1 - 1,000)	Zn	(2 - 10,000)
Cr	(1 - 10,000)	Mn	(5 - 10,000)	Sn	(0.2 - 500)	Zr	(0.5 - 500)
Cs	(0.05 - 500)	Mo	(0.05 - 10,000)	Sr	(0.2 - 10,000)		

To include Hg by AAS (0.01 - 100 ppm) in the suite of elements above,
please request method code ME-MS61m instead of ME-MS61.

Electron Microprobe Analyses

Amphibole, pyroxene, and apatite analyses were carried out on a Cameca SX-50 electron microprobe at Oregon State University (OSU). The microprobe operated with an accelerating voltage of 15.07 to 15.11 kV and a beam current of 29.31 nA to 49.99 nA. Before each run the microprobe was calibrated with multiple analyses on 10 natural mineral standards that included flogpc1, kanopc1, kaugbas1, labrpc1, tugt, sani, baslpc1, crom, pymn, and flap (Table A1.4). Elements analyzed included the following:

Amphibole: Si, Al, Mg, Ca, Na, K, Fe, Ti, Cr, Mn, F, Cl.

Pyroxene: Si, Al, Mg, Ca, Na, K, Fe, Ti, Cr, Mn.

Apatite: P, Mg, Ca, Na, Fe, F, Cl, S.

Oxide weight percent and atomic proportions per formula unit were calculated by computer using Cameca software from the raw data. Fe^{+2} and Fe^{+3} was calculated from the total oxide Fe as FeO* for all amphiboles using an Excel spread sheet format designed by Eric Klemetti (Spreadsheet 1, recalc3-11_iron, Appendix) based on the calculation procedure after Leake et al. (1997) for the standard amphibole formula. Total volatile concentrations as H_2O percent, and atomic proportions per oxygen for Cl and F were also calculated for the amphiboles using the same spread sheet. Molecular Al IV and Al IV were recalculated from Al_2O_3 for all amphibole compositions from spread sheet 1 using a second EXCEL spreadsheet designed by Eric Klemetti (Spreadsheet 2, recalc3-11_dhz, CD Appendix VI). The Al in hornblende was used to calculate the amphibole barometer in Spreadsheet 2 after Johnson and Rutherford (1989).

Reproducibility was checked for all elements by test-analyzing one spot in an amphibole of sample DN-16 for 10 repetitive runs. The level of analytical uncertainty for the analyses fell within a 95% confidence interval around the mean for each element in the study. Three line analyses on the kaugbas1 pyroxene standard were used to check accuracy and precision of the analyses (CD Appendix VI). Total oxide percent in the standard ranged between 99.9 and 101.78 and all analyses were well within a 2-sigma confidence level for the standard deviation around the mean for the calculated oxide/cation data (standard deviations ranged from 0.005 to 0.45).

Samples included 18 standard thin sections of andesite and dacite volcanic and dome rocks from Yanacocha prepared and polished by Montrose Petrographics and Spectrum Petrographics. The polished thin sections were carbon-coated at OSU using high-vacuum evaporative techniques and the evaporative coater.

Table A1.4 List of standards used to calibrate the analyses

Standard	Type	Elements	X-ray	Crystal Detection	Peak 2θ	Counts/sec Pk-Bg
flogpc1	F-phlogopite	F	Kα	PCl	31291	20k-10k
kanopc1	anorthoclase	Na	Kα	TAP	46403	10k-5k
kaugbas	pyroxene	Si	Kα	TAP	27739,	10k-5k
		Mg			38535	10k-5k
kaugbas	augite	Ca	Kα	PET	38387	10k-5k
labrpc1	labradorite	Al	Kα	TAP	32479	20k-10k
tugt	tugtupite	Cl	Kα	PET	54039	20k-10k
sani	sanadine	K	Kα	PET	42753	10k-5k
baslpc1	basalt glass	Fe	Kα	LIF	48081	20k-10k
baslpc1	basalt glass	Ti	Kα	PET	31418	20k-10k
crom	chromite	Cr	Kα	LIF	56859	20k-10k
flap	fluoroapatite	P,Cl,F,S	Kα	PC1	31391	20k-10k
pymn	pyroxmangite	Mn	Kα	LIF	52199	10k-5k

Sulfur Isotope Analyses

Alunite samples used for geochronology in the study were analyzed for the $^{34}S/^{32}S$ isotopic ratio to test for hypogene origin for each alunite. Coarse alunite samples were hand picked to 80-90% purity, and fine samples where sieved -80+100 mesh removing coarse contaminants (55-65% purity). All samples were analyzed by XRD to check purity. A total of 26 samples were submitted for analysis. Duplicates were analyzed for CQ-37, QN-1 and CN-1, and sample TAP-169 had two analyses one with alunite and some pyrite (TAP-169-1) and another of pure alunite (TAP-169-2A). Also, two samples of pyrite coexisting with alunite were collected from samples YN-105 (Yanacocha Norte) and TAP-169 (Tapado) and analyzed. Results are presented in standard permil notation relative to Canyon Diablo trolite standard ($\delta\,^{34}S_{cdt}$) in table and figure .

Samples were sent to Dr. Kéiko H. Hattori at the University of Ottawa and analyzed at the G.G. Hatch Isotope Laboratories (Ottawa, Ontario, Canada) employing a FinniganMAT Delta^{plus} mass spectrometer with online GC/C and EA. The mass spectrometer is operated in dual-inlet and continuous-flow modes and is coupled with an elemental analyzer for on-line combustion, a PreCon device, and a gas chromatograph for separation of carbon, nitrogen, and sulfur gases for isotopic analyses. The elemental analyzer provides the mass spectrometer with a bulk sample preparation and inlet system that can handle microgram quantities of sample. It is a furnace that converts sulfur-bearing compounds to SO_2, carbon-bearing compounds to CO_2, and nitrogen-bearing compounds to N_2, which are then analyzed for their isotope ratios.

Each sample was weighed and mixed with V_2O_5 (1:3 weight ratio) by Monika at G.H. Hatch Laboratory. The mixture was placed in tin foil and injected into a CE Elemental Analyzer. The samples were combusted at ~1700°C to release SO_2 gas. The gas was passed through 7ml of silicate at 1000°C and a Cu-filter at 600°C to buffer the oxygen isotope composition and reduce any SO_3. Pure SO_2 gas was than

introduced to a Finnigan-MAT Delta[plus] mass spectrometer for the isotope analysis. Standards used were IAEA-S1 (-0.3 permil $^{34}S_{CDT}$) and IAES-S2 (+21.7 permil $^{34}S_{CDT}$).

During these analyses, the G.G. Hatch Isotope Laboratory operated under the direction of Dr. Ian Clark, and the technical support team was Paul Middlestead, Gilles St-Jean, Wendy Abdi, and Patricia Wickham.

X-Ray Diffraction

X-ray diffraction (XRD) was conducted on 29 samples that included advance argillic altered volcanic rocks, hydrothermal breccia, and previously-altered accidental fragments in the San Jose ignimbrite sequence (Table A1.4). Samples were analyzed at Oregon State University with a Philips XRG 3100 automated X-ray diffractometer using a long fine focus ceramic Cu-Kα tube operating at 40kV and 35 mA and emitting Cu-Kα radiation with λ=1.54178Å. The unit has a scan rate of 1°2θ/minute and compensating slits, and the quartz reference intensity of the 3.33 A peak is 40,000 cps. Computer software Jade 3.1® was used for mineral identification by matching 2θ-peaks to characteristic peaks of known minerals. Sample results are reported in Table A1.5 and Figures A1.1 to A1.4. Samples were analyzed with XRD to verify the presence of alunite, its composition, and its purity prior to 40Ar/39Ar dating and isotope analysis.

XRD analyses are semi-quantitative, and samples with know amounts of alunite can be run in conjunction with unknowns to compare peak intensities and estimate percent alunite and impurities in the unknown sample. Mixtures of alunite and quartz were made with 29, 37, and 83 weight percent alunite, and used as internal standards. These mixtures help estimate quartz/alunite ratios or abundance in the samples, and most samples analyzed had minor quartz included with the alunite.
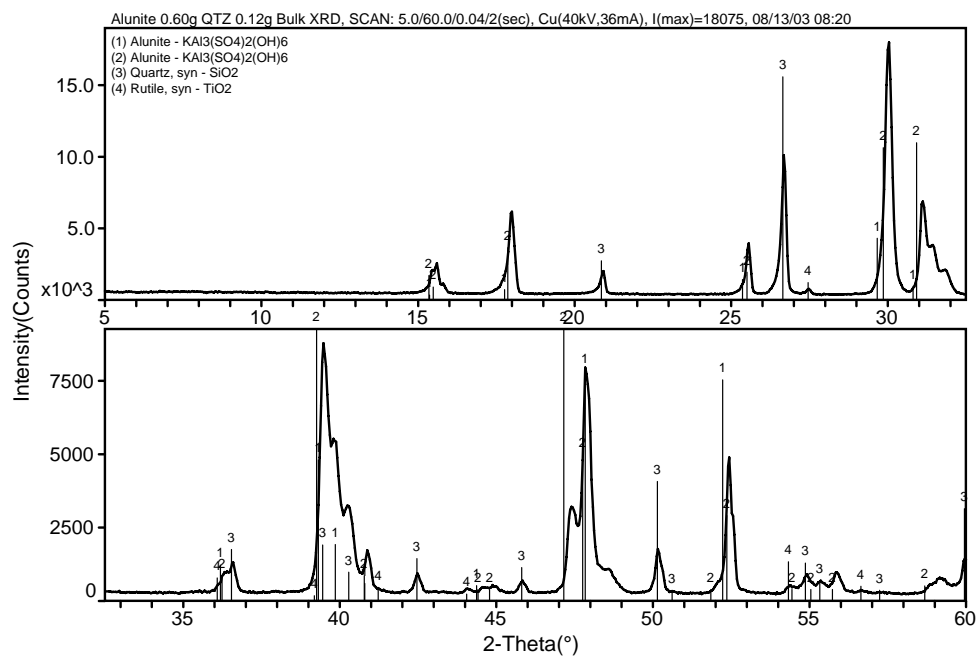
Figure A1.1. XRD patterns for the mixture from sample CLL-2 and quartz from CNE-25. The mixture is 83% alunite and 17% quartz.
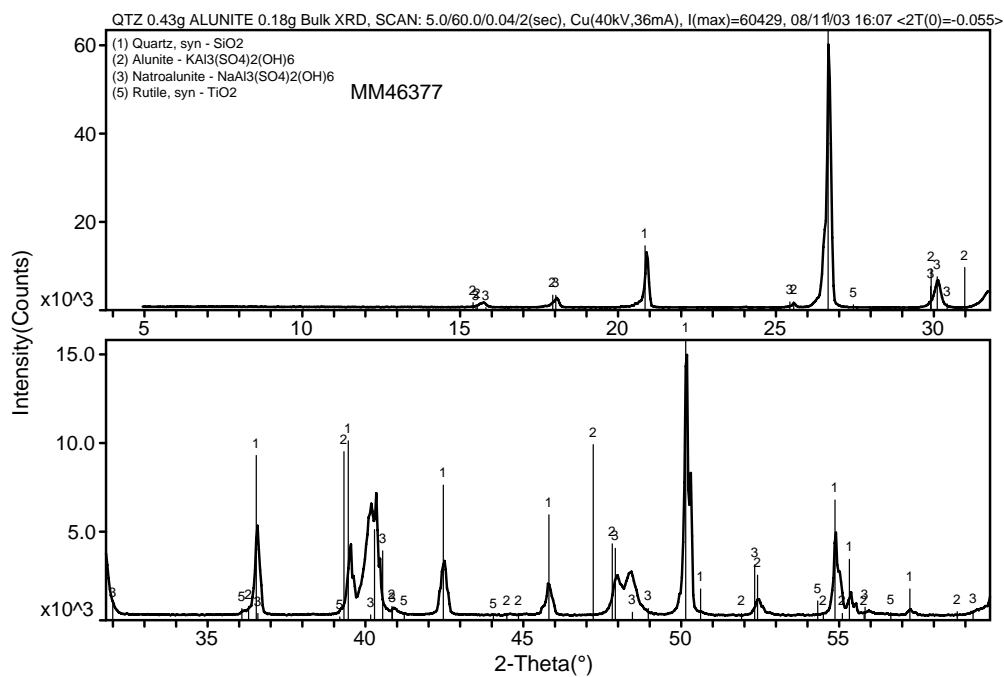

Figure A1.2. XRD patterns for the mixture of pure alunite from sample MM-46377 and pure quartz. The mixture is 29% natroalunite and 71% quartz.
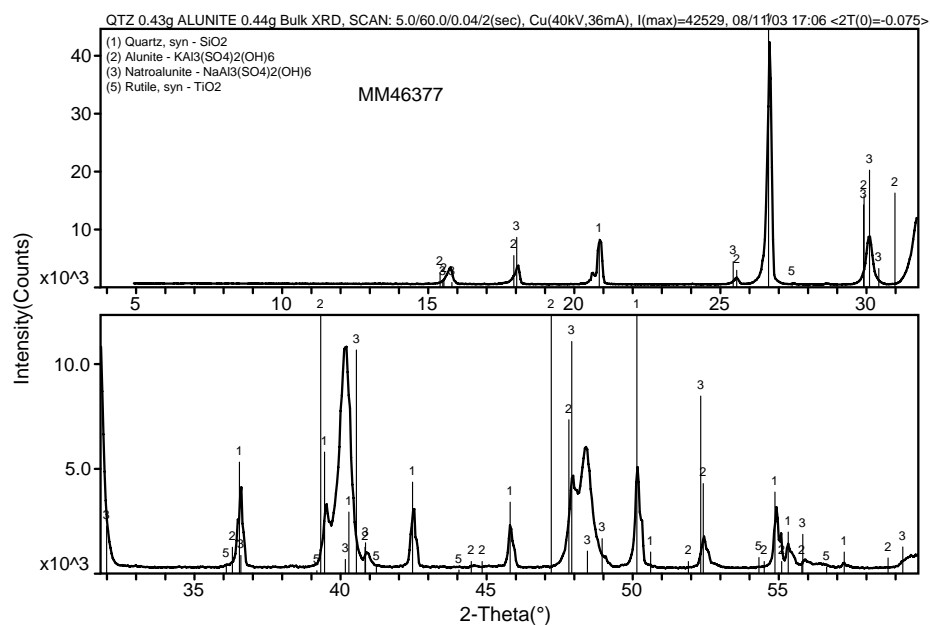
Figure A1.3. XRD patterns for the mixture of pure alunite from sample MM-46377 and pure quartz. The mixture is 37% natroalunite and 63% quartz.
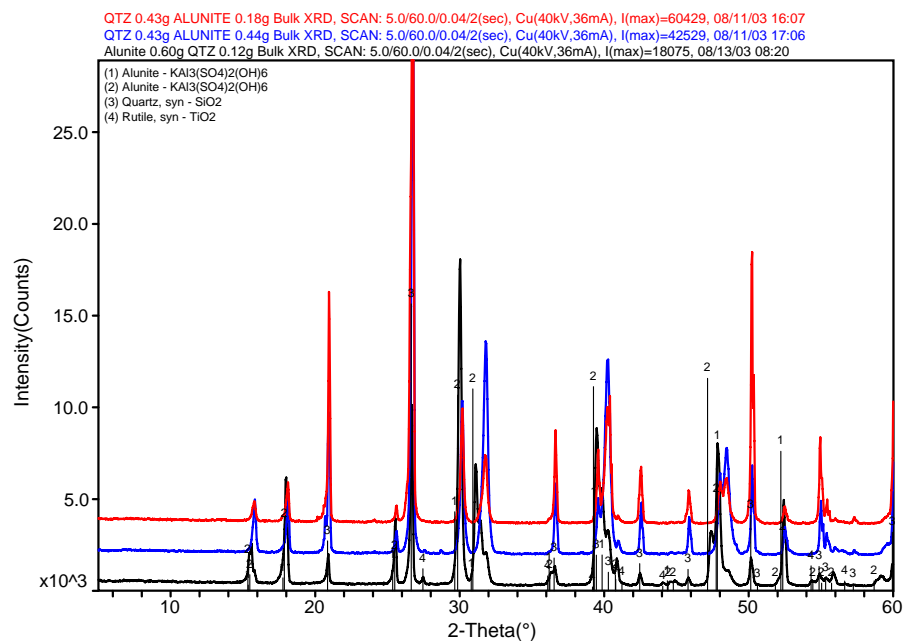

Figure A1.4. XRD patterns that display the results of the three mixtures.

Table A1.5a. XRD results for samples of hypogene advanced argillic altered rocks, alunite-matrix breccia, and alunite veins at Yanacocha.

SAMPLE NAME	SAMPLE DESCRIPTION	MINERAL
Baul-1	Massive pink alunite vein from Cerro Baul that crosscuts a eutaxitic ash-flow in the San Jose ignimbrite with abundant previously-altered accidental fragments.	Natroalunite – $NaAl_3(SO_4)_2(OH)_6$ Quartz – SiO_2 ~10% Rutile– TiO_2
CB-64	Large 30-cm accidental previously-altered fragment from base of an ash-flow (CB-74 11.29±0.08Ma) in the San Jose ignimbrite sequence at Alta Machay. 18 ppb Au, 38 ppm Cu, , 11.1 ppm Mo, 60 ppm As, 163.5 ppm Pb, 86 ppm Zn.	Quartz Cristobilite Sanadine, disordered $K(Si_3Al)O_8$ Hematite Sillimanite Al_2SiO_5
CB-68 A	Large accidental previously-altered and brecciated SM fragment from base of an ash-flow (CB-74) in the San Jose ignimbrite sequence at Alta Machay. 69 ppb Au, 66 ppm Cu, 3.4 ppm Mo, 42 ppm As, 475 ppm Pb, 61 ppm Zn.	Quartz Cristobilite Sanadine, potassium disordered Hematite Sillimanite Montmerillonite
CB-68B	Previously altered and mineralized fragment in the San Jose ignimbrite sequence at Alta Machay. 69 ppb Au, 66 ppm Cu, 42 ppm As, 475 ppm Pb	Quartz Cristobilite Sanadine, potassium disordered Hematite Sillimanite Montmerillonite
CLL-1	Coarse alunite (0.5mm) in vugs of a quartz-alunite altered quartz-bearing lithic tuff with SM fragments.	Quartz 35-40% Natroalunite Minamiite – $(Na,Ca)_{1-x} Al_3(SO_4)_2(OH)_6$ Rutile
CLL-2	Alunite vein x-cut SM on summit of Cerro Collotan Standard for Alunite	Alunite Minamiite Natroalunite
CLL-3	Silica patchy altered rock in road cut below Cerro Collotan	Pyrophyllite – Al2Si4O10(OH)2 Sodium Pharmacosiderite – (Na,K)2Fe4(AsO4)3(OH)5 7H2O Natroalunite pyrite
COR-39 213m	Massive fine grained alunite (<0.002-0.10mm) with granular silica from drill hole COR-39 at Corimayo	Quartz 32% Alunite
COR-49 180.5m	SA altered porphyritic rock at Corimayo Massive fine grained alunite from drill hole COR-49 at Corimayo	Quartz Alunite Opal – $SiO_2 \cdot xH_2O$ Cristobalite
CNE-25 28-30m	Powdery tan and white SA? Zone where textures are TO 0.2 g Au	Quartz Rutile

Table A1.5b

SAMPLE NAME	SAMPLE DESCRIPTION	MINERAL
CNE-26 76-77m	SA? Altered P rock with phenocrysts altered to alunite? Barren	Quartz Cristobilite
CN-1	Coarse alunite (≤0.5mm) in vugs of a quartz-alunite altered vuggy porphyritc rock at Cerro Negro Oeste	Alunite Minamiite Quartz 20% Rutile
CQ-37 110m	Alunite from the Quilish deposit with 3.16 ppm Au	Quartz 15-20% Alunite Sanadine, potassian, disordered $(Na,K)(Si_3Al)O_8$
CS-1	Late pink alunite healed breccia at Chaquicocha Sur with coarse alunite crystals (<0.05-0.5mm)	Quartz 20-25% Alunite Rutile
ENC-6 137-138m	Alunite with a stage 2 breccia with milled and angular SM fragments and fragments within fragments of an early BXH.	Alunite Osarizawaite? – $Pb(Al_2Cu)(SO_4)_2(OH)_6$ Quartz <5% Rutile Hematite Jarosite Cristobilite
KUP-003 94m	Patchy SA altered to vuggy silica – altered porphyritic andesite. Coarse alunite (0.1-0.15-0.5mm)	Quartz 20% Alunite Pyrophyllite 2m1 – $Al_2Si_4O_{10} (OH)_2$ Heulandite – $Ca (Si_7Al_2)O_{18}$ -6H2O
LBQ-40 441.2m	Pink alunite vein x-cut porphyritic dacite in La Quinua basin at 441.2 meters depth.	Alunite Minamiite Quartz 5-10%
MM-46377	Coarse pink alunite vein that crosscuts porphyritic andesite at Cerro Sugares. This has the most Na-rich alunite phase analyzed in this study.	Natroalunite Rutile
MM-314 259.8m	SAP to wormy alunite with pink to white fine grained alunite (0.02-0.25mm) with sulfur at Maqui-Maqui Deep.	Quartz 10% Alunite Rutile
MS-8	"QSP" alteration with quartz stockwork veins at La Sorpresa, 143 ppb Au, 118.5 ppm As, 57.8 ppm Cu, 5.77 ppm Mo, 23.1 ppm Pb, 6 ppm Zn	Sanadine disordered Quartz Kaolinite $Al_2Si_2O_5(OH)_4$ Rectorite $K_{1.2}Al_4Si_8O_{20}OH_4$ -4H_2O
PNE-03 45-50m	SA altered Punta Negra dacite	Quartz 35% Alunite
PNE-3 325-355m	Punta Negra - Silica patchy altered dacite at 350 meters – rare quartz phenos are present.	Quartz Pyrophyllite – Al2Si4O10(OH)2 Diaspore – AlO(OH) pyrite
QN-1 Quilish Norte	Alunite crystals (≤0.005-0.15mm) in vugs and fractures of a quartz-alunite altered porphyritic andesite.	Quartz 40-45% Alunite Rutile

Table A1.5c

SAMPLE NAME	SAMPLE DESCRIPTION	MINERAL
SJS-1	Bottom of the San Jose Sur Pit in the Baul Fault Zone. White alunite monolithic breccia with fragments of SA-altered feldspar porphyry.	Natroalunite Quartz 20-25%
SJS-3	Coarse alunite xtals in vugs of SV altered Fxf rocks that crop out along the north boundary of the San Jose Sur pit.	Alunite Quartz 60%
TAP-169 382m	White platy finely crystalline alunite replaced fragments and possible xtals in a heterolithic 35-40% fragment-rich Fg rock believed to be a phreatic breccia (BXF). 1-2% py	Alunite Minamiite Quartz 10% Pyrite
YN-105 88.7m	Massive silica breccia healed with late alunite	Quartz 40-45% Alunite Rutile
YO-1	Quartz-alunite healed 2 stage breccia from Encajon at Yanacocha Sur. First healed with quartz and later SM breccia healed with alunite.	Quartz 10% Possible zoned Alunite and Natroalunite Rutile
YS-219 111.8m	Alunite matrix-supported heterolithic breccia from Yanacocha Oeste	Quartz 55-60% Alunite ~25-30% Pyrophyllite ~5-10% Diaspore – AlO(OH) <5%

APPENDIX III
Table for Calculation of the Amphibole Formula

Table A3.1a Table that references the calculation of the amphibole formula.

oxide	Molecular weight (MW)	1 Oxide weight%	2 Molecular Proportions (MP) wt%/MW	3 Atomic Proportions (cations) MP*(#cations)	4 Atomic Proportions (anions) MP*(#oxygens)	5 Anions on the basis of 23 Oxygens Column 4*O factor	6 Cations on the basis of 23 Oxygens Column 3*O factor
SiO$_2$	60.09	46.674	0.77673	0.77673	1.55347	13.57904	6.78952
TiO$_2$	79.88	1.773	0.02220	0.02220	0.04440	0.38808	0.19404
Al$_2$O$_3$	101.92	7.641	0.07497	0.14995	0.22492	1.96603	1.31069
Cr$_2$O$_3$	152	0.013	0.00009	0.00018	0.00026	0.00229	0.00153
FeO	71.85	11.522	0.16036	0.16036	0.16036	1.40176	1.40176
MnO	70.94	0.410	0.00578	0.00578	0.00578	0.05054	0.05054
MgO	40.31	15.921	0.39496	0.39496	0.39496	3.45240	3.45240
CaO	56.08	11.094	0.19783	0.19783	0.19783	1.72924	1.72924
Na$_2$O	61.98	1.681	0.02712	0.05425	0.02712	0.23709	0.47417
K$_2$O	94.2	0.760	0.00807	0.01613	0.00807	0.07051	0.14103
F	19	0.455	0.02393	0.02393	0.02393		6.78952
Cl	35.5	0.149	0.00421	0.00421	0.00421		0.19404
Sum		98.094			2.64532	22.87699	15.54492
O=F,Cl					2.63125		
O factor					8.74111		

O=F,Cl - subtract anions F,Cl as follows = O total (2.64532) – ((0.5*Cl)+(0.5*F))
O factor (factor for recalculation of atomic proportion to 23 O basis) 23/O=F,Cl(2.63125)

Table A3.1b Table that references the calculation of the amphibole formula.

	7		8	9	10			
Ideal site assignment	Pre-Ferric	Cations	$F=2X(1-T/S)$ $\sum Mn$	Normalized Column 8*(T/S)	Column 9 Corrected for Ferric (Fe^{3+})	Oxides	Oxide wt%	Total Oxides wt%
Si	6.790					SiO2	46.674	46.674
Al^{IV}	1.210					TiO2	1.773	1.773
Sum T	8.000					Al2O3	7.641	7.641
Al^{VI}	0.100	Si	6.790	6.744	6.744	Cr2O3	0.013	0.013
Ti	0.194	Al	1.311	1.302	1.302	FeO*	11.522	
Fe^{3+}	0.000	Ti	0.194	0.193	0.193	FeO		5.741
Cr	0.002	Fe3+	0.000	0.000	0.699	Fe2O3		6.425
Mg	3.452	Cr	0.002	0.002	0.002	MnO	0.410	0.410
Fe^{2+}	1.252	Mg	3.452	3.429	3.429	MgO	15.921	15.921
Mn	0.000	Fe2+	1.402	1.392	0.694	CaO	11.094	11.094
Sum C	5.000	Mn	0.051	0.050	0.050	Na2O	1.681	1.681
Mg	0.000	Ca	1.729	1.718	1.718	K2O	0.760	0.760
Fe2+	0.150	Na	0.474	0.471	0.471	Total Ox	98.13	98.134
Mn	0.051	K	0.141	0.140	0.140	**H2O		1.81
Ca	1.729	F	0.024	0.024	0.024	F		0.455
Na	0.070	Cl	0.004	0.004	0.004	Cl		0.149
Sum B	2.000	OH		1.972	1.972	Total + F,Cl		100.55
Na	0.404	total	13.200	15.441	15.441	***O=F		-0.191
K	0.141					***O=Cl		-0.034
Sum A	0.545					Final Total		100.32
Total	15.545							
T = T+C			13					
normalization factor T/S			0.985					
S=$\sum$Mn			13.200					
*F			0.699					

*Equation for estimating Fe^{3+} the number of ferric ions (F) per X oxygens (Droop, 1987): F = 2X(1-T/S) T = 13 (ideal number cations/formula), S = observed cation total/X oxygens calculated assuming all iron is ferrous. F = 46(1-13/$\sum$(cations)). Formula is calculated on the basis of 23 oxygens anhydrous assuming 13 cations ($\sum$Mn) exclusive of Ca, Na and K for calcic-amphiboles.

**H₂O is estimated by assuming 2 (OH) groups are present in the formula 1 O is balanced by 2 H (H2O) and 1 O = F and Cl. After normalizing the entire formula (inc. F and Cl) with the O factor, then F + Cl are subtracted from 2 to estimate the OH⁻ ions in formula (H2O = 2(HO₀.₅)).

***O=F and O=Cl Oxygen equivalent of the fluorine and chlorine weight is calculated as follows (one excess O atom is for F and Cl in the formula): (16/2*(MW of F or Cl))*F or Cl content.

Appendix IV

Descriptions of the photographs for the Yanacocha rock sequences

Figure A4.1 Photographs of the Tual lower andesite lahar sequence
- A. Photograph of the Tual lower andesite lahar sequence north of Cerro Negro and Quebrada Rio Tinte.
- B. Photograph of textures typical of the Tual lower andesite lahar sequence north of Cerro Negro and Quebrada Rio Tinte.
- C. Photograph of textures typical of the Tual lower andesite lahar sequence in outcrops on Cerro Rosa Llorca.
- D. Photograph of textures typical of the Tual lower andesite lahar sequence south of Cerro Quilish and Cerro Antibuyoc in Quebrada Rio Porcon.

Figure A4.2 Photographs of the Chaupiloma lower Andesite lahar sequence.
- A. Photograph of a typical outcrop for the Chaupiloma lower andesite lahar sequence at Alto Machay
- B. Photograph of textures from the Chaupiloma lower andesite lahar sequence.
- C. Photograph of textures typical of the Chaupiloma lower andesite lahar sequence that crops out in the Alto Machay area.

Figure A4.3 Photographs of the different textural types of Cerro Frailes dacite pyroclastic tuffs and lahars.
- A. Biotite dacite lahar with well rounded matrix-supported cobbles of porphyritic dacite.
- B. Thick biotite dacite lahar with man-sized boulders of dacite porphyry and other dacite tuffs. Rare carbonized wood has been found in this outcrops. Cerro Frailes area.
- C. Biotite dacite ignimbrite with coarse biotite up to 3-4mm in width. Quebrada Honda.

Figure A4.4 Photographs of the outcrop exposure typical of Cerro Frailes dacite pyroclastic tuffs and lahars.
- A. Sequence of dacite lahars and tuffs at Cerro Frailes.
- B. Cerro Frailes southeast of Negritos intercalated tuffs and lahars. Typical fraylones structure-tower.
- C. Typical outcrops of Frailones (Fraylones) that are part of the 15 Ma Cerro Frailes pyrocalstic sequence.
- D. Large cliffs of devitrified Cerro Frailes biotite dacite tuffs and intercalated lahars in Quebrada Honda.

Figure A4.5 Photographs of the Cerro Frailes dacite pyroclastic sequence
- A. Cerro Frailes geomorphologic terrane and outcrop patterns north of China Linda.
- B. Outcrops of Cerro Frailes biotite dacite tuff breccia at Cerro Peña Blanca north of the mine site.

Figure A4.6 Photographs of typical (a) lava flow and (b) dome outcrops in the Lower Yanacocha volcanic sequence.
- A. Flow banded pyroxene andesite lava flows in Pampa Cerro Negro.
- B. The central summit lobe of the Cerro Regalado quartz-bearing pyroxene andesite dome complex.

Figure A4.7 Photographs of various geomorphological features and textures in the Lower Yanacocha volcanic sequence.
- A. Looking NNW to the Cerro Atazaico andesite stratocone.
- B. Cerro Regalado andesite dome complex looking south.
- C. Lower Yanacocha pyroxene andesite tuff breccia near Alto Machay (CB-5).
- D. Weathered surface of a flow-foliated pyroxene andesite lava flow. The texture has a eutaxitic-like appearance but is not related and is a lava flow.

E. Lower Yanacocha pyroxene andesite lava flow that filled a channel weatherd into the lower andesite lahar sequence. Road cut on the Cajamarca road below Porcon Bajo.

Figure A4.8 Photographs of the Cori Cospha ash-flow tuff.
    A. Close up of the Cori Cospha ash-flow tuff. Argillite and quartzite fragments are common. The tuff is nonwelded and fines-depleted with with white pumice up to 10-12 cm.
    B. Outcrops of Cori Cospha tuff looking north to the flat area dominated by thin-bedded tuffs and laminated rocks that lie below the Cori Coshpa Tuff.

Figure A4.9 Photographs of the different textural features in dome outcrops of the Upper Yanacocha volcanic sequence (Upha).
    A. Near vertical flow-banding in the Upper Yanacocha Ocucho pyroxene andesite dome.
    B. Vertical flow-banding in the Azufre lobe of the Ocucho dome complex.
    C. Closer picture of the vertical flow banding typical of the dike-like central lobes in the Ocucho dome complex.
    D. Lower angle flow foliations in Upha pyroxene andesite lavas along the dome margins.

Figure A4.10 Photographs of special textures in outcrops of the Upper Yanacocha volcanic sequence.
    A. Monolithic Upha pyroxene andesite tuff breccia.
    B. Flattened elliptical pillow-like structures in an acid-leached granular and vuggy silica porphyritic rock at Pabellon.

Figure A4.11 Photographs of outcrop exposures and textures in the Upper San Jose spatter ignimbrite.
    A. Fluted textured outcrop surfaces from weathering characteristic of the Upper San Jose spatter ignimbrite.
    B. Frailones (fraylones) towers in the Upper San Jose spatter ignimbrite at the Bosque de Piedra.
    C. Spatter blob textures in the spatter ignimbrite.
    D. Fluted weathering in the spatter ignimbrite at the Bosque de Piedra.
    E. Spatter blobs mixed with angular blocks.
    F. Fiamme textures in the spatter ignimbrite at Bosque de Piedra.

Figure A4.12 Photographs of textural features in the Upper San Jose spatter ignimbrite.
    A. Breccia textures with spatter blobs and blocks typical of the spatter ignimbrite.
    B. Similar to above but the finer-grained distal texture.

Figure A4.13 Photographs of the disconformity above the Upha Machay Dome and the lithic concentration at the base of the Middle San Jose ignimbrite.
    A. Coarse basal lithic concentration in the Middle San Jose ignimbrite (Msj) marking the unconformity after the Upha Machay Dome.
    B. Quartz-sanidine-andalusite altered accidental fragments dominate the lithic concentration at the base of the Msj flow.
    C. Massive quartz altered fragment in the fresh Middle San Jose ignimbrite (CB-74).

Figure A4.14 Photographs of outcrop exposures and textures from the Middle San Jose ignimbrite and the Upper San Jose white tuff.
    A. Welded and columnar-jointed Lower San Jose ignimbrite south of the Pozo de Azufre in Quebrada Azufre.
    B. A nearly complete section is exposed at Filo Pabellon south of the Ventanillas de Combayo. Basement limestone is overlain with an unconformity by Cerro Friales tuffs and lahars, the lower San Jose ignimbrite overlies the Cerro Frailes. Middle and Upper San Jose ignimbrites are exposed toward the top of the ridge and appear to spill over the preexisting Lower San Jose and Cerro Frailes paleotopography.
    C. Eutaxitic textures preserved in the quartz-alunite altered San Jose ignimbrite at Cerro Baul.
    D. Same as above.

E. Distal non-welded San Jose ash-flow tuff that overlies the basement limestone above Rio Chonta near Cajamarca (RC-6).
F. Eutaxitic-textured Middle ? San Jose ignimbrite that overlies a biotite dacite lapilli tuff interpreted as Cerro Frailes above Puruay.

Figure A4.16 Select photos of the rock sequences in the Yanacocha district.
A. Charred wood in a lahar from the Cerro Frailes dacite sequence.
B. Typical Yp texture in an intermediate argillic altered feldspar porphyry.
C. Radial fractured block from a block and ash flow in the Upha andesite.
D. Glacial striations and scouring of acid-leached hypogene altered massive and vuggy quartz on Cerro Chaquicocha.
E. Volcanic geomorphology of the Cerro Atazaico composite cone and surrounding monogenetic vent areas.

Figure A4.17 Select photos of the rock sequences in the Yanacocha district.
A. Remnant of a co-ignimbrite lag breccia from an eruption of the San Jose ignimbrite at Alto Machay.
B. Frailones towers in the Negritos rhyolite ignimbrite at ceros de las Negritos.
C. Breccia contact to the Chaupiloma rhyolite in the road cut at Cerro Chaupiloma. Large white breccia fragments are the Chaupiloma rhyolite in a fine rock flour-like matrix.
D. San Jose ignimbrite overlying limestone basement with an angular unconformity was topographically controlled and filled the valley into Rio Chonta.
E. Successive terminal moraines on Cerro Paquerumi looking west from Cerro Chaquicocha.

Figure A4.18 Select photos of the rock sequences in the Yanacocha district.
A. Textures that resemble rheomorphic folding in an hypogene acid-leached ignimbrite with opalite lithic fragments at Chaquicocha Alta on Cerro Chaquicocha.
B. Pabellon diatreme with abunbant well rounded black massive quartz pebbles in a clay-pyrite matrix.
C. Panoramic vista from Escalon looking west at the Carachugo, San Jose and Cerro Yanacocha gold deposits. Photo taken in June 2002. Cerro Quilish is in the distance framed in Quebrada Encajon.
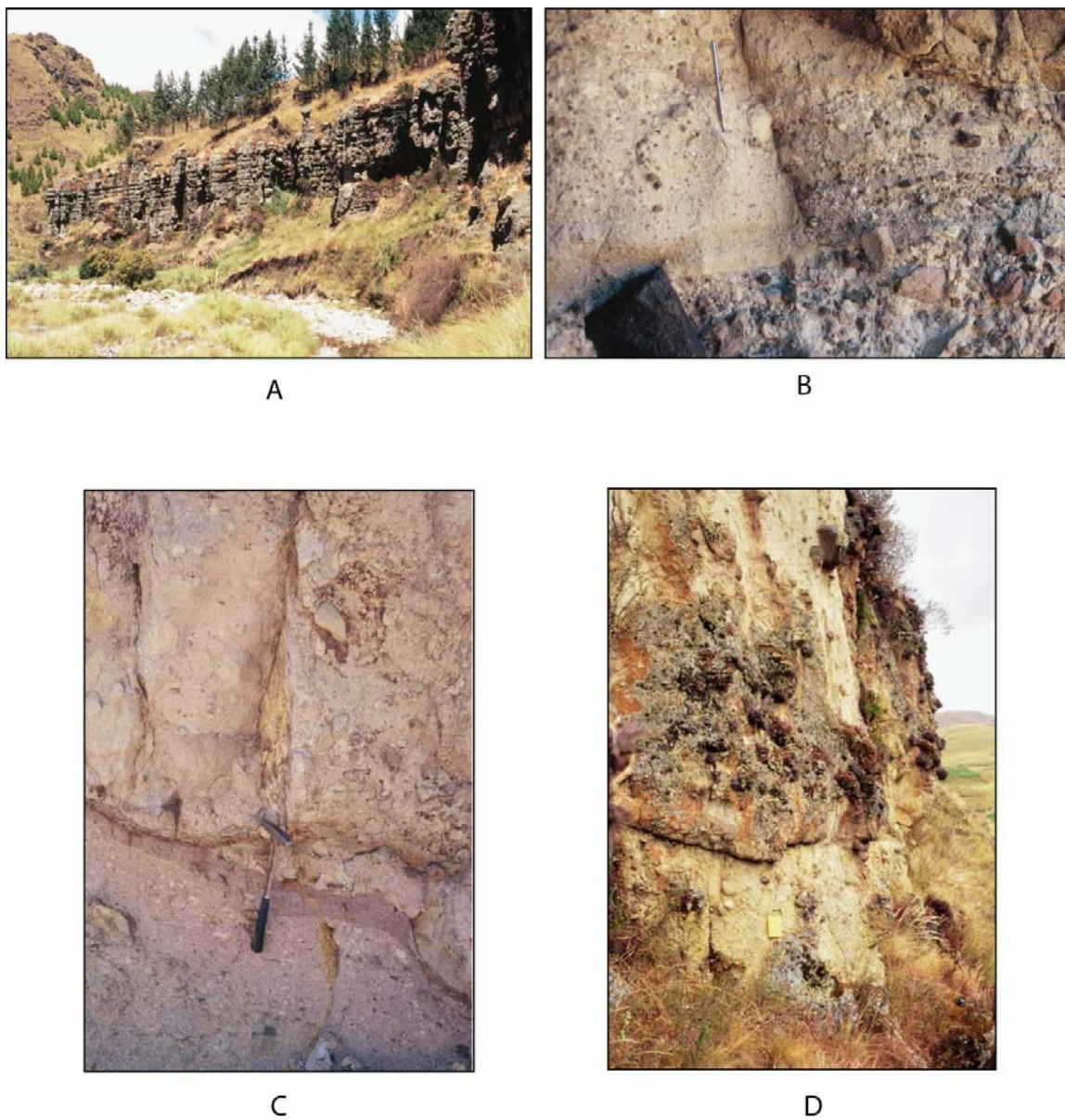
Tual Lower Andesite Lahar Sequence

Figure A4.1 Photographs of the Tual lower amdesite lahar sequence.

Chaupiloma Lower Andesite Lahar Sequence

Figure A4.2 Photographs of the Chaupiloma lower Andeite lahar sequence.

Cerro Frailes Dacite Pyroclastic Rocks

A

B
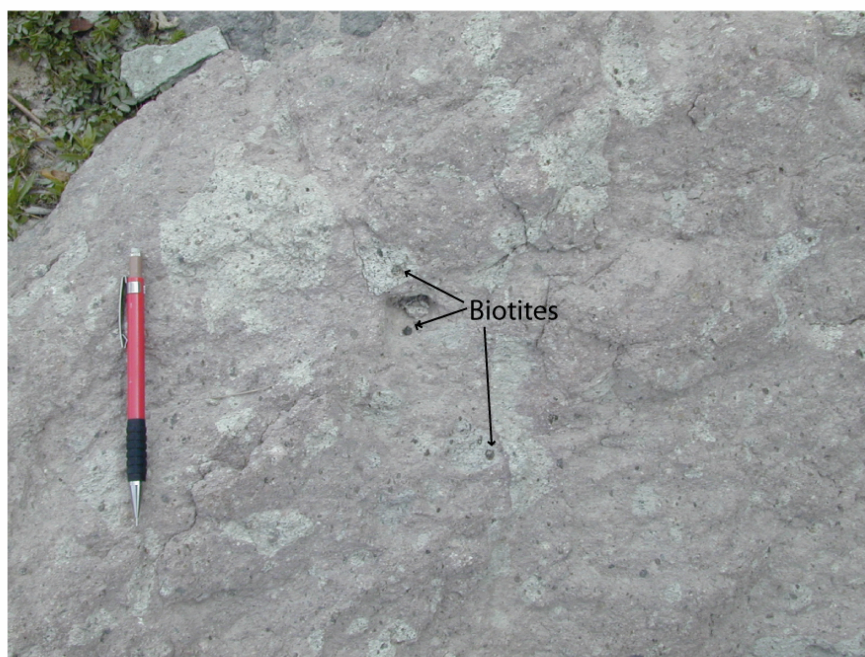
C

Figure A4.3 Photographs of the different textural types of Cerro Frailes dacite pyroclastic tuffs and lahars.

Cerro Frailes Outcrops
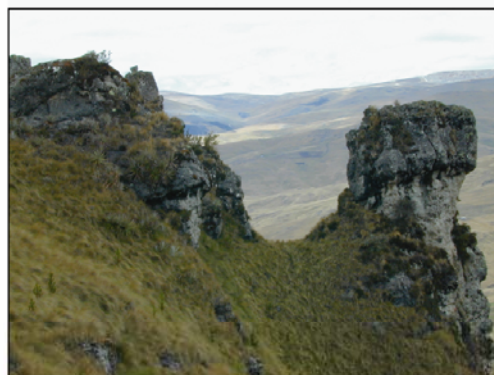
Figure A4.4 Photographs of the outcrop exposure typical of Cerro Frailes dacite pyroclastic tuffs and lahars.

Cerro Frailes Dacite Pyroclastic Sequence
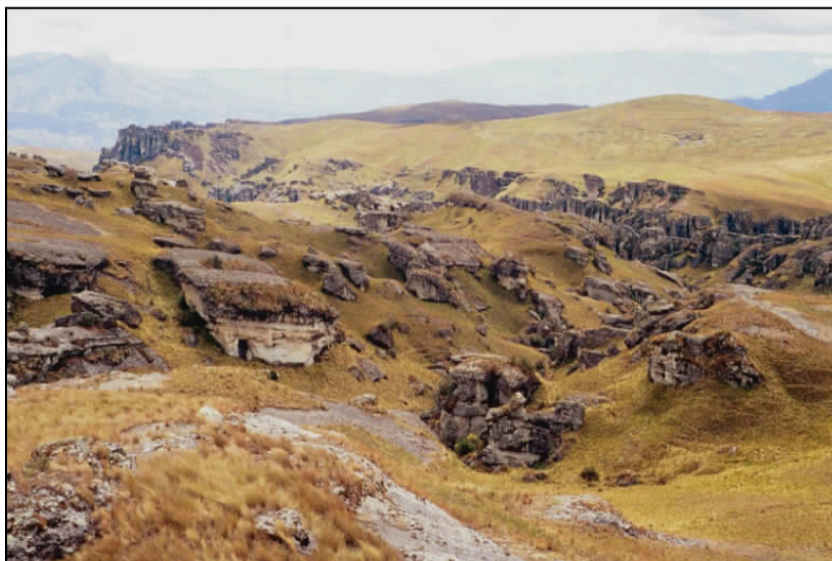
A

B

Figure A4.5 Photographs of the Cerro Frailes dacite pyroclastic sequence.

Lower Yanacocha Volcanic Sequence
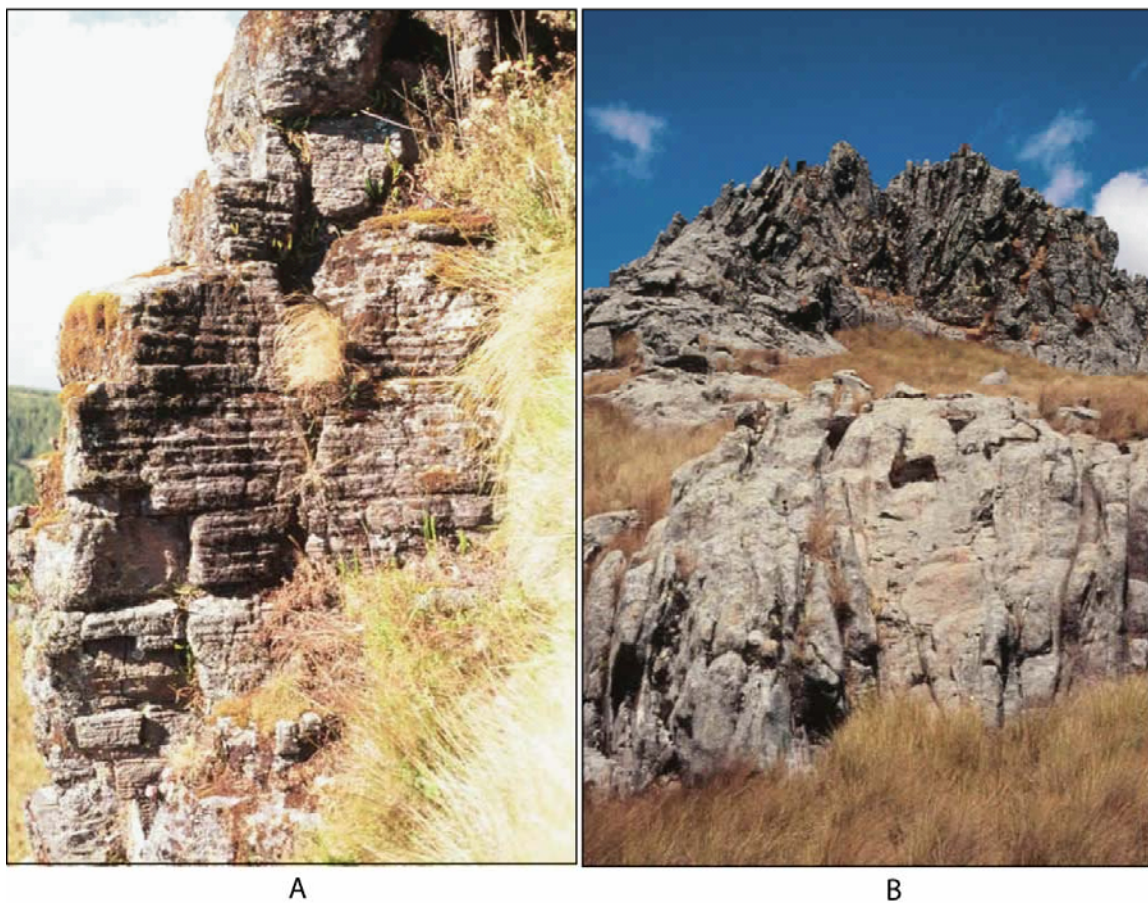
Figure A4.6 Photographs of typical (a) lava flow and (b) dome outcrops in the Lower Yanacocha volcanic sequence.

Figure A4.7 Photographs of various geomorphological features and textures in the Lower Yanacocha volcanic sequence.

Cori Coshpha Ash-Flow Tuff

Figure A4.8 Photographs of the Cori Cospha ash-flow tuff.

Upper Yanacocha Volcanic Sequence - Domes
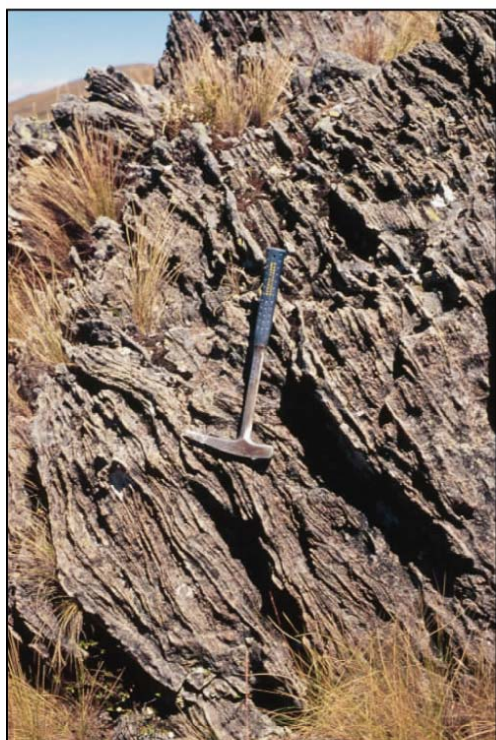
A
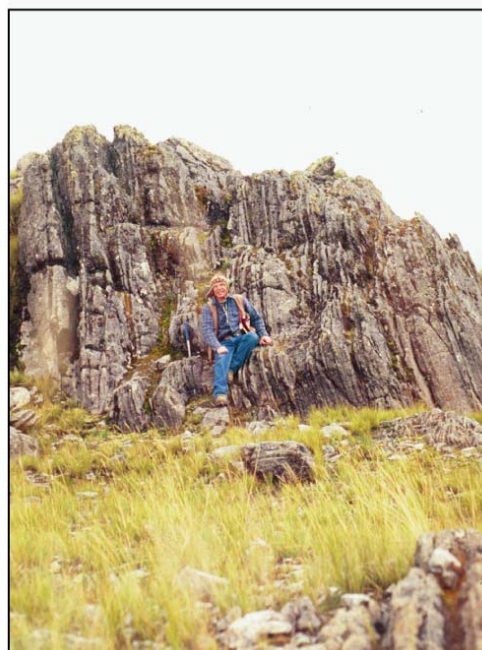
B

C
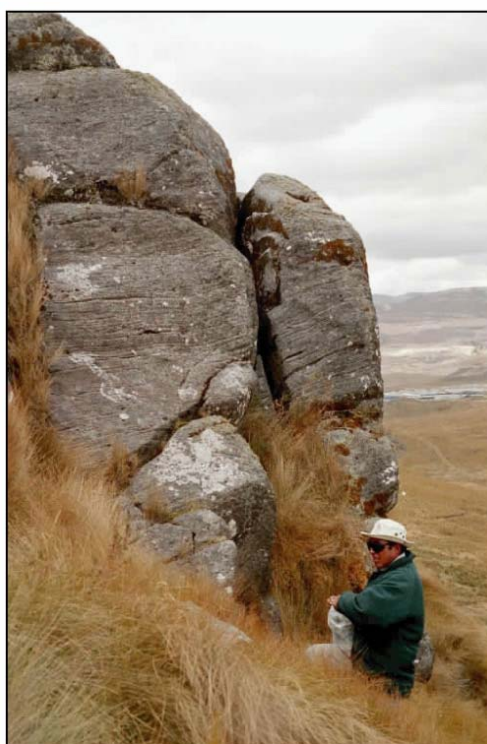
D

Figure A4.9 Photographs of the different textural features in dome outcrops of the Upper Yanacocha volcanic sequence and San Jose related pyroxene dacite domes.

Upha Monolithic Pyroclastic Breccia

A

Upha? Pillow-like textures

B

Figure A4.10 Photographs of special textures in outcrops of the Upper Yanacocha volcanic sequence.
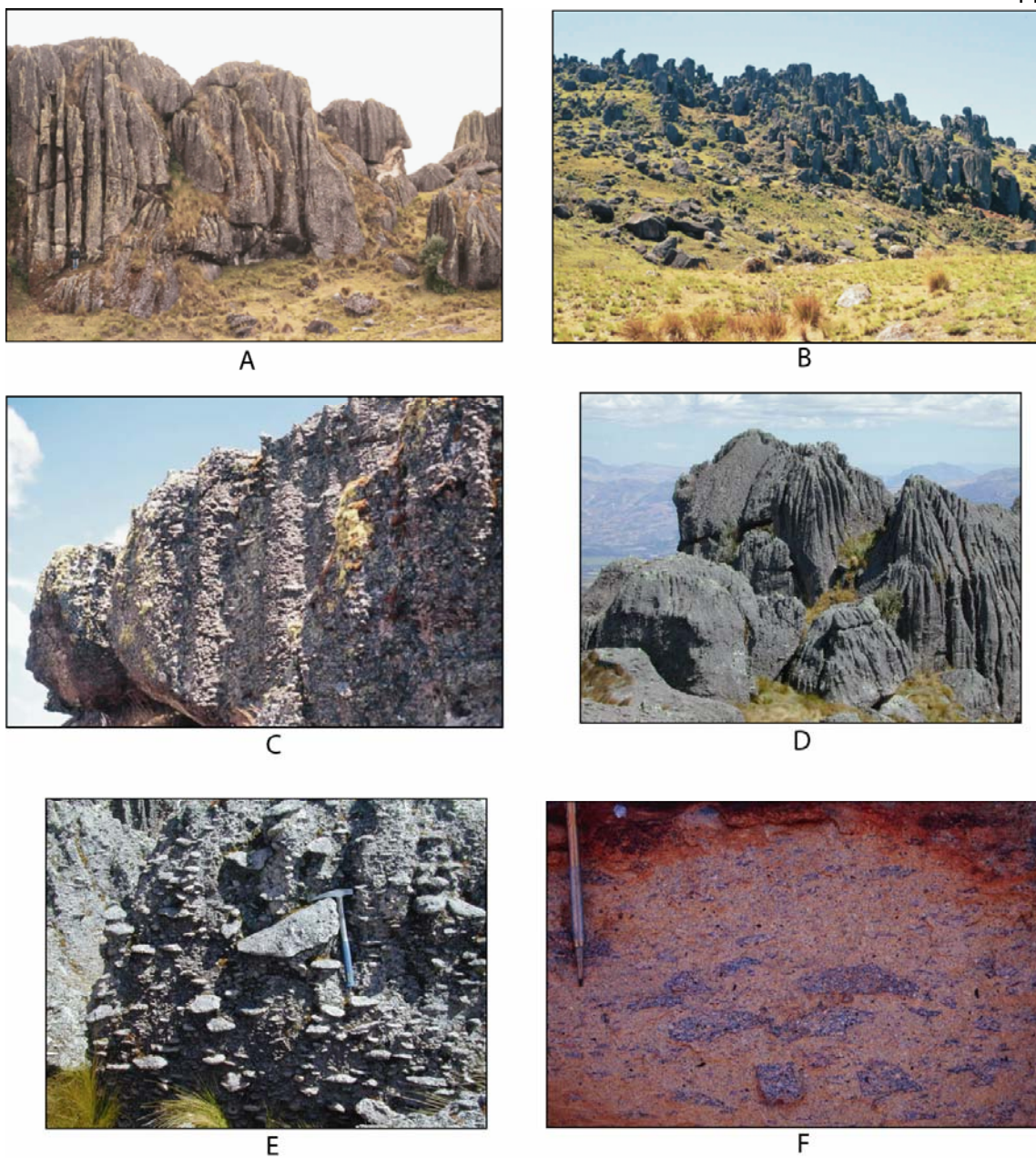
Upper San Jose Spatter Ignimbrite

Figure A4.11 Photographs of outcrop exposures and textures in the Upper San Jose spatter ignimbrite.
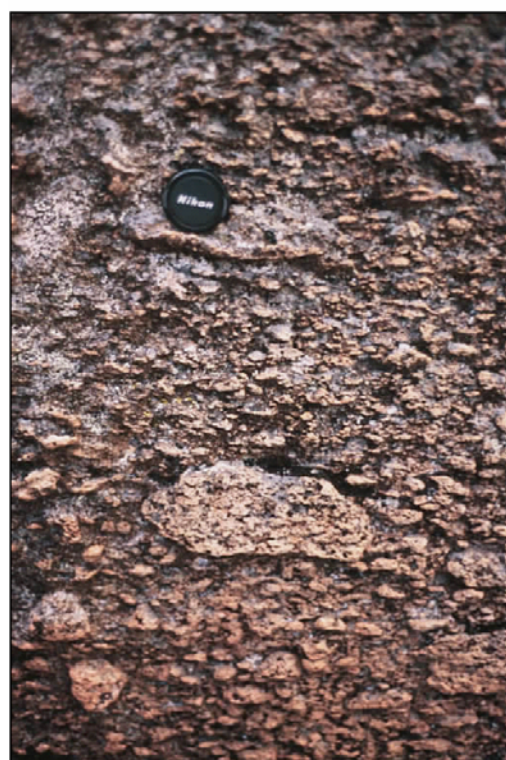
Figure A4.12 Photographs of textural features in the Upper San Jose spatter ignimbrite.
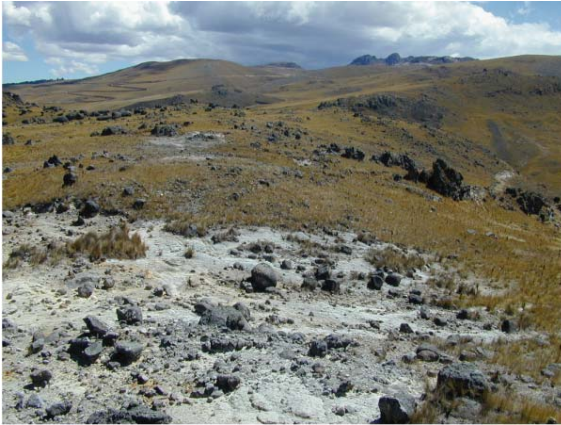
A Coarse lithic concentration at the base of the Msj lies on the unconformity above the Machay Dome The lithics are previously altered accidental fragments.

B Quartz-Sanidine-Andalusite altered accidental fragments at the base of the Msj.

C Massive quartz fragment in the Msj

Quartz-Sanidine-Andalusite altered accidental fragments in the Middle San Jose Ignimbrite

Figure A4.13 Photographs of the disconformity above the Upha Machay Dome and the lithic concentration at the base of the Middle San Jose ignimbrite.
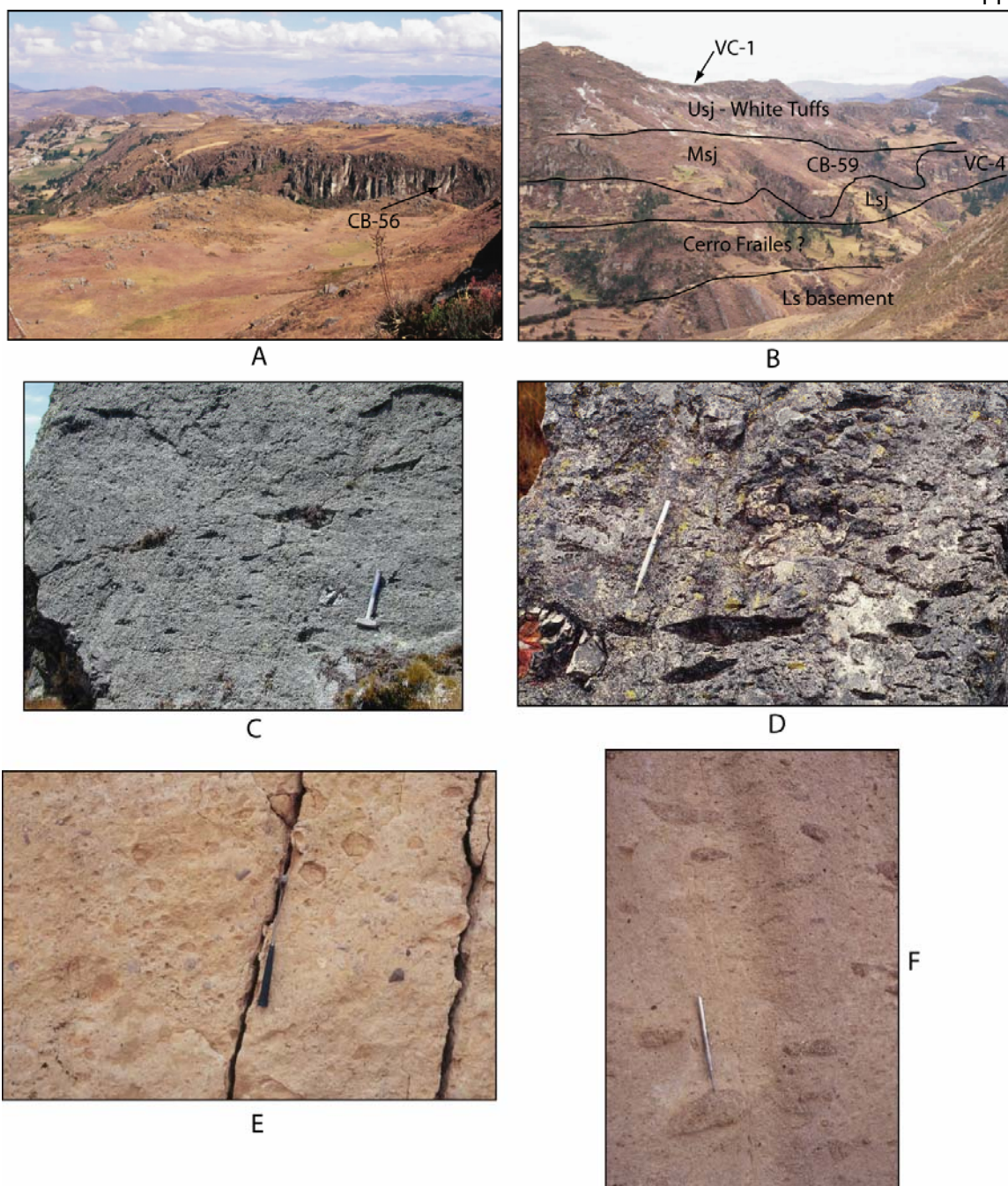
Lower and Middle San Jose Ignimbrites

Figure A4.14 Photographs of outcrop exposures and textures from the Middle San Jose ignimbrite and the Upper San Jose white tuff.
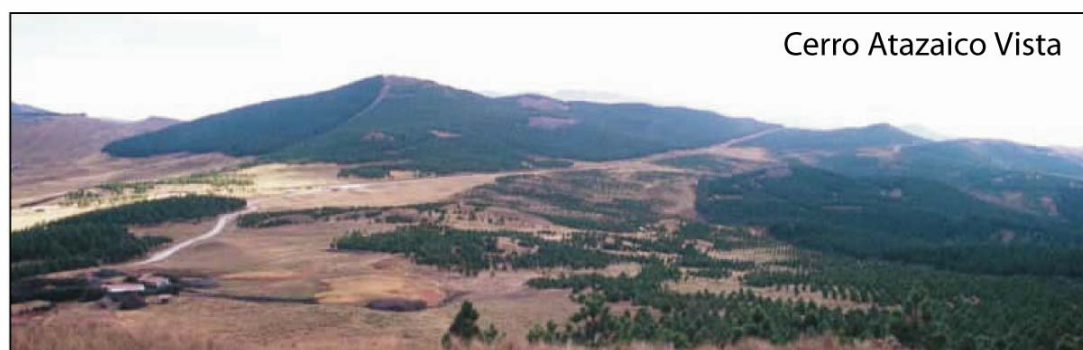
Figure A4.15 Select photos of the Yanacocha district.
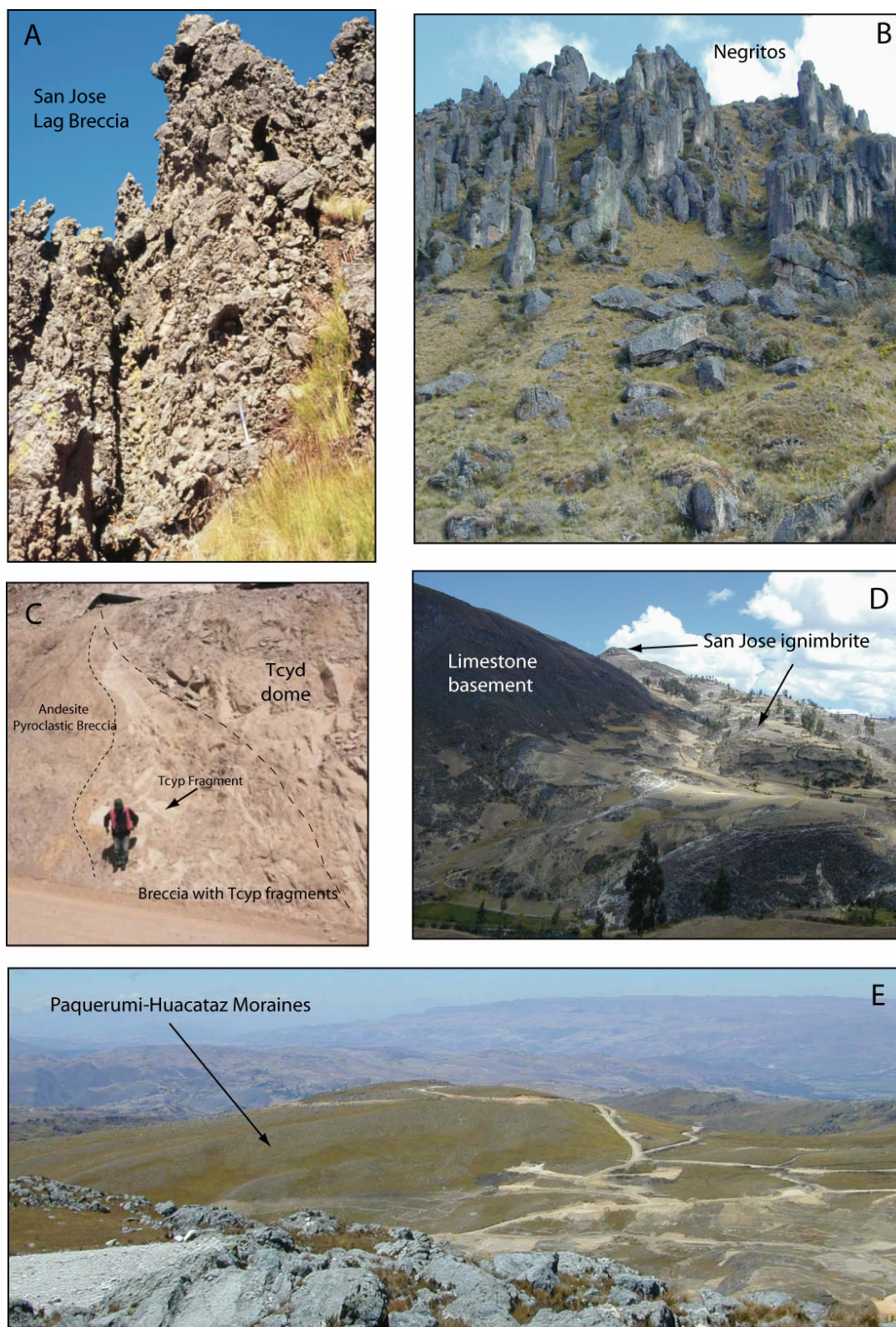
Figure A4.16 Select photos of the rock sequences in the Yanacocha district.

Figure A4.17 Select photos of rock textures.

Appendix V Descriptions of the Scanned Images for the Yanacocha Rock Sequences

Figure A5.1 Scanned images of the Lower Andesite Lahar Sequence:
A. CHQ-97 446.1 meters LAL with crosscutting diatreme-like dikelet. The dikelet has black SM or argillite fragments.
B. Comparison of three fragmental rocks interpreted as LAL-2. CB-32 came from surface outcrops at Alto Machay, CHQ-97 came from 472.6 meters in a diamond drill hole at Chaquicocha Sur, and BS-27 came from 508.3 meters in a DDH at Barranca below MMI and CFP

Figure A5.2 Scanned images comparing the textures of an ignimbrite interpreted as Cerro Frailes dacite to the Maqui Maqui ignimbrite from Barranco drill hole BS-27.
A. Crystal-rich hornblende andesite ignimbrite with rare fiamme and abundant broken phenocrysts and no pyroxene. Interpreted as the Maqui Maqui ignimbrite. Rare accidental fragments of porphyry andesite. Sample collected from drill hole BS-27 56.75 meters at Barranco.
B. Intermediate argillic altered ignimbrite from Barranco drill hole BS-27 at 404.75 meters. The ignimbrite contains fiamme that range from <1 cm to 3 cm in length. Many small fiamme are replaced with pyrite. The ignimbrite contains 2% quartz phenocrysts and lies below the Maqui Maqui ignimbrite (Figure 18) and porphyritic rocks that lack quartz. The unit is interpreted as an ignimbrite flow in the Cerro Frailes dacite pyroclastic sequence, and is similar to ignimbrites described by Loayza (2002) at Cerro Yanacocha drill hole YN-219C 567.2 meters.

Figure A5.3 Scanned images of an ignimbrite that crops out at Chaquicocha Sur and Montura with the Maqui Maqui ignimbrite in the Quebrada Rio Colorado adjacent Maqui Maqui gold deposit.
A. Eutaxitic hornblende trachyandesite tuff at Chaquicocha Sur near Montura. Lithics are black argillite. Interpreted as the Maqui Maqui ignimbrite
B. Eutaxitic hornblende trachyandesite ash-flow tuff at Chaquicocha Sur near Montura. Lithic fragments are black argillite. Interpreted as the Maqui Maqui ignimbrite.
C. Eutaxitic textures in the Maqui Maqui ignimbrite from DDH MM-342 at 242 meters depth.

Figure A5.4 Scanned images of laminated rocks at Yanacocha
A. Laminated rock below Maqui Maqui ignimbrite at Arnacocha. Note white chalcedonic fragments.
B. Laminated rock below Huacataz morane at Chaquicocha. Drill Hole CHQ-81 66.4 meters.
C. Chaquicocha laminated rock on the southwest side. Thin laminated chalcedony
D. Laminated rock at Ocucho Machay upper Lpha contact to Maqui Maqui ignimbrite
E. Laminated rock at Cerro Negro Este.

Figure A5.5 Scanned images of the San Jose ignimbrite. Figure B compares Maqui Maqui ignimbrite DN-7 with the Middle San Jose ignimbrite CB-37 and 38.
A. San Jose ignimbrite that overlies the San Jose gold deposit. Accidental fragments are massive silica and fiamme are rare. Sample is from drill hole SJS-78A 5.0-8.5 meters. The $^{40}Ar/^{39}Ar$ age is 11.24±0.10 Ma.
B. Comparison of the eutaxtic textures in the Maqui Maqui ignimbrite (DN-7) and the San Jose ignimbrite (CB-37 and 38).
C. Eutaxitic textures in the San Jose ignimbrite from 43 meters in DDH SJS-78A over the San Jose Sur deposit.

Figure A5.6 Scanned images of various types of Upper (late) Dacite at Yanacocha.
A. Corimayo Dacite. The upper sample came from diamond drill hole COR-24 at 408 meters depth, and the lower sample came from a surface outcrop at Corimayo.
B. La Quinua Dacite now below the La Quinua leach pad. Similar porphyritic texture to the Corimayo Dacite.
C. Dacite porphyry at Yanacocha (Ypq) from surface outcrops north of Yanacocha Oeste.
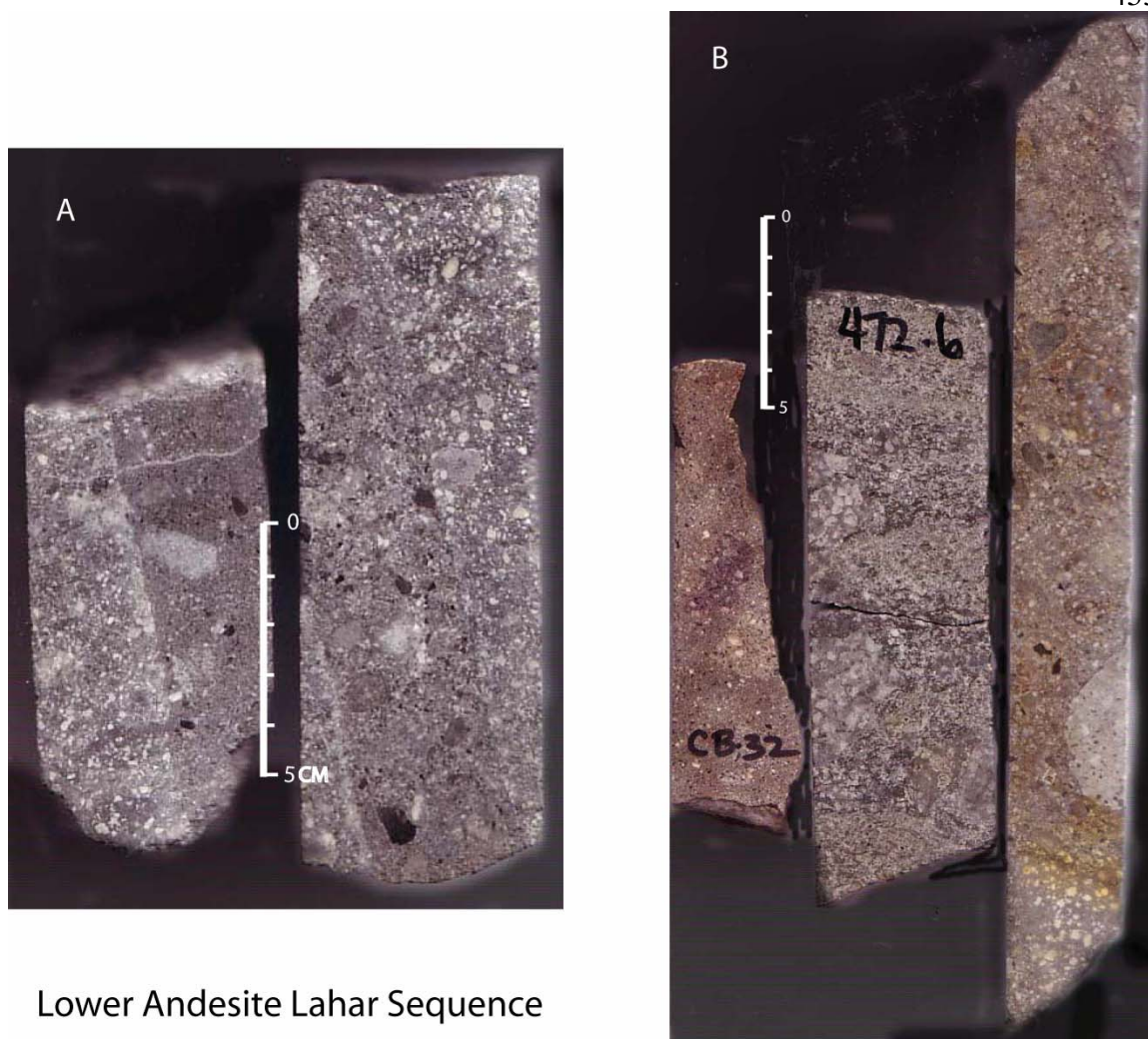
Figure A5.1 Scanned images of the Lower Andesite Lahar Sequence.

BS-27 404.8 meters
Cerro Frailes Ignimbrite

BS-27 57 meters
Maqui Maqui Ignimbrite

Figure A5.2 Scanned images comparing the textures of an ignimbrite interpreted as Cerro Frailes dacite to the Maqui Maqui ignimbrite from Barranco drill hole BS-27.
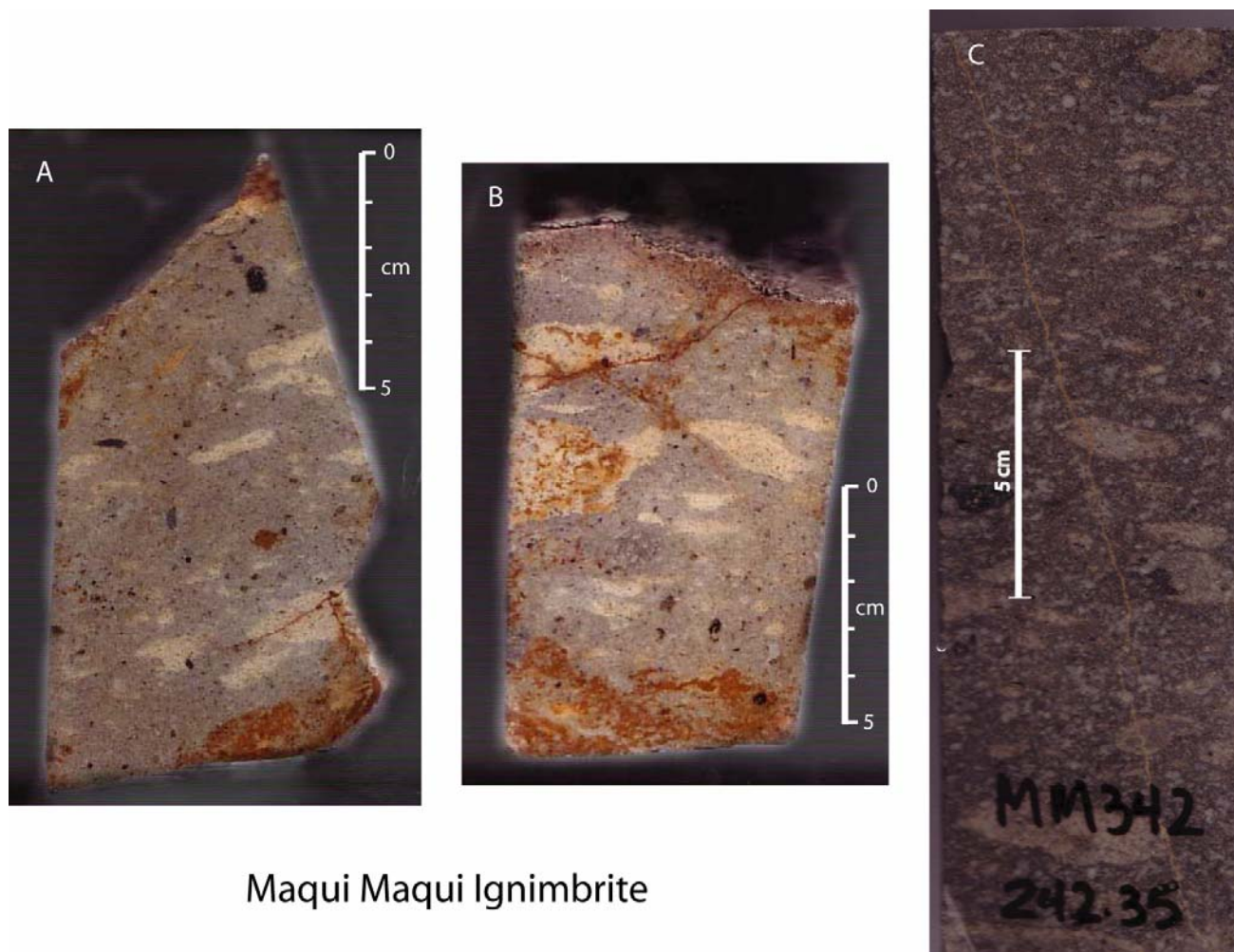
Figure A5.3 Scanned images of an ignimbrite that crops out at Chaquicocha Sur and Montura with the Maqui Maqui ignimbrite in the Quebrada Rio Colorado adjacent Maqui Maqui gold deposit.
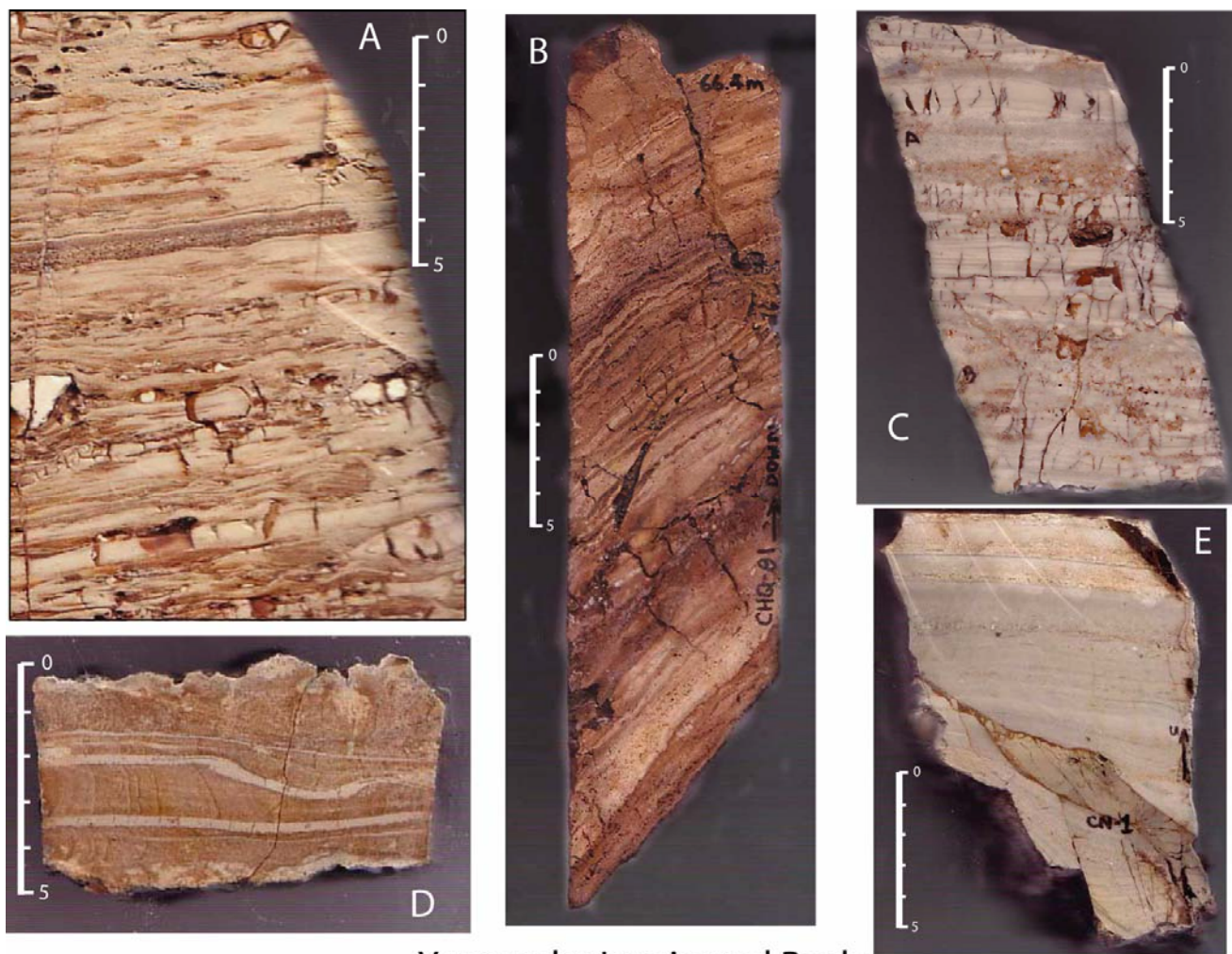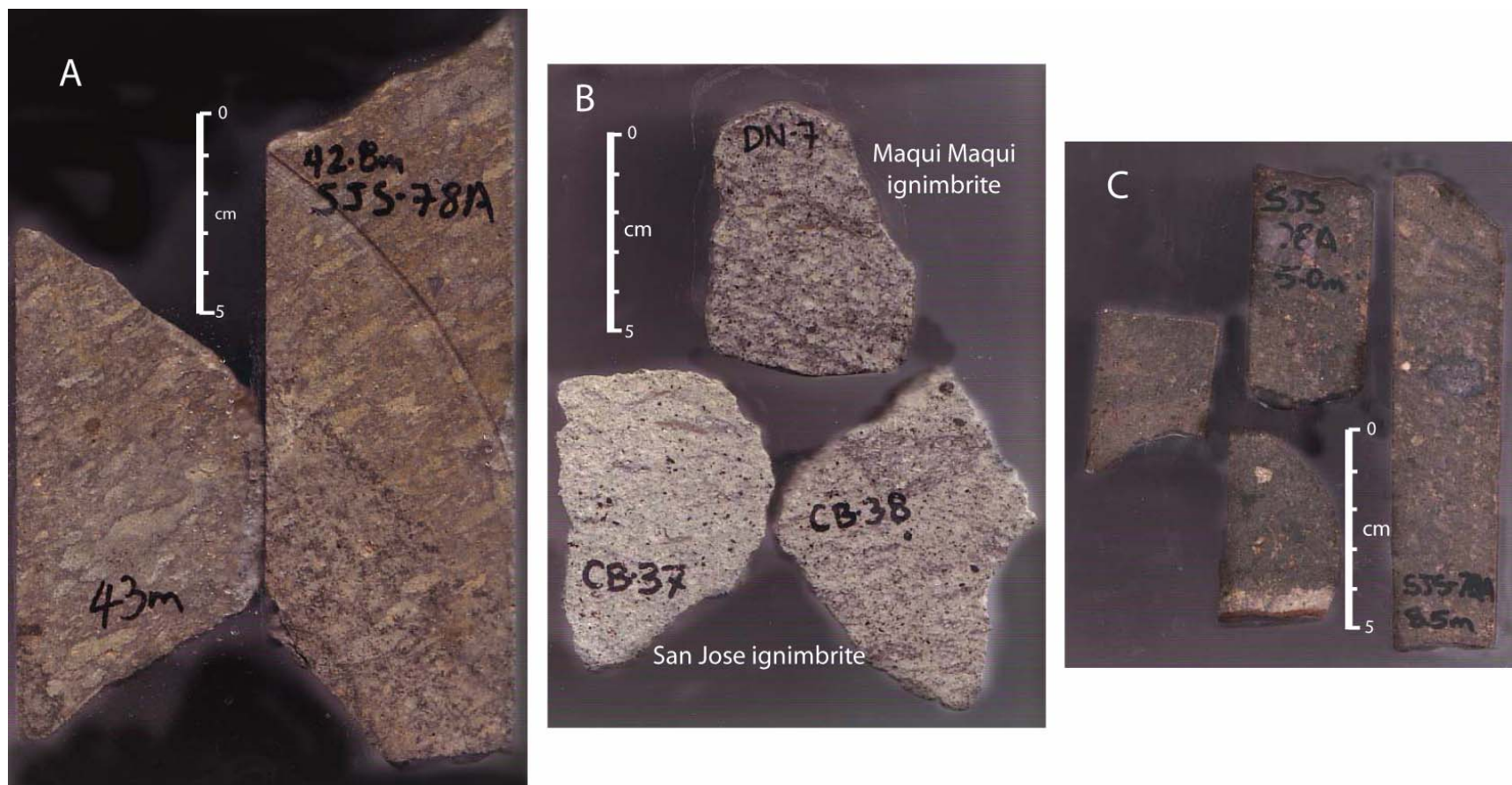
Figure A5.4 Scanned images of laminated rocks at Yanacocha.

San Jose Ignimbrite

Figure A455 Scanned images of the San Jose ignimbrite. Figure B compares Maqui Maqui ignimbrite DN-7 with the Middle San Jose ignimbrite CB-37 and 38.

A

B

C
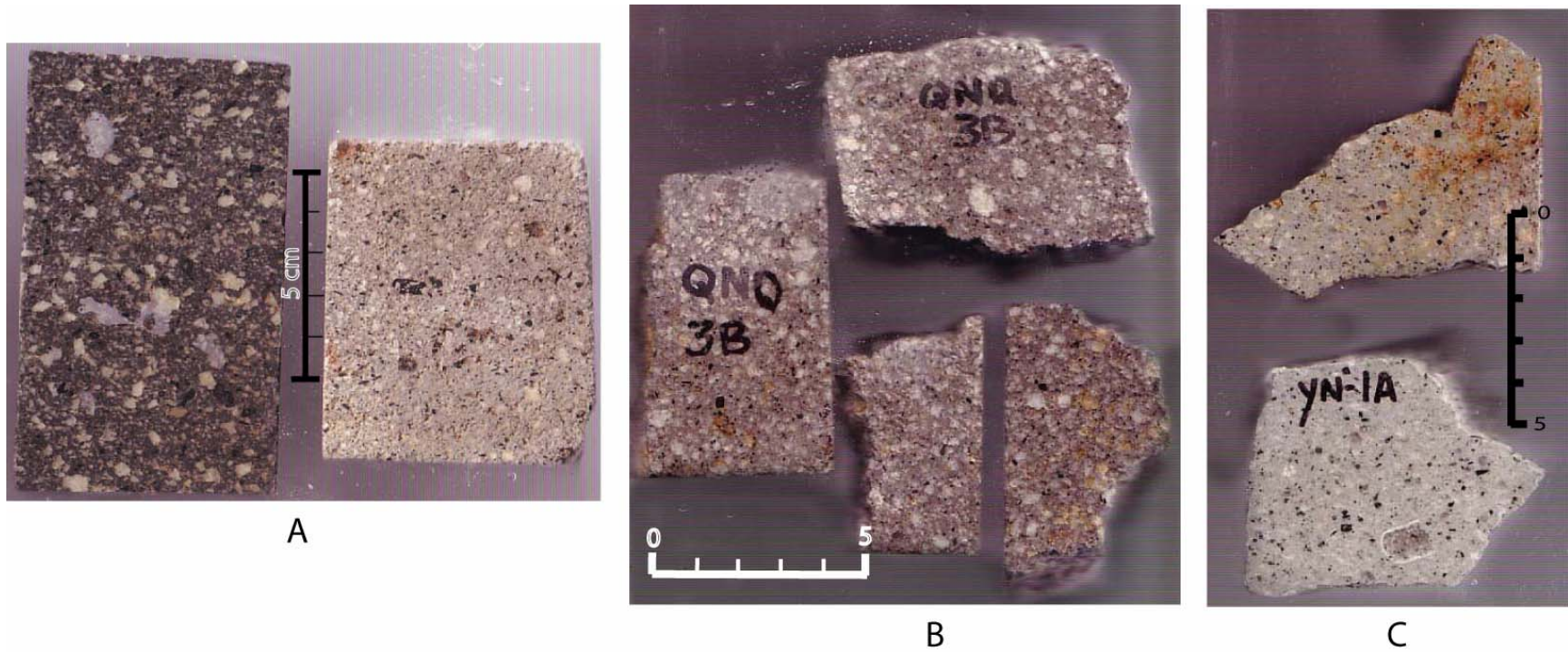
Upper (late) Dacite

Figure A5.6 Scanned images of various types of Upper (late) Dacite at Yanacocha.

Appendix VI Descriptions for the photomicrographs of the Yanacocha rocks

Figure A6.1 Pre-Yanacocha rock sequences
A. Cerro Frailes biotite dacite ash-flow tuff (Fraile 2B)
B. Cerro Frailes biotite-hornblende dacite lapilli tuff (DN-71)
C. Chaupiloma lower andesite lahar (DN-15) with detrital quartz grains.
D. Tual lower andesite pumice-rich lahar flow (CC-18) with hornblende and pyroxene.

Figure A6.2 Upper and Lower Yanacocha Volcanic Sequence
A. Fine-grained trachytic (pilotaxitic) Lower Yanacocha pyroxene andesite lava flow south of Cerro Quilish (DO-43; note 100um scale).
B. Lower Yanacocha pyroxene andesite dome at Cerro Atazaico. Some larger plagioclase (left center) display sieve-cored textures.
C. Lower Yanacocha pyroxene andesite lava flow frim the east district at Elita (AZU-1). Many plagioclase display sieve-rimmed textures with at least three consecutive growth rims.
D. Pilotaxitic textured Upper Yanacocha pyroxene andesite dome lobe in the Otuzco dome complex (DE-2)
E. Near vertical flow foliation in the San Jose-related pyroxene andesite dacite dome called the Chaquicocha Sur dome (CHQS-1).
F. Upper Yanacocha pyroxene andesite tuff at Antonio (DN-83). Plagioclase show oscillatory zoning and most phenocrysts are crystal fragments.

Figure A6.3 Maqui Maqui Ignimbrite
A. Typical fragmental crystal texture with 40-50% phenocrysts in a glassy groundmass (MM-342 158m)
B. Altered ignimbrite that hosts gold ore in the Maqui Maqui deposits. The ignimbrite is fines-depleted with ~50 modal% broken phenocryst in the matrix and less fragments of crystals (~25-30 modal%) in the pumice. MMI at Maqui Maqui Norte (MMN-1).
C. Welded shard textures in glass from a fiamme in the Maqui Maqui ignimbrite west of the Maqui Maqui gold deposi (DN-53).
D Argillite fragment typical of the basement lithics in the Maqui Maqui ignimbrite. Quartzite fragments are also common. (MM-342 169m).
E Typical mineralogy of the non-welded Cori Coshpa ash-flow tuff (DN-30) below the Maqui Maqui Ignimbrite.
F Comparison of a phenocryst-poor pumice fragment and crystal-rich matrix as an example of the fines-depleted character in tuffs in the Maqui Maqui pyroclastic sequence (DN-30; Cori Cospha Tuff).

Figure A6.4 Yanacocha andesite intrusions:
A. Phenocryst-poor, quartz-bearing, pyroxene-hornblende andesite dike at Yanacocha Sur (YSBD) fine-grained pilotaxitic-textured groundmass. Some plagioclase display multiple rims with sieve textures and consecutive growth rims. Pyroxene are altered to calcite.
B. Quartz-bearing pyroxene-hornblende andesite from the Cerro Regalado Dome (CR-4). Orthopyroxene is common.
C. Coarse porphyritic hornblende andesite intrusion at Maqui Maqui Norte (DN-77) with small seriate-textured feldspar laths in a glassy gruondmass. No pyroxene or biotite.
D. Strong trachytic-textured hornblende dacite dike at Corimayo (SL-2 68m). Pyroxene and biotite are absent.

Figure A6.5 Photomicrographs of the San Jose Ignimbrites:
A. Lower San Jose ignimbrite below the Ventanillas de Combayo. The ignimbrite is fines-depleted and the matrix around the pumice fragment contains >50 modal% broken crystals, whereas the pumice fragment may have 25 modal% phenocrysts. The pumice is representative of the phenocryst abundance in the magma (VC-4).
B. Lower or middle San Jose ignimbrite (RC-6) non-welded hornblende±pyroxene dacite ash-flow tuff that overlies the basement limestone above Rio Chonta.
C. Upper San Jose Spatter Ignimbrite (BS-6) a hornblende-pyroxene dacite. The photomicrograph diplays the contact of a juvenile spatter blob to the matrix of the tuff. Phenocrysts are not broken in the spatter blob and the modal% abundance is lower than the matrix. The matrix has 40-50 modal% broken phenocrysts and is fine-depleted. Amphiboles are resorbed oxy-hornblendes.
D Middle to Upper San Jose ignimbrite with strong eutaxitic textures. Most fiamme are smll and rnage from <1 cm to 2 cm in the elongate direction (CB-37, see Figure A3.5B)
E Upper eutaxitic flow in the Lower San Jose ignimbrite (CB-56). Abundant broken pheoncyrsts of plagioclase. The sample contains rare resorbed biotite and small clinopyroxene.
F Middle San Jose ignimbrite that hosts and overlies gold ore at the San Jose gold deposit (SJS-79A 23m). This photomicrograph shows an interesting example of a large broken plagioclase phenocryst bulldozing tiny angular fragments of plagioclase (left side of the large oscillatory zoned and Carlsbad-albite twinned plagioclase.

Figure A6.6 The Lower (early) and Upper (late) Yanacocha Dacite.
A. Early or Lower Dacite at Exaltado in the west district (DO-5). Minerals are plagioclase, hornblende, biotite and quartz. The large subhedral tannish-collered phenocryst in the center is quartz. Some plagioclase display a varity of sieve-textures. The plagioclase bottm center is sive-rimmed with a clear growth rim amd slightly sieve-cored. Upper left is another plagioclase the is strongly sieve-rimmed nearly to the core.
B. Early dacite dome was similar compostions to the sample above (CA-1). The sample was collected from a dacite dome west of Cerro Atazaico.
C. The La Quinua dacite (QNQ-3A) is a late dacite now below the La Quinua leach pad. Minerals consist of quartz (yellowish center and bottom), hornblende (upper left), plagioclase, biotite, and sphene. Siev-textured plagioclase is rare and the amphibole lack opacite rims and resorption textures.
D. Corimayo Dacite (COR-47 238m) at Corimayo with similar mineralogy to the La Quinua dome. Quartz (brown and upper right) is resorbed with ~2-3 modal% abundance. Rare sieve-rimmed plagioclase with clear growth rims are present (left center).
E. Dacite tuff at Corimayo (COR-47 172m) related to the Corimayo dacite. Note the broken phenocrysts with biotite lower right corner.
F. Negritos rhyolite ignimbrite (NG-5) displays abundant broken phenocrysts of plagioclase and quartz. Minerals consist of quartz-plagioclase-biotite-hornblende-sphene.

Figure A6.7 Hypogene Advanced Argillic Alteration:
A. Amorphous silica-kaolinite altered Lower Yanacocha pyroxene-hornblende andesite lava-dome south of Cerro Chaquicocha along the margins of the Ocucho dome. The Ocucho dome post-dates this rock. All phenocryst shapes are preserved.
B. Coarse alunite matrix that surrounds breccia fragments of an earlier vuggy quartz altered dacite tuff at Chaquicocha Sur (CS-1).
C. Irregular-shaped vugs in a fine-grained quartz groundmass lined with coarse alunite above Kupfertal (KUP-3 94m). The vugs resemble phenocryst shapes as often found in vuggy quartz altered rocks. The sample came from the gusano (patchy) textured rocks at Kupfertal.

D. Quartz-alunite altered Punto Negro Dacite at Encajon. Large +1mm resorbed quartz phenocryst (PNE-3 45m). Quartz phenocryst content is ~3 modal% and similar to the Corimayo dacite.
E. Quartz alunite altered Yanacocha dacite porphyry from Cerro Yanacocha. Rounded and embayed quartz phenocrysts at a greater abundance than the Punto Negro dacite. Sample YS-1 SA altered Ypq.
F Heterolithic amorphous silica matrix breccia with fragments of alunite and quartz pebbles all crosscut by late quartz and alunite veinlets. Sample TAP-169 382 meters from the southern margins of Tapado Au deposit.

Figure A6.8 Hypogene Advanced Argillic Alteration and Laminated rocks
A. Rounded and angular quartz-alunite fragments in an amorphous silica groundmass crosscut by late silica-alunite veinlets. The groundmass contains abundant angular fragments of quartz and alunite (<50 μm). Sample TAP-169.
B. Quartz-alunite matrix-supported breccia with heterolithic coarse and fine jigsaw quartz textured fragments. The sample contains anomalous Au (0.11 ppm), Cu (1280 ppm) and Mo (12.15 ppm). Sample YN-105 at 89 meters from Yanacocha Norte.
C. Maqui Maqui laminated rock very thin laminated recrystallized fine-grained jigsaw-textured quartz that may have been amorphous silica or chalcedony. The silica layers contain varying degrees of contamination with fine opaque munerals and rutile.
D Quartz-alunite altered thin bedded, poorly-sorted tuff (QUE-1) above Quebrada Ocucho Machay similar to the thin bedded tuffs and laminated rocks at Pabellon and North Quilish. The textures are similar to TAP-169 in figure A4.7f.
E Chaquicocha laminated rock with varying degrees of recrystallized jigsaw-textured silica with cryptocrystalline silica laminae. This sample contains abundant fine-grained rutile (<5um) and rare zircon (Chaquicocha 2B)
F Arnacocha laminated rock. Very fine-grained, poorly-sorted with occasional fragment, and laminated cyrtocrystalline silica, jigsaw textured quartz, fine opaques (<25um) and rutile.
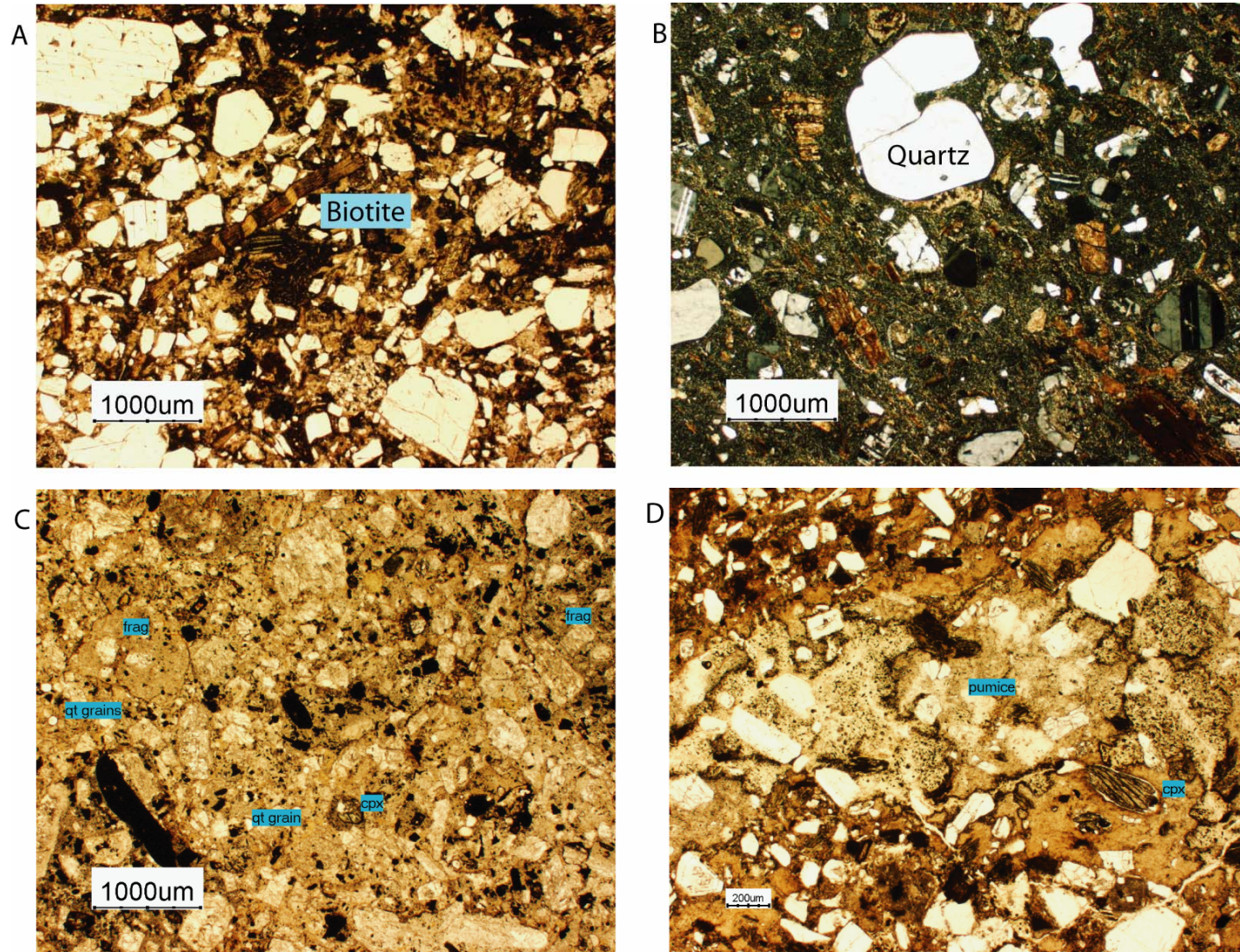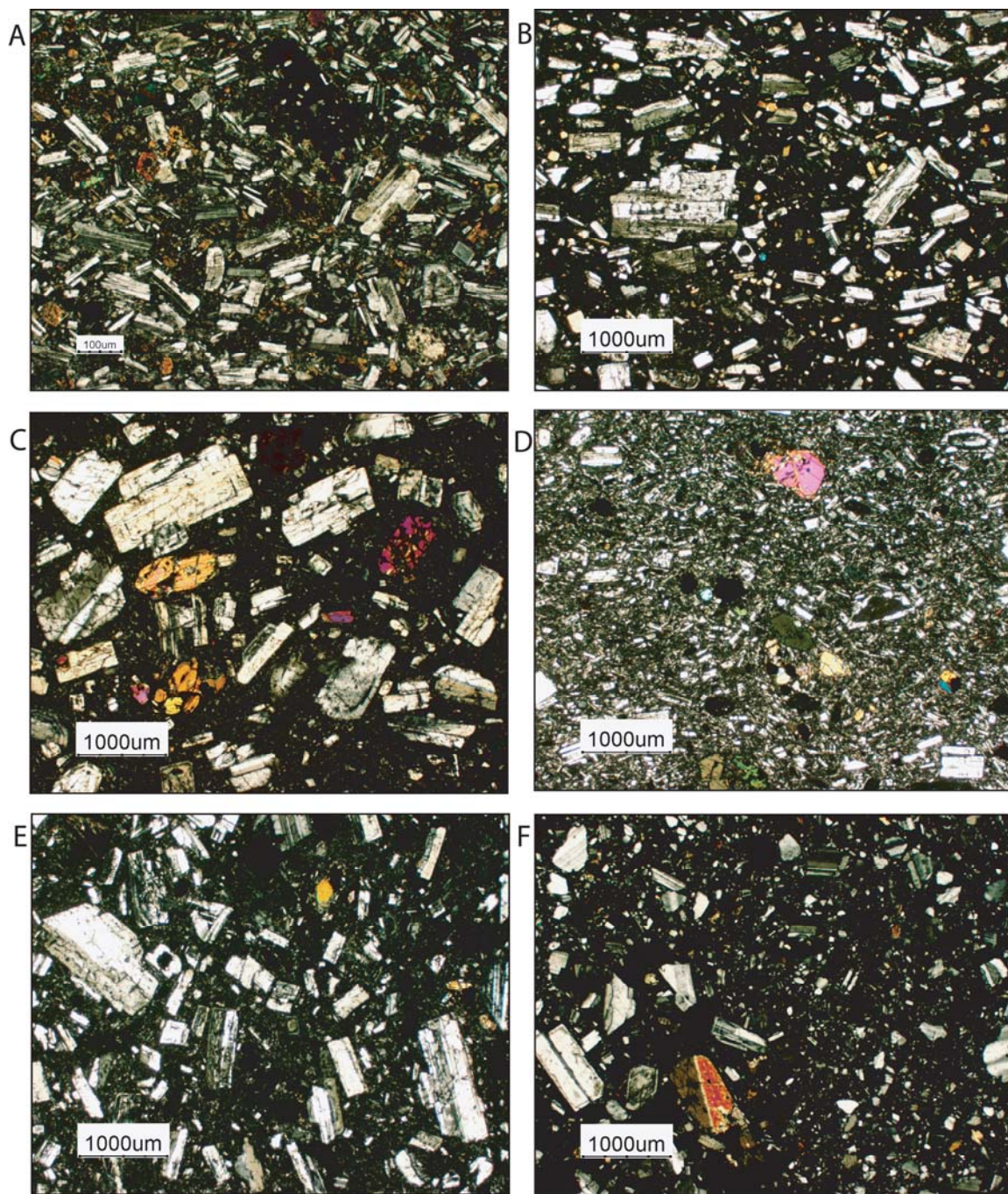
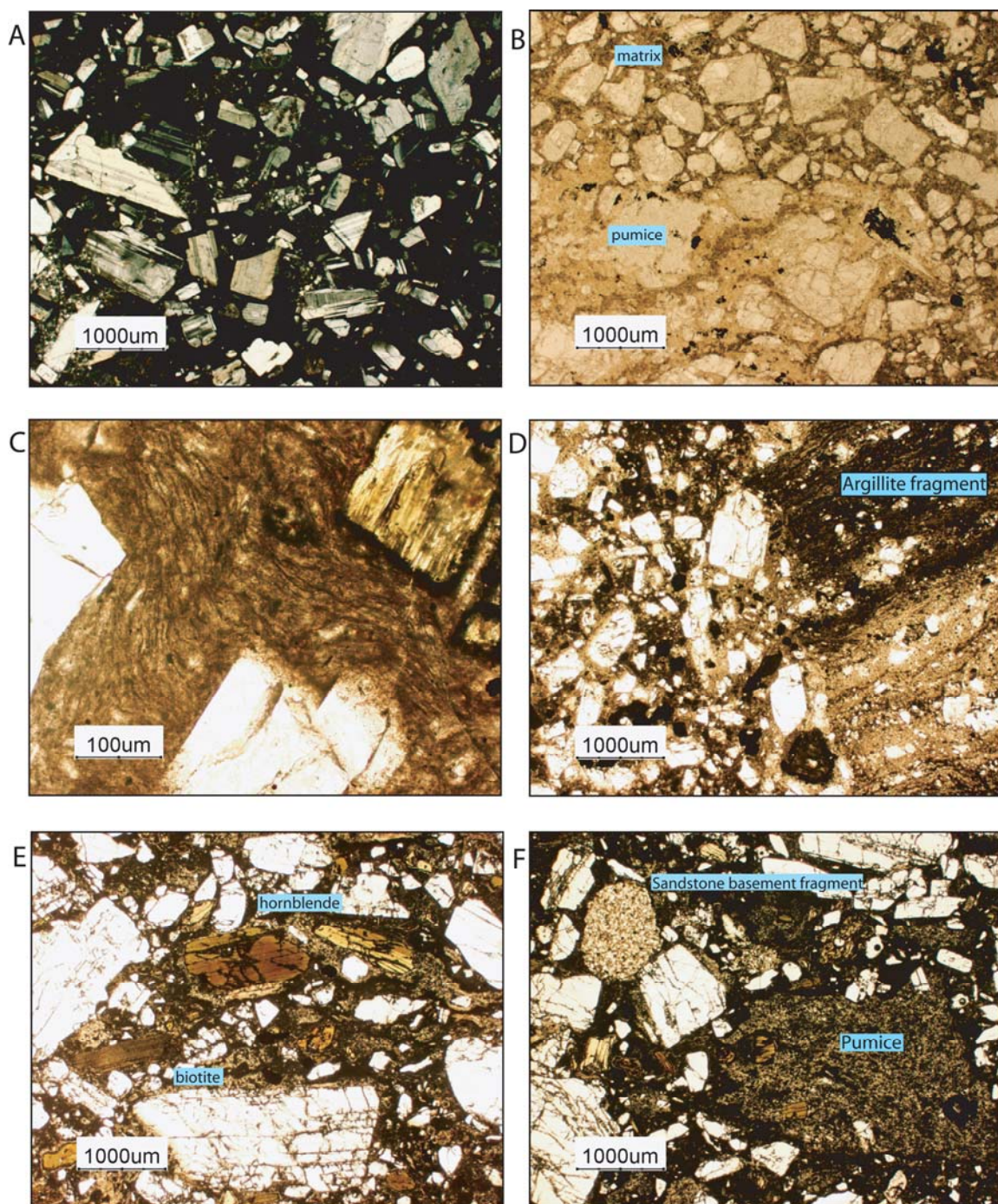Figure A6.1 Photomicrographs of the pre-Yanacocha rock sequences.

Lower and Upper Yanacocha pyroxene-hornblende andesites

Figure A6.2 Photomicrographs of the Upper and Lower Yanacocha volcanic sequences.
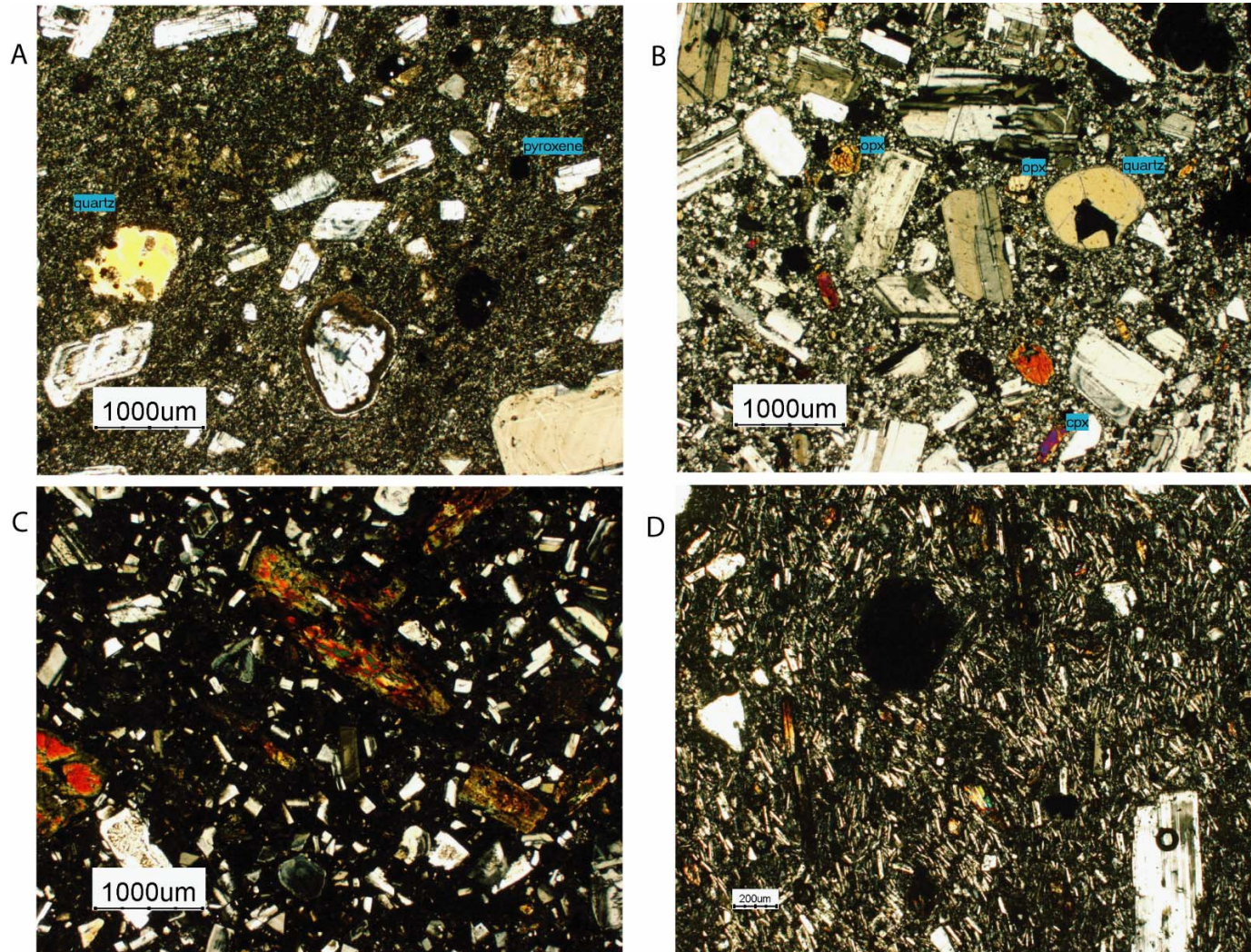
Maqui Maqui Ignimbrite

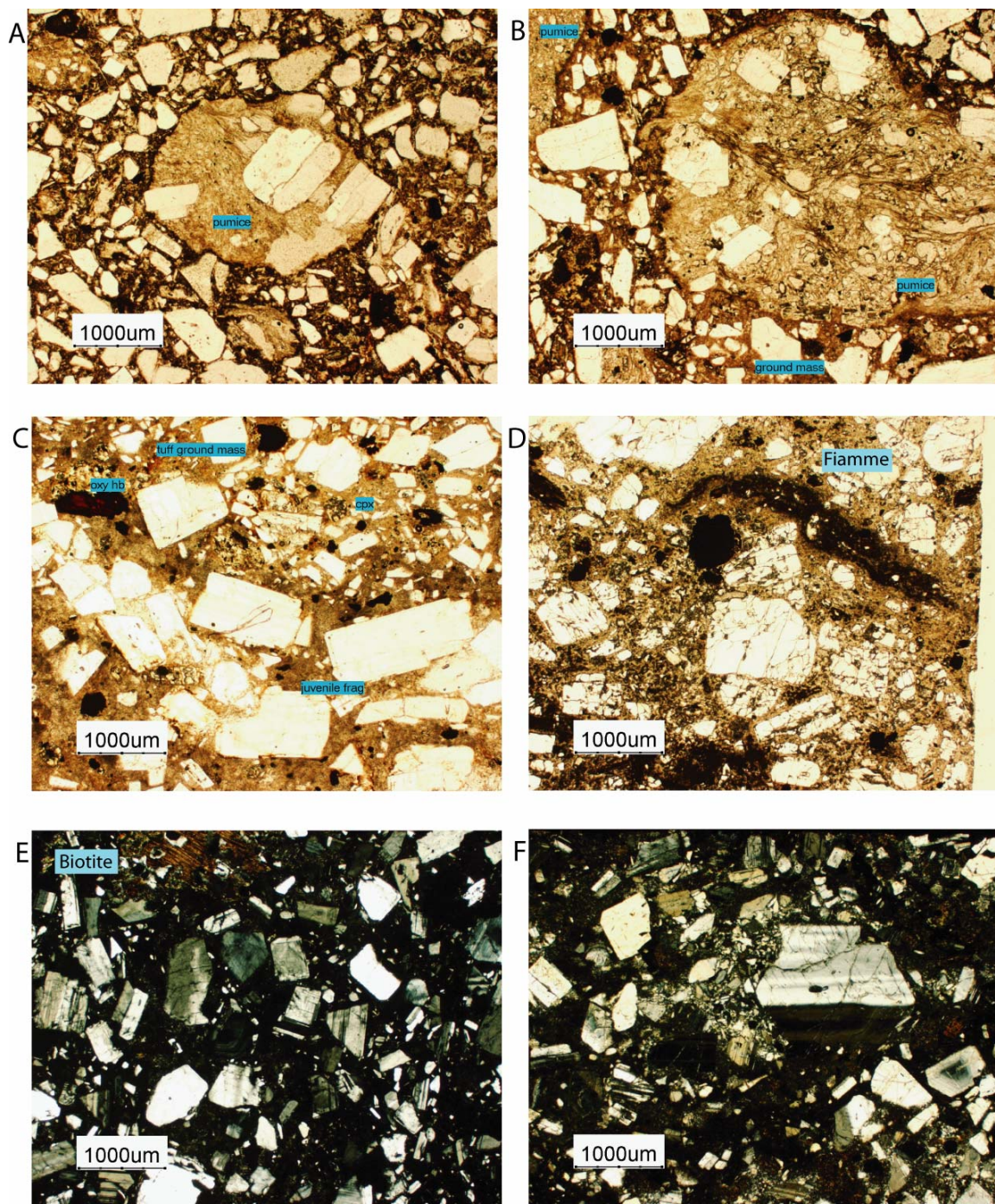Figure A6.3 Photomicrographs of the Maqui Maqui pyroclastic sequence.

Yanacocha Andesite Intrusions

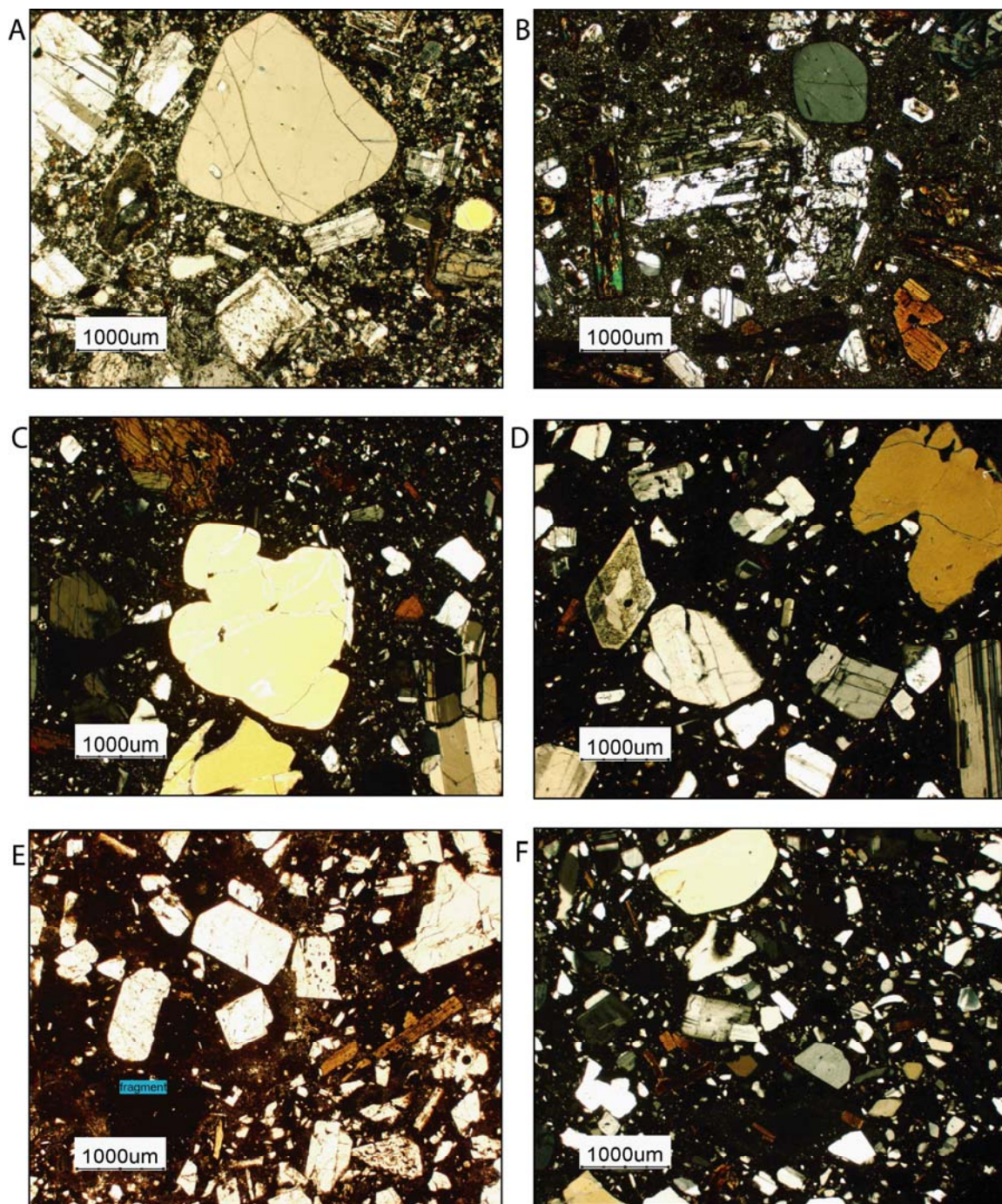Figure A6.4 Photomicrographs of the various Yanacocha andesite intrusions.

San Jose Ignimbrite

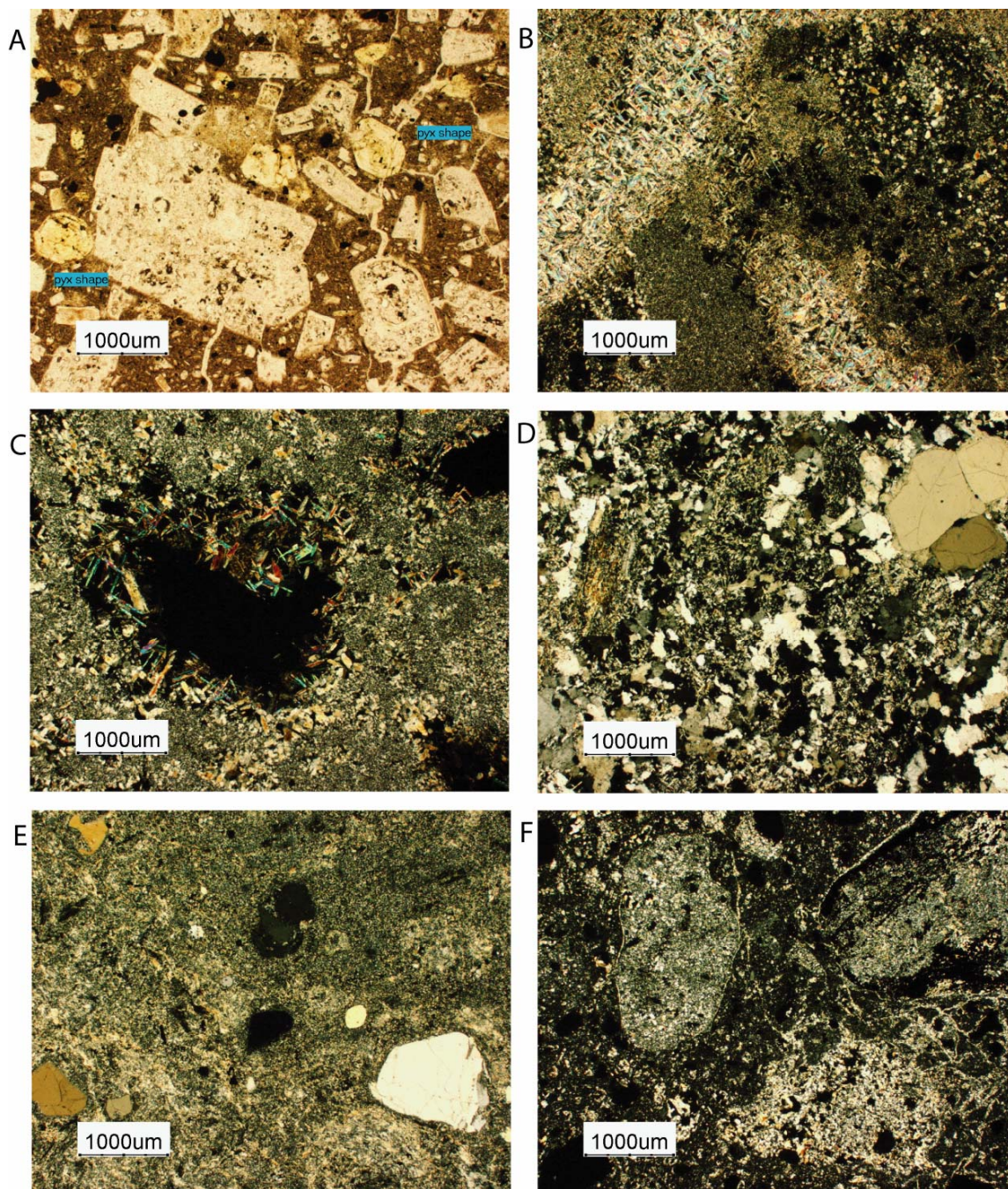Figure A6.5 Photomicrographs of the San Jose ignimbrite sequence.

Lower (early) and Upper (late) Dacites

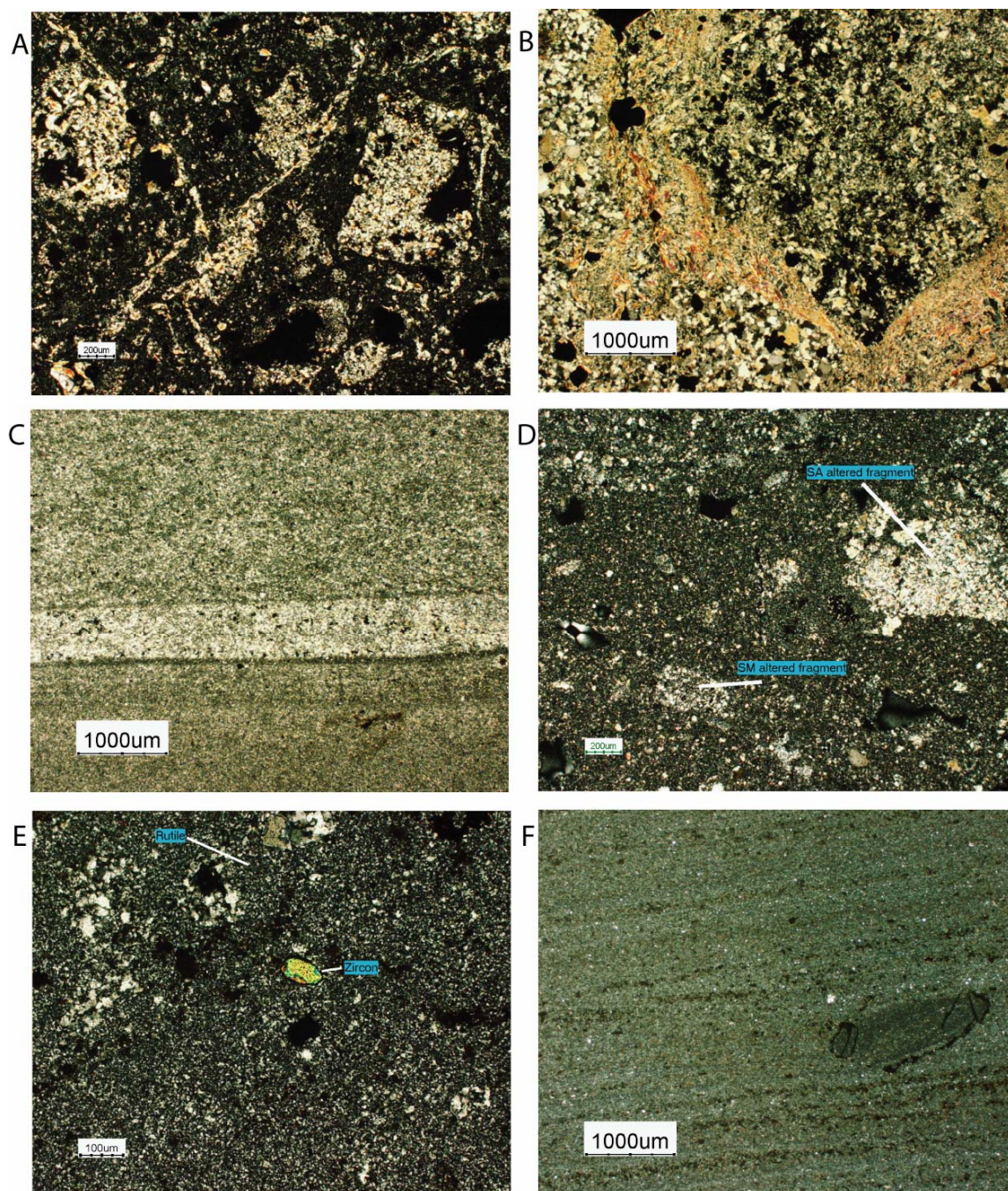Figure A6.6 Photomicrographs of the Lower (early) and Upper (late) Yanacocha Dacite.

Hypogene Advanced Argillic Alteration

Figure A6.7 Photomicrographs of some styles and textures of hypogene advanced argillic alteration. at Yanacocha.

Laminated Rocks and Hypogene Advanced Argillic Alteration

Figure A6.8 Photomicrographs of laminated rocks and some styles and textures of hypogene advanced argillic alteration. at Yanacocha.